frontiers | Research Topics

Tumor microenvironment in cancer hallmarks and therapeutics

Volume II

Edited by
Na Luo, José Alexandre Ferreira and Hongming Miao

Published in
Frontiers in Molecular Biosciences

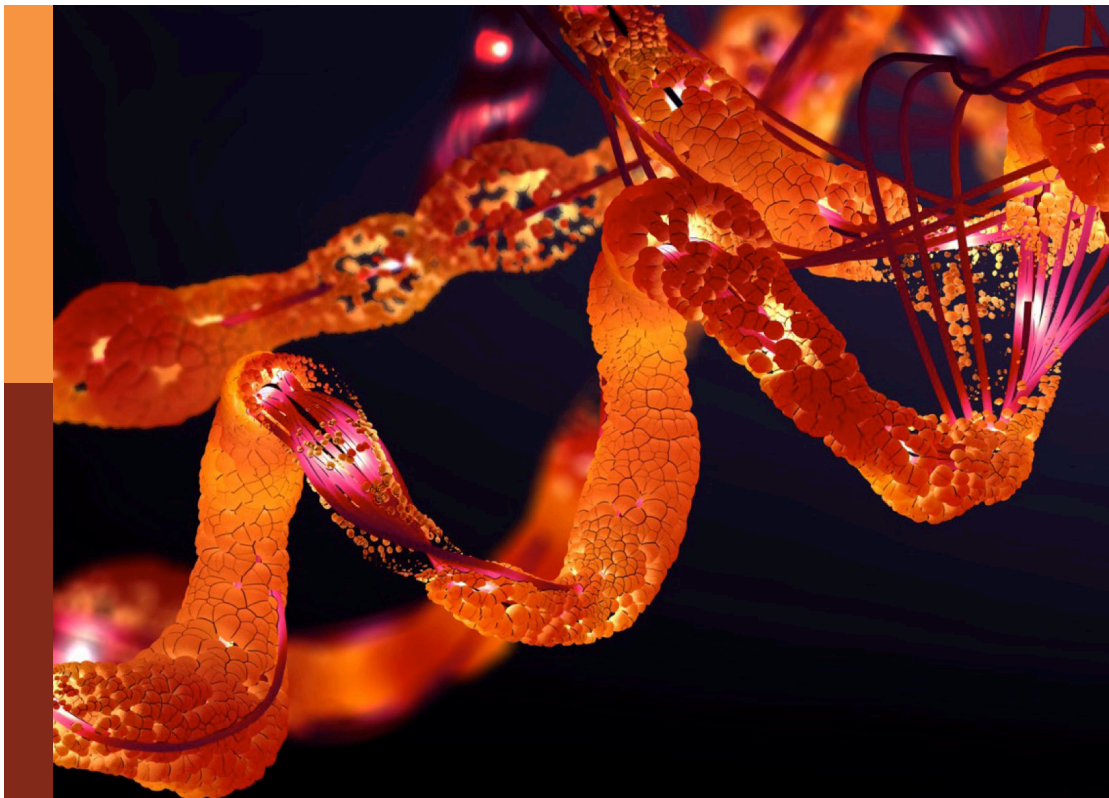

ISSN 1664-8714
ISBN 978-2-83252-154-0
DOI 10.3389/978-2-83252-154-0

About Frontiers

Frontiers is more than just an open access publisher of scholarly articles: it is a pioneering approach to the world of academia, radically improving the way scholarly research is managed. The grand vision of Frontiers is a world where all people have an equal opportunity to seek, share and generate knowledge. Frontiers provides immediate and permanent online open access to all its publications, but this alone is not enough to realize our grand goals.

Frontiers journal series

The Frontiers journal series is a multi-tier and interdisciplinary set of open-access, online journals, promising a paradigm shift from the current review, selection and dissemination processes in academic publishing. All Frontiers journals are driven by researchers for researchers; therefore, they constitute a service to the scholarly community. At the same time, the *Frontiers journal series* operates on a revolutionary invention, the tiered publishing system, initially addressing specific communities of scholars, and gradually climbing up to broader public understanding, thus serving the interests of the lay society, too.

Dedication to quality

Each Frontiers article is a landmark of the highest quality, thanks to genuinely collaborative interactions between authors and review editors, who include some of the world's best academicians. Research must be certified by peers before entering a stream of knowledge that may eventually reach the public - and shape society; therefore, Frontiers only applies the most rigorous and unbiased reviews. Frontiers revolutionizes research publishing by freely delivering the most outstanding research, evaluated with no bias from both the academic and social point of view. By applying the most advanced information technologies, Frontiers is catapulting scholarly publishing into a new generation.

What are Frontiers Research Topics?

Frontiers Research Topics are very popular trademarks of the *Frontiers journals series*: they are collections of at least ten articles, all centered on a particular subject. With their unique mix of varied contributions from Original Research to Review Articles, Frontiers Research Topics unify the most influential researchers, the latest key findings and historical advances in a hot research area.

Find out more on how to host your own Frontiers Research Topic or contribute to one as an author by contacting the Frontiers editorial office: frontiersin.org/about/contact

Volume II: Tumor microenvironment in cancer hallmarks and therapeutics

Topic editors

Na Luo — Nankai University, China

José Alexandre Ferreira — Portuguese Oncology Institute, Portugal

Hongming Miao — Army Medical University, China

Citation

Luo, N., Ferreira, J. A., Miao, H., eds. (2023). *Volume II: Tumor microenvironment in cancer hallmarks and therapeutics*. Lausanne: Frontiers Media SA.

doi: 10.3389/978-2-83252-154-0

Table of contents

frontiers | Frontiers in Molecular Biosciences

TYPE Editorial
PUBLISHED 28 March 2023
DOI 10.3389/fmolb.2023.1182083

OPEN ACCESS

EDITED BY
William C. Cho,
QEH, Hong Kong SAR, China

REVIEWED BY
Haizhou Lou,
Zhejiang University, China

*CORRESPONDENCE
José Alexandre Ferreira,
jose.a.ferreira@ipoporto.min-saude.pt
Na Luo,
luon11@nankai.edu.cn
Hongming Miao,
hongmingmiao@sina.com

†These authors have contributed equally to this work

SPECIALTY SECTION
This article was submitted to Molecular Diagnostics and Therapeutics, a section of the journal Frontiers in Molecular Biosciences

RECEIVED 08 March 2023
ACCEPTED 22 March 2023
PUBLISHED 28 March 2023

CITATION
Shi R, Gao Y, Ferreira JA, Luo N and Miao H (2023), Editorial: Volume II: Tumor microenvironment in cancer hallmarks and therapeutics.
Front. Mol. Biosci. 10:1182083.
doi: 10.3389/fmolb.2023.1182083

Editorial: Volume II: Tumor microenvironment in cancer hallmarks and therapeutics

Rongchen Shi[1,2†], Yuan Gao[2†], José Alexandre Ferreira[3*], Na Luo[4*] and Hongming Miao[2*]

[1]Frontier Medical Training Brigade, Third Military Medical University (Army Medical University), Xinjiang, China, [2]Department of Pathophysiology, College of High Altitude Military Medicine, Third Military Medical University (Army Medical University), Chongqing, China, [3]Experimental Pathology and Therapeutics Group, Research Center of IPO Porto (CI-IPOP)/RISE@CI-IPOP (Health Research Network), Portuguese Oncology Institute of Porto (IPO-Porto)/Porto Comprehensive Cancer Center Raquel Seruca (Porto.CCC), Porto, Portugal, [4]Department of Anatomy and Histology, School of Medicine, Nankai University, Tianjin, China

KEYWORDS

cancer biomarkers, tumor microenvironment, cancer immunotherapy, diagnosis, prognosis

Editorial on the Research Topic
Volume II: Tumor microenvironment in cancer hallmarks and therapeutics

Cancer biomarkers have many important applications in oncology, including risk assessment, diagnosis, prognosis, prediction of treatment response, and disease progression (Sarhadi and Armengol, 2022). In the past, cancer biomarkers were mainly focused on the discovery of mutated genes occurring in cancer cells themselves (Jahangiri and Aghi, 2012; Ganguly et al., 2019). However, tumor cells live in the immunosuppressed tumor microenvironment, and the immune response is also critical to the prognosis of patients. Therefore, there is an urgent need to explore new cancer biomarkers, which could not only indicate prognosis, but also guide tumor therapy, especially tumor immunotherapy (Wu and Dai, 2017; Liu et al., 2022).

This Research Topic is dedicated to publishing new prognostic and therapeutic biomarkers, especially those related to tumor microenvironment (TME), based on large databases and large sample analyses, which will be more beneficial for tumor screening and treatment. A total of 13 articles are included in this Research Topic.

Five articles are devoted to single gene database analysis. Du et al. used the database for somatic mutation analysis and found that FRAS1 Related Extracellular Matrix 2 (FREM2) was one of the genes with the highest mutation frequency in patients with colorectal adenocarcinoma and was closely associated with poor prognosis. Meanwhile, the random forest method was used to construct a prognosis model with good predictive function based on FREM2 mutation. The prediction accuracy was high (83.9%), and a total of 13 prognostic pattern characteristic genes related to overall survival were identified. These results suggest that FREM2 mutation may be a potential prognostic marker for colon cancer. Another research found that collagen triple helix repeat containing 1 (CTHRC1), a glycosylated protein, was significantly expressed in cancer tissues of colorectal adenocarcinoma patients and was associated with poor patient outcomes. More importantly, authors found that CTHRC1 expression was positively correlated with a variety of immune cell infiltration, including $CD8^+$ T cells, $CD4^+$ T cells, neutrophils, macrophages, and dendritic cells, which

may provide a theoretical basis for the development of new immunotherapeutic targets based on CTHRC1. Liu et al. found that interleukin-1 receptor-associated kinases1 (IRAK1), an active kinase that plays a key role in the IL-1/TLR signaling pathway, is upregulated in more than two dozen cancers. And the expression level of IRAK1 is closely related to the efficacy of anti-PDL1, which may be a reliable marker for predicting the efficacy of tumor immunotherapy. In addition, pan-cancer analysis of targeted type 2 mannose receptor C (MRC2) suggested significant associations with immune cell infiltration, immunomodulators, and immunotherapeutic markers, particularly in patients with metastatic melanoma and advanced urothelial carcinoma. Bai et al. also found that the expression of laminin subunit gamma 1 (LAMC1) in different types of renal cancer was completely opposite to the prognosis, and database analysis suggested that this might be closely related to the different tumor immune microenvironment.

Another five papers are devoted to multigene database analysis. A retrospective study of breast cancer samples by Zhu et al. showed that the Systemic Inflammation Index (SIRI) can independently predict breast cancer survival. Lower SIRI predicted increased disease-free survival and overall survival. In addition, Sun et al. developed a considerable nomogram. Trp-related immune gene (TRIG) scores were negatively correlated with immune activation and overall survival. At the same time, TRIG score was also significantly correlated with immune cell infiltration and immune checkpoint expression in TME, which might provide new strategies for prognosis assessment and tumor immunotherapy in lung adenocarcinoma patients. Ephrin family genes (EFNs) and the prognostic and immunological characteristics of liver cancer patients were analyzed in another research. The authors found that EFNA3, EFNA4 and EFNB1 were independent prognostic factors and were closely related to tumor immunity. Zhou et al. conducted a comprehensive analysis of the relationship between genes related to single carbon metabolism and prognosis, chemotherapy resistance and immunotherapy in patients with lung adenocarcinoma. According to the expression of 7 prognostic related genes in 497 LUAD samples, the authors divided the sample into two clusters, and pointed out that cluster 1 had worse prognosis and stronger chemotherapy resistance, but cluster 1 had more significant immunotherapy efficacy, providing a theoretical basis for immunotherapy in LUAD patients. In a study of the association between cuproptosis-related genes and papillary renal cell carcinoma (PRCC) development, prognosis, and treatment, authors created and validated a risk score for predicting overall survival, indicating that the lower the risk score, the better the tumor immune microenvironment, the longer the overall survival, and the stronger the sensitivity to chemotherapy drugs.

In addition, Liu et al. analyzed the tumor immune microenvironment and found that the survival rate of cervical cancer patients with low immune level in tumor was lower than that of patients with high immune level, which may be related to the reduced level of immune infiltration caused by the high methylation level in the TME. This finding is of great significance for hierarchical management of patients and precise targeted therapy.

Finally, two reviews are included in this Research Topic. One paper summarized the role of cytokines most associated with EMT in tumor progression, invasion, migration, and metastasis formation of bladder cancer. The other provides a comprehensive discussion of exosomes and their role in various aspects of cancer biology. Both these cytokines and exosomes might serve as new biomarkers for efficient diagnosis.

In conclusion, recent studies have used large databases and other state-of-art technologies to accurately analyze the significance of one or more genes that are misregulated in a specific TME for tumor diagnosis, prognosis, and treatment. These studies have greatly expanded our current understanding of tumor biomarkers and will facilitate further development.

Author contributions

RS and YG drafted this editorial article using the comments from all the other listed authors. All authors listed approved it for publication.

Acknowledgments

Thanks to all authors for their contributions to this Research Topic.

Conflict of interest

The authors declare that the research was conducted in the absence of any commercial or financial relationships that could be construed as a potential conflict of interest.

Publisher's note

References

Ganguly, A., Frank, D., Kumar, N., Cheng, Y. C., and Chu, E. (2019). Cancer biomarkers for integrative oncology. *Curr. Oncol. Rep.* 21 (4), 32. doi:10.1007/s11912-019-0782-6

Jahangiri, A., and Aghi, M. K. (2012). Biomarkers predicting tumor response and evasion to anti-angiogenic therapy. *Biochim. Biophys. Acta* 1825 (1), 86–100. doi:10.1016/j.bbcan.2011.10.004

Liu, K., Cui, J. J., Zhan, Y., Ouyang, Q. Y., Lu, Q. S., Yang, D. H., et al. (2022). Reprogramming the tumor microenvironment by genome editing for precision cancer therapy. *Mol. Cancer* 21 (1), 98. doi:10.1186/s12943-022-01561-5

Sarhadi, V. K., and Armengol, G. (2022). Molecular biomarkers in cancer. *Biomolecules* 12 (8), 1021. doi:10.3390/biom12081021

Wu, T., and Dai, Y. (2017). Tumor microenvironment and therapeutic response. *Cancer Lett.* 387, 61–68. doi:10.1016/j.canlet.2016.01.043

frontiers in Molecular Biosciences

ORIGINAL RESEARCH
published: 18 February 2022
doi: 10.3389/fmolb.2022.839617

Identification and Comprehensive Analysis of FREM2 Mutation as a Potential Prognostic Biomarker in Colorectal Cancer

Hanpeng Du[1†], Haiyue Wang[2†], Fandong Kong[1], Mingjian Wu[1], Wei Chen[3], Jin Lyu[4], Sitong Zhou[5] and Ronghua Yang[6]**

[1]Department of Gastrointestinal Surgery, Panyu Maternal and Child Care Service Centre of Guangzhou (He Xian Memorial Affiliated Hospital of Southern Medical University), Guangzhou, China, [2]Department of Nutrition, The First Hospital of Hebei Medical University, Shijiazhuang, China, [3]Department of Pancreaticobiliary Surgery, The First Affiliated Hospital of Sun Yat-sen University, Guangzhou, China, [4]Department of Pathology, The First People's Hospital of Foshan, Foshan, China, [5]Department of Dermatology, The First People's Hospital of Foshan, Foshan, China, [6]Department of Burn and Plastic Surgery, Guangzhou First People's Hospital, School of Medicine, South China University of Technology, Guangzhou, China*

OPEN ACCESS

Edited by:
Na Luo,
Nankai University, China

Reviewed by:
Chengnan Tian,
First Affiliated Hospital of Gannan Medical University, China
Bowen Li,
First Affiliated Hospital of Harbin Medical University, China
Yuanke Liang,
First Affiliated Hospital of Shantou University Medical College, China

***Correspondence:**
Sitong Zhou
sitongzhou@hotmail.com
Ronghua Yang
21720091@qq.com

†These authors have contributed equally to this work and share first authorship

Specialty section:
This article was submitted to Molecular Diagnostics and Therapeutics, a section of the journal Frontiers in Molecular Biosciences

Received: 20 December 2021
Accepted: 28 January 2022
Published: 18 February 2022

Citation:
Du H, Wang H, Kong F, Wu M, Chen W, Lyu J, Zhou S and Yang R (2022) Identification and Comprehensive Analysis of FREM2 Mutation as a Potential Prognostic Biomarker in Colorectal Cancer. Front. Mol. Biosci. 9:839617. doi: 10.3389/fmolb.2022.839617

Gene mutations play an important role in tumor progression. This study aimed to identify genes that were mutated in colorectal cancer (CRC) and to explore their biological effects and prognostic value in CRC patients. We performed somatic mutation analysis using data sets from The Cancer Genome Atlas and International Cancer Genome Consortium, and identified that *FREM2* had the highest mutation frequency in patients with colon adenocarcinoma (COAD). COAD patients were divided into *FREM2*-mutated type ($n = 36$) and *FREM2*-wild type ($n = 278$), and a Kaplan-Meier survival curve was generated to perform prognostic analysis. A *FREM2*-mutation prognosis model was constructed using random forest method, and the performance of the model was evaluated using receiver operating characteristic curve. Next, the random forest method and Cox regression analysis were used to construct a prognostic model based on the gene expression data of 36 *FREM2*-mutant COAD patients. The model showed a high prediction accuracy (83.9%), and 13 prognostic model characteristic genes related to overall survival were identified. Then, the results of tumor mutation burden (TMB) and microsatellite instability (MSI) analyses revealed significant differences in TMB and MSI among the risk scores of different prognostic models. Differentially expressed genes were identified and analyzed for functional enrichment and immune infiltration. Finally, 30 samples of CRC patients were collected for immunohistochemical staining to analyze the FREM2 expression levels, which showed that FREM2 was highly expressed in tumor tissues. In conclusion, CRC patients had a high level of *FREM2* mutations associated with a worse prognosis, which indicated that *FREM2* mutations may be potential prognostic markers in CRC.

Keywords: Frem2, gene mutation, colorectal cancer, prognosis, biomarker

Abbreviations: AUC, Area under the curve; COAD, colon adenocarcinoma; CRC, colorectal cancer; FPKM, Fragments Per Kilobase per Million; GO, Gene Ontology; GSEA, Gene Set Enrichment Analysis; GSVA, Gene Set Variation Analysis; HLA, human leukocyte antigen; HPA, The Human Protein Atlas; ICGC, International Cancer Genome Consortium; IHC, Immunohistochemistry; KEGG, Kyoto encyclopedia of genes and genomes; K–M, Kaplan-Meier; MHC, Major histocompatibility complex; MSI, microsatellite instability; OS, overall survival; RF, random forest; ROC, receiver operating characteristic; TCGA, The Cancer Genome Atlas; TMB, tumor mutation burden; TPM, transcripts per million reads.

INTRODUCTION

Colorectal cancer (CRC) is one of the most common malignant tumors that seriously endanger human health nowadays (Sung et al., 2021). In recent years, changes in dietary structure and living habits have been accompanied by an increase in the incidence and mortality of CRC patients in China (Feng et al., 2019). Nonetheless, the prognosis of CRC patients remains remarkably poor, highlighting the need for further understanding the molecular mechanism of the development of CRC and the identification of new prognostic biomarkers. The pathogenesis of CRC is complex and involves genetic and environmental factors. Previous studies have found that gene mutations leading to abnormal cell signal transduction are closely related to the occurrence and development of CRC (Nakayama and Oshima, 2019).

FRAS1 Related Extracellular Matrix 2 (FREM2), located on 13q13.3, encodes an integral membrane protein that contains a large amount of chondroitin sulfate proteoglycan element repeats and Calx-beta domains (Yu et al., 2018), which confer it with sodium-calcium exchanger activity, permitting this protein to export calcium from the cell. Additionally, FREM2 forms part of the FREM2-FRAS1-FREM1 protein complex, which plays an important role in epidermal-dermal interactions (Kiyozumi et al., 2006). Previous studies have found that FREM2 is related to the development of the eye (Zhang et al., 2019) and kidney epithelium (Al-Hamed et al., 2021). Recently, it has been found that FREM2 is highly expressed in gliomas and that patients with high expression levels of FREM2 show a better prognosis (Jovcevska et al., 2019). However, the role of FREM2 in CRC has not been investigated to date.

In the study, we performed somatic mutation analysis using The Cancer Genome Atlas (TCGA) and International Cancer Genome Consortium (ICGC) databases and we found that *FREM2* had the highest mutation frequency. First, prognostic analysis revealed that CRC patients with *FREM2* mutations had a worse prognosis. Subsequently, a prognostic model was constructed based on the gene expression data of 36 *FREM2*-mutant CRC patients, the efficacy of the model was evaluated, and 13 prognostic model characteristic genes related to OS were identified. Next, the tumor mutation burden (TMB) and microsatellite instability (MSI) were compared between the risk scores of different prognostic models. The genes differentially expressed between *FREM2*-mutant type and *FREM2*-wild type were identified, and functional enrichment and immune infiltration analysis were performed. Finally, the FREM2 protein expression levels were detected using immunohistochemical staining in 30 CRC patient tissues. In conclusion, *FREM2* was highly expressed in CRC and showed a higher level of mutation in CRC patients than in healthy controls. The presence of *FREM2* mutations was associated with a worse prognosis in CRC patients, indicating that *FREM2* mutation may be a potential prognostic biomarker for CRC.

MATERIALS AND METHODS

Data Processing

Gene somatic mutation data (MAF files) were downloaded from the colon adenocarcinoma (COAD) project of TCGA (http://cancergenome.nih.gov/) (Tomczak et al., 2015) and COAD-CN cohorts of ICGC (www.icgc.org). RNAseq data in level 3 HTSeq-FPKM format was downloaded from TCGA-COAD. The RNAseq data in fragments per kilobase per million (FPKM) format was converted into transcripts per million reads (TPM) format and log2 conversion was performed for subsequent analysis. The main goal of the ICGC database is to comprehensively study the genomic changes in a variety of cancers that contribute to the global burden of human disease. It comprises data on about 50 different cancer types (or subtypes), including information about abnormal gene expression, somatic mutations, epigenetic modifications, and clinical data among others. In total, 25,000 tumor genomes are compiled in the ICGC. The corresponding clinicopathological characteristics, such as gender, age, stage, etc., and prognostic information of TCGA-COAD patients were downloaded from the UCSC Xena website (http://xena.ucsc.edu/). RNA sequencing data (count value) of 399 samples (TCGA-COAD) with corresponding mutation and survival data were obtained from TCGA database for subsequent analysis. The GRCh38 version of the genome in the Ensembl database (ftp://ftp.ensembl.org/pub/current_gtf) was used for annotation (Howe et al., 2021). In addition, copy number variation (CNV) data were downloaded from TCGA database. The clinical characteristics of the patients are shown in **Supplementary Table S1**.

Mutation Analysis

With the development of tumor genomics, the mutation annotation format (MAF) is being widely accepted and used to store detected somatic mutations. In this study, the maftools package (Mayakonda et al., 2018) and the GenVisR package (Skidmore et al., 2016) were used to visualize the somatic mutation data downloaded from TCGA. The somatic mutation data of COAD patients from the ICGC were visualized using the GenVisR package. The G3viz package (Guo et al., 2020) was used to visualize the *FREM2* mutations. In addition, to check whether the CNVs of this gene were associated with COAD, GISTIC2.0 of the Genepattern (https://cloud.genepattern.org/) cloud analysis platform was used to analyze the CNV data obtained from TCGA database (Reich et al., 2006).

Analysis of the Effects of *FREM2* Mutations on the Prognosis of Patients With COAD

According to the gene expression data of COAD patients downloaded from TCGA, the patients were divided into mutation group (n = 36) and wild type group (n = 278) according to the *FREM2* mutation status. Survival analysis was performed to study the prognostic difference between the mutation and the wild type groups based on the information

about the prognosis of patients with COAD. Additionally, all patients with COAD, whose gene expression data was available, were randomly divided into training (n = 266) and test (n = 90) sets at a ratio of 3:1. A robust model of *FREM2* mutation prediction was constructed on the training set using the random forest (RF) method (Yperman et al., 2020). The performance of the model was evaluated using the receiver operating characteristic (ROC) curve.

Construction of the Prognostic Model

The gene expression data of 36 *FREM2*-mutant COAD patients with clinical information were used to construct a prognostic model. First, a univariate Cox regression analysis was performed to initially identify the genes related to OS (p value <0.05). Next, a prognostic risk model was established using the RF method and multivariate Cox regression analysis. The risk score calculation formula was:Risk score = exp gene 1 * β gene 1 + exp gene 2 * β gene 2 + exp gene 3 * β gene 3 +. . . exp gene n * β gene n (exp gene n: the expression level of gene n; β gene n: the regression coefficient of the multivariate Cox regression analysis of gene n). Next, correlation analysis of *FREM2* mRNA expression levels with risk scores and the expression levels of characteristic genes in the model were conducted.

Evaluation of the Efficacy and Clinical Relevance of the Prognostic Models

According to the median risk score, *FREM2*-mutant COAD patients with clinical information were divided into high-risk and low-risk groups. Kaplan–Meier (K–M) survival curve analysis and time-dependent ROC were used to analyze overall survival (OS) to evaluate the prediction accuracy of the model. Next, among COAD patients with *FREM2* mutations, univariate and multivariate Cox regression analyses were performed using clinicopathological variants, such as age, gender, clinical stage, and tumor stage, as well as risk score of patients. Lastly, the correlation between the risk score and clinical characteristics was analyzed.

Analysis of TMB and MSI

Considering that different types of *FREM2* mutations may have different roles in tumorigenesis, the expression data of COAD patients were divided into inactivating mutation subgroups and other non-silent mutation subgroups. K–M survival curve and time-dependent ROC were used to analyze the prognosis of the two subgroups.

TMB refers to the total number of somatic mutations in the exon coding region of the genome that have substitutions, insertions, or deletions per Mb base in a tumor sample. The TMB score of each sample depicts the total number of somatic mutations (including non-synonymous point mutations, insertions, and deletions in the exon coding region)/target area size, and the unit is mutations/Mb (Chan et al., 2019). A microsatellite is segment of tandem repeats in the human genome, such as single nucleotide repetitions or dinucleotide repetitions. MSI refers to the change of any length of microsatellite caused by the insertion or deletion of repeat units in tumor tissues compared to normal tissues (Hile et al., 2013). MSI is calculated as the number of insertions or deletions in gene repeats. In his study, we separately analyzed the relationship between the risk score of the prognosis model with TMB and MSI.

Identification of Differentially Expressed Genes

To investigate the effects of *FREM2* mutation on the gene expression levels, samples in TCGA data set were divided into *FREM2*-mutant type and *FREM2*-wild type according to their mutation status. Then, the R package limma was used to analyze the differences between the groups (Ritchie et al., 2015). The thresholds for considering a gene as differentially expressed were set as |log fold change (logFC)| > 0.5 and p value < 0.05. Genes with logFC >0.5 and p value <0.05 were considered to be differentially up-regulated and those with logFC < −0.5 and p value < 0.05 were considered to be differentially down-regulated. The results of this analysis were displayed using heat map and volcano plot.

Gene Function and Pathway Enrichment Analysis

Gene Ontology (GO) enrichment analysis is a common method for large-scale functional enrichment studies of genes in different dimensions and at different levels, generally from three levels: biological process, molecular function, and cellular component (Ashburner et al., 2000). Kyoto encyclopedia of genes and genomes (KEGG) (Kanehisa and Goto, 2000) is a widely used database that contains information about genomes, biological pathways, diseases, and drugs. We used the R software package clusterProfiler (Yu et al., 2012) to perform GO function annotation and KEGG biological pathway enrichment analysis on differentially expressed genes to identify significantly enriched biological processes and pathways. p value <0.05 was considered statistically significant.

Gene Set Enrichment Analysis (GSEA) and Gene Set Variation Analysis (GSVA)

GSEA is a n method used to determine whether a set of predefined genes show statistical differences between two biological states. It is generally used to estimate changes in pathway and biological process activity in expression data sets (Subramanian et al., 2005). In order to study the differences in the biological processes of genes between the *FREM2*-mutant and the *FREM2*-wild type groups, the reference gene sets "C5.go.v7.4.symbols.gmt" and "c2.cp.kegg.v7.4. symbols. gmt" were downloaded from the MSigDB database (Liberzon et al., 2015). The R package "clusterProfiler" was used to perform GSEA on TCGA-COAD gene expression profile data. p value <0.05 was considered statistically significant.

GSVA (Liberzon et al., 2015) is a non-parametric unsupervised analysis method that relies on converting the expression matrix of genes between different samples into the expression matrix of gene sets between samples to evaluate the gene set enrichment results of the transcriptome, and to further evaluate whether different metabolic pathways are enriched in

different samples. In order to study the biological process that were altered in the *FREM2*-mutant group compared to the *FREM2*-wild type group, GSVA was performed using the R package "GSVA" (Hanzelmann et al., 2013). The reference gene set "h.all.v7.4.symbols.gmt" from the MSigDB database was downloaded to calculate the enrichment score of each sample in the data set in each pathway. Finally, the correlation between the GSVA results and the risk score was analyzed.

Immune-Cell Infiltration Analysis

The immune microenvironment is a complex integrated system mainly composed of immune cells, inflammatory cells, fibroblasts, interstitial tissues, and various cytokines and chemokines. Analysis of immune cell infiltration in tissues is an important tool in understanding the pathological mechanisms of a disease and guiding prognosis prediction.

ESTIMATE is an algorithm that quantifies the immune infiltration level in tumor samples based on gene expression data, which can reflect the diversity of the stroma and immune cells. In this study, the estimate package in R (Yoshihara et al., 2013) was used to estimate the content of stromal cells and immune cells in TCGA-COAD. The correlation between the characteristic genes of the prognosis model and the expression levels of *FREM2* and the ESTIMATE score were analyzed.

CIBERSORT is an algorithm that deconvolves the expression matrix of immune cell subtypes based on the principle of linear support vector regression using RNA-Seq data to estimate the abundance of immune cells in the tissue. In this study, the proportion of 22 immune cell subtypes in TCGA-COAD immune microenvironment was evaluated using the CIBERSORT algorithm (Newman et al., 2019) in R software. The number of permutations was set to 1,000, and a p value <0.05 was considered be representative of an accurate sample for calculating the content of immune cells. Using Pearson correlation analysis, the correlation between the expression of characteristic genes of the prognostic model and the expression levels of *FREM2* and 22 types of immune cells in COAD was calculated.

To examine the biological processes and cell signaling pathways that the characteristic genes of the prognostic model may participate in, the immune gene set from the ImmPort database (Bhattacharya et al., 2014) (https://www.immport.org) was downloaded and the relationships between characteristics genes of the prognostic model and *FREM2* and the immune genes were analyzed. Major histocompatibility complex (MHC) is expressed on the cell surface of all nucleated cells, and the human MHC is collectively referred to as human leukocyte antigen (HLA). HLA is a key molecule in antigen presentation and antigen recognition by immune cells. The relationships between the expression levels of members of the HLA family and the risk score of the prognostic model was also analyzed.

Patients Tissue Specimens

A total of 30 patients fulfilling the inclusion criteria (histologically confirmed stage II or III or IV melanoma) at The First People's Hospital of Foshan between 2019 and 2021 were included in the present study (**Supplementary Table S2**). The exclusion criteria were as follows: *1*) Incomplete previous medical history, immunohistochemistry (IHC) information, and follow-up information; *2*) cancer recurrence post-surgery; *3*) patients with multiple tumors; *4*) patients who received radiotherapy/chemotherapy before surgery. Patient-informed consent was obtained and approved by The First People's Hospital of Foshan Subject Review Board.

IHC Staining and Analysis

IHC staining was performed as previously described elsewhere (Yang et al., 2021). Briefly, specimens were incubated with individual primary antibodies (anti-FREM2, 1:50, Atlas Antibodies; anti-Ki-67,1:100, Abcam) and then washed and incubated with horseradish peroxidase–conjugated secondary antibody (goat anti-rabbit, 1:500, Cell Signaling Technology). Colorimetric reaction was using diaminobenzidine (DAB).

All specimens were examined using the cross-product (H score) of the percentage of tumor cell staining at each of the three staining intensities. The intensity of immunopositivity was scored as follows: none, 0; weak, 1; moderate, 2; and strong, 3. For example, a particular tumor may have 50% cell staining at intensity = 1 and 50% of cell staining at intensity = 3, it would have a combined H score of 200 [$(50 \times 1) + (50 \times 3) = 200$], with a range from 0 to 300. The final score was graded by H score as follows: Low, H score 0–100; Moderate, H score 101–200; and High, H score 201–300. All IHC sections were scored blindly by three independent pathologists. The IHC score were agreed upon by at least two out of three pathologists.

Expression Levels of *FREM2* in Pan-Cancer and COAD

UALCAN (http://ualcan.path.uab.edu/index.html) is an effective online analysis and mining website for cancer data, mainly based on the relevant cancer data in TCGA database (Chandrashekar et al., 2017). UALCAN database was used to analyze the expression levels of *FREM2* in pan-cancer and COAD. The Human Protein Atlas (HPA, https://www.proteinatlas.org/) is a comprehensive database that provides the protein expression profiles for a large number of human proteins, presented as immunohistological images from most human tissues. The HPA database was used to detect the expression of FREM2 in COAD tissues.

Statistical Analysis

All data calculation and statistical analysis were performed using R (https://www.r-project.org/, version 4.1.0). Benjamini-Hochberg was used for multiple test correction, and false discovery rate was used in multiple tests to correct for multiple testing. For the comparison of two groups of continuous variables, normally distributed variables were analyzed using independent Student's t test, and non-normally distributed variables were analyzed using Mann-Whitney U test (Wilcoxon rank sum test). The survival package of R (Durisova

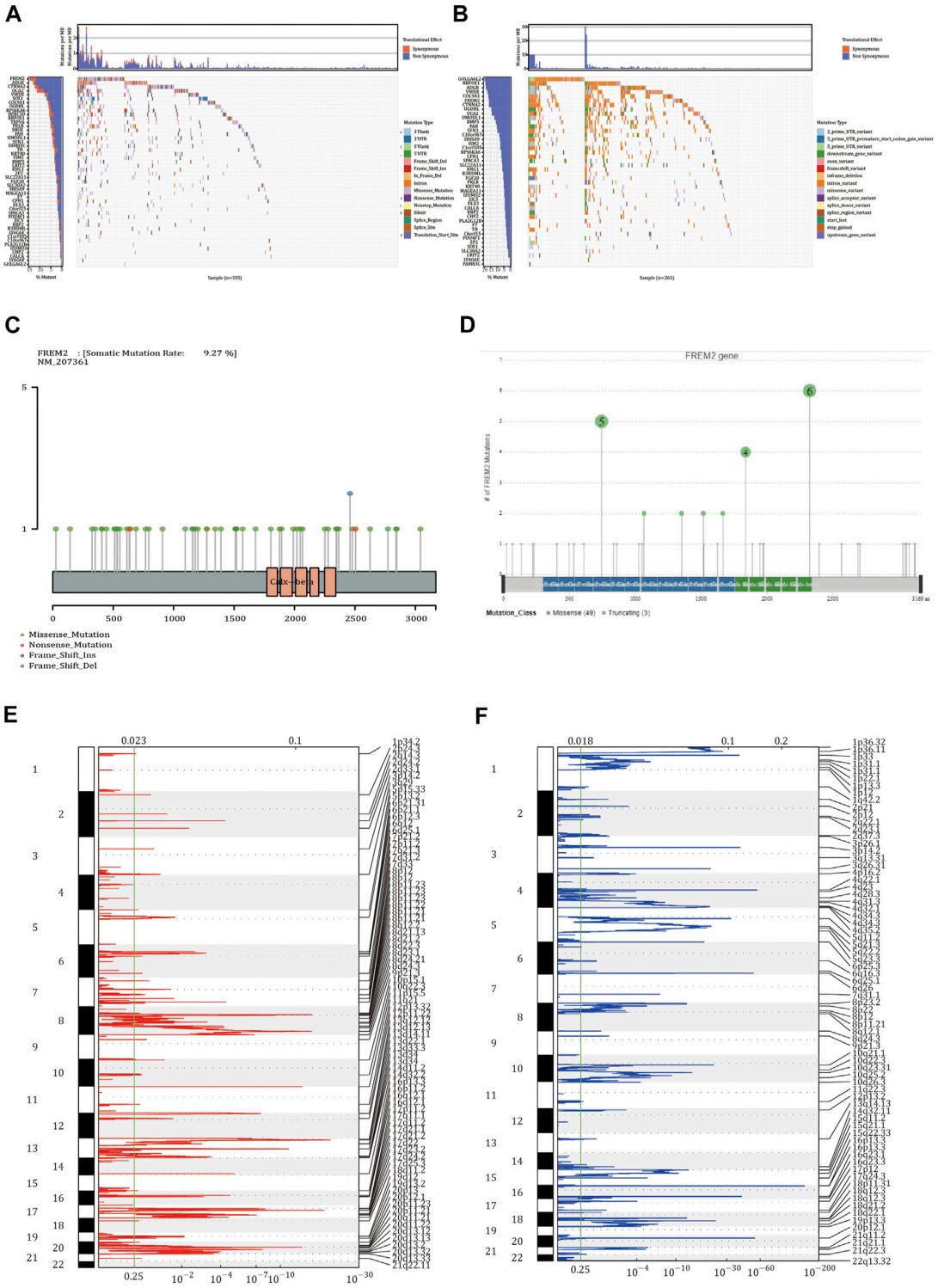

FIGURE 1 | Somatic mutation and copy number variation analysis in colon adenocarcinoma (COAD) patients. **(A)** The 68 genes with the highest mutation frequency in COAD patients from The Cancer Genome Atlas (TCGA). **(B)** The mutations of 68 genes in the International Cancer Genome Consortium (ICGC) database. In the two waterfall charts, the left panel shown genes with high frequency mutations arranged according to their mutation frequency and the right panel shows different types of mutations represented by various color modules. **(C)** The mutations of *FREM2* in TCGA cohort and **(D)** in the ICGC cohort. **(E,F)** Identification the amplification and deletion of *FREM2*. The mRNA located at the focal copy number alteration peak was related to COAD. The false discovery rate (Q value) and the change score of GISTIC2.0 (*x*-axis) correspond to the position of the genome (*y*-axis). The dotted line indicates the centromere. The green line represents the 0.25 Q value cutoff point for determining significance.

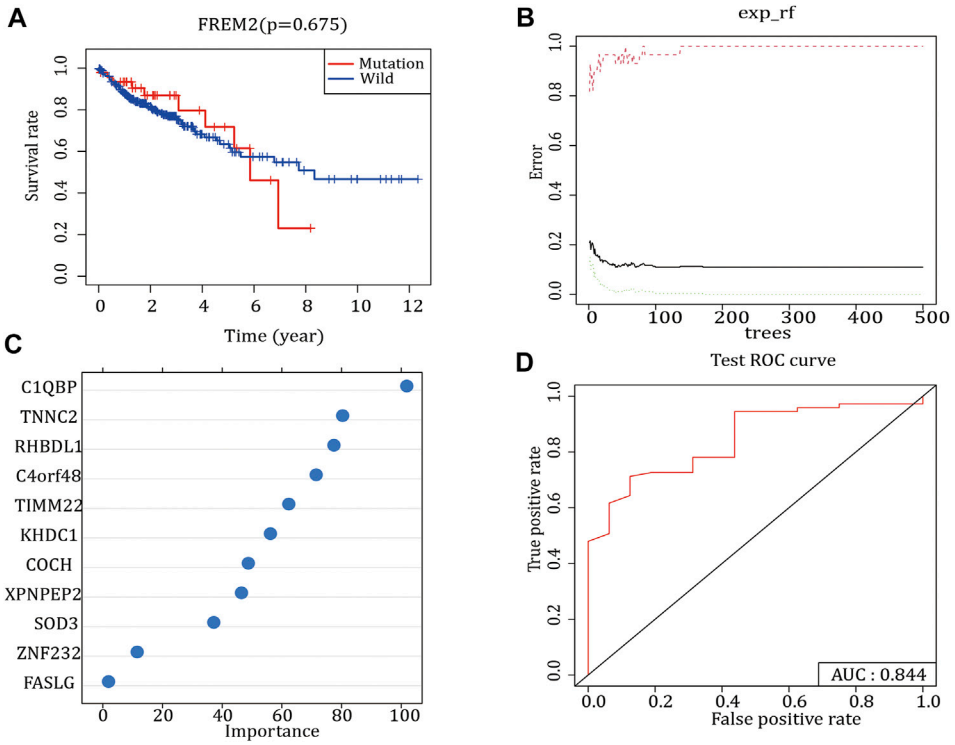

FIGURE 2 | *FREM2* mutation survival analysis and model construction. **(A)** The effect of *FREM2* mutation on the overall survival time of the patients. Blue indicates *FREM2*-wild type, and red indicates *FREM2*-mutant type. **(B,C)** Random Forest method to construct *FREM2* mutation model. **(D)** Performance of the *FREM2* mutation model in the test set.

and Dedik, 1993) was used for survival analysis, the K–M survival curve was used to show the difference in survival, and the log-rank test was used to evaluate the significance of the difference in survival time between the two groups. Univariate and multivariate Cox analyses were used to determine independent prognostic factors. pROC and ROCR packages were used to construct the ROC curve (Sing et al., 2005; Robin et al., 2011), and the area under the curve (AUC) was used to evaluate the accuracy of prognosis estimated by the risk score. All p values were two-sided, and p value <0.05 was considered statistically significant.

RESULTS

Identification of the *FREM2* Mutation Frequency in COAD

We identified 68 genes with somatic mutation data in TCGA-COAD patients obtained from TCGA (**Figure 1A**). Additionally, these 68 genes were also identified in the data downloaded from the ICGC database (**Figure 1B**). As shown in **Figures 1C,D**, the mutation frequency of *FREM2* was relatively high, and the mutation of FREM2 was visualized. We used GISTIC 2.0 to identify genes that exhibited significant amplification or deletion using the CNV data in TCGA. *FREM2* did not show significant amplification or deletion (**Figures 1E,F**).

Construction of *FREM2* Mutation Prediction Model

Survival analysis was performed according to the *FREM2* mutation and prognostic information of patients with COAD. The results showed that *FREM2* mutations significantly impacted the prognosis and survival of patients with COAD (**Figure 2A**). In the training set, the RF method was used to construct a *FREM2* mutation prediction model based on the mRNA data (**Figures 2B,C**). The ROC curve and the AUC were used to evaluate the performance of the model. An AUC value close to 1 indicates that the model has a high sensitivity at a very low false-positive rate. The AUC value of the model in the training cohort was 1.00, and the AUC value in the validation cohort was 84.4% (**Figure 2D**), indicating that the performance of the model was sufficient to effectively predict *FREM2* mutations in other cohorts.

Construction of a Prognostic Model

Using the gene expression data of 36 *FREM*-mutant COAD patients with clinical information, univariate Cox regression analysis was performed to initially identify 20 genes related to OS (p-value <0.05) (**Figure 3A**). Next, we used the RF method to select the most important genes related to prognosis. The results identified a total of 13 genes: *FOXC1, PRRG3, USP29, CCDC116, LRRC52, CTLA4, TCF23, CA7, TM4SF4, SP7, C8G, EFCAB5*, and *PKHD1L1* (**Figure 3B**). Next, multivariate Cox regression analysis clarified the correlation between these 13 genes and

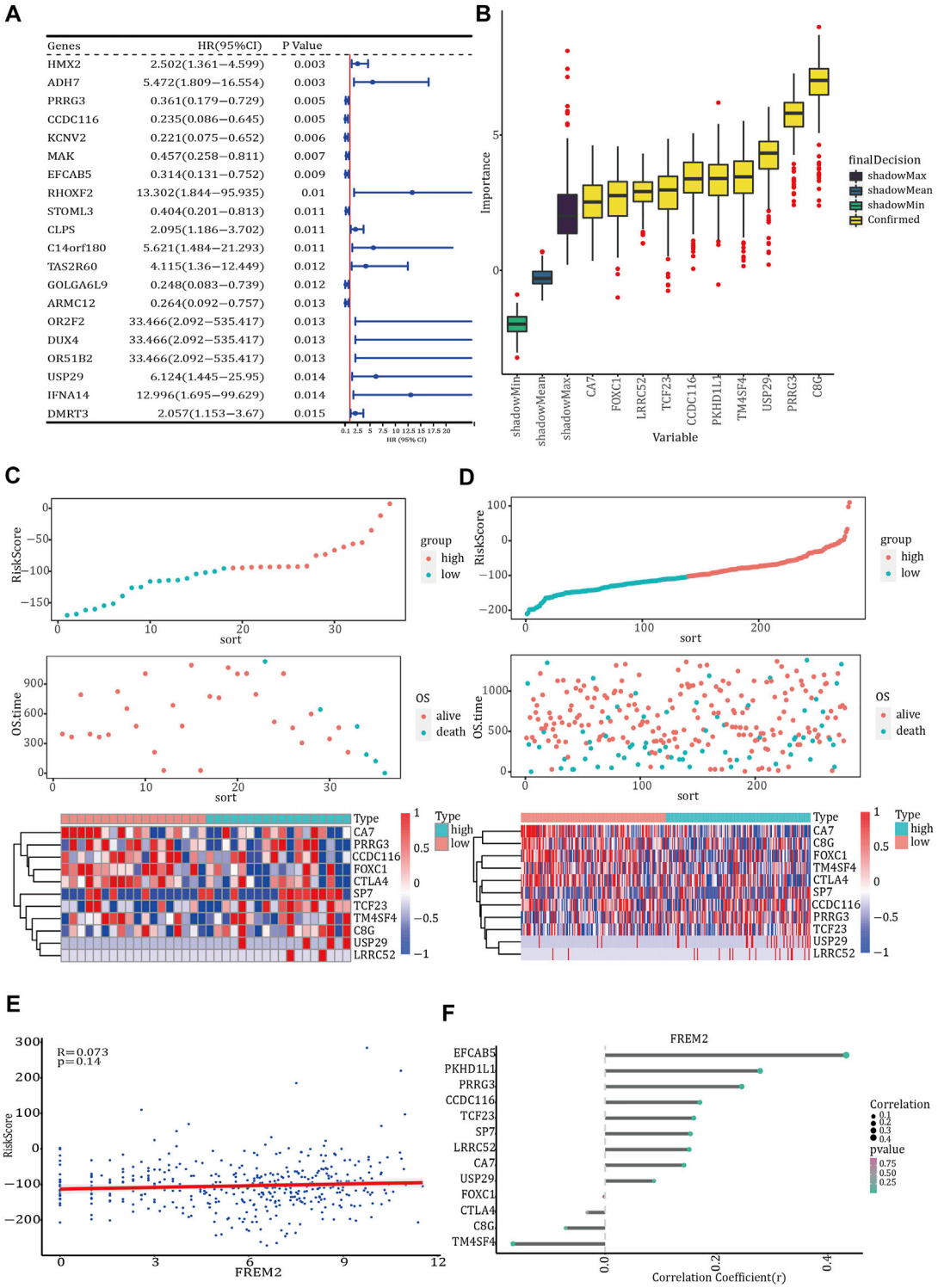

FIGURE 3 | Prognosis model of *FREM2* mutation. **(A)** The forest plot of the top 20 prognosis-related genes obtained by univariate Cox regression analysis. The left side of the vertical dashed line shows the protective gene, and the right-side shows the risk gene. **(B)** The 13 important features selected based on random forest. Risk score, survival status and characteristic gene expression analysis of *FREM2*-mutant type **(C)** and *FREM2*-wild type **(D)**. **(E)** Scatter plot of the correlation between *FREM2* expression and risk score. **(F)** Correlation between the expression levels of *FREM2* and characteristic genes. The size of the dot represents the strength of the correlation between *FREM2* and the characteristic gene; the larger the dot, the stronger the correlation, and vice versa. The color of the point represents the *p* value. The greener the color, the smaller the *p* value, and the pinker the color, the larger the *p* value. *p* value <0.05 was considered statistically significant.

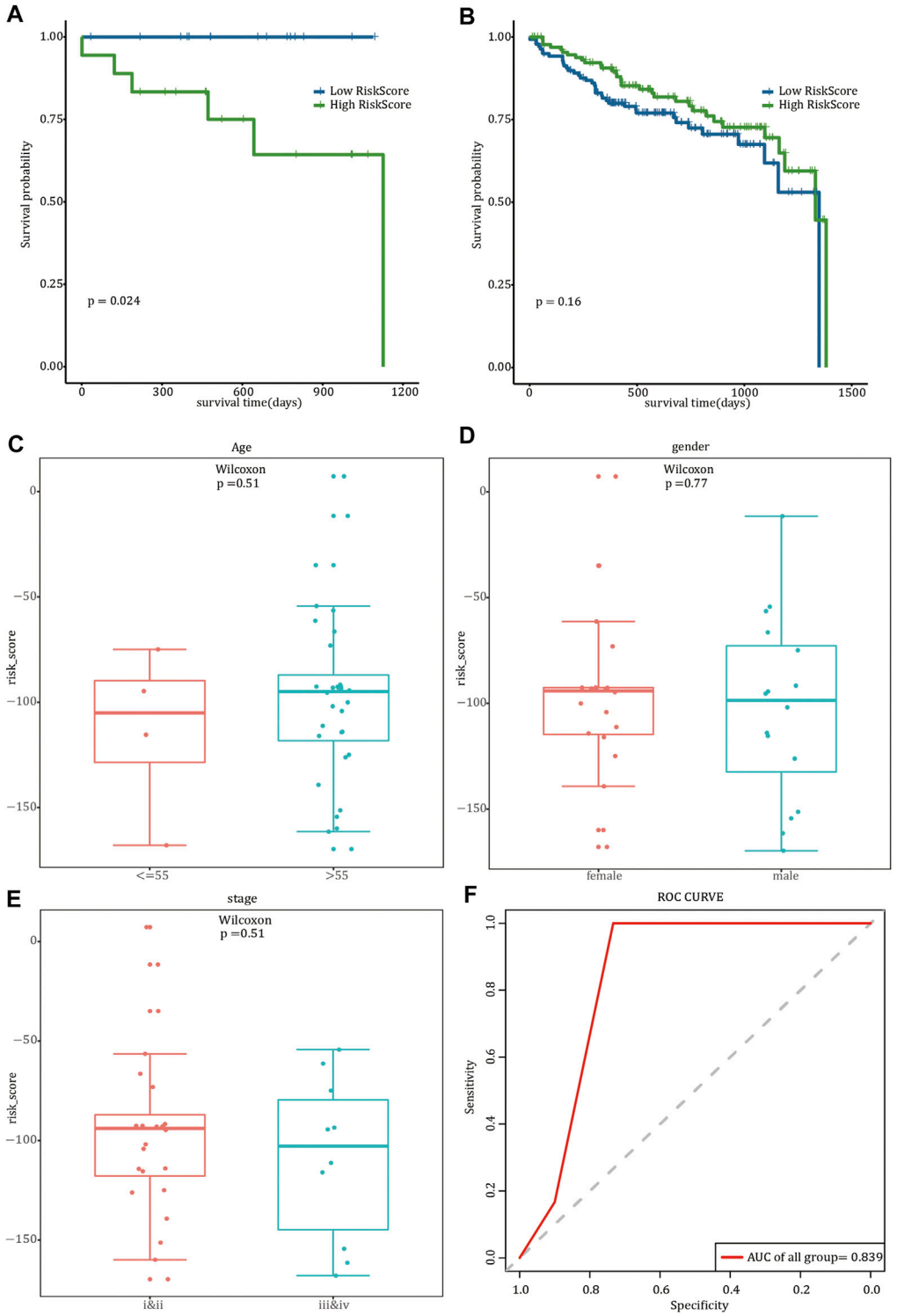

FIGURE 4 | Prognostic model analysis and clinical model construction. The effect of risk score on overall survival of *FREM2*-mutant type **(A)** and *FREM2*-wild type **(B)** patients. Blue indicates low risk score, and green indicates high risk score. Correlation analysis of risk score with age **(C)**, gender **(D)**, and tumor stage **(E)**. **(F)** The receiver operating characteristic curve of the clinical prediction model in 36 *FREM2*-mutant samples.

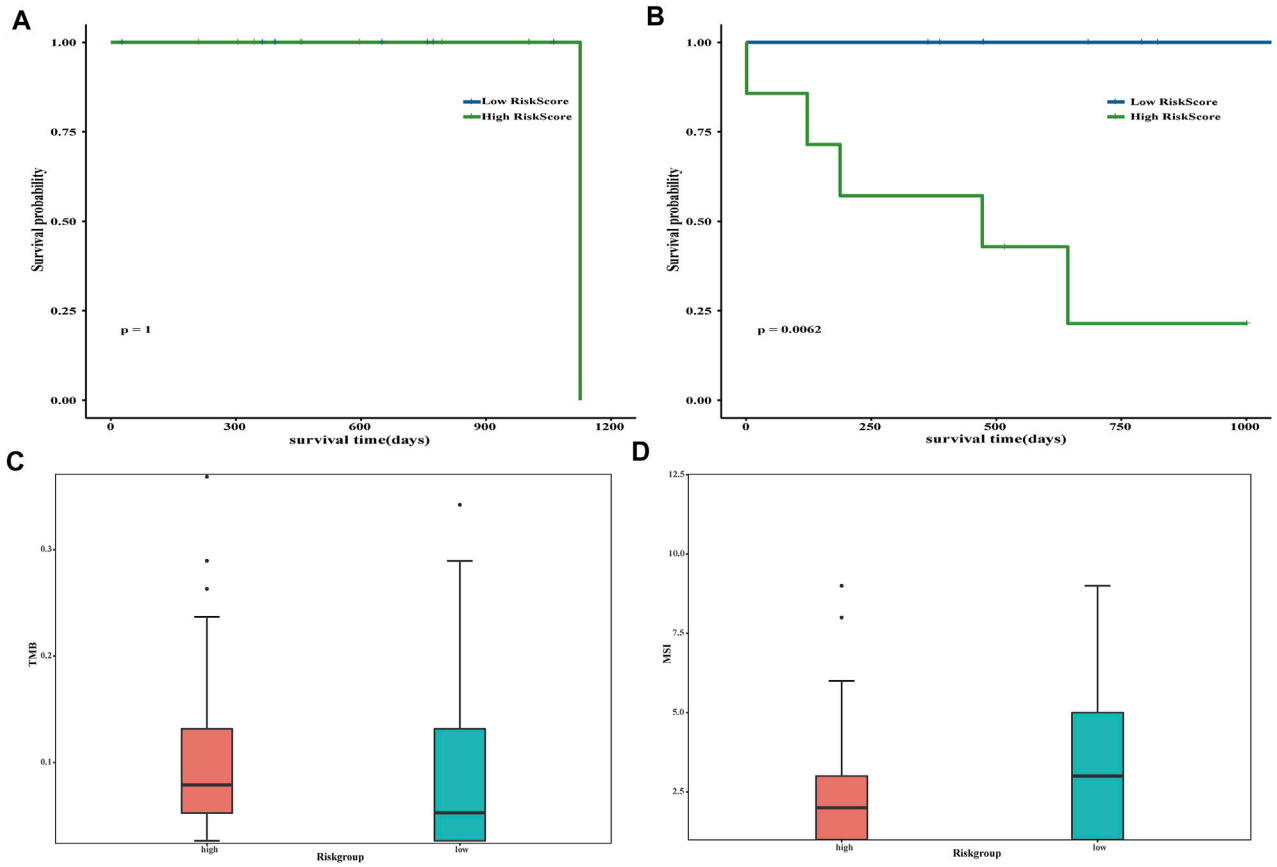

FIGURE 5 | Evaluation of risk score. The impact of risk scores on overall survival in the subgroup of inactivating mutations **(A)** and other non-silent mutations subgroups **(B)**. Blue indicates low-risk scores, and green indicates high-risk scores. Correlation analysis between tumor mutation burden **(C)** and microsatellite instability **(D)** and risk scores. Pink is used to represent the group with high risk, whereas green represents the group with low risk.

OS. The Cox regression coefficients of the 13 characteristic genes were calculated and used to estimate the risk score of each sample, which was calculated as the sum of the expression levels of each characteristic gene multiplied by their regression coefficients.

We evaluated the predictive performance of the prognostic model using the *FREM2*-mutant and *FREM2*-wild type groups. Based on the prognostic model, the risk scores of COAD patients were calculated and sorted, and the survival status of each patient was displayed on a dot plot (**Figures 3C,D**). The correlation between *FREM2* expression levels and risk score and characteristic genes expression levels was analyzed. The expression level of *FREM2* was positively correlated with the risk score (**Figure 3E**). Additionally, the expression level of *FREM2* was significantly positively correlated with that of *PRRG3* (r = 13.651), *USP29* (r = 56.206), CC*DC116* (r = 11.403), *LRRC52* (r = 44.466), TCF*23* (r = 9.083, *TM4SF4* (r = 0.003), *SP7* (r = 8.531), and *EFCAB5* (r = 5.282), and negatively correlated with that of *FOXC1* (r = −10.22), *CTLA4* (r = −5.152), *CA7* (r = −11.705), C8G (r = −2.951), and *PKHD1L1* (r = −20.17) (**Figure 3F**).

Evaluation of the Prognostic Model

According to the median risk score, *FREM2*-mutant COAD patients with clinical information were divided into high-risk and low-risk groups. The results of survival analysis showed that there was a significant difference in OS between the two risk groups in which the 36 *FREM2*-mutant samples had been divided (**Figure 4A**). However, there was no significant difference in OS between the high- and low-risk groups in which the 278 *FREM2*-wild type samples were divided (**Figure 4B**). The correlation analysis between the risk score and the clinical characteristics of the 36 FREM2-mutant samples showed that there were no significant differences in risk scores across different ages, genders, and tumor stages (**Figures 4C–E**). According to the age, gender, tumor stage, and risk score of COAD patients with *FREM2* mutations, univariate Cox analysis and multivariate Cox analysis were performed to construct a clinical prediction model. The efficacy of the model in 36 FREM2-mutant samples was 83.9% (**Figure 4F**).

Analysis of TMB and MSI

Considering that different *FREM2* mutation types may have different roles in the occurrence of rectal cancer, we divided the 36 *FREM2*-mutant COAD patients into two subgroups: patients with inactivating mutations (n = 27, including nonsense mutations and silent mutations), and patients with other non-silent mutation (n = 55).

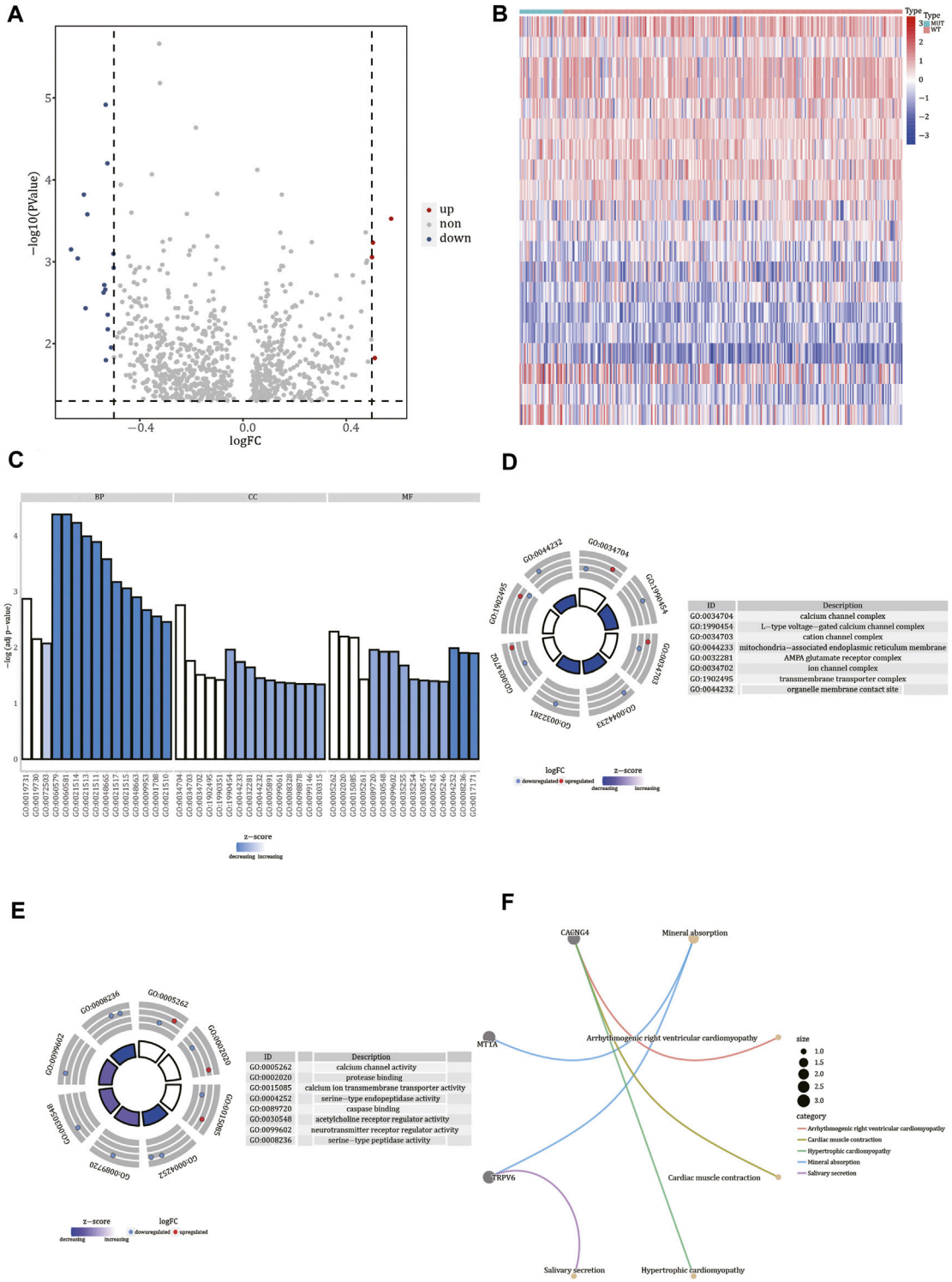

FIGURE 6 | Functional enrichment analysis of differentially expressed genes. **(A)** Volcano plot of differentially expressed genes. The red nodes indicate up-regulation, blue nodes indicate down-regulation, and gray nodes indicate non-significant expression changes. **(B)** Heat map of differentially expressed genes. Red represents high gene expression levels, blue represents low gene expression levels, green annotation bars indicate *FREM2*-mutant samples, and red annotation bars indicate *FREM2*-wild type samples. The result of Gene Ontology functional enrichment analysis of differentially expressed genes **(C)**, and the results of molecular function **(D)** and cell compartment **(E)** terms enrichment analysis are displayed. Blue indicates down-regulation of expression, red indicates up-regulation of expression, the middle quadrilateral indicates the effect of the gene on the enriched Gene Ontology terms, light color indicates inhibition, and dark color indicates activation. **(F)** The top five pathways of Kyoto Encyclopedia of Genes and Genomes enrichment analysis of differentially expressed genes.

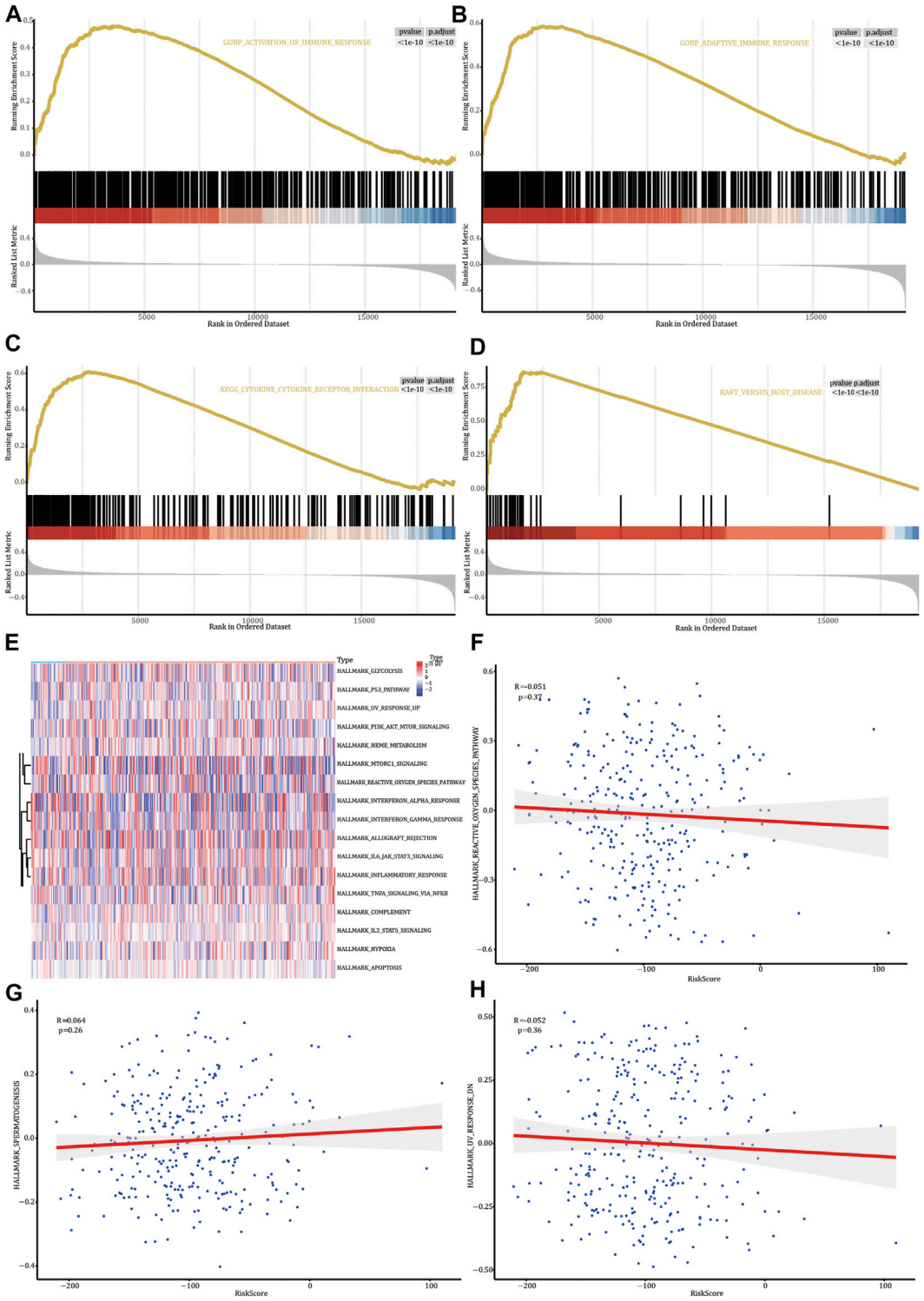

FIGURE 7 | Gene Set Enrichment Analysis (GSEA) and Gene Set Variation Analysis (GSVA). GSEA biological function enrichment analysis shows activation of the immune response **(A)** and adaptive immune response **(B).** GSEA biological pathway enrichment analysis results show cytokine-cytokine receptor interaction **(C)** and adaptive immune response **(D)**. **(E)** Heat map of significant hallmarks analyzed using GSVA. Scatter plot of correlation between significant hallmark and risk score: reactive_oxygen_species_pathway **(F)**, spermatogenesis **(G)**, and uv_response_dn **(H)**.

The prognosis of the low-risk group was significantly better than that of the high-risk group, and limited by the insufficient sample size, we only performed a 1-year time-dependent ROC analysis (**Figures 5A,B**). We obtained TMB scores based on the total number of mutations and calculated the relationship between TMB and the risk scores. Significant differences were shown in TMB between samples with different risk scores (p value <0.05) (**Figure 5C**). Next, the risk score and MSI were analyzed, and there were also significant differences in MSI between samples with different risk scores (p value <0.05) (**Figure 5D**).

Identification of Differentially Expressed Gene and Functional Enrichment Analysis

To identify the differentially expressed genes in *FREM2*-mutant and *FREM2*-wild-type samples, we used the limma R package. Based on the gene expression profile data of 36 *FREM2*-mutant samples and 278 *FREM2*-wild type samples in TCGA-COAD, we found four up-regulated genes (p value <0.05, logFC > 0.5) and 16 down-regulated genes (p value <0.05, logFC < −0.5). Differentially expressed genes were visualized using a volcano plot and a heat map (**Figures 6A,B**).

To determine the functions of the differentially expressed genes, we analyzed the biological processes, cell components, and molecular functions in which they were involved according to GO enrichment analysis (**Figure 6C** and **Supplementary Table S3**). GO analysis results showed that the 20 differentially expressed genes were significantly enriched in calcium channel complex, L-type voltage-gated calcium channel complex, cation channel complex, mitochondria-associated endoplasmic reticulum membrane, AMPA glutamate receptor complex, ion channel complex, transmembrane transporter complex, organelle membrane contact site, and other cellular components (**Figure 6D**). Additionally, these genes were involved in molecular functions, such as calcium channel activity, protein binding, calcium ion transmembrane transporter activity, serine-type endopeptidase activity, caspase binding, acetylcholine receptor regulator activity, serine-type peptidase activity, and neurotransmitter receptor regulator activity (**Figure 6E**). Finally, using KEGG enrichment analysis, we also analyzed the pathways in which the 20 differentially expressed genes were involved (**Supplementary Table S4**). According to the results, these genes were involved in pathways such as mineral absorption, salivary secretion, cardiac muscle contraction, and hypertrophic cardiomyopathy (**Figure 6F**).

GSEA and GSVA

GSEA on the genes differentially expressed in *FREM2*-mutated and *FREM2*-wild type patients showed that the genes were significantly enriched in biological functions, such as the activation of immune response and adaptive immune response (**Figures 7A,B** and **Supplementary Table S5**), and enriched in pathways such as the cytokine-cytokine receptor interaction and graft versus host disease (**Figures 7C,D** and **Supplementary Table S5**).

Next, we analyzed the genes differentially expressed in *FREM2*-mutated and *FREM2*-wild type patients to analyze the role of these genes using GSVA. The results showed that 17 hallmark pathways were differentially enriched in *FREM2*-mutated and *FREM2*-wild type patients (**Figure 7E**). Among them, spermatogenesis was positively correlated with risk score, while reactive_oxygen_species_pathway and uv_response_dn were negatively correlated with risk score. Other correlations were not significant (p value < 0.05) (**Figures 7F–H**).

Immune Cell Infiltration Analysis

We analyzed the relationship between the expression levels of *FREM2, FOXC1, PRRG3, USP29, CCDC116, LRRC52, CTLA4, TCF23, CA7, TM4SF4, SP7, C8G, EFCAB5,* and *PKHD1L1* and the abundance of immune cells and stromal cells (**Figures 8A,B**). Stromal cell abundance was significantly positively correlated with the expression levels of *PRRG3, CTLA4, TCF23, PKHD1L1, FOXC1,* and *SP7*, and significantly negatively correlated with the expression levels of *EFCAB5* and *C8G*. The abundance of immune cell types was significantly positively correlated with the expression levels of *FOXC1, PRRG3, CTLA4, TCF23,* and *PKHD1L1*, and significantly negatively correlated with the expression levels of *FREM2* and *EFCAB5* (p < 0.05). *FREM2* expression levels were significantly related with the expression levels of immune genes such as *TAC1, NFYA,* and *CCL26*; *PKHD1L1* was significantly related with the expression levels of the immune genes *ITGAL* and *NFYA*; *FOXC1* was significantly related with the expression levels of the immune gene *CCL26* (p value < 0.05) (**Figure 8C**). *FREM2* and *PKHD1L1* gene expression levels were significantly correlated with the infiltration rate of 12 types of immune cells; *FOXC1* gene expression levels were significantly correlated with the infiltration rate of 10 immune cells (p value < 0.05) (**Figure 8D**). The expression value of *HLA-DOA* differed in the two different risk groups (**Figure 8E**).

FREM2 Protein Level Analysis

We used the UALCAN database to analyze the expression levels of FREM2 in pan-cancer and found that FREM2 was mainly highly expressed in COAD, glioblastoma multiforme (GBM), stomach adenocarcinoma (STAD), and uterine corpus endometrial carcinoma (UCEC) (**Figure 9A**). Further analysis of COAD tissue samples showed that FREM2 was highly expressed in tumor tissues compared to normal tissues (**Figure 9B**). In addition, the expression levels of FREM2 in COAD tissues was analyzed using the HPA database, and it was found that FREM2 was highly expressed in tumor tissues (**Figure 9D**). Next, we evaluated FREM2 and Ki-67 expression levels in 30 CRC tissues using histochemistry staining. As shown in **Figure 9E**, histological scoring and analysis revealed that FREM2 and Ki-67 were highly expressed in tissue specimens from CRC patients, which was consistent with the results of the previous analysis. Finally, we examined the role of FREM2 molecular function. PDCD1, CD274, CTLA4, LAG3, TIGIT, and HAVCR2 are important immune checkpoints responsible for tumor immune escape. Given the regulatory role of FREM2 in COAD, the relationship of FREM2 to PDCD1, CD274, CTLA4, LAG3, TIGIT, and HAVCR2 was assessed. As shown in

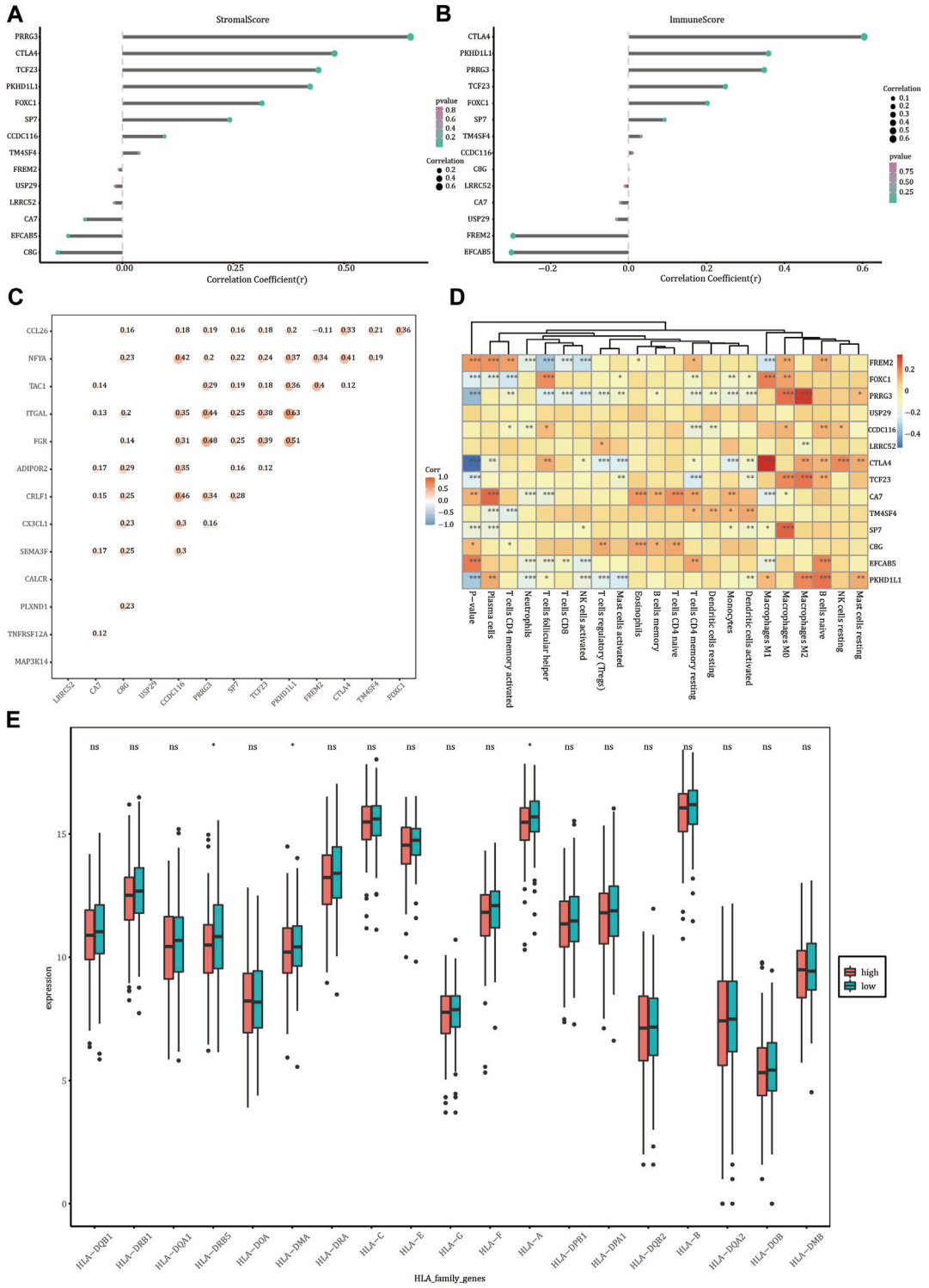

FIGURE 8 | Immune correlation analysis. Correlation of the expression levels of *FREM2* and characteristic genes with the stromal cells **(A)** and the abundance of immune cells **(B)**. **(C)** Correlation between *FREM2* and characteristic genes and immune genes. **(D)** Correlation between *FREM2* and characteristic gene expression levels and immune cell infiltration. **(E)** Correlation between members of the *HLA* family expression levels and risk score.

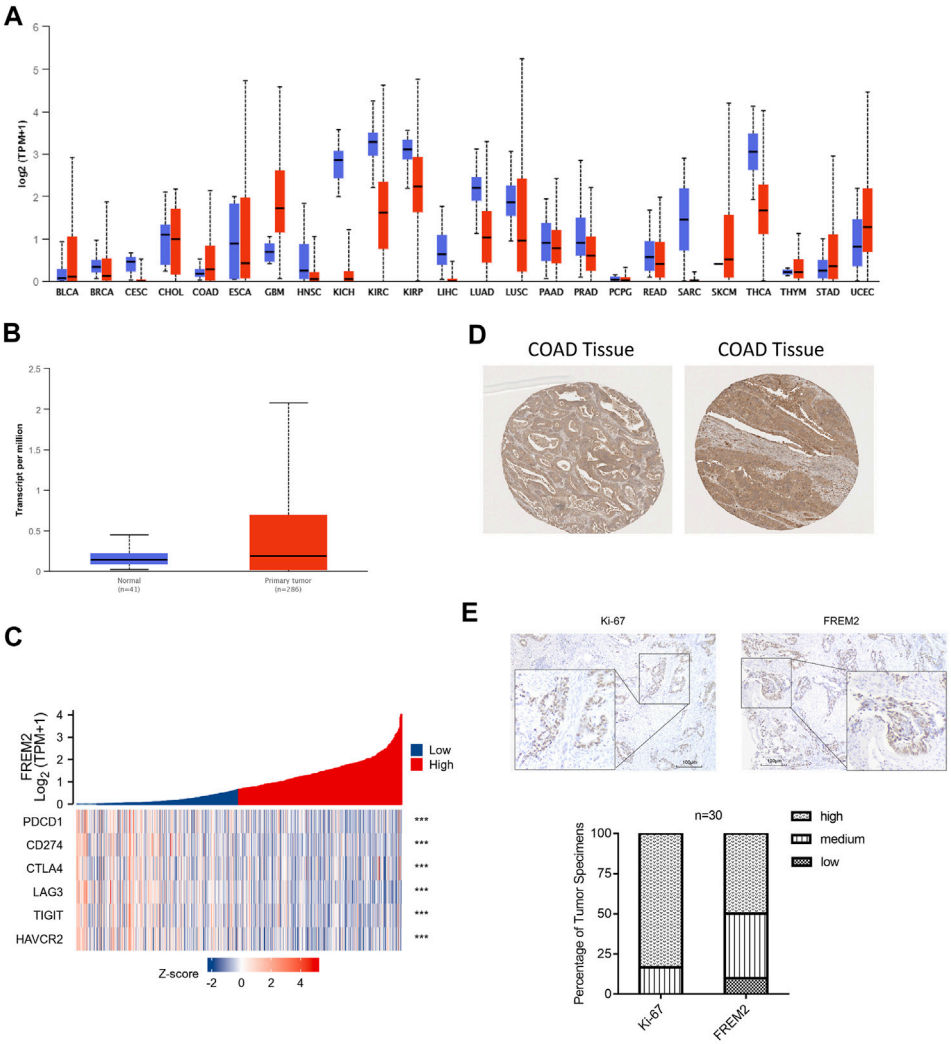

FIGURE 9 | *FREM2* expression analysis. Expression of *FREM2* in pan-cancer, using UALCAN database **(A)**. The expression of *FREM2* in colon adenocarcinoma (COAD), using the data from The Cancer Genome Atlas database **(B)**. Correlation analysis of *FREM2* and immune checkpoints, displayed using a heat map **(C)**. Analysis of FREM2 expression levels in COAD tissues, using the Human Protein Atlas (HPA) database **(D)**. High expression levels of Ki-67 and FREM2 were presented in colorectal cancer tissues (n = 30) by immunohistochemistry (IHC) staining. **(E)** Histogram of the results of analysis of IHC staining. Original magnification is ×100 (inset: IHC stain, DAB, original magnification is ×400).

Figure 9C, FREM2 expression was significantly correlated with that of PDCD1, CD274, CTLA4, LAG3, TIGIT, and HAVCR2. These results suggested that FREM2 was highly expressed in COAD and that tumor immune escape may be involved in FREM2-mediated COAD carcinogenesis.

DISCUSSION

With the wide application of endoscopy technology and the yearly increase in the number of physical examinations, more and more patients with colon cancer are detected early, which increases the chances of a favorable outcome after surgery. Although with the maturity of laparoscopic surgery technology and the development of neoadjuvant chemotherapy have contributed to improve the survival rate of CRC patients after surgery, the 5-year survival rate is still less than 65%. Therefore, it is necessary to identify new prognostic biomarkers in CRC patients. The occurrence of CRC is a multi-step process, including chromosomal abnormalities, gene mutations, and epigenetic changes. These abnormalities may be associated with patient survival. For example, while *KRAS* mutations generally occur relatively early in the evolution of CRC, mainly during the transformation of small to neutral adenomas, mutations in TP53 often occur in later stages. Additionally, previous studies have shown that the number of somatic mutations is positively correlated with the response to immunotherapy (Link and Overman, 2016).

FREM2 is located at 13q13.3 and forms an independent and complete ternary complex structure (FREM2-FRAS1-FREM1)

between the extracellular epithelium and the mesenchyme (Kantaputra et al., 2021). The functions of this complex are similar to those of Collagen VII, and each component of the complex is essential to maintain the stability of the complex structure (Dalezios et al., 2007).

In humans, *FREM2* gene mutations can cause Fraser syndrome, a rare autosomal recessive genetic disease (Jadeja et al., 2005). Additionally, recent studies have shown that *FREM2* mutations cause metabolic reprogramming of mouse embryos during cryptographic development (Zhang et al., 2020), and that loss of function mutations of *FREM2* can disrupt the morphogenesis of the eye (Zhang et al., 2019). Additionally, loss of FREM2 function is an important cause of blood-related kidneys (Al-Hamed et al., 2021), and FREM2 has been suggested to be a candidate prognostic marker in glioma (Vidak et al., 2018).

In this study, we found that *FREM2* had a high mutation frequency in CRC and that *FREM2* mutation was associated with poor prognosis in patients. To further explore the prognostic value of mutations, we divided 36 *FREM2*-mutated patients into high- and a low-risk groups based on the risk scores, constructed a prognostic model, and evaluated its performance. The results suggested that in 36 *FREM2*-mutant patients with CRC, the model showed a higher efficiency, reaching a prediction accuracy of 83.9%. Additionally, we found significant differences in TMB and MSI between the groups with different risk scores. Next, functional enrichment analysis of differentially expressed genes revealed significantly enrichment of genes involved in cytokine-cytokine receptor interaction, immune response, and other pathways. Then, immune infiltration analysis revealed that *FREM2* gene expression was significantly related to the infiltration of 12 immune cell types. Finally, we analyzed the protein expression of FREM2 in pan-cancer and COAD using UALCAN and HPA databases and found that FREM2 was highly expressed in COAD, which was consistent with the results of immunohistochemistry. In addition, since *FREM2* mutation was associated with immune infiltration, we analyzed its association with the expression levels of *PDCD1, CD274, CTLA4, LAG3, TIGIT*, and *HAVCR2,* which are important immune checkpoints responsible for tumor immune escape. FREM2 was significantly correlated with immune checkpoints, which further suggested that FREM2 may regulate immune processes in COAD.

The results of this study should be viewed in light of its limitations. Most of the conclusions were drawn from bioinformatics analysis, and only a small amount of them were validated using clinical samples. In the future, we will continue to further study the functional role of *FREM2* in COAD. Moreover, this study was based on a single omics study, and the understanding of gene function was not comprehensive enough, highlighting the need of more in-depth research in the future. In conclusion, through comprehensive analysis and experimental verification, our results demonstrate that *FREM2* mutations may be prognostic markers for CRC patients.

DATA AVAILABILITY STATEMENT

Publicly available datasets were analyzed in this study. This data can be found at: http://cancergenome.nih.gov/ and http://xena.ucsc.edu/.

ETHICS STATEMENT

Patient-informed consent was obtained and approved by The First People's Hospital of Foshan Subject Review Board.

AUTHOR CONTRIBUTIONS

RY conceived and designed this project. HD and HW performed experiments and acquired data. HD, HW, FK, MW, JL, and SZ analyzed data. All authors participated in writing or revising the manuscript.

FUNDING

This study was supported by the National Natural Science Foundation of China (82002913), GuangDong Basic and Applied Basic Research Foundation (2021A1515011453).

SUPPLEMENTARY MATERIAL

The Supplementary Material for this article can be found online at: https://www.frontiersin.org/articles/10.3389/fmolb.2022.839617/full#supplementary-material

REFERENCES

Al-Hamed, M. H., Sayer, J. A., Alsahan, N., Tulbah, M., Kurdi, W., Ambusaidi, Q., et al. (2021). Novel Loss of Function Variants in FRAS1 and FREM2 Underlie Renal Agenesis in Consanguineous Families. *J. Nephrol.* 34 (3), 893–900. doi:10.1007/s40620-020-00795-0

Ashburner, M., Ball, C. A., Blake, J. A., Botstein, D., Butler, H., Cherry, J. M., et al. (2000). Gene Ontology: Tool for the Unification of Biology. *Nat. Genet.* 25 (1), 25–29. doi:10.1038/75556

Bhattacharya, S., Andorf, S., Gomes, L., Dunn, P., Schaefer, H., Pontius, J., et al. (2014). ImmPort: Disseminating Data to the Public for the Future of Immunology. *Immunol. Res.* 58 (2-3), 234–239. doi:10.1007/s12026-014-8516-1

Chan, T. A., Yarchoan, M., Jaffee, E., Swanton, C., Quezada, S. A., Stenzinger, A., et al. (2019). Development of Tumor Mutation burden as an Immunotherapy Biomarker: Utility for the Oncology Clinic. *Ann. Oncol.* 30 (1), 44–56. doi:10.1093/annonc/mdy495

Chandrashekar, D. S., Bashel, B., Balasubramanya, S. A. H., Creighton, C. J., Ponce-Rodriguez, I., Chakravarthi, B. V. S. K., et al. (2017). UALCAN: A Portal for Facilitating Tumor Subgroup Gene Expression and Survival Analyses. *Neoplasia* 19 (8), 649–658. doi:10.1016/j.neo.2017.05.002

Dalezios, Y., Papasozomenos, B., Petrou, P., and Chalepakis, G. (2007). Ultrastructural Localization of Fras1 in the Sublamina Densa of Embryonic

Epithelial Basement Membranes. *Arch. Dermatol. Res.* 299 (7), 337–343. doi:10.1007/s00403-007-0763-8

Durisová, M., and Dedík, L. (1993). SURVIVAL--an Integrated Software Package for Survival Curve Estimation and Statistical Comparison of Survival Rates of Two Groups of Patients or Experimental Animals. *Methods Find Exp. Clin. Pharmacol.* 15 (8), 535–540.

Feng, R.-M., Zong, Y.-N., Cao, S.-M., and Xu, R.-H. (2019). Current Cancer Situation in China: Good or Bad News from the 2018 Global Cancer Statistics? *Cancer Commun.* 39 (1), 22. doi:10.1186/s40880-019-0368-6

Guo, X., Zhang, B., Zeng, W., Zhao, S., and Ge, D. (2020). G3viz: an R Package to Interactively Visualize Genetic Mutation Data Using a Lollipop-Diagram. *Bioinformatics* 36 (3), 928–929. doi:10.1093/bioinformatics/btz631

Hänzelmann, S., Castelo, R., and Guinney, J. (2013). GSVA: Gene Set Variation Analysis for Microarray and RNA-Seq Data. *BMC Bioinformatics* 14, 7. doi:10.1186/1471-2105-14-7

Hile, S. E., Shabashev, S., and Eckert, K. A. (2013). Tumor-specific Microsatellite Instability: Do Distinct Mechanisms Underlie the MSI-L and EMAST Phenotypes? *Mutat. Research/Fundamental Mol. Mech. Mutagenesis* 743-744, 67–77. doi:10.1016/j.mrfmmm.2012.11.003

Howe, K. L., Achuthan, P., Allen, J., Allen, J., Alvarez-Jarreta, J., Amode, M. R., et al. (2021). Ensembl 2021. *Nucleic Acids Res.* 49 (D1), D884–D891. doi:10.1093/nar/gkaa942

Jadeja, S., Smyth, I., Pitera, J. E., Taylor, M. S., van Haelst, M., Bentley, E., et al. (2005). Identification of a New Gene Mutated in Fraser Syndrome and Mouse Myelencephalic Blebs. *Nat. Genet.* 37 (5), 520–525. doi:10.1038/ng1549

Jovčevska, I., Zottel, A., Šamec, N., Mlakar, J., Sorokin, M., Nikitin, D., et al. (2019). High FREM2 Gene and Protein Expression Are Associated with Favorable Prognosis of IDH-WT Glioblastomas. *Cancers* 11 (8), 1060. doi:10.3390/cancers11081060

Kanehisa, M., and Goto, S. (2000). KEGG: Kyoto Encyclopedia of Genes and Genomes. *Nucleic Acids Res.* 28 (1), 27–30. doi:10.1093/nar/28.1.27

Kantaputra, P. N., Wangtiraumnuay, N., Ngamphiw, C., Olsen, B., Intachai, W., Tucker, A. S., et al. (2021). Cryptophthalmos, Dental Anomalies, Oral Vestibule Defect, and a Novel FREM2 Mutation. *J. Hum. Genet.* 67, 115–118. doi:10.1038/s10038-021-00972-4

Kiyozumi, D., Sugimoto, N., and Sekiguchi, K. (2006). Breakdown of the Reciprocal Stabilization of QBRICK/Frem1, Fras1, and Frem2 at the Basement Membrane Provokes Fraser Syndrome-like Defects. *Proc. Natl. Acad. Sci.* 103 (32), 11981–11986. doi:10.1073/pnas.0601011103

Liberzon, A., Birger, C., Thorvaldsdóttir, H., Ghandi, M., Mesirov, J. P., and Tamayo, P. (2015). The Molecular Signatures Database Hallmark Gene Set Collection. *Cel Syst.* 1 (6), 417–425. doi:10.1016/j.cels.2015.12.004

Link, J. T., and Overman, M. J. (2016). Immunotherapy Progress in Mismatch Repair-Deficient Colorectal Cancer and Future Therapeutic Challenges. *Cancer J.* 22 (3), 190–195. doi:10.1097/PPO.0000000000000196

Mayakonda, A., Lin, D.-C., Assenov, Y., Plass, C., and Koeffler, H. P. (2018). Maftools: Efficient and Comprehensive Analysis of Somatic Variants in Cancer. *Genome Res.* 28 (11), 1747–1756. doi:10.1101/gr.239244.118

Nakayama, M., and Oshima, M. (2019). Mutant P53 in colon Cancer. *J. Mol. Cel Biol* 11 (4), 267–276. doi:10.1093/jmcb/mjy075

Newman, A. M., Steen, C. B., Liu, C. L., Gentles, A. J., Chaudhuri, A. A., Scherer, F., et al. (2019). Determining Cell Type Abundance and Expression from Bulk Tissues with Digital Cytometry. *Nat. Biotechnol.* 37 (7), 773–782. doi:10.1038/s41587-019-0114-2

Reich, M., Liefeld, T., Gould, J., Lerner, J., Tamayo, P., and Mesirov, J. P. (2006). GenePattern 2.0. *Nat. Genet.* 38 (5), 500–501. doi:10.1038/ng0506-500

Ritchie, M. E., Phipson, B., Wu, D., Hu, Y., Law, C. W., Shi, W., et al. (2015). Limma powers Differential Expression Analyses for RNA-Sequencing and Microarray Studies. *Nucleic Acids Res.* 43 (7), e47. doi:10.1093/nar/gkv007

Robin, X., Turck, N., Hainard, A., Tiberti, N., Lisacek, F., Sanchez, J.-C., et al. (2011). pROC: an Open-Source Package for R and S+ to Analyze and Compare ROC Curves. *BMC Bioinformatics* 12, 77. doi:10.1186/1471-2105-12-77

Sing, T., Sander, O., Beerenwinkel, N., and Lengauer, T. (2005). ROCR: Visualizing Classifier Performance in R. *Bioinformatics* 21 (20), 3940–3941. doi:10.1093/bioinformatics/bti623

Skidmore, Z. L., Wagner, A. H., Lesurf, R., Campbell, K. M., Kunisaki, J., Griffith, O. L., et al. (2016). GenVisR: Genomic Visualizations in R. *Bioinformatics* 32 (19), 3012–3014. doi:10.1093/bioinformatics/btw325

Subramanian, A., Tamayo, P., Mootha, V. K., Mukherjee, S., Ebert, B. L., Gillette, M. A., et al. (2005). Gene Set Enrichment Analysis: a Knowledge-Based Approach for Interpreting Genome-wide Expression Profiles. *Proc. Natl. Acad. Sci.* 102 (43), 15545–15550. doi:10.1073/pnas.0506580102

Sung, H., Ferlay, J., Siegel, R. L., Laversanne, M., Soerjomataram, I., Jemal, A., et al. (2021). Global Cancer Statistics 2020: GLOBOCAN Estimates of Incidence and Mortality Worldwide for 36 Cancers in 185 Countries. *CA A. Cancer J. Clin.* 71 (3), 209–249. doi:10.3322/caac.21660

Tomczak, K., Czerwińska, P., and Wiznerowicz, M. (2015). Review the Cancer Genome Atlas (TCGA): an Immeasurable Source of Knowledge. *wo* 1A (1A), 68–77. doi:10.5114/wo.2014.47136

Vidak, M., Jovcevska, I., Samec, N., Zottel, A., Liovic, M., Rozman, D., et al. (2018). Meta-Analysis and Experimental Validation Identified FREM2 and SPRY1 as New Glioblastoma Marker Candidates. *Ijms* 19 (5), 1369. doi:10.3390/ijms19051369

Yang, R., Wang, Z., Li, J., Pi, X., Gao, R., Ma, J., et al. (2021). The Identification of the Metabolism Subtypes of Skin Cutaneous Melanoma Associated with the Tumor Microenvironment and the Immunotherapy. *Front. Cel Dev. Biol.* 9, 707677. doi:10.3389/fcell.2021.707677

Yoshihara, K., Shahmoradgoli, M., Martínez, E., Vegesna, R., Kim, H., Torres-Garcia, W., et al. (2013). Inferring Tumour Purity and Stromal and Immune Cell Admixture from Expression Data. *Nat. Commun.* 4, 2612. doi:10.1038/ncomms3612

Yperman, J., Becker, T., Valkenborg, D., Popescu, V., Hellings, N., Wijmeersch, B. V., et al. (2020). Machine Learning Analysis of Motor Evoked Potential Time Series to Predict Disability Progression in Multiple Sclerosis. *BMC Neurol.* 20 (1), 105. doi:10.1186/s12883-020-01672-w

Yu, G., Wang, L.-G., Han, Y., and He, Q.-Y. (2012). clusterProfiler: an R Package for Comparing Biological Themes Among Gene Clusters. *OMICS: A J. Integr. Biol.* 16 (5), 284–287. doi:10.1089/omi.2011.0118

Yu, Q., Lin, B., Xie, S., Gao, S., Li, W., Liu, Y., et al. (2018). A Homozygous Mutation p.Arg2167Trp in FREM2 Causes Isolated Cryptophthalmos. *Hum. Mol. Genet.* 27 (13), 2357–2366. doi:10.1093/hmg/ddy144

Zhang, X., Wang, D., Dongye, M., Zhu, Y., Chen, C., Wang, R., et al. (2019). Loss-of-function Mutations in FREM2 Disrupt Eye Morphogenesis. *Exp. Eye Res.* 181, 302–312. doi:10.1016/j.exer.2019.02.013

Zhang, X., Wang, R., Wang, T., Zhang, X., Dongye, M., Wang, D., et al. (2020). The Metabolic Reprogramming of Frem2 Mutant Mice Embryos in Cryptophthalmos Development. *Front. Cel Dev. Biol.* 8, 625492. doi:10.3389/fcell.2020.625492

Conflict of Interest: The authors declare that the research was conducted in the absence of any commercial or financial relationships that could be construed as a potential conflict of interest.

Publisher's Note: All claims expressed in this article are solely those of the authors and do not necessarily represent those of their affiliated organizations, or those of the publisher, the editors and the reviewers. Any product that may be evaluated in this article, or claim that may be made by its manufacturer, is not guaranteed or endorsed by the publisher.

frontiers in Molecular Biosciences

ORIGINAL RESEARCH
published: 28 February 2022
doi: 10.3389/fmolb.2022.856064

The Systemic Inflammation Response Index as an Independent Predictor of Survival in Breast Cancer Patients: A Retrospective Study

Mengliu Zhu[1], Li Chen[1,2], Xiangyi Kong[1], Xiangyu Wang[1], Yi Fang[1], Xingrui Li[2]* and Jing Wang[1]**

[1]Department of Breast Surgical Oncology, National Cancer Center/National Clinical Research Center for Cancer/Cancer Hospital, Chinese Academy of Medical Sciences and Peking Union Medical College, Beijing, China, [2]Department of Thyroid and Breast Surgery, Tongji Hospital, Tongji Medical College of Huazhong University of Science and Technology, Wuhan, China

OPEN ACCESS

Edited by:
Na Luo,
Nankai University, China

Reviewed by:
Shun Gong,
Northern Theater General Hospital, China
Anqiang Wang,
Peking University Cancer Hospital, China

***Correspondence:**
Yi Fang
fangyi@cicams.ac.cn
Xingrui Li
lixingrui@tjh.tjmu.edu.cn
Jing Wang
wangjing@cicams.ac.cn

Specialty section:
This article was submitted to Molecular Diagnostics and Therapeutics, a section of the journal Frontiers in Molecular Biosciences

Received: 16 January 2022
Accepted: 08 February 2022
Published: 28 February 2022

Citation:
Zhu M, Chen L, Kong X, Wang X, Fang Y, Li X and Wang J (2022) The Systemic Inflammation Response Index as an Independent Predictor of Survival in Breast Cancer Patients: A Retrospective Study. Front. Mol. Biosci. 9:856064. doi: 10.3389/fmolb.2022.856064

There is a close relationship between inflammatory cells and tumors, but the pathways that connect the two remain unclear. This research explores the clinical and prognostic value of the systemic inflammation response index (SIRI) in breast cancer patients. The study included 477 breast cancer patients who underwent neoadjuvant chemotherapy and 308 breast cancer patients who did not in our center between January 1998 and December 2016. Optimal SIRI threshold values were determined using the receiver operating characteristic curve (ROC). Patients were then reclassified as SIRI ≥0.80 group (High SIRI group) and SIRI <0.80 group (Low SIRI group). The outcomes were analyzed by statistical methods. The univariate and multivariate analyses demonstrated that SIRI independently predicted survival in breast cancer. The disease-free survival (DFS) and overall survival (OS) in patients with low SIRI scores were significantly longer in contrast to those with high SIRI scores (41.50 vs. 37.63 months, and 64.57 vs. 58.42 months). Further subgroup analyses revealed that low SIRI score patients who also had either early breast cancer, advanced breast cancer, or different molecular subtypes also possessed longer mean survival time of DFS and OS in contrast to those with high SIRI levels ($\chi2 = 2.379$, $p = 0.123$, and $\chi2 = 5.153$, $p = 0.023$; $\chi2 = 11.080$, $p = 0.0009$ and $\chi2 = 15.900$, $p < 0.0001$; $\chi2 = 16.020$, $p < 0.0001$ and $\chi2 = 22.050$, $p < 0.0001$, respectively). SIRI serves as an easily accessible, replicable, and minimally invasive prognostic tool in breast cancer patients. Lower SIRI scores were predictive of a longer DFS and OS after surgery in breast cancer patients. SIRI may serve as a marker to guide clinical management and prognostication of breast cancer.

Keywords: breast cancer, neoadjuvant chemotherapy, systemic inflammation response index (SIRI), prognosis, disease-free survival (DFS), overall survival (OS)

INTRODUCTION

Breast cancer is among the most frequently diagnosed cancers in females. This malignancy exerts a deleterious effect on patient quality of life and is a significant public health issue (Dan et al., 2020). The GLOBOCAN 2018 Research reports that there are more than 2 million new cases of breast cancer annually, with more than 600,000 deaths due to breast cancer occurring each year. There is a

concerning trend towards a younger age of the first diagnosis, along with an overall higher number of breast cancer cases (Bray et al., 2020). Recent data in China shows a marked rise in breast cancer incidence, especially in its developed coastal cities. Experts predict that breast cancer incidences in China are expected to reach a staggering 100 cases per 100,000 postmenopausal women in the future (Li et al., 2019). Despite the comprehensiveness of current treatment modalities of breast cancer that includes surgery, adjuvant chemotherapy, radiotherapy, targeted therapy, immunotherapy, and Chinese medicine treatment, patient outcomes are still unsatisfactory (Chen et al., 2017).

The tumor microenvironment, which includes the extracellular matrix, stromal cells, lymphatic and blood vessels, as well as resident immune cells, has been found to be a key determinant in dictating tumor behavior. Of interest is the role of inflammation, which is postulated to be influential in tumor progression and metastasis (Singh et al., 2019). Recent studies have confirmed that various markers of the systemic inflammatory response, for example, the C-reactive Protein (CRP), Platelet to Lymphocyte Ratio (PLR), Lymphocyte to Monocyte Ratio (LMR), and Neutrophil to Lymphocyte Ratio (NLR), all correlate to the prognosis of a myriad of tumors such as high-grade glioma (He et al., 2021b), colorectal cancer (Dagmura et al., 2021), head and neck cancer (Saroul et al., 2021), oral squamous cell cancer (Yamagata et al., 2021), and gastric cancer (Liu et al., 2021). The latest evidence also suggests that a similar tumor-inflammation relationship exists for breast cancer, indicating that quantifying the inflammatory response may be useful in treating and prognosticating breast cancer (Dong et al., 2021). Common blood indices, including platelets (P), monocytes (M), neutrophils (N), hemoglobin (Hb), total red blood cell count (R), total white blood cell count (WBC), and serum albumin (ALB), along with its derivatives, NLR, MLR, LMR, PLR, D-NLR, prognostic nutritional value [PNI, 10 × serum ALB (g/dL) + 0.005 × total lymphocyte count], and SIRI (Neutrophil × Platelet/Lymphocyte) may all be reflective of malignant tumor states (Mantovani et al., 2008). Breast cancer is currently diagnosed by a combination of pathological assessments of tissue samples taken via core needle biopsy (CNB) and various imaging modalities including breast ultrasound, mammography, and magnetic resonance imaging (MRI) (Al-Hattali et al., 2019). Nevertheless, the concept of being able to prognosticate breast cancer based on routine peripheral blood examinations is attractive given the ease of access, replicability, and lower cost. This investigation seeks to determine the utility of common inflammatory markers in the context of breast cancer.

MATERIALS AND METHODS

Study Population

Our study comprised 785 breast cancer patients. Of these, 477 underwent surgery and received neoadjuvant chemotherapy (NACT) in our center between January 1998 to December 2016 were included in our study. The control cohort comprised308 breast cancer patients who received surgical treatment only at the same center and during the same timeframe. All participants underwent routine examination and examination on admission, a comprehensive assessment of their condition, and provided written informed consent prior to study inclusion. All patients were diagnosed by CNB or histopathology. TNM staging was carried out in accordance with the eighth edition AJCC (American Joint Committee on Cancer) and the Union for International Cancer Control (UICC) (Weigelt and Reis-Filho, 2009; Cserni et al., 2018).

Inclusion and Exclusion Criteria

The inclusion criterion was as follows: 1) Breast cancer was confirmed by CNB or pathological examination; 2) Zubrod-Ecog-WHO (ZPS) between 0 and 2 and Karnofsky Performance Scores (KPS) ≥80; 3) Expected to survive more than 3 months; 4) Patients did not receive anti-tumor treatment before admission, including chemotherapy, radiotherapy, immunotherapy, interventional therapy, and traditional Chinese medicine treatment; 5) Surgery was performed after the completion of NACT; 6) Admission examination showed no obvious abnormalities in liver, kidney, lung, heart, brain, and bone marrow; 7) Inpatient medical records and postoperative follow-up data were complete.

The following was our exclusion criteria: 1) The possibility of distant organ metastasis was not able to be excluded on imaging examinations such as abdominal B-ultrasound, chest Computed Tomography (CT), and breast MRI, or the breast tumor was not able to be resected due to the definite presence of metastasis; 2) Patients received anti-tumor therapy, such as radiotherapy, chemotherapy, and targeted therapy; 3) The presence of serious comorbidities that were refractory to treatment such as hypertension, heart disease, and diabetes; 4) Advanced breast cancer, including breast cancer ulcers, inflammatory breast cancer, and infected tumors; 5) Blood transfusion history within 1 month before receiving NACT; 6) Patients who were poorly compliant and not cooperative with treatment.

Chemotherapy Regimen

The NACT treatment regimen included anthracyclines and/or taxanes. Protocols used included the AC regimen, ACF regimen, CT regimen, ACT regimen, AT regimen, and TP regimen.

Peripheral Venous Blood Collection Method

All patients took an early morning fasting peripheral venous blood sample of 2–5 ml. Peripheral venous blood specimens were obtained within 7 days before surgery in patients without neoadjuvant chemotherapy. And others were obtained within 7 days before neoadjuvant chemotherapy. WBC, neutrophils, hemoglobin, lymphocytes, monocytes, platelets, eosinophils, basophils, and other hematological parameters in peripheral venous blood were evaluated using the XE-2100 hematology analyzer (Sysmex, KOBE, Japan). SIRI was calculated based on the following formula: (neutrophils × monocytes)/lymphocyte count.

Evaluation Assays

The size of the tumor, invasion depth, and the degree of lymph node metastasis were determined by breast ultrasound, mammography, and MRI. Tumor diameters were taken as

their largest measurable diameter. The eighth edition of AJCC guided TNM staging (Weigelt and Reis-Filho, 2009; Cserni et al., 2018). The main pathological types of breast cancer were invasive lobular carcinoma, invasive ductal carcinoma, and other types. Molecular classification of breast cancer were triple-negative breast cancers, HER2 overexpressing tumors, Luminal B/HER-2-negative, Luminal B/HER2-positive, and Luminal A types (He et al., 2021a). The Miller and Payne histological grade (MPG) allowed for evaluation of the reduction of tumor cells after NACT and is divided into five grades (Therasse et al., 2000). The efficacy of NACT on tumor lesions after treatment was done in accordance with the 2000 RECIST criteria (Amat et al., 2002). The histological classification of breast cancer is based on the Nottingham Joint Histological Classification (Elston and Ellis modification of the Scarff-Bloom-Richardson grading protocol) (Kaba et al., 2004). NACT toxicity and adverse effects were assessed based on the National Cancer Institute Common Toxicity Criteria (NCI-CTC) (Diakos et al., 2014).

Follow-Up

Follow-up was performed according to the NCCN (2020) guidelines: 1) every 3 months for 1–2 years postoperatively, 2) every 6 months for 3–5 years postoperatively, and 3) every year after 5 years until death. Disease-Free Survival (DFS) was the duration between postoperative day 1 until tumor recurrence, distant metastasis, or death from other causes. The duration between postoperative day 1 until the last follow-up or death was defined as Overall Survival (OS). The duration between postoperative day 1 until death or the last follow-up was deemed as survival.

Statistical Methods

SPSS 17.0 (version 17.0; SPSS Inc., Chicago, IL, United States) and GraphPad Prism Software (Version 8.0; GraphPad Inc., La Jolla, CA, United States) were used to carry out all statistical analyses. The critical optimal threshold values of related variables were identified utilizing receiver operating characteristic curves (ROC), while the area under the curve (AUC) value was used to evaluate the prognostic accuracy. Qualitative data was depicted in terms of the number of cases (%), with intergroup comparisons carried out *via* the χ^2 test or Fisher's exact test. OS was determined *via* the Kaplan-Meier test. The survival rate between the two groups was contrasted with the log-rank method. Univariate and multivariate Cox proportional hazards regression models were used to discern potential prognostic factors. The association between various parameters and breast cancer prognosis was determined using hazard ratios (HRs) and 95% confidence intervals (CIs). A two-tailed p value of less than 0.05 was interpreted as achieving statistical significance.

RESULTS

SIRI is Predictive of Clinical Outcomes in Breast Cancer Before Neoadjuvant Chemotherapy

We applied the ROC curve to confirm that the optimal SIRI threshold was 0.80. Based on the optimal threshold, two SIRI groups were formed: SIRI <0.80 group (Low SIRI group) and SIRI ≥0.80 group (High SIRI group). All enrolled patients were female between ages 22–82 years. The average age of 47 ± 10 years, and the median age of 47 years 756 patients (96.31%) were married, and 29 patients (3.69%) were unmarried. BMI ranged from 16.36 to 38.19, with a median BMI of 24.00 and a mean BMI of 24.45 ± 3.55. 292 patients were postmenopausal (37.20%), and 493 patients were premenopausal (62.80%). ABO blood group distribution showed that there were 214 patients with type A (27.26%), 262 patients with type B (33.38%), 234 patients with type O (29.81%), and 75 patients with type AB (9.55%). All patients received surgical treatment, among which 606 cases (77.20%) underwent total resection of breast cancer and 179 cases (22.80%) underwent breast-conserving surgery. There were 758 cases of ductal carcinoma (96.56%), 13 cases of lobular carcinoma (1.66%), and 14 cases of other types of breast cancer (1.78%). The histological classification of breast cancer included 133 cases of grade I (16.94%), 431 cases of grade II (54.90%), and 221 cases of grade III (28.15%). There were 516 cases (65.73%) who received postoperative chemotherapy and 269 cases (34.27%) who did not receive postoperative chemotherapy. 483 cases (61.53%) received endocrine therapy after breast cancer surgery, and 302 cases (38.47%) did not receive endocrine therapy. 202 cases (25.73%) received targeted therapy after breast cancer surgery, while 583 cases (74.27%) did not receive targeted therapy. The clinical data of 785 breast cancer patients are depicted in **Table 1**.

1) In all breast cancer patients, there were 484 cases in the low SIRI group and 301 cases in the high SIRI group. Statistical analysis showed that BMI ($\chi2 = 4.801$, $p = 0.028$), clinical T stage ($\chi2 = 19.137$, $p = 0.0007$), clinical N stage ($\chi2 = 14.841$, $p = 0.005$), clinical TNM stage ($\chi2 = 12.114$, $p = 0.002$), postoperative chemotherapy regimen ($\chi2 = 16.590$, $p = 0.005$), postoperative chemotherapy ($\chi2 = 10.404$, $p = 0.001$), postoperative chemotherapy times ($\chi2 = 13.066$, $p = 0.0003$), and postoperative targeted therapy ($\chi2 = 9.697$, $p = 0.002$) demonstrated statistically significant differences between the two SIRI groups.
2) In the NACT group (477 patients), there were 267 cases in the low SIRI group and 210 cases in the high SIRI group. Statistical analysis showed that clinical T stage ($\chi2 = 10.284$, $p = 0.036$), neoadjuvant chemotherapy regimen ($\chi2 = 46.320$, $p < 0.0001$), postoperative chemotherapy ($\chi2 = 9.882$, $p = 0.043$), postoperative chemotherapy times ($\chi2 = 5.320$, $p = 0.021$) and postoperative targeted ($\chi2 = 4.153$, $p = 0.042$) were statistically significant.
3) In the non-NACT group (308 breast cancer patients), there were 217 cases in the low SIRI group and 91 cases in the high SIRI group. Statistical analysis showed that postoperative chemotherapy ($\chi2 = 13.250$, $p = 0.021$) was statistically significant.

Hematological Parameters

Breast cancer patient nutritional statuses were evaluated using several parameters, with their median values shown in brackets: ALB (45.2 g/L), blood glucose (GLU) (5.33 mmol/L), alkaline

TABLE 1 | Demographic and clinicopathologic characteristics of 785 patients with breast cancer.

Parameters	N	SIRI 785				N	SIRI 477				N	SIRI 308			
Cases (n)	785	Low SIRI 484	High SIRI 301	χ2	p value		Low SIRI 267	High SIRI 210	χ2	p value		Low SIRI 217	High SIRI 91	χ2	p value
Age (years)				0.193	0.660				0.054	0.816				1.504	0.220
<47	386 (49.17%)	235 (48.55%)	151 (50.17%)			230 (48.22%)	130 (48.69%)	100 (47.62%)			156 (50.65%)	105 (48.39%)	51 (56.04%)		
≥47	399 (50.83%)	249 (51.45%)	150 (49.83%)			247 (51.78%)	137 (51.31%)	110 (52.38%)			152 (49.35%)	112 (51.61%)	40 (43.96%)		
Marital status				0.117	0.732				0.690	0.406				3.013	0.083
Married	756 (96.31%)	467 (96.49%)	289 (96.01%)			457 (95.81%)	254 (95.13%)	203 (96.67%)			299 (97.08%)	213 (98.16%)	86 (94.51%)		
Unmarried	29 (3.69%)	17 (3.51%)	12 (3.99%)			20 (4.19%)	13 (4.87%)	7 (3.33%)			9 (2.92%)	4 (1.84%)	5 (5.49%)		
Occupation				3.276	0.194				0.133	0.936				7.681	0.022
Mental worker	358 (45.61%)	226 (46.69%)	132 (43.85%)			238 (49.90%)	135 (50.56%)	103 (49.05%)			120 (38.96%)	91 (41.94%)	29 (31.87%)		
Manual worker	125 (15.92%)	83 (17.15%)	42 (13.95%)			66 (13.84%)	37 (13.86%)	29 (13.81%)			59 (19.16%)	46 (21.20%)	13 (14.29%)		
Others	302 (38.47%)	175 (36.16%)	127 (42.19%)			173 (36.27%)	95 (35.58%)	78 (37.14%)			129 (41.88%)	80 (36.87%)	49 (53.85%)		
Weight (kg)				1.014	0.314				0.677	0.411				0.465	0.495
<62.00	383 (48.79%)	243 (50.21%)	140 (46.51%)			235 (49.27%)	136 (50.94%)	99 (47.14%)			148 (48.05%)	107 (49.31%)	41 (45.05%)		
≥62.00	402 (51.21%)	241 (49.79%)	161 (53.49%)			242 (50.73%)	131 (49.06%)	111 (52.86%)			160 (51.95%)	110 (50.69%)	50 (54.95%)		
Height (m)				1.696	0.193				0.036	0.850				2.244	0.134
<1.60	337 (42.93%)	199 (41.12%)	138 (45.85%)			218 (45.70%)	121 (45.32%)	97 (46.19%)			119 (38.64%)	78 (35.94%)	41 (45.05%)		
≥1.60	448 (57.07%)	285 (58.88%)	163 (54.15%)			259 (54.30%)	146 (54.68%)	113 (53.81%)			189 (61.36%)	139 (64.06%)	50 (54.95%)		
BMI				4.801	0.028				2.674	0.102				3.186	0.074
<24.00	391 (49.81%)	256 (52.89%)	135 (44.85%)			245 (51.36%)	146 (54.68%)	99 (47.14%)			146 (47.40%)	110 (50.69%)	36 (39.56%)		
≥24.00	394 (50.19%)	228 (47.11%)	166 (55.15%)			232 (48.64%)	121 (45.32%)	111 (52.86%)			162 (52.60%)	107 (49.31%)	55 (60.44%)		
Menarche age (year)				1.076	0.300				0.484	0.487				0.246	0.620
<14	308 (39.24%)	183 (37.81%)	125 (41.53%)			196 (41.09%)	106 (39.70%)	90 (42.86%)			112 (36.36%)	77 (35.48%)	35 (38.46%)		
≥14	477 (60.76%)	301 (62.19%)	176 (58.47%)			281 (58.91%)	161 (60.30%)	120 (57.14%)			196 (63.64%)	140 (64.52%)	56 (61.54%)		
Menopause				1.119	0.290				2.674	0.102				0.083	0.773
No	493 (62.80%)	297 (61.36%)	196 (65.12%)			280 (58.70%)	148 (55.43%)	132 (62.86%)			213 (69.16%)	149 (68.66%)	64 (70.33%)		
Yes	292 (37.20%)	187 (38.64%)	105 (34.88%)			197 (41.30%)	119 (44.57%)	78 (37.14%)			95 (30.84%)	68 (31.34%)	27 (29.67%)		
ABO blood type				2.449	0.654				4.406	0.354				2.856	0.582
A	214 (27.26%)	129 (26.65%)	85 (28.24%)			132 (27.67%)	68 (25.47%)	64 (30.48%)			82 (26.62%)	61 (28.11%)	21 (23.08%)		
B	262 (33.38%)	168 (34.71%)	94 (31.23%)			145 (30.40%)	83 (31.09%)	62 (29.52%)			117 (37.99%)	85 (39.17%)	32 (35.16%)		

(Continued on following page)

TABLE 1 | (*Continued*) Demographic and clinicopathologic characteristics of 785 patients with breast cancer.

Parameters	N	SIRI 785				N	SIRI 477				N	SIRI 308			
Cases (n)	**785**	**Low SIRI 484**	**High SIRI 301**	**χ2**	***p* value**		**Low SIRI 267**	**High SIRI 210**	**χ2**	***p* value**		**Low SIRI 217**	**High SIRI 91**	**χ2**	***p* value**
O	234 (29.81%)	146 (30.17%)	88 (29.24%)			146 (30.61%)	90 (33.71%)	56 (26.67%)			88 (28.57%)	56 (25.81%)	32 (35.16%)		
AB	75 (9.55%)	41 (8.47%)	34 (11.30%)			54 (11.32%)	26 (9.74%)	28 (13.33%)			21 (6.82%)	15 (6.91%)	6 (6.59%)		
Tumor site				0.049	0.824				1.404	0.236				2.417	0.120
Right	369 (47.01%)	226 (46.69%)	143 (47.51%)			233 (48.85%)	124 (46.44%)	109 (51.90%)			136 (44.16%)	102 (47.00%)	34 (37.36%)		
Left	416 (52.99%)	258 (53.31%)	158 (52.49%)			244 (51.15%)	143 (53.56%)	101 (48.10%)			172 (55.84%)	115 (53.00%)	57 (62.64%)		
Clinical T stage				19.137	0.001				10.284	0.036				3.161	0.531
T1	168 (21.40%)	113 (23.35%)	68 (22.59%)			65 (13.63%)	43 (16.10%)	22 (10.48%)			103 (33.44%)	70 (32.26%)	33 (36.26%)		
T2	413 (52.61%)	269 (55.58%)	132 (43.85%)			226 (47.38%)	133 (49.81%)	93 (44.29%)			187 (60.71%)	136 (62.67%)	51 (56.04%)		
T3	131 (16.69%)	71 (14.67%)	59 (19.60%)			115 (24.11%)	62 (23.22%)	53 (25.24%)			16 (5.19%)	9 (4.15%)	7 (7.69%)		
T4	73 (9.30%)	31 (6.40%)	42 (13.95%)			71 (14.88%)	29 (10.86%)	42 (20.00%)			2 (0.65%)	2 (0.92%)	0 (0.00%)		
Clinical N stage				14.841	0.005				0.665	0.956				5.613	0.230
N0	299 (38.09%)	210 (43.39%)	90 (29.90%)			73 (15.30%)	44 (16.48%)	29 (13.81%)			226 (73.38%)	166 (76.50%)	60 (65.93%)		
N1	233 (29.68%)	135 (27.89%)	97 (32.23%)			164 (34.38%)	90 (33.71%)	74 (35.24%)			69 (22.40%)	45 (20.74%)	24 (26.37%)		
N2	160 (20.38%)	88 (18.18%)	72 (23.92%)			151 (31.66%)	84 (31.46%)	67 (31.90%)			9 (2.92%)	4 (1.84%)	5 (5.49%)		
N3	93 (11.85%)	51 (10.54%)	42 (13.95%)			89 (18.66%)	49 (18.35%)	40 (19.05%)			4 (1.30%)	2 (0.92%)	2 (2.20%)		
Clinical TNM stage				12.114	0.002				1.930	0.381				0.555	0.758
I	92 (11.72%)	66 (13.64%)	26 (8.64%)			14 (2.94%)	10 (3.75%)	4 (1.90%)			78 (25.32%)	56 (25.81%)	22 (24.18%)		
II	382 (48.66%)	248 (51.24%)	134 (44.52%)			168 (35.22%)	97 (36.33%)	71 (33.81%)			214 (69.48%)	151 (69.59%)	63 (69.23%)		
III	311 (39.62%)	170 (35.12%)	141 (46.84%)			295 (61.84%)	160 (59.93%)	135 (64.29%)			16 (5.19%)	10 (4.61%)	6 (6.59%)		
Neoadjuvant Chemotherapy															
Chemotherapy regimen									46.320	<0.0001					
EC/ECF						28 (5.87%)	21 (7.87%)	7 (3.33%)							
CT/ECT						27 (5.66%)	21 (7.87%)	6 (2.86%)							
ET						223 (46.75%)	131 (49.06%)	92 (43.81%)							
TP						141 (29.56%)	61 (22.85%)	80 (38.10%)							
Others						58 (12.16%)	33 (12.36%)	25 (11.90%)							

(Continued on following page)

TABLE 1 | (*Continued*) Demographic and clinicopathologic characteristics of 785 patients with breast cancer.

Parameters	N	SIRI 785				N	SIRI 477				N	SIRI 308			
Cases (n)	**785**	**Low SIRI 484**	**High SIRI 301**	**χ2**	***p* value**		**Low SIRI 267**	**High SIRI 210**	**χ2**	***p* value**		**Low SIRI 217**	**High SIRI 91**	**χ2**	***p* value**
Chemotherapy times									3.407	0.065					
<6						134 (28.09%)	84 (31.46%)	50 (23.81%)							
≥6						343 (71.91%)	183 (68.54%)	160 (76.19%)							
Response									1.326	0.857					
CR						7 (1.47%)	6 (2.25%)	1 (0.48%)							
PR						312 (65.41%)	169 (63.30%)	143 (68.10%)							
SD						151 (31.66%)	86 (32.21%)	65 (30.95%)							
PD						7 (1.47%)	6 (2.25%)	1 (0.48%)							
Miller and Payne grade									9.371	0.053					
1						22 (4.61%)	11 (4.12%)	11 (5.24%)							
2						126 (26.42%)	70 (26.22%)	56 (26.67%)							
3						177 (37.11%)	112 (41.95%)	65 (30.95%)							
4						62 (13.00%)	26 (9.74%)	36 (17.14%)							
5						90 (18.87%)	48 (17.98%)	42 (20.00%)							
Pathological response									0.024	0.876					
pCR						72 (15.09%)	40 (14.98%)	32 (15.24%)							
non-pCR						405 (84.91%)	229 (85.77%)	176 (83.81%)							
Post-chemotherapy regimen				16.590	0.005				6.457	0.264				13.250	0.021
EC/ECF	125 (15.92%)	88 (18.18%)	37 (12.29%)			43 (9.01%)	25 (9.36%)	18 (8.57%)			82 (26.62%)	63 (29.03%)	19 (20.88%)		
CT/ECT	125 (15.92%)	75 (15.50%)	50 (16.61%)			30 (6.29%)	20 (7.49%)	10 (4.76%)			95 (30.84%)	55 (25.35%)	40 (43.96%)		
ET	97 (12.36%)	71 (14.67%)	26 (8.64%)			37 (7.76%)	25 (9.36%)	12 (5.71%)			60 (19.48%)	46 (21.20%)	14 (15.38%)		
TP	61 (7.77%)	37 (7.64%)	24 (7.97%)			39 (8.18%)	23 (8.61%)	16 (7.62%)			22 (7.14%)	14 (6.45%)	8 (8.79%)		
Others	108 (13.76%)	68 (14.05%)	40 (13.29%)			81 (16.98%)	48 (17.98%)	33 (15.71%)			27 (8.77%)	20 (9.22%)	7 (7.69%)		
NO	269 (34.27%)	145 (29.96%)	124 (41.20%)			247(51.78%)	126 (47.19%)	121 (57.62%)			22 (7.14%)	19 (8.76%)	3 (3.30%)		
Type of surgery				0.082	0.775				0.037	0.848				0.654	0.419
Mastectomy	606 (77.20%)	372 (76.86%)	234 (77.74%)			406 (85.12%)	228 (85.39%)	178 (84.76%)			200 (64.94%)	144 (66.36%)	56 (61.54%)		
Breast-conserving surgery	179 (22.80%)	112 (23.14%)	67 (22.26%)			71 (14.88%)	39 (14.61%)	32 (15.24%)			108 (35.06%)	73 (33.64%)	35 (38.46%)		
Tumor size (cm)				0.785	0.675				0.512	0.774				0.016	0.992

(Continued on following page)

TABLE 1 | (*Continued*) Demographic and clinicopathologic characteristics of 785 patients with breast cancer.

Parameters	N	SIRI 785				N	SIRI 477				N	SIRI 308			
Cases (n)	**785**	**Low SIRI 484**	**High SIRI 301**	**χ2**	***p* value**		**Low SIRI 267**	**High SIRI 210**	**χ2**	***p* value**		**Low SIRI 217**	**High SIRI 91**	**χ2**	***p* value**
≤2 cm	437 (55.67%)	267 (55.17%)	170 (56.48%)			263 (55.14%)	144 (53.93%)	119 (56.67%)			174 (56.49%)	123 (56.68%)	51 (56.04%)		
> 2 and <5 cm	299 (38.09%)	189 (39.05%)	110 (36.54%)			172 (36.06%)	100 (37.45%)	72 (34.29%)			127 (41.23%)	89 (41.01%)	38 (41.76%)		
≥5 cm	49 (6.24%)	28 (5.79%)	21 (6.98%)			42 (8.81%)	23 (8.61%)	19 (9.05%)			7 (2.27%)	5 (2.30%)	2 (2.20%)		
Histologic type				1.481	0.477				0.906	0.636				3.556	0.169
Ductal	758 (96.56%)	470 (97.11%)	288 (95.68%)			461 (96.65%)	258 (96.63%)	203 (96.67%)			297 (96.43%)	212 (97.70%)	85 (93.41%)		
Lobular	13 (1.66%)	6 (1.24%)	7 (2.33%)			7 (1.47%)	3 (1.12%)	4 (1.90%)			6 (1.95%)	3 (1.38%)	3 (3.30%)		
Others	14 (1.78%)	8 (1.65%)	6 (1.99%)			9 (1.89%)	6 (2.25%)	3 (1.43%)			5 (1.62%)	2 (0.92%)	3 (3.30%)		
Histologic grade				3.881	0.144				3.327	0.190				5.327	0.070
I	133 (16.94%)	76 (15.70%)	57 (18.94%)			108 (22.64%)	54 (20.22%)	54 (25.71%)			25 (8.12%)	22 (10.14%)	3 (3.30%)		
II	431 (54.90%)	279 (57.64%)	152 (50.50%)			244 (51.15%)	146 (54.68%)	98 (46.67%)			187 (60.71%)	133 (61.29%)	54 (59.34%)		
III	221 (28.15%)	129 (26.65%)	92 (30.56%)			125 (26.21%)	67 (25.09%)	58 (27.62%)			96 (31.17%)	62 (28.57%)	34 (37.36%)		
Pathological TNM classification															
Pathological T stage				4.021	0.403				2.050	0.727				1.824	0.768
Tis/T0	92 (11.72%)	50 (10.33%)	42 (13.95%)			88 (18.45%)	46 (17.23%)	42 (20.00%)			4 (1.30%)	4 (1.84%)	0 (0.00%)		
T1	302 (38.47%)	187 (38.64%)	115 (38.21%)			190 (39.83%)	108 (40.45%)	82 (39.05%)			112 (36.36%)	79 (36.41%)	33 (36.26%)		
T2	326 (41.53%)	208 (42.98%)	118 (39.20%)			149 (31.24%)	85 (31.84%)	64 (30.48%)			177 (57.47%)	123 (56.68%)	54 (59.34%)		
T3	45 (5.73%)	29 (5.99%)	16 (5.32%)			34 (7.13%)	21 (7.87%)	13 (6.19%)			11 (3.57%)	8 (3.69%)	3 (3.30%)		
T4	20 (2.55%)	10 (2.07%)	10 (3.32%)			16 (3.35%)	7 (2.62%)	9 (4.29%)			4 (1.30%)	3 (1.38%)	1 (1.10%)		
Pathological N stage				2.054	0.726				1.523	0.823				1.628	0.804
N0	326 (41.53%)	201 (41.53%)	125 (41.53%)			176 (36.90%)	96 (35.96%)	80 (38.10%)			150 (48.70%)	105 (48.39%)	45 (49.45%)		
N1	175 (22.29%)	115 (23.76%)	60 (19.93%)			101 (21.17%)	62 (23.22%)	39 (18.57%)			74 (24.03%)	53 (24.42%)	21 (23.08%)		
N2	122 (15.54%)	71 (14.67%)	51 (16.94%)			77 (16.14%)	42 (15.73%)	35 (16.67%)			45 (14.61%)	29 (13.36%)	16 (17.58%)		
N3	162 (20.64%)	97 (20.04%)	65 (21.59%)			123 (25.79%)	67 (25.09%)	56 (26.67%)			39 (12.66%)	30 (13.82%)	9 (9.89%)		
Pathological TNM stage				2.384	0.666				1.795	0.773				1.621	0.805
Tis/T0	74 (9.43%)	43 (8.88%)	31 (10.30%)			71 (14.88%)	40 (14.98%)	31 (14.76%)			3 (0.97%)	3 (1.38%)	0 (0.00%)		
I	157 (20.00%)	96 (19.83%)	61 (20.27%)			83 (17.40%)	44 (16.48%)	39 (18.57%)			74 (24.03%)	52 (23.96%)	22 (24.18%)		
II	262 (33.38%)	171 (35.33%)	91 (30.23%)			118 (24.74%)	72 (26.97%)	46 (21.90%)			144 (46.75%)	99 (45.62%)	45 (49.45%)		
III	292 (37.20%)	174 (35.95%)	118 (39.20%)			205 (42.98%)	111 (41.57%)	94 (44.76%)			87 (28.25%)	63 (29.03%)	24 (26.37%)		

(Continued on following page)

TABLE 1 | (*Continued*) Demographic and clinicopathologic characteristics of 785 patients with breast cancer.

Parameters	N	SIRI 785				N	SIRI 477				N	SIRI 308			
Cases (n)	**785**	**Low SIRI 484**	**High SIRI 301**	**χ2**	***p* value**		**Low SIRI 267**	**High SIRI 210**	**χ2**	***p* value**		**Low SIRI 217**	**High SIRI 91**	**χ2**	***p* value**
Total lymph nodes				0.204	0.652				2.866	0.091				0.047	0.829
<21	391 (49.81%)	238 (49.17%)	153 (50.83%)			202 (42.35%)	104 (38.95%)	98 (46.67%)			189 (61.36%)	134 (61.75%)	55 (60.44%)		
≥21	394 (50.19%)	246 (50.83%)	148 (49.17%)			275 (57.65%)	163 (61.05%)	112 (53.33%)			119 (38.64%)	83 (38.25%)	36 (39.56%)		
Positive lymph nodes				0.103	0.749				0.175	0.676				0.109	0.742
<1	329 (41.91%)	205 (42.36%)	124 (41.20%)			179 (37.53%)	98 (36.70%)	81 (38.57%)			150 (48.70%)	107 (49.31%)	43 (47.25%)		
≥1	456 (58.09%)	279 (57.64%)	177 (58.80%)			298 (62.47%)	169 (63.30%)	129 (61.43%)			158 (51.30%)	110 (50.69%)	48 (52.75%)		
Postoperative complications				0.002	0.968				0.017	0.898				0.375	0.540
No	728 (92.74%)	449 (92.77%)	279 (92.69%)			449 (94.13%)	251 (94.01%)	198 (94.29%)			279 (90.58%)	198 (91.24%)	81 (89.01%)		
Yes	57 (7.26%)	35 (7.23%)	22 (7.31%)			28 (5.87%)	16 (5.99%)	12 (5.71%)			29 (9.42%)	19 (8.76%)	10 (10.99%)		
Postoperative chemotherapy				10.404	0.001				5.120	0.024				2.881	0.090
No	269 (34.27%)	145 (29.96%)	124 (41.20%)			247 (51.78%)	126 (47.19%)	121 (57.62%)			22 (7.14%)	19 (8.76%)	3 (3.30%)		
Yes	516 (65.73%)	339 (70.04%)	177 (58.80%)			230 (48.22%)	141 (52.81%)	89 (42.38%)			286 (92.86%)	198 (91.24%)	88 (96.70%)		
Postoperative chemotherapy times				13.066	0.0003				5.320	0.021				1.473	0.225
<4	374 (47.64%)	206 (42.56%)	168 (55.81%)			340 (71.28%)	179 (67.04%)	161 (76.67%)			34 (11.04%)	27 (12.44%)	7 (7.69%)		
≥4	411 (52.36%)	278 (57.44%)	133 (44.19%)			137 (28.72%)	88 (32.96%)	49 (23.33%)			274 (88.96%)	190 (87.56%)	84 (92.31%)		
Postoperative radiotherapy				0.496	0.481				0.118	0.732				2.750	0.097
No	196 (24.97%)	125 (25.83%)	71 (23.59%)			119 (24.95%)	65 (24.34%)	54 (25.71%)			77 (25.00%)	60 (27.65%)	17 (18.68%)		
Yes	589 (75.03%)	359 (74.17%)	230 (76.41%)			358 (75.05%)	202 (75.66%)	156 (74.29%)			231 (75.00%)	157 (72.35%)	74 (81.32%)		
Postoperative endocrine therapy				1.927	0.165				0.059	0.808				1.563	0.211
No	302 (38.47%)	177 (36.57%)	125 (41.53%)			206 (43.19%)	114 (42.70%)	92 (43.81%)			96 (31.17%)	63 (29.03%)	33 (36.26%)		
Yes	483 (61.53%)	307 (63.43%)	176 (58.47%)			271 (56.81%)	153 (57.30%)	118 (56.19%)			212 (68.83%)	154 (70.97%)	58 (63.74%)		
Postoperative targeted therapy				9.697	0.002				4.153	0.042				2.753	0.097
No	583 (74.27%)	378 (78.10%)	205 (68.11%)			332 (69.60%)	196 (73.41%)	136 (64.76%)			251 (81.49%)	182 (83.87%)	69 (75.82%)		
Yes	202 (25.73%)	106 (21.90%)	96 (31.89%)			145 (30.40%)	71 (26.59%)	74 (35.24%)			57 (18.51%)	35 (16.13%)	22 (24.18%)		

TABLE 2 | The correlations between nutritional parameters/blood parameters and SIRI.

Parameters	N	SIRI 785				N	SIRI 477				N	SIRI 308			
Cases (*n*)	**785**	**Low SIRI 484**	**High SIRI 301**	**χ^2**	***p* value**		**Low SIRI 267**	**High SIRI 210**	**χ^2**	***p* value**		**Low SIRI 217**	**High SIRI 91**	**χ^2**	***p* value**
ALT (U/L)				0.820	0.365				0.071	0.791				1.699	0.192
<15	370 (47.13%)	234 (48.35%)	136 (45.18%)			208 (43.61%)	115 (43.07%)	93 (44.29%)			162 (52.60%)	119 (54.84%)	43 (47.25%)		
≥15	416 (52.99%)	250 (51.65%)	166 (55.15%)			269 (56.39%)	152 (56.93%)	117 (55.71%)			147 (47.73%)	98 (45.16%)	49 (53.85%)		
AST (U/L)				0.092	0.762				0.153	0.696				0.444	0.505
<18	378 (48.15%)	231 (47.73%)	147 (48.84%)			211 (44.23%)	116 (43.45%)	95 (45.24%)			167 (54.22%)	115 (53.00%)	52 (57.14%)		
≥18	407 (51.85%)	253 (52.27%)	154 (51.16%)			266 (55.77%)	151 (56.55%)	115 (54.76%)			141 (45.78%)	102 (47.00%)	39 (42.86%)		
LDH (U/L)				4.337	0.037				3.509	0.061				0.056	0.813
<167	376 (47.90%)	246 (50.83%)	130 (43.19%)			193 (40.46%)	118 (44.19%)	75 (35.71%)			183 (59.42%)	128 (58.99%)	55(60.44%)		
≥167	409 (52.10%)	238 (49.17%)	171 (56.81%)			284 (59.54%)	149 (55.81%)	135 (64.29%)			125 (40.58%)	89 (41.01%)	36 (39.56%)		
GGT (U/L)				2.314	0.128				1.413	0.235				0.084	0.772
<17	366 (46.62%)	236 (48.76%)	130 (43.19%)			203 (42.56%)	120 (44.94%)	83 (39.52%)			163 (52.92%)	116 (53.46%)	47 (51.65%)		
≥17	419 (53.38%)	248 (51.24%)	171 (56.81%)			274 (57.44%)	147 (55.06%)	127 (60.48%)			145 (47.08%)	101 (46.54%)	44 (48.35%)		
ALP (U/L)				0.273	0.601				2.149	0.143				1.369	0.242
<64	377 (48.03%)	236 (48.76%)	141 (46.84%)			227 (47.59%)	135 (50.56%)	92 (43.81%)			150 (48.70%)	101 (46.54%)	49 (53.85%)		
≥64	408 (51.97%)	248 (51.24%)	160 (53.16%)			250 (52.41%)	132 (49.44%)	118 (56.19%)			158 (51.30%)	116 (53.46%)	42 (46.15%)		
GLU (mmol/L)				0.093	0.761				0.002	0.962				0.013	0.909
<5.33	391 (49.81%)	239 (49.38%)	152 (50.50%)			247 (51.78%)	138 (51.69%)	109 (51.90%)			144 (46.75%)	101 (46.54%)	43 (47.25%)		
≥5.33	394 (50.19%)	245 (50.62%)	149 (49.50%)			230 (48.22%)	129 (48.31%)	101 (48.10%)			164 (53.25%)	116 (53.46%)	48 (52.75%)		
ALB (g/L)				3.817	0.051				0.007	0.933				9.576	0.002
<45.2	392 (49.94%)	255 (52.69%)	137 (45.51%)			235 (49.27%)	132 (49.44%)	103 (49.05%)			157 (50.97%)	123 (56.68%)	34 (37.36%)		
≥45.2	393 (50.06%)	229 (47.31%)	164 (54.49%)			242 (50.73%)	135 (50.56%)	107 (50.95%)			151 (49.03%)	94 (43.32%)	57 (62.64%)		
CRP (mg/dl)				17.198	<0.0001				2.475	0.116				11.798	0.001
<0.02	384 (48.92%)	265 (54.75%)	119 (39.53%)			187 (39.20%)	113 (42.32%)	74 (35.24%)			197 (63.96%)	152 (70.05%)	45 (49.45%)		
≥0.02	401 (51.08%)	219 (45.25%)	182 (60.47%)			290 (60.80%)	154 (57.68%)	136 (64.76%)			111 (36.04%)	65 (29.95%)	46 (50.55%)		
CA125 (U/ml)				5.051	0.025				2.956	0.086				0.784	0.376
<13.35	392 (49.94%)	257 (53.10%)	135 (44.85%)			221 (46.33%)	133 (49.81%)	88 (41.90%)			171 (55.52%)	124 (57.14%)	47 (51.65%)		
≥13.35	393 (50.06%)	227 (46.90%)	166 (55.15%)			256 (53.67%)	134 (50.19%)	122 (58.10%)			137 (44.48%)	93 (42.86%)	44 (48.35%)		
CA153 (U/ml)				0.236	0.627				0.723	0.395				2.060	0.151

(Continued on following page)

TABLE 2 | (*Continued*) The correlations between nutritional parameters/blood parameters and SIRI.

Parameters	N	SIRI 785				N	SIRI 477				N	SIRI 308			
Cases (*n*)	**785**	**Low SIRI 484**	**High SIRI 301**	**χ2**	***p* value**		**Low SIRI 267**	**High SIRI 210**	**χ2**	***p* value**		**Low SIRI 217**	**High SIRI 91**	**χ2**	***p* value**
<11.63	392 (49.94%)	245 (50.62%)	147 (48.84%)			208 (43.61%)	121 (45.32%)	87 (41.43%)			184 (59.74%)	124 (57.14%)	60 (65.93%)		
≥11.63	393 (50.06%)	239 (49.38%)	154 (51.16%)			269 (56.39%)	146 (54.68%)	123 (58.57%)			124 (40.26%)	93 (42.86%)	31 (34.07%)		
CEA (ng/ml)				2.025	0.155				2.025	0.155				2.174	0.140
<1.66	392 (49.94%)	232 (47.93%)	160 (53.16%)			212 (44.44%)	111 (41.57%)	101 (48.10%)			180 (58.44%)	121 (55.76%)	59 (64.84%)		
≥1.66	393 (50.06%)	252 (52.07%)	141 (46.84%)			265 (55.56%)	156 (58.43%)	109 (51.90%)			128 (41.56%)	96 (44.24%)	32 (35.16%)		
D-D (mg/L)				0.147	0.702				0.039	0.844				5.007	0.025
<0.29	387 (49.30%)	236 (48.76%)	151 (50.17%)			200 (41.93%)	113 (42.32%)	87 (41.43%)			187 (60.71%)	123 (56.68%)	64 (70.33%)		
≥0.29	398 (50.70%)	248 (51.24%)	150 (49.83%)			277 (58.07%)	154 (57.68%)	123 (58.57%)			121 (39.29%)	94 (43.32%)	27 (29.67%)		
FIB (g/L)				14.320	0.0002				11.241	0.001				1.468	0.226
<2.85	388 (49.43%)	265 (54.75%)	123 (40.86%)			216 (45.28%)	139 (52.06%)	77 (36.67%)			172 (55.84%)	126 (58.06%)	46 (50.55%)		
≥2.85	397 (50.57%)	219 (45.25%)	178 (59.14%)			261 (54.72%)	128 (47.94%)	133 (63.33%)			136 (44.16%)	91 (41.94%)	45 (49.45%)		
INR				4.218	0.040				0.884	0.347				0.425	0.515
<0.93	365 (46.50%)	239 (49.38%)	126 (41.86%)			177 (37.11%)	104 (38.95%)	73 (34.76%)			188 (61.04%)	135 (62.21%)	53 (58.24%)		
≥0.93	420 (53.50%)	245 (50.62%)	175 (58.14%)			300 (62.89%)	163 (61.05%)	137 (65.24%)			120 (38.96%)	82 (37.79%)	38 (41.76%)		
FDP (ug/ml)				4.691	0.030				0.300	0.584				2.025	0.155
<1.40	367 (46.75%)	241 (49.79%)	126 (41.86%)			137 (28.72%)	74 (27.72%)	63 (30.00%)			230 (74.68%)	167 (76.96%)	63 (69.23%)		
≥1.40	418 (53.25%)	243 (50.21%)	175 (58.14%)			340 (71.28%)	193 (72.28%)	147 (70.00%)			78 (25.32%)	50 (23.04%)	28 (30.77%)		
White blood cell (W) ($\times10^9$/L)				75.436	<0.0001				57.819	<0.0001				20.949	<0.0001
<6.01	389 (49.55%)	299 (61.78%)	90 (29.90%)			239 (50.10%)	175 (65.54%)	64 (30.48%)			150 (48.70%)	124 (57.14%)	26 (28.57%)		
≥6.01	396 (50.45%)	185 (38.22%)	211 (70.10%)			238 (49.90%)	92 (34.46%)	146 (69.52%)			158 (51.30%)	93 (42.86%)	65 (71.43%)		
Red blood cell (R) ($\times10^{12}$/L)				7.107	0.008				5.283	0.022				1.887	0.170
<4.40	389 (49.55%)	258 (53.31%)	131 (43.52%)			235 (49.27%)	144 (53.93%)	91 (43.33%)			154 (50.00%)	114 (52.53%)	40 (43.96%)		
≥4.40	396 (50.45%)	226 (46.69%)	170 (56.48%)			242 (50.73%)	123 (46.07%)	119 (56.67%)			154 (50.00%)	103 (47.47%)	51 (56.04%)		
Hemoglobin (Hb) ($\times10^9$/L)				7.361	0.007				4.887	0.027				4.100	0.043
<132	382 (48.66%)	254 (52.48%)	128 (42.52%)			243 (50.94%)	148 (55.43%)	95 (45.24%)			139 (45.13%)	106 (48.85%)	33 (36.26%)		
≥132													58 (63.74%)		

(Continued on following page)

TABLE 2 | (*Continued*) The correlations between nutritional parameters/blood parameters and SIRI.

Parameters	N	SIRI 785				N	SIRI 477				N	SIRI 308			
Cases (*n*)	**785**	**Low SIRI 484**	**High SIRI 301**	**$\chi2$**	***p* value**		**Low SIRI 267**	**High SIRI 210**	**$\chi2$**	***p* value**		**Low SIRI 217**	**High SIRI 91**	**$\chi2$**	***p* value**
	403 (51.34%)	230 (47.52%)	173 (57.48%)			234 (49.06%)	119 (44.57%)	115 (54.76%)			169 (54.87%)	111 (51.15%)			
Neutrophil (N) ($\times10^9$/L)				142.491	<0.0001				98.716	<0.0001				42.839	<0.0001
<3.68	392 (49.94%)	323 (66.74%)	69 (22.92%)			229 (48.01%)	182 (68.16%)	47 (22.38%)			163 (52.92%)	141 (64.98%)	22 (24.18%)		
≥3.68	393 (50.06%)	161 (33.26%)	232 (77.08%)			248 (51.99%)	85 (31.84%)	163 (77.62%)			145 (47.08%)	76 (35.02%)	69 (75.82%)		
Lymphocyte (L) ($\times10^9$/L)				7.843	0.005				1.884	0.170				4.817	0.028
<1.76	391 (49.81%)	222 (45.87%)	169 (56.15%)			258 (54.09%)	137 (51.31%)	121 (57.62%)			133 (43.18%)	85 (39.17%)	48 (52.75%)		
≥1.76	394 (50.19%)	262 (54.13%)	132 (43.85%)			219 (45.91%)	130 (48.69%)	89 (42.38%)			175 (56.82%)	132 (60.83%)	43 (47.25%)		
Monocyte (M) ($\times10^9$/L)				124.109	<0.0001				100.469	<0.0001				26.521	<0.0001
<0.35	367 (46.75%)	302 (62.40%)	65 (21.59%)			216 (45.28%)	175 (65.54%)	41 (19.52%)			151 (49.03%)	127 (58.53%)	24 (26.37%)		
≥0.35	418 (53.25%)	182 (37.60%)	236 (78.41%)			261 (54.72%)	92 (34.46%)	169 (80.48%)			157 (50.97%)	90 (41.47%)	67 (73.63%)		
Eosinophils (E) ($\times10^9$/L)				3.395	0.065				0.041	0.839				6.697	0.010
<0.06	356 (45.35%)	207 (42.77%)	149 (49.50%)			241 (50.52%)	136 (50.94%)	105 (50.00%)			115 (37.34%)	71 (32.72%)	44 (48.35%)		
≥0.06	429 (54.65%)	277 (57.23%)	152 (50.50%)			236 (49.48%)	131 (49.06%)	105 (50.00%)			193 (62.66%)	146 (67.28%)	47 (51.65%)		
Basophils (B) ($\times10^9$/L)				9.429	0.002				2.588	0.108				9.248	0.002
<0.02	224 (28.54%)	157 (32.44%)	67 (22.26%)			136 (28.51%)	84 (31.46%)	52 (24.76%)			88 (28.57%)	73 (33.64%)	15 (16.48%)		
≥0.02	561 (71.46%)	327 (67.56%)	234 (77.74%)			341 (71.49%)	183 (68.54%)	158 (75.24%)			220 (71.43%)	144 (66.36%)	76 (83.52%)		
Platelet (P) ($\times10^9$/L)				13.231	0.0003				8.329	0.004				3.482	0.062
<243	388 (49.43%)	264 (54.55%)	124 (41.20%)			224 (46.96%)	141 (52.81%)	83 (39.52%)			164 (53.25%)	123 (56.68%)	41 (45.05%)		
≥243	397 (50.57%)	220 (45.45%)	177 (58.80%)			253 (53.04%)	126 (47.19%)	127 (60.48%)			144 (46.75%)	94 (43.32%)	50 (54.95%)		

TABLE 3 | Survival analyses based on univariate and multivariate Cox regression methods for predicting breast cancer patient DFS and OS.

Parameters	DFS				OS				*p* value
	Univariate analysis		Multivariate analysis		Univariate analysis		Multivariate analysis		
	Hazard ratio (95%CI)	*p* value	Hazard ratio (95%CI)	*p* value	Hazard ratio (95%CI)	*p* value	Hazard ratio (95%CI)		
Menopause		0.011		0.001		0.007			0.014
No	1 (reference)		1 (reference)		1 (reference)		1 (reference)		
Yes	1.598 (1.113–2.295)		1.487 (1.180–1.873)		1.392 (1.094–1.771)		1.344 (1.063–1.700)		
GLU (mmol/L)		0.003		0.006		0.013			0.018
<5.33	1 (reference)		1 (reference)		1 (reference)		1 (reference)		
≥5.33	0.662 (0.502–0.872)		0.732 (0.585–0.915)		0.692 (0.518–0.924)		0.749 (0.590–0.952)		
CA125 (U/ml)		0.013		0.026		0.018			0.049
<13.35	1(reference)		1 (reference)		1 (reference)		1 (reference)		
≥13.35	1.395 (1.073–1.813)		1.295 (1.032–1.624)		1.330 (1.050–1.685)		1.261 (1.001–1.589)		
CA153 (U/ml)		0.073				0.002			0.012
<11.63	1 (reference)				1 (reference)		1 (reference)		
≥11.63	1.291 (0.976–1.708)				1.554 (1.171–2.063)		1.331 (1.065–1.664)		
Neutrophil (N)×10^9/L		0.482				0.278			
<3.68	1 (reference)				1 (reference)				
≥3.68	0.875 (0.603–1.269)				0.806 (0.545–1.190)				
Lymphocyte (L)×10^9/L		0.481				0.412			
<1.76	1 (reference)				1 (reference)				
≥1.76	0.898 (0.668–1.209)				1.133 (0.840–1.527)				
Monocyte (M)×10^9/L		0.004		<0.0001		<0.0001			<0.0001
<0.35	1 (reference)		1 (reference)		1 (reference)		1 (reference)		
≥0.35	1.419 (1.118–1.799)		1.627 (1.275–2.078)		1.869 (1.396–2.503)		1.637 (1.269–2.110)		
Eosinophils (E)×10^9/L		0.015		0.008		0.001			0.010
<0.06	1 (reference)		1 (reference)		1 (reference)		1 (reference)		
≥0.06	0.717 (0.548–0.937)		0.740 (0.592–0.925)		0.636 (0.483–0.839)		0.744 (0.594–0.932)		
Platelet (P)×10^9/L		0.137				0.304			
<243	1 (reference)				1 (reference)				
≥243	0.839 (0.666–1.058)				0.874 (0.678–1.128)				
Systemic inflammation response index (SIRI)		0.016		0.013		<0.0001			<0.0001
<112	1 (reference)		1 (reference)		1 (reference)		1 (reference)		
≥112	1.461 (1.074–1.988)		1.475 (1.085–2.005)		1.970 (1.431–2.712)		1.637 (1.269–2.110)		
Clinical stage									
Clinical N stage		0.230				0.001			<0.0001
N0	1 (reference)				1 (reference)		1 (reference)		
N1	0.934 (0.622–1.401)				1.532 (1.101–2.132)		1.371 (1.053–1.786)		
N2	0.883 (0.439–1.777)				1.704 (1.010–2.934)		1.400 (1.010–1.942)		
N3	1.476 (0.689–3.160)				3.525 (1.852–6.708)		3.034 (2.080–4.427)		
Histologic type		0.021		0.028		0.002			0.017
Ductal	1 (reference)		1 (reference)		1 (reference)		1 (reference)		
Lobular	2.581 (1.129–5.899)		2.495 (1.096–5.683)		3.006 (1.255–7.198)		1.943 (1.064–4.019)		
Others	2.046 (1.083–4.537)		1.987 (1.115–4.405)		2.948 (1.332–6.522)		2.357 (1.140–4.870)		
Pathological TNM classification									
Pathological N stage		0.014		<0.0001		0.0002			<0.0001
N0	1 (reference)		1 (reference)		1 (reference)		1 (reference)		

(Continued on following page)

TABLE 3 | (*Continued*) Survival analyses based on univariate and multivariate Cox regression methods for predicting breast cancer patient DFS and OS.

Parameters	DFS				OS				*p* value
	Univariate analysis		Multivariate analysis		Univariate analysis		Multivariate analysis		
	Hazard ratio (95%CI)	*p* value	Hazard ratio (95%CI)	*p* value	Hazard ratio (95%CI)	*p* value	Hazard ratio (95%CI)		
N1	2.901 (1.031–8.668)		1.518 (1.148–2.008)		2.001 (1.493–5.981)		1.330 (1.004–1.776)		
N2	3.928 (1.004–15.47)		1.499 (1.077–2.086)		6.029 (1.702–21.35)		1.495 (1.061–2.105)		
N3	6.219 (1.574–24.56)		1.897 (1.420–2.535)		10.24 (2.861–36.69)		2.006 (1.465–2.748)		
Pathological TNM stage		0.255				0.006			0.012
Tis/T0	1 (reference)				1 (reference)		1 (reference)		
I	2.662 (0.732–9.671)				2.600 (1.399–9.454)		1.986 (1.126–3.503)		
II	3.251 (0.862–12.26)				3.626 (1.043–13.70)		2.236 (1.098–4.844)		
III	1.998 (0.418–9.555)				2.532 (1.337–4.796)		2.645 (1.428–4.899)		
Positive lymph nodes		0.306				0.725			
<1	1 (reference)				1 (reference)				
≥1	0.509 (0.140–1.853)				0.788 (0.210–2.959)				
Postoperative pathology (IHC)									
Molecular subtype		0.018		0.029		0.097			
Luminal A	1 (reference)		1 (reference)		1 (reference)				
Luminal B HER2+	0.395 (0.216–0.724)		0.391 (0.213–0.716)		0.259 (0.093–0.722)				
Luminal B HER2-	0.535 (0.330–0.868)		0.468 (0.287–0.763)		0.535 (0.307–0.933)				
HER2 enriched	0.357 (0.193–0.662)		0.429 (0.233–0.790)		0.287 (0.096–0.853)				
Triple negative	0.534 (0.309–0.924)		0.455 (0.262–0.790)		0.557 (0.271–1.145)				
ER status		0.105				0.725			
Negative	1 (reference)				1 (reference)				
Positive	0.658 (0.397–1.090)				0.913 (0.551–1.512)				
PR status		0.257				0.155			
Negative	1 (reference)				1 (reference)				
Positive	1.253 (0.847–1.854)				1.306 (0.903–1.887)				
HER2 status		0.101				0.182			
Negative (0--++)	1 (reference)				1 (reference)				
Positive (+++)	2.115 (0.864–5.178)				1.826 (0.754–4.420)				
Ki-67 status		0.003		0.005		0.004			0.010
Negative (≤14%)	1 (reference)		1 (reference)		1 (reference)		1 (reference)		
Positive (> 14%)	1.687 (1.190–2.391)		1.650 (1.167–2.333)		1.662 (1.172–2.356)		1.576 (1.116–2.225)		
CK5/6 status		0.011		0.001		0.017			<0.0001
Negative	1 (reference)		1 (reference)		1 (reference)		1 (reference)		
Positive	1.786 (1.142–2.792)		1.752 (1.265–2.426)		1.769 (1.107–2.825)		1.919 (1.386–2.659)		
E-cad status		0.279				<0.0001			<0.0001
Negative	1 (reference)				1 (reference)		1 (reference)		
Positive	1.212 (0.855–1.719)				2.379 (1.622–3.490)		2.320 (1.709–3.150)		
Lymph vessel invasion		0.040		<0.0001		0.012			0.004
Negative	1 (reference)		1 (reference)		1 (reference)		1 (reference)		
Positive	1.406 (1.016–1.945)		1.636 (1.285–2.083)		1.523 (1.097–2.114)		1.458 (1.131–1.880)		
Postoperative chemotherapy		<0.0001		<0.0001		<0.0001			0.004
No	1 (reference)		1 (reference)		1 (reference)		1 (reference)		

(Continued on following page)

TABLE 3 | (*Continued*) Survival analyses based on univariate and multivariate Cox regression methods for predicting breast cancer patient DFS and OS.

Parameters	DFS				OS				*p* value
	Univariate analysis		Multivariate analysis		Univariate analysis		Multivariate analysis		
	Hazard ratio (95%CI)	*p* value	Hazard ratio (95%CI)	*p* value	Hazard ratio (95%CI)	*p* value	Hazard ratio (95%CI)		
Yes	2.182 (1.489–3.198)		1.636 (1.285–2.083)		2.000 (1.359–2.942)		1.458 (1.131–1.880)		
Postoperative radiotherapy		0.183				0.089			
No	1 (reference)				1 (reference)				
Yes	1.254 (0.898–1.751)				1.348 (0.955–1.901)				
Postoperative endocrine therapy		0.015		0.032		0.080			
No	1 (reference)		1 (reference)		1 (reference)				
Yes	1.544 (1.088–2.190)		1.388 (1.029–1.874)		1.301 (0.969–1.747)				
Postoperative targeted therapy		<0.0001		<0.0001		0.004			<0.0001
No	1 (reference)		1 (reference)		1 (reference)		1 (reference)		
Yes	2.608 (1.799–3.781)		2.105 (1.638–2.706)		1.709 (1.188–2.456)		1.791 (1.397–2.296)		

phosphatase (ALP) (64.00 U/L), γ-glutamyl transpeptidase (GGT) (17.00 U/L), lactate dehydrogenase (LDH) (167.00 U/L), alanine aminotransferase (ALT) (15.00 U/L), and aspartate aminotransferase (AST) (18.00 U/L).

The following are other parameters obtained with their respective median values shown in brackets: CRP (0.20 mg/dl), carbohydrate antigen 125 (CA125) (13.35 U/mL), carbohydrate antigen (CA15-3) (11.63 U/mL), carcinoembryonic antigen (CEA) (1.66 ng/ml), plasma D-dimer (D-D) (0.29 mg/L), fibrinogen (FIB) (2.85 g/L), international standardized ratio of prothrombin time (INR) (0.93), fibrinogen degradation products (FDP) (1.40 μg/mL), and W (6.01×10^9/L), R (4.40×10^{12}/L), Hb (132 g/L), N (3.68×10^9/L), L (1.76×10^9/L), M (0.35×10^9/L), E (0.06×10^9/L), B (0.02×109/L), and P (243×109/L).

1) In all breast cancer patients, the parameters of LDH ($\chi^2 = 4.337$, $p = 0.037$), CRP ($\chi^2 = 17.198$, $p < 0.0001$), CA125 ($\chi^2 = 5.051$, $p = 0.025$), FIB ($\chi^2 = 14.320$, $p < 0.0001$), $p = 0.0002$, INR ($\chi^2 = 4.218$, $p = 0.040$), FDP ($\chi^2 = 4.691$, $p = 0.030$), W ($\chi^2 = 75.436$, $p < 0.0001$), R ($\chi^2 = 7.107$, $p = 0.008$), Hb ($\chi^2 = 7.361$, $p = 0.007$), N ($\chi^2 = 142.491$, $p < 0.0001$), L ($\chi^2 = 7.843$, $p = 0.005$), M ($\chi^2 = 124.109$, $p < 0.0001$), B ($\chi^2 = 9.429$, $p = 0.002$), P ($\chi^2 = 13.231$, $p < 0.0001$), L ($\chi^2 = 7.843$, $p < 0.0001$), $p = 0.0003$ were statistically significant between high and low SIRI groups. The results are shown in **Table 2**.
2) In the NACT group (477 patients), FIB ($\chi^2 = 11.241$, $p = 0.0008$), W ($\chi^2 = 57.819$, $p < 0.0001$), R ($\chi^2 = 5.283$, $p = 0.022$), Hb ($\chi^2 = 4.887$, $p = 0.027$), N ($\chi^2 = 98.716$, $p < 0.0001$), M ($\chi^2 = 100.469$, $p < 0.0001$) and P ($\chi^2 = 8.329$, $p = 0.004$) were statistically significant.
3) In the non-NACT group (308 breast cancer patients), ALB ($\chi^2 = 9.576$, $p = 0.002$), CRP ($\chi^2 = 11.798$, $p = 0.0006$), D-D ($\chi^2 = 5.007$, $p = 0.025$), W ($\chi^2 = 20.949$, $p < 0.0001$), Hb ($\chi^2 = 4.100$, $p = 0.043$), N ($\chi^2 = 42.839$, $p < 0.0001$), L ($\chi^2 = 4.817$, $p = 0.028$), M ($\chi^2 = 26.521$, $p < 0.0001$), E ($\chi^2 = 6.697$, $p = 0.010$) and B ($\chi^2 = 9.248$, $p = 0.002$) were statistically significant.

Survival Analysis Based on Univariate and Multivariate Cox Regression Survival Analyses

Through univariate analysis, we found that menopausal status, GLU, CA125, M, E, SIRI, histological type, pathological N stage, molecular type, Ki-67, CK5/6, lymph vessel invasion (LVI), postoperative targeted therapy, postoperative endocrine therapy, and postoperative chemotherapy were independent factors for improving DFS and OS. After multivariate analysis, we found that menopausal status, blood glucose, CA125, CA153, M, E, SIRI, histological grade, clinical N stage, pathological N and TNM stages, Ki-67, CK5/6, E-cadherin (E-cad), LVI, postoperative chemotherapy, and postoperative targeted therapy were independent factors for improving DFS and OS. **Table 3** depicts all of the above results.

Disease-Free Survival and Overall Survival

SIRI was found to be an independent factor that improved DFS and OS on both univariate and multivariate analyses, and the optimal threshold value for SIRI was 0.80. Univariate analysis demonstrated that low SIRI significantly improved DFS and OS (HR: 1.461, 95% CI: 1.074–1.988, $p = 0.016$ and HR: 1.475, 95% CI: 1.085–2.005, $p = 0.013$). Multivariate analysis showed that a low SIRI significantly improved DFS and OS (HR: 1.970, 95% CI: 1.431–2.712, $p < 0.0001$ and HR: 1.637, 95% CI: 1.269–2.110, $p < 0.0001$). Patients with low SIRI scores had mean survival times of DFS and OS of 41.50 months (3.10–238.00 months) and 64.57 months (6.43–260.00 months), respectively. The average DFS and OS survival time of SIRI in the high group was 37.63 months (3.13–238.00 months) and 58.42 months (10.77–256.40 months), respectively. The log-rank analysis shown that the average DFS and OS survival time of SIRI in the low group were remarkably longer in contrast to that of SIRI in the high group ($\chi^2 = 14.290$, $p = 0.0002$, and $\chi^2 = 20.690$, $p < 0.0001$), as shown in **Figure 1**.

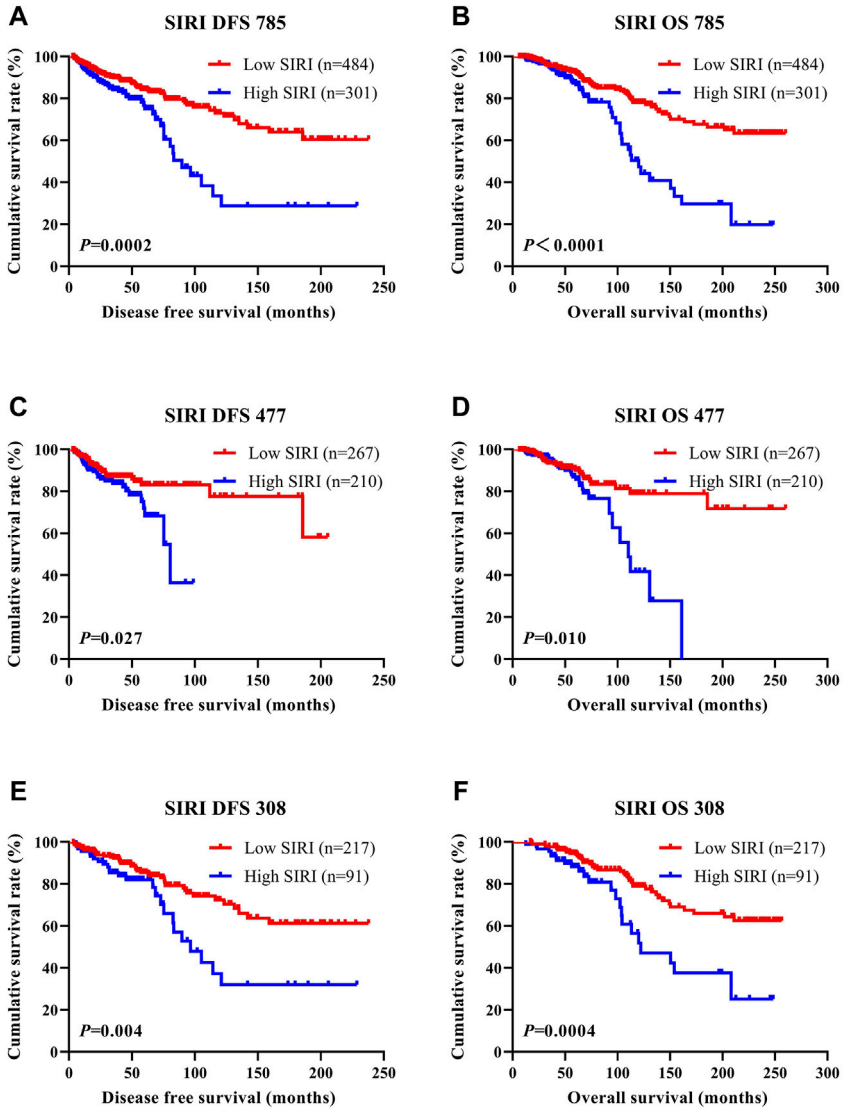

FIGURE 1 | DFS and OS of breast cancer patients. DFS and OS of breast cancer patients. **(A)** Kaplan-Meier analysis of DFS for the SIRI of all patients with breast cancer. **(B)** Kaplan-Meier analysis of OS for the SIRI of all patients with breast cancer. **(C)** Kaplan-Meier analysis of DFS for the SIRI of patients with breast cancer (NACT group). **(D)** Kaplan-Meier analysis of OS for the SIRI of patients with breast cancer (NACT group). **(E)** Kaplan-Meier analysis of DFS for the SIRI of patients with breast cancer (non-NACT group). **(F)** Kaplan-Meier analysis of OS for the SIRI of patients with breast cancer (non-NACT group).

The Association Between SIRI Scores and Tumor Node Metastasis (TNM) Stage

The N stage was an independent predictor of DFS and OS, as revealed by univariate and multivariate analyses. The pathological TNM stage is an independent factor of OS. The ability of SIRI to determine breast cancer prognosis was further assessed by examining the relationship between SIRI and the TNM stage. Early breast cancer was determined to be pathological stages Tis/T0 and I, while advanced breast cancer was pathological stages II and III. Both early and advanced forms of breast cancer were subjected to log-rank analysis to determine their respective DFS and OS.

Early breast cancer patients and low SIRI scores had notably longer DFS and OS in contrast to those high SIRI score patients (χ^2 = 2.379, p = 0.123, and χ^2 = 5.153, p = 0.023), as shown in **Figure 2A** and **Figure 2B**. 2). Similarly, patients with advanced breast cancer and low SIRI scores also had remarkably longer average DFS and OS in contrast to patients with elevated SIRI scores (χ^2 = 11.080, p = 0.0009 and χ^2 = 15.900, p < 0.0001), as shown in **Figure 2C** and **Figure 2D**. The DFS and OS of SIRI and TNM stage of the NACT and non-NACT cohorts are shown in **Figures 2E–L**, respectively.

The Association Between Systemic Inflammatory Response Index Scores and Breast Cancer Molecular Subtype

We found that the molecular subtype of breast cancer was an independent risk factor of DFS based on univariate and

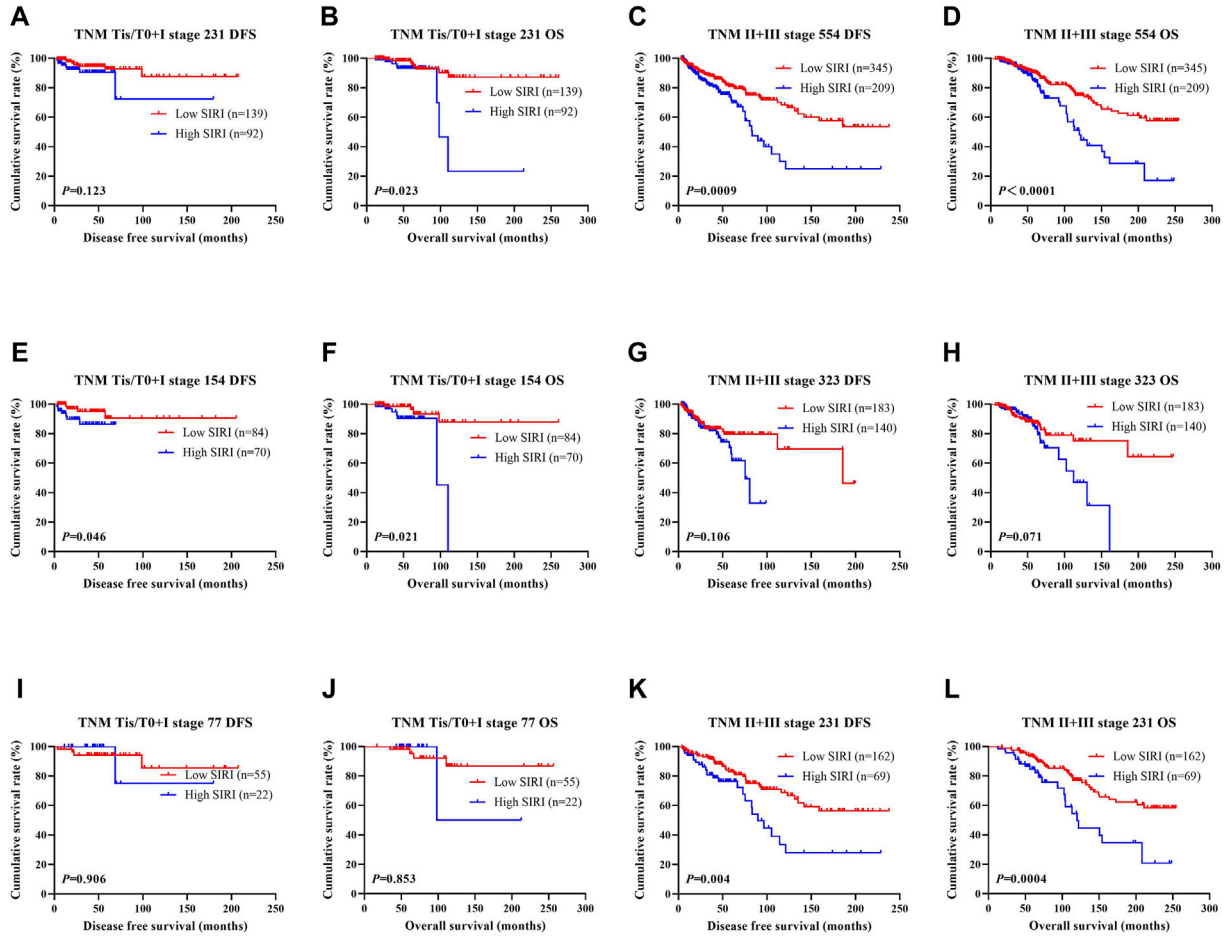

FIGURE 2 | DFS and OS based on SIRI scores of patients with breast cancer of different pathological stage. DFS and OS based on SIRI scores of patients with breast cancer of different pathological stage. **(A)** Kaplan-Meier analysis of DFS for the SIRI of patients with early breast cancer. **(B)** Kaplan-Meier analysis of OS for the SIRI of patients with early breast cancer. **(C)** Kaplan-Meier analysis of DFS for the SIRI of patients with advanced breast cancer. **(D)** Kaplan-Meier analysis of OS for the SIRI of patients with advanced breast cancer. **(E)** Kaplan-Meier analysis of DFS for the SIRI of patients with early breast cancer (NACT group). **(F)** Kaplan-Meier analysis of OS for the SIRI of patients with early breast cancer (NACT group). **(G)** Kaplan-Meier analysis of DFS for the SIRI of patients with advanced breast cancer (NACT group). **(H)** Kaplan-Meier analysis of OS for the SIRI of patients with advanced breast cancer (NACT group). **(I)** Kaplan-Meier analysis of DFS for the SIRI of patients with early breast cancer (non-NACT group). **(J)** Kaplan-Meier analysis of OS for the SIRI of patients with early breast cancer (non-NACT group). **(K)** Kaplan-Meier analysis of DFS for the SIRI of patients with advanced breast cancer (non-NACT group). **(L)** Kaplan-Meier analysis of OS for the SIRI of patients with advanced breast cancer (non-NACT group).

multivariate analyses. Of the 785 patients with breast cancer, 171 cases were triple-negative type, 98 cases were Luminal B HER2-positive type, 325 cases were Luminal B HER2-negative type, 62 cases were Luminal A type, and 129 cases were HER2-overexpressing type. **Table 4** shows the detailed information of the molecular type of breast cancer.

1) In all breast cancer patients, HER2 (χ^2 = 8.077, p = 0.005), E-cad (χ^2 = 21.406, p < 0.0001), epidermal growth factor receptor (EGFR) (χ^2 = 6.339, p = 0.012), topoisomerase (DNA) II alpha (TOP2A) (χ^2 = 5.595, p = 0.018), and LVI (χ^2 = 4.403, p = 0.036). were statistically significant.
2) In the NACT group (477 patients), there were no significant statistically between them.
3) In the non-NACT group (308 breast cancer patients), HER2 (χ^2 = 5.660, p = 0.017), E-cad (χ^2 = 14.686, p = 0.0001), EGFR (χ^2 = 6.983, p = 0.008), TOP2A (χ^2 = 8.526, p = 0.004) and LVI (χ^2 = 11.377, p = 0.007) were statistically significant.

The relationship between SIRI and molecular type of breast cancer was assessed to ascertain the prognostic value of SIRI (shown in **Figure 3**, **Figure 4**, **Figure 5**). The log-rank analysis demonstrated that the average DFS and OS in the low SIRI group was drastically longer in contrast to patients with high SIRI scores.

The Association Between Systemic Inflammatory Response Index Scores and Lymph Vessel Invasion

LVI was found to be an independent factor of DFS and OS based on univariate and multivariate analyses. Of the 785 cases of breast cancer, 227 cases were associated with LVI, and 558 cases were

TABLE 4 | The relationship between SIRI scores and molecular breast cancer subtype.

Parameters	N	SIRI 785				N	SIRI 477				N	SIRI 308			
Cases (n)	**785**	**Low SIRI 484**	**High SIRI 301**	**χ2**	***p* value**		**Low SIRI 267**	**High SIRI 210**	**χ2**	***p* value**		**Low SIRI 217**	**High SIRI 91**	**χ2**	***p* value**
Core needle biopsy (N = 477)															
Molecular subtype									3.520	0.475					
Luminal A						25 (5.24%)	15 (5.62%)	10 (4.76%)							
Luminal B HER2+						67 (14.05%)	31 (11.61%)	36 (17.14%)							
Luminal B HER2-						186 (38.99%)	105 (39.33%)	81 (38.57%)							
HER2 enriched						91 (19.08%)	51 (19.10%)	40 (19.05%)							
Triple negative						108 (22.64%)	65 (24.34%)	43 (20.48%)							
ER status									0.042	0.838					
Negative						191 (40.04%)	108 (40.45%)	83 (39.52%)							
Positive						286 (59.96%)	159 (59.55%)	127 (60.48%)							
ER status									0.929	0.920					
0–25%						228 (47.80%)	129 (48.31%)	99 (47.14%)							
26–50%						42 (8.81%)	26 (9.74%)	16 (7.62%)							
51–75%						33 (6.92%)	18 (6.74%)	15 (7.14%)							
76–100%						174 (36.48%)	94 (35.21%)	80 (38.10%)							
PR status									0.964	0.326					
Negative						189 (39.62%)	111 (41.57%)	78 (37.14%)							
Positive						288 (60.38%)	156 (58.43%)	132 (62.86%)							
PR status									2.467	0.651					
0–25%						286 (59.96%)	165 (61.80%)	121 (57.62%)							
26–50%						67 (14.05%)	35 (13.11%)	32 (15.24%)							
51–75%						45 (9.43%)	21 (7.87%)	24 (11.43%)							
76–100%						79 (16.56%)	46 (17.23%)	33 (15.71%)							
HER2 status									1.743	0.187					
Negative (0--++)						313 (65.62%)	182 (68.16%)	131 (62.38%)							
Positive (+++)						164 (34.38%)	85 (31.84%)	79 (37.62%)							
Ki-67 status									1.455	0.118					
Negative (≤14%)						84 (17.61%)	52 (19.48%)	32 (15.24%)							
Positive (> 14%)															

(Continued on following page)

TABLE 4 | (*Continued*) The relationship between SIRI scores and molecular breast cancer subtype.

Parameters	N	SIRI 785				N	SIRI 477				N	SIRI 308			
Cases (n)	**785**	**Low SIRI 484**	**High SIRI 301**	**χ2**	***p* value**		**Low SIRI 267**	**High SIRI 210**	**χ2**	***p* value**		**Low SIRI 217**	**High SIRI 91**	**χ2**	***p* value**
						393 (82.39%)	215 (80.52%)	178 (84.76%)							
Ki-67 status									1.218	0.875					
0–25%						161 (33.75%)	92 (34.46%)	69 (32.86%)							
26–50%						189 (39.62%)	109 (40.82%)	80 (38.10%)							
51–75%						88 (18.45%)	45 (16.85%)	43 (20.48%)							
76–100%						39 (8.18%)	21 (7.87%)	18 (8.57%)							
Postoperative pathology (IHC)															
Molecular subtype				8.634	0.125				5.449	0.364				12.370	0.030
Luminal A	62 (7.90%)	41 (8.47%)	21 (6.98%)			41 (8.60%)	22 (8.24%)	19 (9.05%)			21 (6.82%)	19 (8.76%)	2 (2.20%)		
Luminal B HER2+	98 (12.48%)	52 (10.74%)	46 (15.28%)			61 (12.79%)	28 (10.49%)	33 (15.71%)			37 (12.01%)	24 (11.06%)	13 (14.29%)		
Luminal B HER2-	325 (41.40%)	211 (43.60%)	114 (37.87%)			166 (34.80%)	96 (35.96%)	70 (33.33%)			159 (51.62%)	115 (53.00%)	44 (48.35%)		
HER2 enriched	129 (16.43%)	70 (14.46%)	59 (19.60%)			96 (20.13%)	53 (19.85%)	43 (20.48%)			33 (10.71%)	17 (7.83%)	16 (17.58%)		
Triple negative	171 (21.78%)	110 (22.73%)	61 (20.27%)			113 (23.69%)	68 (25.47%)	45 (21.43%)			58 (18.83%)	42 (19.35%)	16 (17.58%)		
ER status				0.465	0.495				0.286	0.593				1.884	0.170
Negative	296 (37.71%)	178 (36.78%)	118 (39.20%)			195 (40.88%)	112 (41.95%)	83 (39.52%)			101 (32.79%)	66 (30.41%)	35 (38.46%)		
Positive	489 (62.29%)	306 (63.22%)	183 (60.80%)			282 (59.12%)	155 (58.05%)	127 (60.48%)			207 (67.21%)	151 (69.59%)	56 (61.54%)		
ER status				3.061	0.548				0.530	0.971				6.402	0.171
0–25%	375 (47.77%)	232 (47.93%)	143 (47.51%)			235 (49.27%)	134 (50.19%)	101 (48.10%)			140 (45.45%)	98 (45.16%)	42 (46.15%)		
26–50%	66 (8.41%)	41 (8.47%)	25 (8.31%)			31 (6.50%)	16 (5.99%)	15 (7.14%)			35 (11.36%)	25 (11.52%)	10 (10.99%)		
51–75%	48 (6.11%)	24 (4.96%)	24 (7.97%)			27 (5.66%)	14 (5.24%)	13 (6.19%)			21 (6.82%)	10 (4.61%)	11 (12.09%)		
76–100%	296 (37.71%)	187 (38.64%)	109 (36.21%)			184 (38.57%)	103 (38.58%)	81 (38.57%)			112 (36.36%)	84 (38.71%)	28 (30.77%)		
PR status				1.168	0.280				0.007	0.933				1.720	0.190
Negative	315 (40.13%)	187 (38.64%)	128 (42.52%)			210 (44.03%)	118 (44.19%)	92 (43.81%)			105 (34.09%)	69 (31.80%)	36 (39.56%)		
Positive	470 (59.87%)	297 (61.36%)	173 (57.48%)			267 (55.97%)	149 (55.81%)	118 (56.19%)			203 (65.91%)	148 (68.20%)	55 (60.44%)		
PR status				6.924	0.140				1.764	0.779				2.296	0.682
0–25%	502 (63.95%)	301 (62.19%)	201 (66.78%)			335 (70.23%)	187 (70.04%)	148 (70.48%)			167 (54.22%)	114 (52.53%)	53 (58.24%)		
26–50%	90 (11.46%)	57 (11.78%)	33 (10.96%)			48 (10.06%)	28 (10.49%)	20 (9.52%)			42 (13.64%)	29 (13.36%)	13 (14.29%)		

(Continued on following page)

TABLE 4 | (*Continued*) The relationship between SIRI scores and molecular breast cancer subtype.

Parameters	N	SIRI 785				N	SIRI 477				N	SIRI 308			
Cases (n)	**785**	**Low SIRI 484**	**High SIRI 301**	**χ2**	***p* value**		**Low SIRI 267**	**High SIRI 210**	**χ2**	***p* value**		**Low SIRI 217**	**High SIRI 91**	**χ2**	***p* value**
51–75%	55 (7.01%)	29 (5.99%)	26 (8.64%)			38 (7.97%)	18(6.74%)	20 (9.52%)			17 (5.52%)	11 (5.07%)	6 (6.59%)		
76–100%	138 (17.58%)	97 (20.04%)	41 (13.62%)			56 (11.74%)	34 (12.73%)	22 (10.48%)			82 (26.62%)	63 (29.03%)	19 (20.88%)		
HER2 status				8.077	0.005				1.824	0.177				5.660	0.017
Negative (0--++)	557 (70.96%)	361 (74.59%)	196 (65.12%)			320 (67.09%)	186 (69.66%)	134 (63.81%)			237 (76.95%)	175 (80.65%)	62 (68.13%)		
Positive (+++)	228 (29.04%)	123 (25.41%)	105 (34.88%)			157 (32.91%)	81 (30.34%)	76 (36.19%)			71 (23.05%)	42 (19.35%)	29 (31.87%)		
Ki-67 status				0.423	0.516				0.072	0.788				2.802	0.094
Negative (≤14%)	219 (27.90%)	139 (28.72%)	80 (26.58%)			153 (32.08%)	87 (32.58%)	66 (31.43%)			66 (21.43%)	52 (23.96%)	14 (15.38%)		
Positive (**>** 14%)	566 (72.10%)	345 (71.28%)	221 (73.42%)			324 (67.92%)	180 (67.42%)	144 (68.57%)			242 (78.57%)	165 (76.04%)	77 (84.62%)		
Ki-67 status				5.107	0.277				4.227	0.376				1.436	0.838
0–25%	342 (43.57%)	215 (44.42%)	127 (42.19%)			233 (48.85%)	134 (50.19%)	99 (47.14%)			109 (35.39%)	81 (37.33%)	28 (30.77%)		
26–50%	257 (32.74%)	163 (33.68%)	94 (31.23%)			139 (29.14%)	81 (30.34%)	58 (27.62%)			118 (38.31%)	82 (37.79%)	36 (39.56%)		
51–75%	137 (17.45%)	83 (17.15%)	54 (17.94%)			70 (14.68%)	38 (14.23%)	32 (15.24%)			67 (21.75%)	45 (20.74%)	22 (24.18%)		
76–100%	49 (6.24%)	23 (4.75%)	26 (8.64%)			35 (7.34%)	14 (5.24%)	21 (10.00%)			14 (4.55%)	9 (4.15%)	5 (5.49%)		
AR status				1.209	0.272				0.018	0.892				0.040	0.841
Negative	666 (84.84%)	416 (85.95%)	250 (83.06%)			362 (75.89%)	202 (75.66%)	160 (76.19%)			304 (98.70%)	214 (98.62%)	90 (98.90%)		
Positive	119 (15.16%)	68 (14.05%)	51 (16.94%)			115 (24.11%)	65 (24.34%)	50 (23.81%)			4 (1.30%)	3 (1.38%)	1 (1.10%)		
AR status				1.665	0.797				3.144	0.534				0.021	0.885
0–25%	688 (87.64%)	424 (87.60%)	264 (87.71%)			383 (80.29%)	209 (78.28%)	174 (82.86%)			305 (99.03%)	215 (99.08%)	90 (98.90%)		
26–50%	25 (3.18%)	13 (2.69%)	12 (3.99%)			25 (5.24%)	13 (4.87%)	12 (5.71%)			0 (0.00%)	0 (0.00%)	0 (0.00%)		
51–75%	29 (3.69%)	20 (4.13%)	9 (2.99%)			29 (6.08%)	20 (7.49%)	9 (4.29%)			0 (0.00%)	0 (0.00%)	0 (0.00%)		
76–100%	43 (5.48%)	27 (5.58%)	16 (5.32%)			40 (8.39%)	25 (9.36%)	15 (7.14%)			3 (0.97%)	2 (0.92%)	1 (1.10%)		
CK5/6 status				1.336	0.248				0.940	0.332				0.003	0.954
Negative	684 (87.13%)	427 (88.22%)	257 (85.38%)			406 (85.12%)	231 (86.52%)	175 (83.33%)			278 (90.26%)	196 (90.32%)	82 (90.11%)		
Positive	101 (12.87%)	57 (11.78%)	44 (14.62%)			71 (14.88%)	36 (13.48%)	35 (16.67%)			30 (9.74%)	21 (9.68%)	9 (9.89%)		
E-cad status				21.406	<0.0001				3.593	0.058				14.686	0.0001
Negative	353 (44.97%)	249 (51.45%)	104 (34.55%)			170 (35.64%)	105 (39.33%)	65 (30.95%)			183 (59.42%)	144 (66.36%)	39 (42.86%)		
Positive	432 (55.03%)	235 (48.55%)	197 (65.45%)			307 (64.36%)	162 (60.67%)	145 (69.05%)			125 (40.58%)	73 (33.64%)	52 (57.14%)		
EGFR status				6.339	0.012				0.494	0.482				6.983	0.008
Negative	589 (75.03%)	378 (78.10%)	211 (70.10%)			335 (70.23%)	191 (71.54%)	144 (68.57%)			254 (82.47%)	187 (86.18%)	67 (73.63%)		
Positive			90 (29.90%)				76 (28.46%)	66 (31.43%)				30 (13.82%)			

(Continued on following page)

TABLE 4 | (*Continued*) The relationship between SIRI scores and molecular breast cancer subtype.

Parameters	N	SIRI 785				N	SIRI 477				N	SIRI 308			
Cases (n)	**785**	**Low SIRI 484**	**High SIRI 301**	**χ2**	***p* value**		**Low SIRI 267**	**High SIRI 210**	**χ2**	***p* value**		**Low SIRI 217**	**High SIRI 91**	**χ2**	***p* value**
	196 (24.97%)	106 (21.90%)				142 (29.77%)					54 (17.53%)		24 (26.37%)		
P53 status				0.642	0.423				0.303	0.582				0.528	0.467
Negative	395 (50.32%)	249 (51.45%)	146 (48.50%)			243 (50.94%)	139 (52.06%)	104 (49.52%)			152 (49.35%)	110 (50.69%)	42 (46.15%)		
Positive	390 (49.68%)	235 (48.55%)	155 (51.50%)			234 (49.06%)	128 (47.94%)	106 (50.48%)			156 (50.65%)	107 (49.31%)	49 (53.85%)		
P53 status				1.755	0.781				3.412	0.491				0.082	0.960
0–25%	576 (73.38%)	362 (74.79%)	214 (71.10%)			353 (74.00%)	204 (76.40%)	149 (70.95%)			223 (72.40%)	158 (72.81%)	65 (71.43%)		
26–50%	80 (10.19%)	49 (10.12%)	31 (10.30%)			45 (9.43%)	25 (9.36%)	20 (9.52%)			35 (11.36%)	24 (11.06%)	11 (12.09%)		
51–75%	108 (13.76%)	61 (12.60%)	47 (15.61%)			58 (12.16%)	26 (9.74%)	32 (15.24%)			50 (16.23%)	35 (16.13%)	15 (16.48%)		
76–100%	21 (2.68%)	12 (2.48%)	9 (2.99%)			21 (4.40%)	12 (4.49%)	9 (4.29%)			0 (0.00%)	0 (0.00%)	0 (0.00%)		
TOP2A status				5.595	0.018				0.101	0.750				8.526	0.004
Negative	299 (38.09%)	200 (41.32%)	99 (32.89%)			165 (34.59%)	94 (35.21%)	71 (33.81%)			134 (43.51%)	106 (48.85%)	28 (30.77%)		
Positive	486 (61.91%)	284 (58.68%)	202 (67.11%)			312 (65.41%)	173 (64.79%)	139 (66.19%)			174 (56.49%)	111 (51.15%)	63 (69.23%)		
TOP2A status				4.005	0.405				1.690	0.793				15.817	0.003
0–25%	575 (73.25%)	366 (75.62%)	209 (69.44%)			354 (74.21%)	200 (74.91%)	154 (73.33%)			221 (71.75%)	166 (76.50%)	55 (60.44%)		
26–50%	158 (20.13%)	90 (18.60%)	68 (22.59%)			88 (18.45%)	45 (16.85%)	43 (20.48%)			70 (22.73%)	45 (20.74%)	25 (27.47%)		
51–75%	49 (6.24%)	26 (5.37%)	23 (7.64%)			33 (6.92%)	21 (7.87%)	12 (5.71%)			16 (5.19%)	5 (2.30%)	11 (12.09%)		
76–100%	3 (0.38%)	2 (0.41%)	1 (0.33%)			2 (0.42%)	1 (0.37%)	1 (0.48%)			1 (0.32%)	1 (0.46%)	0 (0.00%)		
Lymph vessel invasion				4.403	0.036				0.048	0.826				11.377	0.001
Negative	558 (71.08%)	357 (73.76%)	201 (66.78%)			320 (67.09%)	178 (66.67%)	142 (67.62%)			238 (77.27%)	179 (82.49%)	59 (64.84%)		
Positive	227 (28.92%)	127 (26.24%)	100 (33.22%)			157 (32.91%)	89 (33.33%)	68 (32.38%)			70 (22.73%)	38 (17.51%)	32 (35.16%)		
Neural invasion				0.0004	0.984				0.470	0.493				0.059	0.808
Negative	670 (85.35%)	413 (85.33%)	257 (85.38%)			384 (80.50%)	212 (79.40%)	172 (81.90%)			286 (92.86%)	201 (92.63%)	85 (93.41%)		
Positive	115 (14.65%)	71 (14.67%)	44 (14.62%)			93 (19.50%)	55 (20.60%)	38 (18.10%)			22 (7.14%)	16 (7.37%)	6 (6.59%)		

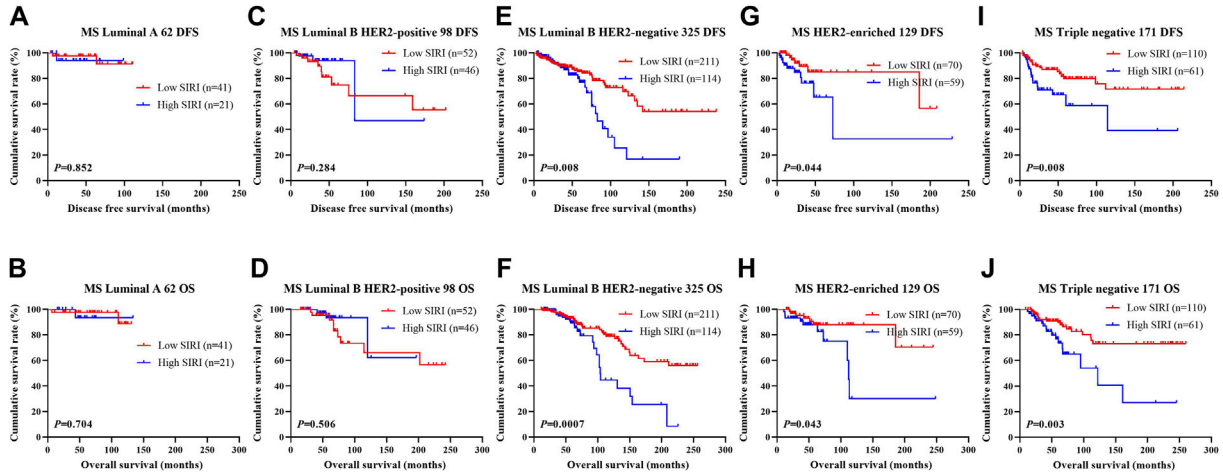

FIGURE 3 | DFS and OS based on SIRI scores in patients with breast cancer of various molecular subtypes. DFS and OS based on SIRI scores in patients with breast cancer of various molecular subtypes. **(A)** Kaplan-Meier analysis of DFS for the SIRI of patients with luminal A breast cancer. **(B)** Kaplan-Meier analysis of OS for the SIRI of patients with luminal A breast cancer. **(C)** Kaplan-Meier analysis of DFS for the SIRI of patients with luminal B HER2-positive breast cancer. **(D)** Kaplan-Meier analysis of OS for the SIRI of patients with luminal B HER2-positive breast cancer. **(E)** Kaplan-Meier analysis of DFS for the SIRI of patients with luminal B HER2-negative breast cancer. **(F)** Kaplan-Meier analysis of OS for the SIRI of patients with luminal B HER2-negative breast cancer. **(G)** Kaplan-Meier analysis of DFS for the SIRI of patients with HER2-enriched breast cancer. **(H)** Kaplan-Meier analysis of OS for the SIRI of patients with HER2-enriched breast cancer. **(I)** Kaplan-Meier analysis of DFS for the SIRI of patients with triple-negative breast cancer. **(J)** Kaplan-Meier analysis of OS for the SIRI of patients with triple-negative breast cancer.

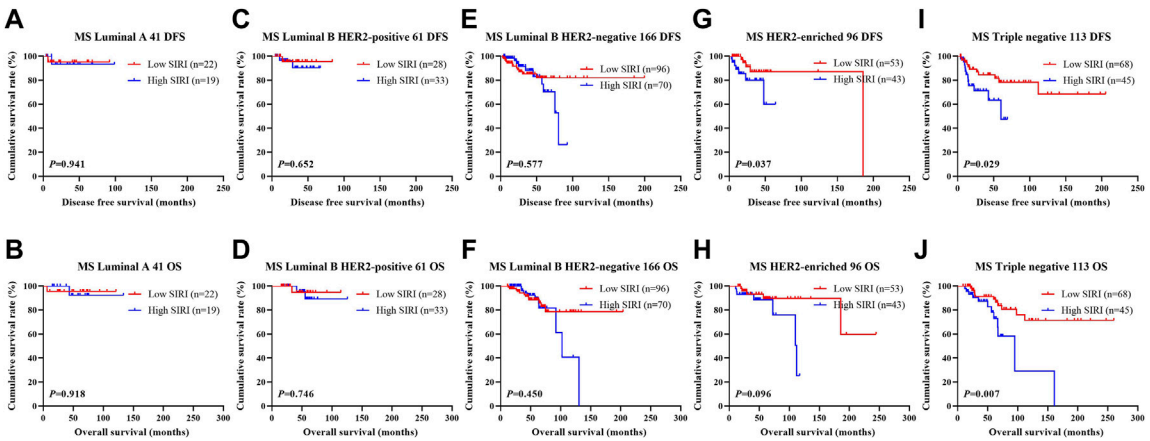

FIGURE 4 | DFS and OS based on SIRI scores in patients with breast cancer of various molecular subtypes (NACT group). DFS and OS based on SIRI scores in patients with breast cancer of various molecular subtypes (NACT group). **(A)** Kaplan-Meier analysis of DFS for the SIRI of patients with luminal A breast cancer. **(B)** Kaplan-Meier analysis of OS for the SIRI of patients with luminal A breast cancer. **(C)** Kaplan-Meier analysis of DFS for the SIRI of patients with luminal B HER2-positive breast cancer. **(D)** Kaplan-Meier analysis of OS for the SIRI of patients with luminal B HER2-positive breast cancer. **(E)** Kaplan-Meier analysis of DFS for the SIRI of patients with luminal B HER2-negative breast cancer. **(F)** Kaplan-Meier analysis of OS for the SIRI of patients with luminal B HER2-negative breast cancer. **(G)** Kaplan-Meier analysis of DFS for the SIRI of patients with HER2-overexpressing breast cancer. **(H)** Kaplan-Meier analysis of OS for the SIRI of patients with HER2-overexpressing breast cancer. **(I)** Kaplan-Meier analysis of DFS for the SIRI of patients with triple-negative breast cancer. **(J)** Kaplan-Meier analysis of OS for the SIRI of patients with triple-negative breast cancer.

not. The relationship between SIRI and LVI was analyzed to determine the prognostic value of SIRI. The average DFS and OS in patients who did not have LVI were 50.96 and 79.65 months, respectively. The average DFS and OS in patients who had LVI were 28.97 and 53.37 months, respectively. Patients without LVI had notably longer mean DFS and OS in comparison to patients who had LVI ($\chi^2 = 20.940$, $p < 0.0001$ and $\chi^2 = 26.540$, $p < 0.0001$), as shown in **Figure 6A** and **Figure 6B**. Among the 558 patients without LVI, patients who had low SIRI scores had mean DFS and OS of 46.40 and 69.37 months, respectively; The average DFS and OS of high SIRI score patients were 30.00 and 54.43 months, respectively. Similarly, low SIRI group patients had notably longer mean DFS and OS in contrast to those with high SIRI scores, as evaluated using log-rank analysis ($\chi^2 = 16.020$, $p < 0.0001$

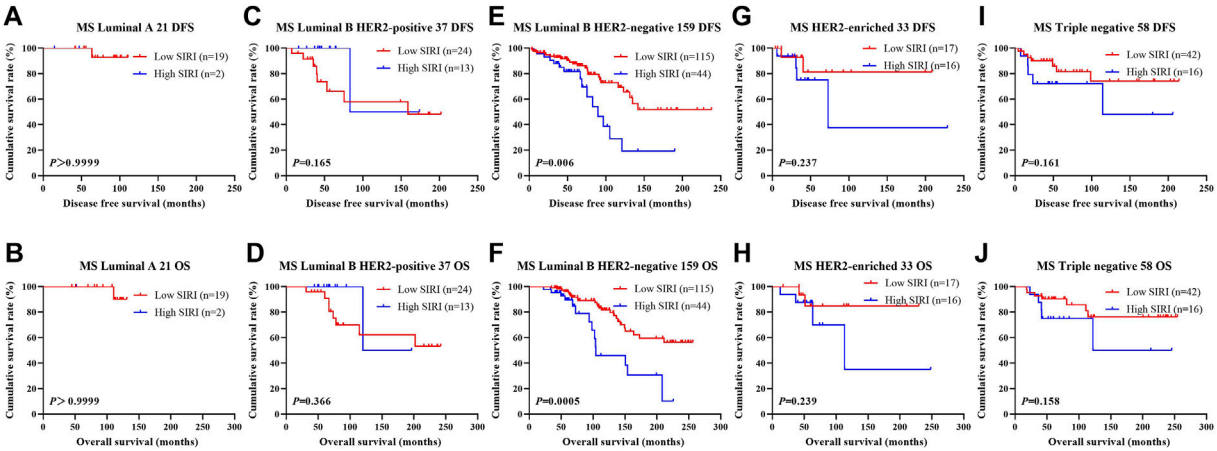

FIGURE 5 | DFS and OS based on SIRI scores in patients with breast cancer of various molecular subtype (Non-NACT group). DFS and OS based on SIRI scores in patients with breast cancer of various molecular subtype (Non-NACT group). **(A)** Kaplan-Meier analysis of DFS for the SIRI of patients with luminal A breast cancer. **(B)** Kaplan-Meier analysis of OS for the SIRI of patients with luminal A breast cancer. **(C)** Kaplan-Meier analysis of DFS for the SIRI of patients with luminal B HER2-positive breast cancer. **(D)** Kaplan-Meier analysis of OS for the SIRI of patients with luminal B HER2-positive breast cancer. **(E)** Kaplan-Meier analysis of DFS for the SIRI of patients with luminal B HER2-negative breast cancer. **(F)** Kaplan-Meier analysis of OS for the SIRI of patients with luminal B HER2-negative breast cancer. **(G)** Kaplan-Meier analysis of DFS for the SIRI of patients with HER2-overexpressing breast cancer. **(H)** Kaplan-Meier analysis of OS for the SIRI of patients with HER2-overexpressing breast cancer. **(I)** Kaplan-Meier analysis of DFS for the SIRI of patients with triple-negative breast cancer. **(J)** Kaplan-Meier analysis of OS for the SIRI of patients with triple-negative breast cancer.

and $\chi^2 = 22.050$, $p < 0.0001$). Among the 227 patients with LVI, the mean DFS and OS were much longer in those with low SIRI scores in contrast to the high SIRI score group ($\chi^2 = 0.257$, $p = 0.612$, and $\chi^2 = 0.705$, $p = 0.401$), as shown in **Figures 6C–F**. The DFS and OS of SIRI and LVI of the NACT and non-NACT cohorts are shown in **Figure 7** and **Figure 8**, respectively.

The Association Between Systemic Inflammatory Response Index Scores and Neoadjuvant Chemotherapy/Postoperative Chemotherapy

In the NACT group, 141 patients underwent TP neoadjuvant chemotherapy, 28 patients received AC/ACF neoadjuvant chemotherapy, 223 patients received AT neoadjuvant chemotherapy, 27 patients received CT/ACT neoadjuvant chemotherapy, and 58 patients received other neoadjuvant chemotherapy regimens. All 477 patients received surgical treatment after neoadjuvant chemotherapy. 247 patients were not treated with postoperative chemotherapy, while 230 patients did. Of the 230 who received postoperative chemotherapy, 39 patients received TP chemotherapy, 37 patients received AT chemotherapy, 30 patients were treated with CT/ACT chemotherapy, 43 patients received AC/ACF chemotherapy, and 81 patients received other chemotherapy regimens. The clinical benefit rate (CR + PR + SD) was 98.53% (470/477), and the clinical objective response rate (CR + PR) was 66.88% (319/477). The MPG grade system was used to evaluate the pathological response of neoadjuvant chemotherapy. There were 22 MPG 1 cases (4.61%), 126 MPG 2 cases (26.42%), 177 MPG 3 cases (37.11%), 62 MPG 4 cases (13.00%), and 90 MPG 5 cases (18.87%). 72 cases (15.09%) achieved pCR, while 405 cases (84.90%) did not. The relationship between SIRI and MPG grade was analyzed to determine the prognostic value of SIRI. Log-rank analysis showed that mean DFS and OS were significantly different among various MPG grades ($\chi^2 = 18.290$, $p < 0.0001$ and $\chi^2 = 18.020$, $p < 0.0001$), as shown in **Figure 9**.

We further scrutinized how SIRI was related to response to neoadjuvant chemotherapy was scrutinized to determine the prognostic value of SIRI. Log-rank analysis demonstrated the average DFS and OS among different response groups were statistically significant ($\chi^2 = 12.540$, $p = 0.006$ and $\chi^2 = 10.820$, $p = 0.013$), as shown in **Figure 10**.

The Association Between Systemic Inflammatory Response Index Scores and Chemotherapy Toxicity and Adverse Effects

Toxicity and adverse effects experienced by patients who received two cycles of NACT were evaluated. In the NACT group, common chemotherapeutic side effects included anorexia, alopecia, oral ulcers, diarrhea, vomiting, nausea, other gastrointestinal reactions, hepatic dysfunction, myelosuppression, thrombocytopenia, neutropenia, leucopenia, anemia, and peripheral neurotoxicity. There were no chemotherapy-related deaths during treatment. The degree of liver dysfunction was statistically different between the two groups ($\chi^2 = 7.146$, $p = 0.028$) (**Table 5**).

DISCUSSION

Breast cancer is a very common female malignancy whose incidence has surpassed that of lung cancer (Siegel et al., 2020). According to the 2020 World Health Organization (WHO) and International Agency for Research on Cancer

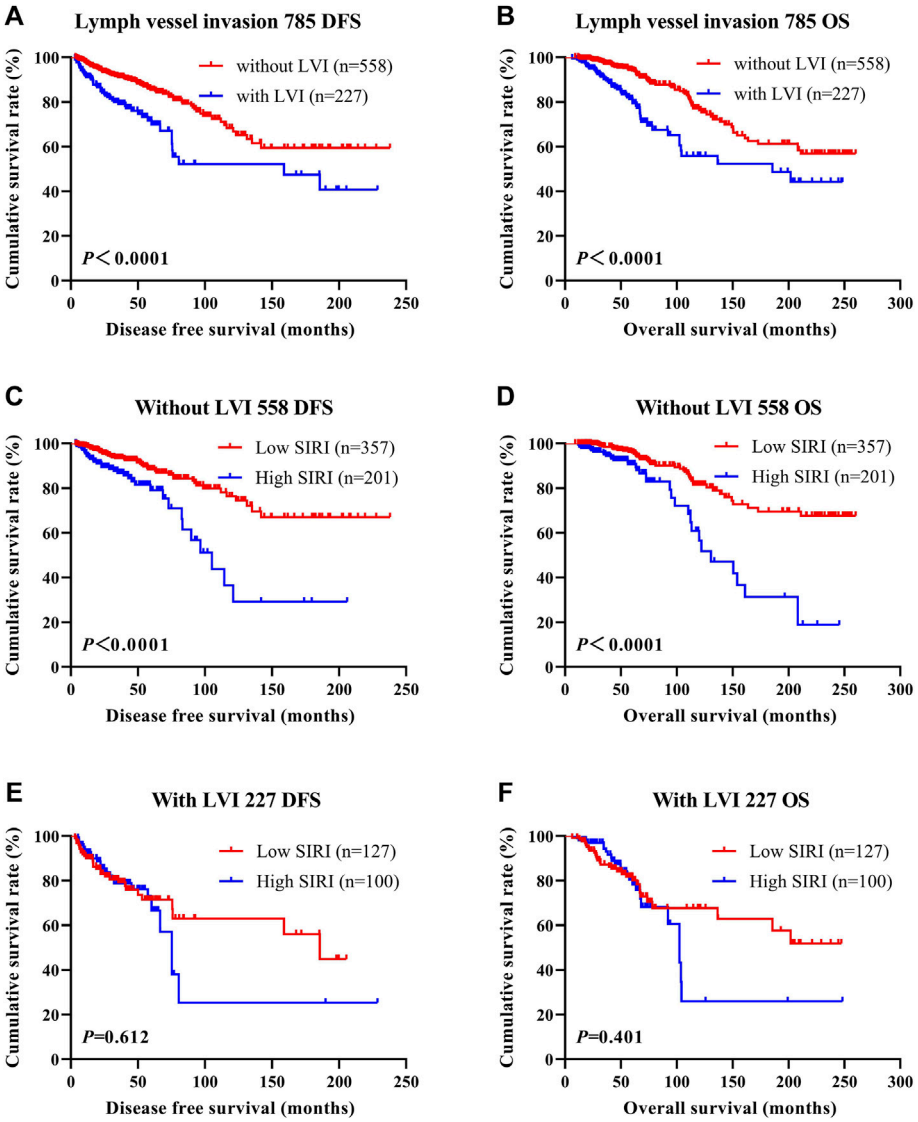

FIGURE 6 | DFS and OS based on the presence of lymph vessel invasion in breast cancer patients. DFS and OS based on the presence of lymph vessel invasion in breast cancer patients. **(A)** Kaplan-Meier analysis of DFS for the SIRI of all patients with breast cancer. **(B)** Kaplan-Meier analysis of OS for the SIRI of all patients with breast cancer. **(C)** Kaplan-Meier analysis of DFS for the SIRI of breast cancer patients without lymph vessel invasion. **(D)** Kaplan-Meier analysis of OS for the SIRI of breast cancer patients without lymph vessel invasion. **(E)** Kaplan-Meier analysis of DFS for the SIRI of breast cancer patients with lymph vessel invasion. **(F)** Kaplan-Meier analysis of OS for the SIRI of breast cancer patients with lymph vessel invasion.

(IARC) research, 19.29 million additional breast cancer cases are diagnosed every year. There are currently 2.26 million breast cancer cases worldwide, exceeding the 2.2 million cases of lung cancer (Siegel et al., 2020). Similar proportions are reported by the China National Cancer Center, which shows that China diagnoses 420,000 new female breast cancer patients every year, with 120,000 women dying from the disease. Patients are being diagnosed at an increasingly younger age, with mortality also increasing every year in spite of the current comprehensive breast cancer management protocols that involve surgery, supplemented by a combination of radiotherapy, chemotherapy, targeted therapy, and endocrine therapy (Tufano et al., 2021). At present, individualized treatment based on tumor characteristics, patient characteristics, and treatment response has emerged as the preferred means of treatment. These methods have greatly reduced patient mortality. Nevertheless, breast cancer is a heterogeneous disease with not all subtypes amenable to current therapies, cementing the position of this disease as the primary instigator of malignancy-associated mortalities in females around the world. NACT is an important part of systemic management of breast cancer, and is effective in reducing tumor size, clinical stage, improve surgical treatment outcomes while having an aesthetic effect (Colomer et al., 2019).

With the development of the field of tumor biology, several investigations have discovered that inflammation is involved in

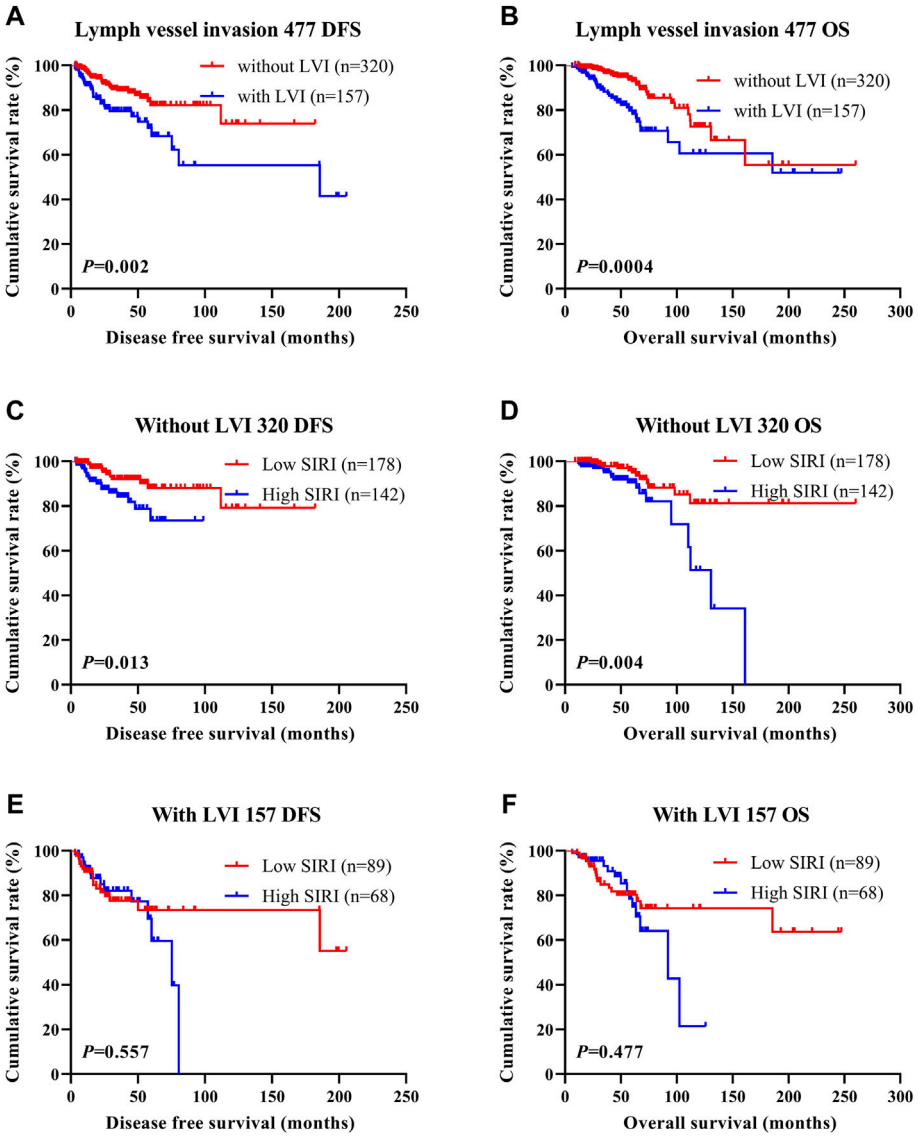

FIGURE 7 | DFS and OS based on the presence of lymph vessel invasion in breast cancer patients (NACT group). DFS and OS based on the presence of lymph vessel invasion in breast cancer patients (NACT group). **(A)** Kaplan-Meier analysis of DFS for the SIRI of all patients with breast cancer. **(B)** Kaplan-Meier analysis of OS for the SIRI of all patients with breast cancer. **(C)** Kaplan-Meier analysis of DFS for the SIRI of breast cancer patients without lymph vessel invasion. **(D)** Kaplan-Meier analysis of OS for the SIRI of breast cancer patients without lymph vessel invasion. **(E)** Kaplan-Meier analysis of DFS for the SIRI of breast cancer patients with lymph vessel invasion. **(F)** Kaplan-Meier analysis of OS for the SIRI of breast cancer patients with lymph vessel invasion.

the initiation, development, and metastasis of tumors. Peripheral platelets, monocytes, lymphocytes, and neutrophils, are associated with the initiation and degree of inflammation (Xie et al., 2018). Many inflammatory markers have been used to predict the occurrence, progression, stage, and prognosis of tumors (Zhu et al., 2018). The reason may be that tumor tissues stimulate the proliferation of inflammatory cells in peripheral blood by secreting a number of pro-inflammatory substances (Li et al., 2018). Studies have confirmed cancer progression and recurrence are more likely to occur when the numbers of inflammatory cells such as neutrophils and monocytes in peripheral blood are relatively increased, and the numbers of immune cells such as lymphocytes and monocytes are relatively decreased (Qi et al., 2021). Inflammation directly brings about changes in the tumor microenvironment that directly promotes and augments malignant cellular transformation, invasion, and metastasis. A number of studies have shown that inflammatory markers in the tumor microenvironment can predict how breast cancer progresses along with its prognosis, with the inflammatory response representing an important marker of breast cancer outcomes. This carries significant implications regarding the role of inflammation in clinical disease assessment and treatment strategy formulation (Chen et al., 2020; Hua et al., 2020). Therefore, it is of great

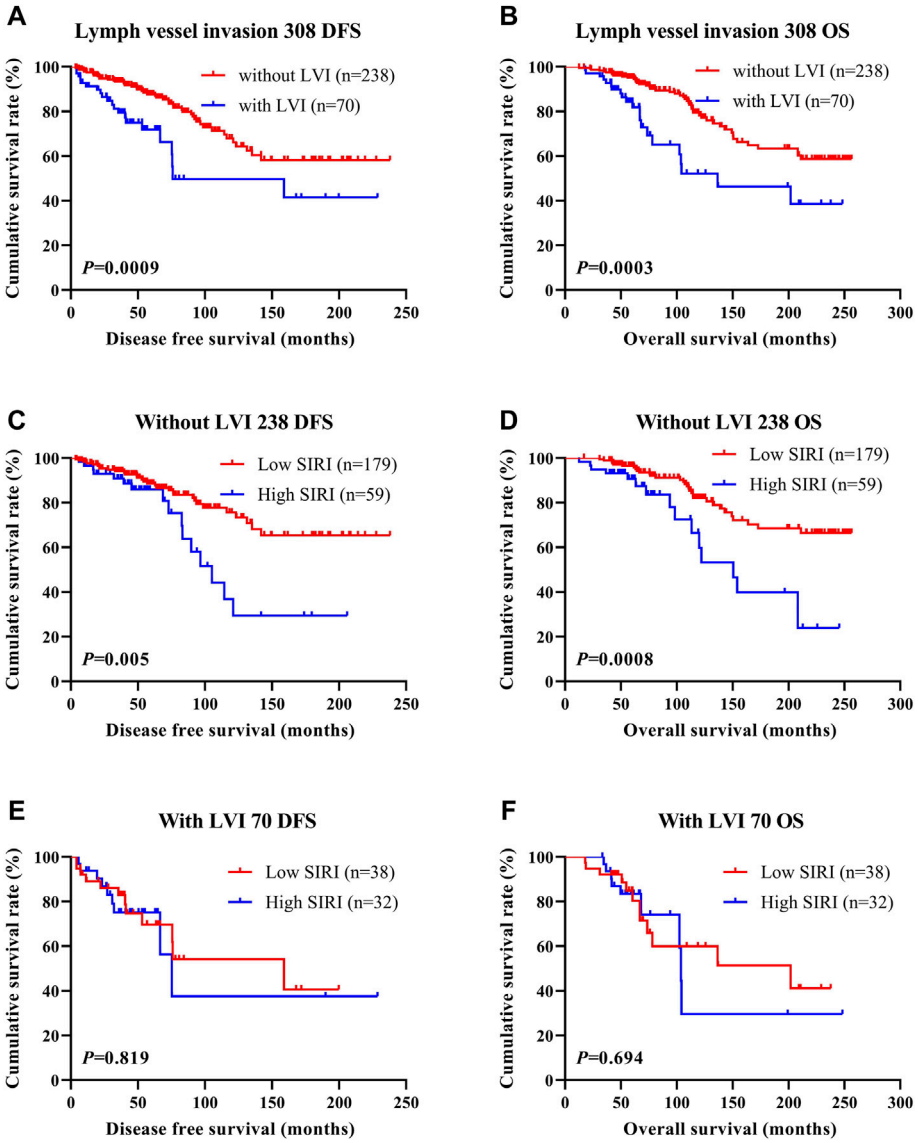

FIGURE 8 | DFS and OS based on the presence of lymph vessel invasion in breast cancer patients (non-NACT group). DFS and OS based on the presence of lymph vessel invasion in breast cancer patients (non-NACT group). **(A)** Kaplan-Meier analysis of DFS for the SIRI of all patients with breast cancer. **(B)** Kaplan-Meier analysis of OS for the SIRI of all patients with breast cancer. **(C)** Kaplan-Meier analysis of DFS for the SIRI of breast cancer patients without lymph vessel invasion. **(D)** Kaplan-Meier analysis of OS for the SIRI of breast cancer patients without lymph vessel invasion. **(E)** Kaplan-Meier analysis of DFS for the SIRI of breast cancer patients with lymph vessel invasion. **(F)** Kaplan-Meier analysis of OS for the SIRI of breast cancer patients with lymph vessel invasion.

research significance to actively dissect the relationship between common peripheral blood markers and breast cancer patient prognosis.

Several cancers have demonstrated evidence of a systemic inflammatory response, although the exact cause of this phenomenon has not been completely reported (Topkan et al., 2020). Various inflammatory cells comprising of lymphocytes, monocytes, and neutrophils correlate to the prognosis of many tumors (Galdiero et al., 2018). Neutrophils augment tumor progression primarily by promoting the production of interleukin-6 (IL-6), arginase-1 (Arginase-1), and vascular endothelial growth factor (VEGF) (Corbeau et al., 2020). Lymphocytes are critical in tumor immune surveillance and are able to inhibit tumor progression and metastasis and directly kill tumor cells by stimulating natural killer cells (NK cells) and macrophages (Morrow et al., 2019). On the other hand, neutrophils inhibit lymphocytes, thereby inhibiting the anti-tumor immune response (Oba et al., 2021). Monocytes can differentiate into TAMs, and tumors secrete chemokines to recruit TAMs in the microenvironment. Some TAMs secrete growth factors and cytokines, promote angiogenesis, and facilitate immune escape, thus accelerating tumor progression (Olingy et al., 2019).

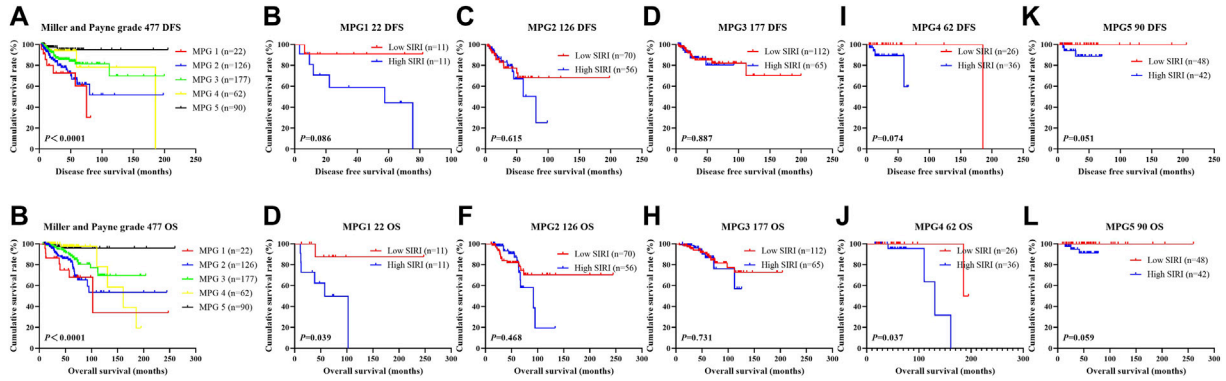

FIGURE 9 | DFS and OS based on Miller and Payne grade (MPG) in breast cancer patients who received NACT. DFS and OS based on Miller and Payne grade (MPG) in breast cancer patients who received NACT. **(A)** Kaplan-Meier analysis of DFS based on MPG for the SIRI of patients with breast cancer. **(B)** Kaplan-Meier analysis of OS based on MPG for the SIRI of patients with breast cancer. **(C)** Kaplan-Meier analysis of DFS based on MPG1 for the SIRI of patients with breast cancer. **(D)** Kaplan-Meier analysis of OS based on MPG1 for the SIRI of patients with breast cancer. **(E)** Kaplan-Meier analysis of DFS for the SIRI of patients with breast cancer (MPG2). **(F)** Kaplan-Meier analysis of OS for the SIRI of patients with breast cancer (MPG2). **(G)** Kaplan-Meier analysis of DFS for the SIRI of patients with breast cancer (MPG3). **(H)** Kaplan-Meier analysis of OS for the SIRI of patients with breast cancer (MPG3). **(I)** Kaplan-Meier analysis of DFS for the SIRI of patients with breast cancer (MPG4). **(J)** Kaplan-Meier analysis of OS for the SIRI of patients with breast cancer (MPG4). **(K)** Kaplan-Meier analysis of DFS for the SIRI of patients with breast cancer (MPG5). **(L)** Kaplan-Meier analysis of OS for the SIRI of patients with breast cancer (MPG5).

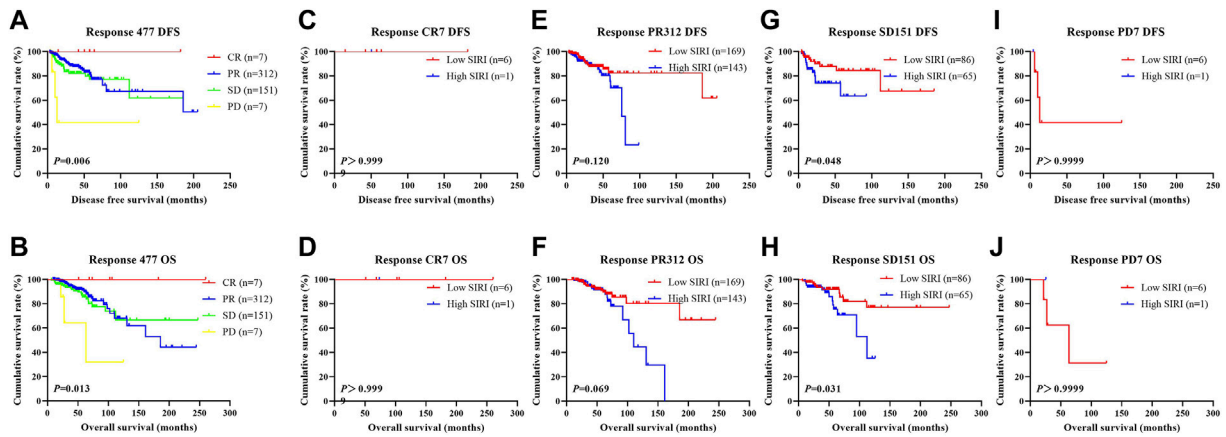

FIGURE 10 | DFS and OS derived from response to neoadjuvant chemotherapy in breast cancer patient who received NACT. DFS and OS derived from response to neoadjuvant chemotherapy in breast cancer patient who received NACT. **(A)** Kaplan-Meier analysis of DFS for the SIRI of patients with breast cancer. **(B)** Kaplan-Meier analysis of OS for the SIRI of patients with breast cancer. **(C)** Kaplan-Meier analysis of DFS for the SIRI of patients with breast cancer. **(D)** Kaplan-Meier analysis of OS for the SIRI of patients with breast cancer. **(E)** Kaplan-Meier analysis of DFS for the SIRI of patients with breast cancer. **(F)** Kaplan-Meier analysis of OS for the SIRI of patients with breast cancer. **(G)** Kaplan-Meier analysis of DFS for the SIRI of patients with breast cancer. **(H)** Kaplan-Meier analysis of OS for the SIRI of patients with breast cancer. **(I)** Kaplan-Meier analysis of DFS for the SIRI of patients with breast cancer. **(J)** Kaplan-Meier analysis of OS for the SIRI of patients with breast cancer.

SIRI is an effective indicator of the immune status of malignant tumors that is established on peripheral venous lymphocyte, monocyte, and neutrophil counts (Wang et al., 2021). Research has revealed SIRI as an independent prognostic factor in several malignancies (Wei et al., 2020; Zhang et al., 2020). Hua et al. (2020) reported that SIRI was prognostic for postmenopausal breast cancer patients who undergo surgery, with patients with higher SIRI scores experiencing worse OS. Wang et al. (2020) used SIRI, histological grading, TNM stage, and a number of other indicators to build models that were able to predict 5-years and 10-years breast cancer survival rates. They found that the changes in SIRI scores 4 weeks after breast cancer surgery were correlated to survival. Breast cancer patients with more varied SIRI scores had worse overall survival (Wang et al., 2020). However, research on SIRI in breast cancer patients who undergo NACT treatment are scarce. Therefore, this study retrospectively studied the impact of SIRI on the survival and prognosis of breast cancer patients undergoing NACT.

This investigation outlines the relationship between SIRI and clinical pathology in breast cancer patients. A low SIRI score significantly influenced clinicopathological characteristics of

TABLE 5 | Correlation between SIRI and toxicity assessment.

Parameters	N	SIRI 477			
Cases (n)		Low SIRI 267	High SIRI 210	$\chi 2$	*p* value
Decreased appetite				1.825	0.177
No	70 (14.68%)	34 (12.73%)	36 (17.14%)		
Yes	407 (85.32%)	233 (87.27%)	174 (82.86%)		
Nausea				1.982	0.159
No	59 (12.37%)	28 (10.49%)	31 (14.76%)		
Yes	418 (87.63%)	239 (89.51%)	179 (85.24%)		
Vomiting				3.391	0.066
No	234 (49.06%)	121 (45.32%)	113 (53.81%)		
Yes	243 (50.94%)	146 (54.68%)	97 (46.19%)		
Diarrhea				0.286	0.593
No	444 (93.08%)	250 (93.63%)	194 (92.38%)		
Yes	33 (6.92%)	17 (6.37%)	16 (7.62%)		
Mouth ulcers				1.398	0.237
No	463 (97.06%)	257 (96.25%)	206 (98.10%)		
Yes	14 (2.94%)	10 (3.75%)	4 (1.90%)		
Alopecia				0.767	0.381
No	222 (46.54%)	129 (48.31%)	93 (44.29%)		
Yes	255 (53.46%)	138 (51.69%)	117 (55.71%)		
Peripheral neurotoxicity				2.559	0.110
No	390 (81.76%)	225 (84.27%)	165 (78.57%)		
Yes	87 (18.24%)	42 (15.73%)	45 (21.43%)		
Anemia				0.526	0.769
Grade 0	257 (53.88%)	144 (53.93%)	113 (53.81%)		
Grade 1–2	215 (45.07%)	121 (45.32%)	94 (44.76%)		
Grade 3–4	5 (1.05%)	2 (0.75%)	3 (1.43%)		
Leukopenia				1.138	0.566
Grade 0	138 (28.93%)	72 (26.97%)	66 (31.43%)		
Grade 1–2	233 (48.85%)	134 (50.19%)	99 (47.14%)		
Grade 3–4	106 (22.22%)	61 (22.85%)	45 (21.43%)		
Neutropenia				1.714	0.425
Grade 0	143 (29.98%)	76 (28.46%)	67 (31.90%)		
Grade 1–2	179 (37.53%)	107 (40.07%)	72(34.29%)		
Grade 3–4	155 (32.49%)	84 (31.46%)	71 (33.81%)		
Thrombocytopenia				0.553	0.758
Grade 0	372 (77.99%)	210 (78.65%)	162 (77.14%)		
Grade 1–2	98 (20.55%)	54 (20.22%)	44 (20.95%)		
Grade 3–4	7 (1.47%)	3 (1.12%)	4 (1.90%)		
Gastrointestinal reaction				1.485	0.476
Grade 0	38 (7.97%)	18 (6.74%)	20 (9.52%)		
Grade 1–2	433 (90.78%)	245 (91.76%)	188 (89.52%)		
Grade 3–4	6 (1.26%)	4 (1.50%)	2 (0.95%)		
Myelosuppression				0.357	0.836
Grade 0	90 (18.87%)	50 (18.73%)	40 (19.05%)		
Grade 1–2	175 (36.69%)	101 (37.83%)	74 (35.24%)		
Grade 3–4	212 (44.44%)	116 (43.45%)	96 (45.71%)		
Hepatic dysfunction				7.146	0.028
Grade 0	371 (77.78%)	196 (73.41%)	175 (83.33%)		
Grade 1–2	105 (22.01%)	70 (26.22%)	35 (16.67%)		
Grade 3–4	1 (0.21%)	1 (0.37%)	0 (0.00%)		

patients, such as clinical data (BMI, US tumor size, US-LNM, clinical N, T, and overall TNM stages, postoperative chemotherapy regimen, operative time, postoperative chemotherapy and the frequency of treatment, postoperative targeted therapy), as well as nutritional and hematological parameters (LDH, CRP, CA125, FIB, INR, FDP, W, R, HB, N, L, M, B, and P). Univariate and multivariate analyses revealed that menopausal status, GLU, CA125, M, E, SIRI, histological grade, pathological N stage, Ki-67, CK5/6, LVI, postoperative chemotherapy, and postoperative targeted therapy were independent predictors of improved DFS and OS. The optimal threshold value for SIRI was 0.80, as determined using a ROC curve. The average DFS and OS survival times of those with low SIRI scores were notably prolonged (achieving statistical significance) compared to those with high SIRI scores.

We also scrutinized the association between SIRI scores and the pathological TNM stage. Data analyses revealed that the average DFS and OS in both early breast cancer and advanced breast cancer were longer in those in the low SIRI group in

contrast to the high SIRI group, especially in advanced breast cancer. Similar findings were also seen in the NACT group, although the variability between the two cohorts was not significant. We also analyzed the relationship between SIRI and breast cancer molecular subtypes. There were differences in DFS and OS between high and low SIRI groups across all the analyzed molecular subtypes. While these differences were statistically significant in the three subtypes of Luminal B HER2-negative, HER2-overexpressed, and triple-negative breast cancer, no statistical significance was gained for the Luminal A type and Luminal B HER2-positive types.

Studies have pointed out that lymphatic vessel density and lymphatic infiltration are related to the prognosis of malignant tumors, with a higher degree of vascular infiltration conferring poorer patient prognosis (Wesch et al., 2014). Yamagata et al. (2021). reiterated that the presence of LVI was a crucial prognosticator in lymph node-positive breast cancer patients (Yamano et al., 2020). Our study also demonstrated that the DFS and OS of breast cancer patients with LVI were lower in contrast to those without LVI. Therefore, this study aimed to establish the association between SIRI and LVI. We found that the mean DFS and OS in breast cancer patients without LVI were longer in those with low SIRI scores compared to those with high SIRI scores. However, there was no significant variability between the two SIRI groups of breast cancer patients with LVI. For patients with LVI who received NACT, there was also no significant variability between in SIRI groups. We further assessed the relationship between SIRI, MPG, and response to chemotherapy. In different MPGs, the average DFS and OS survival times in patients with low SIRI scores were longer in contrast to those with high SIRI scores, although these differences failed to achieve statistical significance. In different responses, the average DFS and OS of the low SIRI group were longer compared to the high SIRI group (statistically significant). At the same time, we also analyzed the relationship between SIRI and the toxic side effects of NACT. Low SIRI scores correlated to improved liver function.

Many studies have described a robust inflammatory response to tumor occurrence and development. Quantifying the inflammatory response appears to be significant in clinical diagnosis as the degree of inflammation dictates the occurrence, progress, and outcomes of diseases. Neutrophils and monocytes both result from macrophage progenitor differentiation and possess similar roles in the inflammatory process. Both release a myriad of inflammatory mediators that includes the tumor necrosis factor, epidermal growth factor, and vascular endothelial growth factor; both promote tumor cell proliferation and blood vessel formation; both can inhibit the activity of T lymphocyte-mediated tumor escape from immune surveillance. Lymphocytes are also critical regulators of the tumor immune response and modulate the ability of tumors to hide from immune detection. The increase in the absolute value of neutrophils and monocytes and the decrease in the absolute value of lymphocytes in peripheral blood is associated with the occurrence, proliferation, and progression of tumors. SIRI takes into consideration peripheral blood neutrophils, lymphocytes, and monocytes to reflect the body's inflammatory response. Therefore, SIRI can be used as a practical clinical indicator of tumor progression and prognosis. We previously noted that SIRI is not widely used as a prognostic indicator in breast cancer patients treated with neoadjuvant chemotherapy. China faces a problem of rising numbers of breast cancer patients. Coupled with the unequal distribution of healthcare resources in the country, the discovery of a commonly used, reproducible, and minimally invasive prognostic parameter that can also guide clinical management would greatly benefit breast cancer patients.

In conclusion, this investigation outlines the relationship between SIRI and breast cancer. Lower SIRI scores appear to confer a better prognosis in breast cancer. Nevertheless, our study is limited due to its small sample size and single-center origin. Future studies would benefit from multicenter patient data collection. The optimal threshold value of SIRI is related to the number of patients included and pathological conditions. Further studies are required to verify the SIRI threshold value of 0.80 that was obtained in this study.

DATA AVAILABILITY STATEMENT

The original contributions presented in the study are included in the article/Supplementary Material, further inquiries can be directed to the corresponding authors.

ETHICS STATEMENT

The studies involving human participants were reviewed and approved by the National Cancer Center/National Clinical Research Center for Cancer/Cancer Hospital, Chinese Academy of Medical Sciences and Peking Union Medical College (reference NCC2018-034). The patients/participants provided their written informed consent to participate in this study.

AUTHOR CONTRIBUTIONS

MZ: Data curation (Equal), Methodology (Equal), and Writing-original draft (Equal). LC: Investigation (Equal), Writing-original draft (Equal), and Writing-review and editing (Equal). XK: Formal analysis (Lead), and Methodology (Lead). XW: Data curation (Lead), and Software (Lead). YF: Funding acquisition (Equal), and Supervision (Equal). XL: Supervision (Equal), and Validation (Equal). JW: Funding acquisition (lead); Project administration (lead).

FUNDING

This work was supported by the Natural Science Foundation of China (No. 81872160), the Natural Science Foundation of China (No. 82072940), the China National Key R&D (or Research and Development) Program (Nos.

2020AAA0105000 and 2020AAA0105004), the Beijing Municipal Natural Science Foundation (Key Project) (No. 7191009), the Beijing Municipal Natural Science Foundation (No. 7204293), the Special Research Fund for Central Universities, Peking Union Medical College (No. 3332019053).

ACKNOWLEDGMENTS

The authors thank the helpful comments of Department of Breast Surgical Oncology, National Cancer Center/National Clinical Research Center for Cancer/Cancer Hospital.

REFERENCES

Al-Hattali, S., Vinnicombe, S. J., Gowdh, N. M., Evans, A., Armstrong, S., Adamson, D., et al. (2019). Breast MRI and Tumour Biology Predict Axillary Lymph Node Response to Neoadjuvant Chemotherapy for Breast Cancer. *Cancer Imaging* 19 (1), 91. doi:10.1186/s40644-019-0279-4

Amat, S., Penault-Llorca, F., Cure, H., Le Bouedec, G., Achard, J.-L., Van Praagh, I., et al. (2002). Scarff-Bloom-Richardson (SBR) Grading: a Pleiotropic Marker of Chemosensitivity in Invasive Ductal Breast Carcinomas Treated by Neoadjuvant Chemotherapy. *Int. J. Oncol.* 20 (4), 791–796. doi:10.3892/ijo.20.4.791

Bray, F., Ferlay, J., Soerjomataram, I., Siegel, R. L., Torre, L. A., and Jemal, A. (2020). Erratum: Global Cancer Statistics 2018: GLOBOCAN Estimates of Incidence and Mortality Worldwide for 36 Cancers in 185 Countries. *CA Cancer J. Clin.* 70 (4), 313. doi:10.3322/caac.21609

Chen, W., Zheng, R., Zheng, R., Zhang, S., Zeng, H., Zuo, T., et al. (2017). Cancer Incidence and Mortality in China in 2013: an Analysis Based on Urbanization Level. *Chin. J. Cancer Res.* 29 (1), 1–10. doi:10.21147/j.issn.1000-9604.2017.01.01

Chen, L., Kong, X., Wang, Z., Wang, X., Fang, Y., and Wang, J. (2020). Pretreatment Systemic Inflammation Response Index in Patients with Breast Cancer Treated with Neoadjuvant Chemotherapy as a Useful Prognostic Indicator. *Cancer Manag. Res.* 12, 1543–1567. doi:10.2147/cmar.s235519

Colomer, R., Saura, C., Sánchez-Rovira, P., Pascual, T., Rubio, I. T., Burgués, O., et al. (2019). Neoadjuvant Management of Early Breast Cancer: A Clinical and Investigational Position Statement. *Oncologist* 24 (5), 603–611. doi:10.1634/theoncologist.2018-0228

Corbeau, I., Jacot, W., and Guiu, S. (2020). Neutrophil to Lymphocyte Ratio as Prognostic and Predictive Factor in Breast Cancer Patients: A Systematic Review. *Cancers (Basel)* 12 (4), 958. doi:10.3390/cancers12040958

Cserni, G., Chmielik, E., Cserni, B., and Tot, T. (2018). The New TNM-Based Staging of Breast Cancer. *Virchows Arch.* 472 (5), 697–703. doi:10.1007/s00428-018-2301-9

Dagmura, H., Daldal, E., and Okan, I. (2021). The Efficacy of Hemoglobin, Albumin, Lymphocytes, and Platelets as a Prognostic Marker for Survival in Octogenarians and Nonagenarians Undergoing Colorectal Cancer Surgery. *Cancer Biother. Radiopharm.* doi:10.1089/cbr.2020.4725

Dan, J., Tan, J., Huang, J., Zhang, X., Guo, Y., Huang, Y., et al. (2020). The Dynamic Change of Neutrophil to Lymphocyte Ratio Is Predictive of Pathological Complete Response after Neoadjuvant Chemotherapy in Breast Cancer Patients. *Breast Cancer* 27 (5), 982–988. doi:10.1007/s12282-020-01096-x

Diakos, C. I., Charles, K. A., McMillan, D. C., and Clarke, S. J. (2014). Cancer-related Inflammation and Treatment Effectiveness. *Lancet Oncol.* 15 (11), E493–E503. doi:10.1016/S1470-2045(14)70263-3

Dong, J., Sun, Q., Pan, Y., Lu, N., Han, X., and Zhou, Q. (2021). Pretreatment Systemic Inflammation Response index Is Predictive of Pathological Complete Response in Patients with Breast Cancer Receiving Neoadjuvant Chemotherapy. *BMC Cancer* 21 (1), 700. doi:10.1186/s12885-021-08458-4

Galdiero, M. R., Marone, G., and Mantovani, A. (2018). Cancer Inflammation and Cytokines. *Cold Spring Harb. Perspect. Biol.* 10 (8), a028662. doi:10.1101/cshperspect.a028662

He, Q., Li, J.-Y., and Ren, Q.-L. (2021a). Efficacy of Neoadjuvant Single or Dual Anti-HER-2 Therapy Combined with Chemotherapy in Patients with HER-2-Positive Breast Cancer: A Single-Center Retrospective Study. *Asian Pac. J. Cancer Prev.* 22 (5), 1467–1475. doi:10.31557/apjcp.2021.22.5.1467

He, Q., Li, L., and Ren, Q. (2021b). The Prognostic Value of Preoperative Systemic Inflammatory Response Index (SIRI) in Patients with High-Grade Glioma and the Establishment of a Nomogram. *Front. Oncol.* 11, 671811. doi:10.3389/fonc.2021.671811

Hua, X., Long, Z. Q., Huang, X., Deng, J. P., Wen, W., He, Z. Y., et al. (2020). The Preoperative Systemic Inflammation Response index (SIRI) Independently Predicts Survival in Postmenopausal Women with Breast Cancer. *Curr. Probl. Cancer* 44 (4), 100560. doi:10.1016/j.currproblcancer.2020.100560

Kaba, H., Fukuda, H., Yamamoto, S., and Ohashi, Y. (2004). Reliability at the National Cancer Institute-Common Toxicity Criteria Version 2.0. *Gan To Kagaku Ryoho* 31 (8), 1187–1192.

Li, B., Wang, Y., Dong, B., Pan, J., Zhu, Y., Sha, J., et al. (2018). Pretreatment Systemic Inflammation Response index as an Independent Prognostic Indicator for Prostate Cancer Patients Treated with Maximal Androgen Blockade. *Chin. J. Urol.* 39 (7), 527–531.

Li, N., Deng, Y., Zhou, L., Tian, T., Yang, S., Wu, Y., et al. (2019). Global burden of Breast Cancer and Attributable Risk Factors in 195 Countries and Territories, from 1990 to 2017: Results from the Global Burden of Disease Study 2017. *J. Hematol. Oncol.* 12 (1), 140. doi:10.1186/s13045-019-0828-0

Liu, Z., Ge, H., Miao, Z., Shao, S., Shi, H., and Dong, C. (2021). Dynamic Changes in the Systemic Inflammation Response Index Predict the Outcome of Resectable Gastric Cancer Patients. *Front. Oncol.* 11, 577043. doi:10.3389/fonc.2021.577043

Mantovani, A., Allavena, P., Sica, A., and Balkwill, F. (2008). Cancer-related Inflammation. *Nature* 454 (7203), 436–444. doi:10.1038/nature07205

Morrow, E. S., Roseweir, A., and Edwards, J. (2019). The Role of Gamma delta T Lymphocytes in Breast Cancer: a Review. *Transl. Res.* 203, 88–96. doi:10.1016/j.trsl.2018.08.005

Oba, T., Maeno, K., Amitani, M., Shimizu, T., Ohno, K., Ono, M., et al. (2021). Prognostic Significance of Neutrophil-To-Lymphocyte Ratio for Long-Term Outcomes in Patients with Poorly Differentiated Thyroid Cancer. *Endocr. J.* 68, 1329. doi:10.1507/endocrj.ej21-0237

Olingy, C. E., Dinh, H. Q., and Hedrick, C. C. (2019). Monocyte Heterogeneity and Functions in Cancer. *J. Leukoc. Biol.* 106 (2), 309–322. doi:10.1002/jlb.4ri0818-311r

Qi, W.-X., Xiang, Y., Zhao, S., and Chen, J. (2021). Assessment of Systematic Inflammatory and Nutritional Indexes in Extensive-Stage Small-Cell Lung Cancer Treated with First-Line Chemotherapy and Atezolizumab. *Cancer Immunol. Immunother.* 70, 3199. doi:10.1007/s00262-021-02926-3

Saroul, N., Puechmaille, M., Lambert, C., Hassan, A. S., Biau, J., Lapeyre, M., et al. (2021). Prognosis in Head and Neck Cancer: Importance of Nutritional and Biological Inflammatory Status. *Otolaryngol. Head Neck Surg.* 166, 118. doi:10.1177/01945998211004592

Siegel, R. L., Miller, K. D., and Jemal, A. (2020). Cancer Statistics, 2020. *CA Cancer J. Clin.* 70 (1), 7–30. doi:10.3322/caac.21590

Singh, N., Baby, D., Rajguru, J., Patil, P., Thakkannavar, S., and Pujari, V. (2019). Inflammation and Cancer. *Ann. Afr. Med.* 18 (3), 121–126. doi:10.4103/aam.aam_56_18

Therasse, P., Arbuck, S. G., Eisenhauer, E. A., Wanders, J., Kaplan, R. S., Rubinstein, L., et al. (2000). New Guidelines to Evaluate the Response to Treatment in Solid Tumors. *J. Natl. Cancer Inst.* 92 (3), 205–216. doi:10.1093/jnci/92.3.205

Topkan, E., Mertsoylu, H., Kucuk, A., Besen, A. A., Sezer, A., Sezen, D., et al. (2020). Low Systemic Inflammation Response Index Predicts Good Prognosis in Locally Advanced Pancreatic Carcinoma Patients Treated with Concurrent Chemoradiotherapy. *Gastroenterol. Res. Pract.* 2020, 5701949. doi:10.1155/2020/5701949

Tufano, A. M., Teplinsky, E., and Landry, C. A. (2021). Updates in Neoadjuvant Therapy for Triple Negative Breast Cancer. *Clin. Breast Cancer* 21 (1), 1–9. doi:10.1016/j.clbc.2020.07.001

Wang, L., Zhou, Y., Xia, S., Lu, L., Dai, T., Li, A., et al. (2020). Prognostic Value of the Systemic Inflammation Response index (SIRI) before and after Surgery in Operable Breast Cancer Patients. *Cancer Biomark* 28 (4), 537–547. doi:10.3233/cbm-201682

Wang, T.-C., An, T.-Z., Li, J.-X., and Pang, P.-F. (2021). Systemic Inflammation Response Index Is a Prognostic Risk Factor in Patients with Hepatocellular Carcinoma Undergoing TACE. *Risk Manag. Healthc. Pol.* 14, 2589–2600. doi:10.2147/rmhp.s316740

Wei, L., Xie, H., and Yan, P. (2020). Prognostic Value of the Systemic Inflammation Response index in Human Malignancy A Meta-Analysis. *Medicine* 99 (50), e23486. doi:10.1097/md.0000000000023486

Weigelt, B., and Reis-Filho, J. S. (2009). Histological and Molecular Types of Breast Cancer: Is There a Unifying Taxonomy? *Nat. Rev. Clin. Oncol.* 6 (12), 718–730. doi:10.1038/nrclinonc.2009.166

Wesch, D., Peters, C., and Siegers, G. M. (2014). Human Gamma delta T Regulatory Cells in Cancer: Fact or Fiction? *Front. Immunol.* 5, 598. doi:10.3389/fimmu.2014.00598

Xie, H., Wei, B., Shen, H., Gao, Y., Wang, L., and Liu, H. (2018). BRAF Mutation in Papillary Thyroid Carcinoma (PTC) and its Association with Clinicopathological Features and Systemic Inflammation Response index (SIRI). *Am. J. Transl. Res.* 10 (8), 2726–2736.

Yamagata, K., Fukuzawa, S., Ishibashi-Kanno, N., Uchida, F., and Bukawa, H. (2021). Association between the C-Reactive Protein/albumin Ratio and Prognosis in Patients with Oral Squamous Cell Carcinoma. *Scientific Rep.* 11 (1), 5446. doi:10.1038/s41598-021-83362-2

Yamano, T., Yamauchi, S., Igeta, M., Takenaka, Y., Song, J., Kimura, K., et al. (2020). Combination of Preoperative Tumour Markers and Lymphovascular Invasion with TNM Staging as a Cost and Labour Efficient Subtyping of Colorectal Cancer. *Sci. Rep.* 10 (1), 10238. doi:10.1038/s41598-020-66652-z

Zhang, Y., Liu, F., and Wang, Y. (2020). Evidence of the Prognostic Value of Pretreatment Systemic Inflammation Response Index in Cancer Patients: A Pooled Analysis of 19 Cohort Studies. *Dis. Markers* 2020, 8854267. doi:10.1155/2020/8854267

Zhu, Z., Xu, L., Zhuang, L., Ning, Z., Zhang, C., Yan, X., et al. (2018). Role of Monocyte-To-Lymphocyte Ratio in Predicting Sorafenib Response in Patients with Advanced Hepatocellular Carcinoma. *Onco. Targets Ther.* 11, 6731–6740. doi:10.2147/ott.s173275

Conflict of Interest: The authors declare that the research was conducted in the absence of any commercial or financial relationships that could be construed as a potential conflict of interest.

Publisher's Note: All claims expressed in this article are solely those of the authors and do not necessarily represent those of their affiliated organizations, or those of the publisher, the editors and the reviewers. Any product that may be evaluated in this article, or claim that may be made by its manufacturer, is not guaranteed or endorsed by the publisher.

frontiers in Molecular Biosciences

ORIGINAL RESEARCH
published: 01 March 2022
doi: 10.3389/fmolb.2022.849771

Application Potential of *CTHRC1* as a Diagnostic and Prognostic Indicator for Colon Adenocarcinoma

Chen Pang[1], *Hongwei Wang*[1], *Chengcheng Shen*[2]* *and Houjie Liang*[1]*

[1]*Department of Oncology and Southwest Cancer Centre, Southwest Hospital, Third Military Medical University (Army Medical University), Chongqing, China,* [2]*Department of Dermatology, The First Affiliated Hospital of Chongqing Medical University, Chongqing, China*

Colon adenocarcinoma (COAD), ranking third in incidence and second in mortality, is one of the most common cancer types in the world. The initial stages of COAD usually show no obvious clinical symptoms; moreover, effective screening or diagnostic indicators with high sensitivity and specificity are lacking, which often leads to missed treatment opportunities. Collagen triple helix repeat containing 1 (*CTHRC1*) is a glycosylated protein secreted during tissue repair, which reduces collagen matrix deposition and promotes cell migration. Under physiological conditions, the expression of *CTHRC1* is conducive to wound healing; however, the pathological overexpression of *CTHRC1* promotes tumour growth and proliferation. In this study, we evaluated the application potential of *CTHRC1* as an early diagnosis and prognostic survival monitoring biomarker for COAD in addition to unravelling its molecular mechanism in the development of COAD and exploring new therapeutic targets. Therefore, various tumour databases were used to investigate the expression of *CTHRC1* in COAD at the mRNA and protein levels. *CTHRC1* expression was found to be significantly increased in COAD, regardless of clinical cancer stage, age, sex or race. Moreover, *CTHRC1* expression was significantly correlated with poor prognosis and positively correlated with $CD8^+$ T cell, $CD4^+$ T cell, neutrophil, macrophage and dendritic cell infiltration. The relevant function pathways and neighbouring proteins to *CTHRC1* in COAD were identified as ROR2, VAPA, LY6E and several collagen family proteins. Therefore, this study suggests that *CTHRC1* is a potential diagnostic and prognostic biomarker for patients with COAD.

Keywords: collagen triple helix repeat containing 1 (CTHRC1), colon adenocarcinoma (COAD), diagnosis, prognosis, immune infiltration, function pathway

OPEN ACCESS

Edited by:
Na Luo,
Nankai University, China

Reviewed by:
Fei Peng,
Dalian Medical University, China
Xiawei Wei,
Sichuan University, China

***Correspondence:**
Chengcheng Shen
shencc2020@163.com
Houjie Liang
lianghoujie@sina.com

Specialty section:
This article was submitted to Molecular Diagnostics and Therapeutics, a section of the journal Frontiers in Molecular Biosciences

Received: *06 January 2022*
Accepted: *04 February 2022*
Published: *01 March 2022*

Citation:
Pang C, Wang H, Shen C and Liang H (2022) Application Potential of CTHRC1 as a Diagnostic and Prognostic Indicator for Colon Adenocarcinoma. Front. Mol. Biosci. 9:849771. doi: 10.3389/fmolb.2022.849771

INTRODUCTION

A recent study by the American Cancer Society reported that colorectal cancer has the third highest (10.0%) incidence rate after female breast cancer (11.7%) and lung cancer (11.4%) (Sung et al., 2021). The incidence rate of colorectal cancer in developed countries is approximately four times higher than that in developing countries (Fidler et al., 2016). Based on the current prediction models, the global incidence of colorectal cancer has been estimated to reach approximately 2.2 million new cases/year by 2030, accounting for 20% of all patients with cancer (Araghi et al., 2018). Colorectal carcinoma has the second-highest death rate of 9.4% after lung cancer. The official statistics on the prognosis of patients with colorectal cancer published by the American Cancer Society report that

the 5 year survival rate is approximately 64% (Sung et al., 2021). Specifically, early diagnosis or detection of colorectal cancer at stage I, stage IIA or IIB increases the 5 years survival rate to approximately 90%; however, delayed diagnosis decreases the survival rate of patients with pathological stage IV tumour to approximately 14% (Pilonis et al., 2020). Although the current screening of colorectal cancer has been strengthened, resulting in a slight decrease in late diagnosis case numbers, up to 90% of cases are diagnosed after symptoms appear (Vanessa and Karen, 2016).

The occurrence of colorectal cancer is attributed to complex genetic and environmental factor interactions, involving multiple genes at different stages. The main pathways include the chromosomal instability pathway, CpG island methylator phenotype pathway, microsatellite instability pathway and the serrated pathway (Harrison and Benziger, 2011). Colon adenocarcinoma (COAD) is the main manifestation of colorectal cancer, with more than 80% of colorectal cancers being diagnosed as COAD (Li and Gu, 2005). The initial stage of COAD usually shows no obvious clinical symptoms, and the lack of effective screening or highly sensitive and specific diagnostic indicators often lead to missed treatment opportunities (Garborg et al., 2013). Therefore, it is crucial to establish an effective screening mechanism to improve the early diagnosis rate.

Collagen triple helix repeat containing 1 (CTHRC1) protein was first identified in the injured arteries of rats as an extracellular secretory protein, which is expressed in the injured part and smooth muscle cells of neointima, mainly promoting the growth and proliferation of newly generated cells (Leclair and Lindner, 2007). CTHRC1 regulates the occurrence and development of cervical, pancreatic and liver carcinoma by participating in cell proliferation, cell migration, type I collagen synthesis and damaged vascular repair (Tameda et al., 2014). Studies have shown that promoting CTHRC1 expression increased the migration and invasion of primary gastrointestinal stromal tumour cells, whereas silencing CTHRC1 expression inhibited the epithelial–mesenchymal transformation of glioblastoma cells (Ma et al., 2014). CTHRC1 promotes the proliferation of colorectal cancer by activating the Wnt/PCP signalling pathway (Yang et al., 2015). Additionally, CTHRC1 plays an important role in the pathogenesis of systemic lupus erythematosus and other diseases (Wu et al., 2018).

This study, therefore, aimed to evaluate the application potential of CTHRC1 as an early diagnosis and prognostic survival monitoring biomarker for COAD. Additionally, the molecular mechanism of COAD occurrence and development along with various novel therapeutic targets were explored. Therefore, the expression of CTHRC1 in COAD at the mRNA and protein levels was investigated using various tumour databases. By evaluating the expression of CTHRC1 in patients with COAD under different physiological and pathological conditions, the application potential of CTHRC1 as a diagnostic indicator was determined. Moreover, the effects of different expression levels and genetic mutations of *CTHRC1* on COAD survival rate was analysed, including the immune infiltration of CTHRC1 in COAD. Further, the associated proteins and pathways of CTHRC1 in tumorigenesis are also discussed.

MATERIALS AND METHODS

Oncomine Analysis

The Oncomine platform (https://www.oncomine.org/) is a publicly accessible, online tumour-related gene microarray database that collects disease-related gene expression profiles and relevant clinical information. The expression level of *CTHRC1* in different cancers was investigated *via* Oncomine. When compared to corresponding normal tissues, the transcriptional levels were considered statistically significant at fold change >1.5 and p-value < 0.001. The threshold value of gene rank was set to "top 10%", and the data type was set to "mRNA" (Rhodes et al., 2004).

TIMER 2.0 Analysis

TIMER 2.0 (http://timer.comp-genomics.org/) was employed to investigate the expression levels of *CTHRC1* in various tumour tissues. Additionally, data of 32 tumour types from more than 10,000 samples were collected from the TCGA database and used for immune infiltration analysis via TIMER 2.0, which ascertains the abundance of tumour infiltrates based on gene expression levels. *CTHRC1* was chosen as the input and tumour cells were detected under the Immune Association module. B cells, $CD8^+$ T cells, $CD4^+$ T cells, neutrophils, macrophages and dendritic cells were selected as the test types based on the study by Li et al. and Danaher et al. (Li et al., 2016; Danaher et al., 2017). Gene expression values were converted to Log2 RNA-Seq by Expectation-Maximization values.

Human Protein Atlas Analysis

The Human Protein Atlas (https://www.proteinatlas.org) is an online dataset that collects the expression characteristics of various functional proteins *via* immunohistochemistry from tumours and corresponding normal tissues (Asplund et al., 2012). The Human Protein Atlas was used to compare the expression of CTHRC1 proteins in normal and COAD tissues using the images of immunohistochemical staining.

UALCAN Analysis

UALCAN (http://ualcan.path.uab.edu) is an open-access web platform that contains cancer-related clinical data, which can be obtained from the TCGA database. This was used to compare the *CTHRC1* expression levels between the COAD and normal tissues, along with the relationship between gene expression and pathologic features in these tissues (Chandrashekar et al., 2017). In the website, TCGA was chosen, and the corresponding tumour type was selected. The student's t-test was used to compare the transcription levels of *CTHRC1* between the tissue types, and $p < 0.05$ was considered statistically significant.

GEPIA Analysis

GEPIA (http://gepia.cancer-pku.cn/index.html) was used to analyse the relationship between *CTHRC1* expression and

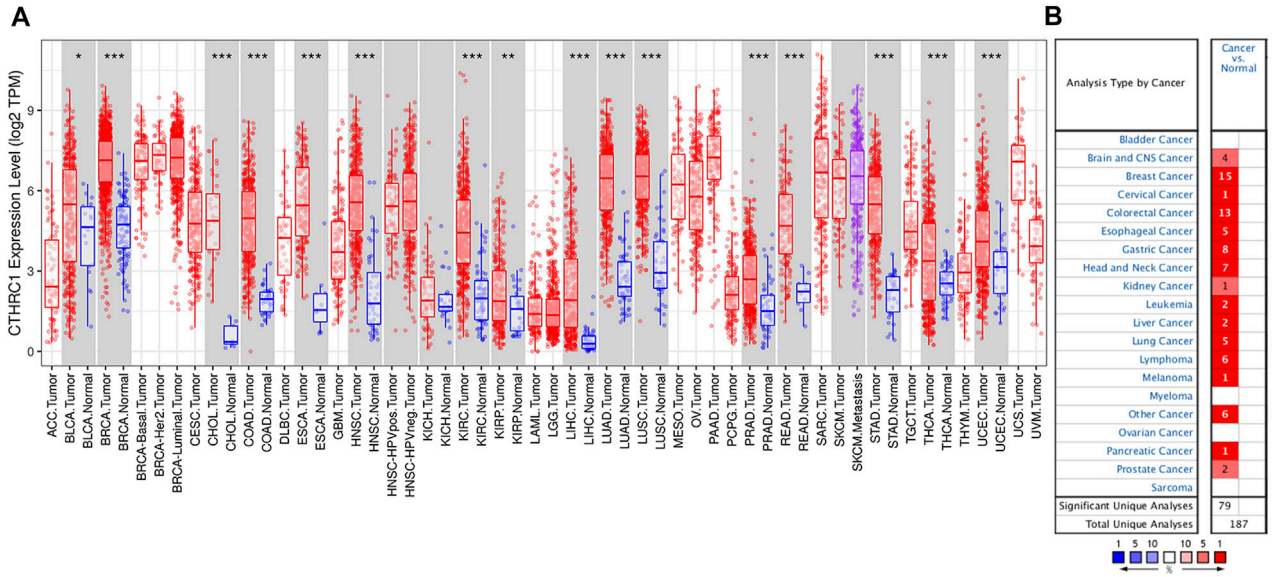

FIGURE 1 | Expression levels of CTHRC1 in different types of tumour tissues. **(A)** *CTHRC1* expression in various tumour tissues *via* TIMER analysis. **(B)** *CTHRC1* expression in different cancer types *via* Oncomine analysis (*$p < 0.05$; **$p < 0.01$; ***$p < 0.001$).

overall survival (OS) or disease-free survival (DFS) prognosis in patients with COAD based on the parameters of hazard ratios and log-rank *p*-values. After logging onto the database, Single Gene Analysis was firstly chosen. After entering *CTHRC1*, "survival plots" was selected. Survival analysis was performed using the following parameters: Group Cut-off: Median; Hazards Ratio: Yes; 95% Confidence Interval: Yes (Tang et al., 2017).

cBioPortal Analysis

cBioPortal (http://www.cbioportal.org/) was used to analyse the alteration frequency of *CTHRC1* gene mutations. Putative copy-number calls on 478 cases were determined using GISTIC 2.0. In the module Comparison/Survival, the influence of the alterations on prognostic survival in patients with COAD was analysed using default parameters (Gao et al., 2013).

Functional Analysis

GeneMANIA was used to identify the physical interaction and co-expression of CTHRC1 with 20 related proteins using the *Homo sapiens* datasets with default parameters (Mostafavi et al., 2008). GO enrichment and KEGG pathway analyses (FDR cutoff <0.05) of related gene were conducted using ShinyGO v0.741 (http://bioinformatics.sdstate.edu/go/).

RESULTS

Expression of *CTHRC1* in COAD

RNA-seq data extracted from TCGA database showed a consistent trend of abnormally high *CTHRC1* expression in more than 16 types of tumour tissues compared with the corresponding normal tissues, such as COAD, breast invasive carcinoma and stomach adenocarcinoma (**Figure 1A**). Similarly, Oncomine analysis of the pathological samples showed that the transcriptional levels of *CTHRC1* mRNA were significantly up-regulated in various cancer types including colorectal cancer (**Figure 1B**). Further comparison of the expression levels of CTHRC1 protein between the normal and COAD tissue using immunohistochemical data from the Human Protein Atlas dataset showed that CTHRC1 protein expression in COAD was consistent with the mRNA detected (**Figure 2**). These findings strongly suggest the positive role of *CTHRC1* in COAD tumorigenesis.

Expression of *CTHRC1* in Patients With COAD Under Different Physiological or Pathological States

UALCAN analysis showed that the expression level of *CTHRC1* was significantly higher in the patients with primary COAD than that in normal tissues (**Figure 3A**). Notably, this abnormally high expression pattern is generally applicable to patients with different clinicopathological characteristics, such as clinical cancer stage, age, sex or race. However, no significant difference in expression level was observed among patients diagnosed with different states, apart from the high expression in patients aged 21–40 years (**Figures 3B–F**). Importantly, *CTHRC1* showed a strong abnormal expression in patients with early stage COAD, *i.e.*, *CTHRC1* has shown significant high expression in stage I COAD, which substantiates the potential role of *CTHRC1* as an early diagnostic biomarker for COAD.

Prognostic Value of *CTHRC1* Expression in Patients With COAD

The GEPIA dataset was employed to assess the prognostic value of *CTHRC1* expression in patients with COAD. *CTHRC1* proves to be

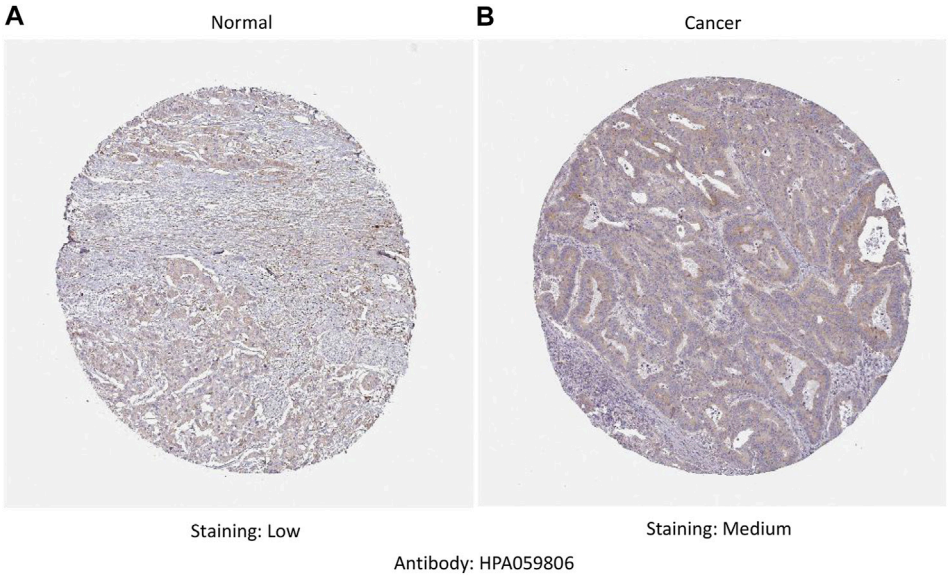

FIGURE 2 | Analysis of CTHRC1 protein expression in colon adenocarcinoma tissue collected from the Human Protein Atlas dataset. **(A)** The control (normal) tissue with low staining; **(B)** The colon adenocarcinoma tissue with medium staining. Primary antibody: HPA059806.

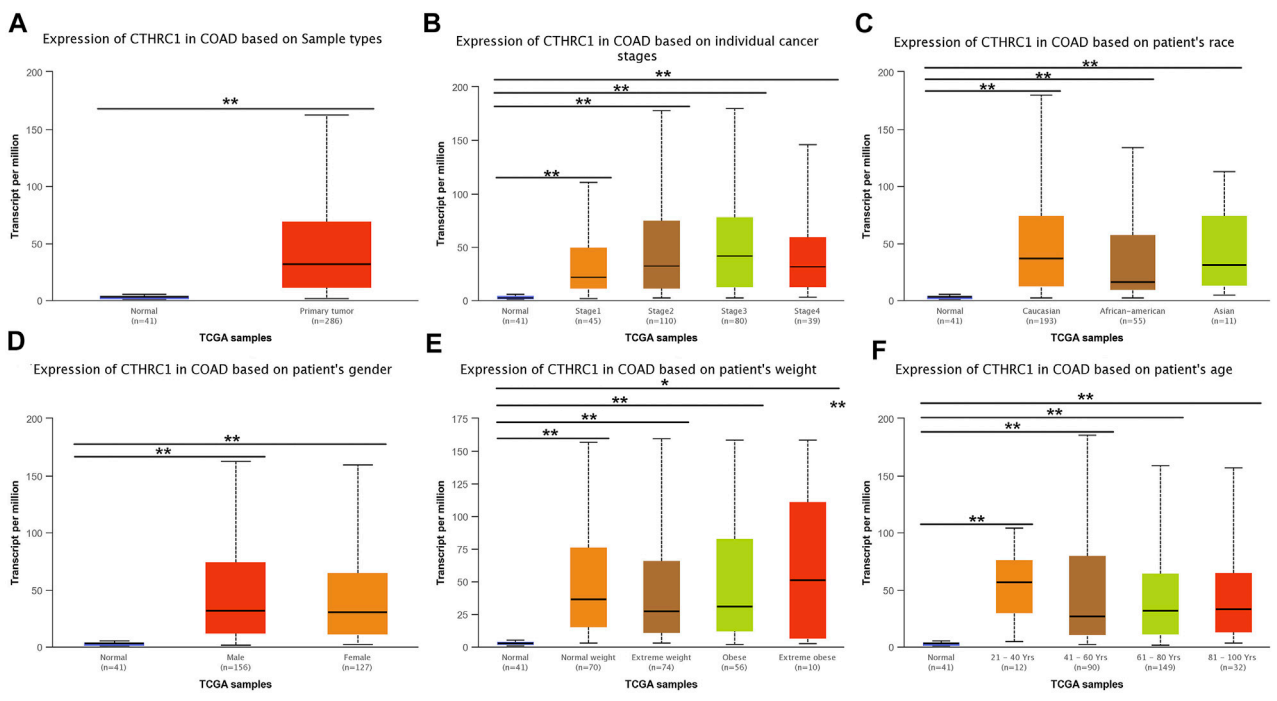

FIGURE 3 | Analysis of *CTHRC1* expression in patients with colon adenocarcinoma (COAD) under different physiological or pathological states using UALCAN. **(A–F)** *CTHRC1* expression in COAD patients of various physiological and pathological states (* denotes $0.01 < p < 0.05$, ** denotes $p < 0.01$).

a promising prognostic indicator due to the high expression level of *CTHRC1*, which indicates poor OS and DFS prognosis with a same high hazard ratio of 1.8 (**Figure 4**). Investigation of the alteration frequency of *CTHRC1* using the TCGA database revealed approximately 7.1% gene alteration in 634 colorectal cancer cases (**Figure 5A,B**). However, these mutations did not significantly affect the OS and DFS of patients (**Figure 5C,D**), indicating that *CTHRC1* has considerable stability as a prognostic indicator.

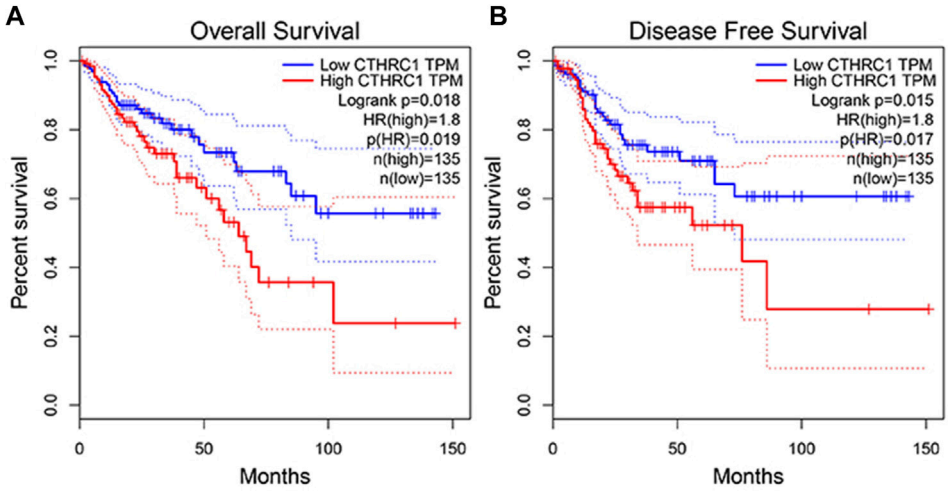

FIGURE 4 | Correlation analysis between CTHRC1 expression and prognostic survival in patients with colon adenocarcinoma (COAD) using GEPIA. **(A)** Correlation analysis between *CTHRC1* expression and overall survival in patients with COAD; **(B)** Correlation analysis between *CTHRC1* expression and disease free survival in patients with COAD.

Correlation Analysis Between *CTHRC1* Expression and Immune Cell Infiltration in COAD Tissue

TIMER 2.0 was used to analyse the correlation between *CTHRC1* expression and immune cell infiltration levels, including B cells, $CD8^+$ T cells, $CD4^+$ T cells, neutrophils, macrophages and dendritic cells. *CTHRC1* expression was significantly positively correlated with all the test immune cells except B cells (p = 0.0644). Among them, macrophages had the strongest correlation with *CTHRC1*, with a high partial correlation coefficient of 0.608 and a p-value of $3.36e^{-42}$ (**Figure 6**). To clarify the immune response mechanism induced by *CTHRC1* and develop new immunotherapeutic targets, the expression correlation between *CTHRC1* and immune cell subsets was investigated. *CTHRC1* was significantly correlated with most of the corresponding biomarker genes of the test immune cell subsets (**Supplementary Table S1**).

Co-Expression and Interaction Analysis of *CTHRC1* in COAD Tissue

CTHRC1 was co-expressed with *ROR2*, *VAPA*, *LY6E* and several collagen family proteins via GeneMANIA analysis (**Figure 7**). These associated molecules are mainly involved in collagen fibril, extracellular matrix/structure and external encapsulating structure organisations of biological processes; the collagen type I trimer, fibrillar collagen trimer and banded collagen fibril of cellular component construction; the platelet-derived growth factor binding, FFAT motif binding, extracellular matrix structural constituent conferring tensile strength and Wnt-protein binding of molecular function. Moreover, KEGG analysis using ShinyGO showed that *CTHRC1* and its related proteins were predominantly enriched in the signalling pathways of AGE-RAGE, Relaxin and Pl3K-Akt; the pathological processes of small cell lung cancer, amoebiasis and human papillomavirus infection; and the physiological functions of protein digestion and absorption, ECM-receptor interaction, focal adhesion and platelet activation (**Figure 8**).

DISCUSSION

Biomarkers are key tools for early diagnosis, prediction of survival and prognosis, and evaluation of treatment responses. Effective biomarkers benefit clinical decision-making and improve the patient's survival rate and life quality (Ogunwobi et al., 2020). With the development of omics technology, many potential indicator genes have been screened for various diseases, such as adenomatous polyposis, transforming growth factor β and several tumour suppressors, which are widely used in the auxiliary diagnosis of tumorigenesis (Fodde et al., 2001; Gyorffy et al., 2013; Seoane and Gomis, 2017). However, the clinical application of these indicator genes is limited due to the lack of sufficient systematic research.

CTHRC1 is a glycosylated protein secreted during tissue repair, which functions by reducing the collagen matrix deposition, thereby promoting cell migration. The expression of *CTHRC1* under physiological conditions promotes wound healing; however, the pathological overexpression of *CTHRC1* promotes tumour cell growth and invasion (Cheng et al., 2019). Studies have shown that *CTHRC1* promotes colorectal cancer metastasis by inducing the Wnt/PCP signal transduction (Yang et al., 2015). In hepatocellular carcinoma, supressing *CTHRC1* expression can inhibit integrin β, and thereby inhibiting cell migration and invasion and inducing apoptosis (Zhou et al., 2019). Additionally, *CTHRC1* promotes the invasion of human epithelial ovarian cancer cells by activating the epidermal growth factor receptor signalling pathway (Ye et al., 2016). In short, the tumour promoting mechanism of *CTHRC1* involves multiple targets.

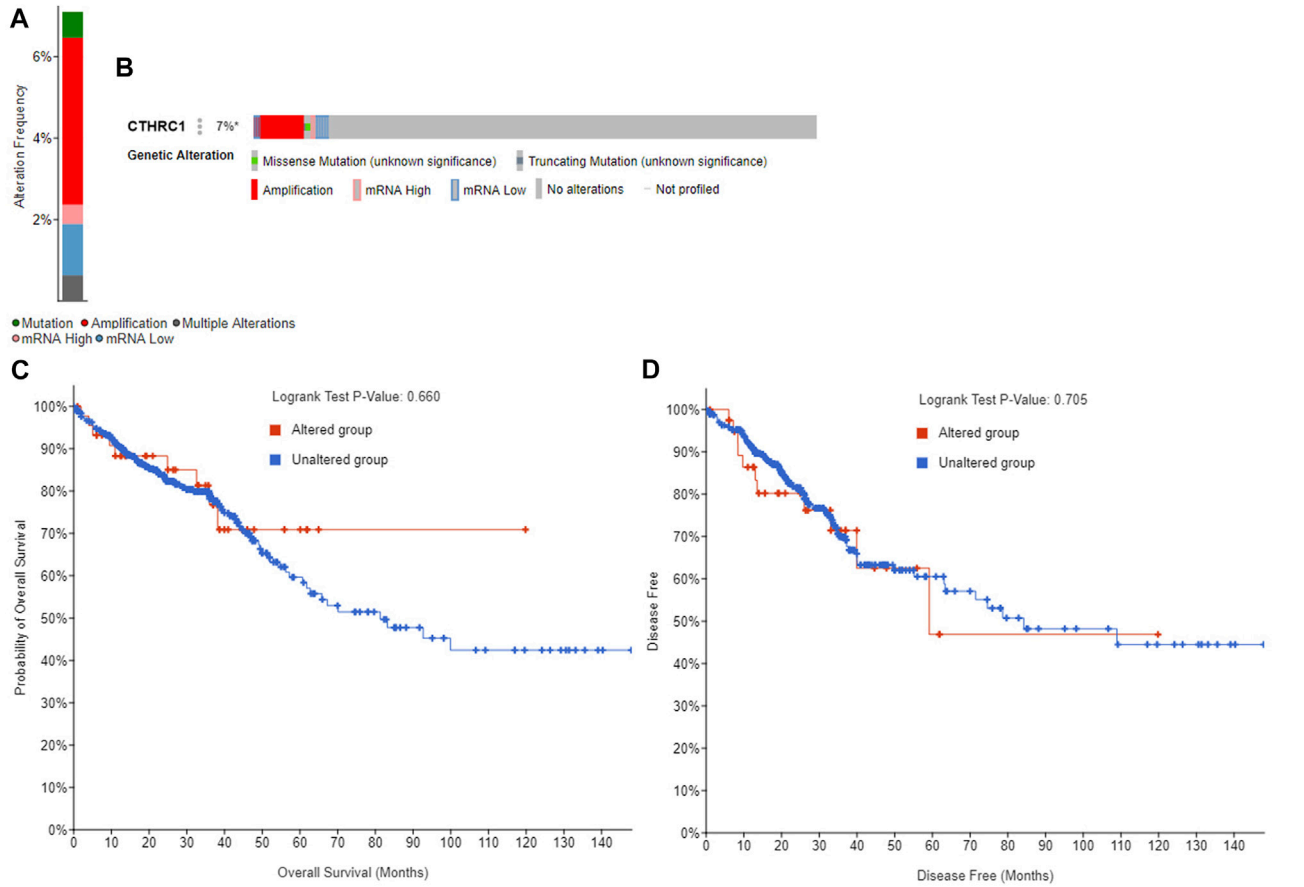

FIGURE 5 | Alteration frequency analysis of *CTHRC1* and its influence on prognosis in patients with colorectal cancer using cBioPortal. **(A)** Alteration frequency of *CTHRC1* in patients with colorectal cancer. **(B)** Effect of *CTHRC1* alteration on the overall survival of COAD patients. **(C)** Effect of *CTHRC1* alteration on the disease free survival of COAD patients. **(D)** Effect of *CTHRC1* alteration on the disease free survival of COAD patients.

The occurrence and development of COAD have the common characteristics of tumorigenesis. It promotes the massive proliferation of cells by avoiding growth inhibitory factors and apoptosis-related genes and the production of tumour blood vessels to induce tumour development. Tumorigenesis mechanisms are also attributed to unstable gene expression, tumour microenvironment change, genetic diversity and inflammatory factor activation (Goubran et al., 2014). To understand the mechanism of *CTHRC1* in COAD and evaluate its potential as a diagnostic and prognostic indicator in patients with COAD, various online public databases were used to systematically investigate *CTHRC1* expression profiles in COAD tissue, its impact on patient survival and immunity, and its related functional pathways and associated proteins. The consistently high expression of *CTHRC1* in patients with COAD under different physiological and pathological states reflects its stability as a diagnostic indicator. Moreover, *CTHRC1* was highly expressed in at least 16 tumour types (Tang et al., 2006), which broadened the application of *CTHRC1* in early disease detection. Tumours usually have the characteristics of high metastasis tendency. Hence, patients aged 21–40 years and/or with Stage I COAD are more likely to obtain satisfying treatment responses; however, they are not easily diagnosed at the early stages. Notably, *CTHRC1* was obviously highly-expressed in these patients, which further highlights its value as an indicator gene. Further analysis of the prognostic value revealed that the characteristics of the high hazard ratio of *CTHRC1* expression and significant differences in prognostic survival indicate the superiority of *CTHRC1* as a prognostic biomarker, even the high mutation frequency would not offset its indicating effect on prognosis. Therefore, these data emphasise the high value of *CTHRC1* as a diagnostic and prognostic indicator for patients with COAD.

During tumorigenesis, due to the intervention of non-coding RNA, such as microRNA, the expression level of mRNA may be inconsistent with that of the associated protein (Macfarlane and Murphy, 2010). Taking this into account, the gene and protein levels were detected separately, revealing that in transcriptional and translational level, *CTHRC1* was both highly expressed in COAD tissues. Since the time-consuming, laborious and expensive method of protein level detection, the follow-up investigation is mainly based on the analysis of mRNA level, which ensures the effectiveness and improves the convenience of *CTHRC1* for future clinical research and application.

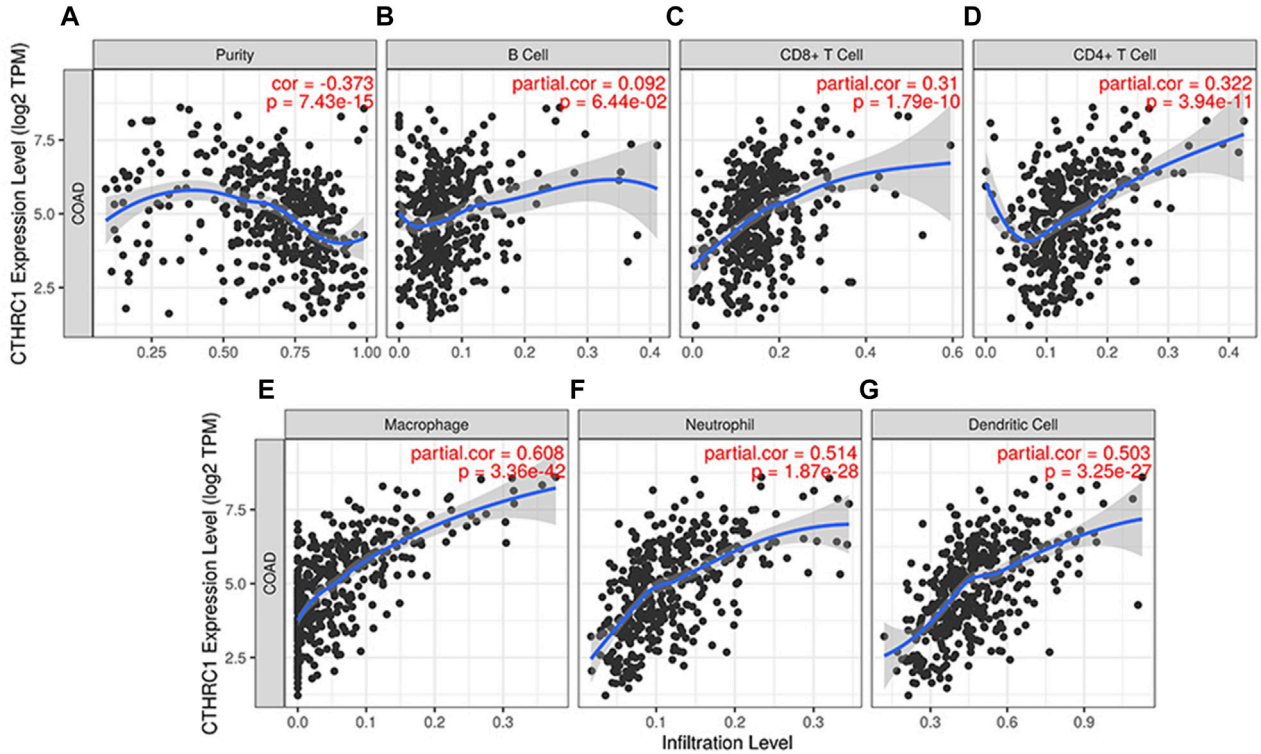

FIGURE 6 | Correlation between *CTHRC1* expression and immune cell infiltration levels in colon adenocarcinoma tissue analysed via TIMER 2.0. **(A–G)** The correlation between *CTHRC1* expression and immune cell infiltration in COAD patients (*n* = 458).

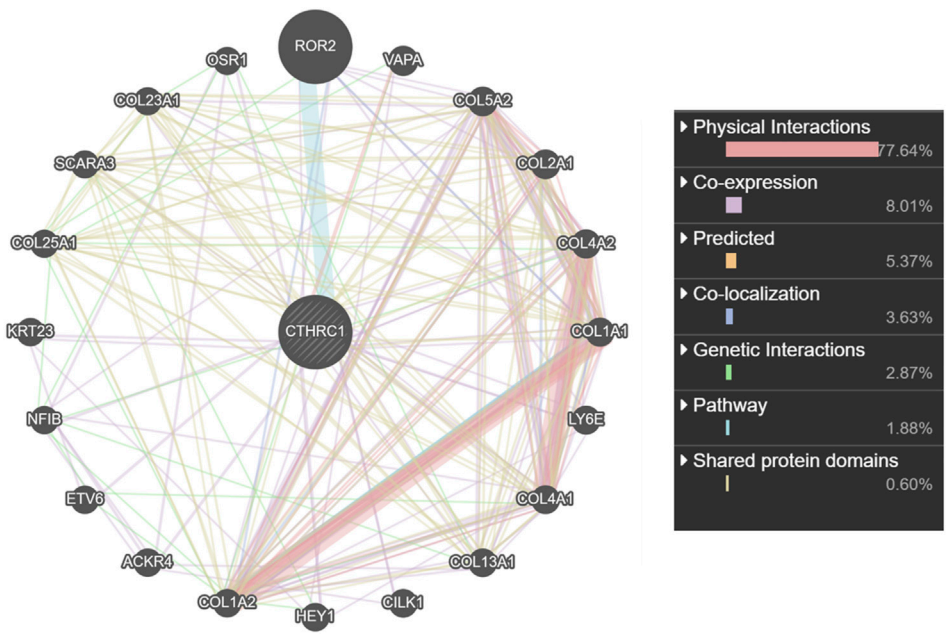

FIGURE 7 | Interaction network analysis of CTHRC1 and its most similar proteins using GeneMANIA.

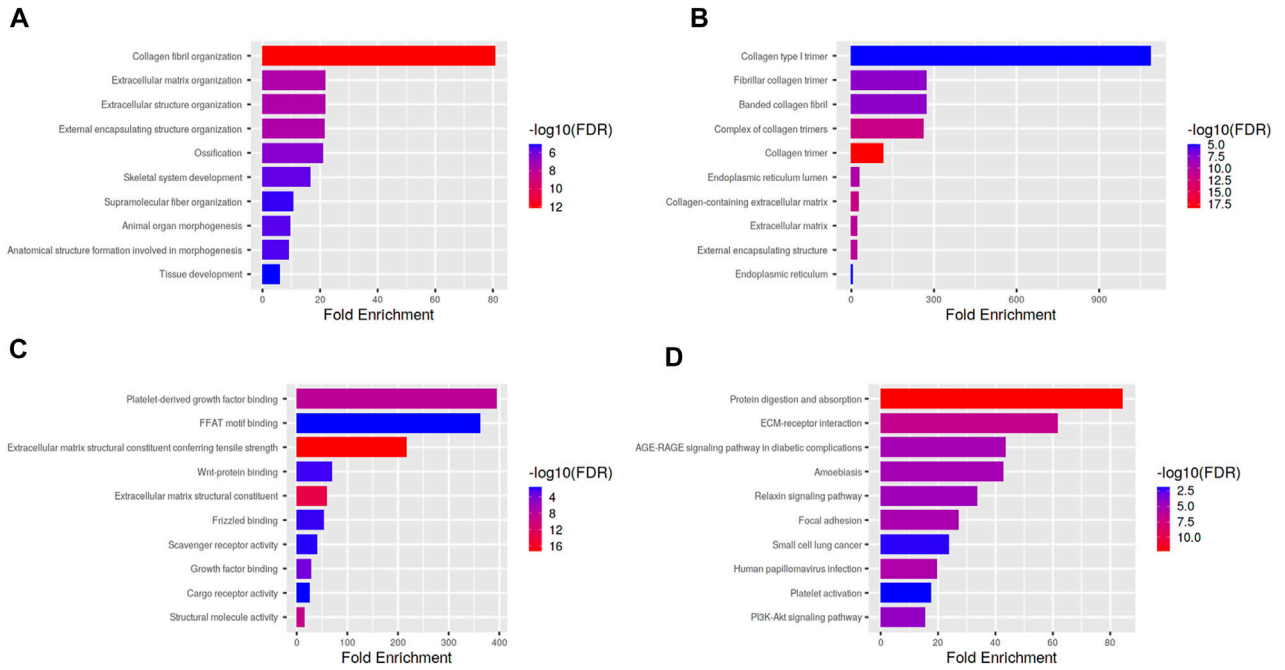

FIGURE 8 | Enrichment analysis of the Kyoto Encyclopedia of Genes and Genomes functional pathways of CTHRC1 and their related proteins using ShinyGO. **(A)** GO enrichment analysis of CTHRC1 in biological process of COAD. **(B)** GO enrichment analysis of CTHRC1 in cellular components of COAD. **(C)** GO enrichment analysis of CTHRC1 in molecular function of COAD. **(D)** KEGG pathway enrichment analysis of CTHRC1 in COAD.

The response mechanism of the immune system in tumorigenesis has always been a popular research topic. The fluctuation of the tumour microenvironment is strongly related to the progress and treatment of the tumour. Understanding the tumour microenvironment provides an insight into tumour diagnosis, therapeutic targets and prognostic biomarkers (Goubran et al., 2014). The correlation analysis between *CTHRC1* level and B cell infiltration showed no significant correlation, which suggests that COAD avoided the immune effect of B cells. However, this observation needs further verification by deeper and profound studies. *CTHRC1* showed a close correlation (>0.5) with the infiltration levels of macrophages, neutrophils, dendritic cells and immune cell biomarker genes, which could be used as early screening targets for immunotherapy.

Through the enrichment analyses of GO and KEGG, the mechanism of *CTHRC1* in biological processes, not only its cellular components and molecular function were defined, but also the specific regulatory pathways (such as AGE-RAGE, Relaxin and Pl3K signalling pathways) and action targets (including protein digestion and absorption, ECM-receptor interaction, focal adhesion and platelet activation) were identified, most of which are classical regulatory models that promote tumorigenesis or are involved in tumour development (Feng et al., 2009; Bao et al., 2019; Waghela et al., 2021). Therefore, unravelling the tumour promoting mechanism of *CTHRC1*could narrow the scope of further research and drug screening.

The promoting effect of *CTHRC1* on tumour metastasis and proliferation could be considered a contributing factor to its abnormal high expression in various cancers including COAD. After systematic analysis, this study recommends *CTHRC1* as a biomarker gene for the early diagnosis and prognostic monitoring of COAD. This study aims to provide a base for future research, regarding the molecular mechanism and therapeutics development for COAD. However, verification of the clinical applications is still lacking although this study uses many databases for comprehensive analyses and comparison.

DATA AVAILABILITY STATEMENT

The original contributions presented in the study are included in the article/**Supplementary Material**, further inquiries can be directed to the corresponding authors.

AUTHOR CONTRIBUTIONS

HL and CP designed the research; CP, CS, and HW analyzed the data; CP wrote the manuscript. All authors read and approved the manuscript.

SUPPLEMENTARY MATERIAL

The Supplementary Material for this article can be found online at: https://www.frontiersin.org/articles/10.3389/fmolb.2022.849771/full#supplementary-material

REFERENCES

Araghi, M., Soerjomataram, I., Jenkins, M., Brierley, J., Morris, E., Bray, F., et al. (2018). Global Trends in Colorectal Cancer Mortality: Projections to the Year 2035. *Int. J. Cancer* 144 (12), 2992–3000. doi:10.1002/ijc.32055

Asplund, A., Edqvist, P.-H. D., Schwenk, J. M., and Pontén, F. (2012). Antibodies for Profiling the Human Proteome-The Human Protein Atlas as a Resource for Cancer Research. *Proteomics* 12, 2067–2077. doi:10.1002/pmic.201100504

Bao, Y., Wang, L., Shi, L., Yun, F., Liu, X., Chen, Y., et al. (2019). Transcriptome Profiling Revealed Multiple Genes and ECM-Receptor Interaction Pathways that May Be Associated with Breast Cancer. *Cell Mol Biol Lett* 24, 38. doi:10.1186/s11658-019-0162-0

Chandrashekar, D. S., Bashel, B., Balasubramanya, S. A. H., Creighton, C. J., Ponce-Rodriguez, I., Chakravarthi, B. V. S. K., et al. (2017). UALCAN: a portal for Facilitating Tumor Subgroup Gene Expression and Survival Analyses. *Neoplasia* 19, 649–658. doi:10.1016/j.neo.2017.05.002

Cheng, X.-N., Shao, M., and Shi, D.-L. (2019). Collagen Triple helix Repeat Containing 1a (Cthrc1a) Regulates Cell Adhesion and Migration during Gastrulation in Zebrafish. *Exp. Cell Res.* 381 (1), 112–120. doi:10.1016/j.yexcr.2019.04.033

Danaher, P., Warren, S., Dennis, L., D'Amico, L., White, A., Disis, M. L., et al. (2017). Gene Expression Markers of Tumor Infiltrating Leukocytes. *J. Immunotherapy Cancer* 5, 18–32. doi:10.1186/s40425-017-0215-8

Feng, S., Agoulnik, I. U., Li, Z., Han, H. D., Lopez-Berestein, G., Sood, A., et al. (2009). Relaxin/RXFP1 Signaling in Prostate Cancer Progression. *Ann. N Y Acad. Sci.* 1160, 379–380. doi:10.1111/j.1749-6632.2008.03793.x

Fidler, M. M., Soerjomataram, I., and Bray, F. (2016). A Global View on Cancer Incidence and National Levels of the Human Development index. *Int. J. Cancer* 139, 2436–2446. doi:10.1002/ijc.30382

Fodde, R., Smits, R., and Clevers, H. (2001). *APC*, Signal Transduction and Genetic Instability in Colorectal Cancer. *Nat. Rev. Cancer* 1 (1), 55–67. doi:10.1038/35094067

Gao, J., Aksoy, B. A., Dogrusoz, U., Dresdner, G., Gross, B., Sumer, S. O., et al. (2013). Integrative Analysis of Complex Cancer Genomics and Clinical Profiles Using the cBioPortal. *Sci. Signal.* 6, pl1. doi:10.1126/scisignal.2004088

Garborg, K., Holme, Ø., Løberg, M., Kalager, M., Adami, H. O., and Bretthauer, M. (2013). Current Status of Screening for Colorectal Cancer. *Ann. Oncol.* 24 (8), 1963–1972. doi:10.1093/annonc/mdt157

Goubran, H. A., Kotb, R. R., Stakiw, J., Emara, M. E., and Burnouf, T. (2014). Regulation of Tumor Growth and Metastasis: the Role of Tumor Microenvironment. *Cancer Growth Metastasis* 7, 9–18. doi:10.4137/CGM.S11285

Gyorffy, B., Surowiak, P., Budczies, J., and Lánczky, A. (2013). Online Survival Analysis Software to Assess the Prognostic Value of Biomarkers Using Transcriptomic Data in Non-small-cell Lung Cancer. *PLoS ONE* 8, e82241.

Harrison, S., and Benziger, H. (2011). The Molecular Biology of Colorectal Carcinoma and its Implications: a Review. *The Surgeon* 9 (4), 200–210. doi:10.1016/j.surge.2011.01.011

Leclair, R., and Lindner, V. (2007). The Role of Collagen Triple Helix Repeat Containing 1 in Injured Arteries, Collagen Expression, and Transforming Growth Factor β Signaling. *Trends Cardiovasc. Med.* 17 (6), 202–205. doi:10.1016/j.tcm.2007.05.004

Li, B., Severson, E., Pignon, J.-C., Zhao, H., Li, T., Novak, J., et al. (2016). Comprehensive Analyses of Tumor Immunity: Implications for Cancer Immunotherapy. *Genome Biol.* 17 (1), 174–189. doi:10.1186/s13059-016-1028-7

Li, M., and Gu, J. (2005). Changing Patterns of Colorectal Cancer in China over a Period of 20 Years. *Wjg* 11 (30), 4685–4688. doi:10.3748/wjg.v11.i30.4685

Ma, M.-Z., Zhuang, C., Yang, X.-M., Zhang, Z.-Z., Ma, H., Zhang, W.-M., et al. (2014). CTHRC1 Acts as a Prognostic Factor and Promotes Invasiveness of Gastrointestinal Stromal Tumors by Activating Wnt/PCP-Rho Signaling. *Neoplasia* 16 (3), 265–278. doi:10.1016/j.neo.2014.03.001

Macfarlane, L.-A., and R. Murphy, P. (2010). MicroRNA: Biogenesis, Function and Role in Cancer. *Cg* 11 (7), 537–561. doi:10.2174/138920210793175895

Mostafavi, S., Ray, D., Warde-Farley, D., Grouios, C., and Morris, Q. (2008). GeneMANIA: a Real-Time Multiple Association Network Integration Algorithm for Predicting Gene Function. *Genome Biol.* 9, S4. doi:10.1186/gb-2008-9-s1-s4

Ogunwobi, O. O., Mahmood, F., and Akingboye, A. (2020). Biomarkers in Colorectal Cancer: Current Research and Future Prospects. *Ijms* 21 (15), 5311. doi:10.3390/ijms21155311

Pilonis, N. D., Bugajski, M., Wieszczy, P., Franczyk, R., Didkowska, J., Wojciechowska, U., et al. (2020). Long-term Colorectal Cancer Incidence and Mortality after a Single Negative Screening Colonoscopy. *Ann. Intern. Med.* 173 (2), 81–91. doi:10.7326/m19-2477

Rhodes, D. R., Yu, J., Shanker, K., Deshpande, N., Varambally, R., Ghosh, D., et al. (2004). ONCOMINE: a Cancer Microarray Database and Integrated Data-Mining Platform. *Neoplasia* 6, 1–6. doi:10.1016/s1476-5586(04)80047-2

Seoane, J., and Gomis, R. R. (2017). TGF-β Family Signaling in Tumor Suppression and Cancer Progression. *Cold Spring Harb Perspect. Biol.* 9 (12), 9a022277. doi:10.1101/cshperspect.a022277

Sung, H., Ferlay, J., Siegel, R. L., Laversanne, M., Soerjomataram, I., Jemal, A., et al. (2021). Global Cancer Statistics 2020: GLOBOCAN Estimates of Incidence and Mortality Worldwide for 36 Cancers in 185 Countries. *CA A. Cancer J. Clin.* 71 (3), 209–249. doi:10.3322/caac.21660

Tameda, M., Sugimoto, K., Shiraki, K., Yamamoto, N., Okamoto, R., Usui, M., et al. (2014). Collagen Triple helix Repeat Containing 1 Is Overexpressed in Hepatocellular Carcinoma and Promotes Cell Proliferation and Motility. *Int. J. Oncol.* 45 (2), 541–548. doi:10.3892/ijo.2014.2445

Tang, L., Dai, D. L., Su, M., Martinka, M., Li, G., and Zhou, Y. (2006). Aberrant Expression of Collagen Triple helix Repeat Containing 1 in Human Solid Cancers. *Clin. Cancer Res.* 12 (12), 3716–3722. doi:10.1158/1078-0432.ccr-06-0030

Tang, Z., Li, C., Kang, B., Gao, G., Li, C., and Zhang, Z. (2017). GEPIA: a Web Server for Cancer and normal Gene Expression Profiling and Interactive Analyses. *Nucleic Acids Res.* 45, W98–W102. doi:10.1093/nar/gkx247

Vanessa, B., and Karen, S. (2016). Colorectal Cancer Development and Advances in Screening. *Clin. Interventions Aging* 11, 967–976.

Waghela, B. N., Vaidya, F. U., Ranjan, K., Chhipa, A. S., Tiwari, B. S., and Pathak, C. (2021). AGE-RAGE Synergy Influences Programmed Cell Death Signaling to Promote Cancer. *Mol. Cell Biochem* 476, 585–598. doi:10.1007/s11010-020-03928-y

Wu, Q., Yang, Q., and Sun, H. (2018). Collagen Triple Helix Repeat Containing-1: A Novel Biomarker Associated With Disease Activity in Systemic Lupus Erythematosus. *Lupus* 27(13), 2076–2085. doi:10.1177/0961203318804877

Yang, X. M., You, H. Y., Li, Q., Ma, H., Wang, Y. H., Zhang, Y. L., et al. (2015). CTHRC1 Promotes Human Colorectal Cancer Cell Proliferation and Invasiveness by Activating Wnt/PCP Signaling. *Int. J. Clin. Exp. Pathol.* 8 (10), 12793–12801.

Ye, J., Chen, W., Wu, Z. Y., Zhang, J. H., Fei, H., Zhang, L. W., et al. (2016). Upregulated CTHRC1 Promotes Human Epithelial Ovarian Cancer Invasion through Activating EGFR Signaling. *Oncol. Rep.* 36, 3588–3596. doi:10.3892/or.2016.5198

Zhou, H., Su, L., Liu, C., Li, B., Li, H., Xie, Y., et al. (2019). CTHRC1 May Serve as a Prognostic Biomarker for Hepatocellular Carcinoma. *Ott* 12, 7823–7831. doi:10.2147/ott.s219429

Conflict of Interest: The authors declare that the research was conducted in the absence of any commercial or financial relationships that could be construed as a potential conflict of interest.

frontiers | Frontiers in Molecular Biosciences

ORIGINAL RESEARCH
published: 19 April 2022
doi: 10.3389/fmolb.2022.872932

Identification of Tumor Microenvironment and DNA Methylation-Related Prognostic Signature for Predicting Clinical Outcomes and Therapeutic Responses in Cervical Cancer

Bangquan Liu[1], Jiabao Zhai[1], Wanyu Wang[1], Tianyu Liu[1], Chang Liu[1], Xiaojie Zhu[1], Qi Wang[1], Wenjing Tian[1] and Fubin Zhang[2]**

[1]Department of Epidemiology, College of Public Health, Harbin Medical University, Harbin, China, [2]Department of Gynecological Oncology, Harbin Medical University Cancer Hospital, Harbin, China

OPEN ACCESS

Edited by:
Na Luo,
Nankai University, China

Reviewed by:
Yiran Li,
Tongji University, China
Xingchen Li,
Peking University People's Hospital, China

***Correspondence:**
Wenjing Tian
tianwenjing@ems.hrbmu.edu.cn
orcid.org/0000-0002-0449-6643
Fubin Zhang
zfbwy163@163.com

Specialty section:
This article was submitted to Molecular Diagnostics and Therapeutics, a section of the journal Frontiers in Molecular Biosciences

Received: 10 February 2022
Accepted: 17 March 2022
Published: 19 April 2022

Citation:
Liu B, Zhai J, Wang W, Liu T, Liu C, Zhu X, Wang Q, Tian W and Zhang F (2022) Identification of Tumor Microenvironment and DNA Methylation-Related Prognostic Signature for Predicting Clinical Outcomes and Therapeutic Responses in Cervical Cancer. Front. Mol. Biosci. 9:872932. doi: 10.3389/fmolb.2022.872932

Background: Tumor microenvironment (TME) has been reported to have a strong association with tumor progression and therapeutic outcome, and epigenetic modifications such as DNA methylation can affect TMB and play an indispensable role in tumorigenesis. However, the potential mechanisms of TME and DNA methylation remain unclear in cervical cancer (CC).

Methods: The immune and stromal scores of TME were generated by the ESTIMATE algorithm for CC patients in The Cancer Genome Atlas (TCGA) database. The TME and DNA methylation-related genes were identified by the integrative analysis of DNA promoter methylation and gene expression. The least absolute shrinkage and selection operator (LASSO) Cox regression was performed 1,000 times to further identify a nine-gene TME and DNA methylation-related prognostic signature. The signature was further validated in Gene Expression Omnibus (GEO) dataset. Then, the identified signature was integrated with the Federation International of Gynecology and Obstetrics (FIGO) stage to establish a composite prognostic nomogram.

Results: CC patients with high immunity levels have better survival than those with low immunity levels. Both in the training and validation datasets, the risk score of the signature was an independent prognosis factor. The composite nomogram showed higher accuracy of prognosis and greater net benefits than the FIGO stage and the signature. The high-risk group had a significantly higher fraction of genome altered than the low-risk group. Eleven genes were significantly different in mutation frequencies between the high- and low-risk groups. Interestingly, patients with mutant *TTN* had better overall survival (OS) than those with wild type. Patients in the low-risk group had significantly higher tumor mutational burden (TMB) than those in the high-risk group. Taken together, the results of TMB, immunophenoscore (IPS), and tumor immune dysfunction and exclusion (TIDE) score suggested that patients in the low-risk group may have greater immunotherapy benefits.

Finally, four drugs (panobinostat, lenvatinib, everolimus, and temsirolimus) were found to have potential therapeutic implications for patients with a high-risk score.

Conclusions: Our findings highlight that the TME and DNA methylation-related prognostic signature can accurately predict the prognosis of CC and may be important for stratified management of patients and precision targeted therapy.

Keywords: tumor microenvironment, DNA methylation, prognostic model, drug response, immunotherapy response, cervical cancer

INTRODUCTION

Cervical cancer (CC) is the fourth leading cause of cancer-related death in women, with more than 300,000 deaths worldwide each year (Cohen et al., 2019), of which adenocarcinoma, squamous cell carcinoma, and adenosquamous carcinoma are common pathological types (Small et al., 2017). The incidence of CC is gradually declining due to the identification of HPV as a causative factor and the introduction of specific vaccines into clinical practice (Wakeham and Kavanagh, 2014; Herrero et al., 2015; Ogilvie et al., 2018). Although goals have been achieved in preventing CC, when patients are diagnosed at an advanced stage, the prognosis is extremely poor, with 5-year overall survival (OS) less than 40% (Lin et al., 2010). Currently, immunotherapy is one of the best treatment strategies for patients with advanced CC (Wendel Naumann and Leath, 2020). However, tumor heterogeneity makes it difficult to accurately assess the prognosis of each patient after immunotherapy, which is also a shortcoming of the Federation International of Gynecology and Obstetrics (FIGO) stage system (Wright et al., 2019). Therefore, accurate molecular predictors are needed to improve the prediction of CC prognosis and guide the individual evaluation of immunotherapy, especially those at high risk of recurrence or death.

Tumor microenvironment (TME) is defined as the environment surrounding the tumor, including various immune cells, stromal cells, extracellular matrix molecules, and cytokines, among which immune cells and stromal cells are closely related to tumor progression and treatment outcome (Hanahan and Coussens, 2012; Binnewies et al., 2018), and the genetic and epigenetic modifications acquired by the TME also play important roles in tumorigenesis and lead to uncontrolled growth of tumor cells (Sharma et al., 2010). Among all epigenetic modifications, DNA methylation is a stable change in gene structure and is one of the most studied mechanisms involved in regulating gene expression (Bird, 2007). DNA hypermethylation in the promoter region of genes encoding inhibitory immune checkpoints, tumor suppressors, and suppressive cytokines can lead to impaired activation of anti-tumor immunity, immune escape, drug resistance, tumor growth, and TME dyshomeostasis and significantly promote the development and progression of cancer (Easwaran et al., 2014; Ali et al., 2017).

In this study, we calculated immune and stromal scores based on the ESTIMATE algorithm to estimate the TME status of each CC patient and found that the immune scores were associated with patients' prognoses. We correlated epigenetic characteristics and TME status by analyzing the multi-omics data (RNA sequencing and DNA methylation array) across different immune groups and identified the TME and DNA methylation-related prognostic signature. We then used microarray data from the Gene Expression Omnibus (GEO) database for validation. Both the developed signature and the nomogram based on the signature and FIGO stage showed high potential for individual risk stratification and prognosis prediction. Furthermore, we sought to understand the relationship between the signature and tumor mutation status, genetic variants, and pathway activation. Finally, we not only identified four agents for these high-risk score patients but also assessed the role of this signature in identifying immune responders to immunotherapy. The results gathered from this study may be valuable in predicting patients' prognosis and facilitating the individualization of immune treatment strategies for CC.

MATERIALS AND METHODS

Data Acquisition and Processing

The Cancer Genome Atlas (TCGA) RNA-seq data, Illumina 450k DNA methylation data, somatic mutation data, copy number variation data, and clinical datasets of 306 CC patients were downloaded from Genomic Data Commons Data Portal (https://portal.gdc.cancer.gov/). FPKM values were transformed into transcripts per kilobase million (TPM) values. Quantile normalized microarray gene expression data and clinical annotations of GSE44001 were obtained from the GEO database (https://www.ncbi.nlm.nih.gov/geo/). All samples with a survival time of 0 or duplicates were deleted, and TCGA 291 samples and GEO 283 samples were used for further analysis. Expression profile data of human cancer cell lines (CCLs) were obtained from the Broad Institute Cancer Cell Line Encyclopedia (CCLE) project (https://portals.broadinstitute.org/ccle/) (Ghandi et al., 2019). The sensitivity data were obtained from the Cancer Therapeutics Response Portal (CTRP v.2.0, released October 2015, https://portals.broadinstitute.org/ctrp) and PRISM Repurposing dataset (19Q4, released December 2019, https://depmap.org/portal/prism/), respectively. In the two datasets, drug sensitivity is measured using the area under the curve (AUC) value and a lower AUC value indicates increased treatment sensitivity. The compounds with more than 20% of missing data were removed, and K-nearest neighbor (k-NN)

imputation was used to impute the missing AUC values (Yang et al., 2021).

Differential Expression Genes (DEGs) and Differential Methylation Genes (DMGs) Analysis

Limma analysis (Ritchie et al., 2015) was carried out to identify DEGs between low- and high-immune score groups. The genes meeting the $|\log_2 FC| > 1.0$ and adjusted p-value < 0.05 were considered as DEGs. DNA methylation level for each gene was estimated by calculating the average beta value of probes in promoter regions including TSS200, 1stExon, TSS1500, and 5′UTR (Jiao et al., 2014). An unpaired t-test was performed to identify DMGs between low- and high-immune score groups. The p-value was adjusted by the Benjamini Hochberg method. DMGs were defined by $|\log_2 FC| > 0.1$ and the false discovery rate corrected p-value < 0.05.

Correlation Analysis Between DNA Promoter Methylation and Genes

The Pearson correlation (r) was calculated between the mean β values of the DNA promoter region and the normalized expression values of the corresponding genes to examine the effect of DNA methylation in the promoter region on gene expression levels. Cut-off for significant correlations was set at $|r| > 0.3$ and p-value < 0.05 (Piao et al., 2012).

Identification of the Prognostic Genes and Calculation of the Risk Score

Robust prognostic genes in TCGA CC samples were identified using multi-step processes. First, univariate Cox regression analysis was performed to screen prognosis-related genes, and genes with p-value less than 0.05 were selected for further analysis. Next, we used the least absolute shrinkage and selection operator (LASSO) Cox regression analysis to assess the correlation between the gene expression and prognosis. This procedure was repeated 1,000 times, and the genes with 100 repetitions were kept for the next step analysis. Further, the concordance index (C-index) was calculated of each possible threshold from one to the number of genes, and the one (k) genes were selected that could reach the largest C-index in the TCGA cohort as the appropriate threshold of the signature. Then, the selected genes were used to perform multivariate Cox regression.

The risk score was calculated by the formula risk score = Σ βi*Expi, where βi is the coefficient of each gene in the multivariate Cox model and Expi represents the normalized expression value of each gene transformed by $\log_2$ and z-score. Patients were divided into high- and low-risk groups using the median risk score as the cut-off.

Construction of Nomogram

Based on the multivariate analysis results, we integrated the FIGO stage and risk signature to construct a composite prognostic model using the Cox proportional hazard regression in the TCGA cohort. Then, the R package "rms" was utilized to generate the nomogram. The consistency between the predicted and actual survival outcomes was assessed using the calibration curves. Moreover, time-dependent C-index and the decision curve analysis (DCA) were performed to compare the predictive accuracy of the nomogram, prognostic signature risk model, and FIGO stage.

Enrichment Analysis and Tumor Immune Signature Analysis

Differentially expressed genes in CC patients between different risk score groups were analyzed by limma. The $\log_2 FC$ value of each gene was used as an input to carry out gene set enrichment analysis (GSEA) (Subramanian et al., 2005). The adjusted $p < 0.05$ was considered significantly enriched. Meanwhile, gene set variation analysis (GSVA) was performed to find significantly associated pathways, and adjusted $p < 0.01$ was considered statistically significant. The gene set "h.all.v7.2.symbols.gmt" was selected as the reference gene set.

Signature-related gene modules in the TCGA expression file were identified by weighted gene co-expression network analysis (WGCNA) (Langfelder and Horvath, 2008). The basic set parameters of the program included setting the scale-free topological fit index (R^2) > 0.85, the minimum cluster size to 30, and the merge threshold function to 0.3. Gene modules with biweight midcorrelation coefficient (r) ≥ 0.5 and p-value < 0.05 were defined as signature-related gene modules.

Immune signatures were evaluated from the gene expression levels of immune checkpoints and human leukocyte antigen (HLA) genes (De Simone et al., 2016; Johnston et al., 2019) and the levels of immune cells infiltrating. The infiltrating immune cells levels were calculated by CIBERSORT (Newman et al., 2015), TIMER (Li et al., 2016), and MCP-counter (Becht et al., 2016) algorithms.

Somatic Variants Analysis and Copy Number Variation Analysis

Logistic regression analysis was performed to adjust for the influence of other clinical pathological features to identify differential mutation patterns, and genes with $p < 0.05$ were defined as significantly mutant genes. Genes with more than five mutations in at least one group were analyzed. The R package "maftools" (Mayakonda et al., 2018) was used to create the visualization of the mutations.

Genomic identification of significant targets in cancer (GISTIC) analysis was used to analyze the copy number variation data and identify the significant amplification and deletion regions and all gene's discrete copy number status between different risk groups, which was performed by the GISTIC 2.0 pipeline (GenePattern, https://genepattern.broadinstitute.org/).

Drug Response Prediction

The CTRP and PRISM datasets were utilized to construct predictive models of drug response. Before subsequent

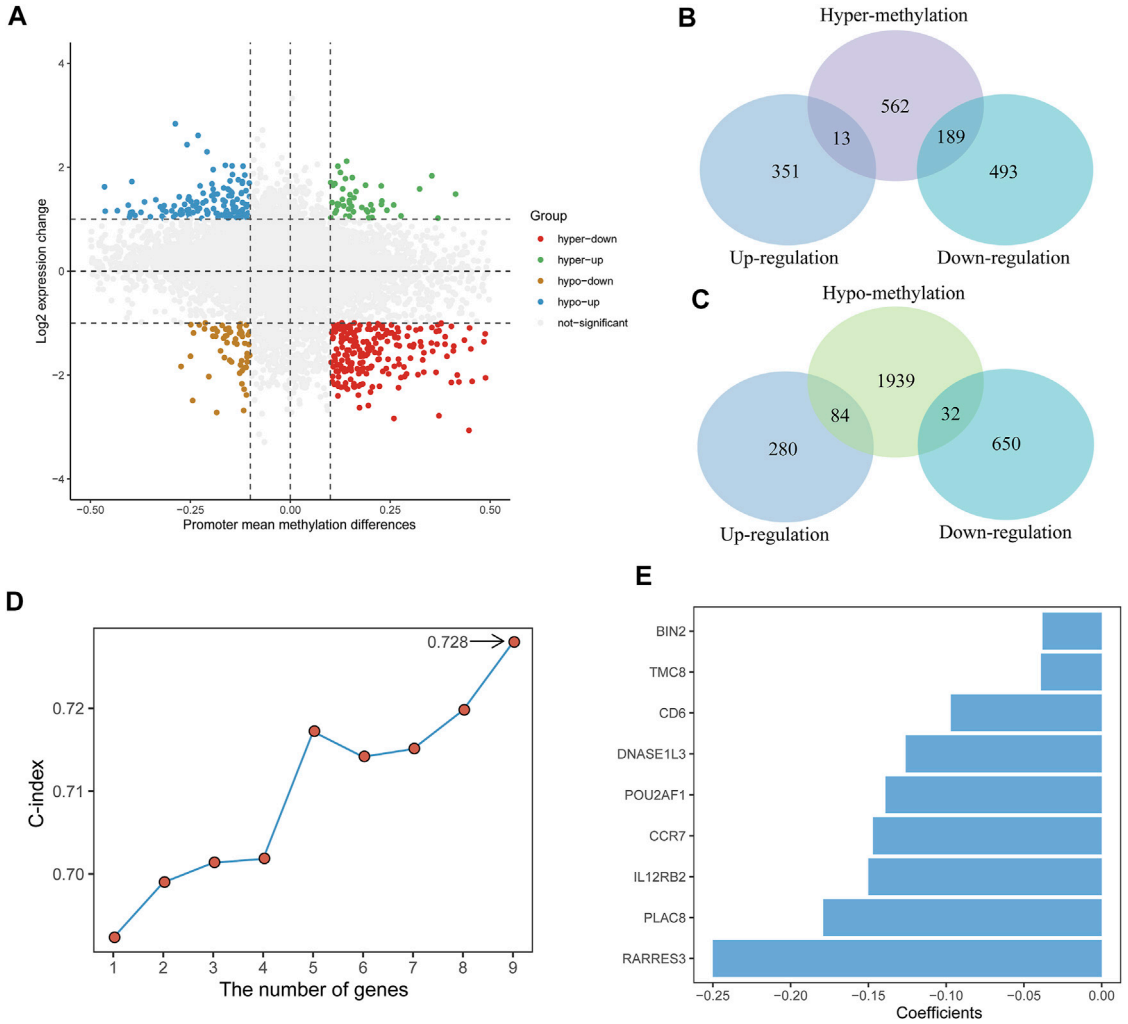

FIGURE 1 | Identification of the TME and DNA methylation-related prognostic signature. **(A)** Scatter plot of promoter mean methylation difference and gene expression levels change. hyper-up, hypermethylated-upregulated; hyper-down, hypermethylated-downregulated; hypo-up, hypomethylated-upregulated; hypo-down, hypomethylated-downregulated. **(B,C)** Venn diagrams showing the intersection between DEGs and hypermethylated genes (top) and between DEGs and hypomethylated genes (bottom). **(D)** The C-index of different genes combinations in the signature. **(E)** The nine genes included in the signature. Corresponding coefficients are depicted by horizontal bars.

analysis, more than 20% of the compounds containing NAs in the samples were excluded. ISOpure algorithm was utilized to reduce the impact of non-tumor components on analysis results (Anghel et al., 2015). A built-in ridge regression model of the "pRRophetic" package was used to estimate the AUC value of each compound in each patient by inputting TCGA purified expression profile and drug sensitivity data.

Immunotherapeutic Response Prediction

The Tumor Immune Dysfunction and Exclusion (TIDE) algorithm (Fu et al., 2020) and immunophenoscore (IPS) (Charoentong et al., 2017) were leveraged to predict the clinical response to immunotherapy of different risk groups based on the gene expression profile of TCGA CC samples. Patients with higher IPS and lower TIDE scores responded better to immunotherapy.

Statistical Analysis

All statistical tests were performed in R statistical software (v3.6.3). Unless otherwise noted, a comparison of a continuous variable in two or more than two groups was performed using Wilcoxon rank-sum test or Kruskal–Wallis test. The correlation between two continuous variables was measured by either Pearson's (r) correlation coefficient or Spearman's rank-order correlation. Immune and stromal scores were estimated to the TCGA cohort using the ESTIMATE algorithm (Yoshihara et al., 2013). Kaplan–Meier (KM) survival analysis was used to assess prognosis between different groups by the log-rank test in the "survival" R package. The time-dependent AUC was performed using the "timeROC" R package. The time-dependent C-index was performed using the "pec" R package. The p-value is two-sided, and $p < 0.05$ was considered statistically significant.

RESULTS

Overview of Workflow

The whole workflow of this study was delineated in **Supplementary Figure S1**, including the identification of hypermethylated-downregulated genes; development and validation of the prognostic signature; the construction of the nomogram; and the analyses of signature-associated immune signature, function enrichment, and genetic features.

Analysis of the Correlation of Immune and Stromal Scores With Clinical Features

The detailed clinical information of patients in the TCGA cohort is shown in **Supplementary Table S1**. Immune scores ranged from −1,203.5 to 3,430.4, and stromal scores of these patients ranged from −2,433.1 to 812.7. The median cut-off values of immune scores and stromal scores were applied to stratify CC patients into high- and low-immune groups and high- and low-stromal groups. KM analysis result showed that the OS of patients in the high-immune group was better than that of the low-immune group, but there was no difference in OS between the high- and low-stromal groups (**Supplementary Figures S2A,B**). We also found a strong negative correlation between immune score and tumor purity (**Supplementary Figure S2C**). However, immune scores were not associated with the FIGO stage (**Supplementary Figure S2D**) and the tumor node metastasis (TNM) stage (**Supplementary Figures S2E–G**).

Identification of DEGs and DMGs Between High- and Low-Immune Groups

We mapped the average β value of the DNA promoter region to genes, and 14,932 genes were obtained (**Figure 1A**). Differential methylation and expression analyses were carried out between high- and low-immune groups. A total of 2,819 DMGs were detected, with 764 hypermethylated genes and 2,055 hypomethylated genes. A total of 1,046 DEGs were detected, with 364 upregulated genes and 682 downregulated genes.

The integrative analysis of gene expression and DNA promoter methylation in CC patients was performed by identifying the intersection between the DEGs and DMGs. Of the 764 hypermethylated genes, 13 genes were upregulated and 189 genes were downregulated (**Figure 1B**). Among the 2,055 hypomethylated genes, 84 genes were upregulated and 32 genes were downregulated (**Figure 1C**). Then, we focused on the hypermethylated-downregulated genes and used the Pearson correlation analysis to examine the impact of DNA promoter methylation on gene expression. Among the 189 hypermethylated-downregulated genes, 111 genes revealed significantly negative correlations (**Supplementary Table S2**), and mRNA expression of these genes is shown in **Supplementary Figure S3**.

Identifying Prognostic Genes and Development of the Risk Score

A total of 291 TCGA CC patients with available clinical information were used to recognize the prognostic signature. We first used univariate Cox proportional hazards regression analysis and identified 55 genes correlated with OS ($p < 0.01$) (**Supplementary Table S3**). After a 1,000-time LASSO Cox regression analysis, we identified nine genes (*CCR7*, *CD6*, *POU2AF1*, *TMC8*, *PLAC8*, *RARRES3*, *BIN2*, *DNASE1L3*, and *IL12RB2*) that were stably associated with prognosis over 100-time iterations (**Supplementary Table S4**).

For all possible thresholds from 1 to 9, a nine-gene set with the largest C-index (0.728) was considered prognosis-associated genes (**Figure 1D**, **Supplementary Table S5**). All nine genes showed a high negative correlation between DNA promoter mean methylation and gene expression (**Supplementary Figure S4**). Furthermore, we estimated the risk score based on the linear combination of the nine-gene expression levels weighted by their multivariate Cox regression coefficients (**Figure 1E**): risk score = (−0.147) × *CCR7* + (−0.097) × *CD6* + (−0.139) × *POU2AF1* + (−0.039) × *TMC8* + (−0.179) × *PLAC8* + (−0.250) × *RARRES3* + (−0.038) × *BIN2* + (−0.126) × *DNASE1L3* + (−0.150) × *IL12RB2*. Then, according to the median risk score, CC patients were divided into low-risk ($n = 145$) and high-risk groups ($n = 146$).

The Prognostic Value of Risk Score

A heatmap of expression levels of the nine identified genes and the scatterplot of OS with a corresponding risk score are illustrated in **Supplementary Figure S5A**. We explored the distribution of the risk score with histological type, TNM stage, and FIGO stage. Patients with a higher M stage and T stage had a higher risk score, and patients in the squamous subtype had a significantly lower risk score than those in other subtypes (**Figure 2A**). We next found that patients with low-risk scores were significantly associated with better OS compared with patients with high-risk scores (**Figure 2B**). Moreover, the accuracy of the risk score in OS prediction was evaluated using the AUC, as shown in **Figures 2C,D**. The AUCs of the risk score model at 1, 3, and 5 years were 0.812, 0.716, and 0.703, respectively.

To confirm that the risk score had a stable prognostic value across different datasets, we corroborated this association in an external validation GEO (GSE44001) dataset. A heatmap of the signature consisting of nine genes and the scatterplot of disease-free survival (DFS) time with corresponding risk score in GEO (GSE44001) are shown in **Supplementary Figure S5B**. Consistent with the above TCGA results, patients with high-risk scores in GSE44001 had a significantly poorer DFS than those with low-risk scores (**Figure 2E**), and AUCs at 1, 3, and 5 years were 0.476, 0.575, and 0.645, respectively (**Figures 2F,G**). The result showed that the risk score did not show high accuracy in predicting the prognosis of CC patients in the validation dataset (GSE44001), which may be caused by the CC patients in the early stage (stages I-II).

The results of univariate and multivariate Cox regression analysis further showed that risk score could be an

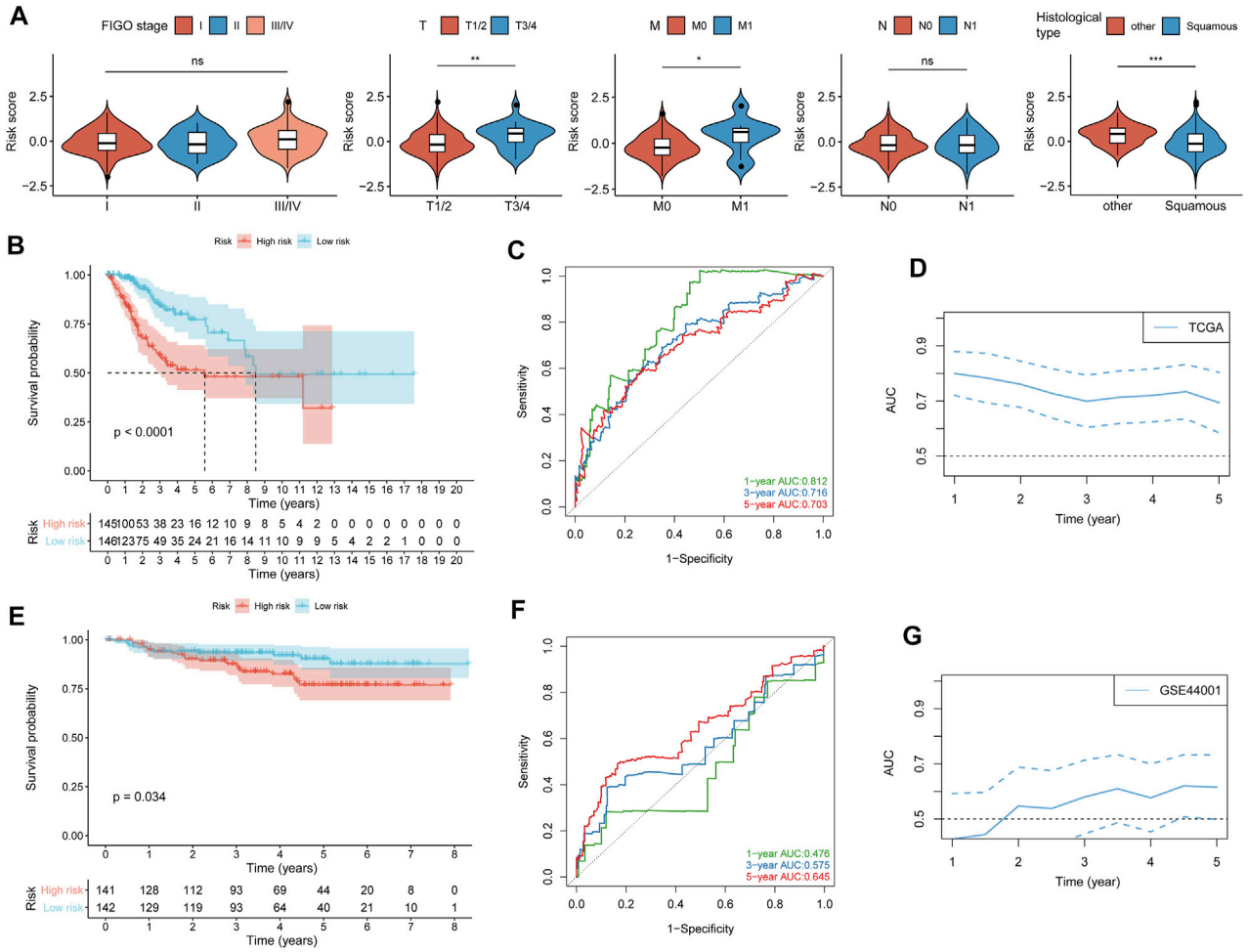

FIGURE 2 | Validation of the prognostic value of the risk score. **(A)** Difference analysis of the distribution of risk scores in different FIGO stages, TNM stages, and histological types. **(B)** Kaplan–Meier curves for differential detection of patients in the TCGA cohort by the log-rank test. **(C)** ROC curves of risk scores used to predict 1-year, 3-year, and 5-year survival in the TCGA cohort. **(D)** Time-dependent ROC curves of the risk score in the TCGA cohorts. **(E)** Kaplan–Meier curves for differential detection of patients in the GSE44001 cohort by the log-rank test. **(F)** ROC curves of risk scores used to predict 1-year, 3-year, and 5-year survival in the GSE44001 cohort. **(G)** Time-dependent ROC curves of the risk score in the GSE44001 cohorts. *$p < 0.05$; **$p < 0.01$; ***$p < 0.001$; ns, not significant.

independent predictor of survival outcome in CC patients after being adjusted for the clinicopathological features (**Figure 3**), suggesting that the TME and DNA methylation-related genes might be involved in CC occurrence and development and could serve as potential therapeutic targets. Meanwhile, we also found that the tumor FIGO stage could be used as an independent predictor.

Construction of Nomogram

To find a more effective method to strongly predict the prognosis of CC patients, we combined tumor FIGO stage and risk score to establish a complete evaluation signature. A nomogram was created to predict the 1-, 3-, and 5-year prognostic survival probabilities of patients with CC (**Figure 4A**). The calibration curve was used to assess the consistency between the actual survival status and the predicted outcomes of CC patients (**Figure 4B**). The result revealed that based on the FIGO stage and risk score, the nomogram could effectively predict the prognosis. Then, we calculated the C-index to confirm this (**Figure 4C**). These results suggested that the ability of the nomogram to predict the prognosis of CC patients is more reliable than a single independent factor. Moreover, the DCA diagram showed that the net benefits of the nomogram were significantly higher than the risk score and FIGO stage, indicating the good clinical applicability of the nomogram (**Figure 4D**).

Risk Score Was Associated With Immune Signature

To elucidate the interrelation of the risk score and immune signature, we examined the correlation between the risk score and immune and stromal scores, HLA family genes, immune checkpoints, and infiltrating immune cells. The results showed that immune and stromal scores were significantly positively

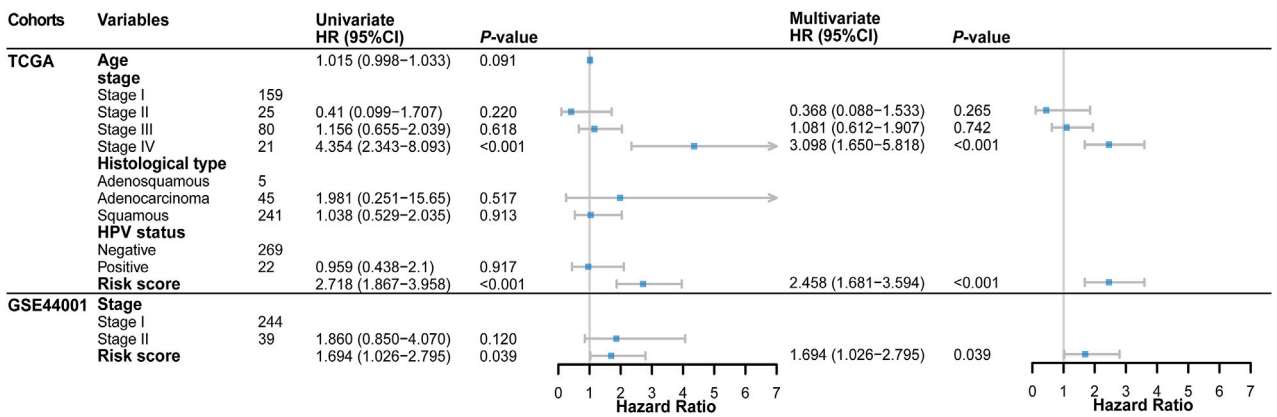

FIGURE 3 | Forest plot of the univariate and multivariate Cox regression analysis in TCGA and GSE44001 cohorts.

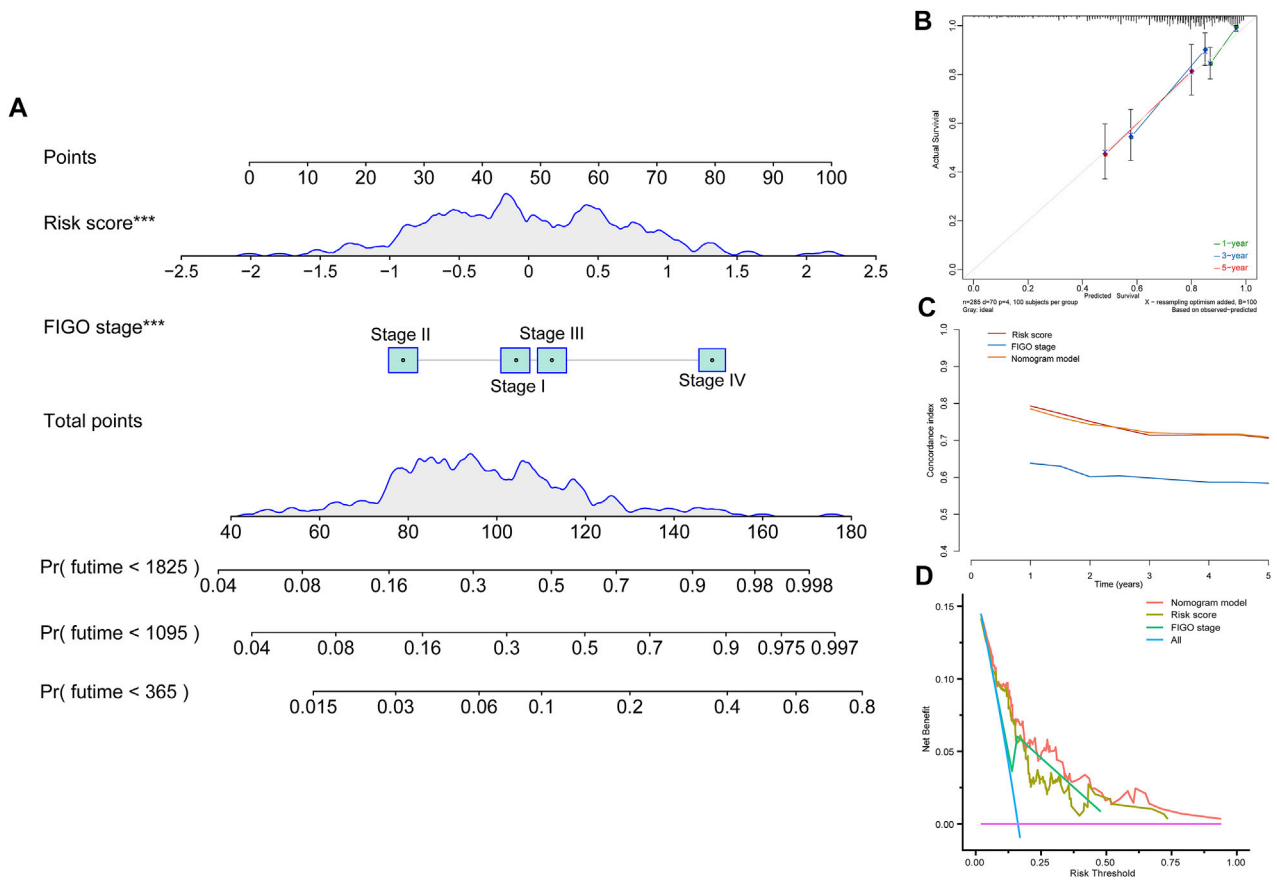

FIGURE 4 | Construction of a nomogram model. **(A)** Nomogram constructed in conjunction with the risk score and FIGO stage for the TCGA cohort. **(B)** Calibration plot of the nomogram. **(C)** C-index curves of the FIGO stage, risk score, and nomogram. **(D)** Decision curve analysis for evaluating the net benefits of FIGO stage, risk score, and nomogram.

correlated with risk scores. Patients in the low-risk score group had higher immune and stromal scores than those in the high-risk score group, and patients in the low-risk score group had lower tumor purity (**Figures 5A–C**). We next found that the gene expression levels of 20 HLA family genes and 41 immune checkpoints were significantly different between the high- and low-risk groups (**Figures 5D,E**, **Supplementary Table S6**), and the risk score was significantly negatively correlated with the

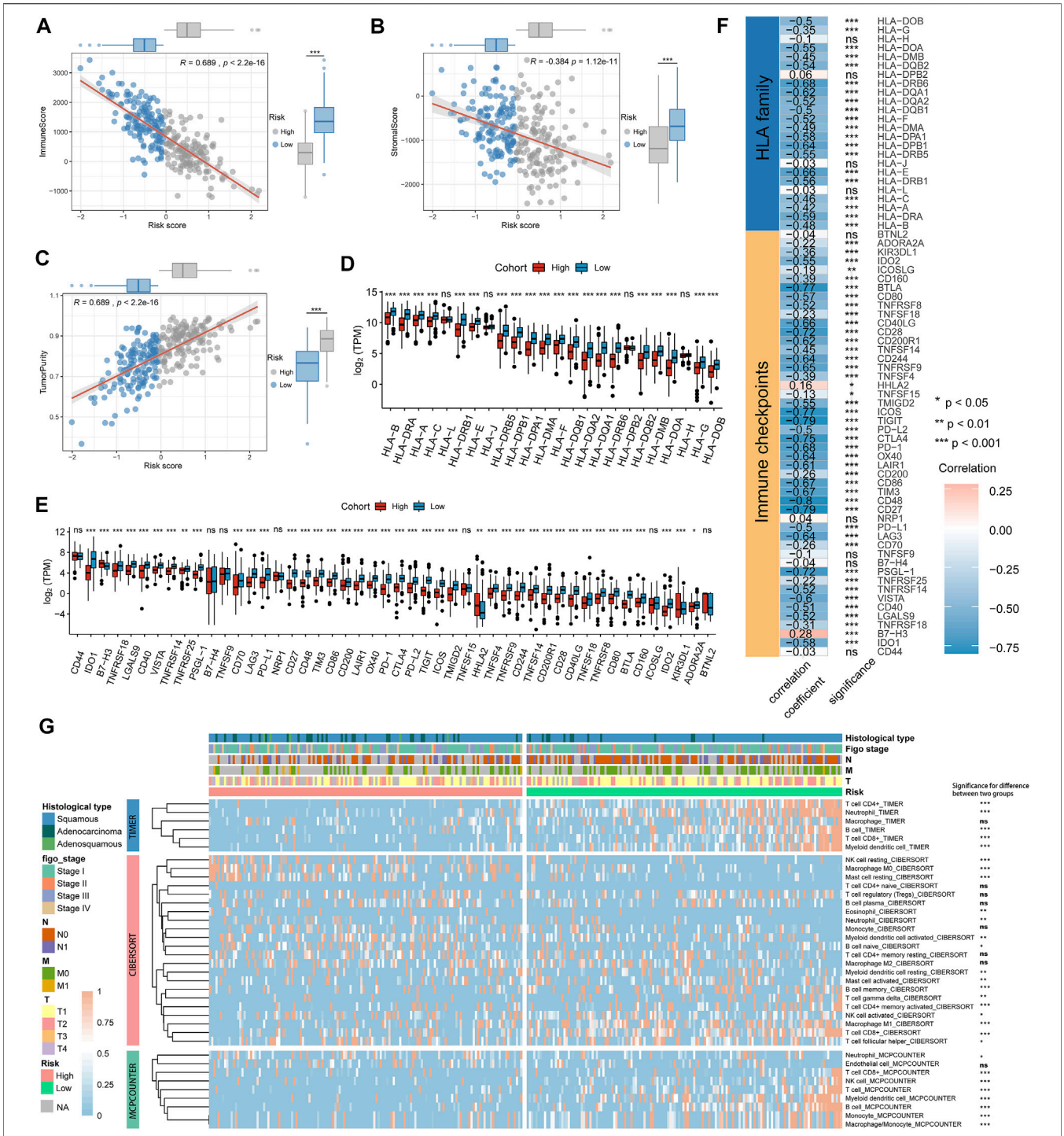

FIGURE 5 | The immune signature between the high- and low-risk groups in the TCGA cohort. **(A–C)** Association between immune score, stromal score, tumor purity, and risk score and their distribution in different risk groups. **(D,E)** Differential analysis of gene expression levels of HLA family genes and immune checkpoints in different risk groups. **(F)** Correlation analysis for the risk score and the gene expression levels of HLA family genes and immune checkpoints. **(G)** The heatmap showing the immune and stromal cell infiltration levels and differences in distribution between different risk groups. *$p < 0.05$; **$p < 0.01$; ***$p < 0.001$; ns, not significant.

expression levels of 20 HLA genes and 43 immune checkpoints, such as *HLA-DOA*, *HLA-DPB1*, *IDO2*, *BTLA*, and *CD27* (**Figure 5F**, **Supplementary Table S7**). TIMER, CIBERSORT, and MCP-counter were performed to estimate the distribution of infiltrating immune cells between the low- and high-risk score groups. Most immune cells and stromal cells were infiltrated more frequently in the low-risk score group. However, antigen presenting cells such as macrophage M0 and T cell regulatory

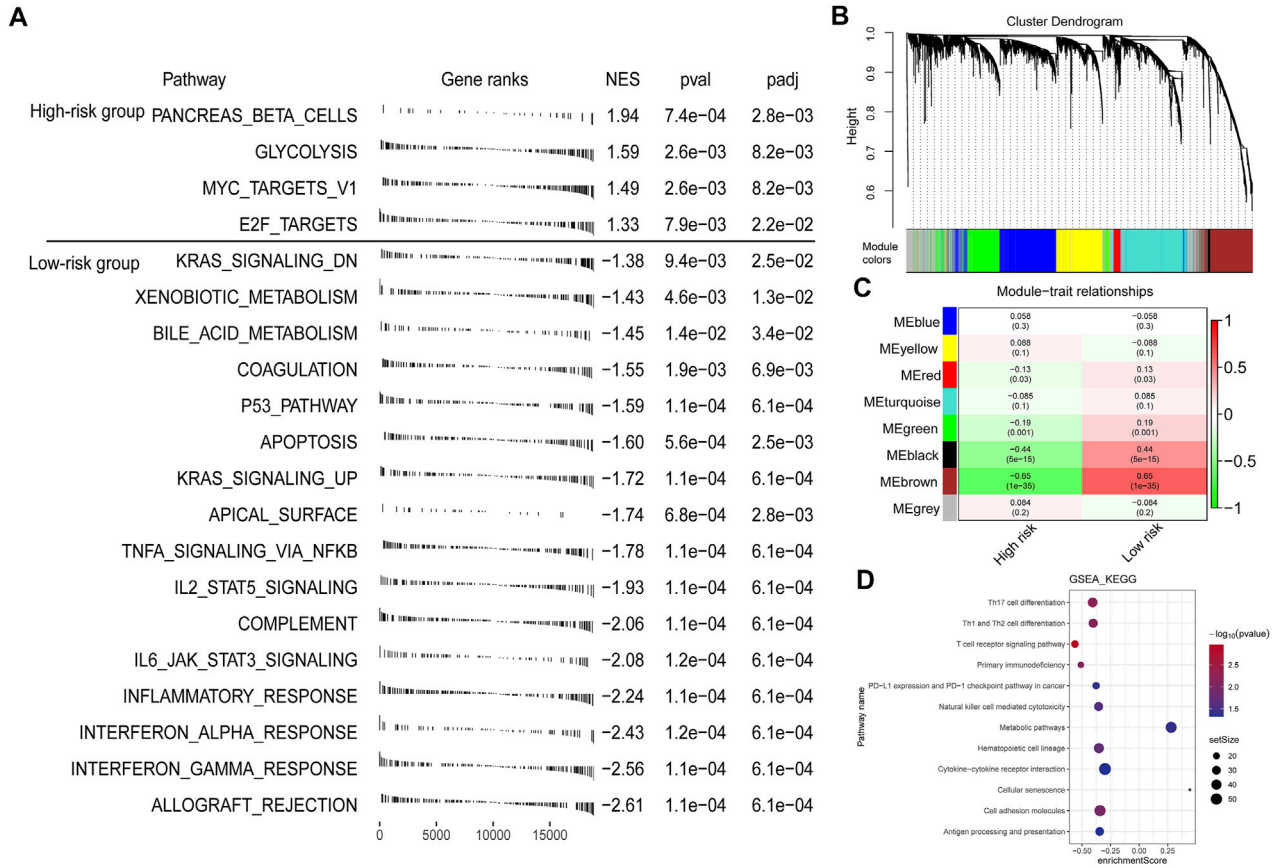

FIGURE 6 | Function analysis of genes correlated with the risk score. **(A)** GSEA enrichment plots showing enriched gene sets against to hallmark dataset in high- and low-risk groups. NES, normalized enrichment score. **(B)** A dendrogram of the top 5,000 genes with the most variation clustered based on the topological overlap together. **(C)** The heatmap showing the association between gene modules and the signature risk score. **(D)** GSEA annotated by KEGG gene sets for the brown module genes.

(Tregs) increased in the high-risk score group (**Figure 5G**, **Supplementary Table S8**). These results indicate that the suppression of stromal and immune components in the tumor microenvironment likely contributes to the worse prognosis in high-risk patients.

Function Analysis of Genes Related to the Risk Score

To explore the underlying mechanisms that lead to different outcomes between the high- and low-risk score groups, we carried out GSEA using annotations of hallmark gene sets. Significantly enriched pathways with adjusted p-value < 0.05 are shown in **Figure 6A**. Genes involved in glycolysis, Myc targets v1, and E2F targets signaling pathway were enriched in the high-risk score group, while genes related to apoptosis, KRAS signaling up, inflammatory response, and p53 signaling pathway were enriched in the low-risk score group.

Furthermore, we performed WGCNA to get the signature-related modules. Based on the median absolute deviation (MAD), the top 5,000 genes with the most variation were selected and the gene expression file of these genes was inputted into the WGCNA. When the lowest soft threshold power was four, the scale-free R2 reached 0.85 (**Supplementary Figure S6**). We constructed a cluster dendrogram with the adjacency matrix; eight-color modules (blue, yellow, red, turquoise, green, black, brown, and grey) were identified (**Figure 6B**). Next, we analyzed the module-trait relationships and found that the brown module was highly significantly correlated with the signature risk score (|r| > 0.5) (**Figure 6C**). We then performed GSEA using the annotations of the KEGG gene set to explore the biological functions of genes in different modules. For brown module genes, the top enriched terms were Th1 and Th2 cell differentiation, T cell receptor signaling pathway, primary immunodeficiency, and PD-L1 and PD-1 checkpoint pathway in cancer, indicating that genes in the brown module are involved in regulating immune system function (**Figure 6D**).

Differences in Genetic Variation and Pathway Activation Between High- and Low-Risk Groups

Tumor mutation burden (TMB) is largely attributed to genomic instability and can indirectly reflect the ability and degree of tumor production of neoantigens and predict the

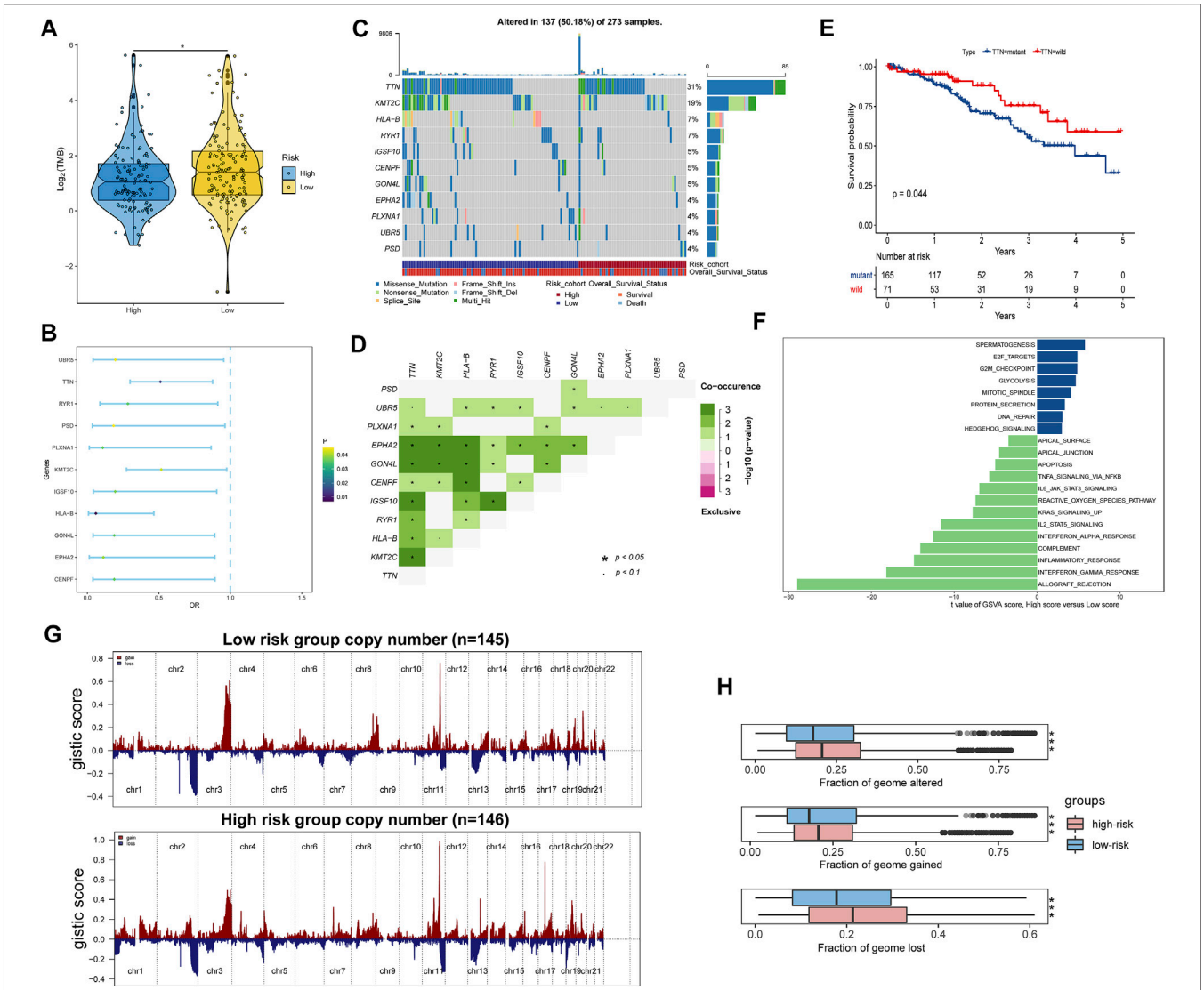

FIGURE 7 | Identification differences of the genetic variation and pathway activation between high- and low-risk groups. **(A)** Tumor mutation burdens were compared among distinct risk groups. **(B)** Forest plot of genes with differences in mutation frequencies between the low- and high-risk groups. **(C)** Waterfall plot of the 11 mutant genes with significant frequency differences between low- and high-risk groups. **(D)** Interaction of differentially mutated genes. **(E)** Kaplan–Meier curve showing that patients with mutant *TTN* have a better OS than those with wild type. **(F)** Differential analysis of GSVA scores among distinct risk groups. **(G)** Copy number alteration gains (red) and losses (blue) between the low- and high-risk groups. **(H)** Differential analysis of altered, lost, and gained genome fractions (%) between the low-risk and high-risk groups. **p* < 0.05; ***p* < 0.01; ****p* < 0.001; ns, not significant.

immunotherapy efficacy of various tumors. We found that TMB was significantly higher in the low-risk score group than in the high-risk score group (**Figure 7A**). We further investigated the somatic mutations across CC patients. Logistic regression analysis showed that 11 genes mutation frequencies were significantly different between high- and low-risk score groups, including *CENPF*, *EPHA2*, *GON4L*, *HLA-B*, *IGSF10*, *KMT2C*, *PLXNA1*, *PSD*, *RYR1*, *TTN*, and *UBR5* (**Figure 7B**). The mutation frequencies of these genes are shown in **Figure 7C**, and there were significant co-occurrences among mutations of these genes (**Figure 7D**). We also found that patients with mutant *TTN* were significantly associated with better OS compared with wild-type patients (**Figure 7E**), suggesting that the *TTN* may be a potential immunotherapy target.

The GSVA also identified significant differences in biological functions between the high- and low-risk groups (**Figure 7F**, **Supplementary Table S9**). Consistent with the GSEA results, the direct comparison revealed that E2F targets, G2M checkpoint, glycolysis, and DNA repair pathways were significantly enriched in the high-risk group. Comparatively, apoptosis, KARS signaling up, and inflammatory response pathways were significantly enriched in the low-risk group. Subsequently, copy number variation analysis showed different patterns of chromosomal alteration between the high- and low-risk groups (**Figure 7G**).

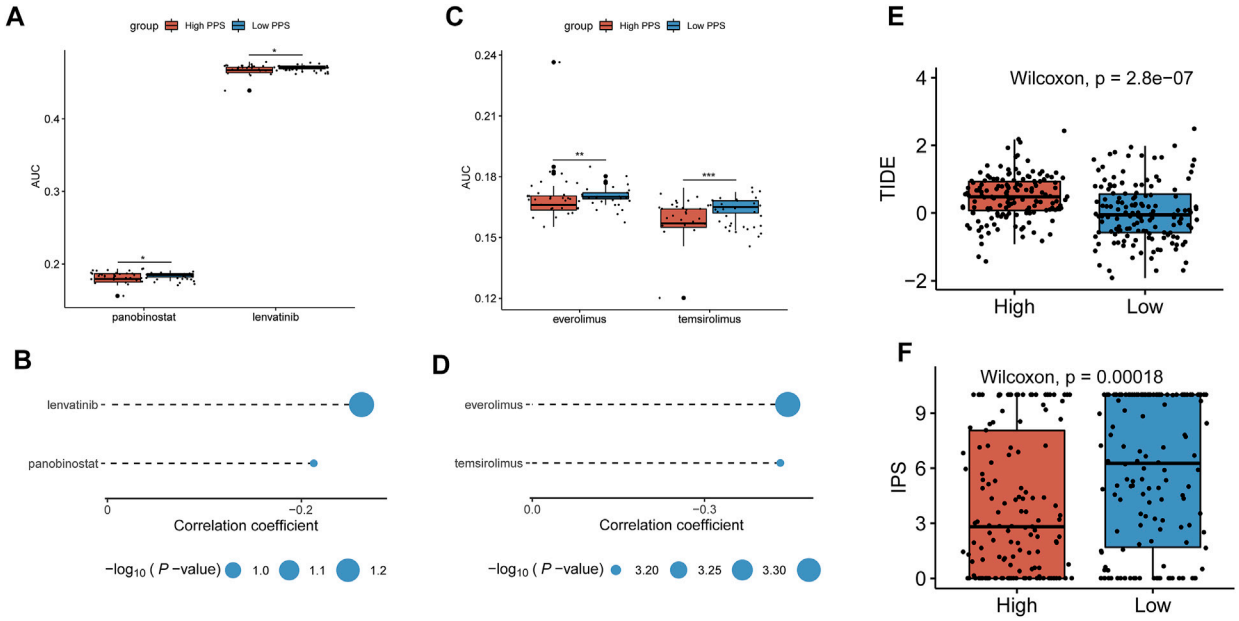

FIGURE 8 | Identification of potential agents and prediction of immunotherapeutic effect. **(A,B)** Differential drug response analysis of the selected agents for CC patients between the higher and lower risk score groups based on the CTRP dataset and Spearman's correlation analysis of CTRP-derived agents and risk score. **(C,D)** Differential drug response analysis of the selected agents for CC patients between the higher and lower risk score groups based on the PRISM dataset and Spearman's correlation analysis of PRISM-derived agents and risk score. **(E,F)** The TIDE score and IPS were compared between the high- and low-risk groups. $^{*}p < 0.05$; $^{**}p < 0.01$; $^{***}p < 0.001$; ns, not significant.

A larger proportion of genomic loss and gain were detected in the high-risk group (**Figure 7H**). Our analysis indicated that activation of tumor-related pathways, production of neoantigens, and amplification and deletion of certain tumor suppressor genes might cause differences in survival between high- and low-risk score groups.

Identification of Potential Agents and Prediction of Immunotherapeutic Effect

Based on the CTRP and PRISM-derived drug response datasets, we used two approaches to identify potential agents for CC patients. First, we performed a differential drug response analysis between high-risk (upper decile) and low-risk (lower decile) groups to identify drugs with significantly different AUC values ($\log_2$FC > 0.01, $p < 0.05$). Next, the Spearman correlation between the risk score and the AUC value was conducted to screen out agents with a significantly negative correlation coefficient ($r < -0.20$ for CTRP and $r < -0.40$ for PRISM, $p < 0.05$). Finally, we determined two CTRP-derived compounds (panobinostat, lenvatinib) (**Figures 8A,B**) and two PRISM-derived compounds (everolimus, temsirolimus) (**Figures 8C,D**) as the potential agents for CC patients with high-risk scores. Moreover, we also calculated the TIDE score and IPS based on the TCGA gene expression profile to determine the immunotherapeutic response in CC patients. We found that patients in the low-risk group had lower TIDE scores and higher IPS (**Figures 8E,F**), suggesting that patients in the low-risk group were more likely to respond to immunotherapy than those in the high-risk group.

DISCUSSION

In this study, the ESTIMATE algorithm was performed to calculate the immune score and the stromal score to estimate the TME infiltration pattern of each CC patient in the TCGA cohort. Because the OS of patients in the high-immune group is better than that of patients in the low-immune group, the TME and DNA methylation-related genes were identified by the integrative analysis of DEGs and DMGs between the low- and high-immune score groups. Based on multiple LASSO Cox regression analysis, we constructed a nine-gene TME and DNA methylation-related prognostic signature to predict prognosis for stratified CC patients and performed external validation for its performance. Then, the signature was combined with the FIGO stage to generate a composite prognostic nomogram that reliably demonstrated the accurate prognosis prediction for patients with CC. Furthermore, we identified the tumor immune signature, function enrichment, genetic variants, and pathway activation associated with the prognostic signature. Finally, we predicted patients' immunotherapy responses by the TIDE score and IPS and provided four potential agents for patients with high-risk scores.

The fundamental role of TME is the dynamic interaction of immune and stromal cells with malignant cells and can influence tumor growth, metastasis, and patient prognosis (Hanahan and Coussens, 2012). Many epigenetic studies have shown that DNA methylation plays a key role in promoting cellular responses to stimuli and regulating immune cell differentiation (Sørensen et al., 2010; Smith and Meissner, 2013). Thus, it is generally

accepted that DNA methylation has a very complex regulatory role on the TME, especially during the development of immune and stromal cells. For example, one study has found that different methylation patterns exist in myeloid and lymphoid lineages in cancer tissues. During the differentiation and activation of macrophages, the global methylation level increased, while it decreased in both T and B lymphocytes (Schuyler et al., 2016). Most importantly, DNA methylation can influence not only the expression levels of genes important for immune cell development but also the tumor immune response in the TME. One study suggested that Th1/Th2 differentiation may be mediated by methylation and demethylation of the FN-γ in naive $CD4^+$ T lymphocytes (Janson et al., 2008). Another report revealed that hypermethylation of genes (*LAX1*, *SIT1*, and *UBASH3A*) leads to enhanced anti-tumor T-cell responses in breast cancer (Dedeurwaerder et al., 2011). Moreover, a previous study showed that in non-small-cell lung cancer, demethylation of the *FOXP3* gene promoter could reduce the activity of DNMTs in Tregs $CD4^+$ lymphocytes and downregulate immune responses in the TME (Ke et al., 2016).

In the present study, we have observed that CC patients with low immunity levels have worse survival than those with high immunity levels, which may be due to a decrease in the immune infiltration levels caused by hypermethylation in the promoter region of immune-related genes affecting gene expression levels. To predict CC patient survival, we constructed a nine-gene TME and DNA methylation-related prognostic signature. In the training and validation datasets, the risk score of the signature was an independent prognosis factor and had a good predictive effect. Among the nine genes included in the signature, their coded proteins correlate with the immune system, such as *CCR7*, which coded protein belonging to the CCR7 chemokine axis. The axis is involved in the trafficking of effector cells for many immune responses and controls the migration and metastasis of tumor cells to the lymphatic system (Salem et al., 2021). CD6 is one kind of type I transmembrane glycoprotein on the lymphocyte surface and is involved in the development and differentiation of lymphocytes (Santos et al., 2016). As a B cell transcriptional coactivator, POU2AF1 regulates the expression of B cell maturation factor TNFRSF17 and stimulates the growth of myeloma cells (Zhao et al., 2008). DNASE1L3 is a kind of deoxyribonuclease and is involved in neutrophil activation and acute inflammatory responses (Jiménez-Alcázar et al., 2017). IL12RB2 is the interleukin-12 receptor. A study found that *IL12RB2* knockout (KO) mice develop autoimmunity, lymphoid proliferation, and B-cell tumors and suggested IL12RB2 functions physiologically in inhibiting aberrant B-cell activation (Airoldi et al., 2005). Moreover, we established a composite nomogram based on the FIGO stage and the signature to guide the prognosis prediction of CC patients more effectively. The composite nomogram demonstrated higher accuracy of prognosis and greater net benefits than the FIGO stage and the signature.

Furthermore, our study results showed that the stromal and immune scores were negatively correlated with the risk score, and patients in the high-risk group had lower immune scores and were more likely to be immunosuppressed. More seriously, patients in the high-risk group had a lower immune activity, including lower immune cell infiltration such as T cell $CD4^+$, T cell $CD8^+$, and downregulation of HLA family genes and immune checkpoints expression such as *HLA-A*, *HLA-B*, *PD1*, and *CTLA4*, which contributed to immunosuppression and tumor immune escape. We further analyzed GSEA pathway enrichment in high- and low-risk groups and found that proliferation-specific pathways were significantly enriched in the high-risk group, such as the Myc targets v1 and E2F targets pathway, while apoptosis, KRAS signaling up, and inflammatory response pathway were significantly enriched in the low-risk group.

Compared to other malignancies, immunotherapy plays an even more important role in cervical cancer. For example, in precancerous abnormalities and early tumors of cervical cancer, restoring the immune response to cancer cells and strengthening immune system function to HPV may stop further progression (Lee et al., 2016). TMB measures the number of nonsynonymous mutations of cancers, and more mutations could generate more neo-antigens, thereby activating the patient's immune system and benefiting cancer immunotherapy (Jardim et al., 2021). Therefore, many studies have suggested that TMB could be a good predictive biomarker of immunotherapy response (Chalmers et al., 2017; Büttner et al., 2019). We found that patients in the low-risk group had higher TMB than those in the high-risk group. Taken together, the results of TMB, IPS, and TIDE scores suggested that patients with lower risk scores may benefit more from immunotherapy. In addition, somatic mutations analysis revealed that the mutation frequency of 11 genes was significantly different between the high- and low-risk groups. There were co-mutations in these genes, suggesting that they may synergistically affect the regulation of TME. Interestingly, patients with mutant *TTN* had better OS than those with the wild type and *TTN* may be a potential immunotherapy target. We also determined that the genetic variants were significantly different between the high- and low-risk groups. The high-risk group had a significantly higher fraction of genome altered than the low-risk group, indicating that patients with high-risk scores had more unstable genomes, and some tumor-promoting pathways were activated, leading to poor prognosis.

Immunotherapy has a demonstrable synergistic activity to alter or enhance the immune system when combined with radiotherapy, chemoradiotherapy, and targeted drugs (Dyer et al., 2021). To identify drugs that synergize with immunotherapy for high-risk patients and facilitate personalized treatment decisions, we identified four potential agents for high-risk CC patients by interaction analysis between the risk signature and drug responses. Among the four candidate agents, lenvatinib is a multikinase inhibitor of receptor tyrosine kinases. Panobinostat is a nonselective HDAC inhibitor. Both everolimus and temsirolimus are inhibitors of mTOR kinase, which is part of the signaling pathway associated with cell growth and proliferation. Many studies have found that the destruction of mTOR leads to the

suppression of the cell cycle and angiogenesis, thereby inhibiting the development of cervical cancer. These studies also validated the reliability of our results (Bossler et al., 2019; Sun et al., 2020; Yang et al., 2020).

Our study has its limitations. First, although our signature is beneficial in evaluating prognosis and conducting therapies for CC patients, it does not yield a satisfactory result in the validation set as their patients are in the early stage of CC. It should be prospectively validated in other datasets. Second, because there are no expression data for CC patients receiving immunotherapy, we only used bioinformatics analysis to predict the effect of immunotherapy in CC patients in the TCGA dataset, and there is no actual immunotherapy benefit of immunotherapy for patients with different risk scores. Third, drug clinical trials and experimental exploration are needed to validate our drug prediction results. In summary, our study highlights the value of the TME and DNA methylation-related signature in predicting prognosis and immune response.

DATA AVAILABILITY STATEMENT

The datasets presented in this study can be found in online repositories. The names of the repository/repositories and accession number(s) can be found in the article/ **Supplementary Material**.

AUTHOR CONTRIBUTIONS

WT, FZ and BL conceived the study. WT, FZ and BL designed the research route. BL performed computational analysis. JZ, TL, WW and CL collected the data. BL wrote the manuscript. XZ and QW revised the manuscript for intellectual content. All authors read the article and approved the submitted version.

FUNDING

This work was supported by grants from the Heilongjiang Provincial Natural Science Foundation of China (LH2020H020).

ACKNOWLEDGMENTS

We thank our colleagues for their encouragement and technical assistance.

SUPPLEMENTARY MATERIAL

The Supplementary Material for this article can be found online at: https://www.frontiersin.org/articles/10.3389/fmolb.2022.872932/full#supplementary-material

REFERENCES

Airoldi, I., Di Carlo, E., Cocco, C., Sorrentino, C., Fais, F., Cilli, M., et al. (2005). Lack of Il12rb2 Signaling Predisposes to Spontaneous Autoimmunity and Malignancy. *Blood* 106 (12), 3846–3853. doi:10.1182/blood-2005-05-2034

Ali, M. A., Matboli, M., Tarek, M., Reda, M., Kamal, K. M., Nouh, M., et al. (2017). Epigenetic Regulation of Immune Checkpoints: Another Target for Cancer Immunotherapy? *Immunotherapy* 9 (1), 99–108. doi:10.2217/imt-2016-0111

Anghel, C. V., Quon, G., Haider, S., Nguyen, F., Deshwar, A. G., Morris, Q. D., et al. (2015). ISOpureR: an R Implementation of a Computational Purification Algorithm of Mixed Tumour Profiles. *BMC Bioinformatics* 16, 156. doi:10.1186/s12859-015-0597-x

Becht, E., Giraldo, N. A., Lacroix, L., Buttard, B., Elarouci, N., Petitprez, F., et al. (2016). Estimating the Population Abundance of Tissue-Infiltrating Immune and Stromal Cell Populations Using Gene Expression. *Genome Biol.* 17 (1), 218. doi:10.1186/s13059-016-1070-5

Binnewies, M., Roberts, E. W., Kersten, K., Chan, V., Fearon, D. F., Merad, M., et al. (2018). Understanding the Tumor Immune Microenvironment (TIME) for Effective Therapy. *Nat. Med.* 24 (5), 541–550. doi:10.1038/s41591-018-0014-x

Bird, A. (2007). Perceptions of Epigenetics. *Nature* 447 (7143), 396–398. doi:10.1038/nature05913

Bossler, F., Hoppe-Seyler, K., and Hoppe-Seyler, F. (2019). PI3K/AKT/mTOR Signaling Regulates the Virus/Host Cell Crosstalk in HPV-Positive Cervical Cancer Cells. *Int. J. Mol. Sci.* 20 (9), 2188. doi:10.3390/ijms20092188

Büttner, R., Longshore, J. W., López-Ríos, F., Merkelbach-Bruse, S., Normanno, N., Rouleau, E., et al. (2019). Implementing TMB Measurement in Clinical Practice: Considerations on Assay Requirements. *ESMO Open* 4 (1), e000442. doi:10.1136/esmoopen-2018-000442

Chalmers, Z. R., Connelly, C. F., Fabrizio, D., Gay, L., Ali, S. M., Ennis, R., et al. (2017). Analysis of 100,000 Human Cancer Genomes Reveals the Landscape of Tumor Mutational burden. *Genome Med.* 9 (1), 34. doi:10.1186/s13073-017-0424-2

Charoentong, P., Finotello, F., Angelova, M., Mayer, C., Efremova, M., Rieder, D., et al. (2017). Pan-cancer Immunogenomic Analyses Reveal Genotype-Immunophenotype Relationships and Predictors of Response to Checkpoint Blockade. *Cel Rep.* 18 (1), 248–262. doi:10.1016/j.celrep.2016.12.019

Cohen, P. A., Jhingran, A., Oaknin, A., and Denny, L. (2019). Cervical Cancer. *Lancet* 393 (10167), 169–182. doi:10.1016/S0140-6736(18)32470-X

De Simone, M., Arrigoni, A., Rossetti, G., Gruarin, P., Ranzani, V., Politano, C., et al. (2016). Transcriptional Landscape of Human Tissue Lymphocytes Unveils Uniqueness of Tumor-Infiltrating T Regulatory Cells. *Immunity* 45 (5), 1135–1147. doi:10.1016/j.immuni.2016.10.021

Dedeurwaerder, S., Desmedt, C., Calonne, E., Singhal, S. K., Haibe-Kains, B., Defrance, M., et al. (2011). DNA Methylation Profiling Reveals a Predominant Immune Component in Breast Cancers. *EMBO Mol. Med.* 3 (12), 726–741. doi:10.1002/emmm.201100801

Dyer, B. A., Feng, C. H., Eskander, R., Sharabi, A. B., Mell, L. K., McHale, M., et al. (2021). Current Status of Clinical Trials for Cervical and Uterine Cancer Using Immunotherapy Combined with Radiation. *Int. J. Radiat. Oncol. Biol. Phys.* 109 (2), 396–412. doi:10.1016/j.ijrobp.2020.09.016

Easwaran, H., Tsai, H.-C., and Baylin, S. B. (2014). Cancer Epigenetics: Tumor Heterogeneity, Plasticity of Stem-like States, and Drug Resistance. *Mol. Cel* 54 (5), 716–727. doi:10.1016/j.molcel.2014.05.015

Fu, J., Li, K., Zhang, W., Wan, C., Zhang, J., Jiang, P., et al. (2020). Large-scale Public Data Reuse to Model Immunotherapy Response and Resistance. *Genome Med.* 12 (1), 21. doi:10.1186/s13073-020-0721-z

Ghandi, M., Huang, F. W., Jané-Valbuena, J., Kryukov, G. V., Lo, C. C., McDonald, E. R., et al. (2019). Next-generation Characterization of the Cancer Cell Line Encyclopedia. *Nature* 569 (7757), 503–508. doi:10.1038/s41586-019-1186-3

Hanahan, D., and Coussens, L. M. (2012). Accessories to the Crime: Functions of Cells Recruited to the Tumor Microenvironment. *Cancer Cell* 21 (3), 309–322. doi:10.1016/j.ccr.2012.02.022

Herrero, R., González, P., and Markowitz, L. E. (2015). Present Status of Human Papillomavirus Vaccine Development and Implementation. *Lancet Oncol.* 16 (5), e206–e216. doi:10.1016/S1470-2045(14)70481-4

Janson, P. C. J., Marits, P., Thörn, M., Ohlsson, R., and Winqvist, O. (2008). CpG Methylation of the IFNG Gene as a Mechanism to Induce Immunosupression in Tumor-Infiltrating Lymphocytes. *J. Immunol.* 181 (4), 2878–2886. doi:10.4049/jimmunol.181.4.2878

Jardim, D. L., Goodman, A., de Melo Gagliato, D., and Kurzrock, R. (2021). The Challenges of Tumor Mutational Burden as an Immunotherapy Biomarker. *Cancer Cell* 39 (2), 154–173. doi:10.1016/j.ccell.2020.10.001

Jiao, Y., Widschwendter, M., and Teschendorff, A. E. (2014). A Systems-Level Integrative Framework for Genome-wide DNA Methylation and Gene Expression Data Identifies Differential Gene Expression Modules under Epigenetic Control. *Bioinformatics* 30 (16), 2360–2366. doi:10.1093/bioinformatics/btu316

Jiménez-Alcázar, M., Rangaswamy, C., Panda, R., Bitterling, J., Simsek, Y. J., Long, A. T., et al. (2017). Host DNases Prevent Vascular Occlusion by Neutrophil Extracellular Traps. *Science* 358 (6367), 1202–1206. doi:10.1126/science.aam8897

Johnston, R. J., Su, L. J., Pinckney, J., Critton, D., Boyer, E., Krishnakumar, A., et al. (2019). VISTA Is an Acidic pH-Selective Ligand for PSGL-1. *Nature* 574 (7779), 565–570. doi:10.1038/s41586-019-1674-5

Ke, X., Zhang, S., Xu, J., Liu, G., Zhang, L., Xie, E., et al. (2016). Non-small-cell Lung Cancer-Induced Immunosuppression by Increased Human Regulatory T Cells via Foxp3 Promoter Demethylation. *Cancer Immunol. Immunother.* 65 (5), 587–599. doi:10.1007/s00262-016-1825-6

Langfelder, P., and Horvath, S. (2008). WGCNA: an R Package for Weighted Correlation Network Analysis. *BMC Bioinformatics* 9, 559. doi:10.1186/1471-2105-9-559

Lee, S.-J., Yang, A., Wu, T.-C., and Hung, C.-F. (2016). Immunotherapy for Human Papillomavirus-Associated Disease and Cervical Cancer: Review of Clinical and Translational Research. *J. Gynecol. Oncol.* 27 (5), e51. doi:10.3802/jgo.2016.27.e51

Li, B., Severson, E., Pignon, J.-C., Zhao, H., Li, T., Novak, J., et al. (2016). Comprehensive Analyses of Tumor Immunity: Implications for Cancer Immunotherapy. *Genome Biol.* 17 (1), 174. doi:10.1186/s13059-016-1028-7

Lin, K., Roosinovich, E., Ma, B., Hung, C.-F., and Wu, T.-C. (2010). Therapeutic HPV DNA Vaccines. *Immunol. Res.* 47 (1-3), 86–112. doi:10.1007/s12026-009-8141-6

Mayakonda, A., Lin, D.-C., Assenov, Y., Plass, C., and Koeffler, H. P. (2018). Maftools: Efficient and Comprehensive Analysis of Somatic Variants in Cancer. *Genome Res.* 28 (11), 1747–1756. doi:10.1101/gr.239244.118

Newman, A. M., Liu, C. L., Green, M. R., Gentles, A. J., Feng, W., Xu, Y., et al. (2015). Robust Enumeration of Cell Subsets from Tissue Expression Profiles. *Nat. Methods* 12 (5), 453–457. doi:10.1038/nmeth.3337

Ogilvie, G. S., van Niekerk, D., Krajden, M., Smith, L. W., Cook, D., Gondara, L., et al. (2018). Effect of Screening with Primary Cervical HPV Testing vs Cytology Testing on High-Grade Cervical Intraepithelial Neoplasia at 48 Months. *JAMA* 320 (1), 43–52. doi:10.1001/jama.2018.7464

Piao, Y., Piao, M., Park, K., and Ryu, K. H. (2012). An Ensemble Correlation-Based Gene Selection Algorithm for Cancer Classification with Gene Expression Data. *Bioinformatics* 28 (24), 3306–3315. doi:10.1093/bioinformatics/bts602

Ritchie, M. E., Phipson, B., Wu, D., Hu, Y., Law, C. W., Shi, W., et al. (2015). Limma powers Differential Expression Analyses for RNA-Sequencing and Microarray Studies. *Nucleic Acids Res.* 43 (7), e47. doi:10.1093/nar/gkv007

Salem, A., Alotaibi, M., Mroueh, R., Basheer, H. A., and Afarinkia, K. (2021). CCR7 as a Therapeutic Target in Cancer. *Biochim. Biophys. Acta Rev. Cancer* 1875 (1), 188499. doi:10.1016/j.bbcan.2020.188499

Santos, R. F., Oliveira, L., and M. Carmo, A. (2016). Tuning T Cell Activation: The Function of CD6 at the Immunological Synapse and in T Cell Responses. *Curr. Drug Targets* 17 (6), 630–639. doi:10.2174/1389450116666150531152439

Schuyler, R. P., Merkel, A., Raineri, E., Altucci, L., Vellenga, E., Martens, J. H. A., et al. (2016). Distinct Trends of DNA Methylation Patterning in the Innate and Adaptive Immune Systems. *Cel Rep.* 17 (8), 2101–2111. doi:10.1016/j.celrep.2016.10.054

Sharma, S., Kelly, T. K., and Jones, P. A. (2010). Epigenetics in Cancer. *Carcinogenesis* 31 (1), 27–36. doi:10.1093/carcin/bgp220

Small, W., Bacon, M. A., Bajaj, A., Chuang, L. T., Fisher, B. J., Harkenrider, M. M., et al. (2017). Cervical Cancer: A Global Health Crisis. *Cancer* 123 (13), 2404–2412. doi:10.1002/cncr.30667

Smith, Z. D., and Meissner, A. (2013). DNA Methylation: Roles in Mammalian Development. *Nat. Rev. Genet.* 14 (3), 204–220. doi:10.1038/nrg3354

Sørensen, A. L., Timoskainen, S., West, F. D., Vekterud, K., Boquest, A. C., Ährlund-Richter, L., et al. (2010). Lineage-specific Promoter DNA Methylation Patterns Segregate Adult Progenitor Cell Types. *Stem Cell Develop.* 19 (8), 1257–1266. doi:10.1089/scd.2009.0309

Subramanian, A., Tamayo, P., Mootha, V. K., Mukherjee, S., Ebert, B. L., Gillette, M. A., et al. (2005). Gene Set Enrichment Analysis: a Knowledge-Based Approach for Interpreting Genome-wide Expression Profiles. *Proc. Natl. Acad. Sci. U.S.A.* 102 (43), 15545–15550. doi:10.1073/pnas.0506580102

Sun, X., Shu, Y., Xu, M., Jiang, J., Wang, L., Wang, J., et al. (2020). ANXA6 Suppresses the Tumorigenesis of Cervical Cancer through Autophagy Induction. *Clin. Transl. Med.* 10 (6), e208. doi:10.1002/ctm2.208

Wakeham, K., and Kavanagh, K. (2014). The burden of HPV-Associated Anogenital Cancers. *Curr. Oncol. Rep.* 16 (9), 402. doi:10.1007/s11912-014-0402-4

Wendel Naumann, R., and Leath, C. A. (2020). Advances in Immunotherapy for Cervical Cancer. *Curr. Opin. Oncol.* 32 (5), 481–487. doi:10.1097/CCO.0000000000000663

Wright, J. D., Matsuo, K., Huang, Y., Tergas, A. I., Hou, J. Y., Khoury-Collado, F., et al. (2019). Prognostic Performance of the 2018 International Federation of Gynecology and Obstetrics Cervical Cancer Staging Guidelines. *Obstet. Gynecol.* 134 (1), 49–57. doi:10.1097/AOG.0000000000003311

Yang, Y., Wang, Q., Song, D., Zen, R., Zhang, L., Wang, Y., et al. (2020). Lysosomal Dysfunction and Autophagy Blockade Contribute to Autophagy-Related Cancer Suppressing Peptide-Induced Cytotoxic Death of Cervical Cancer Cells through the AMPK/mTOR Pathway. *J. Exp. Clin. Cancer Res.* 39 (1), 197. doi:10.1186/s13046-020-01701-z

Yang, C., Huang, X., Li, Y., Chen, J., Lv, Y., and Dai, S. (2021). Prognosis and Personalized Treatment Prediction in TP53-Mutant Hepatocellular Carcinoma: an In Silico Strategy towards Precision Oncology. *Brief Bioinform.* 22 (3), bbaa164. doi:10.1093/bib/bbaa164

Yoshihara, K., Shahmoradgoli, M., Martínez, E., Vegesna, R., Kim, H., Torres-Garcia, W., et al. (2013). Inferring Tumour Purity and Stromal and Immune Cell Admixture from Expression Data. *Nat. Commun.* 4, 2612. doi:10.1038/ncomms3612

Zhao, C., Inoue, J., Imoto, I., Otsuki, T., Iida, S., Ueda, R., et al. (2008). POU2AF1, an Amplification Target at 11q23, Promotes Growth of Multiple Myeloma Cells by Directly Regulating Expression of a B-Cell Maturation Factor, TNFRSF17. *Oncogene* 27 (1), 63–75. doi:10.1038/sj.onc.1210637

Conflict of Interest: The authors declare that the research was conducted in the absence of any commercial or financial relationships that could be construed as a potential conflict of interest.

Publisher's Note: All claims expressed in this article are solely those of the authors and do not necessarily represent those of their affiliated organizations or those of the publisher, the editors, and the reviewers. Any product that may be evaluated in this article, or claim that may be made by its manufacturer, is not guaranteed or endorsed by the publisher.

frontiers | Frontiers in Molecular Biosciences

ORIGINAL RESEARCH
published: 10 May 2022
doi: 10.3389/fmolb.2022.861380

Identification of TRP-Related Subtypes, Development of a Prognostic Model, and Characterization of Tumor Microenvironment Infiltration in Lung Adenocarcinoma

*Sibo Sun, Yu Wang, Min Li and Jianqing Wu**

Department of Geriatrics, The First Affiliated Hospital of Nanjing Medical University, Nanjing, China

The TRP (transient receptor potential) superfamily, as cation channels, is a critical chemosensor for potentially harmful irritants. Their activation is closely related not only to tumor progression and prognosis but also to tumor therapy response. Nevertheless, the TRP-related immune gene (TRIG) expression of the tumor microenvironment (TME) and the associations with prognosis remain unclear. First, we represented the transcriptional and genetic variations in TRIGs in 535 lung adenocarcinoma (LUAD) samples as well as their expression patterns. LUAD samples were divided into two distinct subtypes based on the TRIG variations. Significant differences had been found in prognosis, clinical features, and TME cell-infiltration features between the two subtypes of patients. Second, we framed a TRIG score for predicting overall survival (OS) and validated the predictive capability of the TRIG score in LUAD patients. Accordingly, to enhance the clinical applicability of TRIG score, we developed a considerable nomogram. A low TRIG score, characterized by increased immunity activation, indicated favorable advantages of OS compared with a high TRIG score. Furthermore, the TRIG score was found to have a significant connection with the TME cell-infiltration and immune checkpoint expressions. Our analysis of TRIGs in LUAD showed their potential roles in prognosis, clinical features, and tumor-immune microenvironments. These results may advance our knowledge of TRP genes in LUAD and show a new light on prognosis estimation and the improvement of immunotherapy strategies.

Keywords: TRP superfamily, lung adenocarcinoma, tumor-immune microenvironment, overall survival, immunotherapy

OPEN ACCESS

Edited by:
Na Luo,
Nankai University, China

Reviewed by:
Emanuele Giurisato,
University of Siena, Italy
Maria Beatrice Morelli,
University of Camerino, Italy

****Correspondence:***
Jianqing Wu
jwuny@njmu.edu.cn

Specialty section:
This article was submitted to Molecular Diagnostics and Therapeutics, a section of the journal Frontiers in Molecular Biosciences

Received: *24 January 2022*
Accepted: *30 March 2022*
Published: *10 May 2022*

Citation:
Sun S, Wang Y, Li M and Wu J (2022) Identification of TRP-Related Subtypes, Development of a Prognostic Model, and Characterization of Tumor Microenvironment Infiltration in Lung Adenocarcinoma. Front. Mol. Biosci. 9:861380. doi: 10.3389/fmolb.2022.861380

INTRODUCTION

The TRP (transient receptor potential) superfamily of cation channels, at the very beginning, plays a crucial role in sensory physiology (Venkatachalam and Montell 2007). Mainly regulated by temperature, osmotic pressure, pH values, mechanical force, some endogenous and exogenous ligands, and intracellular signal molecules (Vay et al., 2012), TRP channels have been found to be expressed and functioned in smooth muscle cells of the bronchi, the pulmonary epithelium, the

vasculature, and pulmonary endothelial cells (Taylor-Clark 2016). Nowadays, TRP channels receive potentially harmful irritants in addition to receiving sensory stimulation (Steinritz et al., 2018). When exposed to toxic matters, chemosensory TRP channels, as an important chemosensor for potentially harmful irritative substances, participate in cellular defense mechanisms, thereby affecting cell survival by regulating apoptosis. Toxic inhaled substances involved in lung cancer, such as acrolein, nicotine, nitric oxide, and other components in cigarette smoke, are recognized as TRP channel activators. They further activate *Akt* and *MAPK* signaling pathways through TRP channels (Buch et al., 2018). Also, increased cellular resistance to oxidative stress in lung cancer spheroids is linked to the high expression of *TRPA1*, which is a member of the TRP family (Takahashi et al., 2018).

As the primary subtype of lung cancer, non-small-cell lung cancer (NSCLC) constitutes over 80% of all lung cancers, with lung adenocarcinoma (LUAD) as its primary histological subtype. Despite clinical applications of targeted therapy and immunotherapy, the 5-year overall survival (OS) of LUAD patients remains at 16% as usual (Wood et al., 2016; Bray et al., 2018). Importantly, immunotherapies, whose responses are often durable and come with light toxicity in most people, are now given importance in cancer. However, the responses from people with similar tumors can vary considerably (Zou et al., 2016). Therefore, developing specific prognostic methods for LUAD patients is vital in finding new therapeutic targets so as to improve survival and quality of life. The TRP channel, *TRPV3*, is reported to be overexpressed on NSCLC tissues, compared with para-carcinoma lung tissues. In addition, the overexpression of *TRPV3* is associated with worse survival (Li et al., 2016), and its Ca2+ signaling is important to T-cell activation and differentiation (Majhi et al., 2015). However, there is a lack of studies regarding the impact of the TRP family on immunity and the prognostic potential for LUAD patients.

In this study, we obtained a comprehensive intratumoral immune landscape by fully assessing the expression of TRP channels. First, 21 TRP genes were extracted by gene differential expression analysis between LUAD and normal lung tissues. A total of 535 LUAD patients were divided into two subtypes according to these differentially expressed TRP genes. Second, patients were then stratified into two risk groups according to differentially expressed genes (DEGs) and differentially expressed immunity genes (DEIGs) based on the two TRP-related subtypes. Finally, a nomogram was set up to characterize the immune infiltration and predict OS of LUAD, which might prognose patient responses to immunotherapy and outcomes.

MATERIALS AND METHODS

Datasets

The RNA sequencing (RNA-seq) data of 59 normal human lung samples, along with 535 LUAD patients and their clinical information, were obtained from The Cancer Genome Atlas (TCGA) database, https://portal.gdc.cancer.gov/. We obtained the validation cohort RNA-seq data and clinical features from the Gene Expression Omnibus (GEO) database, https://www.ncbi.nlm.nih.gov/geo/ (ID: GSE3141, GSE31210, GSE30219, GSE37745). Patients lacking survival information were eliminated for further analysis.

Identification of Differentially Expressed TRP Genes

A total of 28 TRP genes were selected from prior reviews (Venkatachalam and Montell 2007). Before comparison, we normalized the TCGA data to fragment per kilobase million (FPKM) values and identified 21 differentially expressed TRP genes by the "limma" package with a p value <0.05. The "maftools" package was used to show the mutation landscape. A PPI (Protein–protein Interaction) network of the 21 TRP genes was formed into Search Tool for the Retrieval of Interacting Genes (STRING), version 11.0. https://string-db.org/ [Accessed 30 July, 2021].

Development of the TRP-Related Gene Molecular Subtypes

Consensus unsupervised subtyping analysis was applied to sort the LUAD samples out into two distinct subtypes by R package "ConsensusClusterPlus" based on TRP gene expression. To identify the clinical value of the two subtypes, we used the Kaplan–Meier analysis to draw the survival curve by "survival" and "survminer" R packages. The Log-rank test was applied to compare the difference between the survival curves. To investigate the differences in the two TRP-related gene subtypes in biological processes, gene set variation analysis (GSVA) was performed with the hallmark gene set (c2.cp.kegg.v7.2) derived from the MSigDB database. We assess the immune, stromal, and estimate scores and the fractions of 22 human immune cell subsets of LUAD patients by the Estimation of STromal and Immune cells in MAlignant Tumour tissues using Expression data (ESTIMATE) and the CIBERSORT algorithm. In addition, the ingle-sample gene set enrichment analysis (ssGSEA) algorithm was used to determine the levels of immune cell infiltration in the tumor microenvironment (TME).

Development and Validation of the Prognostic TRIG Score

A total of 2,483 immune genes were obtained from the ImmPort Resorce website, https://www.immport.org/shared/genelists. DEGs and DEIGs between the two TRP-related gene molecular subtypes were obtained by the R "limma" package ($|\log2FC| \geq 1$ and FDR < 0.05). The TRP-related immune genes (TRIGs) between DEGs and DEIGs based on TRP-related subtypes assessed by the R "Venn" package were applied to estimate the prognostic features. The least absolute shrinkage and selection operator (LASSO)-Cox regression analysis was used to consider the kernel prognostic TRIGs by the R "glmnet" package. Also, the penalty parameter (λ) value was filtered by

the lowest partial likelihood deviance with 10-fold cross-validation. The TRIG score for patients was calculated by the following formula:

Risk score = (−0.00384*CCL17 expression) + (−0.20651*CD40LG expression) + (−0.09076*CIITA expression) + (0.095940*STC1 expression) + (−0.01538*SCGB3A1 expression) + (−0.13689* GDF10 expression).

We divided the TCGA LUAD samples into two groups via the median risk scores and compared OS time through Kaplan–Meier analysis. Principal component analysis (PCA) and the t-distributed stochastic neighbor embedding (t-SNE) algorithm were assessed respectively by the "prcomp" function in the "stats" and "Rtsne" R package. The "time-ROC", "survival", and "survminer" R packages were applied to perform the time-dependent receiver operating characteristic (ROC) curve analysis.

To validate this prognostic TRIG score, we employed four LUAD GEO cohorts (GSE31210, GSE3141, GSE30219, and GSE37745). TRIG expressions were normalized by the "scale" function. Then, we calculated TRIG scores through the exact formula before. In these four GEO datasets, samples were separated into two risk groups for comparison to validate the TRIG score.

Clinical Associations and Stratification Analyses of the TRP-Related Prognostic Model

Univariate and multivariable Cox regression models are used to assess the distinctive character of the TRIG score and clinical features (age, gender, and TNM stage). Moreover, we used the stratified analysis to identify whether the TRIG score was able to maintain the predictive capability in distinct groups (age, gender, and TNM stage).

According to these TRIGs, we estimated the content of tumor-infiltrating immune cells (TIICs) in TME and explored the correlations between the six genes in the TRIG score and portions of 22 TIICs as well as the differential immune checkpoint expression levels between low- and high-risk groups by boxplots.

Foundation and Validation of a Nomogram

A predictive nomogram was formed by extracting clinical features along with TRIG score in accordance with the results of the independent prognosis analysis, and then, time-dependent ROC curves for 1-, 3-, and 5-year survivals were applied to estimate the nomogram. Moreover, we also used calibration plots to show the prognostic value between the 1-, 3-, and 5-year survivals predicted by the nomogram and clinical results.

Statistical Analyses

We used the Mann–Whitney test to compare the immune cell infiltration and immune checkpoints expression between the two groups. R version 4.1.0. Statistical significance was set at $p < 0.05$ in all statistical analyses.

RESULTS

Expression Variations and Genetic Changes of TRP Genes in LUAD

The expression levels of the 28 TRP genes (TRPs) were compared with The Cancer Genome Atlas (TCGA) data from 59 normal lung tissues and 535 tumor tissues, and 21 differentially expressed TRP genes were identified ($p < 0.01$). The RNA expressions of these differentially expressed TRP genes were shown with heatmaps (**Figure 1A**, red: high expression; blue: low expression). Meanwhile, 21 TRP gene mutations were presented in 211 of the 535 samples (about 39.4%) at the genetic

expression level. *TRPA1* and *TRPC4* displayed the highest mutation frequency (**Figure 1B**). Copy number variations (CNVs) of all the 21 TRP genes were detected, and most TRP genes were gathered on copy number amplification (**Figure 1C**). Alterations of the 21 TRP genes with CNVs on the chromosome were also identified (**Figure 1D**). To explore the interactions of 21 TRP genes, a protein–protein interaction (PPI) analysis was conducted (**Figure 1E**). The value of 0.9 (the highest confidence) was set as the minimum required interaction score of the PPI analysis. *TRPC1*, *TRPC3*, *TRPC4*, *TPRC6*, *TRPM2*, and *TRPM3* were considered as hub genes. The correlation network of the 21 TRP genes was also detected (**Figure 1F**, red: positive correlations; blue: negative correlations). The results indicated that CNV changes might lead to abnormal gene expression. Also, the expression levels of TRP genes were linked with LUAD, suggesting that they might consider different characteristics in patients.

Identification of Two Subtypes of LUAD Based on the 21 TRP Genes

Considering the important functions of the TRP family, we conducted the consensus clustering of the 535 LUAD samples based on the TRP family to explore new biological functions. We increased the clustering variable (κ) from 2 to 9 and found that when κ = 2, the intergroup correlations were the lowest and intragroup correlations were the highest, indicating that the 535 LUAD patients could be compartmentalized into two subtypes according to the 21 TRP genes (**Figure 2A**). Between the two subtypes, most TRP gene expression levels were higher in subtype 1 (**Supplementary Figure S1**). Meanwhile, survival benefit of subtype 1 was higher than that of subtype 2 (HR = 1.53, 95% CI: 1.32–2.05. **Figure 2B**). We presented a heatmap of the gene expression profile, along with the clinical features. High expression levels of most TRP genes were identified in subtype 1. Also, subtype 1 was found to have a lower degree of tumor invasion, lymph node metastasis, and distant metastasis. Also, clearly, subtype 2 represented a later stage compared with those in subtype 1. Furthermore, most TRP gene expression levels were higher in subtype 1 (**Figure 2C**). We performed GSVA enrichment analysis to consider the variations in biological behavior between these two subtypes (**Figure 2D**). Subtype 1, compared with subtype 2, demonstrated the enrichment in respect of pathways linked with activation of the immune

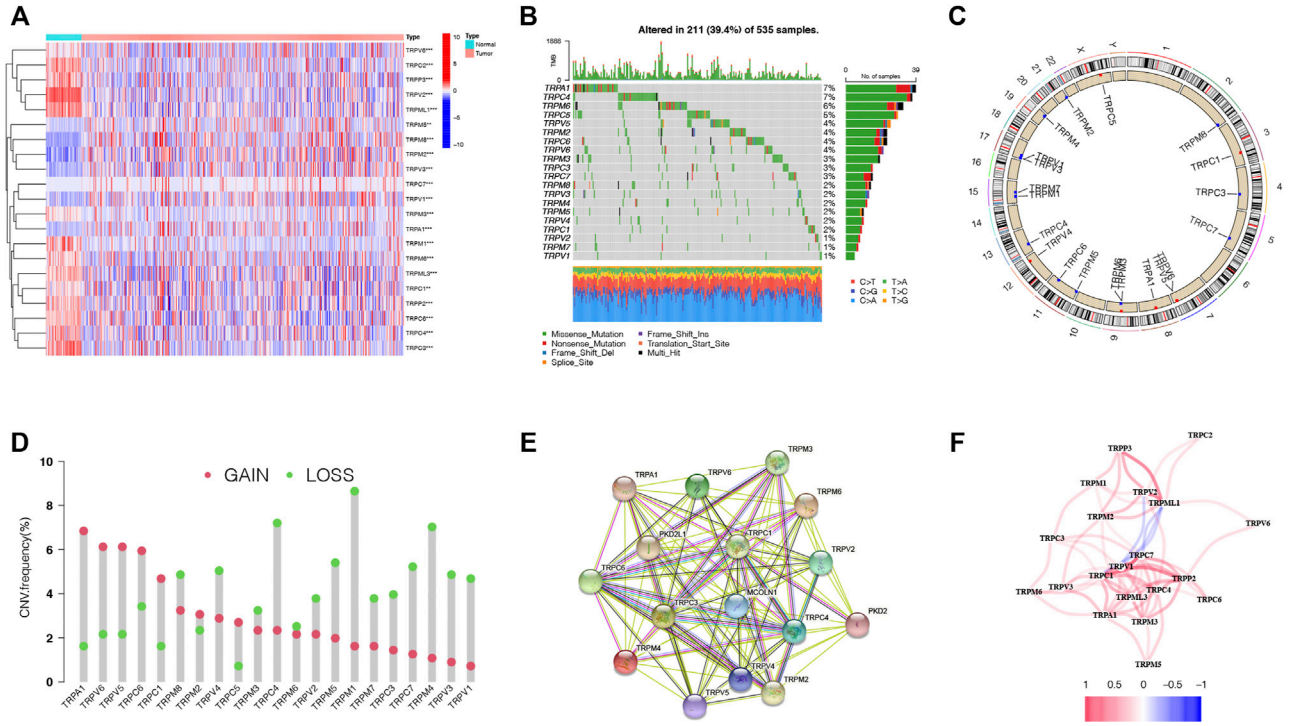

FIGURE 1 | Expressions and correlations of 28 TRP genes in LUAD. **(A)**. Heatmap (red: high expression; blue: low expression) of the TRP genes between normal lung tissues (N, blue) and LUAD tissues (T, red). *p* values were demonstrated as $^{**}p < 0.01$; $^{***}p < 0.001$. **(B)**. Mutation frequencies of TRP genes in LUAD patients from the TCGA cohort. **(C)**. Locations of CNV variations in TRP genes on 23 chromosomes. **(D)**. Frequencies of CNV, non-CNV and gain and loss CNV, among TRP genes. **(E).** PPI network demonstrating the interactions of the TRP genes (interaction score = 0.9). **(F)**. TRP gene correlation network (red string: positive correlation; blue string: negative correlation. The shades of the colors represent the correlation strength).

system (Barclay 2003; Lord et al., 2003; Olivier et al., 2005; Akdis et al., 2016). The results revealed that the two subtypes could be distinguished by the 21 TRP genes, and the lower survival advantage of subtype 2 is mainly related to disorders of the immune system.

TME Infiltration of the Two TRP-Related Subtypes

To explore the immunological features of the two subtypes, 535 LUAD samples of the TCGA cohort were analyzed by ssGSEA analysis with 29 immune gene sets. The TME is considered as the complex multicellular environment in tumor development. It comprises immune cells, including T- and B-lymphocytes, tumor-associated macrophages (TAMs), dendritic cells (DCs), natural killer (NK) cells, neutrophils, myeloid-derived suppressor cells (MDSCs), stromal cells, the extracellular matrix (ECM) and other secreted molecules, and the blood and lymphatic vascular networks (Junttila and de Sauvage 2013). Between them, the immune cells in the TME play vital roles in possessing tumor-antagonizing or tumor-promoting functions (Quail and Joyce 2013).TME features of these two subtypes were identified using the ESTIMATE algorithm. The outcomes demonstrated that subtype 1 had higher expressions of all TME scores, while subtype 2 had lower expressions of these scores (Wilcox test, $p < 0.001$) (**Figure 3A**). Next, we explored immune cell infiltrations by implementing the CIBERSORT algorithm. Subtype 1 showed the enrichment of the activated innate immune cell infiltration, comprising the presence of CD8 T and activated CD4 cells, M1 macrophages, memory B-cells, and resting dendritic cells, thus meeting a significant survival benefit. Subtype 2 was abundant with naive B-cells, plasma cells, M0 macrophages, and activated dendritic cells (**Figure 3B**). We drew to the conclusion that these two subtypes had entirely different human leukocyte antigen (HLA) infiltration characteristics. HLAs are highly polymorphic alloantigens that encode the product of a gene cluster encoding the human major histocompatibility complex (MHC) (D.S. Chen and Mellman 2017). Neoantigens produced by tumors must first be presented on HLAs and recognized by peptide-specific receptors. Then, HLAs and the peptide-specific receptors form the MHC-antigen peptide-specific receptor complex, participating in regulating the immune response of the body (Kalaora et al., 2021). All the HLA gene expression levels were significantly higher in subtype 1 but lower in subtype 2 (Wilcox test, $p < 0.05$), indicating that subtype 1 was inclined to generate protective immunity (D.S. Chen and Mellman 2017) (**Figure 3C**). Besides, to presume the tumor purity of the two subtypes, TME scores (stromal score, immune score, and estimate score) of the two subtypes were investigated through the ESTIMATE package.

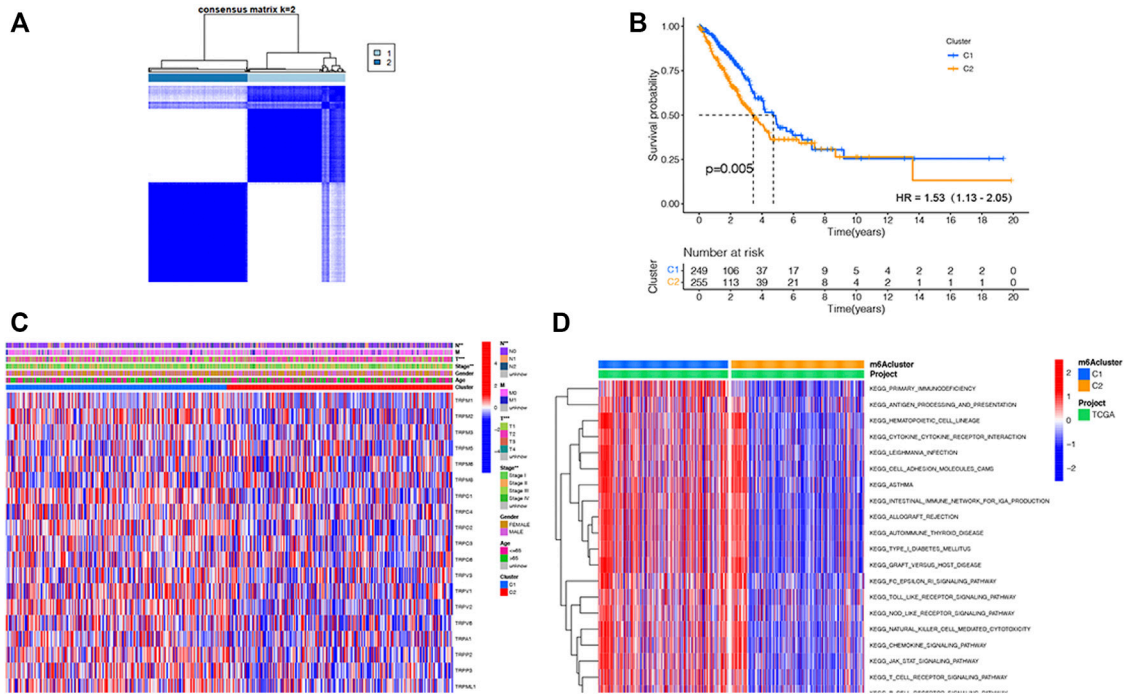

FIGURE 2 | TRP-related subtypes and their clinicopathological features and biological pathways. **(A)**. Consensus matrix heatmap identifying two subtypes ($\kappa = 2$). **(B)**. Kaplan–Meier OS curves of the two subtypes. **(C)**. Variations in clinicopathologic characteristics and TRP gene expression levels between the two distinct subtypes. **(D)**. Biological pathways to two distinct subtypes *via* GSVA (red: activated pathways; blue: inhibited pathways).

For TME scores, the higher stromal scores or immune scores, the higher contents of stromal cells or immunocytes in the TME, and estimated scores represented the comprehensive scores of stromal or immune scores in the TME (Han et al., 2022; W.; Chen et al., 2021) (**Figure 3D**). Our outcomes proved that subtype 1 possessed higher TME scores.

Development of a Prognostic TRIG Score in the TCGA Cohort

Based on those two TRP-related subtypes, we explored the features of tumor-immune interactions and their prognostic potential for LUAD samples. First, 1,469 DEGs were identified with the two subtypes (**Figure 4A**). Subsequently, 1,793 genes were considered as DEIGs according to the ImmPort database (**Figure 4B**). The 367 intersect genes between DEGs and DEIGs were applied to estimate the prognostic features (**Figure 4C**). In order to build a prognostic TRIG score to evaluate each patient, we extracted six of the 367 TRP-related genes by utilization of the LASSO-Cox regression model along with a minimum of λ (**Figures 4D,E**). The formula was identified as follows: risk score = (−0.00384**CCL17* expression) + (−0.20651**CD40LG* expression) + (−0.09076**CIITA* expression) + (0.095940**STC1* expression) + (−0.01538**SCGB3A1* expression) + (−0.13689**GDF10* expression). We used the formula to calculate the median score, according to which two risk groups were then separated from 535 patients (**Figure 5A**). Dimensionality reduction algorithms of PCA (**Figure 5B**) and t-SNE (**Figure 5C**) were used to show discernible dimensions between the low- and high-TRIG-score groups. PCA and t-SNE analysis revealed significant differences between the two subtypes. We performed survival analysis for two risk groups by Kaplan–Meier curves. The high-risk group showed a poorer survival time than the low-risk group (HR = 1.63, 95% CI: 1.21–2.21. **Figure 5D**). We identified a significant variation in survival times and survival statuses of the two groups by the Kaplan–Meier curves. The distribution plot of the risk of TRIG score demonstrated that the survival times decreased, while mortality increased with an increased TRIG score ($p < 0.001$, **Figure 5E**). In addition, we used time-dependent ROC analysis to estimate the predictive efficacy of the TRIG score. The area under the ROC curve (AUC) reached 0.671 for 1-year survival, 0.660 for 2-year survival, and 0.630 for 3-year survival (**Figure 5F**).

Validation of the Prognostic TRIG Score in the GEO Cohorts

Aiming to confirm the reproducibility and stability of prognostic TRIGs of LUAD, we derived the TRIG expression levels and LUAD samples' clinical record from four independent LUAD cohorts from GEO databases (GSE3141, GSE31210, GSE30219, and GSE37745). We calculated the LUAD patients' TRIG scores in the four GEO databases by the median risk score gained before. Kaplan–Meier survival analysis demonstrated that the OS in the low-risk group was significantly better than that of the high-risk group of the four GEO databases (HR = 3.37, 95% CI: 1.69–6.71.

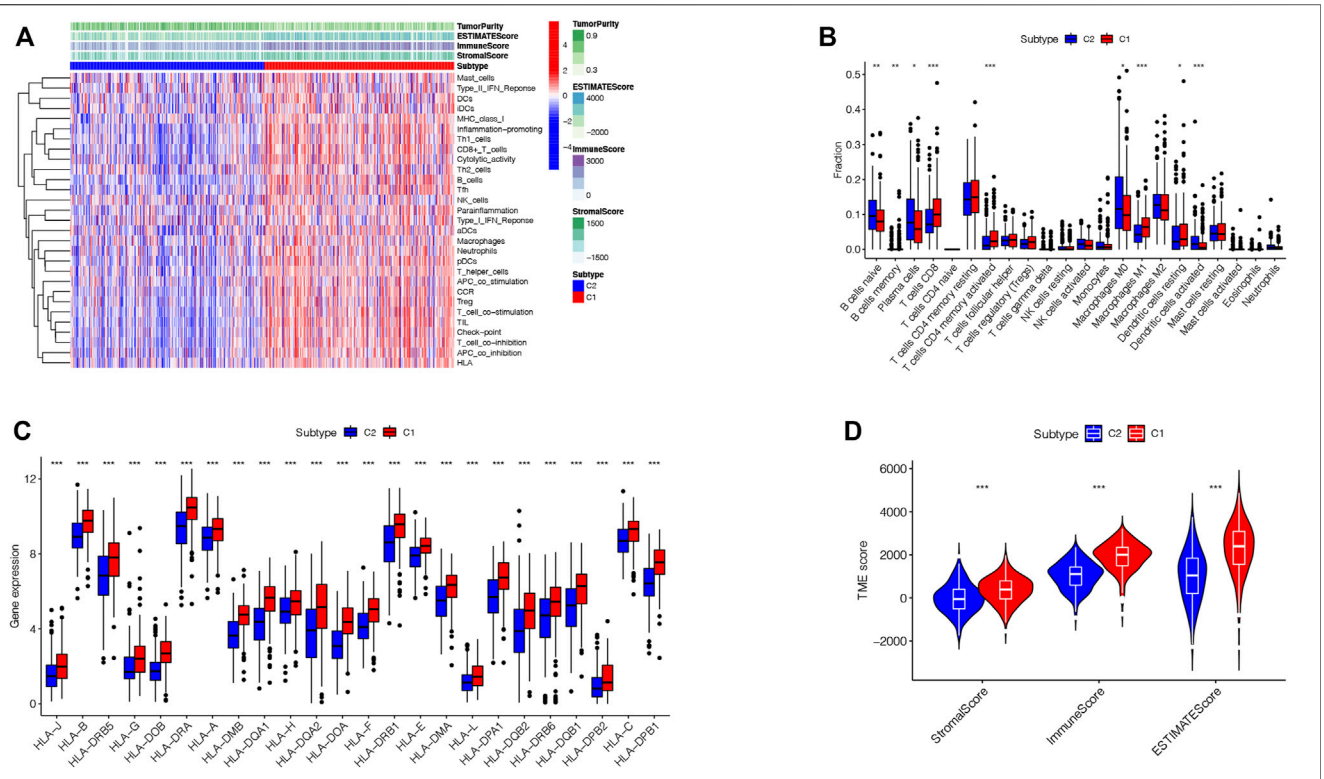

FIGURE 3 | TME infiltration in two subtypes. **(A).** Immunological characteristics of the two subtypes. **(B)**. Correlations of the immune cell infiltration level between two subtypes. **(C)**. Correlations of HLA gene expression level between two subtypes (*$p < 0.05$, **$p < 0.01$, ***$p < 0.001$). **(D)**. Correlations of Stromal-score, Immune-score, ESTIMATE-Score, and TME score between two subtypes.

Figure 6A; HR = 2.05, 95% CI: 1.08–3.87. **Figure 6B**; HR = 1.92, 95% CI: 1.39–2.63. **Figure 6C**; HR = 1.72, 95% CI: 1,14–2.59. **Figure 6D**). Meanwhile, ROC curve analysis made clear that the prognostic TRIG score had good predictive efficacy (**Figures 6E–H**).

Independent Prognostic Value of the Prognostic TRIG Score

In the TCGA cohort, the univariate Cox regression analysis showed that the TRIG score was a prognostic factor for LUAD patients (HR = 3.213, 95% CI: 2.003–5.154. **Figure 7A**). Meanwhile, the multivariate analysis indicated that the TRIG score was an independent factor of survival prediction (HR: 3.008, 95% CI: 1.813–4.990. **Figure 7B**). We still estimated the relationship between TRIG score and clinical traits, including age, gender, and TNM stage in the TCGA cohort (**Figures 7C–H**). All these clinical features, except instance metastasis, were linked with TRIG score. The results indicated that advanced LUAD samples had a higher TRIG score than early LUAD samples. Together, these outcomes indicated that the TRIG score was positively associated with tumor stages, suggesting that TRIG score showed the potential as a clinical indicator to assess the LUAD patient survival rates.

Interrelation of the TRIG Score and Immune Activity

We investigate the variations in the gene functions as well as pathways between the two risk groups. The outcomes of Gene Ontology (GO) enrichment analysis and Kyoto Encyclopedia of Genes and Genomes (KEGG) pathway analysis based on 367 TRIGs demonstrated that TRIGs were mainly linked with the immune response, chemokine-mediated signaling pathways, and inflammatory cell chemotaxis (**Figures 8A,B**). Next, we explored the correlations between the TRIG score and immune cell infiltration, TMB (tumor mutational burden), tumor transcription factors (TFs), and immune checkpoints. On one hand, we explored the correlations between the prognostic TRIG score and the enrichment of TIICs by the Pearson correlation analysis, which referred to the infiltrating immune cells that could be isolated from the tumor tissue when immune cells moved from the blood to the tumor tissue. The infiltration of immune cells in tumors was closely related to clinical prognosis, and immune cells infiltrated in tumors were most likely to serve as immunotherapy targets (Domingues et al., 2016). We found that most TIICs were linked with the six genes (**Figure 8C**). On the other hand, we extracted immune checkpoint genes from prior reviews (Kraehenbuehl et al., 2022; He and Xu 2020; Pardoll 2012) to evaluate their relationships with the TRIG score with the purpose of investigating whether the TRIG score was able to

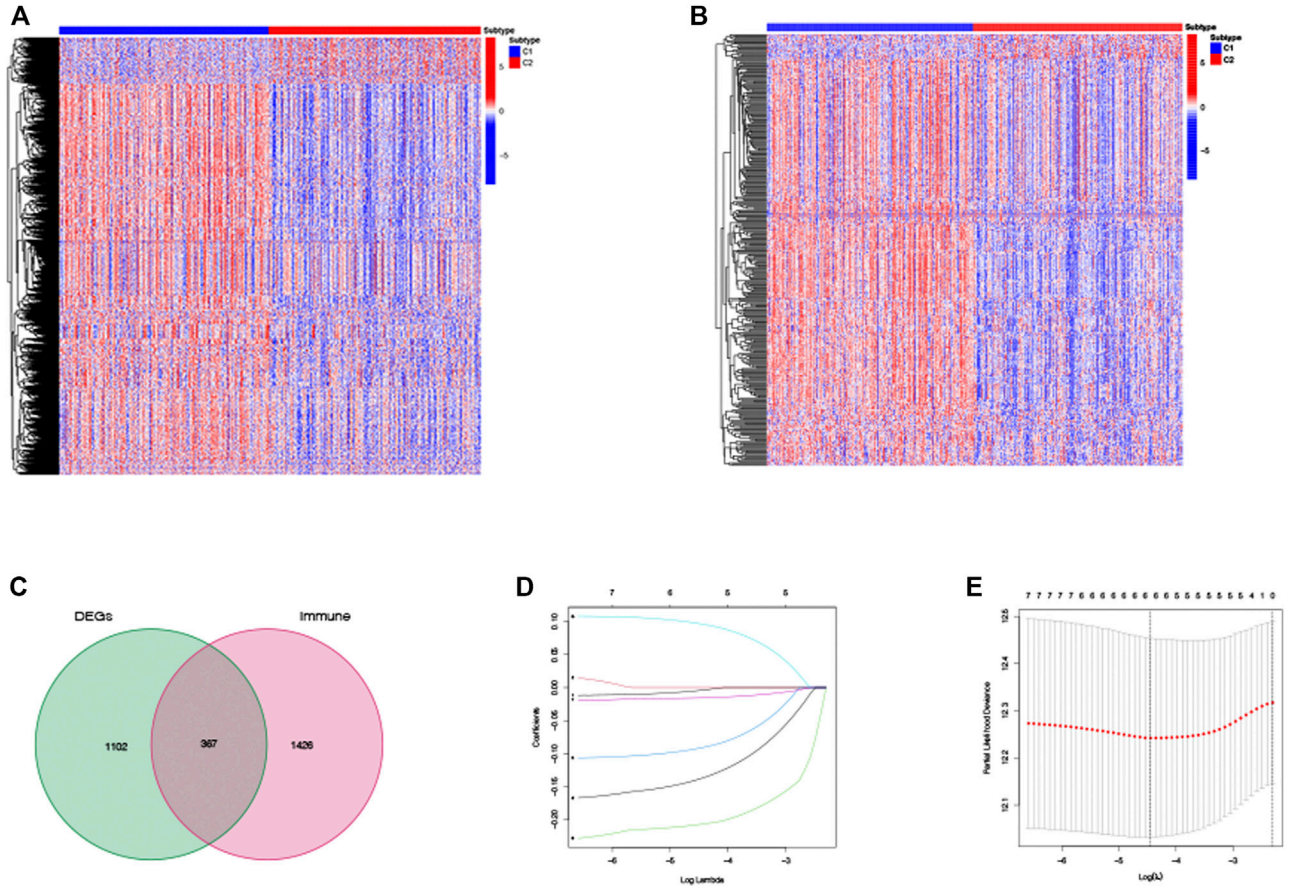

FIGURE 4 | DEG and DEIG expressions and establishment of the prognostic TRIG score in the TCGA cohort. **(A,B)**. Heatmaps of DEGs and DEIGs between two subtypes. **(C)**. TRIGs between two subtypes. **(D)**. LASSO regression of the six TRIGs. **(E)**. Cross-validation of parameter selection of the LASSO regression.

predict the benefits of immune checkpoint inhibitors of LUAD patients via the CIBERSORT algorithm. The results demonstrated that besides *CD276*, all the immune checkpoint expressions were negatively linked with the TRIG score (**Figure 8D**), indicating that TME suppression might be linked with the poor prognosis of high-TRIG patients. TMB was defined as the total number of somatic gene coding errors, base substitutions, and gene insertion or deletion errors detected per megabase and is considered as a biomarker for evaluating the efficacy of PD-1 antibody therapy (Cristescu et al., 2018). Based on the Kruskal–Wallis rank-sum test, the "ggpubr" package in the R language was run to explore the relationship between TMB score and risk groups. We found that the high-risk group showed higher TMB, compared with the low-risk group (**Figure 8E**). We combined the TRIG score and TMB to improve the efficiency of predictive prognosis and stratified all the patients into high TMB/low-risk, high TMB/high-risk, and low TMB/high-risk groups. Significant differences were detected among four groups (Log-rank test, $p < 0.001$). TMB was considered to be a biomarker that could predict the immune checkpoint inhibitors' efficacy, and immune checkpoint inhibitors were proved to be more efficient in the TMB-high subgroup in LUAD (Sha et al., 2020), consistent with our findings that patients in the low TMB/high-risk group showed the worst prognosis compared to the high TMB/high-risk group. There was no significant difference between high TMB/high risk and low TMB/low risk (**Figure 8F**). To explain the role of the immune molecule regulatory network in the process of LUAD, we assessed the relationships between LUAD development-related TFs and the six TRIGs. TFs related to tumorigenesis and the development of LUAD were obtained from the CISTROME project. Then, we extracted the differentially expressed TFs from the intersect genes between DEGs and DEIGs and used Pearson's correlation coefficient analysis to construct the regulatory network of the TFs and the six TRIGs. $|r| > 0.3$ and FDR < 0.01 were set as the cutoffs for a significant correlation. Four of six TRIGs were linked with the corresponding 19 TFs (**Figure 8G**). Therefore, it is reasonable to conclude that immune cell infiltration was significantly linked with the TRIG scores, which might affect the LUAD patient prognosis.

Advancement of a Nomogram to Predict Survival

Finally, we formed a nomogram to expand the scope of the TRIG score clinical application in predicting OS in LUAD

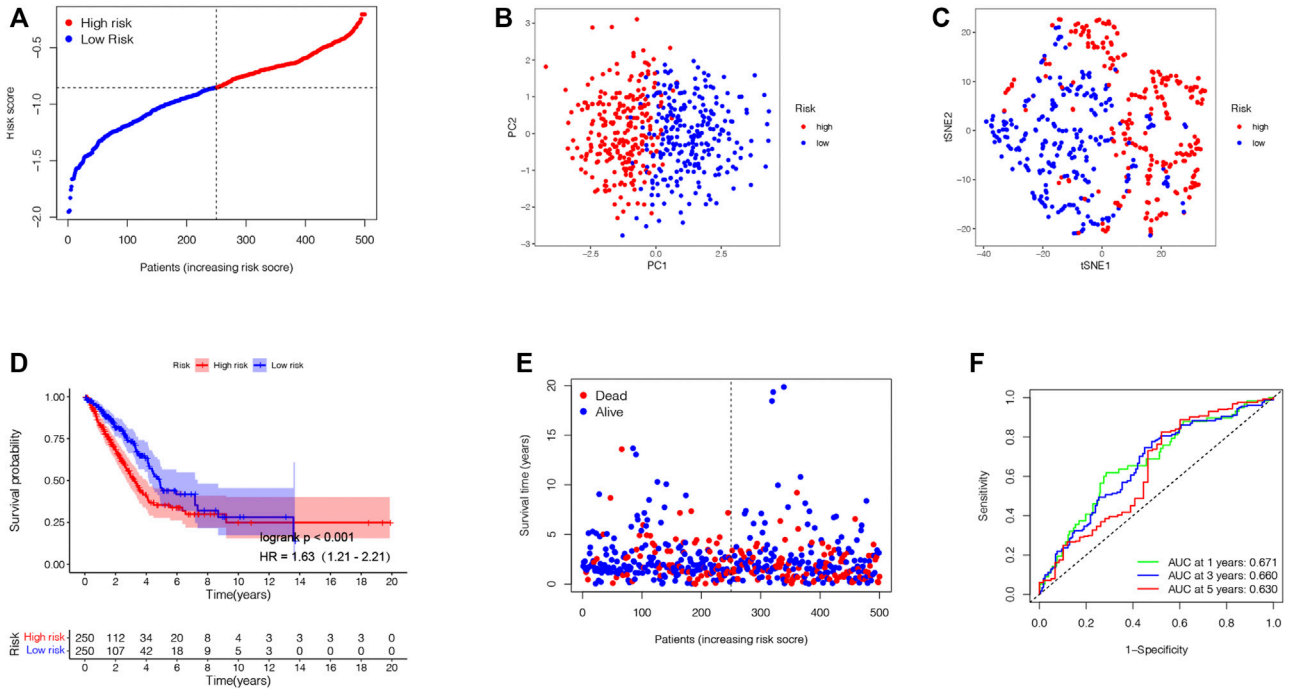

FIGURE 5 | Establishment of the prognostic TRIG score in the TCGA cohort. **(A)**. Spread of survival status and risk scores of the TCGA cohort. **(B,C)**. Variations in the distribution of different TRIGs risk groups. **(D)**. Kaplan–Meier survival curve of OS of LUAD samples in the high- and low-risk groups. **(E)**. Survival status for each patient in low-risk and high-risk populations. **(F)**. AUC of time-dependent ROC curves showed the predictive efficiency of the TRIG score.

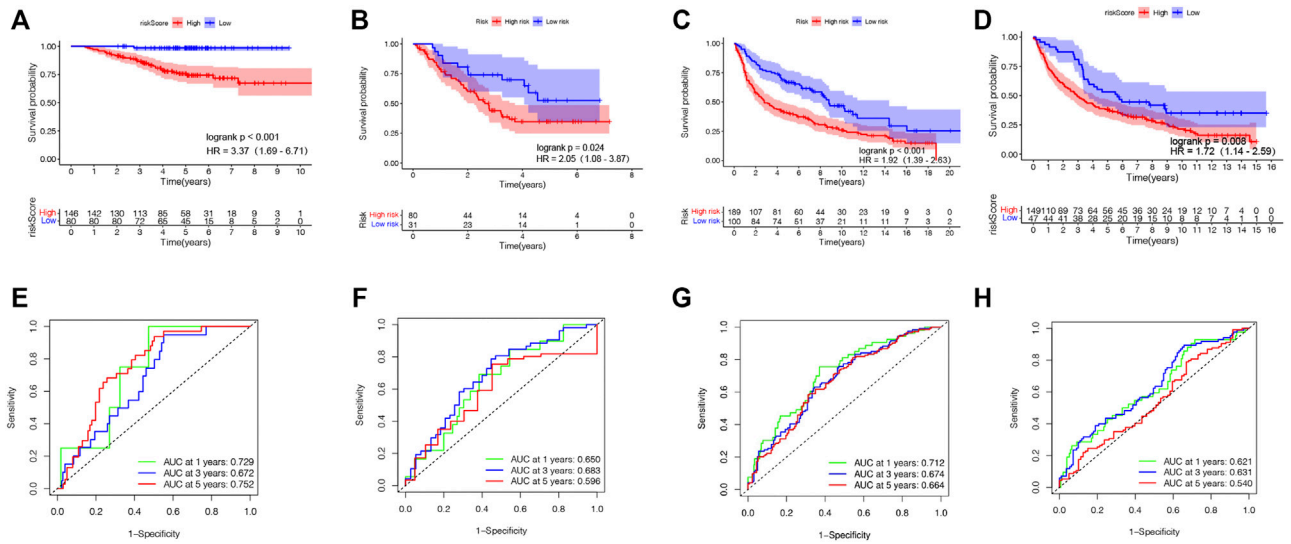

FIGURE 6 | Validation of the prognostic TRIG score in various GEO cohorts of LUAD. **(A-D).** Kaplan–Meier survival curves of OS in four GEO cohorts. **(E-H).** Time-dependent ROC curves for four GEO cohorts. **(A,E)**. GSE31210 (*n* = 226). **(B,F)**. GSE3141 (*n* = 111). **(C,G).** GSE30219 (*n* = 289). **(D,H)**. GSE37745 (*n* = 196).

patients (**Figure 9A**). According to the gender, age, risk ("low risk" represented "low TRIG score"; "high risk" represented "high TRIG score"), and stage, the total point values of every patient were calculated by prognostic parameters. With the increase of the patient total points, the clinical prognosis became worse. The ROC curve supported the good predictive value of the nomogram (**Figure 9B**). Moreover, the calibration plot indicated that the nomogram had a similar performance compared with an ideal model (**Figure 9C**).

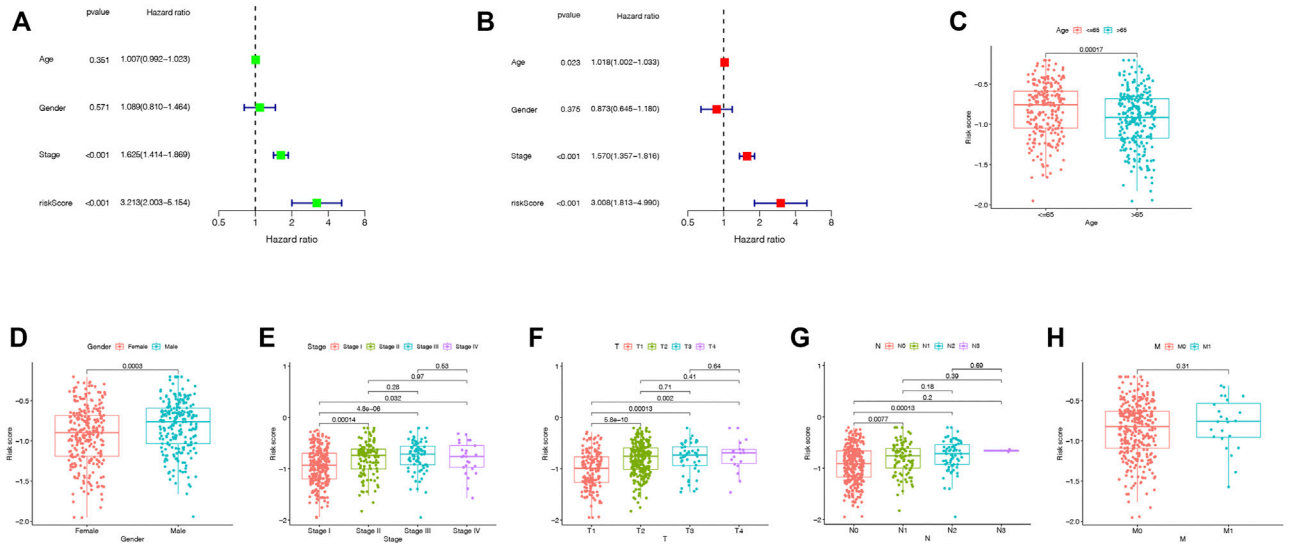

FIGURE 7 | (A,B). Univariate and multivariate Cox regression analysis of the prognostic TRIG score in the TCGA cohort. **(C-H)**. Connections between clinical features and the risk groups.

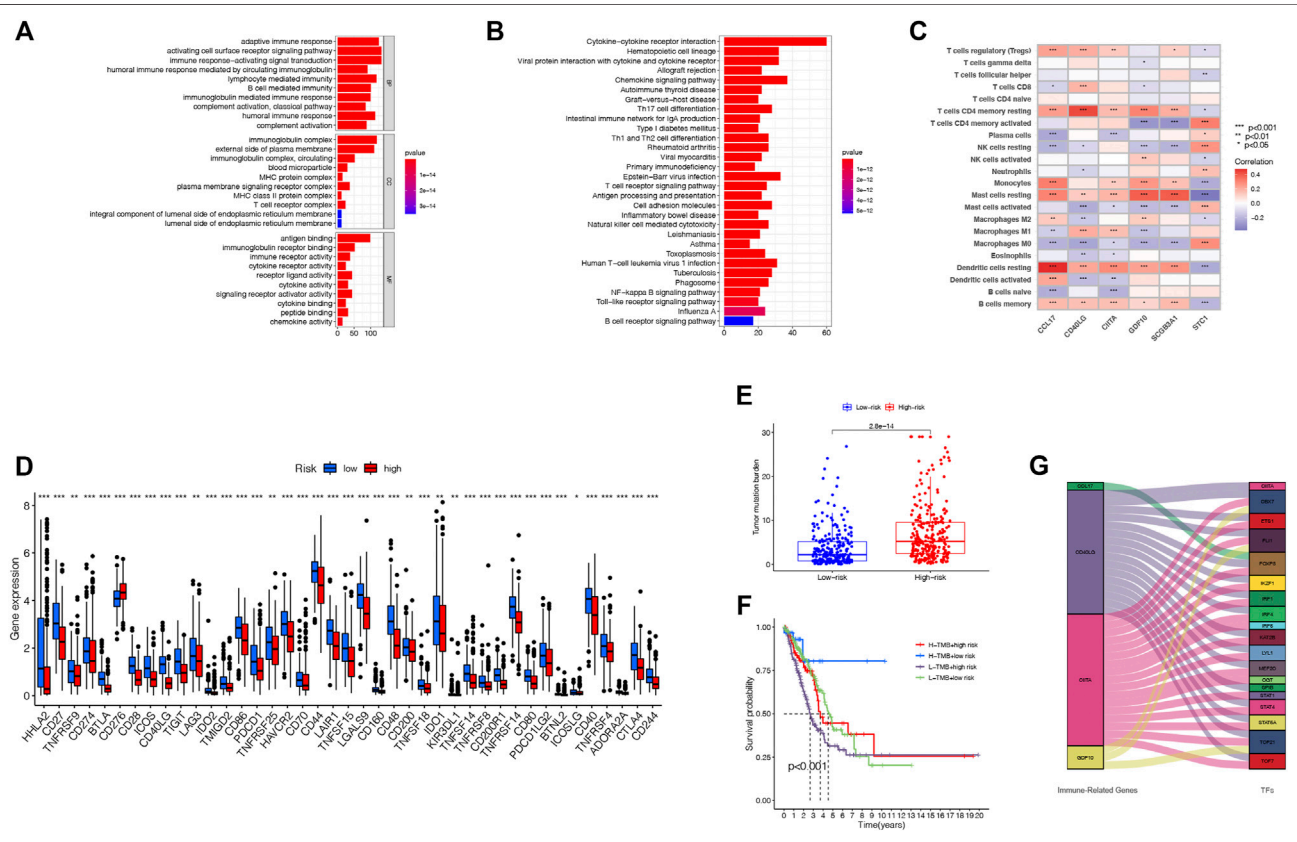

FIGURE 8 | Functional analysis and evaluation of immune activity between the two groups. **(A)**. GO analysis of TRIGs between various risk groups. **(B)**. KEGG analysis of TRIGs between various risk groups. **(C)**. Relationship between TRIG score and immune cell types. **(D)**. Expression of immune checkpoints in the high- and low-risk groups. **(E)**. Comparison of TMB between high- and low-risk groups. **(F)**. Comparison of four groups stratified by combining the TMB and risk groups. **(G)**. Regulatory network of the TRIGs and TFs.

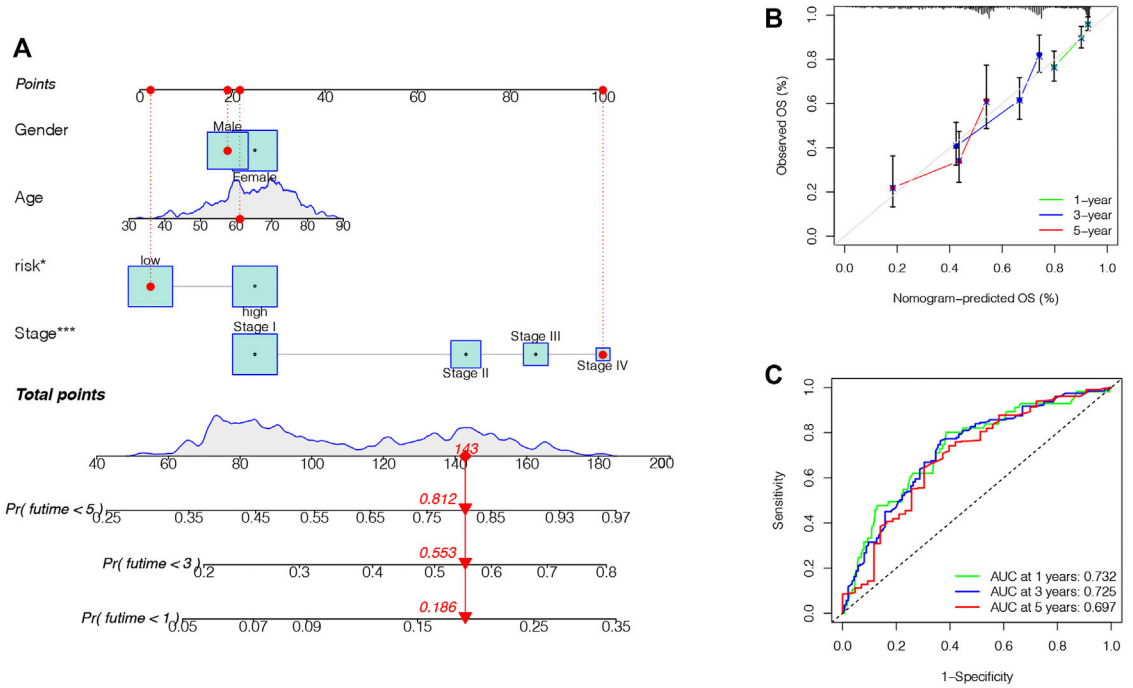

FIGURE 9 | Construction and validation of a nomogram. **(A)**. Nomogram for predicting the 1-, 3-, and 5-year OS of LUAD patients. **(B)**. ROC curve and AUC of the predictions for 1-, 3-, and 5-year OS in the TCGA cohort. **(C)**. Calibration curves of the nomogram for the TCGA cohort.

DISCUSSION

Plenty of research studies have disclosed that the TRP channels played an indispensable role in anti-tumor immune effects (Santoni and Farfariello 2011; Parenti et al., 2016). Most of their major focuses, however, were on a single TRP gene. The total effect and immune infiltration features intervened by the multiple TRP genes have not been fully illustrated. Our study showed variations in TRP genes at the genetic and transcriptional levels in LUAD. According to the differently expressed TRP genes, we classified patients into two subtypes. Between them, subtype 2 patients showed more severe clinical features and worse survival rates. Furthermore, the differences in TME features between two distinct subtypes were significantly linked with immune-related biological pathways, and subtype 1 was identified by a significant immune activation. Therefore, our studies showed that TRP genes might assume the role of a predictor for estimating the immunotherapy response and clinical outcome of LUAD. We further classified LUAD samples in the TCGA into two risk groups based on the DEGs and DEIGs between the two TRP-related subtypes. Moreover, we formed the prognostic TRIG score and revealed its predictive capability. Next, we explored the six TRIG score gene expression levels in LUAD. Patients with low and high TRIG scores were represented, respectively, as immune stimulation and suppression. Moreover, they showed significant differences in prognosis and clinical characteristics, also in the expressions of TME, TMB, and immune checkpoints. Last, by combining the clinical features and TRIG score, we set up a nomogram to facilitate the clinical use of the TRIG score. The prognostic TRIG score will be able to promote a better understanding of the LUAD molecular mechanism as well as provide new inspirations for anti-cancer therapies.

TME is a compound of tumor cells and their ambient cells, primarily composed of TIICs, the tumor vasculature, ECM, lymphocytes, cancer-associated fibroblasts, and bone marrow-derived inflammatory cells. Tumor development, progression, and therapeutic resistance were also reported to be significantly impacted by TME (Quail and Joyce 2013). Immune cells, as significant cellular elements of TME, were engaged in multiple immune activities and responses. For instance, the tumor-related inflammation that can prevent tumor progression is regulated by the immune system (Ribeiro Franco et al., 2020). Cytotoxic T-cell activation in the TME is considered to play vital roles in possessing tumor-antagonizing or tumor-promoting functions (Pardoll 2012). B-cells have been reported to both suppress and support T-cell functions, leading to differential effects on tumorigenesis (Ammirante et al., 2010). Moreover, B-cells have also been shown to promote tumor progression by enhancing pro-tumoral inflammation (Nelson 2010). Mast cell recruitment is related to tumorigenesis and angiogenesis (Coussens et al., 1999; Mantovani and Sica 2010). TAMs can also affect tumor progression depending on their polarization (Yang et al., 2008). LUAD patients are response heterogeneity to immunotherapy; particularly, those with highly expressed tumor neoantigens, tumor-infiltrating lymphocytes, and checkpoints tend to have a poor prognosis (Rosenberg et al., 2011; Rizvi et al., 2015; Verdegaal et al., 2016; Berner et al., 2019; Arrieta et al.,

2020), showing the essential role of TME in LUAD. The TRP channel, *TRPV1*, is proven to be a major Ca2+ channel. In addition, Ca2+ ions, which contributed the important inter- and intracellular messengers to the TME, have been investigated elsewhere (Bong and Monteith 2018; Roberts-Thomson et al., 2019). In this study, the TRP pattern identified by immune suppression showed a higher TRIG score, while, on the contrary, the pattern featured by immune activation was linked with a lower TRIG score. Hence, we discovered that TME features, including the relative abundance of 22 TIICs, varied significantly from two subtypes and different TRIG scores, indicating the key role of TRP genes in LUAD progression.

The tumor-infiltrating T-cell enrichment in LUAD tissues is higher compared with those in normal tissues, and higher enrichment of tumor-infiltrating T-cells indicates a good prognosis (Guo et al., 2018; Stankovic et al., 2018). $CD4^+$ T cells are crucial to driving not only the antibody but also cytotoxic $CD8^+$ T cell response. Moreover, they promote an inflammatory environment that favors antitumor immunity (Tran et al., 2014). Among them, memory $CD4^+$ T cells are reported to play a crucial role in anti-tumor responses to LUAD (Dieu-Nosjean et al., 2016). In this study, the low-risk group and the low TRIG score, accompanied by a higher survival rate, revealed higher resting memory $CD4^+$ T cell expression. At the first time, resting memory $CD4^+$ T cells are extracted from activated T-cells, and then they encounter antigens, followed by multiplying to produce a stronger and faster immune response to, in the second response, the experienced antigens. It has been proved that resting memory $CD4^+$ T cells can regulate tumor growth (McKinstry et al., 2010), which corresponds to our findings. Therefore, we assume that a high percentage of resting memory T-cells can strongly activate effector T-cells and thus favors an ideal result. In addition, the proportion of resting memory $CD4^+$ T cells increased in LUAD patients younger than 65 years old and non-smoking. Nevertheless, resting memory $CD4^+$ T cells can be partitioned into at least five subsets of cells, and which subtypes of memory $CD4^+$ T cells are linked with LUAD prognosis is yet to be found.

B-cells are also proved to participate in the immune response. Evidence showed that enrichment of tumor-infiltrating B-cells is the most powerful prognostic factor of prolonged survival and is strongly linked to *PD-1* blockade responses in soft-tissue sarcomas (Petitprez et al., 2020). Furthermore, tumor-infiltrating B-cells are detected at low levels, accompanied by a poor prognosis in advanced NSCLC (J. Chen et al., 2020; Germain et al., 2014). Meanwhile, higher expressions of B-cell-related genes *IGLL5*, *MZB1*, and *JCHAIN* are identified in patients with responding immune checkpoint blockade than those in non-responders (Helmink et al., 2020). In this study, no significant difference in native B-cell infiltration was found between the two risk groups, while the enrichment of memory B-cells in the low-TRIG-score group with longer OS was significantly higher than those in the high-TRIG-score group. The generation of memory B-cells is reported as a key characteristic of the adaptive immune system. Memory B-cells can activate T-cells and regulatory B-cells, which have been defined as tumor-promoting effects (Wang et al., 2019). Thus, B-cell infiltration restrained tumor progression of LUAD, in accordance with the results of previous studies (J. Chen et al., 2020; Germain et al., 2014).

Macrophages, also named tumor-associated macrophages (TAMs), are the richest immune cell population of tumor tissues. M0 macrophages, the inactive TAMs, can polarize into inhibit-cancer-progression M1 macrophages or promote-cancer-progression M2 macrophages. M1 macrophages generate type I pro-inflammatory cytokines and possess anti-tumor functions. Meanwhile, M2 macrophages promote the matrix-remodeling through immunosuppression and thus favor tumor progression (Qian and Pollard 2010). In LUAD cells, M0 macrophages internalize tumor-derived exosomes and polarize into the M2 phenotype (Pritchard et al., 2020). Meanwhile, in LUAD tissues, M0 macrophages showed a significant infiltration in patients with poor prognosis (Liu et al., 2017; Mo et al., 2020). In our study, neither M1 nor M2 had a significant prognosis for LUAD patients. However, the correlation between poor prognosis and M0 macrophages was observed. In fact, M1 and M2 phenotypes present two extremes of a spectrum of functional states rather than certainly different cell types. Thus, our findings may reflect the polarizing function.

Dendritic cells are essential for the initiation and regulation of both innate and adaptive immune responses. As such, a number of approaches have been advanced to target dendritic cells to improve immunotherapy, such as antigens with immunomodulators that assemble and activate endogenous dendritic cells, as well as dendritic cell-based vaccines (Wculek et al., 2020). In LUAD patients, the lack of resting dendritic cells in tumor tissues is linked with worse anti-*PD*-(*L*)1 response, leading to a poor prognosis (Leader et al., 2021). Mast cells are also critical to tumor angiogenesis as well as metastases (Paolino et al., 2019). Mast cells are considered key regulators of the cancer stroma and coordinators of anti-tumor immunity and have been involved in tumor cell innate characteristics. Therefore, mast cells are an under-recognized but very promising target for cancer immunotherapy (Lichterman and Reddy 2021). In LUAD, high mast cell infiltration is considered an indicator of a good prognosis (Welsh et al., 2005; Carlini et al., 2010; Shikotra et al., 2016). These findings are consistent with our study that resting dendritic cells and mast cells were enriched in the low-TRIG-score group, indicating that they might benefit from immunotherapy.

In our study, the immune checkpoint gene expressions are also considered to differ between the two subtypes. Our study formed a model featuring six TRG (*CCL17*, *CD40LG*, *CIITA*, *GDF10*, *SCGB3A1*, and *STC1*) and identified that it could forecast OS in LUAD patients. Four of the six TRG (*CCL17*, *CD40LG*, *CIITA*, and *STC1*) are reported to be linked with immune checkpoints. Immune checkpoint blockades, such as sole and dual *CTLA-4* and *PD-1/PD-L1* blockades, have already represented a clinical benefit for several cancers including LUAD (Skoulidis et al., 2018; de Miguel and Calvo 2020). Chemokine (C–C motif) ligand 17 (*CCL17*), also named T(H)2-attracting chemokine (*TARC*), can recruit regulatory T-cells to TME. Regulatory T-cell accumulation in TME is reported to reduce anti-tumor immune response and is considered to be an

essential driver of tumor immune evasion (Robles et al., 2020). Meanwhile, patients treated with combined immune checkpoint inhibitors represent the lowest expression of *CCL17* (Fiegle et al., 2019). In advanced melanoma patients treated with dendritic cell-based therapy, high serum levels of *CCL17* are related to improved progression-free survival (Cornforth et al., 2009). The *CD40* receptor and its ligand *CD40L*, widely expressed in various cells, is one of the master molecular pairs of the stimulatory immune checkpoint. The *CD40*/*CD40L*-targeted therapies show promising clinical efficacy in LUAD (Tang et al., 2021). The class II trans-activator (*CIITA*) is the most crucial regulator of the major histocompatibility complex (MHC) gene expression. In LUAD, loss of *CIITA* reduced cancer cell-specific MHCII and transformed LUAD from anti-*PD-1*-sensitive to anti-*PD-1*-resistant (Johnson et al., 2020). Expression of tumor stanniocalcin 1 (*STC1*) is reported to be related to immunotherapy efficacy and is negatively linked with patient survival in LUAD by tumor immune evasion and immunotherapy resistance. In murine tumor models, a gain of *STC1* favors tumor progression and allows tumor resistance to checkpoint blockade (Lin et al., 2021). All these studies correspond to our observations that high expression of *CCL17*, the *CD40* receptor-ligand gene (*CD40LG*), and *CIITA* and low expression of *STC1* are found in the low-TRIG-score group, indicating that patients in the low-TRIG-score group might benefit from immunotherapy. Another two TRIGs in this model, *SCGB3A1* (alias *HIN-1*) and *GDF10*, are both considered as tumor immune suppressors, which are correlated with clinicopathological variables (Garcia-Baquero et al., 2013; Cheng et al., 2016). These are consistent with our observations that high expressions of *SCGB3A1* and *GDF10* are identified in the low-TRIG-score group. Combined with our findings, these two TRIGs might have the potential to respond to immune checkpoint inhibitors.

Our study still had some limitations. First, all analyses were based on data from public databases. Thus, the results might have an innate case selection bias. Reliable *in vitro* and *in vivo* experiments along with large-scale prospective clinical trials are required to confirm our findings. Moreover, data on several critical clinical variables, including neoadjuvant chemotherapy, surgery, chemotherapy, targeted therapy, and immunotherapy, were unavailable in most datasets, which may have exerted an influence on the prognosis of immune responses.

DATA AVAILABILITY STATEMENT

Publicly available datasets were analyzed in this study. These data can be found here: The Cancer Genome Atlas (TCGA) database, https://portal.gdc.cancer.gov/, the Gene Expression Omnibus (GEO) database, https://www.ncbi.nlm.nih.gov/geo/ (ID: GSE3141, GSE31210, GSE30219, GSE37745), and Search Tool for the Retrieval of Interacting Genes (STRING), version 11.0. https://string-db.org/the ImmPort Resource website. https://www.immport.org/shared/genelists.

ETHICS STATEMENT

Written informed consent was obtained from the individual(s) for the publication of any potentially identifiable images or data included in this article.

AUTHOR CONTRIBUTIONS

SS led the bioinformatic and biostatistical data analysis, made the figures, and wrote the manuscript, YW collected the literature. ML edited and made significant revisions to the manuscript. JW contributed to the study design and project supervision. All authors contributed to the article and approved the submitted version.

FUNDING

The National Natural Science Foundation of China, 81871115, the Jiangsu Provincial Key Discipline of Medicine, ZDXKA2016003, and the National Key R&D Program of China, Nos. 2018YFC2002100 and 2018YFC2002102, provided the funding for the work.

SUPPLEMENTARY MATERIAL

The Supplementary Material for this article can be found online at: https://www.frontiersin.org/articles/10.3389/fmolb.2022.861380/full#supplementary-material

REFERENCES

Akdis, M., Aab, A., Altunbulakli, C., Azkur, K., Costa, R. A., Crameri, R., et al. (2016). Interleukins (From IL-1 to IL-38), Interferons, Transforming Growth Factor β, and TNF-α: Receptors, Functions, and Roles in Diseases. *J. Allergy Clin. Immunol.* 138 (4), 984–1010. doi:10.1016/j.jaci.2016.06.033

Ammirante, M., Luo, J.-L., Grivennikov, S., Nedospasov, S., and Karin, M. (2010). B-cell-derived Lymphotoxin Promotes Castration-Resistant Prostate Cancer. *Nature* 464 (7286), 302–305. doi:10.1038/nature08782

Arrieta, O., Barrón, F., Ramírez-Tirado, L. A., Zatarain-Barrón, Z. L., Cardona, A. F., Díaz-García, D., et al. (2020). Efficacy and Safety of Pembrolizumab Plus Docetaxel vs Docetaxel Alone in Patients with Previously Treated Advanced Non-small Cell Lung Cancer. *JAMA Oncol.* 6 (6), 856–864. doi:10.1001/jamaoncol.2020.0409

Barclay, A. N. (2003). Membrane Proteins with Immunoglobulin-like Domains-A Master Superfamily of Interaction Molecules. *Semin. Immunol.* 15 (4), 215–223. doi:10.1016/s1044-5323(03)00047-2

Berner, F., Bomze, D., Diem, S., Ali, O. H., Fässler, M., Ring, S., et al. (2019). Association of Checkpoint Inhibitor-Induced Toxic Effects with Shared Cancer and Tissue Antigens in Non-small Cell Lung Cancer. *JAMA Oncol.* 5 (7), 1043–1047. doi:10.1001/jamaoncol.2019.0402

Bong, A. H. L., and Monteith, G. R. (2018). Calcium Signaling and the Therapeutic Targeting of Cancer Cells. *Biochim. Biophys. Acta (Bba) - Mol. Cel Res.* 1865 (11 Pt B), 1786–1794. doi:10.1016/j.bbamcr.2018.05.015

Bray, F., Ferlay, J., Soerjomataram, I., Siegel, R. L., Torre, L. A., and Jemal, A. (2018). Global Cancer Statistics 2018: GLOBOCAN Estimates of Incidence and

Mortality Worldwide for 36 Cancers in 185 Countries. *CA: A Cancer J. Clinicians* 68 (6), 394–424. doi:10.3322/caac.21492

Büch, T., Büch, E., Boekhoff, I., Steinritz, D., and Aigner, A. (2018). Role of Chemosensory TRP Channels in Lung Cancer. *Pharmaceuticals* 11 (4), 90. doi:10.3390/ph11040090

Carlini, M. J., Dalurzo, M. C. L., Lastiri, J. M., Smith, D. E., Vasallo, B. C., Puricelli, L. I., et al. (2010). Mast Cell Phenotypes and Microvessels in Non-small Cell Lung Cancer and its Prognostic Significance. *Hum. Pathol.* 41 (5), 697–705. doi:10.1016/j.humpath.2009.04.029

Chen, D. S., and Mellman, I. (2017). Elements of Cancer Immunity and the Cancer-Immune Set point. *Nature* 541 (7637), 321–330. doi:10.1038/nature21349

Chen, J., Tan, Y., Sun, F., Hou, L., Zhang, C., Ge, T., et al. (2020). Single-cell Transcriptome and Antigen-Immunoglobin Analysis Reveals the Diversity of B Cells in Non-small Cell Lung Cancer. *Genome Biol.* 21 (1), 152. doi:10.1186/s13059-020-02064-6

Chen, W., Huang, J., Xiong, J., Fu, P., Chen, C., Liu, Y., et al. (2021). Identification of a Tumor Microenvironment-Related Gene Signature Indicative of Disease Prognosis and Treatment Response in Colon Cancer. *Oxidative Med. Cell Longevity* 2021, 1–31. doi:10.1155/2021/6290261

Cheng, C.-W., Hsiao, J.-R., Fan, C.-C., Lo, Y.-K., Tzen, C.-Y., Wu, L.-W., et al. (2016). Loss of GDF10/BMP3b as a Prognostic Marker Collaborates with TGFBR3 to Enhance Chemotherapy Resistance and Epithelial-Mesenchymal Transition in Oral Squamous Cell Carcinoma. *Mol. Carcinog.* 55 (5), 499–513. doi:10.1002/mc.22297

Cornforth, A. N., Lee, G. J., Fowler, A. W., Carbonell, D. J., and Dillman, R. O. (2009). Increases in Serum TARC/CCL17 Levels Are Associated with Progression-free Survival in Advanced Melanoma Patients in Response to Dendritic Cell-Based Immunotherapy. *J. Clin. Immunol.* 29 (5), 657–664. doi:10.1007/s10875-009-9299-3

Coussens, L. M., Raymond, W. W., Bergers, G., Laig-Webster, M., Behrendtsen, O., Werb, Z., et al. (1999). Inflammatory Mast Cells Up-Regulate Angiogenesis during Squamous Epithelial Carcinogenesis. *Genes Dev.* 13 (11), 1382–1397. doi:10.1101/gad.13.11.1382

Cristescu, R., Mogg, R., Ayers, M., Albright, A., Murphy, E., Yearley, J., et al. (2018). Pan-tumor Genomic Biomarkers for PD-1 Checkpoint Blockade-Based Immunotherapy. *Science* 362 (6411). doi:10.1126/science.aar3593

de Miguel, M., and Calvo, E. (2020). Clinical Challenges of Immune Checkpoint Inhibitors. *Cancer Cell* 38 (3), 326–333. doi:10.1016/j.ccell.2020.07.004

Dieu-Nosjean, M.-C., Giraldo, N. A., Kaplon, H., Germain, C., Fridman, W. H., and Sautès-Fridman, C. (2016). Tertiary Lymphoid Structures, Drivers of the Anti-tumor Responses in Human Cancers. *Immunol. Rev.* 271 (1), 260–275. doi:10.1111/imr.12405

Domingues, P., González-Tablas, M., Otero, Á., Pascual, D., Miranda, D., Ruiz, L., et al. (2016). Tumor Infiltrating Immune Cells in Gliomas and Meningiomas. *Brain Behav. Immun.* 53, 1–15. doi:10.1016/j.bbi.2015.07.019

Fiegle, E., Doleschel, D., Koletnik, S., Rix, A., Weiskirchen, R., Borkham-Kamphorst, E., et al. (2019). Dual CTLA-4 and PD-L1 Blockade Inhibits Tumor Growth and Liver Metastasis in a Highly Aggressive Orthotopic Mouse Model of Colon Cancer. *Neoplasia* 21 (9), 932–944. doi:10.1016/j.neo.2019.07.006

García-Baquero, R., Puerta, P., Beltran, M., Alvarez, M., Sacristan, R., Alvarez-Ossorio, J. L., et al. (2013). Methylation of a Novel Panel of Tumor Suppressor Genes in Urine Moves Forward Noninvasive Diagnosis and Prognosis of Bladder Cancer: a 2-center Prospective Study. *J. Urol.* 190 (2), 723–730. doi:10.1016/j.juro.2013.01.105

Germain, C., Gnjatic, S., Tamzalit, F., Knockaert, S., Remark, R., Goc, J., et al. (2014). Presence of B Cells in Tertiary Lymphoid Structures Is Associated with a Protective Immunity in Patients with Lung Cancer. *Am. J. Respir. Crit. Care Med.* 189 (7), 832–844. doi:10.1164/rccm.201309-1611OC

Guo, X., Zhang, Y., Zheng, L., Zheng, C., Song, J., Zhang, Q., et al. (2018). Global Characterization of T Cells in Non-small-cell Lung Cancer by Single-Cell Sequencing. *Nat. Med.* 24 (7), 978–985. doi:10.1038/s41591-018-0045-3

Han, J., Yang, Y., Li, X., Wu, J., Sheng, Y., Qiu, J., et al. (2022). Pan-cancer Analysis Reveals Sex-specific Signatures in the Tumor Microenvironment. *Mol. Oncol.* doi:10.1002/1878-0261.13203

He, X., and Xu, C. (2020). Immune Checkpoint Signaling and Cancer Immunotherapy. *Cell Res* 30 (8), 660–669. doi:10.1038/s41422-020-0343-4

Helmink, B. A., Reddy, S. M., Gao, J., Zhang, S., Basar, R., Thakur, R., et al. (2020). B Cells and Tertiary Lymphoid Structures Promote Immunotherapy Response. *Nature* 577 (7791), 549–555. doi:10.1038/s41586-019-1922-8

Johnson, A. M., Bullock, B. L., Neuwelt, A. J., Poczobutt, J. M., Kaspar, R. E., Li, H. Y., et al. (2020). Cancer Cell-Intrinsic Expression of MHC Class II Regulates the Immune Microenvironment and Response to Anti-PD-1 Therapy in Lung Adenocarcinoma. *J. Immunol.* 204 (8), 2295–2307. doi:10.4049/jimmunol.1900778

Junttila, M. R., and de Sauvage, F. J. (2013). Influence of Tumour Microenvironment Heterogeneity on Therapeutic Response. *Nature* 501 (7467), 346–354. doi:10.1038/nature12626

Kalaora, S., Nagler, A., Nejman, D., Alon, M., Barbolin, C., Barnea, E., et al. (2021). Identification of Bacteria-Derived HLA-Bound Peptides in Melanoma. *Nature* 592 (7852), 138–143. doi:10.1038/s41586-021-03368-8

Kraehenbuehl, L., Weng, C.-H., Eghbali, S., Wolchok, J. D., and Merghoub, T. (2022). Enhancing Immunotherapy in Cancer by Targeting Emerging Immunomodulatory Pathways. *Nat. Rev. Clin. Oncol.* 19 (1), 37–50. doi:10.1038/s41571-021-00552-7

Leader, A. M., Grout, J. A., Maier, B. B., Nabet, B. Y., Park, M. D., Tabachnikova, A., et al. (2021). Single-cell Analysis of Human Non-small Cell Lung Cancer Lesions Refines Tumor Classification and Patient Stratification. *Cancer Cell* 39, 1594–1609. doi:10.1016/j.ccell.2021.10.009

Li, X., Zhang, Q., Fan, K., Li, B., Li, H., Qi, H., et al. (2016). Overexpression of TRPV3 Correlates with Tumor Progression in Non-small Cell Lung Cancer. *Ijms* 17 (4), 437. doi:10.3390/ijms17040437

Lichterman, J. N., and Reddy, S. M. (2021). Mast Cells: A New Frontier for Cancer Immunotherapy. *Cells* 10 (6), 1270. doi:10.3390/cells10061270

Lin, H., Kryczek, I., Li, S., Green, M. D., Ali, A., Hamasha, R., et al. (2021). Stanniocalcin 1 Is a Phagocytosis Checkpoint Driving Tumor Immune Resistance. *Cancer Cell* 39 (4), 480–493 e6. doi:10.1016/j.ccell.2020.12.023

Liu, X., Wu, S., Yang, Y., Zhao, M., Zhu, G., and Hou, Z. (2017). The Prognostic Landscape of Tumor-Infiltrating Immune Cell and Immunomodulators in Lung Cancer. *Biomed. Pharmacother.* 95, 55–61. doi:10.1016/j.biopha.2017.08.003

Lord, S. J., Rajotte, R. V., Korbutt, G. S., and Bleackley, R. C. (2003). Granzyme B: a Natural Born Killer. *Immunol. Rev.* 193, 31–38. doi:10.1034/j.1600-065x.2003.00044.x

Majhi, R. K., Sahoo, S. S., Yadav, M., Pratheek, B. M., Chattopadhyay, S., and Goswami, C. (2015). Functional Expression of TRPV Channels in T Cells and Their Implications in Immune Regulation. *FEBS J.* 282 (14), 2661–2681. doi:10.1111/febs.13306

Mantovani, A., and Sica, A. (2010). Macrophages, Innate Immunity and Cancer: Balance, Tolerance, and Diversity. *Curr. Opin. Immunol.* 22 (2), 231–237. doi:10.1016/j.coi.2010.01.009

McKinstry, K. K., Strutt, T. M., and Swain, S. L. (2010). The Potential of CD4 T-Cell Memory. *Immunology* 130 (1), 1–9. doi:10.1111/j.1365-2567.2010.03259.x

Mo, Z., Yu, L., Cao, Z., Hu, H., Luo, S., and Zhang, S. (2020). Identification of a Hypoxia-Associated Signature for Lung Adenocarcinoma. *Front. Genet.* 11, 647. doi:10.3389/fgene.2020.00647

Nelson, B. H. (2010). CD20+ B Cells: the Other Tumor-Infiltrating Lymphocytes. *J. Immunol.* 185 (9), 4977–4982. doi:10.4049/jimmunol.1001323

Olivier, M., Gregory, D. J., and Forget, G. (2005). Subversion Mechanisms by Which Leishmania Parasites Can Escape the Host Immune Response: a Signaling point of View. *Clin. Microbiol. Rev.* 18 (2), 293–305. doi:10.1128/CMR.18.2.293-305.2005

Paolino, G., Corsetti, P., Moliterni, E., Corsetti, S., Didona, D., Albanesi, M., et al. (2019). Mast Cells and Cancer. *G Ital. Dermatol. Venereol.* 154 (6), 650–668. doi:10.23736/S0392-0488.17.05818-7

Pardoll, D. M. (2012). The Blockade of Immune Checkpoints in Cancer Immunotherapy. *Nat. Rev. Cancer* 12 (4), 252–264. doi:10.1038/nrc3239

Parenti, A., De Logu, F., Geppetti, P., and Benemei, S. (2016). What Is the Evidence for the Role of TRP Channels in Inflammatory and Immune Cells? *Br. J. Pharmacol.* 173 (6), 953–969. doi:10.1111/bph.13392

Petitprez, F., de Reyniès, A., Keung, E. Z., Chen, T. W.-W., Sun, C.-M., Calderaro, J., et al. (2020). B Cells Are Associated with Survival and Immunotherapy Response in Sarcoma. *Nature* 577 (7791), 556–560. doi:10.1038/s41586-019-1906-8

Pritchard, A., Tousif, S., Wang, Y., Hough, K., Khan, S., Strenkowski, J., et al. (2020). Lung Tumor Cell-Derived Exosomes Promote M2 Macrophage Polarization. *Cells* 9 (5), 1303. doi:10.3390/cells9051303

Qian, B.-Z., and Pollard, J. W. (2010). Macrophage Diversity Enhances Tumor Progression and Metastasis. *Cell* 141 (1), 39–51. doi:10.1016/j.cell.2010.03.014

Quail, D. F., and Joyce, J. A. (2013). Microenvironmental Regulation of Tumor Progression and Metastasis. *Nat. Med.* 19 (11), 1423–1437. doi:10.1038/nm.3394

Ribeiro Franco, P. I., Rodrigues, A. P., de Menezes, L. B., and Pacheco Miguel, M. (2020). Tumor Microenvironment Components: Allies of Cancer Progression. *Pathol. - Res. Pract.* 216 (1), 152729. doi:10.1016/j.prp.2019.152729

Rizvi, N. A., Hellmann, M. D., Snyder, A., Kvistborg, P., Makarov, V., Havel, J. J., et al. (2015). Mutational Landscape Determines Sensitivity to PD-1 Blockade in Non-small Cell Lung Cancer. *Science* 348 (6230), 124–128. doi:10.1126/science.aaa1348

Roberts-Thomson, S. J., Chalmers, S. B., and Monteith, G. R. (2019). The Calcium-Signaling Toolkit in Cancer: Remodeling and Targeting. *Cold Spring Harb Perspect. Biol.* 11 (8), a035204. doi:10.1101/cshperspect.a035204

Robles, O., Jackson, J. J., Marshall, L., Talay, O., Chian, D., Cutler, G., et al. (2020). Novel Piperidinyl-Azetidines as Potent and Selective CCR4 Antagonists Elicit Antitumor Response as a Single Agent and in Combination with Checkpoint Inhibitors. *J. Med. Chem.* 63 (15), 8584–8607. doi:10.1021/acs.jmedchem.0c00988

Rosenberg, S. A., Yang, J. C., Sherry, R. M., Kammula, U. S., Hughes, M. S., Phan, G. Q., et al. (2011). Durable Complete Responses in Heavily Pretreated Patients with Metastatic Melanoma Using T-Cell Transfer Immunotherapy. *Clin. Cancer Res.* 17 (13), 4550–4557. doi:10.1158/1078-0432.CCR-11-0116

Santoni, G., and Farfariello, V. (2011). TRP Channels and Cancer: New Targets for Diagnosis and Chemotherapy. *Emiddt* 11 (1), 54–67. doi:10.2174/187153011794982068

Sha, D., Jin, Z., Budczies, J., Kluck, K., Stenzinger, A., and Sinicrope, F. A. (2020). Tumor Mutational Burden as a Predictive Biomarker in Solid Tumors. *Cancer Discov.* 10 (12), 1808–1825. doi:10.1158/2159-8290.CD-20-0522

Shikotra, A., Ohri, C. M., Green, R. H., Waller, D. A., and Bradding, P. (2016). Mast Cell Phenotype, TNFα Expression and Degranulation Status in Non-small Cell Lung Cancer. *Sci. Rep.* 6, 38352. doi:10.1038/srep38352

Skoulidis, F., Goldberg, M. E., Greenawalt, D. M., Hellmann, M. D., Awad, M. M., Gainor, J. F., et al. (2018). STK11/LKB1 Mutations and PD-1 Inhibitor Resistance in KRAS-Mutant Lung Adenocarcinoma. *Cancer Discov.* 8 (7), 822–835. doi:10.1158/2159-8290.CD-18-0099

Stankovic, B., Bjørhovde, H. A. K., Skarshaug, R., Aamodt, H., Frafjord, A., Müller, E., et al. (2018). Immune Cell Composition in Human Non-small Cell Lung Cancer. *Front. Immunol.* 9, 3101. doi:10.3389/fimmu.2018.03101

Steinritz, D., Stenger, B., Dietrich, A., Gudermann, T., and Popp, T. (2018). TRPs in Tox: Involvement of Transient Receptor Potential-Channels in Chemical-Induced Organ Toxicity-A Structured Review. *Cells* 7 (8), 98. doi:10.3390/cells7080098

Takahashi, N., Chen, H.-Y., Harris, I. S., Stover, D. G., Selfors, L. M., Bronson, R. T., et al. (2018). Cancer Cells Co-opt the Neuronal Redox-Sensing Channel TRPA1 to Promote Oxidative-Stress Tolerance. *Cancer Cell* 33 (6), 985–1003 e7. doi:10.1016/j.ccell.2018.05.001

Tang, T., Cheng, X., Truong, B., Sun, L., Yang, X., and Wang, H. (2021). Molecular Basis and Therapeutic Implications of CD40/CD40L Immune Checkpoint. *Pharmacol. Ther.* 219, 107709. doi:10.1016/j.pharmthera.2020.107709

Taylor-Clark, T. E. (2016). Role of Reactive Oxygen Species and TRP Channels in the Cough Reflex. *Cell Calcium* 60 (3), 155–162. doi:10.1016/j.ceca.2016.03.007

Tran, E., Turcotte, S., Gros, A., Robbins, P. F., Lu, Y.-C., Dudley, M. E., et al. (2014). Cancer Immunotherapy Based on Mutation-specific CD4+ T Cells in a Patient with Epithelial Cancer. *Science* 344 (6184), 641–645. doi:10.1126/science.1251102

Vay, L., Gu, C., and McNaughton, P. A. (2012). The Thermo-TRP Ion Channel Family: Properties and Therapeutic Implications. *Br. J. Pharmacol.* 165 (4), 787–801. doi:10.1111/j.1476-5381.2011.01601.x

Venkatachalam, K., and Montell, C. (2007). TRP Channels. *Annu. Rev. Biochem.* 76, 387–417. doi:10.1146/annurev.biochem.75.103004.142819

Verdegaal, E. M. E., de Miranda, N. F. C. C., Visser, M., Harryvan, T., van Buuren, M. M., Andersen, R. S., et al. (2016). Neoantigen Landscape Dynamics during Human Melanoma-T Cell Interactions. *Nature* 536 (7614), 91–95. doi:10.1038/nature18945

Wang, S.-s., Liu, W., Ly, D., Xu, H., Qu, L., and Zhang, L. (2019). Tumor-infiltrating B Cells: Their Role and Application in Anti-tumor Immunity in Lung Cancer. *Cell Mol Immunol* 16 (1), 6–18. doi:10.1038/s41423-018-0027-x

Wculek, S. K., Cueto, F. J., Mujal, A. M., Melero, I., Krummel, M. F., and Sancho, D. (2020). Dendritic Cells in Cancer Immunology and Immunotherapy. *Nat. Rev. Immunol.* 20 (1), 7–24. doi:10.1038/s41577-019-0210-z

Welsh, T. J., Green, R. H., Richardson, D., Waller, D. A., O'Byrne, K. J., and Bradding, P. (2005). Macrophage and Mast-Cell Invasion of Tumor Cell Islets Confers a Marked Survival Advantage in Non-small-cell Lung Cancer. *Jco* 23 (35), 8959–8967. doi:10.1200/JCO.2005.01.4910

Wood, K., Hensing, T., Malik, R., and Salgia, R. (2016). Prognostic and Predictive Value inKRASin Non-small-cell Lung Cancer. *JAMA Oncol.* 2 (6), 805–812. doi:10.1001/jamaoncol.2016.0405

Yang, F.-C., Ingram, D. A., Chen, S., Zhu, Y., Yuan, J., Li, X., et al. (2008). Nf1-Dependent Tumors Require a Microenvironment Containing Nf1+/−- and C-kit-dependent Bone Marrow. *Cell* 135 (3), 437–448. doi:10.1016/j.cell.2008.08.041

Zou, W., Wolchok, J. D., and Chen, L. (2016). PD-L1 (B7-H1) and PD-1 Pathway Blockade for Cancer Therapy: Mechanisms, Response Biomarkers, and Combinations. *Sci. Transl. Med.* 8 (328), 328rv4. doi:10.1126/scitranslmed.aad7118

Conflict of Interest: The authors declare that the research was conducted in the absence of any commercial or financial relationships that could be construed as a potential conflict of interest.

Publisher's Note: All claims expressed in this article are solely those of the authors and do not necessarily represent those of their affiliated organizations or those of the publisher, the editors, and the reviewers. Any product that may be evaluated in this article or claim that may be made by its manufacturer is not guaranteed or endorsed by the publisher.

frontiers | Frontiers in Molecular Biosciences

ORIGINAL RESEARCH
published: 20 May 2022
doi: 10.3389/fmolb.2022.904959

A Pan-Cancer Analysis of IRAK1 Expression and Their Association With Immunotherapy Response

Mengmeng Liu[1,2†], *Yi Que*[1,3†], *Ye Hong*[1,3], *Lian Zhang*[1,3], *Xing Zhang*[1,2*‡] and *Yizhuo Zhang*[1,3*‡]

[1]Sun Yat-sen University Cancer Center, State Key Laboratory of Oncology in South China, Collaborative Innovation Center for Cancer Medicine, Guangzhou, China, [2]Department of Medical Melanoma and Sarcoma, Sun Yat-sen University Cancer Center, Guangzhou, China, [3]Department of Pediatric Oncology, Sun Yat-sen University Cancer Center, Guangzhou, China

OPEN ACCESS

Edited by:
Na Luo,
Nankai University, China

Reviewed by:
Sushil Kumar,
Indian Institute of Technology Roorkee, India
Vikas Singh,
The Rockefeller University, United States

***Correspondence:**
Xing Zhang
zhangxing@sysucc.org.cn
Yizhuo Zhang
zhangyzh@sysucc.org.cn

†These authors have contributed equally to this work and share first authorship

‡These authors have contributed equally to this work

Specialty section:
This article was submitted to Molecular Diagnostics and Therapeutics, a section of the journal Frontiers in Molecular Biosciences

Received: 26 March 2022
Accepted: 29 April 2022
Published: 20 May 2022

Citation:
Liu M, Que Y, Hong Y, Zhang L, Zhang X and Zhang Y (2022) A Pan-Cancer Analysis of IRAK1 Expression and Their Association With Immunotherapy Response. Front. Mol. Biosci. 9:904959. doi: 10.3389/fmolb.2022.904959

IRAK1 is an active kinase which plays a critical role in IL-1/TLR signaling pathway involved in inflammation and innate immune response. Recently, increasing evidence supports a potential role of IRAK1 in cancer progression. However, no immunological pan-cancer analysis of IRAK1 is available. We aimed to explore the prognostic value and the immunological functions of IRAK1. A series of datasets including The Cancer Genome Atlas, GEPIA2, cBioPortal, HPA, TIMER2.0 were performed to explore the oncogenic and immunological roles of IRAK1, including the relationship between IRAK1 and prognosis, genetic mutation, GO and KEGG enrichment pathway analysis, immune state of different tumors, The results showed that IRAK1 levels were upregulated in more than 20 types of cancers compared to the normal tissues. IRAK1 expression was associated with poorer prognosis in different cancer types. For the most frequent DNA alteration of IRAK1 is amplification. And the result of the enrichment analysis suggested that IRAK1 related to immune checkpoint pathway in cancer. IRAK1 inhibitor pacritinib inhibit proliferation and upregulate PD-L1 expression in different cancer cell lines. Moreover, the patients who receiving anti-PD-L1 therapy with low IRAK1 expression had a better prognosis, and the objective response rate to anti-PD-L1 therapy was higher in the low IRAK1 group than in the high IRAK1 group in IMvigor210 cohort. Our study reveals that IRAK1 can function as a prognostic marker in various malignant tumors. And pacritinib upregulated PD-L1 expression in several cancer cell lines, which indicating that IRAK1 can be used as a reliable marker to predict the efficacy of immunotherapy.

Keywords: IRAK1, pan-cancer analysis, PD-L1, prognosis, immunotherapy

INTRODUCTION

Cancer is a complex disease with tumor heterogeneity and regulated by tumor immune microenvironment (Hanahan and Weinberg 2011). As an alternative to traditional anticancer therapies, emerging immune checkpoint inhibitors (ICIs) have been shown to be effective in multiple cancer types (12), such as anti-CTLA-4, anti-PD-L1, and anti-PD-1 (Galluzzi et al., 2020; Vaddepally et al., 2020). Anti-PD-1 inhibitors such as pembrolizumab, toripalimab, and nivolumab have been approved as first-line therapies for patients with unresectable melanoma, non-small cell lung cancer and kidney cancer (Khoja et al., 2015; Keam 2019; Zhao et al., 2020). Existing clinical studies have shown that only part of patients can benefit. Although studies have shown that tumor mutation

burden (TMB), tumor microsatellite instability (MSI), tumor copy-number alterations (CAN) and PD-L1 expression level can be used to predict the prognosis of ICIs (Dudnik et al., 2018; Davis and Patel 2019; Samstein et al., 2019; Lu et al., 2020). However, these biomarkers exhibited certain limitations, for example, the expression levels of PD-L1 cannot be uniform at different tumor. Therefore, it is urgent to identify new markers to find more people suitable for ICIs.

Interleukin-1 receptor-associated kinases comprise a class of serine-threonine kinases, including IRAK1, IRAK2, IRAK3, and IRAK4 (Flannery and Bowie 2010; Rhyasen and Starczynowski 2015). Previous studies suggested that the IRAK family is key to regulating inflammatory, innate immunity, and metabolic diseases (Su, Xu, and Huang 2020). IRAK1 is an active kinase that plays a critical role in the IL-1/TLR signaling pathway involved in inflammation and innate immune responses (Vollmer et al., 2017; Singer et al., 2018). In recent years, IRAK1 expression or alteration has been reported in several cancers. For instance, Wee et al. (Wee et al., 2015) reported that IRAK1 is overexpressed in breast cancers and that IRAK1 inhibition reduces cancer proliferation and metastasis. In addition, Liu et al. showed that IRAK1 contributed to chemoresistance in nasopharyngeal carcinoma through the IRAK1-S100A9 axis (Liu et al., 2021). Interestingly, IRAK1 overexpression was also observed in hepatocellular carcinoma, augmenting cancer stemness and drug resistance (Cheng et al., 2018). Given the potential role of IRAK1 in tumorigenesis, it is essential to conduct a pan-cancer analysis of it.

Moreover, existing papers have not fully elucidated the role of IRAK1 in adaptive immune responses. Thus, our study investigated the potential molecular and immune-related pathways of IRAK1 in various cancer types. We found that IRAK1 is related to immune pathways, including the PD-L1 and PD-1 checkpoint pathway in cancer. Furthermore, inhibitors of IRAK1 pacritinib upregulated PD-L1 expression in several cancer cell lines, indicating that the pharmacological inhibition of IRAK1 could be synergistic with immunotherapy in the future.

METHODS

Data Processing and Expression Analysis

All original data were downloaded from The Cancer Genome Atlas (TCGA) (http://cancergenome.nih.gov/).We used GEPIA database to evaluate the expression of tumor tissues and the normal control of the TCGA data. The violin plots of the IRAK1 expression in different pathological stages were also obtained in the GEPIA database. Additionally, the correlation between the OS and PFS survival and the expression of IRAK1 was evaluated through the "Survival Analysis" module of GEPIA2. The cut-off valued was determined automatically (high expression (50%) vs. low expression (50%)). A log p-value < 0.05 was considered statistically significant.

The total protein expression of IRAK1 in tumor and normal tissues were explored in the UALCAN portal (http://ualcan.path.uab.edu/analysis-prot.html). The datasets of breast cancer, ovarian cancer, clear cell RCC, UCEC and LUAD are available.

The immunohistochemistry (IHC) images of IRAK1 protein expression in normal tissues and tumors tissues, including breast cancer, colorectal cancer, low-grade glioma and ovarian cancer, were downloaded from the HPA (http://www.proteinatlas.org/).

Genetic Mutation Analysis

The frequencies of IRAK1 copy number alterations and mutations were identified in the cBioPortal (http://cbioportal.org), which is an open-access resource. The correlation of IRAK1 mutations and the survival in LSCC was also obtained.

IRAK1- Related Genes Enrichment Analysis

IRAK1 binding proteins related genes were obtained on the STRING website (http://string-db.org/). IRAK1 correlated genes were obtained through the GEPIA2. Then the top five genes which exhibited the most significant correlation were determined and the TIMER2 was used to display the heatmap between the selected five genes and the IRAK1 expression across the pan-cancer types. The partial correlation and p-value was adjusted in the purity spearman's rank correlation test.

The GO and KEGG enrichment pathway analysis were applied to the "clusterProfiler" R package by using the R software (3.6.3 version). Moreover, we used the "ggplot2" R packages for visualization.

Immune-Infiltration Analysis and the IRAK1 Expression Data With Immunotherapy

The heatmaps of correlation between immune-suppressive genes and IRAK1 expression levels were shown by TIMER2.0. The CD274 and IRAK1 mRNA expression correlation was evaluated in different cancer types from the TCGA database using the TIMER2.0 tool. CIBERSORT and TIMER algorithms calculated the putative proportion of the different immune cells and correlated with IRAK1 expression in pan-cancer types. We analyzed IRAK1 expression in different immune subtypes in TISIDB (http://cis.hku.hk/TISIDB/index.php). To determine whether IRAK1 expression predicts the benefits of immunotherapy, we downloaded the IMvigor210 information from the http://research pub.gene.com/IMvigor210CoreBiologies, which include 298 patients with complete clinical data for urothelial carcinoma.

Cell Culture

All cell lines, including MDA-MB-231, U251, Hep3B, Kyse30 and A498 were purchased from ATCC. MDA-MB-231, U251 and Hep3B cells were cultured in Dulbecco's Modified Eagle Medium (DMEM) supplemented with 10% fetal bovine serum. Meanwhile, Kyse30 and A498 cells were cultured in RPMI 1640 supplemented with 10% fetal bovine serum.

RESULTS

IRAK1 Expression in Pan-Cancer From the TCGA Database

We analyzed IRAK1 mRNA expression in tumor and normal tissue samples across 33 pan cancers from the TCGA database. The results indicated that IRAK1 levels upregulated in BLCA, BRCA, CESC,

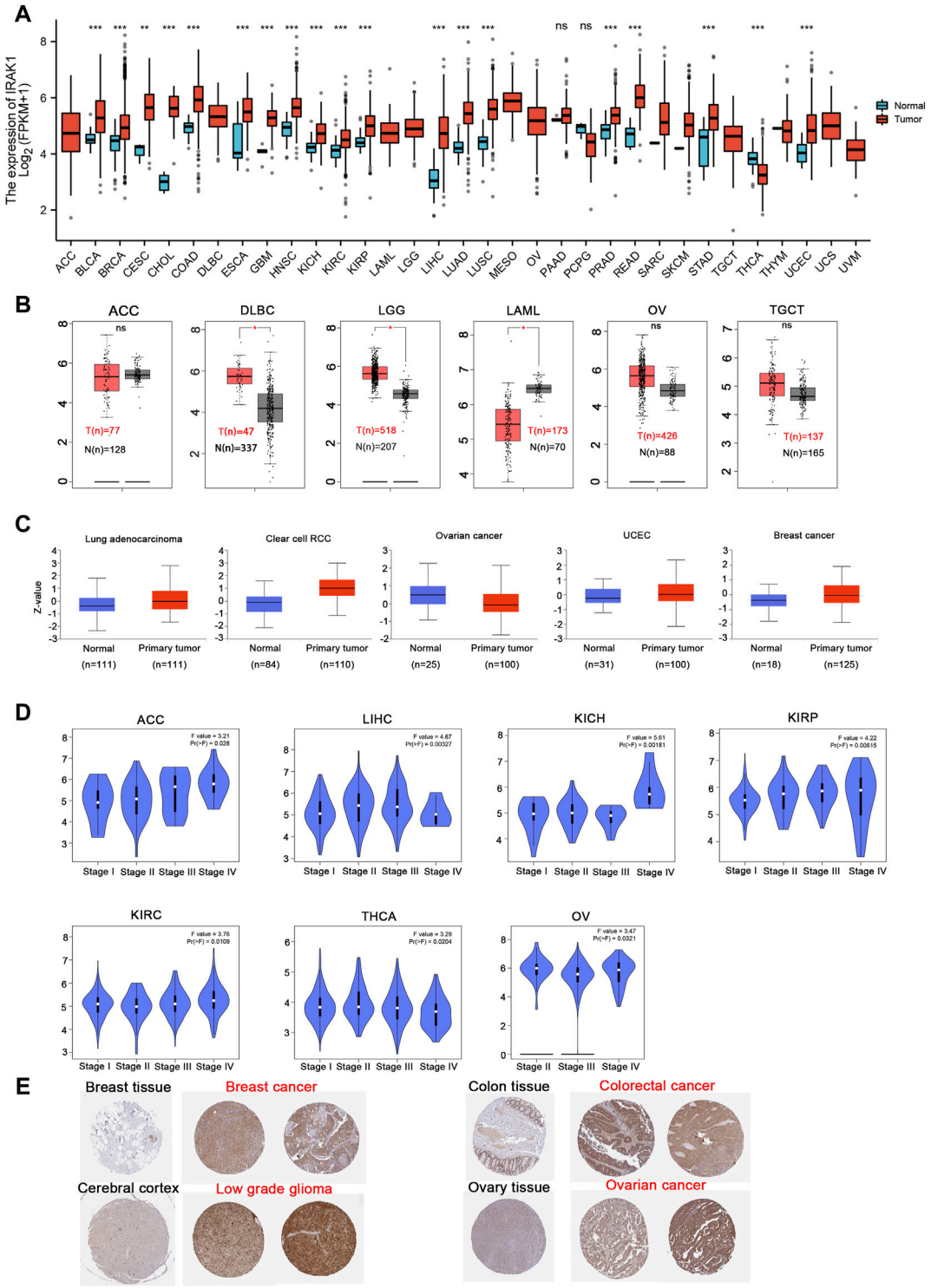

FIGURE 1 | Expression level of IRAK1 in different cancer and pathological stages. **(A)** IRAK1 expression in different cancer types from the TCGA database analyzed by the TIMER database. *$p < 0.05$; **$p < 0.01$; ***$p < 0.001$. **(B)** IRAK1 expression in the cancer type of ACC, DLBC, LGG, LAML, OV, TGCT from TCGA database analyzed by GEPIA database, and the normal tissues were included as controls. **$p < 0.01$. **(C)** The expression level of IRAK1 total protein between normal tissue and primary tissue of lung adenocarcinoma, clear cell RCC, ovarian cancer, UCEC and breast cancer were analyzed from the CPTAC dataset. ***$p < 0.001$. **(D)** The expression of IRAK1 based on the different pathological stages were analyzed in ACC, LIHC, KICH, KIRP, KIRC, THCA, OV in the TCGA database. **(E)** Representative immunohistochemical staining of IRAK1 in breast cancer, colorectal cancer, low grade glioma and ovarian cancer from the HPA (http://www.proteinatlas.org/).

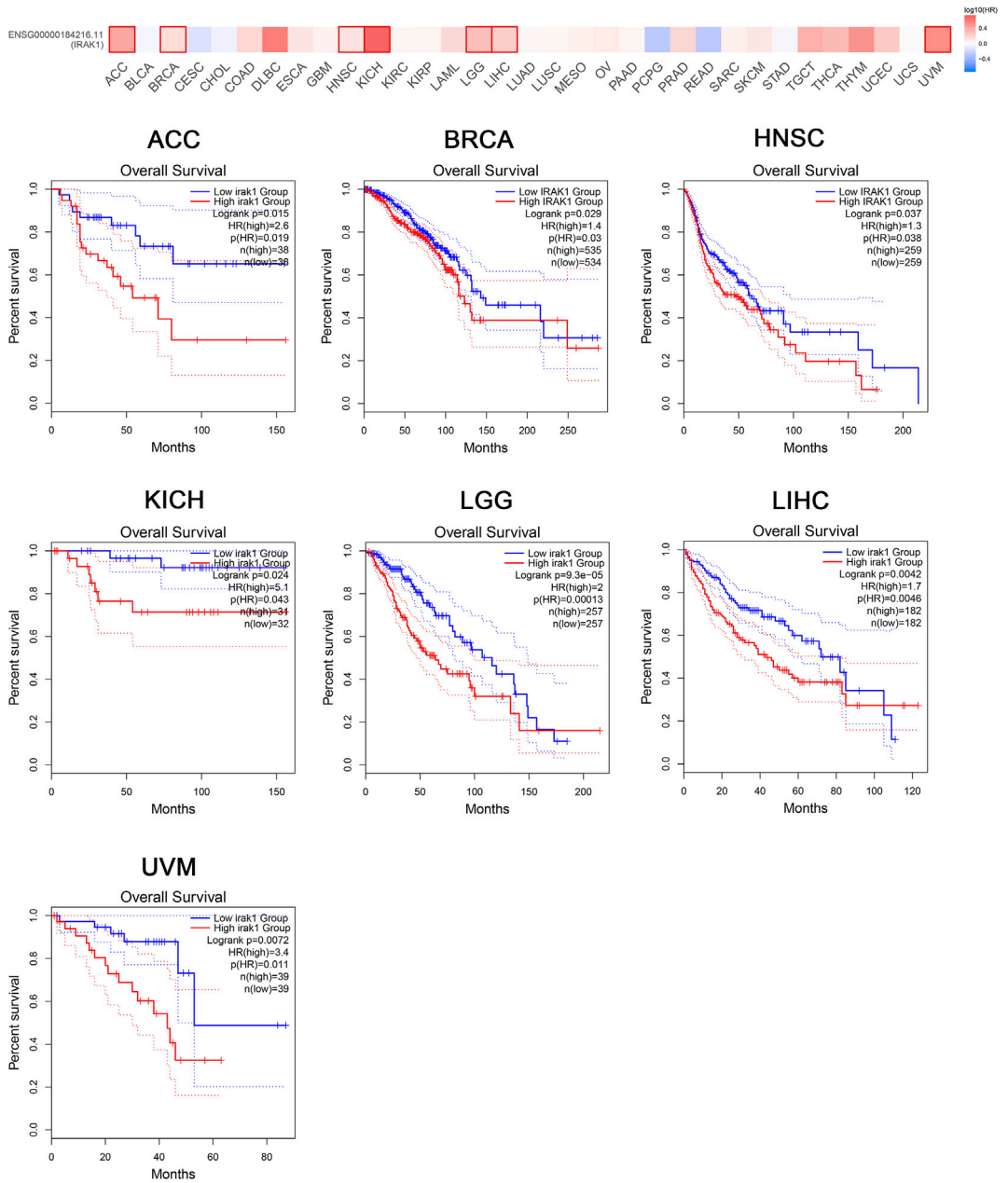

FIGURE 2 | Kaplan-Meier overall survival curve of pan-cancers with high and low expression of IRAK1. Correlations between IRAK1 gene expression and overall survival from TCGA database are showed. The GEPIA2 tool was used to show the survival map and perform the survival curves.

CHOL, COAD, ESCA, GBM, HNSC, KICH, KIRC, KIRP, LIHC, LUAD, LUSC, PRAD, READ, STAD, UCEC, DLBC, and LGG compared to their corresponding normal tissues ($p < 0.05$) (**Figures 1A,B**). However, IRAK1 expressions downregulated in THCA and LAML compared to those in normal tissues. We further evaluated the total protein levels of IRAK1 from the CPTAC dataset; the results revealed higher expressions in the primary tumor of LUAD, clear cell RCC, UCEC, and breast cancer than in normal tissues (**Figure 1C**). In addition, through GEPIA2.0, we found that IRAK1 levels were significantly different in different pathological cancer stages, including ACC, LIHC, KIRP, KIRC, THCA, and OV (**Figure 1D**). Specifically, higher expressions correlated with higher stages in ACC, KICH, KIRP, and KIRC.

Then, we investigated IRAK1 protein expressions from the HPA database, which provided the IHC results of IRAK1 expression in tumor and normal tissues. The analysis showed that normal breast, colon, cerebral cortex, and ovary tissues exhibited a negative or weak staining of IRAK1, while in the corresponding tumor tissues, such expressions displayed moderate or strong staining (**Figure 1E**). Altogether, these

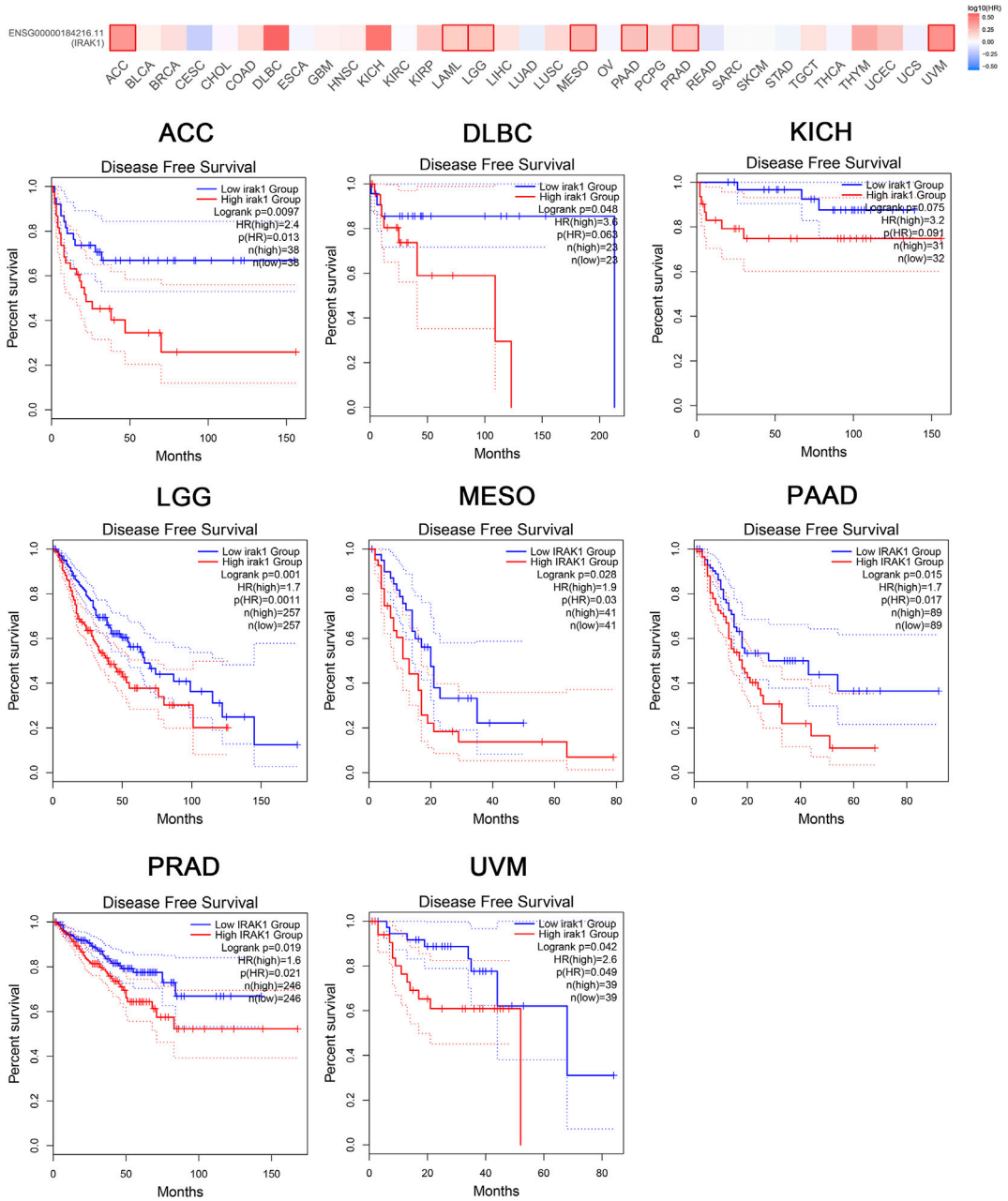

FIGURE 3 | Kaplan-Meier disease-free survival curve of pan-cancers with high and low expression of IRAK1. Correlations between IRAK1 gene expression and disease-free survival from TCGA database are showed. The GEPIA2 tool was used to show the survival map and perform the survival curves.

results indicated that IRAK1 might play a significant role in different cancers.

IRAK1 as a Prognostic Biomarker in Multiple Cancers

The prognostic value of IRAK1 in most human cancers remained unknown. Thus, we aimed to evaluate the prognostic role by analyzing the TCGA cohort using GEPIA2.0. We found that IRAK1 expression was associated with a poorer overall survival (OS) in ACC (p = 0.015, HR (high) = 2.6), BRCA (p = 0.029, HR (high) = 1.4), HNSC (p = 0.037, HR (high) = 1.3), KICH (p = 0.024, HR (high) = 5.1), LGG (p < 0.01, HR (high) = 2), LIHC (p = 0.0042, HR (high) = 1.7), and UVM (p = 0.0072, HR (high) = 3.4) (**Figure 2**).

Moreover, the analysis of DFS data revealed associations between high IRAK1 expression and poor prognosis among patients with ACC (p = 0.0097, HR (high) = 2.4), DLBC (p = 0.048, HR (high) = 3.6), KICH (p = 0.075, HR (high) = 3.2), LGG (p = 0.001, HR (high) = 1.7), MESO (p = 0.028, HR (high) = 1.9), PAAD (p = 0.015, HR (high) = 1.7), PRAD (p = 0.019, HR (high) = 1.6), and UVM (p =

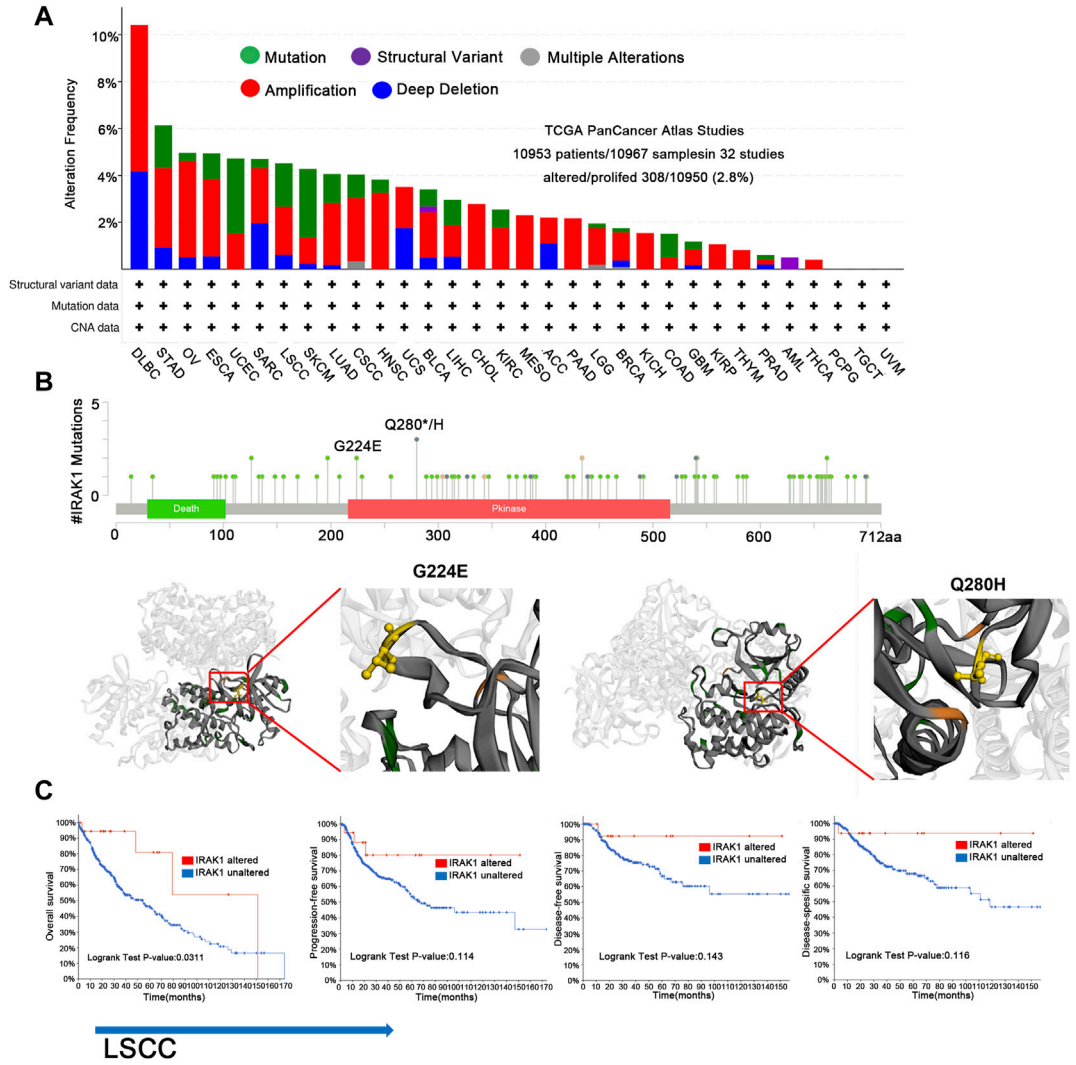

FIGURE 4 | Genetic aberration of IRAK1 in human pan-cancers from TCGA database. **(A)** Display of genetic aberration of IRAK1 by using the cBioportal tool. The alteration frequency was 2.8% (10,953 patients/10967 samples in 32 studies from TCGA pan-cancer panel). **(B)** All mutation sites of IRAK1 were distributed using cBioPortal. The most frequent mutation was Q180H/* in Pkinase site. Another mutation named G224E was also displayed. **(C)** Correlations of mutation status and different survival status of LSCC are shown using cBioPortal.

0.042, HR (high) = 2.6) (**Figure 3**). We further conducted analysis of DSS and PFS data across different cancers by showing forest plots (**Supplementary Figure S1**). The above data indicated IRAK1 as a potential prognostic biomarker in multiple cancers.

Frequencies of IRAK1 Alteration in Multiple Cancers

We then curated a pan-cancer analysis of IRAK1 genetic alteration. In the TCGA pan-cancer panel, the most frequent DNA alteration was amplification. Mutations were likewise distributed in multiple cancers, including STAD, ESCA, UCEC, LSCC, and SKCM (**Figure 4A**). The most frequent mutation was Q180H/*, situated in the Pkinase site. Another frequent mutation was G224E (**Figures 4B**). We then determined the correlation between mutations and prognosis in LSCC. We found that cases with altered IRAK1 depicted a better prognosis in overall survival (p = 0.311) and exhibited a trend of prognostic value in progression-free survival (p = 0.114), disease-free survival (p = 0.143), and disease-specific survival (p = 0.116) compared to cases without altered IRAK1 (**Figure 4C**). These results indicated that a high IRAK1 expression in tumor tissue might be due to gene amplification. Additionally, IRAK1 mutation might reduce its role in cancer, requiring further exploration.

Association of IRAK1 With Immune-Related Pathways Through Enrichment Analysis

We attempted to investigate the molecular mechanism of IRAK1 through analyzing the related and binding genes, then performed

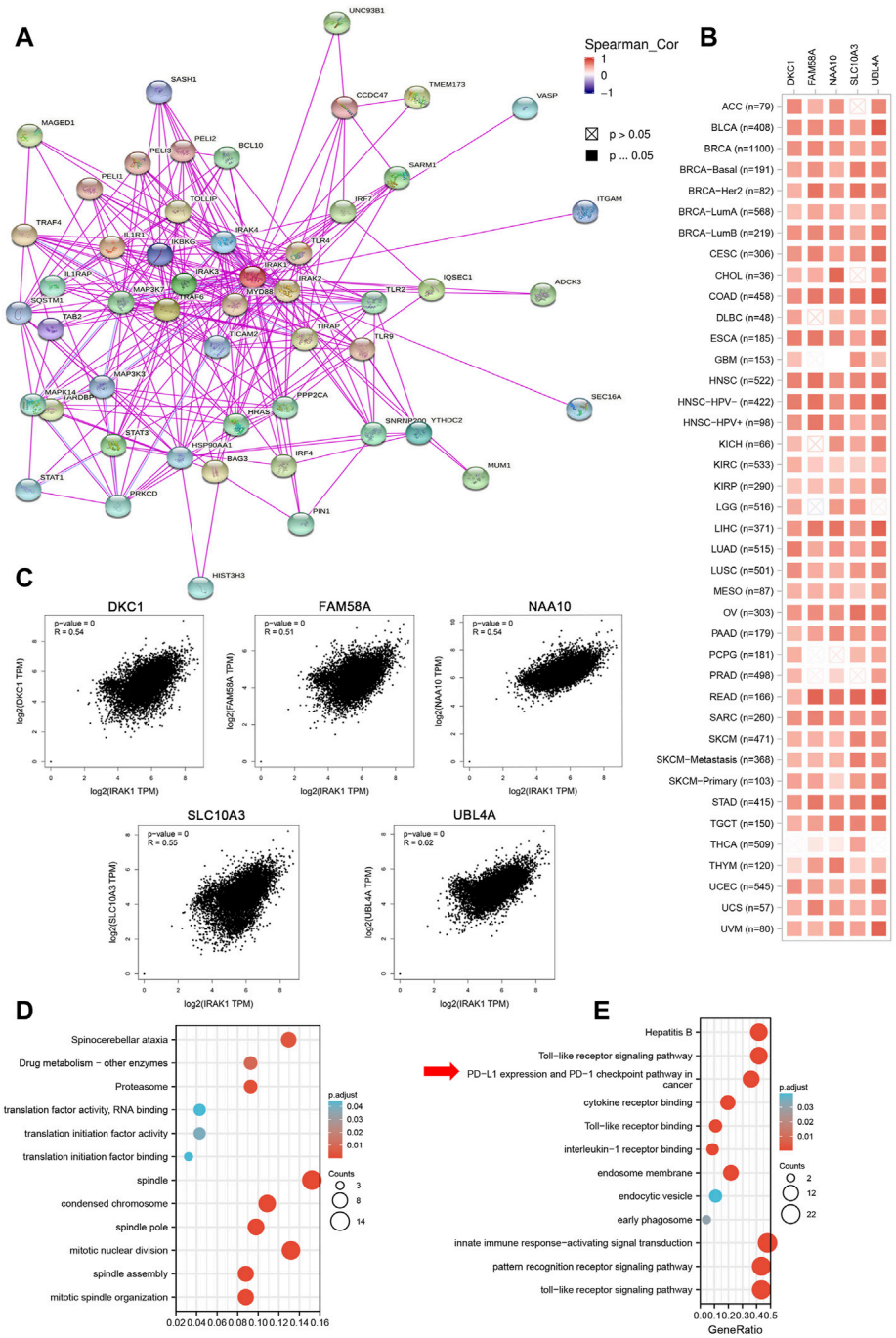

FIGURE 5 | IRAK1-related gene enrichment analysis. **(A)** IRAK1 binding proteins were determined by using STRING tool. **(B)** Top 100 IRAK1 correlated genes were analyzed by using GEPIA2 tool and the correlation of IRAK1 and top five genes (DKC1, FAM58A, NAA10, SLC10A3, UBL4A) were shown. **(C)** The correlation map of IRAK1 and top five correlated genes in TCGA pan-cancer panel was analyzed by using TIMER2.0. **(D)** GO-KEGG pathways analysis was performed based on the IRAK1 correlated genes. **(E)** GO-KEGG pathways analysis was performed based on the IRAK1 binding genes.

the enrichment analysis. As shown in **Figure 5A**, the interactions of IRAK-binding proteins were depicted using the STRING tool. We identified the top five related genes (DKC1, FAM58A, NAA10, SLC10A3, UBL4A) that mostly correlated with IRAK1 by GEPIA2.0; the heatmap displayed the correlation in pan-cancers (**Figure 5B**). In the TCGA pan-cancer cohort, IRAK1 expression positively correlated with DKC1 (R = 0.54), FAM58A (R = 0.51), NAA10 (R = 0.54), SLC10A3 (R = 0.55), and UBLA4 (R = 0.62) (**Figure 5C**). Notably, the KEGG and GO enrichment analysis of IRAK1 correlated genes suggested that

IRAK1 was related to immune pathways, including PD-L1 and PD-1 checkpoint pathway in cancer, Toll-like receptor signaling pathway, interleukin-1 receptor binding, and innate immune response-activating signal transduction (**Figures 5D,E**).

Correlations Between IRAK1 and Immune Checkpoint-Associated Genes and TME

Previous studies have demonstrated that immune checkpoint genes significantly influence tumor microenvironment and response to immunotherapy. Thus, we investigated the associations of IRAK1 expression and 20 primary immune checkpoint genes. The results exhibited strong positive relations with IRAK1 expression in multiple cancer types, including BLCA, BRCA, GBM, KIRC, KIRP, LGG, PCPG, and UVM, suggesting that a high IRAK1 expression might predict the better therapeutic efficacy of immunotherapy in targeting immune checkpoint genes (**Figure 6A**). KEGG and GO enrichment analysis of IRAK1 correlated genes suggested that IRAK1 was related to immune pathways, including PD-L1 and PD-1 checkpoint pathways. We further explored the potential relationship between PD-L1 (CD274) and IRAK1 gene expression in diverse cancer types of TCGA. A positive statistical correlation existed in ACC, BLCA, BRCA, KIRC, GBM, KIRP, LGG, LUAD, LUSC, OV, PCPG, STAD, UCEC, and UVM (**Figure 6B**).

After defining the associations with ICPs, we examined the relationship between IRAK1 and tumor-infiltrating immune cells in cancers using the CIBERSORT algorithm. The results revealed that IRAK1 expression negatively correlated with T cell $CD8^+$ in seven cancer types, but a positive relationship in UVM. Conversely, a statistically positive relationship existed with myeloid dendritic cells activated in five cancer types, macrophage M2 in eight cancer types, and macrophage M1 in ten cancer types (**Figure 7A**). The TIMER algorithm analyzed the relationship between IRAK1 and immune-infiltrating cells for further validation. We further found a strong positive relationship with myeloid dendritic cells and macrophages in multiple cancers from TCGA (**Figure 7A**).

Afterward, we explored the IRAK1 mRNA levels in various immune subtypes using TISDB. Immune subtypes had six types, including C1 (wound healing), C2 (IFN-gamma dominant), C3 (inflammatory), C4 (lymphocyte depleted), C5 (immunologically quiet), and C6 (TGF-b dominant). IRAK1 expression differed significantly in immune subtypes in BLCA, BRCA, LGG, LUAD, LUSC, PARD, STAD, and UCEC (**Figure 7B**). However, no significant difference existed in other cancer types (data not shown). Altogether, these results suggested that IRAK1 significantly influenced the tumor microenvironment and might be a potential target for PD-1 antibody immunotherapy.

IRAK1 Inhibitors Inhibit Proliferation and Upregulate PD-L1 Expression in Different Cancer Cell Lines

Then, we evaluated the effect of IRAK1 inhibitor pacritinib on the growth and proliferation of different cancer lines by the MTT assay, including MDA-MB-231, U251, Hep3B, Kyse30, and A498. The results suggested that pacritinib inhibited the proliferation in different cancer lines. The mean IC50 values ranged from 0.789 to 2.612 μM (**Supplementary Figure S2A**). Additionally, the colony formation assay revealed the inhibitory effect of pacritinib in a dose-dependent manner (**Supplementary Figure S2B**). Finally, to further explore the relationship between the treatment of IRAK1 inhibitor and PD-L1 expression in cancer, we performed a flow cytometry assay to detect PD-L1 levels in different cancer types. The results indicated that pacritinib treatment significantly upregulated protein expressions of PD-L1 in MDA-MB-231, U251, Hep3B, and Kyse30 ($p < 0.001$). However, the expression of PD-L1 in A498 had not significantly changed post-treatment (**Figure 8A**).

The Role of IRAK1 in the Prediction of Immunotherapeutic Benefits

In subsequent analyses, we examined the utility of IRAK1 expression the prediction of immunotherapeutic benefits. For the purposes of the study, patients receiving anti-PD-L1 immunotherapy in the IMvigor210 cohort were assigned high or low IRAK1. Notably, in the IMvigor210 cohort, patients with low IRAK1 had significantly better outcomes than those with high IRAK1 ($p = 0.036$). In the IMvigor210 cohort, the objective response rate to anti-PD-L1 therapy was higher in the low IRAK1 group than in the high IRAK1 group (27 vs. 18%, $p = 0.041$) (**Figure 8B**). Overall, these results indicate that the level of IRAK1 in cancer which could be significant biomarker both for predicting cancer survival and immunotherapy response in ACC, KICH, BRCA, LGG, and UVM.

DISCUSSION

IRAK1 plays a vital role in oncogenesis and tumor progression in multiple cancers and is shown to contribute to the progression of various cancers, including hepatocellular carcinoma (Chen et al., 2020), breast cancer (Wee et al., 2015), endometrial cancer (Wang et al., 2018), non-small cell lung cancer (Behrens et al., 2010) and melanoma (Boukerche et al., 2004; Srivastava et al., 2012). However, the systematic analysis in pan cancer and the relationship with immune system has not been investigated in detail.

In our study, we initially used GEPIA2, TIMER, and HPA databases to determine the mRNA, protein expression level of IRAK1 in cancers compared normal tissues, and found that its expression was significantly higher in 20 tumours. In addition, the expression level of IRAK1 was positively correlated with tumor stage in ACC, KICH, KIRP, and KIRC, suggesting that IRAK1 plays an important role in predicting tumor malignancy and aggressiveness. Then, the relationship between IRAK1 expression and prognosis were explored. The OS analysis indicated that IRAK1 is a risk factor for patients with ACC, BRCA, HNSC, KICH, LGG, LIHC and UVM. And for DFS, the results revealed that IRAK1 acts as a risk factor for patients with ACC, DLBC, KICH, LGG, MESO, PAAD, PRAD and UVM. These results indicated that IRAK1 is

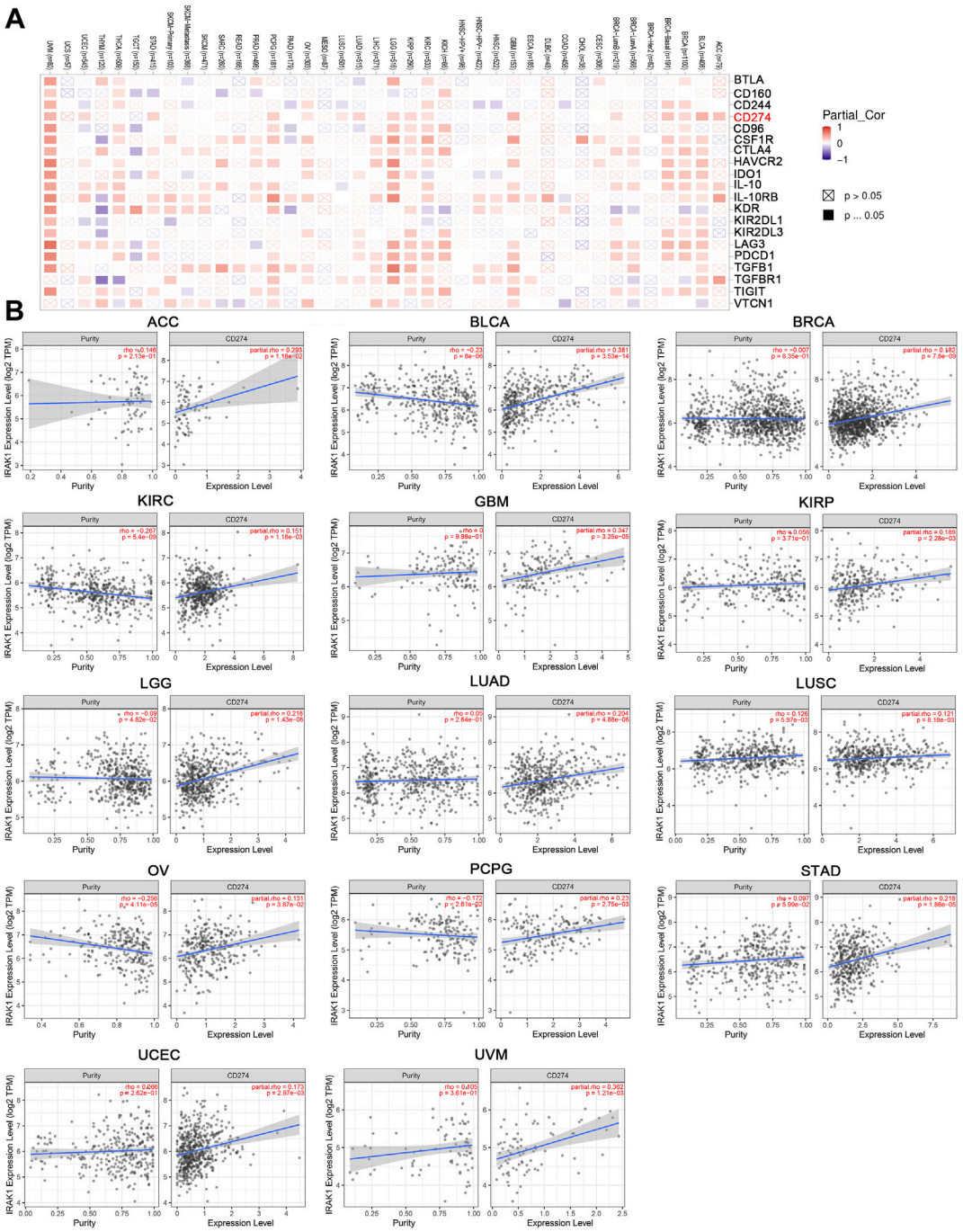

FIGURE 6 | IRAK1 expression is associated with immune checkpoint-associated genes in pan-cancers. **(A)** Heatmap representation of the correlation between IRAK1 expression and immune checkpoint-associated genes across pan-cancer types. **(B)** IRAK1 expression was positive associated with CD274 expression in ACC, BLCA, BRCA, KIRC, GBM, KIRP, LGG, LUAD, LUSC, OV, PCPG, STAD, UCEC and UVM analyzed by using TIMER2.0.

a potential prognostic biomarker and promotes oncogenesis and tumor progression in various cancer types, especially in the ACC and KICH.

We then presented the genetic alteration of IRAK1 across all cancer types in the TCGA cohort, depicting that the most frequent alteration was amplification. Although IRAK1 expression has been reported in several cancers to date, its amplification had not been examined before.

However, the relationship between IRAK1 and immune cells or immune pathways in tumors remains unclear. Therefore, we found that IRAK1 is related to a variety of immune signaling pathways in tumors, including toll-like

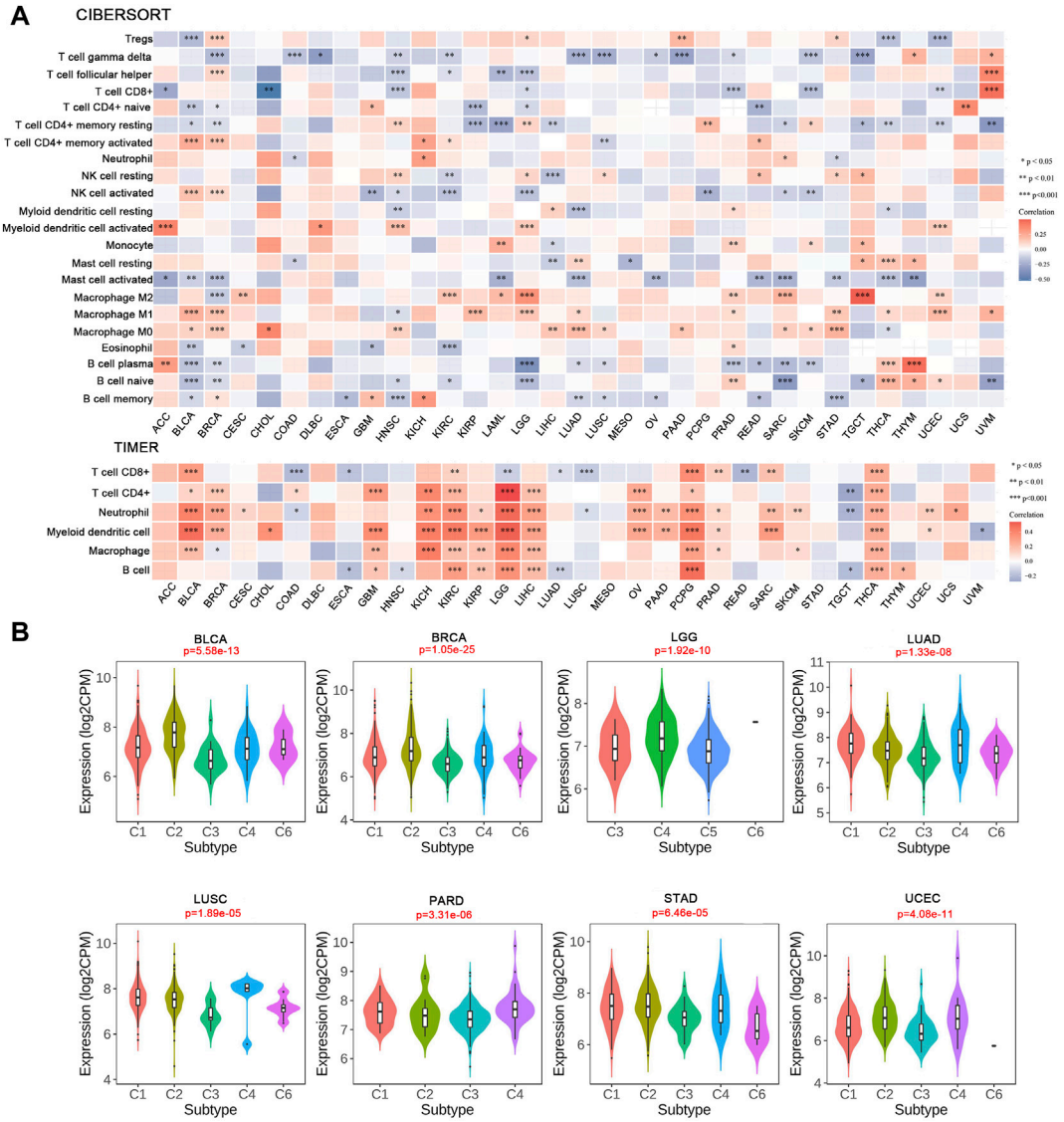

FIGURE 7 | Correlation analysis between IRAK1 expression and tumor-infiltrating immune cells. **(A)** Correlation analysis of IRAK1 mRNA expression with different immune cells from TCGA database by CIBERSORT and TIMER. **(B)** The relationship between IRAK1 expression in pan-cancer immune subtypes. C1 (wound healing); C2(IFN-gamma dominant); C3 (inflammatory); C4 (lymphocyte depleted); C5 (immunologically quiet); C6 (TGF-b dominant).

receptor signaling Pathway, interlekin-1 receptor binding and innate immune response-activating signal transduction and immune checkpoint signaling. The relationship between IRAK1 and autoimmunity has been explored. For example, some studies have examined the potential associations of SNPs in IRAK1 and miRNA-146 and the development of arthritis (Chatzikyriakidou et al., 2010a; Chatzikyriakidou et al., 2010b; Song et al., 2015). Moreover, evidence suggested that anti-IRAK1 exhibited unusual activity in a murine arthritis model (Madan et al., 2012). Another study identified the genetic association between IRAK1 SNPs and the increased risk factors for SLE (Jacob et al., 2009). On the other hand, it has been reported that IRAK1 regulates immune cells to control excessive inflammatory responses *in vivo* and induce chronic inflammation by participating in TLR and Interlekin-1 receptor signaling pathways (Wang et al., 2020; Hu et al., 2021). Further analysis of the relationship between IRAK1 and tumor immune-infiltrating cells showed that IRAK1 was positively correlated with M2 macrophage cells and negatively correlated with CD8+T cells in multiple tumors. It is well-known that M2 tumor-associated macrophages inhibit immune cells against tumor immune responses, leading to the formation of tumor immunosuppressive microenvironment and promoting tumor proliferation and metastasis (Yang et al., 2020). In addition, IRAK1 have reported that promotes the progression of hepatocellular

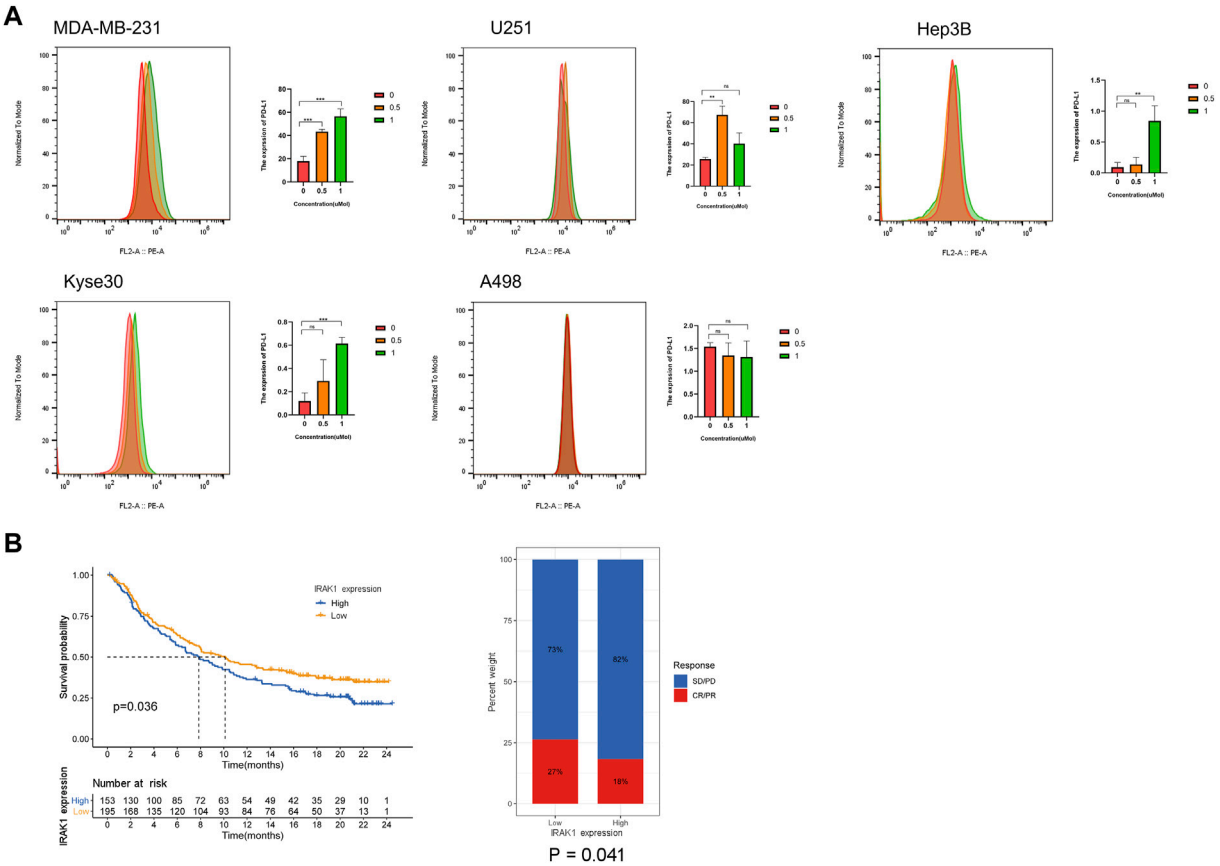

FIGURE 8 | IRAK1 expression predicts the benefits in the immunotherapeutic treatments. **(A)** MDA-MB-231, U251, Hep3B, Kyse30 and A498 cells treated with DMSO control and IRAK1 inhibitors pacritinib (0.5μM, 1 μM) for 48 h were subjected to FACs analysis for cell surface PD-L1 expression. Quantification of PD-L1 is shown. Every experiment was run in three independent experiments. *<0.05, **<0.01, ***$p < 0.001$. **(B)** Patients receiving anti-PD-L1 immunotherapy in the IMvigor210 cohort were assigned high or low IRAK1. Notably, in the IMvigor210 cohort, patients with low IRAK1 had significantly better outcomes than those with high IRAK1 ($p = 0.036$). In the IMvigor210 cohort, the objective response rate to anti-PD-L1 therapy was higher in the low IRAK1 group than in the high IRAK1 group (27 vs. 18%, $p = 0.041$). The IMvigor210 dataset was downloaded from a freely available, fully documented software and data package, under the Creative Commons 3.0 license that can be downloaded from http://research-pub.gene.com/IMvigor210CoreBiologies. A total of 298 urothelial cancer cases with complete clinical information, were analyzed to determine the immunotherapy response.

carcinoma by participating in the chronic inflammation mediated by macrophages, which is consistent with the positive correlation between IRAK1 and macrophage expression in liver cancer found in this study (Li et al., 2015).

To our knowledge, as anti- PD-1/PD-L1 had attained considerable clinical efficacy in various cancer types, the relationship between IRAK1 and PD-1/PD-L1 axis remains unknown, which motivated us to explore the role of IRAK1 in PD-L1 regulation. To understand fully the role of IRAK1 in the regulation of PD-L1 protein expression, we investigated the associations of IRAK1 expression and PD-L1 and other main immune checkpoint genes. The results indicated that strong positive relationships with PD-L1(CD274) and IRAK1 gene expression in diverse cancer types of TCGA. Using IMvigor210 to evaluate patients receiving anti-PD-L1 therapy, we found that patients with low IRAK1 expression had a better prognosis, and the objective response rate of patients with low IRAK1 expression was higher than that of patients with high IRAK1 expression, indicating that IRAK1 can be used as a reliable marker to predict the efficacy of immunotherapy. Overall, this suggests that immunotherapy may benefit patients with low IRAK1 expression.

Although IRAK1 has been proved to play an important role in tumor malignant proliferation, metastasis and drug resistance acquisition in a variety of tumors, the clinical usefulness of IRAK1 inhibitor has not been clarified in clinical studies (Jain, Kaczanowska, and Davila 2014; Wee et al., 2015; Meng et al., 2020). Pacritinib, an IRAK1 inhibitor, which has been shown to be effective in myelofibrosis, and acute myeloid leukemia (Hart et al., 2011; Mesa et al., 2017). We used pacritinib to treat five different tumor cell lines, including esophageal cancer, liver cancer, glioma, breast cancer and kidney cancer, and found that pacritinib effectively inhibited tumor proliferation, suggesting that pacritinib may be a potential anti-pan cancer inhibitor. In addition, pacritinib has also been reported to reduce chemotherapy resistance in nasopharyngeal carcinoma, mainly by regulating the phosphorylation level of IRAK1, thereby inhibiting the expression of S100A9 and reducing the patients

with nasopharyngeal carcinoma resistance to paclitaxel (Liu et al., 2021). In order to verify the relationship between PD-L1 and IRAK1, we used flow cytometry to detect PD-L1 expression in tumor cells treated with different concentrations of pacritinib and found that the level of PD-L1 upregulated, suggesting that IRAK1 correlated with PD-1/PD-L1 axis and mediated immunosuppression. Thus, inhibiting the expression level of IRAK1 in the tumor microenvironment may improve anti-tumor immune responses. In addition, the combination of IRAK1 inhibitor with immunotherapy is expected to be a feasible treatment for patients with cancer with high IRAK1 expression. Pacritinib, a IRAK1 inhibitor which also dual affects the expression of JAK2 and FLT3. And JAK2 and FLT3 have been proved to be important molecules involved in the regulation of PD-L1 in different kind tumors (Prestipino et al., 2018; Brodská et al., 2019). Therefore, there may be differences in the detail mechanism of its regulating PD-L1 in different tumors, which needs to be validated by further research.

Although we performed a comprehensive and systematic analysis on IRAK1 and utilized different databases for verifying the role of IRAK1, there are some limitations in this study. First, the sequencing data from the different databases exhibited differences and lacked granularity and specificity, which might entail systematic bias. Second, *in vivo* and mechanistic experiments are necessary to prove our results on the potential functions of IRAK1, which can increase our research credibility. Finally, the mechanisms by which IRAK1 participates in immune regulation remain unknown, and the exact pathways require further study.

To conclude, more specific and clinical samples are necessary to identify the benefits of anti-IRAK1 in cancer survival. Therefore, prospective studies on targeting IRAK1 to anti-tumor immunotherapy are vital.

DATA AVAILABILITY STATEMENT

The raw data supporting the conclusion of this article will be made available by the authors, without undue reservation.

AUTHOR CONTRIBUTIONS

ML, YQ, and YZ designed and provided financial support for this study. YH performed experiments. LZ performed data analysis. XZ supervised data acquisition and provided feedback and suggestions on the manuscript.

FUNDING

This work was supported by the Key Technology Research Project of Guangzhou Science, Technology and Innovation Committee (No. 201902020001) and the Guangzhou Science and Technology project (No. 201905010004) and National Scientific Foundation of China (No. 82002835).

ACKNOWLEDGMENTS

We would like to thank the participants and staff of this project.

SUPPLEMENTARY MATERIAL

The Supplementary Material for this article can be found online at: https://www.frontiersin.org/articles/10.3389/fmolb.2022.904959/full#supplementary-material

REFERENCES

Behrens, C., Feng, L., Kadara, H., Kim, H.-J., Lee, J. J., Mehran, R., et al. (2010). Expression of Interleukin-1 Receptor-Associated Kinase-1 in Non-small Cell Lung Carcinoma and Preneoplastic Lesions. *Clin. Cancer Res.* 16 (1), 34–44. doi:10.1158/1078-0432.CCR-09-0650

Boukerche, H., Su, Z.-Z., Kang, D.-C., and Fisher, P. B. (2004). Identification and Cloning of Genes Displaying Elevated Expression as a Consequence of Metastatic Progression in Human Melanoma Cells by Rapid Subtraction Hybridization. *Gene* 343 (1), 191–201. doi:10.1016/j.gene.2004.09.002

Brodská, B., Otevřelová, P., Šálek, C., Fuchs, O., Gašová, Z., and Kuželová, K. (2019). High PD-L1 Expression Predicts for Worse Outcome of Leukemia Patients with Concomitant NPM1 and FLT3 Mutations. *Ijms* 20 (11), 2823. doi:10.3390/ijms20112823

Chatzikyriakidou, A., Voulgari, P. V., Georgiou, I., and Drosos, A. A. (2010a). A Polymorphism in the 3'-UTR of Interleukin-1 Receptor-Associated Kinase (IRAK1), a Target Gene of miR-146a, Is Associated with Rheumatoid Arthritis Susceptibility. *Jt. Bone Spine* 77 (5), 411–413. doi:10.1016/j.jbspin.2010.05.013

Chatzikyriakidou, A., Voulgari, P. V., Georgiou, I., and Drosos, A. A. (2010b). The Role of microRNA-146a (miR-146a) and its Target IL-1R-associated Kinase (IRAK1) in Psoriatic Arthritis Susceptibility. *Scand. J. Immunol.* 71 (5), 382–385. doi:10.1111/j.1365-3083.2010.02381.x

Chen, W., Wei, T., Chen, Y., Yang, L., and Wu, X. (2020). Downregulation of IRAK1 Prevents the Malignant Behavior of Hepatocellular Carcinoma Cells by Blocking Activation of the MAPKs/NLRP3/IL-1β Pathway. *Ott* Vol. 13, 12787–12796. doi:10.2147/OTT.S260793

Cheng, B. Y., Lau, E. Y., Leung, H.-W., Leung, C. O.-N., Ho, N. P., Gurung, S., et al. (2018). IRAK1 Augments Cancer Stemness and Drug Resistance via the AP-1/AKR1B10 Signaling Cascade in Hepatocellular Carcinoma. *Cancer Res.* 78 (9), 2332–2342. doi:10.1158/0008-5472.CAN-17-2445

Davis, A. A., and Patel, V. G. (2019). The Role of PD-L1 Expression as a Predictive Biomarker: an Analysis of All US Food and Drug Administration (FDA) Approvals of Immune Checkpoint Inhibitors. *J. Immunother. cancer* 7 (1), 278. doi:10.1186/s40425-019-0768-9

Dudnik, E., Peled, N., Nechushtan, H., Wollner, M., Onn, A., Agbarya, A., et al. (2018). BRAF Mutant Lung Cancer: Programmed Death Ligand 1 Expression, Tumor Mutational Burden, Microsatellite Instability Status, and Response to Immune Check-Point Inhibitors. *J. Thorac. Oncol.* 13 (8), 1128–1137. doi:10.1016/j.jtho.2018.04.024

Flannery, S., and Bowie, A. G. (2010). The Interleukin-1 Receptor-Associated Kinases: Critical Regulators of Innate Immune Signalling. *Biochem. Pharmacol.* 80 (12), 1981–1991. doi:10.1016/j.bcp.2010.06.020

Galluzzi, L., Humeau, J., Buqué, A., Zitvogel, L., and Kroemer, G. (2020). Immunostimulation with Chemotherapy in the Era of Immune Checkpoint Inhibitors. *Nat. Rev. Clin. Oncol.* 17 (12), 725–741. doi:10.1038/s41571-020-0413-z

Hanahan, D., and Weinberg, R. A. (2011). Hallmarks of Cancer: the Next Generation. *Cell.* 144 (5), 646–674. doi:10.1016/j.cell.2011.02.013

Hart, S., Goh, K. C., Novotny-Diermayr, V., Tan, Y. C., Madan, B., Amalini, C., et al. (2011). Pacritinib (SB1518), a JAK2/FLT3 Inhibitor for the Treatment of Acute Myeloid Leukemia. *Blood Cancer J.* 1 (11), e44. doi:10.1038/bcj.2011.43

Hu, Y.-H., Wang, Y., Wang, F., Dong, Y.-M., Jiang, W.-L., Wang, Y.-P., et al. (2021). SPOP Negatively Regulates Toll-like Receptor-Induced Inflammation by Disrupting MyD88 Self-Association. *Cell. Mol. Immunol.* 18 (7), 1708–1717. doi:10.1038/s41423-020-0411-1

Jacob, C. O., Zhu, J., Armstrong, D. L., Yan, M., Han, J., Zhou, X. J., et al. (2009). Identification of IRAK1 as a Risk Gene with Critical Role in the Pathogenesis of Systemic Lupus Erythematosus. *Proc. Natl. Acad. Sci. U.S.A.* 106 (15), 6256–6261. doi:10.1073/pnas.0901181106

Jain, A., Kaczanowska, S., and Davila, E. (2014). IL-1 Receptor-Associated Kinase Signaling and its Role in Inflammation, Cancer Progression, and Therapy Resistance. *Front. Immunol.* 5, 553. doi:10.3389/fimmu.2014.00553

Keam, S. J. (2019). Toripalimab: First Global Approval. *Drugs* 79 (5), 573–578. doi:10.1007/s40265-019-01076-2

Khoja, L., Butler, M. O., Kang, S. P., Ebbinghaus, S., and Joshua, A. M. (2015). Pembrolizumab. *J. Immunother. cancer* 3, 36. doi:10.1186/s40425-015-0078-9

Li, W., Xiao, J., Zhou, X., Xu, M., Hu, C., Xu, X., et al. (2015). STK4 Regulates TLR Pathways and Protects against Chronic Inflammation-Related Hepatocellular Carcinoma. *J. Clin. Invest.* 125 (11), 4239–4254. doi:10.1172/JCI81203

Liu, L., Liu, S., Deng, P., Liang, Y., Xiao, R., Tang, L.-Q., et al. (2021). Targeting the IRAK1-S100a9 Axis Overcomes Resistance to Paclitaxel in Nasopharyngeal Carcinoma. *Cancer Res.* 81 (5), 1413–1425. doi:10.1158/0008-5472.CAN-20-2125

Lu, Z., Chen, H., Li, S., Gong, J., Li, J., Zou, J., et al. (2020). Tumor Copy-Number Alterations Predict Response to Immune-Checkpoint-Blockade in Gastrointestinal Cancer. *J. Immunother. Cancer* 8 (2), e000374. doi:10.1136/jitc-2019-000374

Madan, B., Goh, K. C., Hart, S., William, A. D., Jayaraman, R., Ethirajulu, K., et al. (2012). SB1578, a Novel Inhibitor of JAK2, FLT3, and C-Fms for the Treatment of Rheumatoid Arthritis. *J. I.* 189 (8), 4123–4134. doi:10.4049/jimmunol.1200675

Meng, D.-F., Sun, R., Liu, G.-Y., Peng, L.-X., Zheng, L.-S., Xie, P., et al. (2020). S100A14 Suppresses Metastasis of Nasopharyngeal Carcinoma by Inhibition of NF-kB Signaling through Degradation of IRAK1. *Oncogene* 39 (30), 5307–5322. doi:10.1038/s41388-020-1363-8

Mesa, R. A., Vannucchi, A. M., Mead, A., Egyed, M., Szoke, A., Suvorov, A., et al. (2017). Pacritinib versus Best Available Therapy for the Treatment of Myelofibrosis Irrespective of Baseline Cytopenias (PERSIST-1): an International, Randomised, Phase 3 Trial. *Lancet Haematol.* 4 (5), e225–e236. doi:10.1016/S2352-3026(17)30027-3

Prestipino, A., Emhardt, A. J., Aumann, K., O'Sullivan, D., Gorantla, S. P., Duquesne, S., et al. (2018). Oncogenic JAK2 V617F Causes PD-L1 Expression, Mediating Immune Escape in Myeloproliferative Neoplasms. *Sci. Transl. Med.* 10 (429), eaam7729. doi:10.1126/scitranslmed.aam7729

Rhyasen, G. W., and Starczynowski, D. T. (2015). IRAK Signalling in Cancer. *Br. J. Cancer* 112 (2), 232–237. doi:10.1038/bjc.2014.513

Samstein, R. M., Lee, C.-H., Shoushtari, A. N., Hellmann, M. D., Shen, R., Janjigian, Y. Y., et al. (2019). Tumor Mutational Load Predicts Survival after Immunotherapy across Multiple Cancer Types. *Nat. Genet.* 51 (2), 202–206. doi:10.1038/s41588-018-0312-8

Singer, J. W., Fleischman, A., Al-Fayoumi, S., Mascarenhas, J. O., Yu, Q., and Agarwal, A. (2018). Inhibition of Interleukin-1 Receptor-Associated Kinase 1 (IRAK1) as a Therapeutic Strategy. *Oncotarget* 9 (70), 33416–33439. doi:10.18632/oncotarget.26058

Song, G. G., Bae, S.-C., Seo, Y. H., Kim, J.-H., Choi, S. J., Ji, J. D., et al. (2015). The Association between Susceptibility to Inflammatory Arthritis and miR-146a, miR-499 and IRAK1 Polymorphisms. *Z Rheumatol.* 74 (7), 637–645. doi:10.1007/s00393-014-1493-x

Srivastava, R., Geng, D., Liu, Y., Zheng, L., Li, Z., Joseph, M. A., et al. (2012). Augmentation of Therapeutic Responses in Melanoma by Inhibition of IRAK-1,-4. *Cancer Res.* 72 (23), 6209–6216. doi:10.1158/0008-5472.CAN-12-0337

Su, L.-C., Xu, W.-D., and Huang, A.-F. (2020). IRAK Family in Inflammatory Autoimmune Diseases. *Autoimmun. Rev.* 19 (3), 102461. doi:10.1016/j.autrev.2020.102461

Vaddepally, R. K., Kharel, P., Pandey, R., Garje, R., and Chandra, A. B. (2020). Review of Indications of FDA-Approved Immune Checkpoint Inhibitors Per NCCN Guidelines with the Level of Evidence. *Cancers* 12 (3), 738. doi:10.3390/cancers12030738

Vollmer, S., Strickson, S., Zhang, T., Gray, N., Lee, K. L., Rao, V. R., et al. (2017). The Mechanism of Activation of IRAK1 and IRAK4 by Interleukin-1 and Toll-like Receptor Agonists. *Biochem. J.* 474 (12), 2027–2038. doi:10.1042/BCJ20170097

Wang, H., Zhou, H., Zhang, Q., Poulsen, K. L., Taylor, V., McMullen, M. R., et al. (2020). Inhibition of IRAK4 Kinase Activity Improves Ethanol-Induced Liver Injury in Mice. *J. Hepatology* 73 (6), 1470–1481. doi:10.1016/j.jhep.2020.07.016

Wang, Y., Wang, Y., Duan, X., Wang, Y., and Zhang, Z. (2018). Interleukin-1 Receptor-associated Kinase 1 Correlates with Metastasis and Invasion in Endometrial Carcinoma. *J. Cell. Biochem.* 119 (3), 2545–2555. doi:10.1002/jcb.26416

Wee, Z. N., Yatim, S. M. J. M., Kohlbauer, V. K., Feng, M., Goh, J. Y., Bao, Y., et al. (2015). IRAK1 Is a Therapeutic Target that Drives Breast Cancer Metastasis and Resistance to Paclitaxel. *Nat. Commun.* 6, 8746. doi:10.1038/ncomms9746

Yang, Q., Guo, N., Zhou, Y., Chen, J., Wei, Q., and Han, M. (2020). The Role of Tumor-Associated Macrophages (TAMs) in Tumor Progression and Relevant Advance in Targeted Therapy. *Acta Pharm. Sin. B* 10 (11), 2156–2170. doi:10.1016/j.apsb.2020.04.004

Zhao, X., Shen, J., Ivaturi, V., Gopalakrishnan, M., Feng, Y., Schmidt, B. J., et al. (2020). Model-based Evaluation of the Efficacy and Safety of Nivolumab once Every 4 Weeks across Multiple Tumor Types. *Ann. Oncol.* 31 (2), 302–309. doi:10.1016/j.annonc.2019.10.015

Conflict of Interest: The authors declare that the research was conducted in the absence of any commercial or financial relationships that could be construed as a potential conflict of interest.

Publisher's Note: All claims expressed in this article are solely those of the authors and do not necessarily represent those of their affiliated organizations, or those of the publisher, the editors and the reviewers. Any product that may be evaluated in this article, or claim that may be made by its manufacturer, is not guaranteed or endorsed by the publisher.

GLOSSARY

ACC adrenocortical carcinoma
BLCA bladder urothelial carcinoma
BRCA breast invasive carcinoma
CAN tumor copy-number alterations
CESC cervical squamous cell carcinoma and endocervical adenocarcinoma
CHOL cholangiocarcinoma
COAD colon adenocarcinoma
DMEM dulbecco's modified eagle medium
DLBC lymphoid neoplasm diffuse large B-cell lymphoma
ESCA esophageal carcinoma
GBM glioblastoma multiforme
HNSC head and neck squamous cell carcinoma
ICIs immune checkpoint inhibitors
KICH kidney chromophobe
KIRC kidney renal clear cell carcinoma
KIRP kidney renal papillary cell carcinoma
LGG brain lower grade glioma
LIHC liver hepatocellular carcinoma
LUAD lung adenocarcinoma
LUSC lung squamous cell carcinoma
MESO mesothelioma
MSI tumor microsatellite instability
OV ovarian serous cystadenocarcinoma
PRAD prostate adenocarcinoma
PAAD Pancreatic adenocarcinoma
PCPG pheochromocytoma and paraganglioma
RCC renal carcinoma
READ rectum adenocarcinoma
STAD stomach adenocarcinoma
TCGA the cancer genome atlas
TMB tumor mutation burden
THCA thyroid carcinoma
UVM uveal melanoma
UCEC uterine corpus endometrial carcinoma

frontiers | Frontiers in Molecular Biosciences

TYPE Review
PUBLISHED 10 August 2022
DOI 10.3389/fmolb.2022.939050

OPEN ACCESS

EDITED BY
José Alexandre Ferreira,
Portuguese Oncology Institute,
Portugal

REVIEWED BY
Kamla Kant Shukla,
All India Institute of Medical Sciences
Jodhpur, India
Reetobrata Basu,
Ohio University, United States

*CORRESPONDENCE
Gauri Mishra,
gaurishukla1@gmail.com

†These authors have contributed equally to this work

SPECIALTY SECTION
This article was submitted to Molecular Diagnostics and Therapeutics, a section of the journal Frontiers in Molecular Biosciences

RECEIVED 08 May 2022
ACCEPTED 15 July 2022
PUBLISHED 10 August 2022

CITATION
Mishra LC, Pandey U, Gupta A, Gupta J, Sharma M and Mishra G (2022), Alternating exosomes and their mimetics as an emergent strategy for targeted cancer therapy.
Front. Mol. Biosci. 9:939050.
doi: 10.3389/fmolb.2022.939050

Alternating exosomes and their mimetics as an emergent strategy for targeted cancer therapy

Lokesh Chandra Mishra[1†], Utkarsh Pandey[2], Abhikarsh Gupta[3], Jyotsna Gupta[3], Monal Sharma[4] and Gauri Mishra[2,5*†]

[1]Department of Zoology, Hansraj College, University of Delhi, New Delhi, India, [2]Department of Zoology, Swami Shraddhanand College, University of Delhi, New Delhi, India, [3]Department of Microbiology, Swami Shraddhanand College, University of Delhi, New Delhi, India, [4]Betterhumans Inc., Gainesville, FL, United States, [5]Division Radiopharmaceuticals and Radiation Biology, Institute of Nuclear Medicine and Allied Sciences, New Delhi, India

Exosomes, a subtype of the class of extracellular vesicles and nano-sized particles, have a specific membrane structure that makes them an alternative proposition to combat with cancer through slight modification. As constituents of all most all the primary body fluids, exosomes establish the status of intercellular communication. Exosomes have specific proteins/mRNAs and miRNAs which serve as biomarkers, imparting a prognostic tool in clinical and disease pathologies. They have efficient intrinsic targeting potential and efficacy. Engineered exosomes are employed to deliver therapeutic cargos to the targeted tumor cell or the recipient. Exosomes from cancer cells bring about changes in fibroblast via TGFβ/Smad pathway, augmenting the tumor growth. These extracellular vesicles are multidimensional in terms of the functions that they perform. We herein discuss the uptake and biogenesis of exosomes, their role in various facets of cancer studies, cell-to-cell communication and modification for therapeutic and diagnostic use.

KEYWORDS

exosome, targeted delivery, exosome mimetics, biomarker, therapeutics

Introduction

Exosomes are recognized as a subtype of the class of Extracellular vesicles (EVs). These nano-sized particles appear as small, flattened hemispheres with a diameter of 40–150 nm and a density of 1.13–1.21 g/ml (Kalluri, 2016; Gilligan and Dwyer, 2017; Kalimuthu et al., 2018; You et al., 2018; Głuszko et al., 2019; Zhao and Xie, 2019). The orientation of the surrounding lipid bilayer membrane can be regarded unique as it serves

Abbreviations:: ARF, ADP ribosylation factor; LAMP, lysosome-associated membrane protein; MHC, major histocompatibility complex; MUC1, mucin 1; PGK-1, phosphoglycerate kinase 1; TfR, transferrin receptor.

as a reflection of the intrinsic cell from which the exosomes have originated (Kalluri, 2016; Kalimuthu et al., 2018; Głuszko et al., 2019; Zhao and Xie, 2019). The structural specificity of the membrane confers properties, proving to be useful in cancer treatments through selection of preferably modified exosomes (You et al., 2018).

Exosomes are remarkable constituents of all the major body fluids, including plasma, saliva, urine, cerebrospinal fluid (Zhao and Xie, 2019) and are also present as secretions or discharges of cells such as red blood cells, platelets, lymphocytes, dendritic cells and cancer cells (Głuszko et al., 2019). Nucleic acids like RNA [mRNAs, microRNAs (miRNA) and long noncoding RNA (IncRNA)] (Głuszko et al., 2019; Zhao and Xie, 2019), cellular proteins and lipids represent the contents of exosomes (Kalluri, 2016; Gilligan and Dwyer, 2017; Kalimuthu et al., 2018; You et al., 2018). Noteworthy, the presence of DNA in the exosomes is considered rather contradictory. It is thought to share a relation with the source of the exosomes in consideration (Fais et al., 2013). These contents are protected from degradation and are taken up *via* fusion by the target cell acting as receiver, thus establishing the status of exosomes as means of intercellular communication (Kalluri, 2016; You et al., 2018; Głuszko et al., 2019).

Majority of exosomal proteins are universal and are referred to as "exosome markers" (Głuszko et al., 2019). These include TSG101, ALIX and ESCRT complex (exosome biogenesis), RabGTPases and annexins (exosome delivery and membrane fusion), heat shock proteins (HSP70, HSP90), integrins, tetraspanins (CD9, CD63, CD81 and CD82), MHC class II proteins, epithelial cell adhesion molecules (EpCAM) and members of the human epidermal receptor (HER) family (Fais et al., 2013; Kalluri, 2016; Głuszko et al., 2019). Apart from the signature molecules present within them, there are certain specific proteins and nucleic acids acquired by the exosomes from their native cell types, which can serve as biomarkers for the identification of various diseases including cancer (Fais et al., 2013). Numerous genes and proteins have been identified in lung cancer cells and tissues that can serve as exosomal biomarkers for lung cancer. ZEB1, TRAF4, and TGF-β1 are involved in lung cancer metastasis by EMT proteins while PD-L1, EGFR, TLR7 and TLR8 are involved in inhibiting the immune system. Like other cancers, exosomes derived from breast cancer cells are enriched with certain miNAs that are not abundant in healthy cells. miR-372, miR-101 and miR-373 were not found in significantly higher proportions in exosomes from breast cancer cells. Certain nucleic acid molecules and proteins may also serve as diagnostic biomarkers of colorectal cancer (CRC). Among miRNAs, around 7 to 11 molecules have been identified to be differentially expressed in CRC patients. Similarly, in colorectal Cancer, the cell surface proteoglycan Glypican1 (GPC1) serves as the most prominent biomarker of pancreatic cancer.

Ovarian cancer cells derived exosomes include membrane proteins, Rab proteins, annexin proteins, tetraspanins, heat shock proteins *etc.* can be used to potentially identify the malignancy early in its development. Besides, *Helicobacter pylori* infection is the most common factor that predisposes a person to develop gastric cancer by transporting the virulence factor CagA (mediator of gastric disorders) to epithelial cells and mesenchymal-epithelial transition factor (MET) protein to macrophages. The exosomes are enriched in lipids such as cholesterol, sphingomyelin, hexosylceramides, phosphatidylserine, phosphatidylcholine, phosphatidylethanolamines and saturated fatty acids (Figure 1) (Fais et al., 2013; Kalluri, 2016). Moreover, presence of lipid-raft like domains (due to membrane associated lipid-raft proteins) and/or phospholipid scramblase (responsible for translocating phospholipids of membrane leaflets) have also been consistently reported (Fais et al., 2013).

Exosomes are found to be enriched with the presence numerous classes of RNAs encompassing various expressed and significantly matured miRNAs and mRNAs. They are known to have eminent effects on physiological and developmental aspects of growth, development and regulation of expression in the recipient cell (Kalluri, 2016; Głuszko et al., 2019). Interestingly, recent studies have established a strong notion governing the fact that exosomes are acting as molecular vehicles by showing the presence of placental specific miRNA in the maternal blood exported *via* mature trophoblast, imparting the ability to modify genetic expressions (Fais et al., 2013).

Exosomes: Biogenesis

Exosomes are constitutively produced by cells through the inward budding of the plasma membrane leading to the formation of intracellular endosomes, which further fold in to form multivesicular bodies (MVBs). These MVBs contain nano-sized vesicles which after fusing with the plasma membrane release their contents to the extracellular space leading to the release of exosomes (Fais et al., 2013; Kalluri, 2016).

Exosomes are predominantly generated by the aid of endosomal sorting complexes required for transport complexes (ESCRT complexes) (Figure 2). ESCRT is composed of four complexes namely ESCRT-0, ESCRT-I, ESCRT-II and ESCRT-III along with several associated accessory proteins (ALIX, VPS4, Tsg101, VTA1) which sort ubiquitinated cargo proteins on the inner leaflet of the endosomal membrane and caused subsequent scission thereby releasing the exosomes (Kalluri, 2016; Yue et al., 2020).

Biogenesis begins with endocytosis, enclosing bioactive molecules, forming endosomes. Endosomal membrane further undergoes inward budding, enclosing the molecules and forming multivesicular bodies (MVBs). Exosomes form from these MVBs, either through ESCRT-dependent or ESCRT-independent pathways.

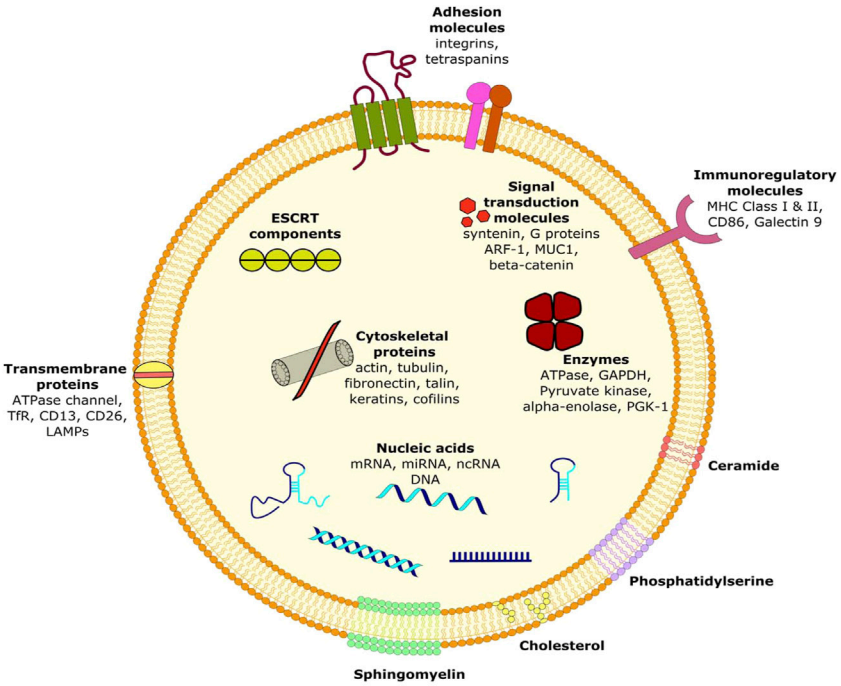

FIGURE 1
Ultrastructure of exosome showing its composition.

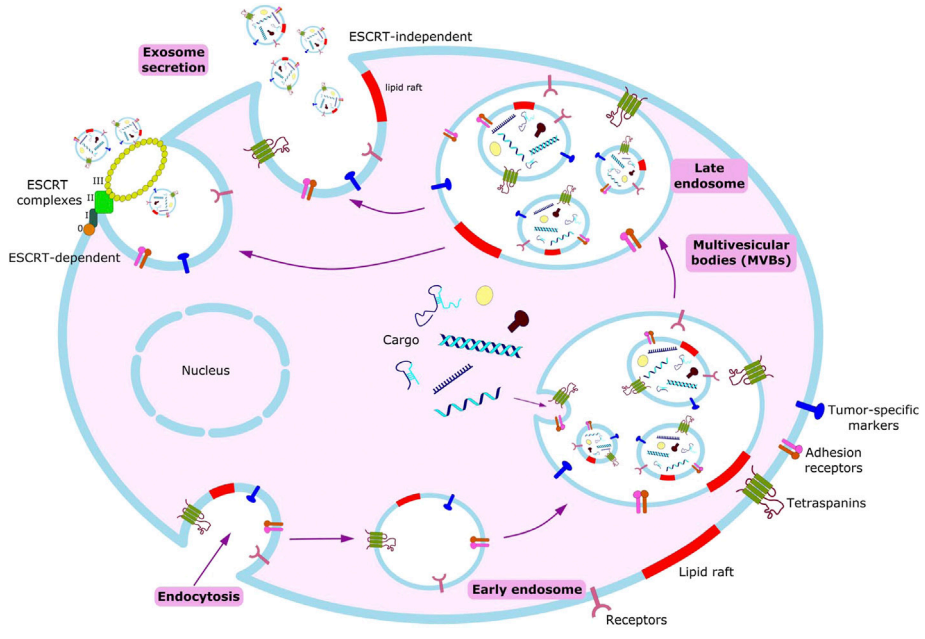

FIGURE 2
Scheme of exosome biogenesis and secretion.

Based on recent studies, a key system has been elucidated called the Syndecan-syntenin pathway which is responsible for controlling the generation of endosomal vesicles that release exosomes as well as delivering cargo inside these vesicles. Syntenin bound to syndecans with the help of extracellular heparansulphate chains communicate with a myriad of signaling and adhesion moieties including ALIX protein which links the Syndecan-syntenin pathway with the ESCRT machinery (Fares et al., 2017; Hessvik and Llorente, 2018).

Remarkably, numerous studies have also indicated the presence of an ESCRT-independent pathway for exosome biogenesis and loading which is mediated by lipids and associated proteins. Proteins such as A2, RAB5/7/27, TSG101 have been identified to play important roles in exosome biogenesis (Kalluri, 2016). Several transmembrane proteins of tetraspanin family such as CD9, CD63, CD82, Tspan8 are also involved in ESCR-independent exosome generation. Another protein namely small integral membrane protein of the lysosome/late endosome (SIMPLE) has also been shown to positively influence the release of exosomes. Apart from proteins, various lipids such as Phosphatidic acid, ceramide, glycosphingolipids, lyso-phospholipid are also inducers of exosomebiogenesis (Hessvik and Llorente, 2018; Yue et al., 2020).

ESCRT-dependent or ESCRT-independent mechanisms are not entirely exclusive. Exosome biogenesis is instead a coordinated and synergistic outcome of these mechanisms wherein their presence or absence in a particular cell type and/or cellular homeostasis manipulates intraluminal vesicle number and size in addition to cargo sorting and loading (Yue et al., 2020). Moreover, exosome secretion is eminently regulated by the conditions of the cellular microenvironment. In tumor cells, stressful conditions arise due to several factors such as chemotherapeutics, irradiation, starvation and most notably hypoxia which together lead to increased production of exosomes (Głuszko et al., 2019).

Exosomes uptake

Exosomes from the extracellular space can adhere to the cell in its proximity nonspecifically (Tian et al., 2013) or be attached *via* a specific ligand-receptor complex (Ohno et al., 2013). They can either exert their functional effects by direct activation of a signaling pathway (Al-Nedawi et al., 2008; Cossetti et al., 2014; Patel et al., 2016) or be internalized to transfer their cargo inside the cell, *via* endosomal maturation: the endosomal-lysosomal degradative pathway (Nakase and Futaki, 2015). Non-specific internalization of exosomes has been shown to occur in both normal and transformed cell lines (Svensson et al., 2013). The uptake depends on the recipient cell and not on the origin of the exosomes (Horibe et al., 2018). It is an energy dependent process, as evidenced by attenuation of the uptake when incubated at 4°C or with compounds interfering with cell function (Morelli et al., 2004). It has been shown that low pH conditions, a consequence of hypoxia in the cell interstitium and a characteristic of tumor microenvironment lead to rupture of the exosomal membrane and subsequent uptake of its cargo through macropinocytosis (Joseph et al., 1996; Gatenby and Gillies, 2004; Taraboletti et al., 2006; Parolini et al., 2009). The two most frequently reported ways of exosomal uptake by cancer cells are Lipid-raft mediated endocytosis and macropinocytosis.

Clathrin-independent endocytosis (CIE) is reported to occur through membrane proteins, CAV-1, flotillin-1 and RhoA that are known to be components of lipid-rafts: the microdomains of plasma membrane that contain high cholesterol and glycosphingolipid concentration, involved in endocytosis (Costa Verdera et al., 2017). Local disruption of actin network and inhibition of dynamin recruitment to plasma membrane: both of which are important in CIE, decreased exosomal uptake, suggesting its role in endocytosis (Tian T. et al., 2014). Although, in a study, CAV1 knock-out cells showed increased uptake of exosomes, in most of them, CAV-1 has been shown to play important role in CIE, as described above (Feng et al., 2010; Chaudhary et al., 2014).

Clathrin-dependent endocytosis (CDE) although shown to be taking part in uptake in some cancer cells, is majorly non-existent (Tian T. et al., 2014).

Macropinocytosis (MP) is another widely discussed pathway of exosomal uptake by cancer cells. Exosomes can themselves induce MP, thus facilitating their uptake (Yan-Liang et al., 2014). EGFR expression has been shown in many tumors, when activated by EFG, enhanced uptake through MP *via* activation of Rac, leading to cytoskeletal organization and subsequent induction of MP (Nakase et al., 2015).

Role of exosomes in mitigating cancer metastasis

Exosomes and their contents function together as a unit, facilitating the promotion of malignancy and tumorigenic effects, aiding the ability of native epithelial cells. Serving as an alternative to conventional cell-based therapies, exosomes are currently being engineered to deliver therapeutic cargos to the targeted recipient or tumor cells (Gilligan and Dwyer, (2017); You et al., 2018; Głuszko et al., 2019). Furthermore, the most presumptuous property of cancer i.e. metastasis is governed by the localized impression of exosome-mediated signaling. The influence is diverse and can be either due to site-production of exosomes or through uptake by a distant recipient cell (Kalluri, 2016). The mediators proffered between tumor and their microenvironments are under constant modulation and are known to play a key role in cancer immunotherapy. Tumor-derived exosomes (TEXs) are one such modification, suitable for imparting chemotherapeutic resistance, influenced by various other strategies, survival time and tumor growth (You et al., 2018).

A study in 2018 accorded for observing induced apoptosis along with a combined outcome of reduced metastasis and prolonged survival when exosomal cargo, siKras^{G12D-1}, in the donor cells of Bone marrow MSCs-derived exosomes (BM-MSC), was electroporated with pancreatic cancer as the tumor model (Melo et al., 2014; Mendt et al., 2018; You et al., 2018). The most talked about are the cancer cell-derived exosomes that have been found accountable for the transformation of benign epithelial cells into malignant cells (Kalluri, 2016). Melo SA *et al.* demonstrated how cancer exosomes differ from normal exosomes as the former possesses the capability of independent transcription of miRNA through a Dicer-dependent pathway (Melo et al., 2014; Kalluri, 2016). It was reported that breast cancer associated exosomes enriched in miRNA exhibit the presence of RISC-Loading Complex (RLC), thus efficiently mediating the process of silencing and miRNA biogenesis (Mendt et al., 2018).

Additionally, a research study in 2015 investigated the chemo-sensitive resistance in tumors displayed by patients with Hepatocellular carcinoma (HCC). A cumulative effect of metastasis, inadequate prognosis and loss of miR-122 encapsulated within exosomes caused the patients to develop a resistance to chemotherapies involving agents such as 5-fluorouracil (5-FU) and doxorubicin (Lou et al., 2015). A subsequent observation was made, while testing, whether a modification revolving around Adipose-derived MSCs (AMSCs) can prove helpful in restoring the lost chemosenstivity *via* expression of miR-122. Reduction in the tumor mass and volume was observed when the engineered exosomes administered intra-tumoral to BALB/c nude mice with HepG2 tumors, combined with sorafenib treatment, thus increasing the HCC cell sensitivity (Lou et al., 2015; Gilligan and Dwyer, 2017).

Likewise, Tumor-derived exosomes (TEXs) regulate the process of tumor formation due to release of immunosuppressive molecules such as Fas-ligand (FasL), the expression of which contributes to resistance and malignant niche selection. Expression of exosomal secretions can also be traced to the responses and correlated levels of Tumor necrosis factor-related apoptosis-inducing ligand (TRAIL), interleukin 10 (IL-10), programmed death-ligand 1 (PD-L1), neo-angiogenesis factors and several other microenvironment conditioning factors, e.g., transforming growth factor β1 (TGF-β1), prostaglandin E2 (PGE2) and ecto-enzymes engaged in the adenosine pathway (CD39 and CD73) (Głuszko et al., 2019).

The current cancer therapeutics deal with targeted destruction of both cancer stem cells (CSCs) alias cancer-initiating cells (CICs) as well as the non-CSCs. Several investigative experiments suggest that the CSC population is not static, and can be effectively reconfigured. The transformation of non-CSCs to CSCs results in regaining or acquiring stemness phenotype in the non-CSC tumor microenvironment which can be achieved by CSC-derived exosomes (Lin et al., 2013; Hu et al., 2015; Donnarumma et al., 2017).

The progressive inter-conversion establishes an equilibrium between the exosomal derived CSCs and non-CSCs, involving various cellular signaling pathways, bio-active cell cargo, molecular sorting and transport. Thus, a prospective scheme can be developed concerning possible mechanisms like cancer initiation, progression, metastasis, relapsing and resistance to therapies by modifying exosome contents in the cancer surrounding. A controlled and regulated interaction between CSCs and non-CSCs can be accomplished, which will prove to be a more beneficial and novel therapeutic strategy (Sun B. et al., 2018).

Role of exosomes in cancer: Signaling

Exosomes are capable of acting as transporters for different molecules aided by several types of signaling mechanisms and pathways that can operate over varying distances (Whiteside, 2017). Significantly, they play important roles in maintaining cancer-related functions such as metastasis, angiogenesis and regulating tumor micro-environment (Rachel et al., 2017; Whiteside, 2017; Sun Z. et al., 2018). Exosomes generated from Cancer Stem Cells (CSCs) are believed to induce stemness in non-CSCs thereby maintaining a state of equilibria in the tumor-microenvironment (Sun Z. et al., 2018). The ability of exosomes to act as communication vehicles is due to the presence of diverse signaling molecules on their surface derived from their parent cell as well as the presence of various nucleic acids, enzymes and factors inside them, thereby making them capable of acting as efficient mediators of cancer metabolism (Whiteside, 2017). Studies have elucidated that EVs from glioblastoma (GBM) under hypoxic conditions produce growth factors and cytokines which in turn activate directed pericyte movement and PI3K/AKT signaling and induce angiogenesis (Matarredona, 2020). Such EVs carry molecules like VEGF-A which straightaway promote angiogenesis (Are, 2016; Kalluri, 2016; Tomasetti et al., 2017). ECS have also shown enhanced sprouting and bifurcation of vessels after being delivered the components of the Notch pathway *via* exosome (Whiteside, 2017).

Exosomes from cancer cells have also been noted to bring about changes in fibroblasts *via* the TGFβ/Smad pathway. Cancer-Associated Fibroblasts (CAFs) can augment or inhibit tumor growth driven by tumor-derived exosomes (Whiteside, 2017; Sun Z. et al., 2018). Another study showed that the transfer of CRE mRNA to normal cells *via* EVs had pronounced immunosuppressive character (Are, 2016). The oncogenic potential of tumor cells is retained by the removal of tumor suppressor miRNAs *via* exosomes. Ras-MEK network is involved in maintaining the RNA-Induced Silencing

Complex (RISC) which in turn leads to the release of miRNA in exosomes (Rachel et al., 2017). The uptake and attachment of exosomes in target cells are mediated by protein interactions *via* several adhesion molecules like integrins and ICAMs whereas heparin sulphate proteoglycans, carbohydrate/lectin receptors, T-cell immunoglobinmucin-binding phosphatidylserines, *etc.* are crucial for their entry inside the cells (Tomasetti et al., 2017). In another tumor microenvironment, the exosomes of prostate cancer cells were rich in H-Ras and K-Ras signaling mechanisms. They contained miRNAs and Rab proteins, which led to aggressive tumors in the recipient target cells. Likewise, cancer-cell derived exosomes having copious presence of Ras and other kinases in the MAP kinase pathway, phosphorylated EGFR, and other growth factors led to an increased longevity of tumor monocytes. It has further been demonstrated that the capability of tumor cells to manipulate healthy distant cells involving exosomes is *via* a mechanism needing Rho GTPase effectors Rac1/PAK2 which possibly is the basis of metastatic spread of tumors (Rachel et al., 2017). The exosomal signaling is not only dependent on growth factors and cytokines but several metabolites as well, which include lactate, proteins, ketone bodies, *etc.* (Whiteside, 2017).

As a new and potent method to combat cancer, targeting the precise signaling pathway of exosomes is an exceedingly promising and emergent aspect of cancer therapy (Sun Z. et al., 2018). Refined manipulation of exosomes, for instance by protein fused to a ligand that allows the targeted delivery of exosomes to neuronal cells is one such successful attempt at modifying and channeling the exosomal signaling mechanism for a noble use of therapeutics (Kalluri, 2016).

Role of exosomes in cancer: Biomarkers

The diverse cargo of exosomes consisting of circulating RNAs, proteins with membrane and cell functions are proving to be recent research tools as potential biomarkers. A number of recent studies are looking into the insights of exosomal release as indicative of patho-physiological conditions and not merely riddance of undesirable components (Lin et al., 2015). The results have been suggestive of superior rates of sensitivity and specificity involving diagnosis of various metabolic and infectious diseases and cancer tumors by exosomal cargo biomarkers (Lin et al., 2015; Wong and Chen, 2019). This ability is credited to potentiate and better coordination of intercellular communication exhibited by exosomes, amongst a deck of other responses such as oncogenic growth, tumor progression and signaling pathways (Ruivo et al., 2017; Batista and Melo, 2019; Mathew et al., 2020). Challenges and shortcomings of existing biomarkers such as invasive and predictive nature, limited responsiveness and incompetency of genomic biomarkers in efficiently determining adaptive immune responses (Conway et al., 2018; Mathew et al., 2020); have paved way for development of novel diagnostic tools: the exosomal engineered biomarkers. Islet autoantibodies, like GAD65, IA-2 also known as ICA512, accurately predict development of type 1 diabetes mellitus; likely reduce with the disease progression and the antibodies gets exhausted as soon as insulin therapy is initiated (Towns and Pietropaolo, 2011; Garcia-Contreras et al., 2017). The cytokine stimulated ß-cells releasing EXOs are hence being utilized for TID diagnosis involving analysis of specific proteins and RNAs preceding isolation by using a surface marker (Palmisano et al., 2012; Garcia-Contreras et al., 2017).

In 2009, a study reported elevated levels of $CD63^{+}$ (scaffolding membrane protein) exosomes in plasma isolated from melanoma patients; qualifying as a tumor-associated marker based on western blot and flow-cytometric analysis (Logozzi et al., 2009; Lin et al., 2015). The tetraspanin family member was also found helpful in carrying out comparison of various human cancers; when quantification data showed lower levels of CD63 in exosomes derived from non-cancer cells. In addition, they also proposed reliability of CD9 and CD81 as marker proteins based on the fact that both of them were profoundly found in all the (four prostate and five breast) cell lines, that they utilized (Yoshioka et al., 2013; Lin et al., 2015). Several other exosomal proteins have also found their place as suitable prognostic tools in clinical and disease pathologies.

Findings of Taylor et al. regarding exosomal associated eight miRNAs (miR-21, -141, -200a, -200b, -200c, -203, -205, -214) are suggestive of the applications in diseases like ovarian cancer as substitute biomarkers; involving plasma biofluid and are reported to overcome the invasive isolation and profiling of biopsy samples (Taylor and Gercel-Taylor, 2008; Lin et al., 2015). In this regard, cell culture medium biofluids; have found predictive use in metastatic gastric cancers. Let-7 family miRNAs enriched extracellular fractions indicated by signal intensity data, confirming the possibility of selective secretion, and consequently revealed a new disease marker (Ohshima et al., 2010; Lin et al., 2015). Thus, exosomal nucleic acids also possess great potential as biomarkers for cancer diagnosis.

Such expositions by researchers are satisfactory and are coaxing others to take this descriptive nature of the published accounts to a further expanded diagnostic setting, particularly development of ideal biomarkers (Tables 1, 2).

Lung cancer

Multiple genes and proteins have been identified in lung cancer cells and tissues that can serve as exosomal biomarkers for lung cancer. The most prominent ones are the proteins (ZEB1, TRAF4, TGF-β, *etc.*) involved in lung cancer metastasis by EMT, proteins (PD-L1, EGFR, TLR7, TLR8) involved in

TABLE 1 Exosomal proteins as biomarkers for diagnosing cancer from serum and plasma.

Type of tumor	Protein biomarker(s)	Prospective use(s)
Lung cancer	NY-ESO-1 (Sandfeld-Paulsen et al., 2016a)	Prognosis
	EGFR, KRAS, Claudins, RAB-family proteins (Clark et al., 2016)	Diagnosis
	CD151, CD171, tetraspanin (Sandfeld-Paulsen et al., 2016b)	Diagnosis
Breast cancer	Her2 (Ciravolo et al., 2012)	Diagnosis
	Fibronectin (Moon et al., 2016a)	Early Diagnosis
	Glypican-1 (Melo et al., 2015)	Diagnosis
	Breast cancer resistance protein (BCPR) (Chen et al., 2015)	Prognosis
	Periostin (Vardaki et al., 2016)	Diagnosis
	Del-1 (Moon et al., 2016b)	Prognosis
Colorectal cancer	CD147 (Tian et al., 2018)	Diagnosis
	CEA (Huber et al., 2005)	Diagnosis
	Hsp60 (Campanella et al., 2015)	Diagnosis/Therapy
	TSAP6/CEA (Silva et al., 2012)	Prognosis/Diagnosis
	Copine III (Sun Z. et al., 2018)	Diagnosis
Prostate cancer	ephrinA2 (Zhu et al., 2018)	Diagnosis
	surviving (Khan et al., 2012)	Diagnosis
	PTEN (Gabriel et al., 2013)	Diagnosis
	PSA (Logozzi et al., 2017)	Early Diagnosis
	CA IX (Logozzi et al., 2020)	Diagnosis
Pancreatic cancer	CD44v6, CD104, Tspan 8, EpCAM (Madhavan et al., 2015)	Prognosis/Diagnosis
Gastric cancer	TRIM3 (Fu H. et al., 2018)	Diagnosis
	GKN1 (Yoon et al., 2018)	Prognosis/Diagnosis
	HER-2neu, EMMPRIN, MAGE-1, C-MET (Baran et al., 2010)	Diagnosis
Ovarian cancer	TGF-β1, MAGE3/6 (Szajnik et al., 2013)	Prognosis/Diagnosis/Therapy Tracking
	EpCAM, CD24, CA-125 (An et al., 2015)	Diagnosis
Melanoma of skin	Hsp70, Hsp90 (Peinado et al., 2012)	Prognosis
	Caveolin-1 (Logozzi et al., 2009)	Diagnosis
	(phospho)Met (Peinado et al., 2012)	Diagnosis
Hematological malignancies	CD9, CD13, CD19, CD30, CD38, CD63 (Caivano et al., 2015)	Diagnosis

inhibiting the immune system, and several Wnt proteins (Wnt5b, Wnt3a) and Interleukins (IL-6, IL-8, IL-10) that allow invasion and proliferation of the tumor (Jiang et al., 2021). A number of miRNAs that are an integral part of the exosomal cargo of the lung cancer cells have also been noted. They include miR-660-p5, miR-29a, miR-21 and miR494 (promote proliferation of lung cancer cells), miR-5100, miR-9, miR-23a (promote metastasis), miR-21, miR-29 (promote angiogenesis), and miR-23a (involved in immunomodulation) (Xu et al., 2021).

Breast cancer

As seen with other cancers, exosomes derived from breast cancer cells are enriched with certain miNAs that are not

TABLE 2 Exosomal nucleic acids as biomarkers for diagnosing Cancer from serum and plasma.

Type of tumor	Nucleic acid biomarker(s)	Prospective use(s)
Lung cancer	miR-151a-5p, miR-30a-3p, miR-100, miR-629 (Cazzoli et al., 2013)	Early Diagnosis
	let-7-g-5p, miR-24-3p, miR-223-3p, miR-7-5p, miR-424-5p (Rodríguez et al., 2014)	Diagnosis
Breast cancer	miR-101, miR-30a-3p, miR-373 (Eichelser et al., 2014)	Diagnosis
	miR-1246, miR-21 (Hannafon et al., 2016)	Diagnosis
Colorectal cancer	miR-19 (Matsumura et al., 2015)	Prognosis
	miR-21 (Tsukamoto et al., 2017)	Prognosis
	miR-221 (Liu et al., 2018)	Prognosis
	miR-4772-3p (Liu et al., 2016)	Prognosis for recurrent stages II and III
	let-7a, miR-1246, miR-150, miR23a (Ogata-Kawata et al., 2014)	Early Diagnosis
Prostate cancer	miR-141 (Li et al., 2016)	Diagnosis
	miR-1290, miR-375 (Huang et al., 2015)	Prognosis
Pancreatic cancer	miR-17-5p, miR-21 (Que et al., 2013)	Prognosis/Diagnosis
	circ-IARS (RNA) (Li et al., 2018)	Diagnosis
	miR-1246, miR-4644, miR-3976, miR-4306 (Madhavan et al., 2015)	Diagnosis
	miR-451a (Takahasi et al., 2018)	Prognosis
	miR-191, miR-21, miR451a (Goto et al., 2018)	Diagnosis
Gastric cancer	miR-423-5p (Yang et al., 2018)	Prognosis/Diagnosis
	LncRNA HOTTIP (Zhao et al., 2018)	Diagnosis
	Circ-KIAA1244 (Tang et al., 2018)	Diagnosis
Ovarian cancer	miR-373, miR-200a, miR-200b, miR-200c (Meng et al., 2016)	Prognosis/Diagnosis
	miR-21, miR-214, miR-203, miR-205, miR-141 (Taylor and Gercel-Taylor, 2008)	Prognosis/Early Diagnosis
	miR-21, miR-100, miR-200b, miR-320 (Pan et al., 2018)	Diagnosis
Hepatocellular carcinoma	miR-718 (Sugimachi et al., 2015)	Prognosis/Diagnosis/Recurrence
	miR-18a, miR-221, miR-222, miR-224 (Sohn et al., 2015)	Diagnosis
	LINC00161 (Xu et al., 2018)	Diagnosis

abundant in healthy cells. miR-372, miR-101, and miR-373 were found in significantly higher proportions in exosomes from breast cancer cells. Further, these miRNA are also indicative of metastasizing cancer while miR-373 is a marker of the highly aggressive triple-negative phenotype of breast cancer (Joyce et al., 2016). Expression levels of proteins such as ER (estrogen receptor), Ki67 (a marker of proliferation Ki-67), PR (progesterone receptor), and HER2 (member of the epidermal growth factor receptor family which is involved in the regulation of cell growth, survival, and differentiation *via* targeting multiple signal transduction pathways) can serve as important biomarkers for breast cancer prognosis and diagnosis (Jafari et al., 2018).

Colorectal cancer

Certain nucleic acid molecules and proteins may also serve as diagnostic biomarkers of colorectal cancer (CRC). Among miRNAs, around 7–11 molecules have been identified to be differentially expressed in CRC patients out of which miR-23a, miR-1246, and miR-21 are considered better markers. Several lncRNAs (colorectal neoplasia differentially expressed-h (CRNDE-h), breast cancer anti-estrogen resistance 4 (BCAR4), mRNA keratin-associated protein 5-4 (KRTAP5-4), and mRNA melanoma antigen family A3 (MAGEA3) have also been found in higher amounts in serum exosomes, thus increasing the scope of using them as predictive as well as diagnostic molecules. Upregulation and downregulation of specific proteins may

serve as another method to screen CRC patients. Heat shock protein 60 (a chaperonin involved in tumorigenesis), glypican-1, and the transmembrane protein CD147 are increasingly expressed in Colorectal Cancer, hence could be potential candidates for diagnosis (Balacescu et al., 2018; Xiao et al., 2020).

Pancreatic cancer

Similar to Colorectal Cancer, the cell surface proteoglycan Glyptican1 (GPC1) is the most prominent biomarker of pancreatic cancer. Exosomes enriched in GPC1 are known to positively regulate cancer and thereby serve as the best biomarker for detecting pancreatic cancer (Melo et al., 2015). Further, based on the study of exosomes isolated from pancreatic cancer cell lines and plasma isolated from patients, miRNAs such as miR-196a, miR-1246, miR-191, miR-21, miR-451a, miRNA-483-3p, miR-155, miR-196a, *etc*. are present in ample amount in the pancreatic cancer tumor microenvironment and may be effectively used to diagnose the same (Gabriel et al., 2020).

Ovarian cancer

Ovarian cancer cells derived exosomes are extracted from either ascites or serum of patients and contain a concoction of specific signature molecules which help in the progress of the tumor. It includes membrane proteins (Alix, TSG 101), Rab proteins, annexin proteins, tetraspanins (CD9, CD82, CD63 and CD81), heat shock proteins (Hsp90, Hsp70), antigens (MHC I and II), Nanog and enzymes (phosphate isomerase, peroxiredoxin, aldehyde reductase, fatty acid synthase), which can be used to potentially identify the malignancy early in itsdevelopment (Feng et al., 2019). Since ovarian cancer is highly lethal yet lacks any early screening test, therefore using exosomalmiRNA biomarkers (miR-100, miR-200b, miR-320, miR-21, miR-362-5p, and miR-1274a *etc*.) for diagnosis and prognosis of ovarian cancer would be of great clinical utility (Yoshida et al., 2020).

Gastric cancer

Helicobacter pylori infection is the most common factor that predisposes a person to develop gastric cancer. Interestingly, studies have found the role of exosomes in *H. pylori* infection and tumorigenesis by transporting the virulence factor CagA (mediator of extragstric disorders) to epithelial cells and mesenchymal-epithelial transition factor (MET) protein to macrophages, thus aiding in disease progression (Tang et al., 2021). Other signature molecules that form a part of the exosomes cargo from GC cells include proteins (UBR2, TRIM3, Apolipoprotein E), miRNAs (miR-423-5p, miR-155-5p, miR-27a, *etc*.), lncRNA (ZFAS1, LINC00152), and circRNA (ciRS-133, circ-KIAA1244) which may be utilized as characteristic biomarker for early diagnosis of gastric cancer (Fu et al., 2019).

Exosomes as therapeutic targets

Modification of exosome content

By default, exosomes are generally engineered under the control and governance of various cellular mechanisms; however, an accelerating number of successful researches are presently being done that involve exploring possibilities of exosomal content modification. The biocompatible traits of exosomes, with several appropriate changes, can trigger the steadiness and efficacy of cellular uptake and prove to be an effective step in improving the picture of current therapeutics. The cognizance of this subject matter is to summarize perspective, passive and lively approaches to unique exosome changes, and examples of the transport molecules (Luan et al., 2017).

Exosomal cargos such as nucleic acid components, heat shock proteins, and various ligand molecules, for example, miR-425-3p, TGF- β, miR-100–5p, and Survivin, are found to be effectively involved with various targeted cells such as TGF- β is with NK cells. These modified exosomes, due to the incorporation of desirable components can prove to be an efficient vehicle in dealing with advancing cases of cancers such as AML, Lung cancers, Hepatocellular cancers, *etc*. A platinum-based chemotherapeutic approach was carried out to monitor a Lung cancer model, utilizing exosomal content modification and miR-425 as the cargo component. It was rendered ineffective resulting in a resistive response to NSCLC which was an outcome of autophagy due to AKT1 inhibition. Similarly, NK cell-mediated suppression controlled by tumor-derived vesicles proved to be therapeutic in instances of AML accompanied by the opposition of suppression by interleukin-15. The study outcome in the case of A549 cells involved DDP resistance and was observed in resident cancer cells due to modulation of mTOR expression. In another study, Exosomes purified from HeLa Cervical Carcinoma cells exhibited revised survival rates due to assistance from IAP and HSPs (Refer to the table).

One such critical group of derived exosomes comes beneath the mega-group of Tumor-derived exosomes. There are an array of attractive components that contributes to the usage of tumor-derived exosomes for the transport of therapeutics and vaccines for immunotherapy. A stage 1 medical trial has recently been accomplished on the discharge of tumor exosomes, which had been earlier presumed to undergo tumor specificity *via* antigens equipped for presentation to immune cells and stimulating the immune structures of glioma sufferers to achieve pure and

TABLE 3 An account of exosomal alterations manifested as therapeutic and restorative in specific cancer treatments.

Exosomal cargos	Targeted cell	Cancer model	Study outcome	Reference
miR-425-3p	PC-9 and SPCA1 cells	Lung Cancer	AKT1 inhibition triggers autophagy, conferring resistance to NSCLC; observed as decrease in clinical response to platinum-based chemotherapy	Zhao and Xie, (2019), Yuwen et al. (2019)
miR-100–5p	A549 cells (Rapamycin signaling pathway)	Lung Cancer	DDP resistance was observed in other cancer cells due to modulation of mTOR expression	Qin et al. (2017), Zhao and Xie, (2019)
miR-222	MCF-7/S (Phosphatase and tensin homolog)	Breast Cancer	Exosomes were found to be acting as MDR arbitrators that transferred Adriamycin-and Docetaxel resistance from donor cells to recipient MCF-7 breast cancer cells	Chen et al. (2014), Zhao and Xie, (2019)
miR-122 and miR-32-5p	HepG2 cells (Sensitive HCC cell)	Hepatocellular cancer	Delivery of miR-122 into HepG2 cells followed by its negative regulation expression; aids the sensitivity of HCC cells to chemotherapeutic agents. miR-32-5p facilitates the activation of PI3K/Akt pathway thus providing MDR to sensitive cells.	Lou et al. (2015), Xiao Fu et al. (2018), Zhao and Xie, (2019)
lnc-ROR and lnc-VLDLR	HepG2 or PLC-PRF5 HCC cells	Hepatocellular cancer	Upregulatory response in HCC cells, reduction in chemotherapy-induced cell death and increased expression level of linc-ROR; and ABCG2.	Takahashi et al. (2014a), Takahashi et al. (2014b), Zhao and Xie, (2019)
TGF- β	NK Cells	AML	NK cell mediated suppression mediated by tumor-derived vesicles which proved to be therapeutic in instances of AML and the fact that interleukin-15 can oppose this suppression, was also established	Szczepanski et al. (2011), Whiteside, (2016)
Hsp72	MDSC	Colon CA	Suppression in the activity of the MDSCs *via* activation of Stat3 triggered by TDE-associated Hsp72 in a TLR2/MyD88-dependent manner *via* autocrine production of IL-6. MDSC expansion was triggered by TDSFs following activation of Erk	Chalmin et al. (2010), Zhao and Xie, (2019)
Survivin	Cervical CA cells	Cervical CA	Exosomes purified from HeLa Cervical Carcinoma cells demonstrated increased survival rates due to assistance to IAP and HSPs	Khan et al. (2011), Zhao and Xie, (2019)
αvβ6 Integrin	Prostate CA cells	Prostate CA	EVs were derived from PCa cell lines and human plasma samples, characterized as to contain ds-gDNA fragments which appears to be an able candidate for cancer biomarker; exhibiting certain specific migration mutations	Lázaro-Ibáñez et al. (2014), Zhao and Xie, (2019)
FasL	Activated T cells	Ovarian CA	An increased immune-suppression of T-cell receptor/CD3-zeta followed by T-cell apoptosis due to modified Fas ligand-containing exosomes obtained from ovarian tumors	Taylor et al. (2003), Matsumura et al. (2015)

ABCG2, ATP-binding cassette sub-family G member 2; AML, acute myeloid leukemia; CA, carcinoma; DDP, Cisplatin [cis-diamminedichloroplatinum(II)]; HCC, hepatocellular carcinoma; Hsp, Heat Shock Protein; IAP, Inhibitor of apoptosis; lnc-ROR, Long Non-coding RNA Reprogramming; lnc-VLDLR, Long Non-coding very low density lipoprotein receptor; MDR, Multi-drug resistance; MDSC, myeloid-derived suppressor cells; miR, micro RNA; mTOR, Mammalian target of rapamycin; NSCLC, Non-small cell lung cancer; NK, natural killer cells; TDE, Tumor derived exosomes; TGF-β, transforming growth factor β; TDSF, Tumor derived Suppressor factor.

ultimate tumor cells after resection (Thomas Jefferson University, 2000).

For example, for the determination of tumor cells and tumor exosomes in excessive numbers in malignant effusions, it has been established that tumor exosomes convey tumor-related antigens unique to the tumors from which they may be derived, in addition to MHC I molecules. A supply of antigens to dendritic cells by tumor exosomes can result in a T-cellular-mediated immune reaction towards tumor cells (Wolfers et al., 2001). In addition, tumor-focused on selective drug transport involves tumor-derived exosomes and has been proposed as an opportunity due to their unique expression of tetraspanins, which preferentially engage with ligands in specific tissues (Rana et al., 2012). Proteases, including urokinase plasminogen activator, which promotes tumor cellular invasion, and cathepsin D, and adhesion modulators, including vimentin, galectin 3-binding protein, and annexin A1, have additionally been determined in tumor-derived exosomes (Harris et al., 2015); miRNAs and different nucleic acids, that may result in malignant adjustments in target cells, had been identified in tumor cellular exosomes (Melo et al., 2014). An account of exosomal alterations manifested as therapeutic and restorative in specific cancer treatments is enlisted below in Table 3.

Modification of exosome surface

Exosomal surface proteins (ligands) can be modified to aid targeted drug delivery. It is carried out to image and track them, make them better adapted to the target cells vis-à-vis anchorage and uptake, increase their therapeutic value, and

TABLE 4 A list of practical changes carried out on exosomal surfaces to assist their involvement in promoting advancements and therapies.

Source of exosome	Molecule involved in expression	Loading and labeling	Consequences and aftermath	Reference
HEK293	GE11 peptide and microRNA Let-7a	Xenolight DiR	Binding of GE11 to EGFR caused the delivery of exosomes to epithelial originated tumors; increase three-fold and assisting in tumor suppressive target delivery	Ohno et al. (2013), Gilligan and Dwyer, (2017)
Murine immature dendritic cells	Membrane protein Lamp2b fused with αγ integrin-specific iRGD peptide	Dox	Delivery of encapsulated Dox with 20% efficacy significantly inhibited tumor growth; demonstrating a prospective approach of modifying exosomes by delivery target of ligand molecules	Yanhua Tian et al. (2014), Gilligan and Dwyer, (2017)
HEK293T cells	IL3-Lamp2B (Lamp2B conjugated with IL3-receptor)	Imatinib or BCR-ABL siRNA	CML infected mice exhibited improved tumor targeting due to exosomal surface modification. IL3-R is overexpressed in CML blasts therefore appearing as a potential receptor to be utilized in drug deliveries; involving cancer cases. Additionally, in cases involving Imatinib group, a slight reduction in tumor growth was observed	Bellavia et al. (2017), Gilligan and Dwyer, (2017)
AuNP coated exosome particles	Lamp2b fusion protein and a neuron-targeted short peptide of RVG	DiI	AuNPs encapsulated with RVG-targeted exosomes, reported elevation in their targeting ability in both *in vitro* as well as *in vivo* blood-brain barrier systems. This could prove beneficial in drug delivery pathway and diagnosis revolving around CNS disorders such as Alzheimer's disease, Parkinson's disease and incidents of brain cancers	Khongkow et al., 2019
CD63-GFP-exosomes	GALA Peptide in cytosol	Dextran, Saponin	Combination of cationic lipids and a pH-sensitive fusogenic peptide caused a substantial increase in cellular uptake and cytosolic release of exosomal contents; without any cytotoxic effects	Nakase and Futaki, (2015), Zhang et al. (2020)

AuNPs, Gold nanoparticles; CML, Chronic Myelogenous Leukemia; DiI, 1,1′-dioctadecyl-3,3,3′,3′-tetramethylindocarbocyanine perchlorate dye; DiR, 1,10-dioctadecyltetramethyl indotricarbocyanine Iodide; Dox, Doxorubicin; EGFR, Epidermal Growth Factor Receptor; GFP, Green fluorescent protein; HEK, Human Embryonic Kidney cell line; RVG, Rabies virus glycoprotein.

give them other possible advantages over unmodified exosomes (Sandfeld-Paulsen et al., 2016a). This specific modification is beneficial in terms of more effective drug delivery, more retention in circulation and more stability. Furthermore, since it augments the targeted delivery, a lesser quantity of exosomes is required for the same effect, thus reducing the need for high yield from parent cells (Zhang et al., 2020).

These modifications are done through various methods, depending upon the requirement, including genetic engineering of parent cells, nanoparticle technology, hydrophobic cargo loading in the lipid bilayer, fusion with liposomes, *etc*. (Xu et al., 2020). Table 4 summarizes a list of practical changes carried out on exosomal surfaces to assist their involvement in promoting advancements and therapies.

The prospects of exosome mimetics

The role of exosomes in multiple cancer types and their potential utility as targeted therapeutics by its alteration or through exosome-mimetics has been widely discussed in this paper. Additionally, since exosomes are functionally involved and produced by almost all types of cells, their application is also omnipresent and is witnessed throughout various ailments. Apart from cancer, exosomes have been studied as ideal vehicles for drug delivery for several neurodegenerative diseases like Alzheimer's disease and Parkinson's disease, cardiovascular disorders, musculoskeletal diseases, Kidney ailments, diabetes, *etc*. (Antimisiaris et al., 2018; Jiang et al., 2019). A revolutionary aspect of exosomes is their ability to act as nanocarriers for the delivery of therapeutic agents in brain to treat disorders pertaining to the CNS (Antimisiaris et al., 2018). Neuron-derived exosomes (NDEs) have also been implied to contain distinguishing biomarkers for HIV-associated neurological disorders (HAND) and Alzheimer's Disease (AD) (Pulliam et al., 2019).

Studies have also been performed to show how circulating EVs might have a functional role in the pathophysiology of several vascular disorders such as Acute Chest Syndrome (ACS) and Sickle Cell Disease (Lapping-Carr et al., 2020). Experimentally, it has been demonstrated that Mesenchymal Stem Cell Derived-Exosomes (MEX) suppresses lung infection by regulating the lung tissue therefore, thereby lies a possible remedial for Pulmonary Arterial Hypertension (Willis et al., 2018). Urinary exosomes as well give an insight into diverse biomarkers that are pointers to different drug-induced kidney toxicities. Furthermore, this aspect can be scaled up after

subsequent research for large-scale drug trials (Griffin et al., 2020).

Preclinical research has displayed the ability of MSC-derived exosomes as an alternative form of therapy for Acute Respiratory Distress Syndrome (ARDS). Furthermore, MSC-derived exosomes behave as silencing complexes; hence they can induce some epigenetic changes in the expression of their cellular receptors, eventually leading to the inability of infection of many RNA viruses like Hepatitis-C, Influenza and Coronavirus. This is suggestive of the underlying aptitude of MSC-derived exosomes to treat COVID-19 infection (Gupta et al., 2020).

\Although the role of exosomes as curative agents is highly promising, there are quite a few limitations that need to be tackled first to unleash its extensive utility. The shortcomings of exosomes therapeutics include scanty yield of exosomes from cells, difficulty in loading drugs and engineering the vesicles, potential unwanted effect at non-target sites, systemic dilution before reaching the target site, change in the conformation of membrane protein (thus affecting organotropism), questionable stability of the engineered-vesicles *etc.* (Antimisiaris et al., 2018; Hu et al., 2020). Thus, the use of exosomes-mimetics, which are membrane-coated nanoparticles having the same functional characteristics and efficacy as endogenous exosomes appear more promising for the same therapeutic purpose. Additionally, it can be quickly produced, engineered and loaded with our desired drug in a reproducible and relatively cost-effective manner (Hu et al., 2020).

Conclusion

This article has comprehensively discussed exosomes and their quintessential involvement in various facets of Cancer Biology. Firstly, there is enough substantial evidence that solidifies the role of exosomes in cell-to-cell communication and signaling and regulation of tumor micro-environment. Secondly, exosomes aid in malignancy of the disease by promoting metastasis and tumor progression. Moreover, they can be characterized to act as biomarkers for efficient diagnostic applications. Thus, these extra-cellular vesicles are multidimensional in terms of the functions that they perform and have thereby emerged as a highly promising niche for cancer therapeutics. It is remarkable to note their efficient, intrinsic targeting potential, biocompatibility, efficacy and physiological stability.

However, numerous aspects, such as purification, administration, standardization and long-term safety effects, require to be studied and monitored. The current studies also lack clinical trials on human models, which are essential to further advancements in this area. Despite their expanded hopes of applications, more advanced and robust technologies are required to isolate surplus exosomes to counter the scanty yield from the current methods. Also, a scalable and economical method for loading drugs/nucleic acids and modifying the surface of exosome mimetics is awaited that also preserves the integrity and innate characteristics of these engineered vesicles.

We have partly unraveled the search for the perfect, fool-proof tool for the cancer treatment, but the quest is yet incomplete until the abovementioned voids are filled. Conclusively, exosomes undeniably carry a plethora of possibilities to revolutionize and significantly optimize Cancer therapeutics and diagnostics. Even, a multitude of research still needs to be performed and analyzed to apply the pre-clinical proof of concept studies to fruition.

Author contributions

LM- Concept and Manuscript preparation GM- Manuscript Preparation, concept and Corresponding Author UP- Figure construction and Editing AG- Manuscript Preparation JG- Manuscript and Table preparation MS- Proof reading.

Conflict of interest

Author MS was employed by Betterhumans Inc.

The remaining authors declare that the research was conducted in the absence of any commercial or financial relationships that could be construed as a potential conflict of interest.

Publisher's note

References

Al-Nedawi, K., Meehan, B., Micallef, J., Lhotak, V., May, L., Guha, A., et al. (2008). Intercellular transfer of the oncogenic receptor EGFRvIII by microvesicles derived from tumour cells. *Nat. Cell. Biol.* 10 (5), 619–624. doi:10.1038/ncb1725

An, T., Qin, S., Xu, Y., Tang, Y., Huang, Y., Situ, B., et al. (2015). Exosomes serve as tumour markers for personalized diagnostics owing to their important role in cancer metastasis. *J. Extracell. Vesicles* 4, 27522. doi:10.3402/jev.v4.27522

Antimisiaris, S. G., Mourtas, S., and Marazioti, A. (2018). Exosomes and exosome-inspired vesicles for targeted drug delivery. *Pharmaceutics* Vol. 10, E218. doi:10.3390/pharmaceutics10040218

Are, W. W. (2016). Review communication by extracellular vesicles : Where we are and where we need to go. *Cell.* 164 (6), 1226–1232. doi:10.1016/j.cell.2016.01.043

Balacescu, O., Sur, D., Cainap, C., Visan, S., Cruceriu, D., Manzat-Saplacan, R., et al. (2018). The impact of miRNA in colorectal cancer progression and its liver metastases. *Int. J. Mol. Sci.* 19 (12), 3711. doi:10.3390/ijms19123711

Baran, J., Bajkrzyworzeka, M., Weglarczyk, K., Szatanek, R., Zembala, M., Barbasz, J., et al. (2010). Circulating tumour-derived microvesicles in plasma of gastric cancer patients. *Cancer Immunol. Immunother.* 59 (6), 841–850. doi:10.1007/s00262-009-0808-2

Batista, I. A., and Melo, S. A. (2019). Exosomes and the future of immunotherapy in pancreatic cancer. *Int. J. Mol. Sci.* 20 (3), 567. doi:10.3390/ijms20030567

Bellavia, D., Raimondo, S., Calabrese, G., Forte, S., Cristaldi, M., Patinella, A., et al. (2017). Interleukin 3- receptor targeted exosomes inhibit in vitro and in vivo Chronic Myelogenous Leukemia cell growth. *Theranostics* 7 (5), 1333–1345. doi:10.7150/thno.17092

Caivano, A., Laurenzana, I., De Luca, L., La Rocca, F., Simeon, V., Trino, S., et al. (2015). High serum levels of extracellular vesicles expressing malignancy-related markers are released in patients with various types of hematological neoplastic disorders. *Tumour Biol.* 36, 9739–9752. doi:10.1007/s13277-015-3741-3

Campanella, C., Rappa, F., Sciumè, C., Marino Gammazza, A., Barone, R., Bucchieri, F., et al. (2015). Heat shock protein 60 levels in tissue and circulating exosomes in human large bowel cancer before and after ablative surgery: Exosomal Hsp60 in Large Bowel Cancer. *Cancer* 121, 3230–3239. doi:10.1002/cncr.29499

Cazzoli, R., Buttitta, F., Di Nicola, M., Malatesta, S., Marchetti, A., Rom, W. N., et al. (2013). microRNAs derived from circulating exosomes as noninvasive biomarkers for screening and diagnosing lung cancer. *J. Thorac. Oncol.* 8, 1156–1162. doi:10.1097/JTO.0b013e318299ac32

Chalmin, F., Ladoire, S., Mignot, G., Vincent, J., Bruchard, M., Remy-Martin, J. P., et al. (2010). Membrane-associated Hsp72 from tumor-derived exosomes mediates STAT3-dependent immunosuppressive function of mouse and human myeloid-derived suppressor cells. *J. Clin. Invest.* 120 (2), 457–471. doi:10.1172/JCI40483

Chaudhary, N., Gomez, G. A., Howes, M. T., Lo, H. P., McMahon, K. A., Rae, J. A., et al. (2014). Endocytic crosstalk: Cavins, caveolins, and caveolae regulate clathrin-independent endocytosis. *PLoS Biol.* 12, e1001832. doi:10.1371/journal.pbio.1001832

Chen, W. X., Liu, X. M., Lv, M. M., Chen, L., Zhao, J. H., Zhong, S. L., et al. (2014). Exosomes from drug-resistant breast cancer cells transmit chemoresistance by a horizontal transfer of microRNAs. *PloS one* 9 (4), e95240. doi:10.1371/journal.pone.0095240

Chen, Y., Wang, L., Zhu, Y., Chen, Z., Qi, X., Jin, L., et al. (2015). Breast cancer resistance protein (BCRP)-containing circulating microvesicles contribute to chemoresistance in breast cancer. *Oncol. Lett.* 10, 3742–3748. doi:10.3892/ol.2015.3806

Ciravolo, V., Huber, V., Ghedini, G. C., Venturelli, E., Bianchi, F., Campiglio, M., et al. (2012). Potential role of HER2-overexpressing exosomes in countering trastuzumab-based therapy. *J. Cell. Physiol.* 227, 658–667. doi:10.1002/jcp.22773

Clark, D. J., Fondrie, W. E., Yang, A., and Mao, L. (2016). Triple SILAC quantitative proteomic analysis reveals differential abundance of cell signaling proteins between normal and lung cancer-derived exosomes. *J. Proteomics* 133, 161–169. doi:10.1016/j.jprot.2015.12.023

Conway, J. R., Kofman, E., Mo, S. S., Elmarakeby, H., and Van Allen, E. (2018). Genomics of response to immune checkpoint therapies for cancer: Implications for precision medicine. *Genome Med.* 10, 93. doi:10.1186/s13073-018-0605-7

Cossetti, C., Iraci, N., Mercer, T. R., Leonardi, T., Alpi, E., Drago, D., et al. (2014). Extracellular vesicles from neural stem cells transfer IFN-γ via Ifngr1 to activate Stat1 signaling in target cells. *Mol. Cell.* 56 (2), 193–204. doi:10.1016/j.molcel.2014.08.020

Costa Verdera, H., Gitz-Francois, J. J., Schiffelers, R. M., and Vader, P. (2017). Cellular uptake of extracellular vesicles is mediated by clathrin-independent endocytosis and macropinocytosis. *J. Control. Release* 266, 100–108. doi:10.1016/j.jconrel.2017.09.019

Donnarumma, E., Fiore, D., Nappa, M., Roscigno, G., Adamo, A., Iaboni, M., et al. (2017). Cancer-associated fibroblasts release exosomal microRNAs that dictate an aggressive phenotype in breast cancer. *Oncotarget* 8, 19592–19608. doi:10.18632/oncotarget.14752

Eichelser, C., Stückrath, I., Müller, V., Milde-Langosch, K., Wikman, H., Pantel, K., et al. (2014). Increased serum levels of circulating exosomal microRNA-373 in receptor-negative breast cancer patients. *Oncotarget* 5, 9650–9663. doi:10.18632/oncotarget.2520

Fais, S., Logozzi, M., Lugini, L., Federici, C., Azzarito, T., Zarovni, N., et al. (2013). Exosomes: The ideal nanovectors for biodelivery. *Biol. Chem.* 394 (1), 1–15. doi:10.1515/hsz-2012-0236

Fares, J., Kashyap, R., and Zimmermann, P. (2017). Syntenin: Key player in cancer exosome biogenesis and uptake? *Cell. adh. Migr.* 11, 124–126. doi:10.1080/19336918.2016.1225632

Feng, D., Zhao, W. L., Ye, Y. Y., Bai, X. C., Liu, R. Q., Chang, L. F., et al. (2010). Cellular internalization of exosomes occurs through phagocytosis. *Traffic* 11, 675–687. doi:10.1111/j.1600-0854.2010.01041.x

Feng, W., Dean, D. C., Hornicek, F. J., Shi, H., and Duan, Z. (2019). Exosomes promote pre-metastatic niche formation in ovarian cancer. *Mol. Cancer* 18 (1), 124. doi:10.1186/s12943-019-1049-4

Fu, H., Yang, H., Zhang, X., Wang, B., Mao, J., Li, X., et al. (2018). Exosomal TRIM3 is a novel marker and therapy target for gastric cancer. *J. Exp. Clin. Cancer Res.* 37, 162. doi:10.1186/s13046-018-0825-0

Fu, M., Gu, J., Jiang, P., Qian, H., Xu, W., Zhang, X., et al. (2019). Exosomes in gastric cancer: Roles, mechanisms, and applications. *Mol. Cancer* 18 (1), 41. doi:10.1186/s12943-019-1001-7

Fu, X., Liu, M., Qu, S., Ma, J., Zhang, Y., Shi, T., et al. (2018). Exosomal microRNA-32-5p induces multidrug resistance in hepatocellular carcinoma via the PI3K/Akt pathway. *J. Exp. Clin. Cancer Res.* 37 (1), 52. doi:10.1186/s13046-018-0677-7

Gabriel, A. N. A., Wang, F., Jiao, Q., Yvette, U., Yang, X., Al-Ameri, S. A., et al. (2020). The involvement of exosomes in the diagnosis and treatment of pancreatic cancer. *Mol. Cancer* 19 (1), 132. doi:10.1186/s12943-020-01245-y

Gabriel, K., Ingram, A., Austin, R., Kapoor, A., Tang, D., Majeed, F., et al. (2013). Regulation of the tumor suppressor pten through exosomes: A diagnostic potential for prostate cancer. *PLoS ONE* 8, e70047. doi:10.1371/journal.pone.0070047

Garcia-Contreras, M., Brooks, R. W., Boccuzzi, L., Robbins, P. D., and Ricordi, C. (2017). Exosomes as biomarkers and therapeutic tools for type 1 diabetes mellitus. *Eur. Rev. Med. Pharmacol. Sci.* 21 (12), 2940–2956.

Gatenby, R. A., and Gillies, R. J. (2004). Why do cancers have high aerobic glycolysis? *Nat. Rev. Cancer* 4 (11), 891–899. doi:10.1038/nrc1478

Gilligan, K. E., and Dwyer, R. M. (2017). Engineering exosomes for cancer therapy. *Int. J. Mol. Sci.* 18 (6), 1122. doi:10.3390/ijms18061122

Głuszko, A., Szczepański, M. J., Ludwig, N., Mirza, S. M., and Olejarz, W. (2019). Exosomes in cancer: Circulating immune-related biomarkers. *BioMed Res. Int.* 1628029, 9. doi:10.1155/2019/1628029

Goto, T., Fujiya, M., Konishi, H., Sasajima, J., Fujibayashi, S., Hayashi, A., et al. (2018). An elevated expression of serum exosomal microRNA-191, −21, −451a of pancreatic neoplasm is considered to be efficient diagnostic marker. *BMC Cancer* 18, 116. doi:10.1186/s12885-018-4006-5

Griffin, B. R., Faubel, S., and Edelstein, C. L. (2020). *U. S. Department of veterans affairs*, 41, 213–226. doi:10.1097/FTD.0000000000000589. Biomarkers

Gupta, A., Kashte, S., Gupta, M., Rodriguez, H. C., Gautam, S. S., Kadam, S., et al. (2020). Mesenchymal stem cells and exosome therapy for COVID-19: Current status and future perspective. *Hum. Cell.* 4, 907–918. doi:10.1007/s13577-020-00407-w

Hannafon, B. N., Trigoso, Y. D., Calloway, C. L., Zhao, Y. D., Lum, D. H., Welm, A. L., et al. (2016). Plasma exosome microRNAs are indicative of breast cancer. *Breast Cancer Res.* 18, 90. doi:10.1186/s13058-016-0753-x

Harris, D. A., Patel, S. H., Gucek, M., Hendrix, A., Westbroek, W., and Taraska, J. W. (2015). Exosomes released from breast cancer carcinomas stimulate cell movement. *PLoS One* 10, e0117495. doi:10.1371/journal.pone.0117495

Hessvik, N. P., and Llorente, A. (2018). Current knowledge on exosome biogenesis and release. *Cell. Mol. Life Sci.* 75, 193–208. doi:10.1007/s00018-017-2595-9

Horibe, S., Tanahashi, T., Kawauchi, S., Murakami, Y., and Rikitake, Y. (2018). Mechanism of recipient cell-dependent differences in exosome uptake. *BMC Cancer* 18 (1), 47. doi:10.1186/s12885-017-3958-1

Hu, Q., Su, H., Li, J., Lyon, C., Tang, W., Wan, M., et al. (2020). Clinical applications of exosome membrane proteins. *Precis. Clin. Med.* 1, 54–66. doi:10.1093/pcmedi/pbaa007

Hu, Y., Yan, C., Mu, L., Huang, K., Li, X., Tao, D., et al. (2015). Fibroblast-derived exosomes contribute to chemoresistance through priming cancer stem cells in colorectal cancer. *PLoS One* 10, e0125625. doi:10.1371/journal.pone.0125625

Huang, X., Yuan, T., Liang, M., Du, M., Xia, S., Dittmar, R., et al. (2015). Exosomal miR-1290 and miR-375 as prognostic markers in castration-resistant prostate cancer. *Eur. Urol.* 67, 33–41. doi:10.1016/j.eururo.2014.07.035

Huber, V., Fais, S., Iero, M., Lugini, L., Canese, P., Squarcina, P., et al. (2005). Human colorectal cancer cells induce T-cell death through release of proapoptotic microvesicles: Role in immune escape. *Gastroenterology* 128, 1796–1804. doi:10.1053/j.gastro.2005.03.045

Jafari, S. H., Saadatpour, Z., Salmaninejad, A., Momeni, F., Mokhtari, M., Nahand, J. S., et al. (2018). Breast cancer diagnosis: Imaging techniques and biochemical markers. *J. Cell. Physiol.* 233 (7), 5200–5213. doi:10.1002/jcp.26379

Jiang, C., Zhang, N., Hu, X., and Wang, H. (2021). Tumor-associated exosomes promote lung cancer metastasis through multiple mechanisms. *Mol. Cancer* 20 (1), 117. doi:10.1186/s12943-021-01411-w

Jiang, L., Dong, H., Cao, H., Ji, X., Luan, S., Liu, J., et al. (2019). Exosomes in pathogenesis, diagnosis, and treatment of alzheimer's disease. *Med. Sci. Monit.* 25, 3329–3335. doi:10.12659/MSM.914027

Joseph, D., Penland Lolita, B. P. O., Tyagi, S., Kramer, F. R., and Group, N. P. (1996). © 1997 nature publishing group. *Group, 4,* 303–308. Available at: http://www.nature.com/naturemedicine. https://doi.org/10.1038/nm0798-822

Joyce, D. P., Kerin, M. J., and Dwyer, R. M. (2016). Exosome-encapsulated microRNAs as circulating biomarkers for breast cancer. *Int. J. Cancer* 139 (7), 1443–1448. doi:10.1002/ijc.30179

Kalimuthu, S., Gangadaran, P., Rajendran, R. L., Zhu, L., Oh, J. M., Lee, H. W., et al. (2018). A new approach for loading anticancer drugs into mesenchymal stem cell-derived exosome mimetics for cancer therapy. *Front. Pharmacol.* 9, 1116. doi:10.3389/fphar.2018.01116

Kalluri, R. (2016). The biology and function of exosomes in cancer. *J. Clin. Invest.* 126 (4), 1208–1215. doi:10.1172/JCI81135

Khan, S., Jutzy, J. M. S., Valenzuela, M. M. A., Turay, D., Aspe, J. R., Ashok, A., et al. (2012). Plasma-derived exosomal survivin, a plausible biomarker for early detection of prostate cancer. *PLoS One* 7 (10), e46737. doi:10.1371/journal.pone.0046737

Khan, S., Jutzy, J. M., Aspe, J. R., McGregor, D. W., Neidigh, J. W., Wall, N. R., et al. (2011). Survivin is released from cancer cells via exosomes. *Apoptosis* 16 (1), 1–12. doi:10.1007/s10495-010-0534-4

Khongkow, M., Yata, T., Boonrungsiman, S., Ruktanonchai, U. R., Graham, D., Namdee, K., et al. (2019). Surface modification of gold nanoparticles with neuron-targeted exosome for enhanced blood-brain barrier penetration. *Sci. Rep.* 9 (1), 8278. doi:10.1038/s41598-019-44569-6

Lapping-Carr, G., Gemel, J., Mao, Y., and Beyer, E. C. (2020). Circulating extracellular vesicles and endothelial damage in Sickle cell disease. *Front. Physiol.* 11. doi:10.3389/fphys.2020.01063

Lázaro-Ibáñez, E., Sanz-Garcia, A., Visakorpi, T., Escobedo-Lucea, C., Siljander, P., Ayuso-Sacido, A., et al. (2014). Different gDNA content in the subpopulations of prostate cancer extracellular vesicles: Apoptotic bodies, microvesicles, and exosomes. *Prostate* 74 (14), 1379–1390. doi:10.1002/pros.22853

Li, J., Li, Z., Jiang, P., Peng, M., Zhang, X., Chen, K., et al. (2018). Circular RNA IARS (circIARS) secreted by pancreatic cancer cells and located within exosomes regulates endothelial monolayer permeability to promote tumor metastasis. *J. Exp. Clin. Cancer Res.* 37 (1), 177. doi:10.1186/s13046-018-0822-3

Li, Z., Ma, Y.-Y., Wang, J., Zeng, X.-F., Li, R., Kang, W., et al. (2016). Exosomal microRNA-141 is upregulated in the serum of prostate cancer patients. *Onco. Targets. Ther.* 9, 139–148. doi:10.2147/OTT.S95565

Lin, J., Li, J., Huang, B., Liu, J., Chen, X., Chen, X. M., et al. (2015). Exosomes: Novel biomarkers for clinical diagnosis. *ScientificWorldJournal.* 2015, 657086. doi:10.1155/2015/657086

Lin, R., Wang, S., and Zhao, R. C. (2013). Exosomes from human adipose-derived mesenchymal stem cells promote migration through Wnt signaling pathway in a breast cancer cell model. *Mol. Cell. Biochem.* 383, 13–20. doi:10.1007/s11010-013-1746-z

Liu, C., Eng, C., Shen, J., Lu, Y., Takata, Y., Mehdizadeh, A., et al. (2016). Serum exosomal miR-4772-3p is a predictor of tumor recurrence in stage II and III colon cancer. *Oncotarget* 7, 76250–76260. doi:10.18632/oncotarget.12841

Liu, L., Meng, T., Yang, X.-H., Sayim, P., Lei, C., Jin, B., et al. (2018). Prognostic and predictive value of long non-coding RNA GAS5 and mircoRNA-221 in colorectal cancer and their effects on colorectal cancer cell proliferation, migration and invasion. *Cancer Biomark.* 22, 283–299. doi:10.3233/CBM-171011

Logozzi, M., Angelini, D. F., Iessi, E., Mizzoni, D., Di Raimo, R., Federici, C., et al. (2017). Increased PSA expression on prostate cancer exosomes in in vitro condition and in cancer patients. *Cancer Lett.* 403, 318–329. doi:10.1016/j.canlet.2017.06.036

Logozzi, M., De Milito, A., Lugini, L., Borghi, M., Calabrò, L., Spada, M., et al. (2009). High levels of exosomes expressing CD63 and caveolin-1 in plasma of melanoma patients. *PloS one* 4 (4), e5219. doi:10.1371/journal.pone.0005219

Logozzi, M., Mizzoni, D., Capasso, C., Del Prete, S., Di Raimo, R., Falchi, M., et al. (2020). Plasmatic exosomes from prostate cancer patients show increased carbonic anhydrase IX expression and activity and low pH. *J. Enzyme Inhib. Med. Chem.* 35, 280–288. doi:10.1080/14756366.2019.1697249

Lou, G., Song, X., Yang, F., Wu, S., Wang, J., Chen, Z., et al. (2015). Exosomes derived from miR-122-modified adipose tissue-derived MSCs increase chemosensitivity of hepatocellular carcinoma. *J. Hematol. Oncol.* 8, 122. doi:10.1186/s13045-015-0220-7

Luan, X., Sansanaphongpricha, K., Myers, I., Chen, H., Yuan, H., and Sun, D. (2017). Engineering exosomes as refined biological nanoplatforms for drug delivery. *Acta Pharmacol. Sin.* 38, 754–763. doi:10.1038/aps.2017.12

Madhavan, B., Yue, S., Galli, U., Rana, S., Gross, W., Müller, M., et al. (2015). Combined evaluation of a panel of protein and miRNA serum-exosome biomarkers for pancreatic cancer diagnosis increases sensitivity and specificity. *Int. J. Cancer* 136 (11), 2616–2627. doi:10.1002/ijc.29324

Matarredona, E. R., and Pastor, A. M. (2020). Extracellular vesicle-mediated communication. *Cells* 9 (1), 96–103. doi:10.3390/cells9010096

Mathew, M., Zade, M., Mezghani, N., Patel, R., Wang, Y., Momen-Heravi, F., et al. (2020). Extracellular vesicles as biomarkers in cancer immunotherapy. *Cancers* 12 (10), 2825. doi:10.3390/cancers12102825

Matsumura, T., Sugimachi, K., Iinuma, H., Takahashi, Y., Kurashige, J., Sawada, G., et al. (2015). Exosomal microRNA in serum is a novel biomarker of recurrence in human colorectal cancer. *Br. J. Cancer* 113, 275–281. doi:10.1038/bjc.2015.201

Melo, S. A., Sugimoto, H., O'Connell, J. T., Kato, N., Villanueva, A., Vidal, A., et al. (2014). Cancer exosomes perform cell-independent microRNA biogenesis and promote tumorigenesis. *Cancer Cell.* 26 (5), 707–721. doi:10.1016/j.ccell.2014.09.005

Melo, S. A., Luecke, L. B., Kahlert, C., Fernandez, A. F., Gammon, S. T., Kaye, J., et al. (2015). Glypican-1 identifies cancer exosomes and detects early pancreatic cancer. *Nature* 523, 177–182. doi:10.1038/nature14581

Mendt, M., Kamerkar, S., Sugimoto, H., McAndrews, K. M., Wu, C. C., Gagea, M., et al. (2018). Generation and testing of clinical-grade exosomes for pancreatic cancer. *JCI Insight* 3, e99263. doi:10.1172/jci.insight.99263

Meng, X., Müller, V., Milde-Langosch, K., Trillsch, F., Pantel, K., Schwarzenbach, H., et al. (2016). Diagnostic and prognostic relevance of circulating exosomal miR-373, miR-200a, miR-200b and miR-200c in patients with epithelial ovarian cancer. *Oncotarget* 7 (13), 16923–16935. doi:10.18632/oncotarget.7850

Moon, P.-G., Lee, J.-E., Cho, Y.-E., Lee, S. J., Chae, Y. S., Jung, J. H., et al. (2016a). Fibronectin on circulating extracellular vesicles as a liquid biopsy to detect breast cancer. *Oncotarget* 7, 40189–40199. doi:10.18632/oncotarget.9561

Moon, P.-G., Lee, J.-E., Cho, Y.-E., Lee, S. J., Jung, J. H., Chae, Y. S., et al. (2016b). Identification of developmental endothelial locus-1 on circulating extracellular vesicles as a novel biomarker for early breast cancer detection. *Clin. Cancer Res.* 22, 1757–1766. doi:10.1158/1078-0432.CCR-15-0654

Morelli, A. E., Larregina, A. T., Shufesky, W. J., Sullivan, M. L. G., Stolz, D. B., Papworth, G. D., et al. (2004). Endocytosis, intracellular sorting, and processing of exosomes by dendritic cells. *Blood* 104 (10), 3257–3266. doi:10.1182/blood-2004-03-0824

Nakase, I., Kobayashi, N. B., Takatani-Nakase, T., and Yoshida, T. (2015). Active macropinocytosis induction by stimulation of epidermal growth factor receptor and oncogenic Ras expression potentiates cellular uptake efficacy of exosomes. *Sci. Rep.* 5, 10300. doi:10.1038/srep10300

Nakase, I., and Futaki, S. (2015). Combined treatment with a pH-sensitive fusogenic peptide and cationic lipids achieves enhanced cytosolic delivery of exosomes. *Sci. Rep.* 5, 10112. doi:10.1038/srep10112

Ogata-Kawata, H., Izumiya, M., Kurioka, D., Honma, Y., Yamada, Y., Furuta, K., et al. (2014). Circulating exosomal microRNAs as biomarkers of colon cancer. *PLoS ONE* 9, e92921. doi:10.1371/journal.pone.0092921

Ohno, S. I., Takanashi, M., Sudo, K., Ueda, S., Ishikawa, A., Matsuyama, N., et al. (2013). Systemically injected exosomes targeted to EGFR deliver antitumor microrna to breast cancer cells. *Mol. Ther.* 21 (1), 185–191. doi:10.1038/mt.2012.180

Ohshima, K., Inoue, K., Fujiwara, A., Hatakeyama, K., Kanto, K., Watanabe, Y., et al. (2010). Let-7 microRNA family is selectively secreted into the extracellular environment via exosomes in a metastatic gastric cancer cell line. *PloS one* 5 (10), e13247. doi:10.1371/journal.pone.0013247

Palmisano, G., Jensen, S. S., Le Bihan, M. C., Lainé, J., McGuire, J. N., Pociot, F., et al. (2012). Characterization of membrane-shed microvesicles from cytokine-stimulated β-cells using proteomics strategies. *Mol. Cell. Proteomics* 11 (8), 230–243. doi:10.1074/mcp.M111.012732

Pan, C., Stevic, I., Müller, V., Ni, Q., Oliveira-Ferrer, L., Pantel, K., et al. (2018). Exosomal microRNAs as tumor markers in epithelial ovarian cancer. *Mol. Oncol.* 12, 1935–1948. doi:10.1002/1878-0261.12371

Parolini, I., Federici, C., Raggi, C., Lugini, L., Palleschi, S., De Milito, A., et al. (2009). Microenvironmental pH is a key factor for exosome traffic in tumor cells. *J. Biol. Chem.* 284 (49), 34211–34222. doi:10.1074/jbc.M109.041152

Patel, B., Patel, J., Cho, J. H., Manne, S., Bonala, S., Henske, E., et al. (2016). Exosomes mediate the acquisition of the disease phenotypes by cells with normal genome in tuberous sclerosis complex. *Oncogene* 35 (23), 3027–3036. doi:10.1038/onc.2015.358

Peinado, H., Alečković, M., Lavotshkin, S., Matei, I., Costasilva, B., Morenobueno, G., et al. (2012). Melanoma exosomes educate bone marrow progenitor cells toward a pro-metastatic phenotype through MET. *Nat. Med.* 18 (6), 883–891. doi:10.1038/nm.2753

Pulliam, L., Sun, B., Mustapic, M., Chawla, S., and Kapogiannis, D. (2019). Plasma neuronal exosomes serve as biomarkers of cognitive impairment in HIV infection and Alzheimer's disease. *J. Neurovirol.* 25 (5), 702–709. doi:10.1007/s13365-018-0695-4

Qin, X., Yu, S., Zhou, L., Shi, M., Hu, Y., Xu, X., et al. (2017). Cisplatin-resistant lung cancer cell-derived exosomes increase cisplatin resistance of recipient cells in exosomal miR-100-5p-dependent manner. *Int. J. Nanomedicine* 12, 3721–3733. doi:10.2147/IJN.S131516

Que, R., Ding, G., Chen, J., and Cao, L. (2013). Analysis of serum exosomal microRNAs and clinicopathologic features of patients with pancreatic adenocarcinoma. *World J. Surg. Oncol.* 11, 219. doi:10.1186/1477-7819-11-219

Rachel, E. S., Gabriel, M., Steve, K., Philip, A. P., and Asfar, S. A. (2017). Ras and exosome signaling Rachel. *Physiol. Behav.* 176, 139–148. doi:10.1016/j.semcancer.2019.02.004

Rana, S., Yue, S. J., Stadel, D., and Zoller, M. (2012). Toward tailored exosomes: The exosomal tetraspanin web contributes to target cell selection. *Int. J. Biochem. Cell. Biol.* 44, 1574–1584. doi:10.1016/j.biocel.2012.06.018

Rodríguez, M., Silva, J., Lópezalfonso, A., Lópezmuñiz, M. B., Peña, C., Domínguez, G., et al. (2014). Different exosome cargo from plasma/bronchoalveolar lavage in non-small-cell lung cancer. *Genes. Chromosom. Cancer* 53 (9), 713–724. doi:10.1002/gcc.22181

Ruivo, C. F., Adem, B., Silva, M., and Melo, S. A. (2017). The biology of cancer exosomes: Insights and new perspectives. *Cancer Res.* 77 (23), 6480–6488. doi:10.1158/0008-5472.CAN-17-0994

Sandfeld-Paulsen, B., Aggerholm-Pedersen, N., Baek, R., Jakobsen, K. R., Meldgaard, P., Folkersen, B. H., et al. (2016a). Exosomal proteins as prognostic biomarkers in non-small cell lung cancer. *Mol. Oncol.* 10, 1595–1602. doi:10.1016/j.molonc.2016.10.003

Sandfeld-Paulsen, B., Jakobsen, K. R., Bæk, R., Folkersen, B. H., Rasmussen, T. R., Meldgaard, P., et al. (2016b). Exosomal proteins as a diagnostic biomarkers in lung cancer. *J. Thorac. Oncol.* 11 (10), 1701–1710. doi:10.1016/j.jtho.2016.05.034

Silva, J., Garcia, V., Rodriguez, M., Compte, M., Cisneros, E., Veguillas, P., et al. (2012). Analysis of exosome release and its prognostic value in human colorectal cancer. *Genes. Chromosom. Cancer* 51, 409–418. doi:10.1002/gcc.21926

Sohn, W., Kim, J., Kang, S. H., Yang, S. R., Cho, J.-Y., Cho, H. C., et al. (2015). Serum exosomal microRNAs as novel biomarkers for hepatocellular carcinoma. *Exp. Mol. Med.* 47, e184. doi:10.1038/emm.2015.68

Sugimachi, K., Matsumura, T., Hirata, H., Uchi, R., Ueda, M., Ueo, H., et al. (2015). Identification of a bona fide microRNA biomarker in serum exosomes that predicts hepatocellular carcinoma recurrence after liver transplantation. *Br. J. Cancer* 112, 532–538. doi:10.1038/bjc.2014.621

Sun, B., Li, Y., Zhou, Y., Ng, T. K., Zhao, C., Gan, Q., et al. (2018). Circulating exosomal CPNE3 as a diagnostic and prognostic biomarker for colorectal cancer. *J. Cell. Physiol.* 234, 1416–1425. doi:10.1002/jcp.26936

Sun, Z., Wang, L., Dong, L., and Wang, X. (2018). Emerging role of exosome signalling in maintaining cancer stem cell dynamic equilibrium. *J. Cell. Mol. Med.* 22, 3719–3728. doi:10.1111/jcmm.13676

Svensson, K. J., Christianson, H. C., Wittrup, A., Bourseau-Guilmain, E., Lindqvist, E., Svensson, L. M., et al. (2013). Exosome uptake depends on ERK1/2-heat shock protein 27 signaling and lipid raft-mediated endocytosis negatively regulated by caveolin-1. *J. Biol. Chem.* 288 (24), 17713–17724. doi:10.1074/jbc.M112.445403

Szajnik, M., Derbis, M., Lach, M., Patalas, P., Michalak, M., Drzewiecka, H., et al. (2013). Exosomes in plasma of patients with ovarian carcinoma: Potential biomarkers of tumor progression and response to therapy. *Gynecol. Obstet.* 4, 3. doi:10.4172/2161-0932.S4-003

Szczepanski, M. J., Szajnik, M., Welsh, A., Whiteside, T. L., and Boyiadzis, M. (2011). Blast-derived microvesicles in sera from patients with acute myeloid leukemia suppress natural killer cell function via membrane-associated transforming growth factor-beta1. *Haematologica* 96 (9), 1302–1309. doi:10.3324/haematol.2010.039743

Takahashi, K., Yan, I. K., Kogure, T., Haga, H., and Patel, T. (2014a). Extracellular vesicle-mediated transfer of long non-coding RNA ROR modulates chemosensitivity in human hepatocellular cancer. *FEBS open bio* 4, 458–467. doi:10.1016/j.fob.2014.04.007

Takahashi, K., Yan, I. K., Wood, J., Haga, H., and Patel, T. (2014b). Involvement of extracellular vesicle long noncoding RNA (linc-VLDLR) in tumor cell responses to chemotherapy. *Mol. Cancer Res.* 12 (10), 1377–1387. doi:10.1158/1541-7786.MCR-13-0636

Takahasi, K., Iinuma, H., Wada, K., Minezaki, S., Kawamura, S., Kainuma, M., et al. (2018). Usefulness of exosome-encapsulated microRNA-451a as a minimally invasive biomarker for prediction of recurrence and prognosis in pancreatic ductal adenocarcinoma. *J. Hepatobiliary. Pancreat. Sci.* 25, 155–161. doi:10.1002/jhbp.524

Tang, W., Fu, K., Sun, H., Rong, D., Wang, H., Cao, H., et al. (2018). CircRNA microarray profiling identifies a novel circulating biomarker for detection of gastric cancer. *Mol. Cancer* 17 (1), 137. doi:10.1186/s12943-018-0888-8

Tang, X. H., Guo, T., Gao, X. Y., Wu, X. L., Xing, X. F., Ji, J. F., et al. (2021). Exosome-derived noncoding RNAs in gastric cancer: Functions and clinical applications. *Mol. Cancer* 20 (1), 99. doi:10.1186/s12943-021-01396-6

Taraboletti, G., D'Ascenzo, S., Giusti, I., Marchetti, D., Borsotti, P., Millimaggi, D., et al. (2006). Bioavailability of VEGF in tumor-shed vesicles depends on vesicle burst induced by acidic pH. *Neoplasia* 8 (2), 96–103. doi:10.1593/neo.05583

Taylor, D. D., and Gercel-Taylor, C. (2008). MicroRNA signatures of tumor-derived exosomes as diagnostic biomarkers of ovarian cancer. *Gynecol. Oncol.* 110 (1), 13–21. doi:10.1016/j.ygyno.2008.04.033

Taylor, D. D., Gerçel-Taylor, C., Lyons, K. S., Stanson, J., and Whiteside, T. L. (2003). T-cell apoptosis and suppression of T-cell receptor/CD3-zeta by Fas ligand-containing membrane vesicles shed from ovarian tumors. *Clin. Cancer Res.* 9 (14), 5113–5119.

Thomas Jefferson University (2000). "Pilot immunotherapy trial for recurrent malignant gliomas," in *ClinicalTrials.gov* [Internet] (Bethesda (MD): National Library of Medicine US).

Tian, T., Zhu, Y. L., Hu, F. H., Wang, Y. Y., Huang, N. P., Xiao, Z. D., et al. (2013). Dynamics of exosome internalization and trafficking. *J. Cell. Physiol.* 228 (7), 1487–1495. doi:10.1002/jcp.24304

Tian, T., Zhu, Y. L., Zhou, Y. Y., Liang, G. F., Wang, Y. Y., Hu, F. H., et al. (2014). Exosome uptake through clathrin-mediated endocytosis and macropinocytosis and mediating miR-21 delivery. *J. Biol. Chem.* 289, 22258–22267. doi:10.1074/jbc.M114.588046

Tian, Y., Li, S., Song, J., Ji, T., Zhu, M., Anderson, G. J., et al. (2014). A doxorubicin delivery platform using engineered natural membrane vesicle exosomes for targeted tumor therapy. *Biomaterials* 35 (7), 2383–2390. doi:10.1016/j.biomaterials.2013.11.083

Tian, Y., Ma, L., Gong, M., Su, G., Zhu, S., Zhang, W., et al. (2018). Protein profiling and sizing of extracellular vesicles from colorectal cancer patients via flow cytometry. *ACS Nano* 12, 671–680. doi:10.1021/acsnano.7b07782

Tomasetti, M., Lee, W., Santarelli, L., and Neuzil, J. (2017). Exosome-derived microRNAs in cancer metabolism: Possible implications in cancer diagnostics and therapy. *Exp. Mol. Med.* 49, e285. doi:10.1038/emm.2016.153

Towns, R., and Pietropaolo, M. (2011). GAD65 autoantibodies and its role as biomarker of type 1 diabetes and latent autoimmune diabetes in adults (LADA). *Drugs Future* 36 (11), 847. doi:10.1358/dof.2011.036.11.1710754

Tsukamoto, M., Iinuma, H., Yagi, T., Matsuda, K., and Hashiguchi, Y. (2017). Circulating exosomal MicroRNA-21 as a biomarker in each tumor stage of colorectal cancer. *Oncology* 92, 360–370. doi:10.1159/000463387

Vardaki, I., Ceder, S., Rutishauser, D., Baltatzis, G., Foukakis, T., Panaretakis, T., et al. (2016). Periostin is identified as a putative metastatic marker in breast cancer-derived exosomes. *Oncotarget* 7 (46), 74966–74978. doi:10.18632/oncotarget.11663

Whiteside, T. L. (2017). *HHS public access*. doi:10.1016/bs.acc.2015.12.005

Whiteside, T. L. (2016). Tumor-derived exosomes and their role in cancer progression. *Adv. Clin. Chem.* 74, 103–141. doi:10.1016/bs.acc.2015.12.005

Willis, G. R., Fernandez-Gonzalez, A., Reis, M., Mitsialis, S. A., and Kourembanas, S. (2018). Macrophage immunomodulation: The gatekeeper for mesenchymal stem cell derived-exosomes in pulmonary arterial hypertension? *Int. J. Mol. Sci.* 19. doi:10.3390/ijms19092534

Wolfers, J., Lozier, A., Raposo, G., Regnault, A., Thery, C., and Masurier, C. (2001). Tumor-derived exosomes are a source of shared tumor rejection antigens for CTL cross-priming. *Nat. Med.* 7, 297–303. doi:10.1038/85438

Wong, C. H., and Chen, Y. C. (2019). Clinical significance of exosomes as potential biomarkers in cancer. *World J. Clin. Cases* 7 (2), 171–190. doi:10.12998/wjcc.v7.i2.171

Xiao, Y., Zhong, J., Zhong, B., Huang, J., Jiang, L., Jiang, Y., et al. (2020). Exosomes as potential sources of biomarkers in colorectal cancer. *Cancer Lett.* 476, 13–22. doi:10.1016/j.canlet.2020.01.033

Xu, K., Zhang, C., Du, T., Gabriel, A., Wang, X., Li, X., et al. (2021). Progress of exosomes in the diagnosis and treatment of lung cancer. *Biomed. Pharmacother.* 134, 111111. doi:10.1016/j.biopha.2020.111111

Xu, M., Su, Y., Liu, X., Xu, M., Chen, X., Zhu, Y., et al. (2018). Serum and exosome long non coding RNAs as potential biomarkers for hepatocellular carcinoma. *J. Cancer* 9 (15), 2631–2639. doi:10.7150/jca.24978

Xu, M., Sun, X., Wang, Y., Yang, Q., Sun, X., and Wang, Y. (2020). Recent advancements in the loading and modification of therapeutic exosomes. *Front. Bioeng. Biotechnol.* 8, 586130. doi:10.3389/fbioe.2020.586130

Yan-Liang, Z., Yue-Yuan, Z., Gao-Feng, L., Yuan-Yuan, W., Fei-Hu, H., and Zhong-Dang, X. (2014). Exosome uptake through clathrin-mediated endocytosis and macropinocytosis and mediating miR-21 delivery. *J. Biol. Chem.* 289 (32), 22258–22267. doi:10.1074/jbc.M114.588046

Yang, H., Fu, H., Wang, B., Zhang, X., Mao, J., Li, X., et al. (2018). Exosomal miR-423-5p targets SUFU to promote cancer growth and metastasis and serves as a novel marker for gastric cancer. *Mol. Carcinog.* 57, 1223–1236. doi:10.1002/mc.22838

Yoon, J. H., Ham, I.-H., Kim, O., Ashktorab, H., Smoot, D. T., Nam, S. W., et al. (2018). Gastrokine 1 protein is a potential theragnostic target for gastric cancer. *Gastric Cancer* 21, 956–967. doi:10.1007/s10120-018-0828-8

Yoshida, K., Yokoi, A., Kato, T., Ochiya, T., and Yamamoto, Y. (2020). The clinical impact of intra- and extracellular miRNAs in ovarian cancer. *Cancer Sci.* 111 (10), 3435–3444. doi:10.1111/cas.14599

Yoshioka, Y., Konishi, Y., Kosaka, N., Katsuda, T., Kato, T., Ochiya, T., et al. (2013). Comparative marker analysis of extracellular vesicles in different human cancer types. *J. Extracell. Vesicles* 2, 20424. doi:10.3402/jev.v2i0.20424

You, B., Xu, W., and Zhang, B. (2018). Engineering exosomes: A new direction for anticancer treatment. *Am. J. Cancer Res.* 8 (8), 1332–1342. Published 2018 Aug 1.

Yue, B., Yang, H., Wang, J., Ru, W., Wu, J., Huang, Y., et al. (2020). Exosome biogenesis, secretion and function of exosomal miRNAs in skeletal muscle myogenesis. *Cell. Prolif.* 53, e12857. doi:10.1111/cpr.12857

Yuwen, D., Ma, Y., Wang, D., Gao, J., Li, X., Xue, W., et al. (2019). Prognostic role of circulating exosomal miR-425-3p for the response of NSCLC to platinum-based chemotherapy. *Cancer Epidemiol. Biomarkers Prev.* 28 (1), 163–173. doi:10.1158/1055-9965.EPI-18-0569

Zhang, Y., Bi, J., Huang, J., Tang, Y., Du, S., Li, P., et al. (2020). Exosome: A review of its classification, isolation techniques, storage, diagnostic and targeted therapy applications. *Int. J. Nanomedicine* 15, 6917–6934. doi:10.2147/IJN.S264498

Zhao, R., Zhang, Y., Zhang, X., Yang, Y., Zheng, X., Li, X., et al. (2018). Exosomal long noncoding RNA HOTTIP as potential novel diagnostic and prognostic biomarker test for gastric cancer. *Mol. Cancer* 17 (1), 68. doi:10.1186/s12943-018-0817-x

Zhao, Y. J., and Xie, L. (2019). Potential role of exosomes in cancer therapy. *Precis. Radiat. Oncol.* 3, pro6.66. doi:10.1002/pro6.66

Zhu, J., Zhao, Y., Chen, W., Yin, L., Zhu, J., Zhang, H., et al. (2018). Exosomal ephrinA2 derived from serum as a potential biomarker for prostate cancer. *J. Cancer* 9 (15), 2659–2665. doi:10.7150/jca.25201

frontiers | Frontiers in Molecular Biosciences

TYPE Original Research
PUBLISHED 16 August 2022
DOI 10.3389/fmolb.2022.943384

OPEN ACCESS

EDITED BY
José Alexandre Ferreira,
Portuguese Oncology Institute,
Portugal

REVIEWED BY
Ashutosh Kumar Pandey,
Rutgers, The State University of New Jersey, United States
Carmine Giorgio,
University of Parma, Italy

*CORRESPONDENCE
Jianbing Wu,
ndefy93008@ncu.edu.cn

†These authors have contributed equally to this work and share first authorship

SPECIALTY SECTION
This article was submitted to Molecular Diagnostics and Therapeutics, a section of the journal Frontiers in Molecular Biosciences

RECEIVED 13 May 2022
ACCEPTED 13 July 2022
PUBLISHED 16 August 2022

CITATION
Huang S, Dong C, Zhang J, Fu S, Lv Y and Wu J (2022), A comprehensive prognostic and immunological analysis of ephrin family genes in hepatocellular carcinoma.
Front. Mol. Biosci. 9:943384.
doi: 10.3389/fmolb.2022.943384

A comprehensive prognostic and immunological analysis of ephrin family genes in hepatocellular carcinoma

Shenglan Huang[1,2†], Cairong Dong[3†], Jian Zhang[1,2†], Shumin Fu[1,2], Yaqin Lv[1,2] and Jianbing Wu[1,2*]

[1]Department of Oncology, The Second Affiliated Hospital of Nanchang University, Nanchang, Jiangxi, China, [2]Jiangxi Key Laboratory of Clinical and Translational Cancer Research, Nanchang, Jiangxi, China, [3]Department of Hepatobiliary Surgery, The Second Affiliated Hospital of Nanchang University, Nanchang, Jiangxi, China

Background: Ephrins, a series of Eph-associated receptor tyrosine kinase ligands, play an important role in the tumorigenesis and progression of various cancers. However, their contributions to hepatocellular carcinoma (HCC) remain unclear. Thus, we aimed to explore their prognostic value and immune implications in HCC.

Methods: Multiple public databases, such as TCGA, GTEx, and UCSC XENA, were used to analyze the expression of ephrin genes across cancers. Kaplan-Meier analysis and Cox regression were used to explore the prognostic role of ephrin genes in HCC. A logistic regression model was utilized to evaluate the association between ephrin gene expression and clinical characteristics. Gene set enrichment analysis (GSEA) was conducted to elucidate their potential biological mechanisms. Various immune algorithms were utilized to investigate the correlation between ephrin genes and tumor immunity. We also analyzed their association with drug sensitivity, and gene mutations. Finally, RT–qPCR was performed to validate the expression of ephrin family genes in HCC cells and clinical tissues.

Results: The expression of EFNA1, EFNA2, EFNA3, EFNA4, EFNB1, and EFNB2 was upregulated in most cancer types, while EFNA5 and EFNB3 was downregulated in most cancers. In HCC, the expression levels of EFNA1, EFNA3, EFNA4, EFNB1, and EFNB2 were significantly higher in tumor tissues than in normal tissues. High expression of EFNA3, EFNA4, and EFNB1 was associated with tumor progression and worse prognosis in HCC patients. The expression of EFNA3 and EFNA4 was negatively associated with the stromal/ESTIMATE scores, while EFNB1 was positively correlated with the immune/stromal/ESTIMATE scores. Moreover, these ephrin genes were closely relevant to the infiltration of immune cells, such as B cells, $CD4^+$ T cells, $CD8^+$ T cells, neutrophil cells, macrophage cells, and dendritic cells. EFNB1 expression was positively associated with most immune-related genes, while EFNA3/EFNA4 was positively related to TMB and MSI. In addition, EFNA3, EFNA4, and EFNB1 were related to drug sensitivity and affected the mutation frequency of some genes in HCC.

Conclusion: EFNA3, EFNA4, and EFNB1 are independent prognostic factors for HCC patients and are closely correlated with tumor immunity, which may provide a new direction for exploring novel therapeutic targets and biomarkers for immunotherapy.

KEYWORDS

ephrin family, prognosis, immune, biomarker, hepatocellular carcinoma

Introduction

Hepatocellular carcinoma (HCC) is one of the most prevalent malignant tumors and ranks fourth among the most common causes of cancer-related death worldwide (Yang J. D. et al., 2019). Several factors, including chronic hepatitis B and hepatitis C, cirrhosis, alcohol abuse, nonalcoholic fatty liver disease and exposure to dietary toxins such as aristolochic acid and aflatoxins, remarkably increase the occurrence risk of HCC (Yang J. D. et al., 2019; Kulik and El-Serag, 2019; Llovet et al., 2021). Early-stage HCC can be treated curatively by surgical excision, local ablation, or liver transplantation. However, the majority of HCC patients are diagnosed at an advanced stage and are unsuitable for curative treatments (Fitzmaurice et al., 2017). Multiple kinase inhibitors and immune checkpoint inhibitors (ICIs) have been proven to be effective treatment options for advanced-stage HCC in recent years. The prognosis of HCC remains unsatisfactory, with cancer-specific mortality still increasing in many countries and an overall 5-year survival rate of only approximately 18% (Galle et al., 2021). The poor prognosis and high mortality of HCC patients are mainly attributed to molecular heterogeneity and the lack of early and effective indictive markers (Yang J. D. et al., 2019; Kulik and El-Serag, 2019). Thus, exploring reliable prognostic biomarkers and effective therapeutic targets is critically important to improve the clinical outcomes of HCC patients.

Erythropoietin-producing hepatocellular carcinoma (Eph) and Eph receptor interacting ligands (ephrins, EFNs) are the largest family of membrane-bound receptor tyrosine kinases, which consist of fourteen Eph receptors and eight ephrin ligands (Kullander and Klein, 2002). Ephs and ephrins are widely expressed on the surface of various cells. Characteristic bidirectional signaling is induced through Eph–ephrin interactions in receptor- and ligand-expressing cells; Eph receptors activated by ephrin ligands are referred to as "forward signaling," resulting in phosphorylation of the receptors and activation of downstream signaling molecules, while "reverse signaling" is defined as Eph receptor-mediated activation of ephrin ligands (Héroult et al., 2006; Lin et al., 2021). The Eph-ephrin complexes are involved in a wide spectrum of physiological and pathological processes and affect cell biological functions during development, such as neurogenesis and angiogenesis, cell proliferation and differentiation, cell segregation, cellular motility and adhesion (Brückner and Klein, 1998; Shu et al., 2016). The Eph-ephrin signaling system promotes cell migration by regulating the reorganization of the actin cytoskeleton and increasing intercellular adhesiveness (Pasquale, 2008), suggesting that the common characteristics and molecular mechanisms of cancer cells can be modulated by them. Therefore, the Eph-ephrin complex can be used as a new diagnostic biomarker and potential molecular therapeutic target in cancers.

Ephrin ligands are divided in A-subclass (ephrin-A1-A5) and B subclass (ephrin-B1-B3) groups based on their sequence conservation. Ephrin-As are glycosyl phosphatidyl inositol (GPI)-anchored molecules and are usually bound by EphA receptors, while ephrin-Bs are transmembrane proteins with an extracellular binding domain for EphB receptors and cytoplasmic SAM/PDZ-binding motif (Kullander and Klein, 2002). Ephrin ligands have been extensively studied in morphogenesis and neural development. Recently, increasing attention has been given to its significance in the tumorigenesis and progression of various cancers. Substantial evidence indicates that ephrins play a vital role in tumor angiogenesis, invasion, metastasis, and tumor stemness maintenance (Lodola et al., 2017). Many ephrin ligands have been shown to be upregulated in multiple tumors and associated with poor prognosis, such as lung adenocarcinoma (Deng et al., 2021), breast cancer (Kaenel et al., 2012), colorectal cancer (Papadakos et al., 2022), prostate cancer (Zhao et al., 2021), bladder cancer (Mencucci et al., 2020), and other cancers (Surawska et al., 2004). Lin et al. (2021) reported that EFNA4 is highly expressed in cancer tissues and leads to poor prognosis in patients with HCC. In addition, recent studies have highlighted important roles of Eph-ephrin signaling in the tumor microenvironment (TME) and tumor immunity (Janes et al., 2021). The ephrin ligand members are widely expressed on diverse immune cell types and participate in regulating cell adhesion, migration, and activation of B and T lymphocytes (Jin et al., 2011; Mori et al., 2013). Moreover, they also recruit immunosuppressive cells such as myeloid-derived suppressor cells (MDSCs) and tumor-associated macrophages (TAMs) to the TME, inhibit the activity of cytotoxic T cells, and, thus, support tumor survival (Hanahan and Coussens, 2012). A recent study suggested that EFNA3 acts as an independent prognostic factor and correlates with immune cell infiltration in gastric cancer and lung adenocarcinoma (Deng et al., 2021; Zheng et al.,

2021). However, the expression level and prognostic value of ephrin family genes and their association with tumor immunity have been less explored in HCC.

In this study, we performed a comprehensive analysis of ephrin family genes in HCC based on The Cancer Genome Atlas (TCGA), Genotype-Tissue Expression dataset (GTEx), Tumor Immune Evaluation Resource (TIMER) database, and some online bioinformatics analysis websites. We first explored the expression patterns of ephrin genes among 31 human cancer types. Then, the prognostic role of ephrin genes was discussed in HCC patients, and the association between prognosis-related ephrin genes and the TME, immune cell infiltration, immune subtypes, immune checkpoint biomarkers, gene mutation landscape, and drug response in HCC was further highlighted. Moreover, the differential expression of ephrins was validated in multiple HCC cell lines and 40 paired clinical tissue samples using RT–qPCR. The results of this study revealed the potential role of ephrin family genes as predictive biomarkers of prognosis and immunotherapy in patients with HCC, which warrants further in-depth study.

Materials and methods

Clinical tissue samples and ethics approval

In total, 40 paired fresh HCC tumorous and adjacent tissues were collected from the Second Affiliated Hospital of Nanchang University (Nanchang, China) between January 2021 and December 2021. The tissue samples were immediately frozen in liquid nitrogen after surgical resection and stored at −80°C until further analysis. The usage of tumor and adjacent normal tissues in this study was approved by The Second Affiliated Hospital of Nanchang University Medical Research Ethics Committee. All of the patients enrolled in this study provided written informed consent in accordance with the Helsinki Declaration and related guidelines.

Public data acquisition and processing

RNA-seq data in the TPM (transcripts per million reads) format of pan-cancer datasets were downloaded from the UCSC XENA (https://xenabrowser.net/datapages/), which were processed by the Toil process (Vivian et al., 2017), and the samples were derived from the TCGA and GTEx datasets. All expression data were normalized on a log2 (TPM +1) scale. The cancer types with fewer than 3 samples were removed, and we ultimately obtained the expression data of 15,521 samples from 31 cancer types. Meanwhile, transcriptome profiling data of HCC projects harmonized to TPM were downloaded from TCGA (https://portal.gdc.cancer.gov/), including 374 tumor tissues and 50 normal samples. Furthermore, we also obtained clinical information and prognostic outcomes of HCC from the UCEC database, which was derived from a prognostic study of the TCGA dataset (Liu et al., 2018), including age, sex, histological grade, pathological stage, vascular invasion status, overall survival (OS), progression-free interval (PFI), and disease-specific survival (DSS).

Expression patterns of ephrin genes in pan-cancer and their diagnostic value in HCC

Ephrin gene expression between tumor tissues and unpaired normal tissues in pan-cancer was analyzed and visualized using the Sangerbox online platform (http://sangerbox.com/) based on TCGA targeted GTEx datasets. The differential expression analysis of EFNs in HCC tissues compared with paired normal tissues was conducted in TCGA datasets by using the "limma" and "ggplot2" packages of R 4.0.5 software (http://www.r-project.org/). The Wilcoxon rank sum test was applied for statistical analyses, and a value of $p < 0.05$ was considered to be statistically significant.

Receiver operating characteristic (ROC) curves and the area under the ROC curve (AUC) were employed to estimate the diagnostic ability of ephrin family genes, and "pROC" and "ggplot2" of R packages were used for visualization and analysis. An AUC of 0.5–0.7 indicates a lower level of diagnostic accuracy, an AUC of 0.7–0.9 suggests moderate accuracy, and an AUC above 0.9 indicates higher diagnostic accuracy.

Subsequently, we explored the correlation among ephrin genes at the mRNA expression level with Pearson's correlation analysis, in which the "corrplot" R package was used to calculate the correlation coefficient (Pearson's R), and Pearson's R > 0.3 was considered statistically significant.

Prognostic values and clinical feature correlation analyses of ephrin genes in HCC

First, we integrated the mRNA expression data of ephrin genes with clinical information based on the HCC project from the TCGA database. After removing the samples with incomplete follow-up information, the remaining patients were divided into high- and low-expression groups based on the best cutoff values of the expression of each ephrin gene. Kaplan-Meier analysis was performed to explore the relationship between EFN gene expression and prognostic indicators, including OS, PFI, and DSS. The "survminer" and "survival" R packages were used for statistical analysis and data visualization. The statistical significance was obtained with the log-rank test. In addition, independent prognostic factors for OS were identified by

univariate and multivariate Cox regression analyses, integrating the following clinical features: age, sex, histological grade, and pathological stage. The results are presented as a hazard ratio (HR) and 95% confidence interval (CI), and statistical significance was defined as $p < 0.05$. The ephrin genes that significantly and independently affected OS were chosen for further analyses.

To further investigate the correlation between ephrin ligand genes and clinicopathological parameters, we compared the expression levels of ephrin genes with different clinical T stages, pathological stages, histological grades, and vascular invasion status in HCC patients. Student's t test or one-way ANOVA was used to verify expression differences. Moreover, the binary logistic regression model was utilized to evaluate the association between ephrin gene expression and clinical characteristics, such as age (>60 vs. ≤ 60), sex (male vs. female), T stage (T3&T4 vs. T1&T2), N stage (N1 vs. N0), M stage (M1 vs. M0), pathological stage (stage III& IV vs. stage I&II), histological grade (G3&G4 vs. G1&G2), vascular invasion status (yes vs. no), AFP (ng/ml) (>400 vs. ≤400), and Child–Pugh grade (B&C vs. A). The patients were divided into high- or low-expression groups according to the median expression value of ephrin genes, and the expression grouping was used as the independent variable. The clinical characteristics were dependent variables, and the right factors in parentheses were used as references. The results are presented with odds ratios and *p values*, and a *p value* of less than 0.05 ($p < 0.05$) was considered significant.

Protein interaction and gene set enrichment analysis

The GeneMANIA online website (http://www.genemania.org) was applied to explore the interaction network of ephrin ligand members (EFNA3, EFNA4, and EFNB1), in which a large number of genomic and proteomic data were used to identify interactional genes with similar functions (Franz et al., 2018). The website mainly provides protein–protein interaction (PPI) predictions, including physical interaction, co-expression, co-localization, sharing of protein domains, genetic interactions, and signaling pathways. Furthermore, we also used the STRING database (https://string-db.org/) to clarify the interactive relationships among ephrin family genes and displayed the 50 most relevant proteins that interact with ephrin genes.

To investigate the biological role and uncover the potential biological mechanisms of ephrin genes in HCC, we conducted GSEA based on GSEA v.4.1.0 software (http://www.gsea-msigdb.org/gsea/index.jsp) and "c2. cp.kegg.v7.4. symbols.gmt," which was downloaded from MSigDB (http://www.gseamsigdb.org/gsea/msigdb/collections.jsp). Gene sets with a *p value* < 0.05 and a false discovery rate (FDR) of q-value < 0.25 were considered significantly enriched pathways.

Correlation of ephrin genes with the tumor microenvironment and tumor immunity

Previous studies have indicated that ephrin ligands and the Eph receptor signaling pathway significantly affect immune cell infiltration and change the tumor microenvironment (TME) (Yu et al., 2004; Yu et al., 2006; Lu et al., 2017). Thus, in this study, we explored the correlation between the expression of ephrin genes and TME and tumor immune cell infiltration. First, immune and stromal scores were calculated by the ESTIMATE algorithm using the "estimate" R package, which represents the infiltration levels of immune and stromal cells in different tumors, respectively. ESTIMATE scores are the sum of immune and stromal scores and show an inverse correlation with tumor purity. Then, Spearman correlation analysis was performed to analyze the correlation between the expression of ephrin ligand genes and immune scores, stromal scores, ESTIMATE scores, and tumor purity. The results are presented with scatterplots, and $p < 0.05$ was considered statistically significant.

Thereafter, the Tumor Immune Evaluation Resource (TIMER) database (http://timer.comp-genomics.org/), an online platform for comprehensive analysis of the specific gene(s) associated with tumor immune infiltrating cells (TIICs), was used to evaluate the association between the expression of ephrin family members and the infiltration levels of various immune cells in HCC samples. TIMER2.0 provides multiple immune infiltration estimations, including the TIMER, XCELL, QUANTISEQ, MCPCOUNTER, EPIC, CIBERSORT-ABS, and CIBERSORT algorithms. In this study, we selected the "Gene" module and used Spearman correlation analysis in TIMER 2.0, with a focus on exploring the association of ephrin genes with the infiltration levels of B cells, $CD4^+$ T cells, $CD8^+$ T cells, neutrophil cells, macrophage cells, and dendritic cells. A p value < 0.05 was considered statistically significant. The results are presented with scatterplots. In addition, we downloaded immune cell infiltration estimates for all TCGA tumor samples from the TIME2.0 database, which included immune cell infiltration levels in each HCC sample based on the XCELL, QUANTISEQ, MCPCOUNTER, EPIC, CIBERSORT-ABS, and CIBERSORT algorithms. We further integrated the immune cell infiltration data and ephrin gene expression to comprehensively analyze the correlation between ephrin gene expression and tumor immunity in HCC tissues by using the "scales," "ggplot2," and "ggtext" R packages. Spearman correlation coefficients were calculated to measure the strength of the statistical correlation between two variables. The results with $p < 0.05$ were considered significant and are presented with bubble plots.

Immune subtypes in cancers could effectively reflect intratumoral immune states. Six immune subtypes have been identified based on immune expression signatures and represent

different immune functions, including C1 (wound healing), C2 (IFN-gamma dominant), C3 (inflammatory), C4 (lymphocyte depleted), C5 (immunologically quiet), and C6 (TGF-beta dominant) (Thorsson et al., 2018). To identify the relationship between the expression of ephrin genes and immune subtypes in HCC, we used the online TISIDB web portal (http://cis.hku.hk/TISIDB/) and the Kruskal–Wallis test to compare the expression of ephrin genes between different immune subtypes. $P < 0.05$ was considered statistically significant.

Correlation analysis of ephrin family genes with immune checkpoint inhibitors (ICIs) biomarkers

Gene expression profiling within the tumor microenvironment could assess active innate and adaptive immune responses and may identify robust biomarkers for predicting the clinical benefit of checkpoint inhibitor strategies (Gibney et al., 2016). Thus, we utilized Spearman correlation analysis to assess the co-expression relationship between ephrin ligand genes and 47 immune checkpoint-related genes in HCC. The R packages "limma," "reshape2" and "RColorBrewer" were used to conduct the co-expression analysis. The results are displayed with a heatmap. Furthermore, we thoroughly analyzed the expression connection between ephrin genes and four key immune-related genes: PDCD1 (PD-1), CTLA4, CD274 (PD-L1), and PDCD1LG2 (PD-L2). The results are presented with scatter plots, and a p value less than 0.05 ($p < 0.05$) indicated a significant correlation.

Tumor mutation burden (TMB) is defined as the total number of mutations per million bases detected in each tumor sample, including gene coding errors, base substitution, gene insertion or deletion errors. Microsatellite instability (MSI) is a hypermutator phenotype with hypermutability of short repetitive sequences in the genome and impaired DNA mismatch repair (MMR) in tumors (Cortes-Ciriano et al., 2017). Increasing studies have indicated that TMB and MSI are primary drivers of tumor immune responses and have been proven to be predictive biomarkers for ICIs (Lengyel, 2021; McGrail et al., 2021). In our study, we explored the correlation of ephrin family genes with TMB and MSI in HCC. First, gene mutation data in "varscan 2" format were downloaded from the TCGA database and then transformed to TMB data using Perl 5.30.0 software (https://www.perl.org/). MSI data of HCC patients were directly acquired from previous studies (Hause et al., 2016; Yang G. et al., 2019). Then, we compared EFN gene expression between the high- and low-TMB/MSI subgroups and further explored their association using Spearman correlation analysis. The "limma," "ggpubr" and "reshape2" R packages were used for data analysis and visualization.

Prediction of response to chemotherapy and targeted therapy

To date, chemotherapy and antiangiogenic targeted therapy are the main treatments for advanced HCC patients. Thus, we investigated the role of ephrin genes in predicting the sensitivity of HCC patients to chemotherapies and targeted drugs. In our study, six commonly used chemotherapeutic and targeted agents of HCC were selected, namely, camptothecin, cisplatin, doxorubicin, mitomycin C, gemcitabine, and sorafenib. First, the pRRophetic algorithm and "pRRophetic" R package were used to calculate the drug half-maximal inhibitory concentration (IC50) of common chemotherapy and targeted therapy drugs based on the Cancer Genome Project (CGP) cell lines data (Geeleher et al., 2014). Then, we compared the drug sensitivity of the six common drugs in HCC between the high- and low-expression subgroups of ephrin family members. Statistical significance was determined as a *p value* less than 0.05.

Associations between the expression of ephrin family genes and mutational landscape genes

Single nucleotide polymorphisms (SNPs) refer to DNA sequence polymorphisms caused by variation in a single nucleotide at the genome level and widely exist in human genomic DNA. Abnormal SNPs promote the occurrence and development of tumors and contribute to treatment resistance. In our study, we analyzed the correlation between ephrin gene expression and SNPs in HCC. First, the format (MAF) file of somatic mutation information of HCC was obtained from the TCGA database, which was previously processed by the "varscan" method. The gene mutation frequency was calculated with the "maftools" R package. The top 15 genes with the highest mutation frequency were selected for comparison between the high- and low-expression groups of ephrin genes. We compared the genes and the mutational incidence rate between the two subgroups using the chi-squared test. $p < 0.05$ served as the significance threshold.

Cell lines and cell culture

Five HCC cell lines (HCC-LM3, MHCC97-H, SMMC7721, Huh7, and HepG2) were purchased from Procell Life Science & Technology Co. Ltd. (Wuhan, China). The normal liver cell Line L02 was previously acquired from the Chinese Academy of Science. All cells were cultured in Dulbecco's modified Eagle medium (DMEM; Solarbio, Beijing, China) supplemented with 10% FBS (Gibco, Grand Island, NY, United States), 100 μg/ml streptomycin and 100 U/ml penicillin sodium (Biotechnology,

TABLE 1 Primers for RT-qPCR analysis targeting ephrin genes.

Gene name	Sequences (5′—3′)
EFNA1	F: TCAGGCCCATGACAATCCAC; R: GTGACCGATGCTATGTAGAACC
EFNA2	F: TACGCCGTCTACTGGAACC; R: GAGCCTCGTACAGGGTCTC
EFNA3	F: CATGCGGTGTACTGGAACAG; R: AGATAGTCGTTCACGTTCACCT
EFNA4	F: CTC CGCCACGTAGTCTACTG; R: TACAAAGCAAACGTCTCGGGG
EFNA5	F: CGCTACGCTGTCTACTGGAAC; R: TTCTGGGACGGAGTCCTCATA
EFNB1	F: CGTGTTGGTCACCTGCAATAG; R: CAGGCTTCCATTGGATGTTGA
EFNB2	F: TATGCAGAACTGCGATTTCCAA; R: TGGGTATAGTACCAGTCCTTGTC
EFNB3	F: CTCGGCGAATAAGAGGTTCCA; R: GTGAAGCGGAGATCCAGGTC
GAPDH	F: GGAGCGAGATCCCTCCAAAAT; R: GGCTGTTGTCATACTTCTCATGG

qRT-PCR, quantitative real-time reverse transcription polymerase chain reaction.
F, forward primer; R, reverse primer.

Beijing, China) in a humidified cell incubator containing 5% CO_2 at 37°C. Subsequently, the mRNA levels of EFNs in each cell line were detected using real-time reverse transcription-quantitative polymerase chain reaction (RT–qPCR). The L-02 cell line served as a control.

RNA extraction and RT–qPCR

Total RNA isolation from HCC cells and tissue samples was carried out by using TRIzol Reagent (Invitrogen, Carlsbad, CA, United States) according to the product manual. Subsequently, the RNA was reverse transcribed to complementary DNA (cDNA) using EasyScript® One-Step gDNA Removal and cDNA Synthesis SuperMix (AE311-03, TransGen Biotech, Beijing, China). Then, real-time quantitative PCR (qPCR) was performed using TB Green® Premix Ex Taq™ II (RR820A, TaKaRa, China). Glyceraldehyde 3-phosphate dehydrogenase (GAPDH) was used as the endogenous control. The relative gene expression of HCC cells was calculated according to the $2^{-\Delta\Delta CT}$ method, and $2^{-\Delta CT}$ was used to determine the mRNA expression in HCC tissues. qPCR assays were performed in triplicate. The gene primers for qPCR are listed in Table 1.

Statistical analysis

R software (https://www.r-project.org/, version 4.0.4) and Perl 5.30.0 software (https://www.perl.org/) were applied to conduct bioinformatics analyses. Student's t test, one-way ANOVA, or the Wilcoxon rank sum test was used to assess the differences between groups. The log-rank test and Cox regression analysis were used for survival analysis. Spearman correlation was used in the correlation analyses. The differential gene expression in HCC cells or tissue samples was analyzed with Student's t test or one-way ANOVA using GraphPad Prism 9.0 software (GraphPad Prism Software, Inc., La Jolla, CA, United States). All experiments were repeated in triplicate to calculate the mean ± standard deviation (SD). All statistical tests were two-sided, and statistical significance was set at $p < 0.05$.

Results

Ephrin family ligands are aberrantly expressed in pan-cancer

Based on the expression analysis of eight ephrin ligand genes (EFNA1, EFNA2, EFNA3, EFNA4, EFNA5, EFNB1, EFNB2, EFNB3) in 15,521 samples of 31 cancer types from TCGA and GTEx datasets, we found that EFNA1 expression was upregulated in 21 cancer types, including GBM, LGG, UCEC, BRCA, CESC, LUAD, ESCA, STES, COAD, PRAD, STAD, HNSC, KIRC, LIHC, BLCA, OV, PAAD, TGCT, ALL, LAML, and CHOL. In contrast, EFNA1 expression was downregulated in LUSC, WT, SKCM, THCA, and KICH (Supplementary Figure S1A). The mRNA expression of EFNA2 in tumor tissues of GBM, LGG, UCEC, BRCA, CESC, LUAD, ESCA, STES, KIRP, COAD, PRAD, STAD, KIRC, LUSC, WT, SKCM, BLCA, THCA, OV, PAAD, TGCT, UCS, ALL, LAML, PCPG, and ACC was higher than that in corresponding normal tissues. Significant downregulation of EFNA2 was observed in LIHC, READ, and KICH (Supplementary Figure S1B). EFNA3 was upregulated in most cancer types, except for GBM, SKCM, and KICH (Supplementary Figure S1C). The expression level of EFNA4 was higher in 27 tumor tissues than in corresponding normal tissues, including GBM, LGG, UCEC, BRCA, CESC, LUAD, ESCA, STES, KIRP, COAD, PRAD, STAD, HNSC, LUSC, LIHC, WT, BLCA, THCA, READ, OV, PAAD, TGCT, UCS, ALL, LAML, ACC, and CHOL (Supplementary Figure S1D). EFNA5 gene expression was found to be upregulated in 13 tumor tissues but downregulated in 15 cancer types (Supplementary Figure S1E). EFNB1 was significantly distinctly expressed in 26 cancer types, with higher expression

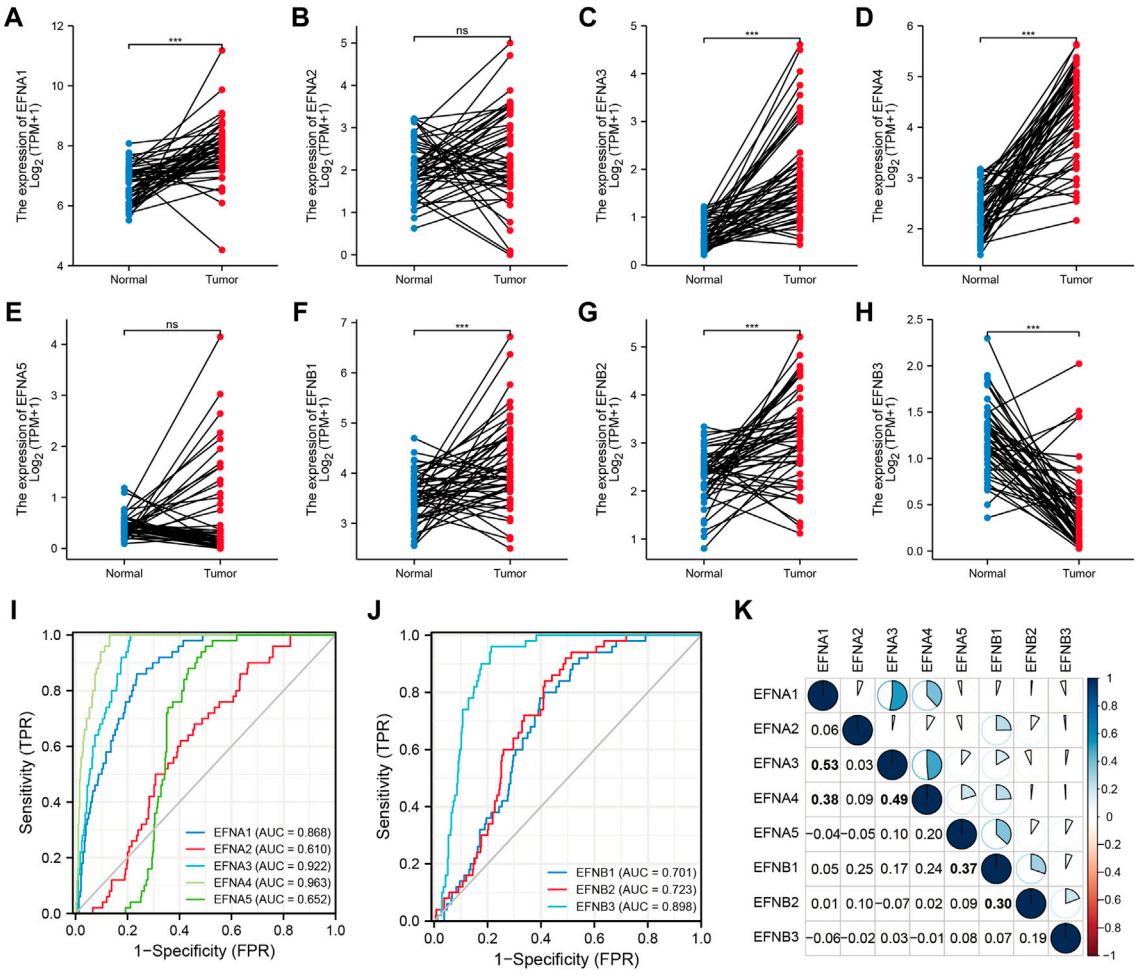

FIGURE 1
The expression levels and diagnostic significance of ephrin members in HCC tissues based on TCGA database. **(A–H)** The differential expression of EFNs (EFNA1, EFNA2, EFNA3, EFNA4, EFNA5, EFNB1, EFNB2, EFNB3) in tumor tissues compared with paired normal tissues in HCC. ns: no significance; ***$p < 0.001$; **(I,J)** The diagnostic role of EFNs identified by receiver operating characteristic (ROC) curves. **(K)** Correlation analysis of each EFN member based on Pearson's correlation analysis. The bold values represent significant correlations between the EFN members.

in cancer tissues observed in GBM, LGG, CESC, ESCA, STES, COAD, STAD, HNSC, LIHC, WT, OV, PAAD, UCS, ALL, LAML, and CHOL and lower expression observed in UCEC, BRCA, LUAD, KIRP, PRAD, KIRC, SKCM, THCA, PCPG, and KICH (Supplementary Figure S1F). EFNB2 was aberrantly expressed in 26 cancer types (Supplementary Figure S1G). The expression of EFNB3 was downregulated in multiple cancer types, including LIHC (Supplementary Figure S1H).

The expression levels and diagnostic significance of ephrin family genes in HCC

Based on the TCGA datasets related to HCC, the mRNA expression levels of EFNs were detected in 50 paired tumor tissues and corresponding normal samples. As shown in Figures 1A–H, the expression of EFNA1, EFNA3, EFNA4, EFNB1, and EFNB2 was significantly increased in tumor tissues compared with normal tissues. EFNB3 expression was evidently decreased in tumor tissues, and no significant difference was observed in EFNA2 and EFNA5 expression between tumor and normal tissues. The differential expression results in paired HCC tissues of EFNA1, EFNA3, EFNA4, EFNB1, EFNB2, and EFNB3 coincided with the above pan-cancer analysis.

According to the expression levels of ephrin genes, we further evaluated the diagnostic accuracy of EFNs by calculating the AUC values of ROC curves. The results indicated that EFNA3 (AUC = 0.922) and EFNA4 (AUC = 0.963) showed higher diagnostic accuracy; EFNB1 (AUC = 0.701), EFNB2 (AUC = 0.723), and EFNB3 (AUC = 0.898) exhibited moderate diagnostic

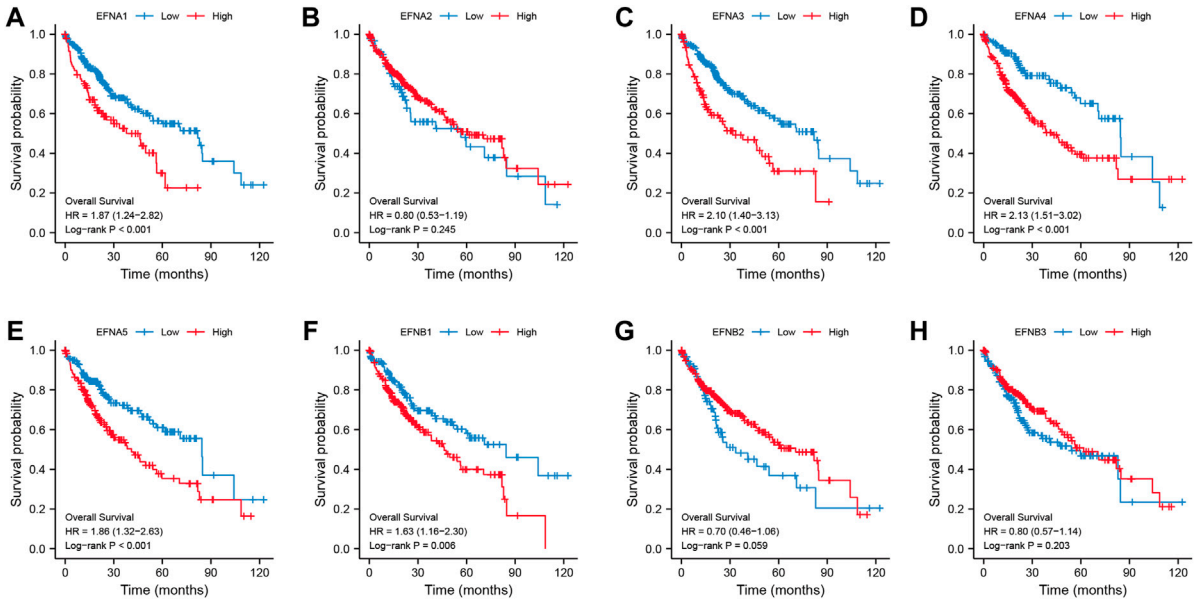

FIGURE 2
Correlation of ephrin genes expression with overall survival (OS) in patients with HCC based on Kaplan-Meier analysis **(A–H)**.

performance; and EFNA2 and EFNA5 exhibited a lower level of diagnostic accuracy, with an AUC <0.7 (Figures 1I,J).

Moreover, we also investigated the co-expression correlation among the eight ephrin genes using Pearson's correlation analysis. The results (Figure 1K) showed that the expression of EFNA1 was positively correlated with EFNA3 (R = 0.53) and EFNA4 (R = 0.38); EFNA3 showed a positive correlation with EFNA4 (R = 0.49); EFNA5 expression was positively associated with EFNB1 (R = 0.37); and EFNB1 was related to EFNB2 expression (R = 0.3). However, the expression of EFNA2 and EFNB3 was not significantly associated with other ephrin genes.

The association of ephrin genes with prognosis and clinical characteristics in HCC

We found that ephrin family genes were differentially expressed in patients with HCC. To further explore the prognostic influence of the eight EFNs on OS, PFI, and DSS in HCC patients, the Kaplan-Meier method and log-rank test were performed in patients with HCC. For OS (Figure 2), the results suggested that the patients in the high-expression groups of EFNA1 ($p < 0.001$), EFNA3 ($p < 0.001$), EFNA4 ($p < 0.001$), EFNA5 ($p < 0.001$), and EFNB1 ($p = 0.006$) showed worse OS than those in the low-expression groups, while there was no significant correlation between the expression of EFNA2, EFNB2, EFNB3 and OS. We next explored the effect of ephrin genes on PFI. As shown in Supplementary Figure S2A, higher EFNA3 and EFNA4 expression was related to shorter PFI ($p = 0.006$ and $p = 0.008$, respectively), while the opposite result was observed for EFNA2 ($p = 0.047$) and EFNB3 ($p = 0.007$); the expression of EFNA1, EFNA5, EFNB1, and EFNB2 was not significantly associated with PFI. The DSS results of Kaplan-Meier analysis indicated that the expression of EFNA1 ($p = 0.002$), EFNA3 ($p = 0.001$), EFNA4 ($p = 0.001$), EFNA5 ($p = 0.027$), and EFNB1 ($p = 0.004$) was negatively correlated with DSS in patients with HCC (Supplementary Figure S2B). Subsequently, univariate and multivariate Cox regression analyses were performed to identify the prognostic factors for OS by integrating the EFN expression and clinical factors (age, sex, histological grade, and pathological stage). Univariate Cox analysis suggested that the expression of EFNA3, EFNA4, and EFNB1 and pathological stage were risk factors for OS ($p < 0.05$; Figure 3A). Remarkably, these factors were proven to be independent prognostic factors for OS in HCC based on multifactor Cox regression analysis (Figures 3B–D). In brief, these results showed that EFNA3, EFNA4, and EFNB1 could serve as effective prognostic predictors in patients with HCC. We therefore focused on EFNA3, EFNA4, and EFNB1 for our subsequent analysis.

To address how the ephrin genes affect survival outcomes, we further investigated the relationship between prognosis-related genes and clinicopathology features in HCC, including T stages, pathological stages, histological grades, and vascular invasion

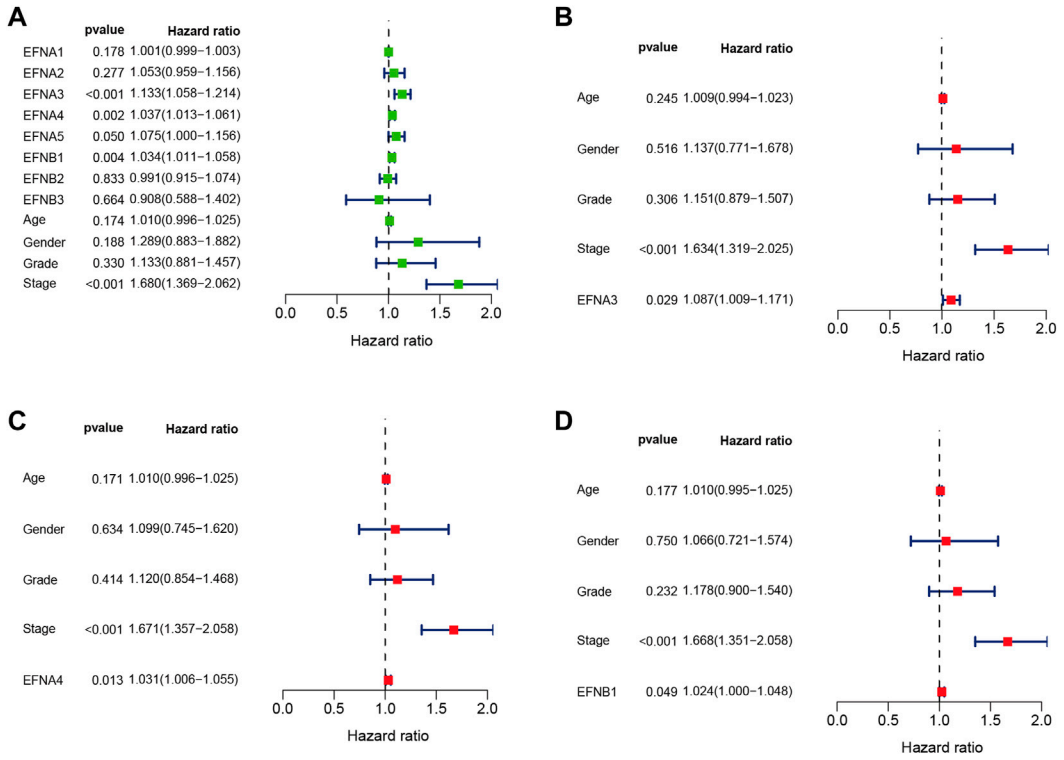

FIGURE 3
Univariate and multivariate Cox regression analyses of EFN members and clinicopathological parameters in HCC displayed with forest plots. **(A)** Univariate Cox regression analysis of EFNs and clinicopathological parameters. **(B–D)** Multivariate Cox regression analysis of ephrin members with significant prognostic significance.

status. The results indicated that patients with more advanced T stages and pathological stages tended to have higher expression levels of EFNA3 and EFNA4 (Figures 4A,B,E,F). Similarly, the expression of EFNA3 and EFNA4 was positively correlated with histological grade (Figures 4C,G). We also found that patients with vascular invasion showed higher expression of EFNA3 (Figure 4D), but no significant difference was observed in EFNA4 (Figure 4H). However, there was no significant difference in EFNB1 expression among different T stages, pathological stages, histological grades, and vascular invasion statuses (Figures 4I–L). In addition, binary logistic regression analysis was used to explore the association between EFNs expression and different clinical characteristics. As shown in Table 2, we found that the patients in the high EFNA3 expression group exhibited a higher T stage (T3&T4 vs. T2&T1, $p < 0.001$) and pathological stage (Stage III& IV vs. Stage I& II, $p < 0.001$) and vascular invasion (Yes vs. No, $p = 0.005$) than those in the low EFNA3 expression group. The patients with high EFNA4 expression were associated with a higher histological grade (G3&G4 vs. G1&G2, $p < 0.001$) and AFP levels (>400 ng/ml vs. ≤400 ng/ml, $p < 0.011$). Similarly, high expression of EFNB1 tended to correlate with higher tumor size (T3&T4 vs. T1&T2, $p = 0.034$) and advanced TNM stage (Stages III & IV vs. Stages I & II, $p = 0.028$). However, the expression of EFNA3, EFNA4, and EFNB1 showed no significant difference between age subgroups (>60 vs. ≤60), sex subgroups (male vs. female), N stages (N1 vs. N0), M stages (M1 vs. M0), and Child–Pugh grades (B&C vs. A).

Protein interactions and gene set enrichment analysis of prognosis-related ephrin genes in HCC

To explore the interactional proteins of prognosis-related ephrin genes (EFNA3, EFNA4, and EFNB1), protein–protein interaction networks were constructed by using STRING. The network diagram in Figure 5A shows the 50 proteins most correlated with EFNA3, EFNA4, and EFNB1 and their interaction network based on the STRING database. GeneMANIA is available to explore gene interactions, and the results displayed the top 20 genes with the most relevance to EFNA3, EFNA4, and EFNB1 in accordance with physical interactions, co-expression, co-location, genetic interaction, pathway, and shared protein domains (Figure 5B). We found that both in the gene and protein levels, the prognosis-related

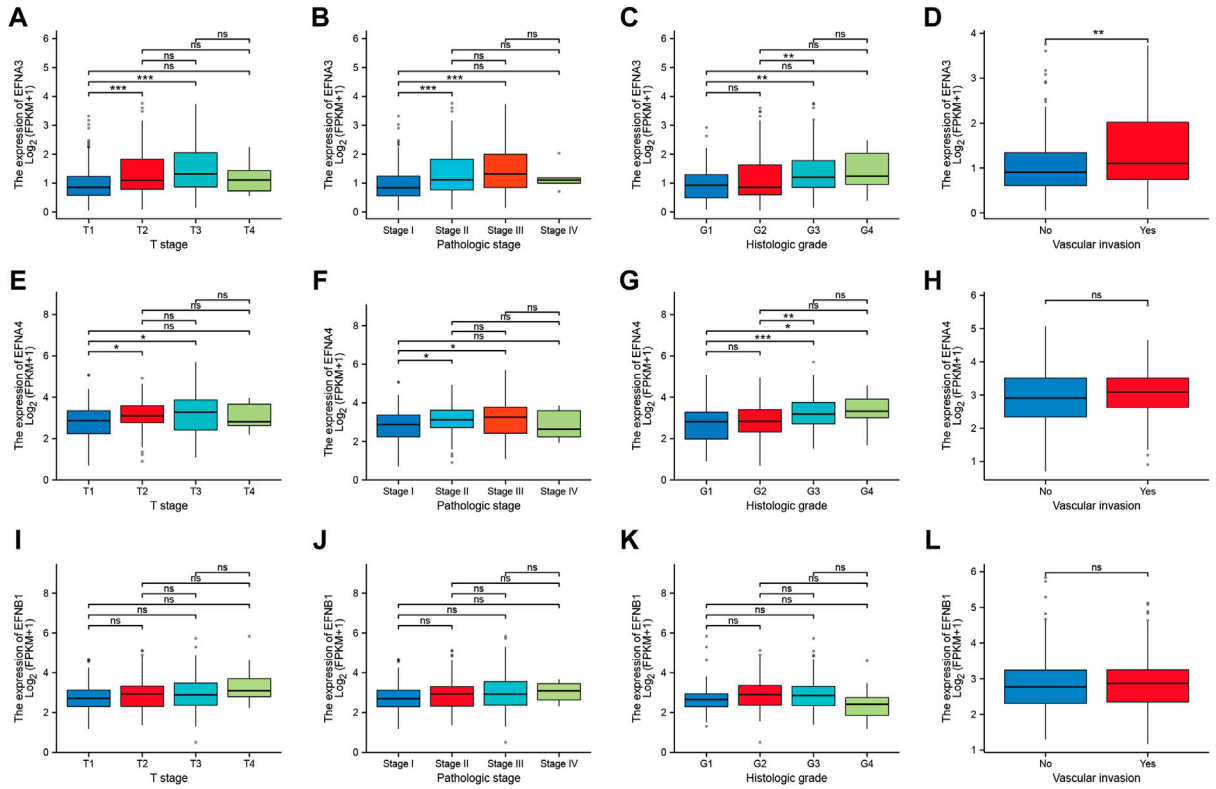

FIGURE 4
Correlation between prognosis-related ephrins and tumor stage, pathological stage, histological grade, and vascular invasion status in HCC. **(A–D)** The differential expression of EFNA3 associated with different tumor stages **(A)**, pathological stages **(B)**, histological grades **(C)**, and vascular invasion **(D)**. **(E–H)** The expression levels of EFNA4 for different tumor stages **(E)**, pathological stages **(F)**, histological grades **(G)**, and vascular invasion **(H)**. **(I–L)** The correlation between EFNB1 expression and tumor stage **(I)**, pathological stage **(J)**, histological grade **(K)**, and vascular invasion **(L)**. ns: no significance; *$p < 0.05$; **$p < 0.01$; ***$p < 0.001$.

TABLE 2 The correlation between prognosis-related ephrin genes expression and clinicopathology characteristics.

Characteristics	Total(N)	EFNA3		EFNA4		EFNB1	
		Odds ratio	*p*-value	Odds ratio	*p*-value	Odds ratio	*p*-value
Age (>60 vs. ≤ 60)	373	0.73 (0.49–1.10)	0.132	0.93 (0.62–1.39)	0.719	0.80 (0.53–1.20)	0.275
Gender (Male vs. Female)	374	0.80 (0.52–1.24)	0.320	0.93 (0.60–1.43)	0.740	0.69 (0.45–1.07)	0.098
T stage (T3&T4 vs. T1&T2)	371	2.78 (1.70–4.63)	<0.001	1.44 (0.90–2.33)	0.128	1.67 (1.04–2.71)	0.034
N stage (N1 vs. N0)	258	2.64 (0.33–53.85)	0.402	2.83 (0.36–57.36)	0.373	NA	0.994
M stage (M1 vs. M0)	272	2.58 (0.33–52.59)	0.414	0.87 (0.10–7.37)	0.894	1.14 (0.14–9.65)	0.894
Pathologic stage (Stage III & IV vs. Stage I& II)	350	2.94 (1.78–4.98)	<0.001	1.41 (0.87–2.30)	0.161	1.72 (1.06–2.82)	0.028
Histologic grade (G3&G4 vs. G1&G2)	369	2.94 (1.90–4.60)	<0.001	2.37 (1.54–3.68)	<0.001	0.96 (0.63–1.47)	0.860
Vascular invasion (Yes vs. No)	318	1.97 (1.24–3.16)	0.005	1.51 (0.95–2.41)	0.082	1.46 (0.92–2.33)	0.111
AFP (ng/ml) (>400 vs. ≤ 400)	280	1.53 (0.88–2.70)	0.137	2.10 (1.19–3.78)	0.011	0.89 (0.50–1.55)	0.674
Child-Pugh grade (B&C vs. A)	241	0.50 (0.18–1.23)	0.144	0.61 (0.24–1.48)	0.285	0.60 (0.22–1.48)	0.282

EFNs were mainly associated with Eph receptors, such as EPHA3, EPHA1, EPHA4, EPHA10, and EPHA2. Gene function prediction suggested that these genes were mostly involved in ephrin receptor activity, neuron projection guidance, protein kinase activity, axonogenesis, and peptidyl-tyrosine modification (Figure 5B).

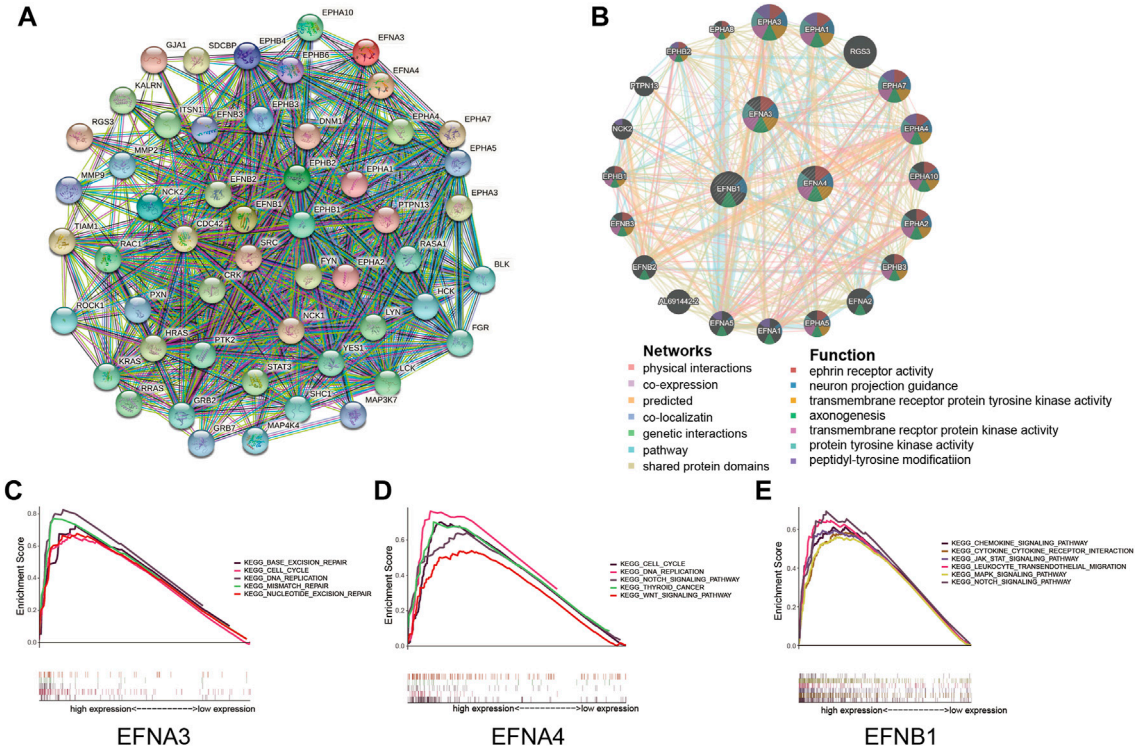

FIGURE 5
Protein interactions and gene set enrichment analysis (GSEA) of prognosis-related ephrin members (EFNA3, EFNA4, and EFNB1). **(A)** Protein–protein interactions (PPIs) based on the STRING database. **(B)** Interaction network for ephrin members based on the GeneMANIA database. **(C–E)** Gene set enrichment analysis (GSEA) of prognosis-related ephrin members, including EFNA3 **(C)**, EFNA4 **(D)**, and EFNB1 **(E)**.

Furthermore, we conducted GSEA to further investigate the potential biological mechanisms of ephrin genes in HCC. The results suggested that high expression of EFNA3 was positively related to 43 gene sets at p value < 0.05 and FDR <0.25. The most significant pathways enriched in the high EFNA3 group were "cell cycle," "DNA replication," "base excision repair," "mismatch repair," and "nucleotide excision repair" (Figure 5C). High expression of EFNA4 was distinctly positively correlated with the "cell cycle," "DNA replication," "thyroid cancer," "NOTCH signaling pathway," and "WNT signaling pathway" (Figure 5D). The GSEA results of EFNB1 showed that "JAK/STAT signaling pathway," "MAPK signaling pathway," "NOTCH signaling pathway," "chemokine signaling pathway," "chemokine and chemokine receptor interaction," and "leukocyte trans-endothelial migration" were enriched in the EFNB1 high-expression group (Figure 5E).

Ephrin family members are correlated with TME and tumor immunity in HCC

To further discuss the potential correlation between ephrin genes and the tumor immune microenvironment, we applied the ESTIMATE algorithm to calculate immune and stromal scores for each HCC sample and then analyzed the association of ephrin genes (EFNA3, EFNA4, and EFNB1) with immune scores, stromal scores, ESTIMATE scores, and tumor purity by using the Spearman correlation method. As shown in Figure 6, the expression of EFNA3 was evidently negatively related to stromal scores (R = −0.27, p = 2.1e-07) and ESTIMAT scores (R = −0.13, p = 0.0099) but positively related to tumor purity (R = 0.13, p = 0.0099) in HCC (Figures 6A–D). Analogously, EFNA4 was negatively correlated with stromal scores (R = −0.24, p = 2.4e-06) and ESTIMAT scores (R = −0.16, p = 0.0015) but positively correlated with tumor purity (R = 0.16, p = 0.0015) (Figures 6E–H). The immune scores (R = 0.31, p = 1.3e-09), stromal scores (R = 0.36, p = 1.4e-12), and ESITIMAT scores (R = 0.35, p = 4.1e-12) showed a significantly positive correlation with EFNB1 expression, while EFNB1 expression was negatively correlated with tumor purity (R = −0.35, p = 4.1e-12) in HCC (Figures 6I–L).

Moreover, the TIMER database and Spearman correlation analysis were used to explore the correlation of ephrin family genes (EFNA3, EFNA4, EFNB1) with the infiltration levels of immune cells in HCC by using TIMER algorithms. The results indicated that EFNA3 was notably positively associated with tumor purity (Rho = 0.137, p = 1.1e-02), B cells (Rho = 0.226,

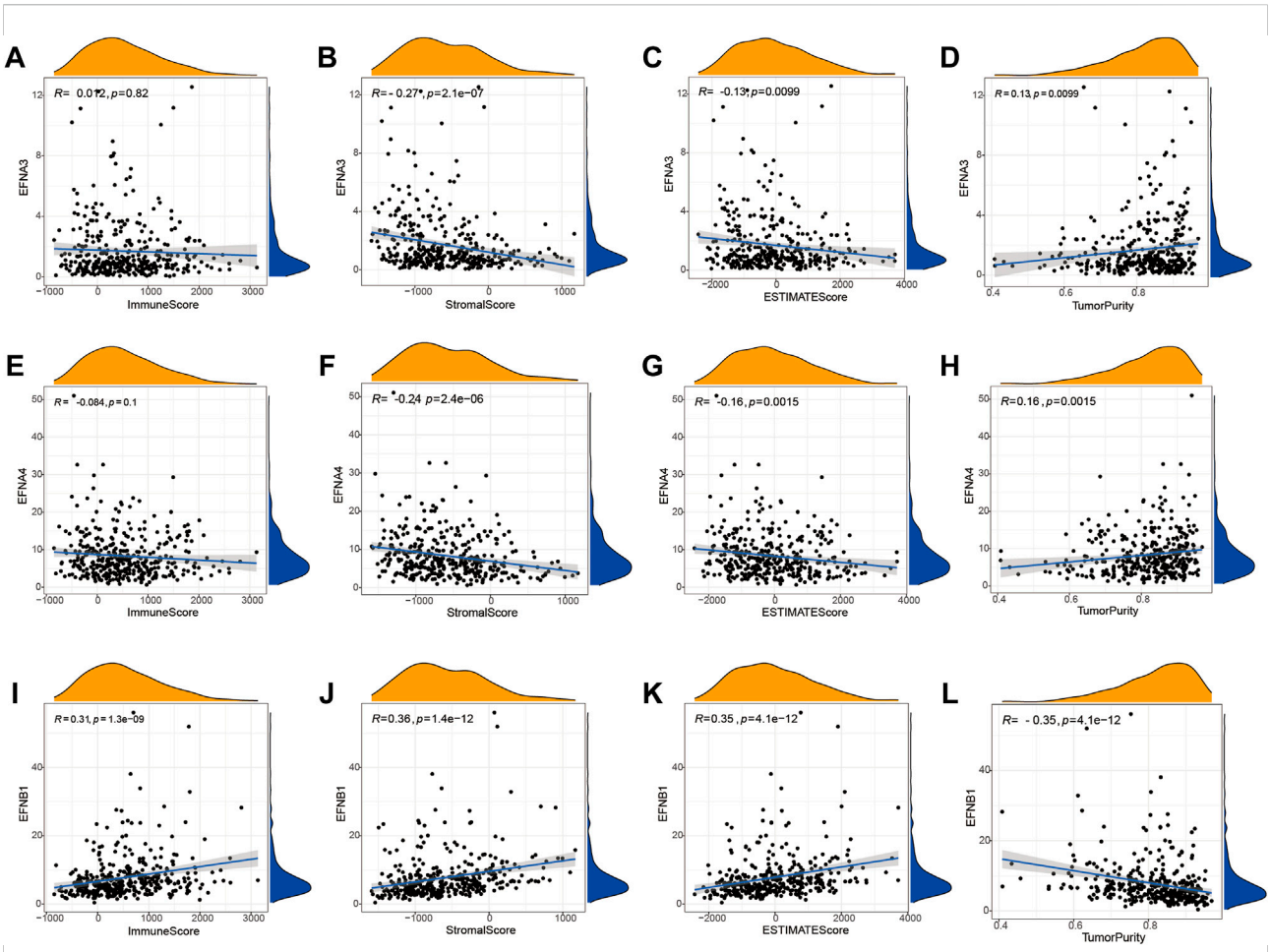

FIGURE 6
Correlation between the expression of prognostic ephrin genes and the tumor microenvironment based on the ESTIMATE algorithm. **(A–D)** The correlation between EFNA3 expression and immune/stromal/ESTIMATE/tumor purity scores. **(E–H)** The correlation between EFNA4 expression and immune/stromal/ESTIMATE/tumor purity scores. **(I–L)** The correlation between EFNB1 expression and immune/stromal/ESTIMATE/tumor purity scores. R: Spearman's rank coefficient.

p = 2.26e-05), $CD4^+$ T cells (Rho = 0.191, p = 3.55e-04), neutrophil cells (Rho = 0.202, p = 1.55e-04), macrophage cells (Rho = 0.219, p = 4.11e-05), and dendritic cells (Rho = 0.304, p = 8.24e-09) in HCC (Figure 7A). The expression of EFNA4 showed positive associations with tumor purity (Rho = 0.184, p = 5.9e-04), B cells (Rho = 0.297, p = 1.87e-08), $CD4^+$ T cells (Rho = 0.192, p = 3.25e-04), neutrophil cells (Rho = 0.334, p = 2.0e-10), macrophage cells (Rho = 0.195, p = 2.72e-04), and dendritic cells (Rho = 0.385, p = 2.59e-12) (Figure 7B). However, no correlation was observed between EFNA3/EFNA4 expression and the infiltration levels of $CD8^+$ T cells (Figures 7A,B). EFNB1 was found to have a statistically significant negative correlation with tumor purity (Rho = −0.247, p = 3.3e-06) and a positive correlation with B cells (Rho = 0.171, p = 1.45e-03), $CD4^+$ T cells (Rho = 0.334, p = 2.02e-10), $CD8^+$ T cells (Rho = 0.157, p = 3.45e-03), neutrophil cells (Rho = 0.342, p = 6.73e-11), macrophage cells (Rho = 0.433, p = 3.44e-17), and dendritic cells (Rho = 0.427, p = 9.29e-17) (Figure 7C). In addition, we applied other algorithms, such as XCELL, QUANTISEQ, MCPCOUNTER, EPIC, CIBERSORT-ABS, and CIBERSORT, to comprehensively analyze the association of prognostic ephrin genes with tumor immunity. The results showed that EFNA3 expression was evidently correlated with most immune cells, such as hematopoietic stem cells (XCELL, Rho = −0.394, p = 3.06E-15), endothelial cells (XCELL, Rho = −0.39, p = 6.36E-15), and common lymphoid progenitors (XCELL, Rho = 0.311, p = 8.53E-10) (Supplementary Figure S3; Supplementary Table S1). Similarly, there were significant associations between EFNA4 expression and various immune cells (Supplementary Figure S4; Supplementary Table S2). We also found that the expression of EFNB1 was positively related to most immune and stromal cells in HCC tissues, such as cancer-associated fibroblasts, myeloid dendritic cells, and M2 macrophages (Supplementary Figure S5; Supplementary Table S3).

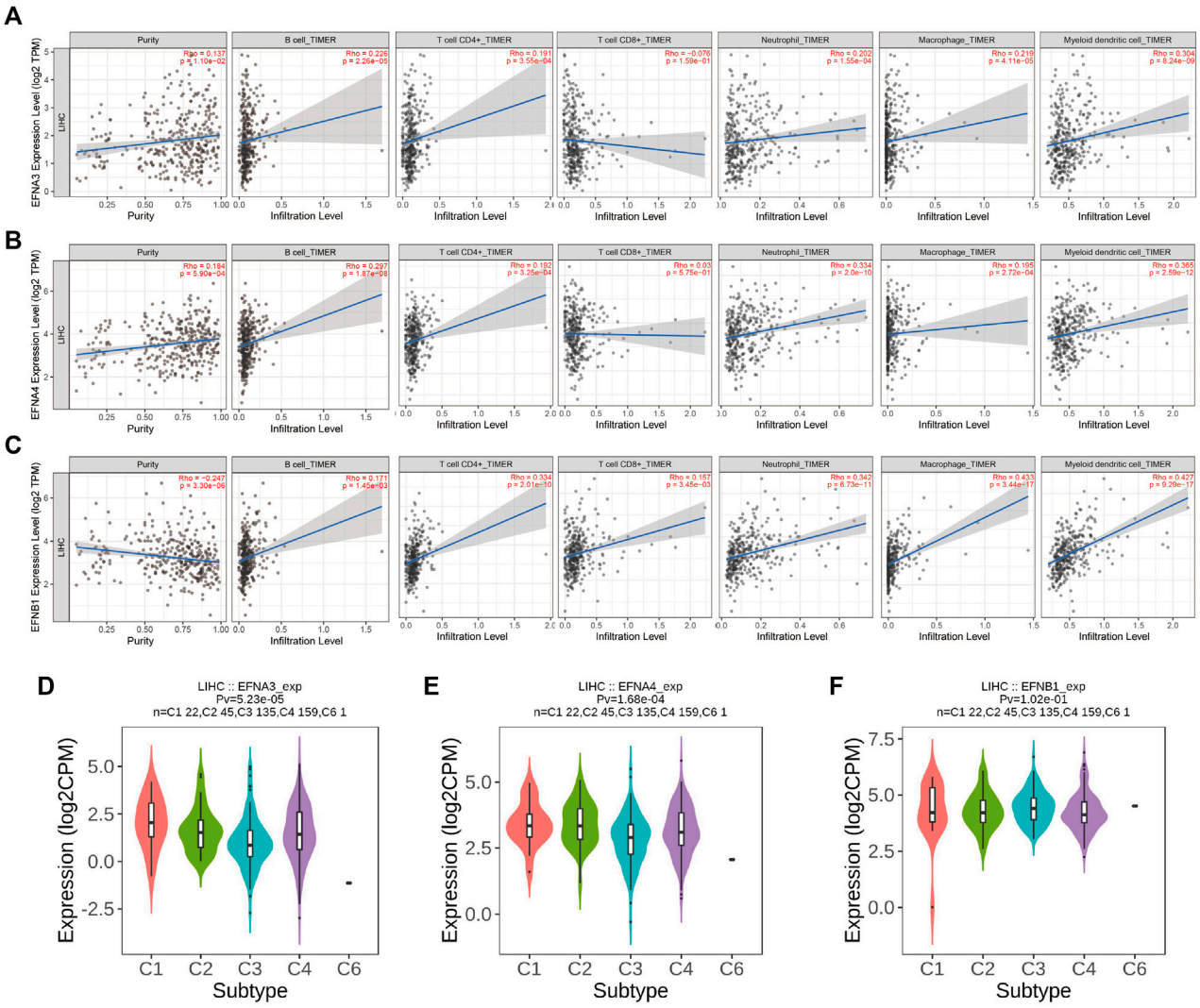

FIGURE 7
Correlation of significant prognostic ephrin genes with tumor-infiltrating immune cells and immune subtypes in HCC using TIMER algorithms. **(A)** EFNA3; **(B)** EFNA4; and **(C)** EFNB1. Tumor purity is shown in the panels on the left. **(D–F)** The correlation between prognostic ephrin genes (EFNA3, EFNA4, and EFNB1) expression and immune subtypes in HCC using TISIDB. Rho, Spearman's rank coefficient; Pv, *p* value; C1, wound healing; C2, IFN-gamma dominant; C3, inflammatory; C4, lymphocyte depleted; C5, immunologically quiet; C6, TGF-b dominant.

In addition, we further investigated the potential relevance between ephrin family genes (EFNA3, EFNA4, EFNB1) and different immune subtypes of HCC, and the results revealed that the expression of EFNA3 and EFNA4 was prominently correlated with immune subtype (p = 5.23e-05, p = 1.68e-04, respectively). EFNA3 and EFNA4 were highly expressed in the C1 subtype but expressed at low levels in the C3 subtype (Figures 7D,E). This finding indicated that EFNA3 and EFNA4 may be more involved in wound healing but less involved in inflammatory processes. However, no significant association was observed between EFNB1 expression and immune subtype (Figure 7F).

Relationship between ephrin gene expression and ICIs

It was reported that immune checkpoint-related genes, TMB, and MSI can serve as effective predictors for ICIs. Thus, we assessed the latent correlations of prognosis-related ephrin genes (EFNA3, EFNA4, EFNB1) with these ICIs biomarkers in HCC. A multigene correlation heatmap of gene co-expression analyses showed that EFNA3 expression was significantly related to 24 immune checkpoint-related genes, EFNA4 was significantly correlated with 23 immune-related genes, and there was a highly positive correlation between EFNB1 expression and immune-related

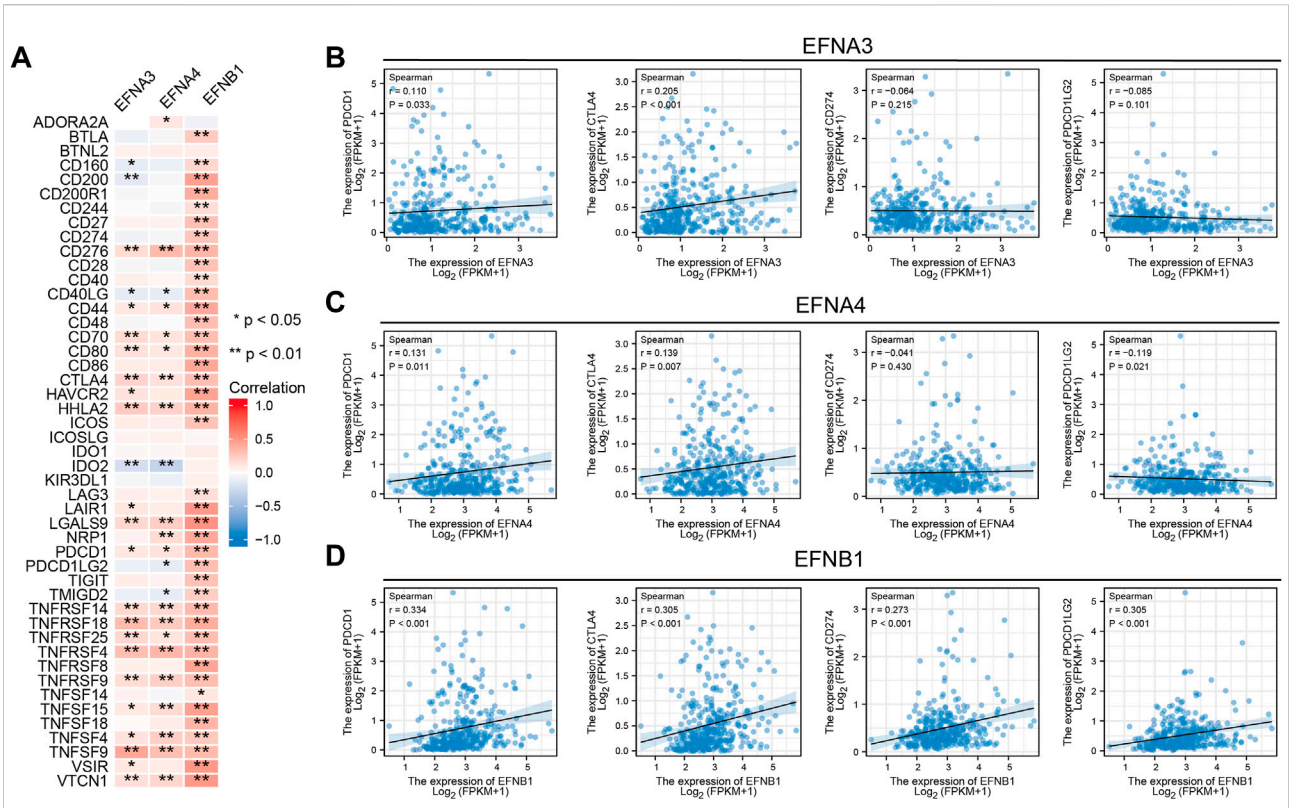

FIGURE 8
Relationship between significant prognostic ephrin members and immune checkpoint-related genes in HCC. **(A)** Heatmap displaying the coexpression relationship between prognosis-related ephrins and 47 immune checkpoint-related genes. **(B–D)** Scatterplots displaying the association of EFNA3 **(B)**, EFNA4 **(C)**, and EFNB1 **(D)** expression with four key immune checkpoint-related genes (PDCD1, CTLA4, CD274, and PDCD1LG2) with Spearman correlation analysis. r: Spearman's rank coefficient; *$p < 0.05$; **$p < 0.01$.

genes (Figure 8A). We highlighted the association between ephrin genes expression and four key immune checkpoint-related genes (PDCD1, CTLA4, CD274, and PDCD1LG2) using Spearman correlation analysis. The scatter plots showed that the expression of PDCD1 and CTLA4 was positively correlated with EFNA3 expression (r = 0.11, p = 0.033; r = 0.205, $p < 0.001$), while no association was found between EFNA3, CD274 and PDCD1LG2 (Figure 8B). EFNA4 exhibited a significant positive correlation with PDCD1 (r = 0.131, p = 0.011) and CTLA4 (r = 0.139, p = 0.007) but a negative correlation with PDCD1LG2 (r = –0.119, p = 0.021) (Figure 8C). Remarkably, EFNB1 expression was significantly positively associated with PDCD1 (r = 0.334, $p < 0.001$), CTLA4 (r = 0.305, $p < 0.001$), CD274 (r = 0.273, $p < 0.001$), and PDCD1LG2 (r = 0.305, $p < 0.001$) (Figure 8D).

Furthermore, we performed an investigation to analyze the association of ephrin genes with TMB and MSI by integrating gene expression and TMB/MSI data. We found that HCC patients with a high TMB highly expressed EFNA3 (p = 0.046) and EFNA4 (p = 0.048) (Figures 9A,B), and Spearman correlation analysis also indicated that TMB levels were positively correlated with the expression of EFNA3 (R = 0.13, p = 0.015) and EFNA4 (R = 0.15, p = 0.0039) (Figures 9D,E). However, there was no significant association between EFNB1 expression and TMB scores (Figures 9C,F). Similarly, HCC patients with high MSI exhibited higher EFNA3 (p = 0.0046) and EFNA4 (p = 0.004) expression than those with low MSI (Figures 9G,H), and the expression levels of EFNA3 (R = 0.14, p = 0.0075) and EFNA4 (R = 0.15, p = 0.003) were significantly positively related to MSI scores based on Spearman correlation analysis (Figures 9J,K). No significant relationship was observed between EFNB1 expression and MSI status (Figures 9I,L).

Ephrin genes predict the response to chemotherapy and targeted therapy in HCC

To probe the correlation between prognosis-related ephrin genes (EFNA3, EFNA4, and EFNB1) and drug sensitivity to chemotherapy and targeted therapy, we compared the

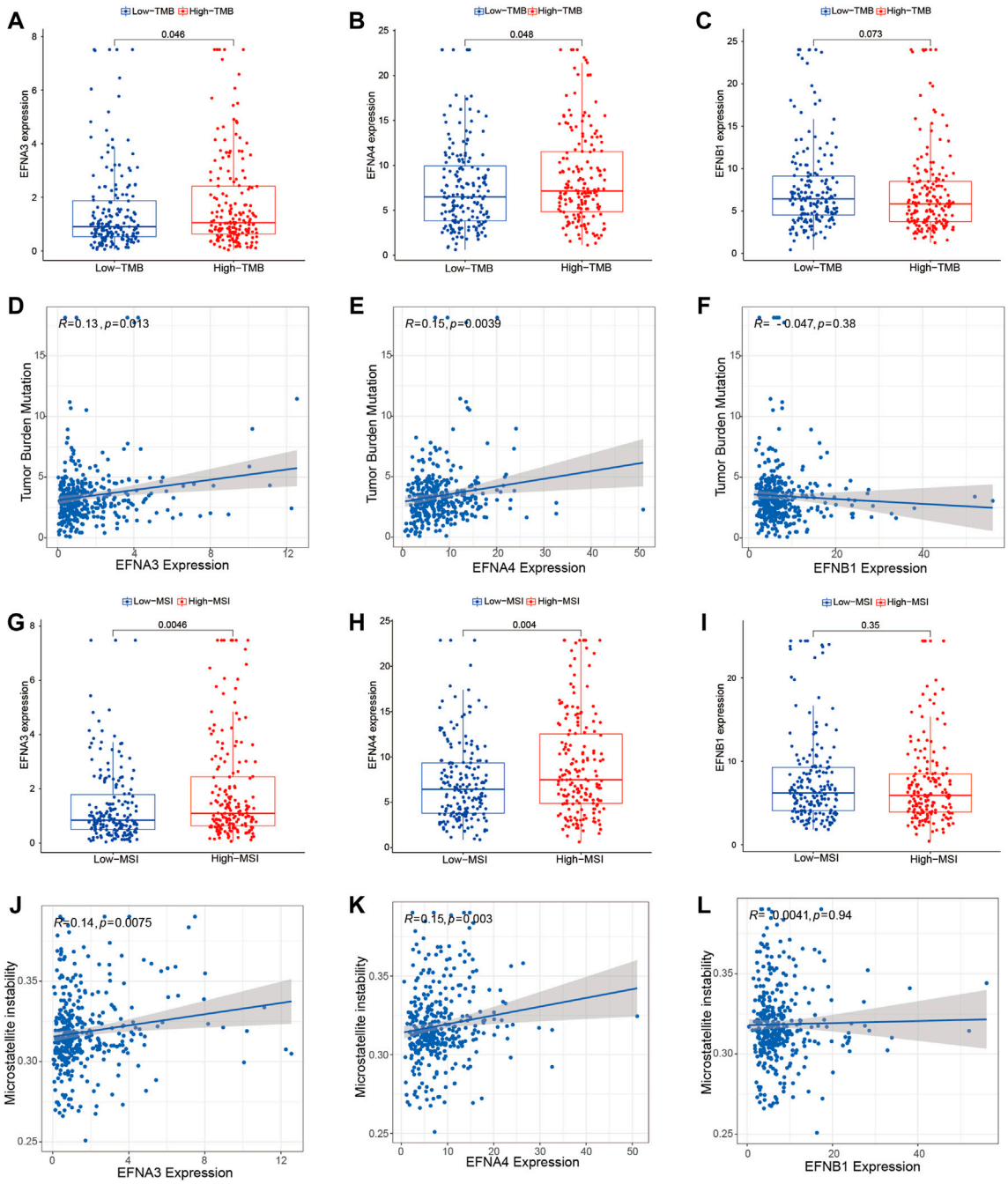

FIGURE 9
Association of prognosis-related ephrins with tumor mutation burden (TMB) and microsatellite instability (MSI) in HCC. **(A–C)** The differential expression of EFNA3, EFNA4, and EFNB1 in the low- and high-TMB groups. **(D–F)** Scatterplots displaying the association between TMB scores and EFNA3 expression **(D)**, EFNA4 expression **(E)**, and EFNB1 expression **(F)**. **(G–I)** The differential expression of EFNA3, EFNA4, and EFNB1 in the low- and high-MSI groups. **(J–L)** Scatterplots displaying the association between MSI scores and EFNA3 expression **(J)**, EFNA4 expression **(K)**, and EFNB1 expression **(L)**. r: Spearman's rank coefficient.

IC50 values of six commonly used drugs (camptothecin, cisplatin, gemcitabine, doxorubicin, mitomycin C, and sorafenib) in the high- and low-EFNs expression subgroups using pRRophetic algorithm. As shown in Figures 10A–R, a lower IC50 of cisplatin (p = 0.0092), doxorubicin (p = 0.0025), gemcitabine (p = 3.1e-11), and mitomycin C (p = 1.4e-10) was present in the high EFNA3 expression group compared with the low expression group, indicating that HCC patients with high

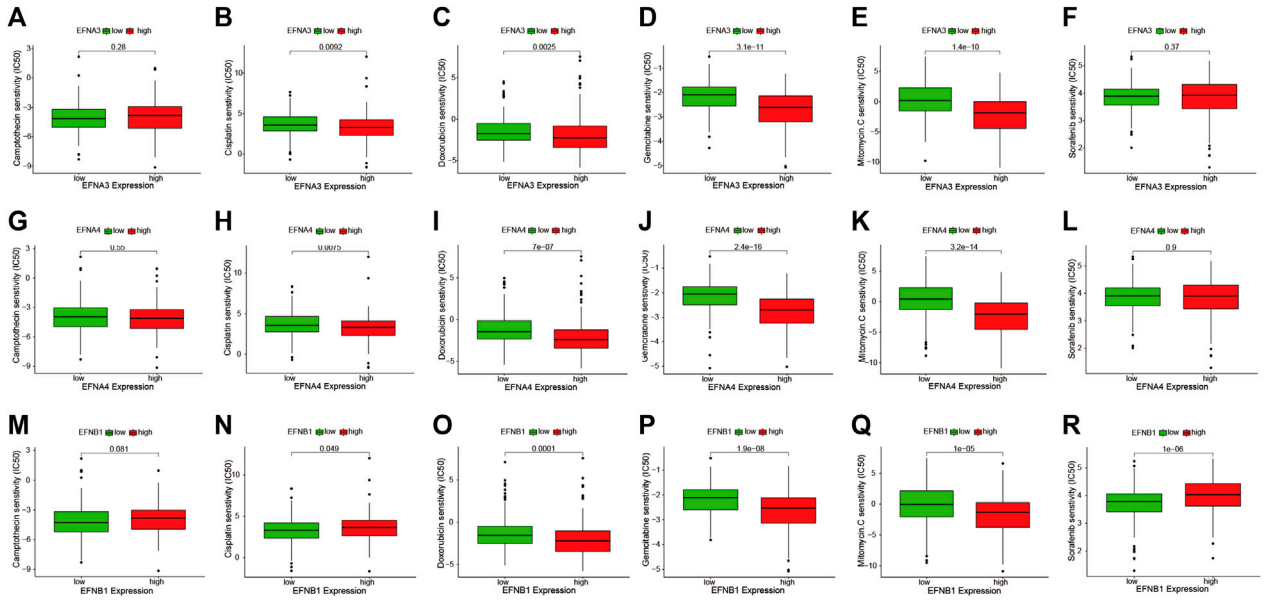

FIGURE 10
The IC50 values of six commonly used drugs (camptothecin, cisplatin, doxorubicin, gemcitabine, mitomycin C, and sorafenib) were compared between high- and low-expression subgroups of prognostic ephrin genes in HCC. **(A–F)** EFNA3, **(G–L)** EFNA4, and **(M–R)** EFNB1.

EFNA3 expression appeared to be more susceptible to these drugs. However, no significant difference was observed between camptothecin and sorafenib (Figures 10A–F). The expression of EFNA4 was also significantly related to the IC50 of cisplatin (p = 0.0075), doxorubicin (p = 7e-07), gemcitabine (p = 2.4e-16), and mitomycin C (p = 3.2e-14), showing that the high-expression populations were more sensitive to these drugs, but the IC50 of camptothecin and sorafenib was not evidently different in the high- and low-expression groups (Figures 10G–L). Regarding the correlation between EFNB1 and drug sensitivity, we found that HCC patients with high EFNB1 expression exhibited a better drug response to doxorubicin (p = 0.0001), gemcitabine (p = 1.91e-8), and mitomycin C (p = 1e-05) than those with low EFNB1 expression, while the opposite results were discovered for cisplatin (p = 0.049) and sorafenib (p = 1e-06) (Figures 10M–R). In brief, the results indicated that EFNs expression may contribute to evaluating the response to chemotherapy and targeted therapy in patients with HCC. Regrettably, the IC50 of immune checkpoint inhibitors is currently not available in GDC cell lines, thus we could not predict the response to ICIs by using "pRRophetic" R package.

Correlation between ephrin gene expression and gene mutational landscape

In the HCC project of TCGA database, a total of 369 samples were included for detecting genetic mutations. Then, we integrated the gene expression and mutation data and further compared gene mutational frequency in high- and low-expression groups of ephrin genes (EFNA3, EFNA4, and EFNB1). The results are highlighted in Supplementary Figure S6. The top 15 genes with the highest mutational frequency are presented in the Waterfall plots. The mutational frequency of the 15 genes showed significant differences in the high- and low-expression groups of EFNA3, including TP53 (p = 8.6e-04), ABCA13 (p = 5.4e-04), RB1 (p = 0.04), DCHS2 (p = 0.03), HELZ (p = 0.04), DOCK10 (p = 0.04), MICAL3 (p = 0.02), COL3A1 (p = 0.02), ITGAD (p = 0.02), DENND4A (p = 0.02), CHSY3 (p = 0.04), ADGRB1 (p = 0.04), FAM65B (p = 0.04), BNC2 (p = 0.04), and FAM205A (p = 0.04) (Supplementary Figure S6A). With regard to EFNA4, we found that gene mutations were more common in the high expression group compared with the low expression group, such as TP53 (p = 8.6e-04), CTNNB1 (p = 5.3e-03), MUC4 (p = 0.04), RYR2 (p = 0.02), HMCN1 (p = 0.04), PREX2 (p = 0.03), MUC5B (p = 0.01), TDRD5 (p = 8.7e-03), SVEP1 (p = 0.04), ROBO1 (p = 0.03), EP300 (p = 0.04), and ARFGEF3 (p = 0.02), while higher mutation of IL6ST, DMBT1, and DOCK8 was observed in low EFNA4 expression group (Supplementary Figure S6B). The association between EFNB1 expression and the gene mutational landscape indicated that the mutational frequency of the ten mutated genes was higher in the high EFNB1 expression group, while the other five gene mutations occurred more commonly in the low expression group (Supplementary Figure S6C). In brief, it can be concluded that high expression of EFNA3, EFNA4, and EFNB1 may be relevant to more gene mutations and, thus, drive oncogenesis and tumor progression of HCC.

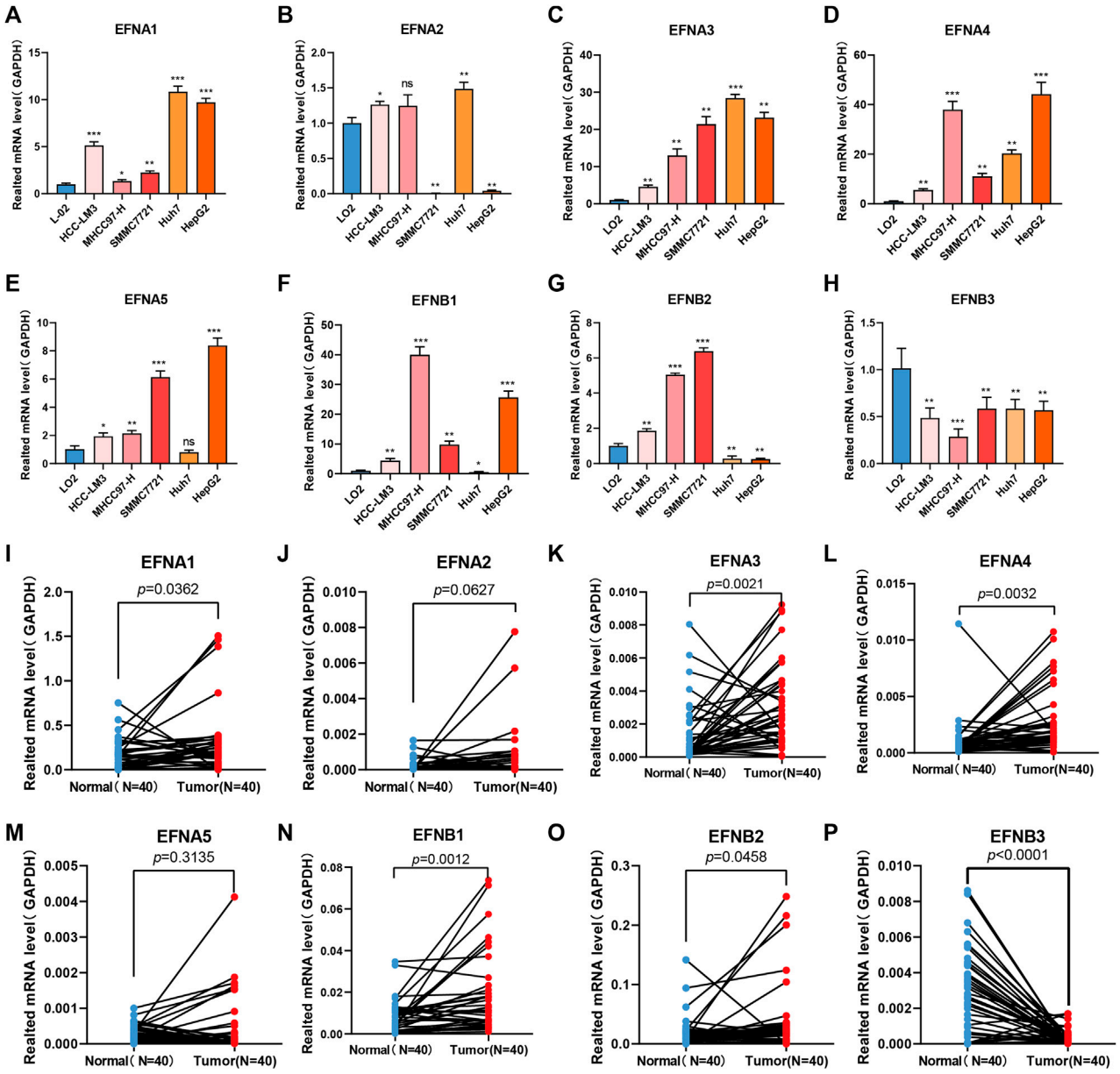

FIGURE 11
Ephrin family genes are abnormally expressed in HCC cell lines and HCC tissues. **(A–H)** RT–qPCR analysis of the mRNA expression of ephrin genes in five HCC cell lines (HCC-LM3, MHCC97-H, SMMC 7721, Huh-7, and HepG2) and a normal liver cell line (LO2). EFNA1 **(A)**, EFNA2 **(B)**, EFNA3 **(C)**, EFNA4 **(D)**, EFNA5 **(E)**, EFNB1 **(F)**, EFNB2 **(G)**, and EFNB3 **(H)**. **(I–P)** The mRNA expression of ephrin genes in 40 pairs of HCC tissues and adjacent para-carcinoma tissues was evaluated using qPCR. EFNA1 **(I)**, EFNA1 **(I)**, EFNA2 **(J)**, EFNA3 **(K)**, EFNA4 **(L)**, EFNA5 **(M)**, EFNB1 **(N)**, EFNB2 **(O)**, and EFNB3 **(P)**. GAPDH was used as an internal control. Error bars represent the means ± SEM (triplicate experiments). *$p < 0.05$; **$p < 0.01$; ***$p < 0.001$.

Expression levels of ephrin genes in HCC cells and clinical tissues were identified by qPCR

In the above bioinformatics analysis based on the TCGA dataset, we found that some ephrin genes (EFNA1, EFNA3, EFNA4, EFNB1, EFNB2) were significantly upregulated in HCC tissues, and EFNB3 was downregulated in HCC tissues, while EFNA2 and EFNA5 showed no significant differences between cancer tissues and adjacent normal tissues. To validate the results of the bioinformatics analysis, RT-qPCR was applied to detect mRNA expression in five HCC cell lines

(HCC-LM3, MHCC97-H, SMMC 7721, Huh-7, and HepG2) and 40 paired HCC tissues. The results suggested that the mRNA expression of EFNA1, EFNA3 and EFNA4 was evidently higher in five HCC cell lines (HCC-LM3, MHCC97-H, SMMC 7721, Huh-7, and HepG2) ($p < 0.05$) (Figures 11A,C,D) and tumor tissues ($p = 0.0362$, $p = 0.0021$ and $p = 0.0032$, respectively) (Figures 11I,K,L) than in a normal liver cell line (L-02) and paired para-cancerous tissues. EFNA2 and EFNA5 were highly expressed in certain cell lines (Figures 11B,E) and showed no significant differences between cancer tissues and adjacent normal tissues (Figures 11J,M). The expression of EFNB1 was significantly increased in HCC-LM3, MHCC97-H, SMMC 7721, and HepG2 cells compared with the normal liver cell line (L-02), while EFNB1 expression was decreased in Huh-7 cells compared with the L-02 control ($p < 0.05$) (Figure 11F). Similarly, EFNB1 expression was significantly higher in cancer tissues than in paired adjacent normal tissues ($p = 0.0012$) (Figure 11N). The expression of EFNB2 was obviously higher in HCC cell lines (HCC-LM3, MHCC 97-H, SMMC 7721) but lower in Huh7 and HepG2 compared to the expression in normal liver cell line (L-02) (Figure 11G). Moreover, EFNB2 had a higher expression level in cancer tissues than in para-carcinoma tissues ($p = 0.0458$) (Figure 11O). In addition, the level of EFNB3 in the HCC cells and cancerous tissues was significantly reduced compared with the normal liver cell line L-02 ($p<0.05$) (Figure 11H) and the para-carcinoma tissues ($p < 0.0001$) (Figure 11P). These experimental results were consistent with those of the bioinformatics analysis.

Discussion

The Eph/ephrin bidirectional signaling system is composed of a family of tyrosine kinase receptors and their plasma membrane-bound ligands (ephrins), which act as vital regulators for a variety of physiological and biological activities, such as axon guidance, cell–cell interactions, cell migration, and angiogenesis. Recently, an increasing number of studies have focused on its role in tumorigenesis and metastatic potential as related to tumor growth and survival. Aberrant ephrin expression is closely correlated with tumorigenicity, tumor vasculature, invasion, and metastasis in many types of human cancers, including HCC (McCarron et al., 2010). Thus, our study emphasized exploring the expression pattern, prognostic value and potential function of ephrin family genes in HCC, which may play a crucial role in the discovery of novel inhibition targets and therapeutic strategies for patients with HCC.

The ephrin ligands are aberrantly expressed in a variety of tumors and have been implicated in tumor progression, malignancy, and prognosis (Ieguchi and Maru, 2019). In HCC, for example, the expression level of EFNA1 is positively related to microscopic portal invasion after curative resection (Wada et al., 2014). EFNA2 was significantly upregulated in HCC cell lines and tissue samples, and its overexpression was associated with more aggressive tumor behaviors (Feng et al., 2010). EFNA3 was upregulated in HCC tissues, and its overexpression was associated with more aggressive tumor behaviors (Husain et al., 2022). EFNA4 is highly expressed and leads to poor prognosis in patients with HCC (Lin et al., 2021). The expression of EFNB1 is significantly higher in HCC tissues than in nontumor tissues and contributes to tumor progression *in vivo* by promoting neovascularization in HCC (Sawai et al., 2003). Although ephrin family genes have been extensively studied, the role of ephrins in cancers is not yet understood, as some tumors present with elevated levels of ephrin expression, while others demonstrate decreased expression (McCarron et al., 2010). In our study, the expression levels of ephrin members were comprehensively analyzed in 31 human cancer types based on TCGA and GTEx datasets. We found that the expression of EFNA1, EFNA2, EFNA3, EFNA4, EFNB1, and EFNB2 was upregulated in the tumor tissues of most cancers compared with corresponding normal tissues. EFNA5 and EFNB1 showed low expression in most cancers. In addition, this study focused on investigating the expression levels of ephrin genes and their relationship to prognosis in HCC. We found that the expression of EFNA1, EFNA3, EFNA4, EFNB1, and EFNB2 was significantly higher in HCC tissues than in paired normal tissues, and higher expression of EFNA1, EFNA3, EFNA4, EFNA5, and EFNB1 was associated with worse overall survival in patients with HCC. Whereas EFNB3 showed low expression in cancerous tissues, EFNA2 and EFNA5 expression showed no evident difference between tumor and normal tissues. Moreover, we have validated this differential expression results of bioinformatic analysis *via* performing RT-qPCR in HCC cell lines and clinical tissue samples. Besides, all the ephrin genes except EFNA2 and EFNA5 presented high disease diagnostic performance for HCC, with AUC>0.7. Cox regression analysis indicated that EFNA3, EFNA4, and EFNB1 were independent prognostic factors for OS and were defined as prognosis-related ephrin genes. We also discovered a significant correlation between the expression of EFNA3, EFNA4, and EFNB1 and T stage, pathological stage, histological grade, and vascular invasion. In short, these findings suggest that some ephrin genes (EFNA3, EFNA4, and EFNB1) are closely related to malignant biological behavior, such as tumor growth, vascular invasion and distant metastasis, and, thus, could be used as promising diagnostic and prognostic biomarkers in patients with HCC.

It has been reported that ephrins are abnormally expressed in multiple tumors and implicated in tumor development and metastasis, but their specific mechanism is still unclear. In this study, we focused on analyzing the protein–protein correlation and potential biological mechanisms of prognostic ephrin genes (EFNA3, EFNA4,

and EFNB1) in HCC. The PPI network indicated that the three ephrins were mainly associated with Eph receptors and participated in ephrin receptor activity, protein kinase activity, neuron projection guidance, axonogenesis, and peptidyl-tyrosine modification, which was consistent with the results reported in previous work (McCarron et al., 2010). Furthermore, the potential biological mechanisms of EFNA3, EFNA4, and EFNB1 in HCC exhibit large variation based on GSEA. High EFNA3 expression was mainly involved in the following pathways: "cell cycle," "DNA replication," "base excision repair," "mismatch repair," and "nucleotide excision repair." EFNA4 may affect tumor progression by changing pathways such as the "cell cycle," "DNA replication," "thyroid cancer," "NOTCH signaling pathway," and "WNT signaling pathway." EFNB1 mainly participates in cancer-related pathways, such as the "JAK/STAT signaling pathway," "MAPK signaling pathway," and "NOTCH signaling pathway," as well as immune regulation processes, including the "chemokine signaling pathway," "chemokine and chemokine receptor interaction," and "leukocyte transendothelial migration." A previous study reported that suppression of EFNA3 expression promotes cell proliferation, migration, and invasion and regulates EMT in oral squamous cell carcinoma via the PI3K/AKT signaling pathway (Wang et al., 2020). In contrast, EFNA3 contributes to tumor cell self-renewal, proliferation and migration in HCC under hypoxia via SREBP1/ACLY-mediated metabolic rewiring in HCC (Husain et al., 2022). EFNA4 influences the proliferation and migration of HCC cells by promoting EphA2 phosphorylation at Ser897, activating the PIK3R2/GSK3β/β-catenin signaling pathway loop (Lin et al., 2021). A novel anti-EFNA4 drug (PF-06647263) binds specifically to EFNA4-expressing cells and subsequently induces DNA cleavage and apoptosis/cell death in triple-negative breast and ovarian tumors (Damelin et al., 2015; Garrido-Laguna et al., 2019). In general, during the process of tumor progression, ephrins may play critical roles through different mechanisms, which can vary among different genes or cancer types. Therefore, further experiments are needed to elucidate the specific molecular mechanisms of prognosis-related ehprins in HCC.

The tumor microenvironment has crucial roles in the development and progression of HCC, and distinct immune features, such as inflamed and noninflamed classes of HCC, and different genomic signatures are correlated with the immune therapy response (Llovet et al., 2022). Emerging evidence indicates that the Eph/ephrin signaling system plays a pivotal role in remodeling the tumor microenvironment and regulating immune cell infiltration (Janes et al., 2021). Unique microenvironments caused by cancer cells in turn induce the abnormal expression of the Eph/ephrin complex (Iwasaki et al., 2018; Husain et al., 2022). For example, EFNB1, which is widely expressed on T cells, B cells, and monocytes/macrophages, has been proven to mediate various immune events, such as lymphocyte activation and adhesion, T-cell differentiation and survival, regulation of acquired immune responses, and cytokine production (Yu et al., 2004; Luo et al., 2011). EFNB1 and two Eph receptors (EPHB6 and EPHB4) collaborate to repulsively control follicular T-helper cell retention in the germinal center and promote interleukin 21 (IL-21) production by T cells locally (Lu et al., 2017). All previous studies are consistent with the results of functional enrichment analysis in our study showing that EFNB1 is closely involved in immune regulation. However, the function of other EFNs in the tumor immune response is limited. In our study, we systematically analyzed the correlation between EFNs expression and TME scores, tumor immune cell infiltration, and immune subtypes using different immune algorithms. Our results suggest that EFNA3 and EFNA4 were negatively related to stromal and ESTIMATE scores but positively associated with tumor purity in HCC, which is consistent with the results obtained by Deng et al. (2021) in lung adenocarcinoma that EFNA3 is negatively associated with immunity and stromal infiltration. Moreover, EFNA3 and EFNA4 were positively associated with immune cell infiltration of B cells, $CD4^+$ T cells, neutrophils, macrophages, and DCs but were not related to $CD8^+$ T cells. We also discovered that EFNB1 was positively correlated with immune, stromal, and ESTIMATE scores but negatively correlated with tumor purity. Furthermore, we found a significant positive association between EFNB1 and different immune response cells toward cancer, such as B cells, $CD4^+$ T cells, $CD8^+$ T cells, neutrophils, macrophages, and DCs. These findings revealed that high expression of EFNA3, EFNA4, and EFNB1 in HCC tissues is not only related to tumor progression and poor prognosis but also promotes immune cell infiltration, which may improve antitumor immune responses.

In the past decade, antitumor responses have achieved unprecedented rates of long-lasting tumor responses in patients with a variety of cancers, including HCC, which can be realized by antibodies blocking the CTLA-4 or PD-1 pathway, either alone or in combination (Ribas and Wolchok, 2018). In HCC, tremelimumab plus durvalumab yields superior overall survival versus sorafenib (Kelley et al., 2021). The combination of atezolizumab and bevacizumab improves overall survival relative to sorafenib, which has already gained FDA approval for use in patients with HCC (Qin et al., 2021). Despite these major advances, more than half of HCC patients still do not respond to ICIs. Moreover, no reliable predictive biomarker of response to immunotherapy is available to guide personalized treatment and improve survival. Several potential biomarkers,

such as PD-L1 expression, TMB, and specific genomic alterations, have been proposed based on exploratory end points in HCC trials (Pinter et al., 2021). The combined PD-L1 positivity score was associated with response to pembrolizumab and PFS in patients with HCC (Zhu et al., 2018). Patients with higher MSI and TMB may be more sensitive to ICIs based on previous studies in non-small-cell lung cancer and colon cancer (Samstein et al., 2019; Schrock et al., 2019). However, TMB is generally low and MSI is rare in HCC, which may limit their utility as biomarkers to predict ICI outcomes. Based on the current evidence, the incorporation of several predictive factors, such as genetic, TMB, MSI, and microenvironmental factors, may be more likely to estimate the response to ICIs than a single biomarker. Therefore, we performed a comprehensive correlation analysis between EFNs expression and previous biomarkers of ICIs, including immune checkpoint-related genes, TMB, and MSI. The results indicated that EFNA3 and EFNA4 were significantly related to some immune-related genes, TMB, and MSI in HCC; EFNB1 was positively associated with most immune-related genes, such as PD-1, CTLA4, PD-L1, and PD-L2, but unrelated to TMB and MSI scores. These findings suggest that EFNs may be used as integrated biomarkers to predict the therapeutic efficacy of ICIs in HCC. Nevertheless, studies on immunotherapy are still far from mature, especially in the aspect of sensitivity to ICIs, and the IC50 of ICIs has not been included in GDC database, which restricted our analyses to immunotherapy sensitivity *via* EFNs genes expression.

In this study, we found the expression levels of prognosis-related ephrin genes (EFNA3, EFNA4, and EFNB1) were associated with certain drugs sensitivity to chemotherapy and targeted therapy, the patients with higher expression of EFNA3, EFNA4, and EFNB1 may be more susceptible to these drugs. However, the high EFNA3/EFNA4 expression associated with worse overall survival in patients with HCC. How to explain this discrepancy? Firstly, our study is a retrospective data based on a public database, the treatment drugs for these patients was not available in TGCA database, which means the patient with high EFNs expression and poor prognosis probably did not use sensitive drugs. Secondly, in the drugs sensitivity analysis, we used pRRophetic algorithm to compared the IC50 values of common drugs in the high- and low-EFNs expression subgroups, which was based on expression matrix and drug information of the Cancer Genome Project (CGP) cell lines. The clinical roles of this analysis may guide drugs selection and predict drugs response in certain EFNs expression populations. Furthermore, the EFNs expression is associated to other prognostic factors, such as gene mutational landscape and tumor immune microenvironment. In brief, the patient with high EFNs expression exhibiting a better response to certain drugs does not mean a better prognosis.

In summary, we conducted comprehensive analyses of ephrin family members in HCC to explore their expression patterns and prognostic values using multiple databases. We discovered that EFNA3, EFNA4, and EFNB1 were highly expressed in HCC tissues compared with normal samples, and the high expression of these genes was associated with tumor progression and vascular invasion and, thus, led to poor prognosis in patients with HCC. Moreover, we found that prognosis-related EFNs were closely related to the TME, immune cell infiltration, immune subtypes, and biomarkers of ICIs, which may provide a new direction for the discovery of novel therapeutic targets and predictive biomarkers for immunotherapy.

Data availability statement

The original contributions presented in the study are included in the article/Supplementary Material, further inquiries can be directed to the corresponding author.

Ethics statement

The studies involving human participants were reviewed and approved by The Second Affiliated Hospital of Nanchang University Medical Research Ethics Committee. The patients/participants provided their written informed consent to participate in this study.

Author contributions

JW and SH contributed to conception and design of the study. SH, CD, and JZ organized the database. SF and YL performed the statistical analysis. SH wrote the first draft of the manuscript. CD, JZ, and SF wrote sections of the manuscript. All authors contributed to manuscript revision, read, and approved the submitted version.

Funding

This research was supported by the National Natural Science Foundation of China (NO. 82060435).

Conflict of interest

The authors declare that the research was conducted in the absence of any commercial or financial relationships that could be construed as a potential conflict of interest.

Publisher's note

Supplementary material

The Supplementary Material for this article can be found online at: https://www.frontiersin.org/articles/10.3389/fmolb.2022.943384/full#supplementary-material

SUPPLEMENTARY FIGURE S1
The expression levels of ephrin family genes in 31 cancer types based on TCGA and GTEx datasets . **(A–H)** *p < 0.05; **p <0.01; ***p < 0.001.

SUPPLEMENTARY FIGURE S2
Association of ephrin expression with progression-free interval (PFI) **(A)** and disease-specific survival (DSS) **(B)** in HCC based on Kaplan–Meier analysis.

SUPPLEMENTARY FIGURE S3
Correlation between EFNA3 and tumor-infiltrating immune cells in HCC based on the XCELL, QUANTISEQ, MCPCOUNTER, EPIC, CIBERSORT-ABS, and CIBERSORT algorithms.

SUPPLEMENTARY FIGURE S4
Correlation between EFNA4 and tumor-infiltrating immune cells in HCC based on the XCELL, QUANTISEQ, MCPCOUNTER, EPIC, CIBERSORT-ABS, and CIBERSORT algorithms.

SUPPLEMENTARY FIGURE S5
Correlation between EFNB1 and tumor-infiltrating immune cells in HCC based on the XCELL, QUANTISEQ, MCPCOUNTER, EPIC, CIBERSORT-ABS, and CIBERSORT algorithms.

SUPPLEMENTARY FIGURE S6
Correlation between prognosis-related ephrin gene expression and gene mutational landscapes. **(A)** EFNA3; **(B)** EFNA4; and **(C)** EFNB1.

References

Brückner, K., and Klein, R. (1998). Signaling by Eph receptors and their ephrin ligands. *Curr. Opin. Neurobiol.* 8 (3), 375–382. doi:10.1016/s0959-4388(98)80064-0

Cortes-Ciriano, I., Lee, S., Park, W. Y., Kim, T. M., and Park, P. J. (2017). A molecular portrait of microsatellite instability across multiple cancers. *Nat. Commun.* 8, 15180. doi:10.1038/ncomms15180

Damelin, M., Bankovich, A., Park, A., Aguilar, J., Anderson, W., Santaguida, M., et al. (2015). Anti-EFNA4 calicheamicin conjugates effectively target triple-negative breast and ovarian tumor-initiating cells to result in sustained tumor regressions. *Clin. Cancer Res.* 21 (18), 4165–4173. doi:10.1158/1078-0432.CCR-15-0695

Deng, M., Tong, R., Zhang, Z., Wang, T., Liang, C., Zhou, X., et al. (2021). EFNA3 as a predictor of clinical prognosis and immune checkpoint therapy efficacy in patients with lung adenocarcinoma. *Cancer Cell Int.* 21 (1), 535. doi:10.1186/s12935-021-02226-x

Feng, Y. X., Zhao, J. S., Li, J. J., Wang, T., Cheng, S. Q., Yuan, Y., et al. (2010). Liver cancer: EphrinA2 promotes tumorigenicity through rac1/akt/NF-kappaB signaling pathway. *Hepatology* 51 (2), 535–544. doi:10.1002/hep.23313

Fitzmaurice, C., Allen, C., Barber, R. M., Barregard, L., Bhutta, Z. A., et al. (2017). Global, regional, and national cancer incidence, mortality, years of Life lost, years lived with disability, and disability-adjusted life-years for 32 cancer groups, 1990 to 2015: a systematic analysis for the global burden of disease study. *JAMA Oncol.* 3 (4), 524–548. doi:10.1001/jamaoncol.2016.5688

Franz, M., Rodriguez, H., Lopes, C., Zuberi, K., Montojo, J., Bader, G. D., et al. (2018). GeneMANIA update 2018. *Nucleic Acids Res.* 46 (W1), W60–W64. doi:10.1093/nar/gky311

Galle, P. R., Dufour, J. F., Peck-Radosavljevic, M., Trojan, J., and Vogel, A. (2021). Systemic therapy of advanced hepatocellular carcinoma. *Future Oncol.* 17 (10), 1237–1251. doi:10.2217/fon-2020-0758

Garrido-Laguna, I., Krop, I., Burris, H. A., 3rd, Hamilton, E., Braiteh, F., Weise, A. M., et al. (2019). First-in-human, phase I study of PF-06647263, an anti-EFNA4 calicheamicin antibody-drug conjugate, in patients with advanced solid tumors. *Int. J. Cancer* 145 (7), 1798–1808. doi:10.1002/ijc.32154

Geeleher, P., Cox, N., and Huang, R. S. (2014). pRRophetic: an R package for prediction of clinical chemotherapeutic response from tumor gene expression levels. *PLoS One* 9 (9), e107468. doi:10.1371/journal.pone.0107468

Gibney, G. T., Weiner, L. M., and Atkins, M. B. (2016). Predictive biomarkers for checkpoint inhibitor-based immunotherapy. *Lancet. Oncol.* 17 (12), e542–e551. doi:10.1016/s1470-2045(16)30406-5

Hanahan, D., and Coussens, L. M. (2012). Accessories to the crime: functions of cells recruited to the tumor microenvironment. *Cancer Cell* 21 (3), 309–322. doi:10.1016/j.ccr.2012.02.022

Hause, R. J., Pritchard, C. C., Shendure, J., and Salipante, S. J. (2016). Classification and characterization of microsatellite instability across 18 cancer types. *Nat. Med.* 22 (11), 1342–1350. doi:10.1038/nm.4191

Héroult, M., Schaffner, F., and Augustin, H. G. (2006). Eph receptor and ephrin ligand-mediated interactions during angiogenesis and tumor progression. *Exp. Cell Res.* 312 (5), 642–650. doi:10.1016/j.yexcr.2005.10.028

Husain, A., Chiu, Y. T., Sze, K. M., Ho, D. W., Tsui, Y. M., Suarez, E. M. S., et al. (2022). Ephrin-A3/EphA2 axis regulates cellular metabolic plasticity to enhance cancer stemness in hypoxic hepatocellular carcinoma. *J. Hepatology* 77, 383–396. doi:10.1016/j.jhep.2022.02.018

Ieguchi, K., and Maru, Y. (2019). Roles of EphA1/A2 and ephrin-A1 in cancer. *Cancer Sci.* 110 (3), 841–848. doi:10.1111/cas.13942

Iwasaki, K., Ninomiya, R., Shin, T., Nomura, T., Kajiwara, T., Hijiya, N., et al. (2018). Chronic hypoxia-induced slug promotes invasive behavior of prostate cancer cells by activating expression of ephrin-B1. *Cancer Sci.* 109 (10), 3159–3170. doi:10.1111/cas.13754

Janes, P. W., Vail, M. E., Ernst, M., and Scott, A. M. (2021). Eph receptors in the immunosuppressive tumor microenvironment. *Cancer Res.* 81 (4), 801–805. doi:10.1158/0008-5472.Can-20-3047

Jin, W., Qi, S., and Luo, H. (2011). The effect of conditional EFNB1 deletion in the T cell compartment on T cell development and function. *BMC Immunol.* 12, 68. doi:10.1186/1471-2172-12-68

Kaenel, P., Mosimann, M., and Andres, A. C. (2012). The multifaceted roles of Eph/ephrin signaling in breast cancer. *Cell Adh. Migr.* 6 (2), 138–147. doi:10.4161/cam.20154

Kelley, R. K., Sangro, B., Harris, W., Ikeda, M., Okusaka, T., Kang, Y. K., et al. (2021). Safety, efficacy, and pharmacodynamics of tremelimumab plus durvalumab for patients with unresectable hepatocellular carcinoma: randomized expansion of a phase I/II study. *J. Clin. Oncol.* 39 (27), 2991–3001. doi:10.1200/jco.20.03555

Kulik, L., and El-Serag, H. B. (2019). Epidemiology and management of hepatocellular carcinoma. *Gastroenterology* 156 (2), 477–491. doi:10.1053/j.gastro.2018.08.065

Kullander, K., and Klein, R. (2002). Mechanisms and functions of Eph and ephrin signalling. *Nat. Rev. Mol. Cell Biol.* 3 (7), 475–486. doi:10.1038/nrm856

Lengyel, C. G. (2021). Microsatellite instability as a predictor of outcomes in colorectal cancer in the era of immune-checkpoint inhibitors. *Curr. Drug Targets* 22 (9), 968–976. doi:10.2174/1389450122666210325121322

Llovet, J. M., Kelley, R. K., Villanueva, A., Singal, A. G., Pikarsky, E., and Roayaie, S. (2021). Hepatocellular carcinoma. *Nat. Rev. Dis. Prim.* 7 (1), 6. doi:10.1038/s41572-020-00240-3

Lin, J., Zeng, C., Zhang, J., Song, Z., Qi, N., Liu, X., et al. (2021). EFNA4 promotes cell proliferation and tumor metastasis in hepatocellular carcinoma through a PIK3R2/GSK3β/β-catenin positive feedback loop. *Mol. Ther. Nucleic Acids* 25, 328–341. doi:10.1016/j.omtn.2021.06.002

Liu, J., Lichtenberg, T., Hoadley, K. A., Poisson, L. M., Lazar, A. J., Cherniack, A. D., et al. (2018). An integrated TCGA pan-cancer clinical data Resource to drive high-quality survival outcome analytics. *Cell* 173 (2), 400–416. doi:10.1016/j.cell.2018.02.052

Llovet, J. M., Castet, F., Heikenwalder, M., Maini, M. K., Mazzaferro, V., Pinato, D. J., et al. (2022). Immunotherapies for hepatocellular carcinoma. *Nat. Rev. Clin. Oncol.* 19 (3), 151–172. doi:10.1038/s41571-021-00573-2

Lodola, A., Giorgio, C., Incerti, M., Zanotti, I., and Tognolini, M. (2017). Targeting Eph/ephrin system in cancer therapy. *Eur. J. Med. Chem.* 142, 152–162. doi:10.1016/j.ejmech.2017.07.029

Lu, P., Shih, C., and Qi, H. (2017). Ephrin B1-mediated repulsion and signaling control germinal center T cell territoriality and function. *Science* 356 (6339), eaai9264. doi:10.1126/science.aai9264

Luo, H., Charpentier, T., Wang, X., Qi, S., Han, B., Wu, T., et al. (2011). Efnb1 and Efnb2 proteins regulate thymocyte development, peripheral T cell differentiation, and antiviral immune responses and are essential for interleukin-6 (IL-6) signaling. *J. Biol. Chem.* 286 (48), 41135–41152. doi:10.1074/jbc.M111.302596

McCarron, J. K., Stringer, B. W., Day, B. W., and Boyd, A. W. (2010). Ephrin expression and function in cancer. *Future Oncol.* 6 (1), 165–176. doi:10.2217/fon.09.146

McGrail, D. J., Pilié, P. G., Rashid, N. U., Voorwerk, L., Slagter, M., Kok, M., et al. (2021). High tumor mutation burden fails to predict immune checkpoint blockade response across all cancer types. *Ann. Oncol.* 32 (5), 661–672. doi:10.1016/j.annonc.2021.02.006

Mencucci, M. V., Lapyckyj, L., Rosso, M., Besso, M. J., Belgorosky, D., Isola, M., et al. (2020). Ephrin-B1 is a novel biomarker of bladder cancer aggressiveness. Studies in murine models and in human samples. *Front. Oncol.* 10, 283. doi:10.3389/fonc.2020.00283

Mori, T., Maeda, N., Inoue, K., Sekimoto, R., Tsushima, Y., Matsuda, K., et al. (2013). A novel role for adipose ephrin-B1 in inflammatory response. *PLoS One* 8 (10), e76199. doi:10.1371/journal.pone.0076199

Papadakos, S. P., Petrogiannopoulos, L., Pergaris, A., and Theocharis, S. (2022). The EPH/ephrin system in colorectal cancer. *Int. J. Mol. Sci.* 23 (5), 2761. doi:10.3390/ijms23052761

Pasquale, E. B. (2008). Eph-ephrin bidirectional signaling in physiology and disease. *Cell* 133 (1), 38–52. doi:10.1016/j.cell.2008.03.011

Pinter, M., Jain, R. K., and Duda, D. G. (2021). The current landscape of immune checkpoint blockade in hepatocellular carcinoma: a review. *JAMA Oncol.* 7 (1), 113–123. doi:10.1001/jamaoncol.2020.3381

Qin, S., Ren, Z., Feng, Y. H., Yau, T., Wang, B., Zhao, H., et al. (2021). Atezolizumab plus bevacizumab versus sorafenib in the Chinese subpopulation with unresectable hepatocellular carcinoma: phase 3 randomized, open-label IMbrave150 study. *Liver Cancer* 10 (4), 296–308. doi:10.1159/000513486

Ribas, A., and Wolchok, J. D. (2018). Cancer immunotherapy using checkpoint blockade. *Science* 359 (6382), 1350–1355. doi:10.1126/science.aar4060

Samstein, R. M., Lee, C. H., Shoushtari, A. N., Hellmann, M. D., Shen, R., Janjigian, Y. Y., et al. (2019). Tumor mutational load predicts survival after immunotherapy across multiple cancer types. *Nat. Genet.* 51 (2), 202–206. doi:10.1038/s41588-018-0312-8

Sawai, Y., Tamura, S., Fukui, K., Ito, N., Imanaka, K., Saeki, A., et al. (2003). Expression of ephrin-B1 in hepatocellular carcinoma: possible involvement in neovascularization. *J. Hepatol.* 39 (6), 991–996. doi:10.1016/s0168-8278(03)00498-7

Schrock, A. B., Ouyang, C., Sandhu, J., Sokol, E., Jin, D., Ross, J. S., et al. (2019). Tumor mutational burden is predictive of response to immune checkpoint inhibitors in MSI-high metastatic colorectal cancer. *Ann. Oncol.* 30 (7), 1096–1103. doi:10.1093/annonc/mdz134

Shu, Y., Xiao, B., Wu, Q., Liu, T., Du, Y., Tang, H., et al. (2016). The ephrin-A5/EphA4 interaction modulates neurogenesis and angiogenesis by the p-akt and p-ERK pathways in a mouse model of TLE. *Mol. Neurobiol.* 53 (1), 561–576. doi:10.1007/s12035-014-9020-2

Surawska, H., Ma, P. C., and Salgia, R. (2004). The role of ephrins and Eph receptors in cancer. *Cytokine Growth Factor Rev.* 15 (6), 419–433. doi:10.1016/j.cytogfr.2004.09.002

Thorsson, V., Gibbs, D. L., Brown, S. D., Wolf, D., Bortone, D. S., Ou Yang, T. H., et al. (2018). The immune landscape of cancer. *Immunity* 48 (4), 812–830. doi:10.1016/j.immuni.2018.03.023

Vivian, J., Rao, A. A., Nothaft, F. A., Ketchum, C., Armstrong, J., Novak, A., et al. (2017). Toil enables reproducible, open source, big biomedical data analyses. *Nat. Biotechnol.* 35 (4), 314–316. doi:10.1038/nbt.3772

Wada, H., Yamamoto, H., Kim, C., Uemura, M., Akita, H., Tomimaru, Y., et al. (2014). Association between ephrin-A1 mRNA expression and poor prognosis after hepatectomy to treat hepatocellular carcinoma. *Int. J. Oncol.* 45 (3), 1051–1058. doi:10.3892/ijo.2014.2519

Wang, L., Song, Y., Wang, H., Liu, K., Shao, Z., Shang, Z., et al. (2020). MiR-210-3p-EphrinA3-PI3K/AKT axis regulates the progression of oral cancer. *J. Cell. Mol. Med.* 24 (7), 4011–4022. doi:10.1111/jcmm.15036

Yang, G., Zheng, R. Y., and Jin, Z. S. (2019a). Correlations between microsatellite instability and the biological behaviour of tumours. *J. Cancer Res. Clin. Oncol.* 145 (12), 2891–2899. doi:10.1007/s00432-019-03053-4

Yang, J. D., Hainaut, P., Gores, G. J., Amadou, A., Plymoth, A., Roberts, L. R., et al. (2019b). A global view of hepatocellular carcinoma: trends, risk, prevention and management. *Nat. Rev. Gastroenterol. Hepatol.* 16 (10), 589–604. doi:10.1038/s41575-019-0186-y

Yu, G., Luo, H., Wu, Y., and Wu, J. (2004). EphrinB1 is essential in T-cell-T-cell co-operation during T-cell activation. *J. Biol. Chem.* 279 (53), 55531–55539. doi:10.1074/jbc.M410814200

Yu, G., Mao, J., Wu, Y., Luo, H., and Wu, J. (2006). Ephrin-B1 is critical in T-cell development. *J. Biol. Chem.* 281 (15), 10222–10229. doi:10.1074/jbc.M510320200

Zhao, Y., Cai, C., Zhang, M., Shi, L., Wang, J., Zhang, H., et al. (2021). Ephrin-A2 promotes prostate cancer metastasis by enhancing angiogenesis and promoting EMT. *J. Cancer Res. Clin. Oncol.* 147 (7), 2013–2023. doi:10.1007/s00432-021-03618-2

Zheng, P., Liu, X., Li, H., Gao, L., Yu, Y., Wang, N., et al. (2021). EFNA3 is a prognostic biomarker correlated with immune cell infiltration and immune checkpoints in gastric cancer. *Front. Genet.* 12, 796592. doi:10.3389/fgene.2021.796592

Zhu, A. X., Finn, R. S., Edeline, J., Cattan, S., Ogasawara, S., Palmer, D., et al. (2018). Pembrolizumab in patients with advanced hepatocellular carcinoma previously treated with sorafenib (KEYNOTE-224): a non-randomised, open-label phase 2 trial. *Lancet. Oncol.* 19 (7), 940–952. doi:10.1016/S1470-2045(18)30351-6

Glossary

HCC hepatocellular carcinoma

Eph Erythropoietin-producing hepatocellular carcinoma

Ephrins Eph receptor interacting ligands

EFNs Eph receptor interacting ligands

TME tumor microenvironment

TCGA the Cancer Genome Atlas database

GTEx Genotype-Tissue Expression database

TIMER Tumor Immune Evaluation Resource

TPM transcripts per million reads

TMB tumor mutation burden

MSI microsatellite instability

OS Overall Survival

DSS Disease-Specific Survival

PFI Progression Free Interval

ROC Receiver Operating Characteristics

AUC Area Under the ROC Curve

PPI protein-protein interaction

GSEA gene set enrichment analysis

ICIs immune checkpoint inhibitors

SNP Single nucleotide polymorphisms

RT-qPCR real-time reverse transcription-quantitative polymerase chain reaction

qPCR Quantitative Real-time Polymerase Chain Reaction

ACC Adrenocortical carcinoma

BLCA Bladder urothelial carcinoma

BRCA Breast invasive carcinoma

CESC Cervical squamous cell carcinoma and endocervical adenocarcinoma

CHOL Cholangiocarcinoma

COAD Colon adenocarcinoma

DLBC Lymphoid neoplasm diffuse large B cell lymphoma

ESCA Esophageal carcinoma

GBM Glioblastoma multiforme

HNSC Head and neck squamous cell carcinoma

KICH Kidney chromophobe

KIRC Kidney renal clear cell carcinoma

KIRP Kidney renal papillary cell carcinoma

LAML Acute myeloid leukemia

LGG Brain Lower Grade Glioma

LIHC Liver hepatocellular carcinoma

LUAD Lung adenocarcinoma

LUSC Lung squamous cell carcinoma

MESO Mesothelioma

OV Ovarian serous cystadenocarcinoma

PAAD Pancreatic adenocarcinoma

PCPG Pheochromocytoma and paraganglioma

PRAD Prostate adenocarcinoma;

READ Rectum adenocarcinoma

SARC Sarcoma

SKCM Skin cutaneous melanoma

STAD Stomach adenocarcinoma

TGCT Testicular germ cell tumors

THCA Thyroid carcinoma

THYM Thymoma

UCEC Uterine corpus endometrial carcinoma

UCS Uterine carcinosarcoma

UVM Uveal melanoma

frontiers | Frontiers in Molecular Biosciences

TYPE Original Research
PUBLISHED 14 September 2022
DOI 10.3389/fmolb.2022.951636

OPEN ACCESS

EDITED BY
Hongming Miao,
Army Medical University, China

REVIEWED BY
Siyuan Zheng,
The University of Texas Health Science Center at San Antonio, United States
Qianghu Wang,
Nanjing University, China

*CORRESPONDENCE
Yibo Gao,
gaoyibo@cicams.ac.cn
Shuangmei Zou,
zousm@cicams.ac.cn
Xishan Wang,
wxshan1208@126.com

†These authors have contributed equally to this work

SPECIALTY SECTION
This article was submitted to Molecular Diagnostics and Therapeutics, a section of the journal Frontiers in Molecular Biosciences

RECEIVED 24 May 2022
ACCEPTED 01 August 2022
PUBLISHED 14 September 2022

CITATION
Zhao Z, Yang Y, Liu Z, Chen H, Guan X, Jiang Z, Yang M, Liu H, Chen T, Gao Y, Zou S and Wang X (2022), Prognostic and immunotherapeutic significance of mannose receptor C type II in 33 cancers: An integrated analysis. *Front. Mol. Biosci.* 9:951636. doi: 10.3389/fmolb.2022.951636

Prognostic and immunotherapeutic significance of mannose receptor C type II in 33 cancers: An integrated analysis

Zhixun Zhao[1†], Yanwei Yang[2†], Zheng Liu[1†], Haipeng Chen[1†], Xu Guan[1], Zheng Jiang[1], Ming Yang[1], Hengchang Liu[1], Tianli Chen[1], Yibo Gao[3,4,5,6]*, Shuangmei Zou[7]* and Xishan Wang[1]*

[1]Department of Colorectal Surgery, National Cancer Center/National Clinical Research Center for Cancer/Cancer Hospital, Chinese Academy of Medical Sciences and Peking Union Medical College, Beijing, China, [2]Department of Laboratory, National Center for Children's Health/Beijing Children's Hospital, Capital Medical University, Beijing, China, [3]Department of Thoracic Surgery, National Cancer Center/National Clinical Research Center for Cancer/Cancer Hospital, Chinese Academy of Medical Sciences and Peking Union Medical College, Beijing, China, [4]Laboratory of Translational Medicine, National Cancer Center/National Clinical Research Center for Cancer/Cancer Hospital, Chinese Academy of Medical Sciences and Peking Union Medical College, Beijing, China, [5]State Key Laboratory of Molecular Oncology, National Cancer Center/National Clinical Research Center for Cancer/Cancer Hospital, Chinese Academy of Medical Sciences and Peking Union Medical College, Beijing, China, [6]Central Laboratory, National Cancer Center/National Clinical Research Center for Cancer/Cancer Hospital & Shenzhen Hospital, Chinese Academy of Medical Sciences and Peking Union Medical College, Beijing, China, [7]Department of Pathology, National Cancer Center/ National Clinical Research Center for Cancer/ Cancer Hospital, Chinese Academy of Medical Sciences and Peking Union Medical College, Beijing, China

Background: The type 2 mannose receptor C (MRC2) is involved in tumor biological processes and plays a new role in the remodeling of the extracellular matrix turnover. Previous studies have demonstrated MRC2 expression profiling and prognostic relevance in some tumor types. However, the clinical and immunotherapeutic value of MRC2 in pan-cancers remains controversial. Our study aimed to evaluate MRC2 expression pattern, clinical characteristics and prognostic significance in 33 cancers, explore the relationship between MRC2 and immune-related characteristics, and assess the prediction of MRC2 for the immunotherapeutic response.

Methods: Transcriptional and clinical data of 33 cancers were downloaded from The Cancer Genome Atlas database (TCGA) database and two independent immunotherapeutic cohorts were obtained from GSE67501 and the IMvigor210 study. Next, patients stratified by MRC2 expression levels were displayed by Kaplan-Meier plot to compare prognosis-related indexes. Meanwhile, immune infiltrates of different cancers were estimated by tumor immune estimation resources (TIMER) and CIBERSORT. The ESTIMATE algorithm was used to estimate the immune and stromal scores in tumor tissues. MRC2 expression and immunological modulators, including immune inhibitors, immune stimulators, and MHC molecules, were screened through

the TISIDB portal. Gene-set enrichment analysis analyses were performed to explore the underlying biological process of MRC2 across different cancers. The immunotherapeutic response prediction was performed in two independent cohorts (GSE78220: metastatic melanoma with pembrolizumab treatment and IMvigor210: advanced urothelial cancer with atezolizumab intervention).

Results: MRC2 is expressed differently in many cancers and has been shown to have potential prognostic predicting significance. MRC2 was significantly associated with immune cell infiltration, immune modulators, and immunotherapeutic markers. Notably, the immunotherapeutic response group was associated with lower MRC2 expression in metastatic melanoma and advanced urothelial carcinoma cohort.

Conclusion: This study demonstrated that MRC2 could be a prognostic indicator for certain cancer and is critical for tumor immune microenvironments. MRC2 expression level may influence and predict immune checkpoint blockade response as a potential indicator.

KEYWORDS

mannose receptor C type 2 (MRC2), pan-cancer, immunotherapy, immune response, prognosis

Introduction

More recently, although immune checkpoint blockade therapy is considered a promising strategy for cancers, literature has emerged that less than one-third of the patients who received immunotherapy have significant therapeutic effects (Wang et al., 2019). Except for the antigenicity and mutational burden of cancer, the response to immunotherapy is affected by many factors, such as the composition of the tumor-associated extracellular matrix (ECM) (Madsen and Bugge, 2015). Degradation of the surrounding ECM could promote tumor invasion and destroy the normal tissues. Regarding immunotherapy, ECM could hinder tumor immune infiltration and act as ligands for immune inhibitory receptors (Mariathasan et al., 2018). Consequently, the tumor-associated ECM regulation is expected to provide a novel sight for optimizing the immunotherapeutic strategies and improving the prognosis of cancer (He et al., 2021).

The mannose receptor C type 2 (MRC2), also known as uPARAP/Endo180, plays a pivotal role in the remodeling of the extracellular matrix turnover, such as collagen binding and internalization (Honardoust et al., 2006; Rohani et al., 2014). Meanwhile, MRC2 has an impact on cell migration and invasion involved in tissue repair, cancer progression (Melander et al., 2015; Jurgensen et al., 2020), and more pathological lymphangiogenesis (Engelholm et al., 2001; Durre et al., 2018). It has previously been observed that the expression of MRC2 is aberrantly upregulated in a variety of cancers and associated with poor prognosis, upregulated in including breast cancer, prostate cancer, hepatocellular carcinoma, as well as head and neck cancer (Sulek et al., 2007; Wienke et al., 2007; Kogianni et al., 2009; Palmieri et al., 2013; Gai et al., 2014). However, little systematic research has been focused on the MRC2 expression features and prognosis in pan-cancers. Besides, though extensive research has been carried out on the relationship between immune therapy and ECM, no related study clarified the immune-related characteristics and immunotherapeutic prediction of MRC2 in different cancers.

In our study, we evaluated the MRC2 expression and prognosis-related significance across 33 cancer types based on Cancer Genome Atlas (TCGA) data. Furthermore, the associations between MRC2 and tumor-infiltrating immune cells, immune-related modulators, tumor mutation burden, and microsatellite instability in the tumor microenvironments were analyzed. Additionally, the therapy response with different MRC2 expression levels to immunotherapies for melanoma and urothelial carcinoma was further investigated according to the public immunotherapeutic cohorts.

Methods and materials

Data sources

RNA sequencing data and the corresponding clinical information of 33 cancer types were downloaded from TCGA by using the UCSC cancer genome browser (https://tcga.xenahubs.net, accessed April 2020). Totally, 11,007 cases were evaluated in the final analysis and the abbreviations of 33 cancers were summarized in Table 1. Two independent immune therapy cohorts were obtained in this research: The IMvigor210 cohort (advanced urothelial cancer with atezolizumab intervention) was collected from the website

TABLE 1 Abbreviation of 33 human cancers.

Abbreviation	Full name
ACC	Adrenocortical carcinoma
BLCA	Bladder urothelial carcinoma
BRCA	Breast invasive carcinoma
CESC	Cervical squamous cell carcinoma and endocervical adenocarcinoma
CHOL	Cholangiocarcinoma
COAD	Colon adenocarcinoma
DLBC	Lymphoid neoplasm diffuse large B-cell lymphoma
ESCA	Esophageal carcinoma
GBM	Glioblastoma multiforme
HNSC	Head and neck squamous cell carcinoma
KICH	Kidney chromophobe
KIRC	Kidney renal clear cell carcinoma
KIRP	Kidney renal papillary cell carcinoma
LAML	Acute myeloid leukemia
LGG	Brain lower grade glioma
LIHC	Liver hepatocellular carcinoma
LUAD	Lung adenocarcinoma
LUSC	Lung squamous cell carcinoma
MESO	Mesothelioma
OV	Ovarian serous cystadenocarcinoma
PAAD	Pancreatic adenocarcinoma
PCPG	Pheochromocytoma and paraganglioma
PRAD	Prostate adenocarcinoma
READ	Rectum adenocarcinoma
SARC	Sarcoma
SKCM	Skin cutaneous melanoma
STAD	Stomach adenocarcinoma
TGCT	Testicular germ cell tumors
THCA	Thyroid carcinoma
THYM	Thymoma
UCEC	Uterine corpus endometrial carcinoma
UCS	Uterine carcinosarcoma
UVM	Uveal melanoma

based on the Creative Commons 3.0 license (http://research-pub.Gene.com/imvigor210corebiologies) (Mariathasan et al., 2018), and the GSE78220 (metastatic melanoma with pembrolizumab treatment) was downloaded from the Gene Expression Omnibus database (GEO, https://www.ncbi.nlm.nih.gov/geo/).

Clinical features and prognosis associated significance of MRC2 in 33 cancers

Gene expression profiles and corresponding clinical information of 33 tumor types was extracted from TCGA. The univariate Cox model was applied to calculate the associations between MRC2 expression levels and patient survival to compare overall survival (OS), disease-free survival (DFS), disease-specific survival (DSS), and progression-free survival (PFS) across the 33 cancer types. Patients stratified by MRC2 expression levels were evaluated by log-rank test and visualized by Kaplan-Meier (KM) curves. MRC2 activity was generated by single-sample gene-set enrichment analysis (ssGSEA), which was utilized to quantify the enrichment scores of immune cells and immune functions for each cancer types. The difference in MRC2 activity between normal and tumor groups was further investigated. To evaluate differences in MRC2 expression at the protein level, IHC images of MRC2 protein expression in normal tissues and tumors tissues, were downloaded from the

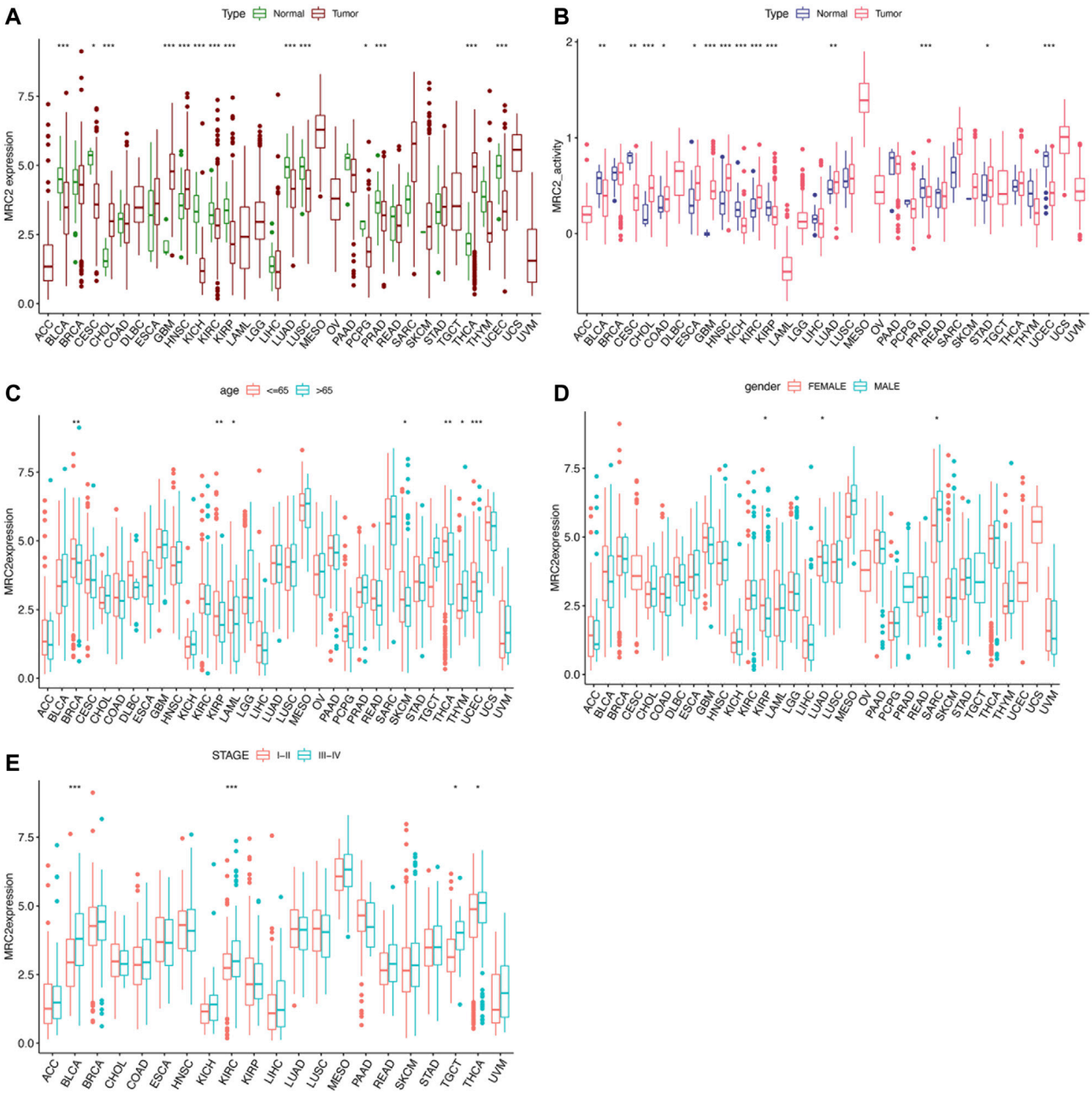

FIGURE 1
The clinical correlation and activity of MRC2. **(A)** The differential expression analysis between tumor and normal groups of MRC2 in 33 cancers; **(B)** The different activity analysis between tumor and normal groups of MRC2 in 33 cancers; **(C)** The correlation between age and MRC2. **(D)**; The correlation between gender and MRC2; **(E)** The correlation between stage and MRC2. "**" indicates $p < 0.01$ and "***" indicates $p < 0.001$.

HPA (http://www.proteinatlas.org/) and analyzed. To evaluate differences in MRC2 expression at the protein level, IHC images of MRC2 protein expression in normal tissues and tumors tissues, were downloaded from the HPA (http://www.proteinatlas.org/) and analyzed. $p < 0.05$ was regarded as a statistical significance.

MRC2 and immune-associated characteristics in 33 cancers

The tumor immune estimation resources (TIMER, https://cistrome.shinyapps.io/timer/) and CIBERSORT((http://cibersort.stanford.edu/) were carried

out to estimate the tumor immune infiltration in different cancers, respectively (Li et al., 2017; Newman et al., 2019). ESTIMATE algorithm was performed to calculate the immune and stromal scores, as well as the correlation with MRC2 expression in tumor tissues. The associations between MRC2 expression and tumor-infiltrating immunocyte related markers were further investigated (Cristescu et al., 2018). The potential relationship between MRC2 expression and immunological modulators, including immune inhibitors, immune stimulators, and MHC molecules, was screened through the TISIDB website (http://cis.hku.hk/TISIDB/index.php). The four most relevant results were then highlighted and presented in plots. The somatic mutation data of all TCGA patients were downloaded (https://tcga.xenahubs.net) and TMB scores and MSI scores were calculated.

Functional enrichment analysis of MRC2

Subsequently, the expression and activity averages of MRC2 were calculated and ranked for 33 cancers to explore the potential characterization of MRC2 expression and activity. To explore the biological functions of MRC2 in cancers with overall survival prognosis, gene-set enrichment analysis (GSEA) analyzes were performed in BRCA, KIRC, LGG, and UVM, respectively.

Immunotherapeutic response analysis MRC2

As mentioned above, data obtained from two related independent immunotherapeutic cohorts were analyzed in current study. Patients in complete remission (CR) or partial response (PR) were classified as responders and the remaining cases with stale disease (SD) and progressive disease (PD) were classified as non-response.

Statistical analysis

In this study, the Wilcox log-rank test was adopted to determine the presence or absence of a markedly increased sum of gene expression z-scores in cancer tissues compared with adjacent normal tissues. Differences in MRC2 expression were also compared in the Kruskal–Wallis test. Survival rates were analyzed using the KM curves, log-rank tests, and Cox proportional hazard regression model models. The Spearman test for correlation analysis. R Language (Version 4.1.1; R Foundation) is available for analysis and the difference of $p < 0.05$ was statistically significant.

Results

Clinical profile of MRC2 expression

As shown in Figure 1A, MRC2 is differentially expressed between tumor and normal tissues in 14 of 33 cancers (Highly expressed in CHOL, GBM, HNSC, and THCA, whereas lowly expressed in BLCA, CESC, KICH, KIRC, KIRP, LUAD, LUSC, PCPG, PRAD, and UCEC). According to the ssGSEA of MRC2 between normal and tumor groups, MRC2 activity was significantly increased in the tumor group of CHOL, ESCA, GBM, HNSC, KIRC, LUAD, and STAD, while decreased in the tumor group of BLCA, CESC, KICH, KIRC, KIRP, PRAD, and UCEC (Figure 1B). Compared to the younger patients (≤65 years old), MRC2 expression decreased in the tumor of elderly patients (>65 years old) in the group of BRCA, KIRP, LAML, SKCM, and UCEC, while the expression pattern was reversed in the THYM group (Figure 1C). With regard to gender, the female group has the higher MRC2 expression in the KRIP and LUAD tumors, while the lower MRC2 level in the SARC tumor (Figure 1D). Besides, MRC2 was positively correlated with the tumor stage of BLCA, KIRC, TCGT, and THCA (Figure 1E). To further explore the differential expression patterns of MRC2 in pan-cancers between tumor and normal tissues, we obtained the related data from the Human Protein Atlas (HPA, https://www.proteinatlas.org). We found that MRC2 was mainly expressed in the tumor stroma, and combined with morphological features, we considered that fibroblasts might be the largest. For tumor cells, we found moderate to strong cytoplasmic positivity was observed in papillary adenocarcinomas of thyroid; a few cases of malignant gliomas, breast, ovarian, endometrial and skin cancers exhibited weak to moderate staining, and remaining malignant cells were mainly negative, which was consistent with our results from pan-cancer analysis (Supplementary Figure S10).

Correlation of MRC2 expression level and prognosis in 33 cancers

Furthermore, high-level MRC2 expression was an unfavorable prognostic indicator for OS in ACC, BLCA, GBM, KICH, KIRC, LAML, LGG, OV, and UVM, as demonstrated in Figure 2A and Supplementary Table S1. In terms of DFS, the higher level of MRC2 was associated with worse outcomes in LGG and PAAD (Supplementary Figure S2A; Supplementary Table S2). Regarding DSS, MRC2 was a risk factor for BLCA, GBM, KICH, KIRC, LGG, OV, PAAD, and UVM (Supplementary Figure S3A; Supplementary Table S3). MRC2 expression was positively correlated with PFS in COAD, KICH, KIRC, PAAD, and UVM and only negatively

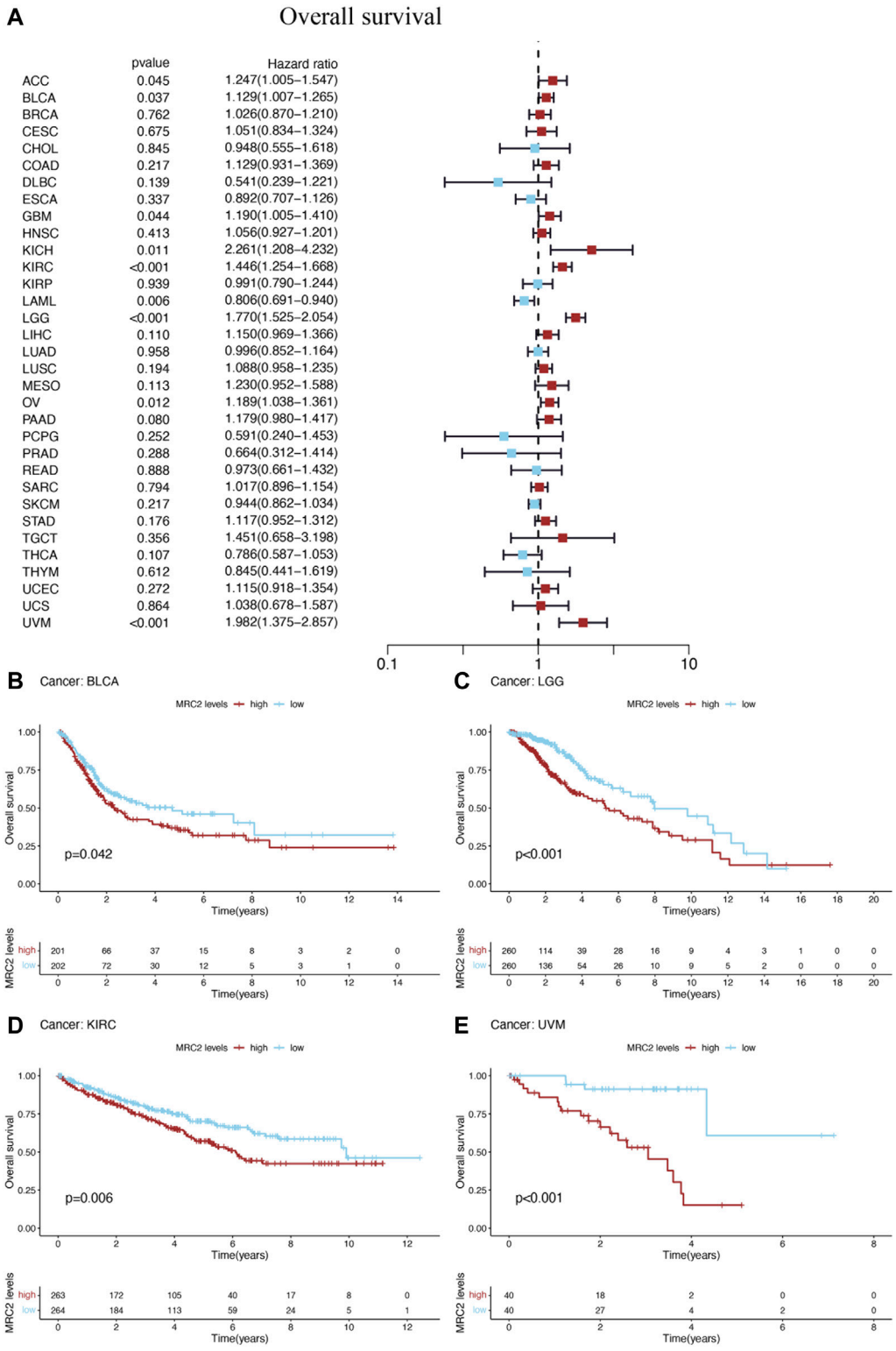

FIGURE 2
The forest plots of univariate Cox regression analyses for overall survival (OS). **(A)** The highlight items mean that MRC2 expression was significantly correlated with prognosis in these cancer types ($p < 0.05$). Items with hazard ratio greater than 1 indicated that the MRC2 expression was a promoting factor of death. The Kaplan–Meier curves were plotted to visualize the OS of MRC2 expression levels in different cancers **(B–E)**.

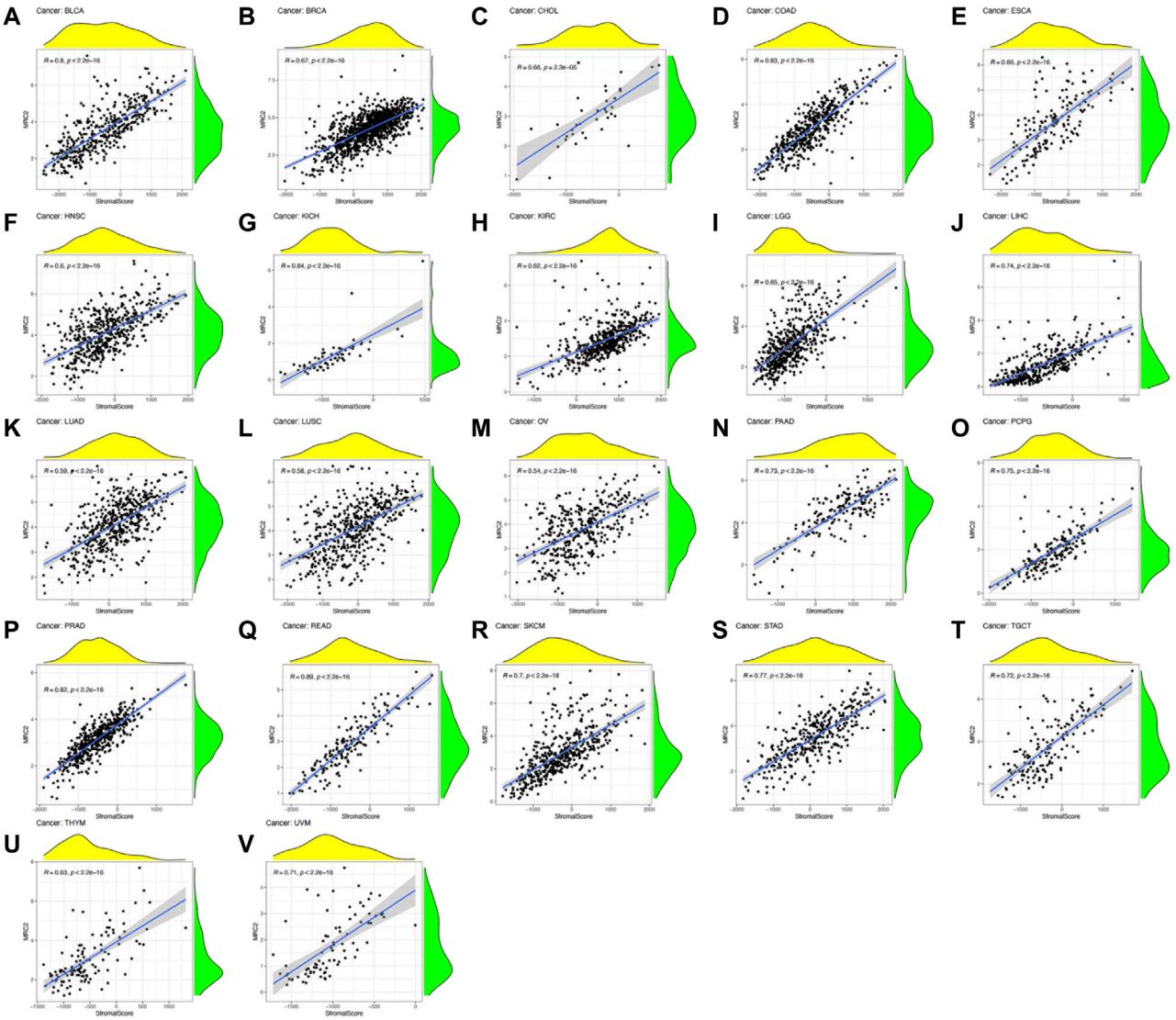

FIGURE 3
The correlation of MRC2 expression with Stromal Score. The correlation filter was set as $p < 0.001$ and $|R| > 0.5$ **(A–V)**.

correlated with DLBC (Supplementary Figure S4A; Supplementary Table S4). Taken all together, MRC2 expression was negatively associated with survival in many tumor types, including ACC, BLCA, GBM, KICH, KIRC, LAML, LGG, OV, and UVM.

The Kaplan–Meier (KM) curves were performed to visualize the prognostic value of MRC2 expression levels in above cancers. High levels of MRC2 expression indicated unfavorable OS in BLCA ($p = 0.042$), LGG ($p < 0.001$), KIRC ($p = 0.006$), and UVM ($p < 0.001$), which was shown in Figures 2B–E. Meanwhile, lower MRC2 was associated with worse DFS in LGG ($p = 0.013$) and PAAD ($p = 0.036$) (Supplementary Figures S2A,C), worse DSS in BLCA ($p = 0.029$), LGG ($p < 0.001$), KIRC ($p = 0.003$), and UVM ($p < 0.001$) (Supplementary Figures S3B–E), worse PFS in COAD ($p = 0.014$), KIRC ($p < 0.001$), LGG ($p < 0.001$), and UVM ($p < 0.001$), and better PFS in only DLBC($p = 0.016$) (Supplementary Figures S4B–F).

Correlation between MRC2 expression level and immune-related characteristics

ESTIMATE algorithm was used to estimate the stromal score and immune score, with the threshold of $p < 0.001$ and $|R| > 0.5$. Remarkably, as can be seen from Figure 3, the MRC2 expression was

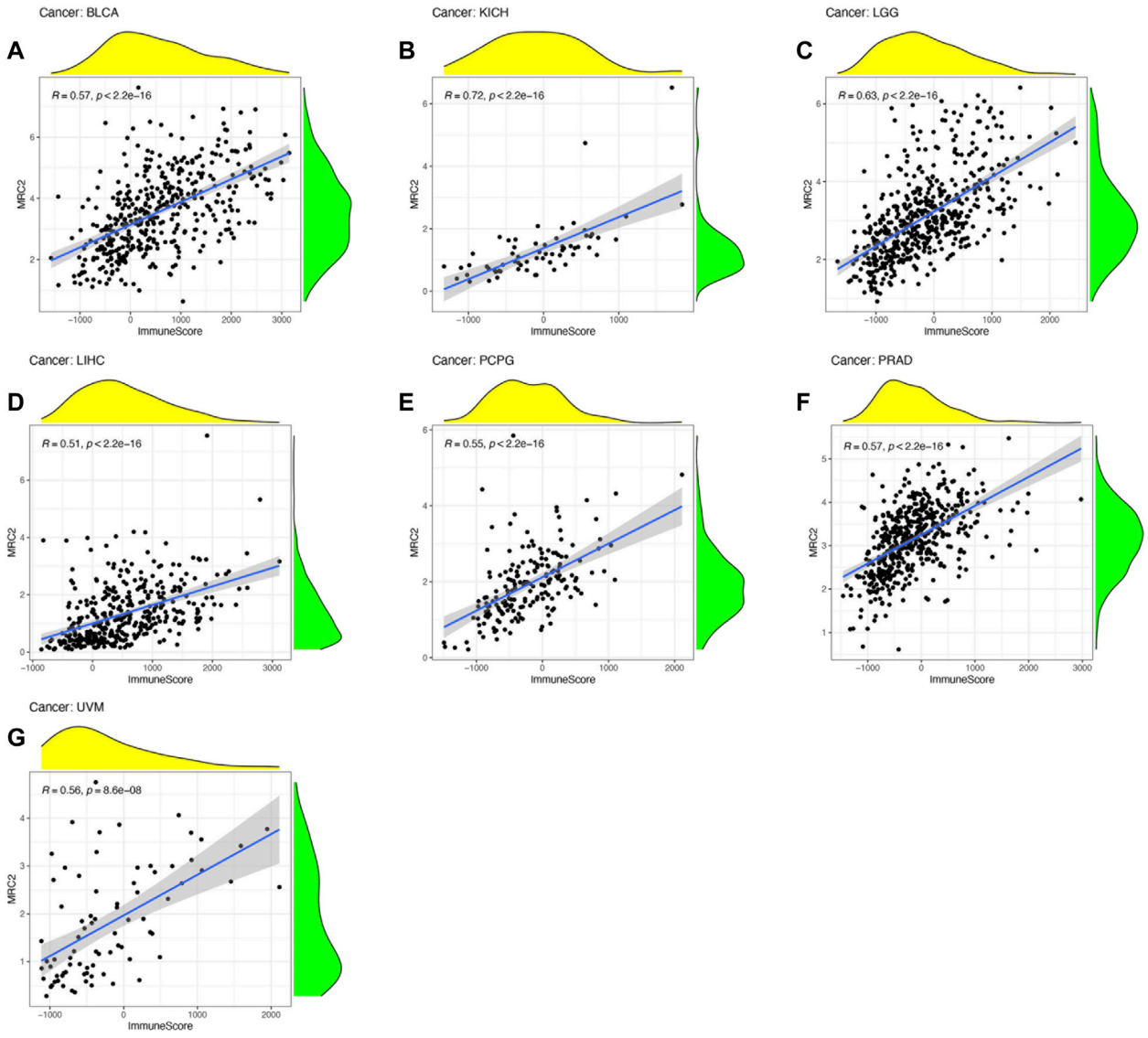

FIGURE 4
The correlation of MRC2 expression with Immune Score. The correlation filter was set as $p < 0.001$ and $|R| > 0.5$ **(A–G)**.

positively correlated with the stromal scores for most the cancer types (BLCA, BRCA, CHOL, COAD, ESCA, HNSC, KICH, KIRC, LGG, LIHC, LUAD, LUSC, OV, PAAD, PCPG, PRAD, READ, SKCM, STAD, TGCT, THYM, and UVM). Relatively, MRC2 is associated with immune scores for BLCA, KICH, LGG, LIHC, PCPG, PRAD, and UVM (Figure 4; Supplementary Table S5). Regarding immune infiltrates (Supplementary Figure S5; Supplementary Table S6), MRC2 expression was positively correlated with the abundance of macrophage M1 and T cells CD8, while negatively with dendritic cells activated in ACC. In TCGT, MRC2 expression was positively correlated with M2 macrophage and negatively associated with B cell naïve and T cells CD4 memory activated. It is also worth mentioning that the MRC2 tended to be correlated to T cells CD8.

To further investigate the underlying mechanisms of MRC2 immune inhibition, the TIMER database was taken to compare MRC2 expression with multiple checkpoint markers across different cancer types (Figure 5A). Notably, MRC2 expression in BLCA, COAD, READ, PAAD, and UMV was positively correlated with LAG3, NRP1, CTLA4, PDCD1 (PD-1), CD274 (PD-L1), and PDCD1LG2(PD-L2). To explore the potential of MRC2 to regulate immunomodulators, the relationship between MRC2 and immunomodulators was analyzed by TISIDB. In immune inhibitors, MRC2 was positively

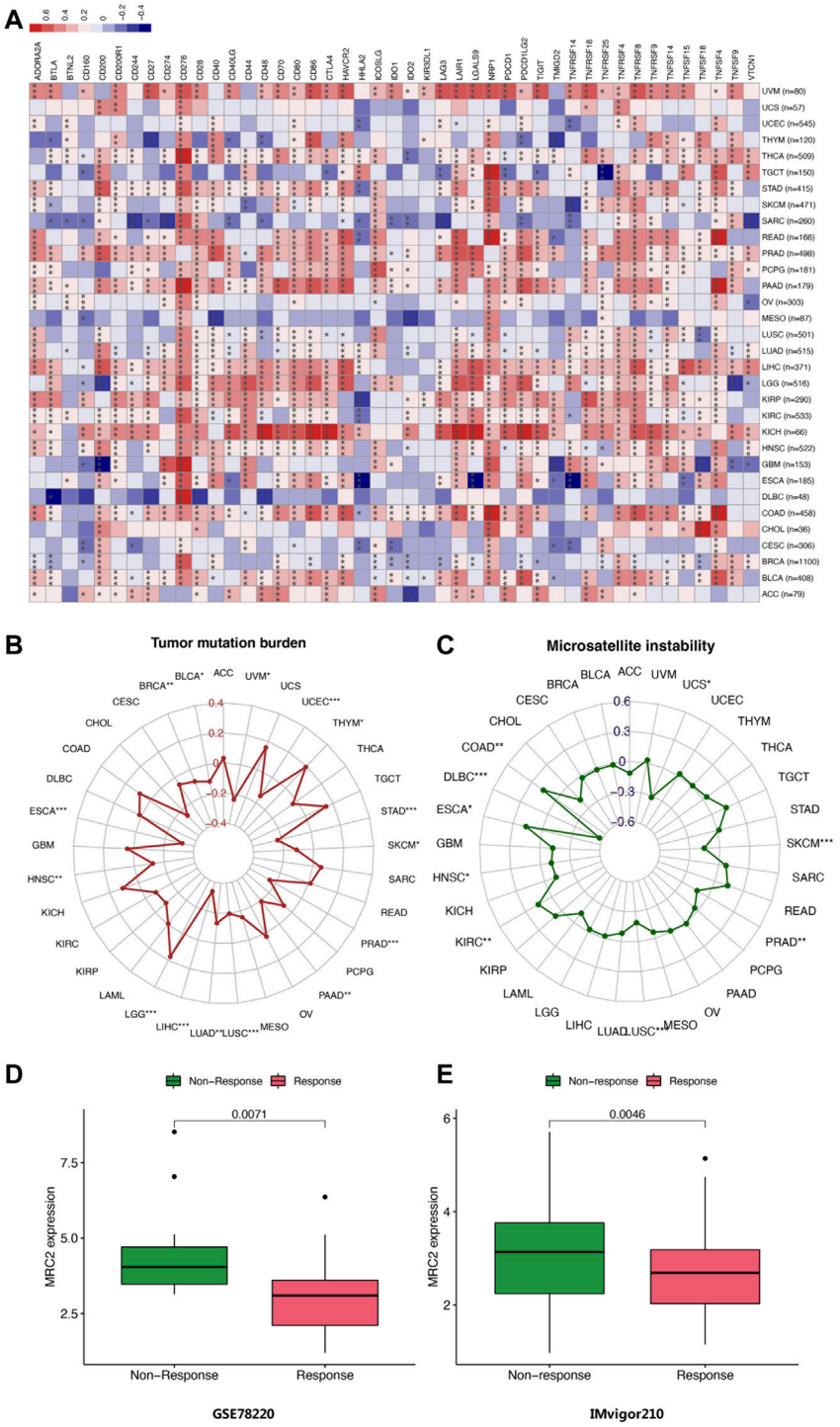

FIGURE 5
(A) Correlation of MRC2 expression with expression of immune checkpoint genes calculated by TIMER. Red indicates positive correlation, whereas blue indicates negative correlation. "*" indicates $p < 0.05$, "**" indicates $p < 0.01$ and "***" indicates $p < 0.001$. **(B)** Correlations between MRC2 expression and TMB. **(B,C)** Correlation between MRC2 and MSI. **(D–E)** Correlations between MRC2 and immunotherapeutic response in immunotherapeutic cohorts.

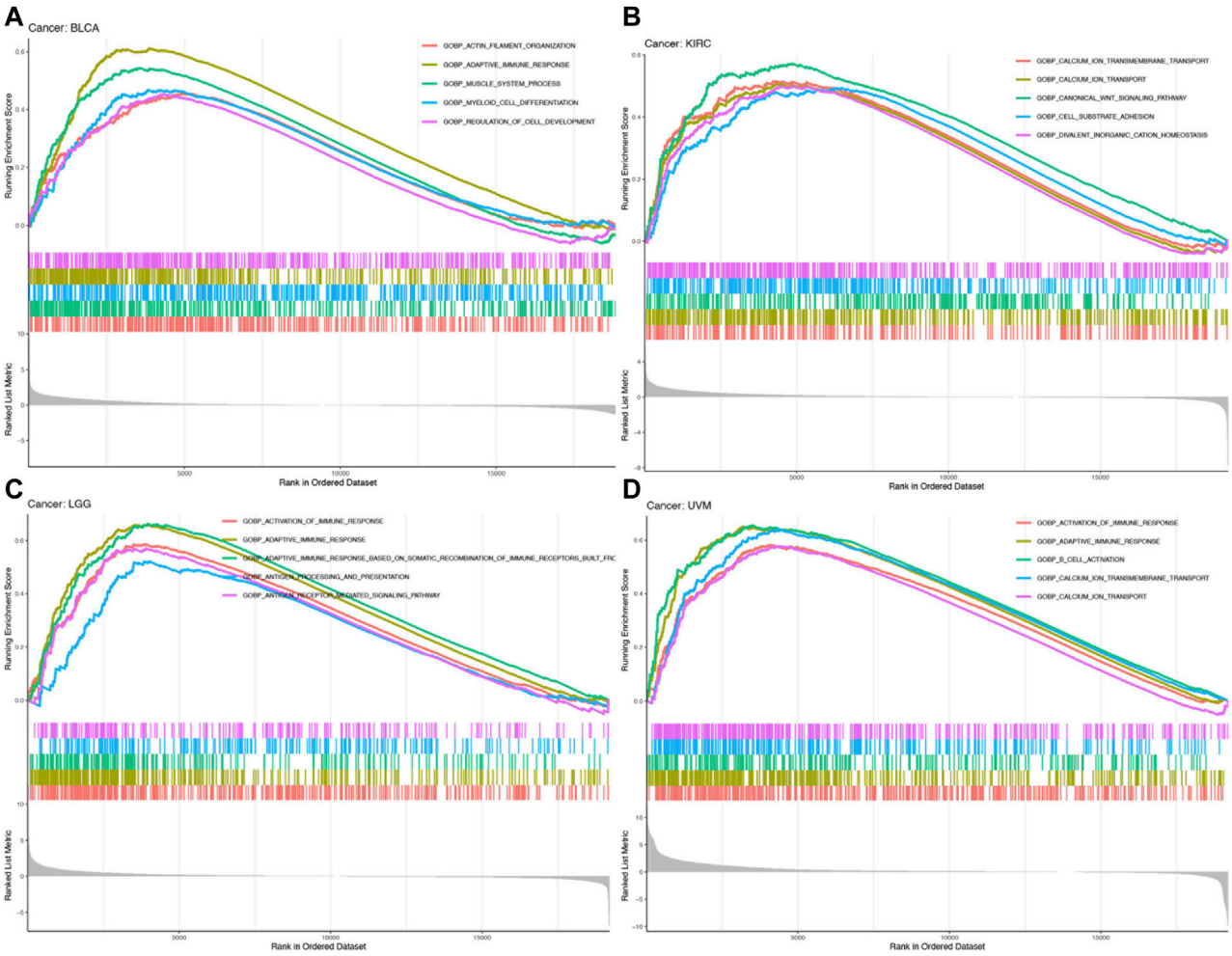

FIGURE 6
GO enrichment analysis of MRC2 in BLCA **(A)**, KIRC **(B)**, LGG **(C)**, and UVM **(D)**.

associated with PDCD1 in BLCA, CSF1R and PDCD1LG2 in KICH, and TGFBR1 in PRAD (Supplementary Figure S6). In immune stimulators analysis, MRC2 expression was positively correlated with CD86 and TNFSF13B in KICH, TMEM173 in LIHC, and C10orf54 in PRAD (Supplementary Figure S7). Meanwhile, MRC2 expression was positively associated with HLA-DOA, HLA-DPB1, HLA-DQA1 and HLA-DRB1 in KICH (Supplementary Figure S8).

Analysis of MRC2 immunotherapy response

The correlation between MRC2 expression and TMB as well as MSI was investigated. As demonstrated in Figure 5B, MRC2 has a positive correlation with TMB in LGG and THYM and is negatively correlated with TMB in BLCA, BRCA, ESCA, HNSC, LIHC, LUAD, LUSC, PAAD, PRAD, SKCM, STAD, UCEC, and UVM. In terms of MSI analysis, MRC2 was positively associated with MSI in COAD, ESCA, and KIRC, but negatively correlated with DLBC, HNSC, LUSC, PRAD, SKCM, and USC (Figure 5C). Intriguingly, when analyzing the immunotherapeutic response in a cohort of GSE78220 and IMvigor210, the response group proved the lower MRC2 expression level in metastatic melanoma with pembrolizumab (p = 0.071, Figure 5D) and advanced urothelial cancer with atezolizumab (p = 0.0046, Figure 5E).

Functional analysis by GSEA

To explore the biological functions of MRC2 in cancers with overall survival prognosis, gene-set enrichment analysis (GSEA) analyzes were performed in BRCA, KIRC, LGG, and UVM,

respectively. Gene Ontology (GO) analysis indicated that MRC2 was mainly enriched to the activation of the immune response, adaptive immune response, and calcium ion transport (Figure 6; Supplementary Table S9). According to Kyoto Encyclopedia of Genes and Genomes (KEGG) analysis demonstrated in Supplementary Figure S9, MRC2 was enriched in many functions or pathways including chemokine signaling pathway, cytokine receptor interaction, focal adhesion, antigen processing and presentation, and calcium signaling pathway.

Discussions

There is also increasing research on ECM regulation in cancer immunity, but there is still some confusion. The components of ECM play a critical role in regulating each step of the cancer immunity cycle, which also highlights the potential of targeting tumor-associated ECM to improve cancer immunotherapy. The "hot tumors" characterized by molecular markers of T cell infiltration and immune activation were highly responsive to immunotherapies such as anti-programmed death-ligand 1 (PD-L1)/PD-1 treatment, while "cold tumors" exhibited significant T cell deletion or exclusion (Gajewski, 2015; Zemek et al., 2019). The MRC2, which is involved in homeostatic maintenance and ECM remodeling, plays a role in physiological (embryonic development, wound healing, tissue repair) and pathological conditions (cancer, inflammation) (Lu et al., 2011). Current research has focused on the relationship between MRC2 and tumor immune response and critically analyzed the role of MRC2 in cancer immunity and its potential combination with cancer immunotherapy.

MRC2 expression levels were altered in a variety of cancers. MRC2 expression was highly expressed in the tumor group of CHOL, GBM, HNSC, and THCA, whereas lowly expressed in BLCA, CESC, KICH, KIRC, KIRP, LUAD, LUSC, PCPG, PRAD, and UCEC. There have been accumulating studies reporting that MRC2 expression is increased aberrantly in a variety of cancers. In GBM, MRC2 is upregulated in tumor tissues and mediates tumor cell invasion through collagen-containing stroma (Huijbers et al., 2010; Takahashi et al., 2011). Sulek et al. found that MRC2 expression increased in HNSC tumor compared to adjacent tumors and was positively associated with poor differentiation (Sulek et al., 2007). Previous studies also suggest that in most solid tumors of epithelial origin, expression of MRC2 is reported to be predominantly restricted to cancer-associated fibroblasts (CAFs) with little or no expression by the tumor cells (Sulek et al., 2007; Sulek et al., 2007; Schnack Nielsen et al., 2002; Curino et al., 2005; Koikawa et al., 2018). There is extensive functional evidence implicating CAFs in tumor progression, via their ability to deposit and remodel the extracellular matrix, to secrete pro-tumorigenic factors and by modulating the immune compartment. Besides, there is also evidence that CAFs can play a role in restraining tumor growth, by acting as a desmoplastic barrier to tumor cell invasion and by the recruitment of anti-tumor immune cells. Therefore, MRC2 may play a similar function in tumorigenesis by regulating CAFs.

Previous studies confirmed that downregulation of MRC2 expression reduced the tumor migration and collagen invasion, suggesting active involvement of MRC2 in glioma cell invasion (Huijbers et al., 2010; Takahashi et al., 2011). There is increasing evidence that MRC2 interferes with lymphatic endothelial cells VEGFR-2 and VEGFR-3, which are associated with cancer progression and metastasis to lymph nodes and distant organs (Cady, 2007; Paupert et al., 2011; Durre et al., 2018). Meanwhile, the genetic ablation of MRC2 affects the contractility and viability of cancer associated fibroblasts, limiting tumor growth and metastasis. Based on the above evidence, we suppose that MRC2 expression may contribute to the selection of clinical strategies for certain cancer types. Interestingly, MRC2 suggests poor PFS in multiple tumors, but better PFS in DLBC alone. In most solid tumors of epithelial origin, expression of MRC2 is reported to be predominantly restricted to CAFs with little or no expression by the tumor cells. CAFs play a role in promoting tumorigenesis, metastasis, and drug resistance. Previous studies have confirmed that CAFs generally indicate poor tumor prognosis. However, as a hematological tumor, the roles of MRC2 and CAFs in DLBC may be quite different from those of conventional solid tumors, so there are differences in the predictive prompts.

Next, we investigated the relationship between MRC2 and immune-related characteristics. The MRC2 expression was positively correlated with the stromal scores in 22/33 tumor types, which is consistent with MRC2 as an extracellular matrix remodeling gene. This is possibly because that CAFs play an important role as a component of tumor stroma, and MRC2 expresses predominantly in fibroblasts. In the meantime, MRC2 is correlated to immune scores for BLCA, KICH, LGG, LIHC, PCPG, PRAD, and UVM by ESTIMATE algorithm, which may be due to the fact that CAFs affects the tumor microenvironment in some types tumors. There is also evidence that CAFs can play a role in the recruitment of anti-tumor immune cells (LeBleu and Kalluri, 2018). In addition, the study found that MRC2 expression was correlated with infiltrating levels of macrophage M1 and T cells CD8 in ACC, M2 macrophage, B cell naïve, and T cells CD4 memory activated in TCGT. In addition, the study found that MRC2 expression was correlated with infiltrating levels of macrophage. GSEA also points out that the biological processes of MRC2 in different types of cancer are involved in the activation of immune response and adaptive immune response. Subsequently, using the TIMER and TISIDE databases, we found that MRC2 is associated with important immunomodulatory molecules in multiple tumors. There are a number of known or ongoing immunotherapy-

related drug targets, including CD274 (PD1), PDCD1 (PD-L1), PDCD1LG2 (PD-L2), CTLA4, and LAG3. Emerging evidence suggests that components of ECM and its proteolytic remodeling products regulate immune responses and act as immune modulators (Pao et al., 2018). Based on the previous research about the linkage between ECM and the immune microenvironment, the collagens might be the different primary components of ECM between "cold" and "hot" tumors (Pao et al., 2018). Moreover, MRC2 mainly acts on tumor-associated fibroblasts, and affects the characteristics of the tumor microenvironment by regulating extracellular matrix remodeling and secreting cytokines. Previous study confirmed that of epithelial origin, expression of MRC2 is reported to be predominantly restricted to CAFs with little or no expression by the tumor cells in most solid tumors. Likewise, we obtained similar results with the HPA database. However, we found that the expression of MRC2 in certain tumors is related to immune cells, and we consider this to be related to the function of CAFs. In previous studies, CAFs can act on the tumor microenvironment in various ways to produce immune suppression effects, which may include inhibiting the maturation of dendritic cells, abnormal differentiation of T cells, and secreting cytokines to inhibit tumor cell activity. Therefore, the high expression of MRC2 may have an immunosuppressive effect through the function of CAFs, thereby affecting the enrichment of immune cells. All above, targeting MRC2 combined with immune checkpoint blockade therapy may modulate the tumor's immune status and potentially influence the immunotherapeutic response.

Notably, we investigated the predictive role of MRC2 expression in immunotherapy efficacy in two PD-1 treated immunotherapy cohorts. The results elucidated the potential immunotherapeutic response prediction function of MRC2 in metastatic melanoma and advanced urothelial carcinoma. In previous studies, CAFs can act on the tumor microenvironment in various ways to produce immune suppression effects, which may include inhibiting the maturation of dendritic cells, abnormal differentiation of T cells, and secreting cytokines to inhibit tumor cell activity (LeBleu and Kalluri, 2018). Therefore, the high expression of MRC2 may have an immunosuppressive effect through the function of CAFs, thereby affecting the efficacy of immunotherapy. In follow-up studies, it is necessary to validate the prognostic role of this gene for immune checkpoint therapy in cohorts of other tumor types and larger samples. In follow-up studies, it is necessary to validate the prognostic role of this gene for immune checkpoint therapy in cohorts of other tumor types and larger samples. It is also worth investigating whether inhibition of MRC2 expression can improve the efficacy of immunotherapies. Combination inhibition of MRC2 and immune checkpoints to improve immunotherapeutic efficacy is also a direction for future exploration.

As an article based on public database analysis, this study has certain limitations. The first point is that there is no private data or independent cohort for validation. Second, this study found the associations between MRC2 and CAFs, which may affect the biological functions and characteristics of immunotherapy efficacy. Therefore, it also requires further in-depth study of the function of MRC2 *in vivo* and *in vitro* experiments. Third, all studies in this study were based on bulk sequencing. The research team also consulted the current tumor-related single-cell sequencing database, but it is difficult to meet the evaluation at the pan-cancer level. Therefore, further analysis at the single-cell level in one or several cancer types may be performed in the future, followed by a more in-depth analysis of MRC2.

Conclusion

In conclusion, we found that MRC2 could be a prognostic indicator for certain cancer and is critical for tumor immune microenvironments. Further exploration of the function of MRC2 might provide influence and predict immune checkpoint blockade response as a potential biomarker.

Data availability statement

The original contributions presented in the study are included in the article/Supplementary Material, further inquiries can be directed to the corresponding authors.

Author contributions

Study design: ZZ, HC, and XW; Data analysis: ZZ, XG, and HL; Manuscript writing: ZZ and YY; Visualization: ZZ and TC; Manuscript review and editing: XW, YG, ZL, SZ, ZJ, and MY; Funding acquisition: XW and ZZ; Project administration: XW, ZL, and YG.

Funding

This work was supported by the National Key R&D Program of China (2020AAA0109500, 2021YFC2501900), Beijing Science and Technology Program (D17110002617004), Beijing Hope Run Special Fund of Cancer Foundation of China (LC2019B14, LC2021A13), National Natural Science Foundation of China (82122053, 81972316), the Beijing Municipal Science & Technology Commission (Z191100006619118), CAMS Innovation Fund for Medical Sciences (CIFMS) (2021-I2M-1-067), Non-profit Central Research Institute Fund of Chinese Academy of Medical Sciences (2021-PT310-001, 2021-RC310-020), Key-Area Research and Development Program of Guangdong Province (2021B0101420005).

Acknowledgments

The authors would like to thank the donors and the Cancer Institute & Hospital, Chinese Academy of Medical Sciences, Peking Union Medical College, Beijing, China for tumor specimens which was provided for the study.

Conflict of interest

The authors declare that the research was conducted in the absence of any commercial or financial relationships that could be construed as a potential conflict of interest.

Publisher's note

All claims expressed in this article are solely those of the authors and do not necessarily represent those of their affiliated organizations, or those of the publisher, the editors and the reviewers. Any product that may be evaluated in this article, or claim that may be made by its manufacturer, is not guaranteed or endorsed by the publisher.

Supplementary material

The Supplementary Material for this article can be found online at: https://www.frontiersin.org/articles/10.3389/fmolb.2022.951636/full#supplementary-material

SUPPLEMENTARY FIGURE S1
(A) The mean expression of MRC2 in 33 cancers (from high to low); **(B)** The mean activity of MRC2 in 33 cancers (from high to low). "**" indicates p < 0.01 and "***" indicates p < 0.001.

SUPPLEMENTARY FIGURE S2
The forest plots of univariate Cox regression analyses for disease-free survival (DFS). The highlight items mean that MRC2 expression was significantly correlated with prognosis in these cancer types ($p < 0.05$). Items with hazard ratio greater than 1 indicated that the MRC2 expression was a promoting factor of death. The Kaplan–Meier curves were plotted to visualize the DFS of MRC2 expression levels in different cancers.

SUPPLEMENTARY FIGURE S3
The forest plots of univariate Cox regression analyses for disease-specific survival (DSS). The highlight items mean that MRC2 expression was significantly correlated with prognosis in these cancer types ($p < 0.05$). Items with hazard ratio greater than 1 indicated that the MRC2 expression was a promoting factor of death. The Kaplan–Meier curves were plotted to visualize the DSS of MRC2 expression levels in different cancers.

SUPPLEMENTARY FIGURE S4
The forest plots of univariate Cox regression analyses for progression-free survival (PFS). The highlight items mean that MRC2 expression was significantly correlated with prognosis in these cancer types ($p < 0.05$). Items with hazard ratio greater than 1 indicated that the MRC2 expression was a promoting factor of death. The Kaplan–Meier curves were plotted to visualize the PFS of MRC2 expression levels in different cancers.

SUPPLEMENTARY FIGURE S5
The correlation of MRC2 expression with immune infiltration level in ACC, DLBC, LAML, TGCT, and UVM. The correlation filter was set as $p < 0.001$ and $|R| > 0.5$.

SUPPLEMENTARY FIGURE S6
Expression correlation between MRC2 expression and immune inhibitors. The top four immune inhibitors with the correlation coefficient of MRC2 expression level were displayed *via* dot plots.

SUPPLEMENTARY FIGURE S7
Expression correlation between MRC2 expression and immune stimulators. The top four immune stimulators with the correlation coefficient of MRC2 expression level were displayed *via* dot plots.

SUPPLEMENTARY FIGURE S8
Expression correlation between MRC2 expression and MHC molecules. The top four MHC molecules with the correlation coefficient of MRC2 expression level were displayed *via* dot plots.

SUPPLEMENTARY FIGURE S9
KEGG enrichment analysis of MRC2 in BLCA **(A)**, KIRC **(B)**, LGG **(C)**, and UVM **(D)**.

SUPPLEMENTARY FIGURE S10
Comparison of MRC2 gene expression immunohistochemistry images in normal (left) and tumor (right) between normal and tumor tissues.

References

Cady, B. (2007). Regional lymph node metastases; a singular manifestation of the process of clinical metastases in cancer: contemporary animal research and clinical reports suggest unifying concepts. *Ann. Surg. Oncol.* 14 (6), 1790–1800. doi:10.1245/s10434-006-9234-2

Cristescu, R., Mogg, R., Ayers, M., Albright, A., Murphy, E., Yearley, J., et al. (2018). Pan-tumor genomic biomarkers for PD-1 checkpoint blockade-based immunotherapy. *Science* 362 (6411), eaar3593. doi:10.1126/science.aar3593

Curino, A. C., Engelholm, L. H., Yamada, S. S., Holmbeck, K., Lund, L. R., Molinolo, A. A., et al. (2005). Intracellular collagen degradation mediated by uPARAP/Endo180 is a major pathway of extracellular matrix turnover during malignancy. *J. Cell Biol.* 169 (6), 977–985. doi:10.1083/jcb.200411153

Durre, T., Morfoisse, F., Erpicum, C., Ebroin, M., Blacher, S., Garcia-Caballero, M., et al. (2018). uPARAP/Endo180 receptor is a gatekeeper of VEGFR-2/VEGFR-3 heterodimerisation during pathological lymphangiogenesis. *Nat. Commun.* 9 (1), 5178. doi:10.1038/s41467-018-07514-1

Engelholm, L. H., Nielsen, B. S., Dano, K., and Behrendt, N. (2001). The urokinase receptor associated protein (uPARAP/endo180): a novel internalization receptor connected to the plasminogen activation system. *Trends cardiovasc. Med.* 11 (1), 7–13. doi:10.1016/s1050-1738(01)00076-7

Gai, X., Tu, K., Lu, Z., and Zheng, X. (2014). MRC2 expression correlates with TGFβ1 and survival in hepatocellular carcinoma. *Int. J. Mol. Sci.* 15 (9), 15011–15025. doi:10.3390/ijms150915011

Gajewski, T. F. (2015). The next hurdle in cancer immunotherapy: Overcoming the non-T-cell-inflamed tumor microenvironment. *Semin. Oncol.* 42 (4), 663–671. doi:10.1053/j.seminoncol.2015.05.011

He, Y., Liu, T., Dai, S., Xu, Z., Wang, L., and Luo, F. (2021). Tumor-associated extracellular matrix: How to Be a potential aide to anti-tumor immunotherapy? *Front. Cell Dev. Biol.* 9, 739161. doi:10.3389/fcell.2021.739161

Honardoust, H. A., Jiang, G., Koivisto, L., Wienke, D., Isacke, C. M., Larjava, H., et al. (2006). Expression of Endo180 is spatially and temporally regulated during wound healing. *Histopathology* 49 (6), 634–648. doi:10.1111/j.1365-2559.2006.02559.x

Huijbers, I. J., Iravani, M., Popov, S., Robertson, D., Al-Sarraj, S., Jones, C., et al. (2010). A role for fibrillar collagen deposition and the collagen internalization

receptor endo180 in glioma invasion. *PLoS One* 5 (3), e9808. doi:10.1371/journal.pone.0009808

Jurgensen, H. J., van Putten, S., Norregaard, K. S., Bugge, T. H., Engelholm, L. H., Behrendt, N., et al. (2020). Cellular uptake of collagens and implications for immune cell regulation in disease. *Cell. Mol. Life Sci.* 77 (16), 3161–3176. doi:10.1007/s00018-020-03481-3

Kogianni, G., Walker, M. M., Waxman, J., and Sturge, J. (2009). Endo180 expression with cofunctional partners MT1-MMP and uPAR-uPA is correlated with prostate cancer progression. *Eur. J. Cancer* 45 (4), 685–693. doi:10.1016/j.ejca.2008.11.023

Koikawa, K., Ohuchida, K., Takesue, S., Ando, Y., Kibe, S., Nakayama, H., et al. (2018). Pancreatic stellate cells reorganize matrix components and lead pancreatic cancer invasion via the function of Endo180. *Cancer Lett.* 412, 143–154. doi:10.1016/j.canlet.2017.10.010

LeBleu, V. S., and Kalluri, R. (2018). A peek into cancer-associated fibroblasts: origins, functions and translational impact. *Dis. Model. Mech.* 11 (4), dmm029447. doi:10.1242/dmm.029447

Li, Q., Li, Y., Xu, J., Wang, S., Li, X., and Cai, S. (2017). Aldolase B overexpression is associated with poor prognosis and promotes tumor progression by epithelial-mesenchymal transition in colorectal adenocarcinoma. *Cell. Physiol. biochem.* 42 (1), 397–406. doi:10.1159/000477484

Lu, P., Takai, K., Weaver, V. M., and Werb, Z. (2011). Extracellular matrix degradation and remodeling in development and disease. *Cold Spring Harb. Perspect. Biol.* 3 (12), a005058. doi:10.1101/cshperspect.a005058

Madsen, D. H., and Bugge, T. H. (2015). The source of matrix-degrading enzymes in human cancer: Problems of research reproducibility and possible solutions. *J. Cell Biol.* 209 (2), 195–198. doi:10.1083/jcb.201501034

Mariathasan, S., Turley, S. J., Nickles, D., Castiglioni, A., Yuen, K., Wang, Y., et al. (2018). TGFβ attenuates tumour response to PD-L1 blockade by contributing to exclusion of T cells. *Nature* 554 (7693), 544–548. doi:10.1038/nature25501

Melander, M. C., Jurgensen, H. J., Madsen, D. H., Engelholm, L. H., and Behrendt, N. (2015). The collagen receptor uPARAP/Endo180 in tissue degradation and cancer (Review). *Int. J. Oncol.* 47 (4), 1177–1188. doi:10.3892/ijo.2015.3120

Newman, A. M., Steen, C. B., Liu, C. L., Gentles, A. J., Chaudhuri, A. A., Scherer, F., et al. (2019). Determining cell type abundance and expression from bulk tissues with digital cytometry. *Nat. Biotechnol.* 37 (7), 773–782. doi:10.1038/s41587-019-0114-2

Palmieri, C., Caley, M. P., Purshouse, K., Fonseca, A. V., Rodriguez-Teja, M., Kogianni, G., et al. (2013). Endo180 modulation by bisphosphonates and diagnostic accuracy in metastatic breast cancer. *Br. J. Cancer* 108 (1), 163–169. doi:10.1038/bjc.2012.540

Pao, W., Ooi, C. H., Birzele, F., Ruefli-Brasse, A., Cannarile, M. A., Reis, B., et al. (2018). Tissue-specific immunoregulation: A call for better understanding of the "immunostat" in the context of cancer. *Cancer Discov.* 8 (4), 395–402. doi:10.1158/2159-8290.CD-17-1320

Paupert, J., Sounni, N. E., and Noel, A. (2011). Lymphangiogenesis in post-natal tissue remodeling: lymphatic endothelial cell connection with its environment. *Mol. Asp. Med.* 32 (2), 146–158. doi:10.1016/j.mam.2011.04.002

Rohani, M. G., Chow, Y. H., Razumova, M. V., Ash, S., Hung, C. F., and Schnapp, L. M. (2014). uPARAP function in cutaneous wound repair. *PLoS One* 9 (3), e92660. doi:10.1371/journal.pone.0092660

Schnack Nielsen, B., Rank, F., Engelholm, L. H., Holm, A., Dano, K., and Behrendt, N. (2002). Urokinase receptor-associated protein (uPARAP) is expressed in connection with malignant as well as benign lesions of the human breast and occurs in specific populations of stromal cells. *Int. J. Cancer* 98 (5), 656–664. doi:10.1002/ijc.10227

Sulek, J., Wagenaar-Miller, R. A., Shireman, J., Molinolo, A., Madsen, D. H., Engelholm, L. H., et al. (2007). Increased expression of the collagen internalization receptor uPARAP/Endo180 in the stroma of head and neck cancer. *J. Histochem. Cytochem.* 55 (4), 347–353. doi:10.1369/jhc.6A7133.2006

Takahashi, S., Yamada-Okabe, H., Hamada, K., Ohta, S., Kawase, T., Yoshida, K., et al. (2011). Downregulation of uPARAP mediates cytoskeletal rearrangements and decreases invasion and migration properties in glioma cells. *J. Neurooncol.* 103 (2), 267–276. doi:10.1007/s11060-010-0398-z

Wang, X., Yu, Q., Ghareeb, W. M., Zhang, Y., Lu, X., Huang, Y., et al. (2019). Downregulated SPINK4 is associated with poor survival in colorectal cancer. *BMC Cancer* 19 (1), 1258. doi:10.1186/s12885-019-6484-5

Wienke, D., Davies, G. C., Johnson, D. A., Sturge, J., Lambros, M. B. K., Savage, K., et al. (2007). The collagen receptor Endo180 (CD280) Is expressed on basal-like breast tumor cells and promotes tumor growth *in vivo*. *Cancer Res.* 67 (21), 10230–10240. doi:10.1158/0008-5472.CAN-06-3496

Zemek, R. M., De Jong, E., Chin, W. L., Schuster, I. S., Fear, V. S., Casey, T. H., et al. (2019). Sensitization to immune checkpoint blockade through activation of a STAT1/NK axis in the tumor microenvironment. *Sci. Transl. Med.* 11 (501), eaav7816. doi:10.1126/scitranslmed.aav7816

frontiers | Frontiers in Molecular Biosciences

TYPE Original Research
PUBLISHED 16 September 2022
DOI 10.3389/fmolb.2022.988777

OPEN ACCESS

EDITED BY
Hongming Miao,
Army Medical University, China

REVIEWED BY
Liudmila Matskova,
Immanuel Kant Baltic Federal University, Russia
Pingping Wang,
Harbin Institute of Technology, China

*CORRESPONDENCE
Zhihua Shen,
szh75@126.com
Botao Luo,
Luobotao707@126.com
Wei Jie,
wei_jie@hainmc.edu

†These authors have contributed equally to this work

SPECIALTY SECTION
This article was submitted to Molecular Diagnostics and Therapeutics, a section of the journal Frontiers in Molecular Biosciences

RECEIVED 07 July 2022
ACCEPTED 06 September 2022
PUBLISHED 16 September 2022

CITATION
Bai J, Zheng A, Ha Y, Xu X, Yu Y, Lu Y, Zheng S, Shen Z, Luo B and Jie W (2022), Comprehensive analysis of LAMC1 expression and prognostic value in kidney renal papillary cell carcinoma and clear cell carcinoma.
Front. Mol. Biosci. 9:988777.
doi: 10.3389/fmolb.2022.988777

Comprehensive analysis of *LAMC1* expression and prognostic value in kidney renal papillary cell carcinoma and clear cell carcinoma

Jianrong Bai[1†], Axiu Zheng[1†], Yanping Ha[1†], Xiaoqing Xu[2], Yaping Yu[2], Yanda Lu[2,3], Shaojiang Zheng[2,3], Zhihua Shen[1*], Botao Luo[1*] and Wei Jie[1,2,3*]

[1]Department of Pathology, School of Basic Medicine Sciences, Pathology Diagnosis and Research Center of Affiliated Hospital, Guangdong Medical University, Zhanjiang, China, [2]Cancer Institute of Hainan Medical University, Haikou, China, [3]Department of Oncology, The First Affiliated Hospital, Hainan Medical University, Haikou, China

Background: Laminin subunit gamma 1 (LAMC1) protein is associated with tumor cell invasion and metastasis. However, its role in kidney cancer remains unclear. In this work, we sought to probe the expression as well as its carcinogenic mechanisms of *LAMC1* in kidney renal papillary cell carcinoma (KIRP) and kidney renal clear cell carcinoma (KIRC).

Methods: Public databases including TIMER, Oncomine, UALCAN, TISIDB, TCGA, Kaplan–Meier plotter, UCSC Xena, cBioPortal, SurvivalMeth, KEGG, GeneMANIA, Metascape, GSCALite and GDSC were adopted, and the expression, clinical pathological correlation, prognostic signatures, dominant factors influencing *LAMC1* expression, DNA methylation levels, gene mutations, copy number variations, functional networks, and drug sensitivity were analyzed. Expression of LAMC1 protein in clinical KIRP and KIRC was validated using tissue array.

Results: *LAMC1* expression in KIRP and KIRC were significantly higher than those in normal tissues. High *LAMC1* expression indicated poor overall survival in KIRP patients and better overall survival in KIRC patients. Through the univariate and multivariate Cox analysis, we found that high *LAMC1* expression was a potential independent marker for poor prognosis in KIRP, however it implied a better prognosis in KIRC by univariate Cox analysis. In addition, the *LAMC1* expression in KIRP and KIRC was negatively correlated with methylation levels of *LAMC1* DNA. Interestingly, *LAMC1* expression was positively correlated with the infiltration of $CD8^+$ T cells, dendritic cells and neutrophils in KIRP; however, it was positively correlated with the infiltration of $CD4^+$ T cells, macrophages and neutrophils but negatively correlated with B cells in KIRC. Moreover, high level of $CD8^+$ T cells is beneficial for KIRC prognosis but opposite for KIRP. *LAMC1* may participate in signaling pathways involved in formation of adherens junction and basement membrane in KIRP

and KIRC, and the high expression of *LAMC1* is resistant to most drugs or small molecules of the Genomics of Drug Sensitivity in Cancer database.

Conclusion: Enhanced *LAMC1* expression suggests a poor prognosis in KIRP while a better prognosis in KIRC, and these opposite prognostic signatures of *LAMC1* may be related to different immune microenvironments.

KEYWORDS

kidney renal papillary cell carcinoma (KIRP), kidney renal clear cell carcinoma (KIRC), LAMC1, expression, prognosis

Introduction

The morbidity of renal cell carcinoma (RCC) has grown by 2% per year globally over the past 20 years (Ljungberg et al., 2019). In 2020, there were 73,750 new cases and 14,830 deaths of RCC patients reported in the United States (Ljungberg et al., 2019; Siegel et al., 2020). Kidney renal clear cell carcinoma (KIRC) and kidney renal papillary cell carcinoma (KIRP) account for 70%–85% and 10%–15% of all RCC patients, respectively, and KIRC is the most common pathological type of RCC. About 20%–30% of KIRC patients are diagnosed with advanced clinical stages (Escudier, 2007; Oudard et al., 2007). Approximately 30% of KIRC patients develop recurrence and progression despite surgical resection of the primary tumor (Ferlay et al., 2013; Hsieh et al., 2017). For non-metastatic KIRC, the recurrence rate is still as high as 20%–40% after partial or radical nephrectomy (Frank et al., 2003). Furthermore, KIRC is a chemo- and radio-resistant neoplasia and alternative treatment options are limited (Geissler et al., 2015). Clinical practice demonstrated that only a small percentage of patients with KIRC can benefit from targeted therapy and immunotherapy (Topalian et al., 2012; Motzer et al., 2015), and the clinical prognosis and treatment of KIRP are limited. Therefore, the identification of new prognostic and therapeutic biomarkers has important clinical significance.

In clinical practice, cancer biomarkers can be used for the purpose of diagnosis or prognosis in personalized medicine. With the deepening of the understanding of the molecular etiology of RCC, several effective targeted therapies have been applied in clinical treatment, including immunotherapies, and use of multiple kinase inhibitors (Hsieh et al., 2017). However, most RCC patients still die from their diseases because of resistance to these therapies (Linehan and Ricketts, 2014). Current studies on renal cancer biomarkers are mainly focusing on the identification of molecular markers of prognostic signatures and the prediction of the metastatic potential of individual tumors (Tunuguntla and Jorda, 2008; Eichelberg et al., 2009). Cell-matrix adhesion is an important pathological process in the malignant progression of tumor cells. As one of the main components of cell-matrix adhesion molecules, laminin uses the C-terminal LG1-3 domain and the LG4-5 domain as binding sites, connects the extracellular matrix to intracellular components by binding to transmembrane receptors (including integrin receptors and non-integrin receptors), and mediates various signaling (Sonnenberg et al., 1988; Aumailley, 2013). Members of laminin family are composed of three chains named α chain (α1-5), β chain (β1-3) and γ chain (γ1-3). *LAMC1*, which encoding the laminin γ one chain, is widely expressed in the basement membrane and is related to tissue development (Engbring and Kleinman, 2003; Schéele et al., 2007; Gritsenko et al., 2012; Aumailley, 2013). The overexpression of LAMC1 is related to tumor progression and poor prognosis in cancers such as endometrial carcinoma (Kunitomi et al., 2020), hepatocellular carcinoma (Zhang et al., 2017), gastric cancer (Han et al., 2021) and meningioma (Ke et al., 2013), highlighting the significance of molecular targeting LAMC1 in cancer treatment. However, the roles and mechanisms of LAMC1 in RCC remain unclear.

In this investigation, we adopted several publicly accessible databases to analyze *LAMC1* expression and its association with the clinical characteristics and prognosis in KIRP and KIRC. Then, a prognostic signature for KIRP and KIRC patients was constructed. We also focused on the relation of *LAMC1* expression to immune cells infiltration and the immunomodulator-related molecules expression. Furthermore, we explored how *LAMC1* may participate in signaling pathways, biological processes, and drug resistance. Our results revealed the expression status and prognostic signature of *LAMC1* in KIRP and KIRC, and uncovered the impacts of *LAMC1* on immune cell infiltration, and immunomodulator-related molecules in RCC.

Materials and methods

Analysis of *LAMC1* gene expression

The Oncomine database (https://www.oncomine.org/), a publicly available microarray database, was used to analyze the mRNA expression level of the LAMC family in different cancers (Rhodes et al., 2007). Tumor tissue was compared with normal controls for the LAMC family members applying *t*-statistics based on the thresholds of *p*-value = 0.0001 and fold change (FC) ≥ 2. The tumor immune estimation resource (TIMER) database (https://cistrome.shinyapps.io/timer/) is a

comprehensive resource for the systematic analysis of immune infiltrates across diverse cancer types by using the Wilcoxon test based on the thresholds of p-value < 0.05 (Li et al., 2017). The *LAMC1* mRNA and protein expression levels were compared between RCC and normal tissues using the DiffExp module of TIMER. We used the University of Alabama Cancer database (UALCAN, http://ualcan.path.uab.edu/), containing RNA sequences and clinical information from 33 types of tumors to assess the correlation between *LAMC1* gene expression levels and clinicopathological features in KIRP and KIRC patient (Chandrashekar et al., 2017). Differences with a p-value < 0.05 were considered statistically significant. The functions and purposes of using various public online databases in this study were detailed in Supplementary Table S1.

Tissue microarray and immunochemistry staining

The tissue microarray was obtained from Shanghai Outdo Biotech Co.,LTD. Statistical cases include 10 normal kidney tissues and 168 tumor tissues samples (KIRC:138; KIRP: 30). The immunochemistry staining (IHC) was performed using DAKO automatic immunohistochemistry instrument with the programs of "Autostainer Link 48 Usage Guide". The array was incubated with primary antibodies against LAMC1 (Cat: ABP55085, Abbkine, Wuhan, China) at 1:25 dilution for overnight at 4°C. Antigenic sites were visualized using a DAB kits. The scores of *LAMC1* were calculated as follows: 0, negative; 1, weak; 2, moderate; or 3, strong. The percentage of positive cells was scored as follows: 1, 0–25% positive cells; 2, 26–50% positive cells; and 3, 51–75% positive cells, and 4, 76–100% positive cells. The total immunoreactive scores were determined by nuclear staining score plus cytoplasm membrane staining score, and the IHC scores were determined independently by two pathologists who were blinded to the patients' clinical data and original pathology reports.

TCGA data collection and Cox regression

The expression data and mRNA expression profiles of patients with KIRP and KIRC and the clinical information related to survival time were retrieved from Genomic Data Commons data portal of The Cancer Genome Atlas (TCGA, https://portal.gdc.cancer.gov/repository) (KIRP, 321 cases including 32 normal samples; KIRC, 604 cases including 72 normal samples; workflow type, HTSeqCounts) (Weinstein et al., 2013). We used block diagrams to visualize the differences in discrete variable expressions. The HTSeq count data of RNA-Seq gene expression in 289 KIRP and 532 KIRC patients were used for further analysis. Wilcoxon symbolic rank test and logistic regression were used to evaluate the association between clinical factors and *LAMC1* expression. Multivariate Cox regression and Kaplan-Meier methods were used to determine the role of *LAMC1* expression related to the overall survival (OS) of RCC patients and clinical features, including age, gender, grade, stage, characteristics of the primary tumor (T) and distant metastasis (M). The low and high expression groups were distinguished by the median risk score for *LAMC1* expression level as the cutoff value.

The correlation analysis between *LAMC1* expression and immunity, neoantigen and tumor mutational burden

We evaluated the correlation between *LAMC1* expression in the RCC samples and the six kinds of infiltrating immune cells including B cells, $CD4^+$ T cells, $CD8^+$ T cells, neutrophils, macrophages, and dendritic cells using "Immune-Gene" module in TIMER2 database. Then we explored the effects of the infiltration immune cell levels on the prognosis of KIRP and KIRC by using the TIMER platform. In addition, the relationship between *LAMC1* expression level and immunoinhibitors and immunostimulators were further studied by the TISIDB database (http://cis.Hku.hk/TISIDB/), a public database for analyzing immune cell and immunoregulatory molecule in different tumors (Ru et al., 2019). The Kaplan–Meier plotter database (http://kmplot.com/analysis/) can be quick and intuitive for prognostic analysis (Nagy et al., 2021), which contains survival data on 54,675 genes from 10,461 cancer samples. We then used this database for prognostic analysis based on *LAMC1* expression levels in related enriched or decreased immune cell subsets including B cells, $CD4^+$ memory T cells, $CD8^+$ T cells, macrophages, natural killer (NK) T cells, regulatory T (Treg) cells, Type 1 T-helper (Th1) cells, and Type 2 T-helper (Th2) cells (grouping conditions: auto select best cutoff). According to the degree of immune infiltration levels, the ESTIMATE algorithm was used to calculate immune scores, stromal scores and estimate immune scores (the sum of immune score and stromal score) for each tumor sample (Yoshihara et al., 2013). We visualized the correlation between *LAMC1* gene expression and these scores using the R software packages "estimate" and "limma". Neoantigen encoded by a mutated gene in tumor cells, coming from biological events such as point mutations, deletion mutations, and gene fusions. The number of neoantigens per tumor sample was calculated by SCANNEO algorithm (Wang et al., 2019). Tumor mutational burden (TMB), as a quantifiable biomarker, can be used to reflect the number of mutations contained in a tumor cell, which was visualized with R software packages "ggstatsplot" (Jardim et al., 2021). In addition, Spearman's rank correlation coefficient was applied to analyze the relationship of *LAMC1* gene expression and tumor immunity, neoantigens and TMB of each tumor sample. These results presented as scatter plots.

Scoring of anti-cancer immunity

With the widespread use of immune checkpoint blockade agents in clinical practice, tumor immunity has been widely concerned in recent years and has received a good clinical response, pointing out a new direction for the treatment of cancer patients. The Cancer-Immunity Cycle can be roughly divided into seven steps (Chen and Mellman, 2013). These seven steps finely modulate the overall direction of antitumor activity. The scores of anti-cancer immunity were calculated by using ssGSEA algorithm with R package "GSEABase" based on specific gene set. The median value of *LAMC1* were used as the cutoff value and our cohort were divided into high expression group and low expression. These results were presented with boxplot with the assistance of online web-Sangerbox 3.0 (http://vip.sangerbox.com/home.html) with *t*-test.

Analysis of copy number variation and DNA methylation

To investigate the possible factors influencing *LAMC1* expression, the California Santa Cruz Cancer Genomics Browser (UCSC Xena, http://xena.ucsc.edu/) database was used (Goldman et al., 2020). In addition, to confirm the prognostic value of *LAMC1* methylation and copy number variation (CNV) in KIRP and KIRC, UCSC Xena databases was searched to investigate the effects of *LAMC1* methylation and CNV on OS. The alteration frequency and CNV of the *LAMC1* gene was also analyzed via the cBioPortal database (http://www.cbioportal.org/). We used SurvivalMeth database (http://bio-bigdata.hrbmu.edu.cn/survivalmeth/) to study the differences in *LAMC1* DNA methylation in region of whole gene between normal kidney tissues and KIRP and KIRC tissues (Method: *t*-test, Threshold Value: 0.01, Grouping Strategy: Maxstate) (Zhang et al., 2021).

Pathway, Co-expression network, and functional enrichment analyses

To explore whether *LAMC1* gene and a set of genomes with the highest correlation are differentially expressed (high or low groups were distinguished by the median value of *LAMC1* expression level), we used GSEA algorithm analysis (https://www.gsea-msigdb.org/gsea/index.jsp) based on TCGA data of KIRP and KIRC (Subramanian et al., 2005). Gene sets with p-value < 0.05 and false discovery rate (FDR) Q-value < 0.25 were considered the thresholds. The results of gene enrichment analysis were plotted using R packages such as "ggplot2" and "grid" in R software (https://www.R-project.org, Version 4.0.4). We obtained the gene interacting with *LAMC1* through the GeneMANIA network (http://genemania.org/), which could establish genetic interactions, protein–DNA interactions, and protein–protein interactions (PPI) (Warde-Farley et al., 2010). When the gene mane "*LAMC1*" was typed in the search interface, GeneMANIA automatically searches related public databases to establish a co-expression network. In addition, we carried out Gene Ontology (GO) and Kyoto Encyclopedia of Genes and Genomes (KEGG) functional enrichment analysis of the interacting genes using the Metascape portal (http://metascape.org/gp/index.html) (Zhou et al., 2019).

Gene set enrichment and drug resistance analysis

GSCALite database (http://bioinfo.life.hust.edu.cn/web/GSCALite/) offers multiple types of cancer gene set analyses, including mRNA expression, single nucleotide variation (SNV), methylation, cancer-related pathways, and miRNA networks (Liu et al., 2018). We analyzed the effect of *LAMC1* in cancer-related signaling, the expression of some genes of interest, and the miRNA network between them. In addition, we analyzed the correlation between *LAMC1* expression and drug sensitivity based on the Genomics of Drug Sensitivity in Cancer (GDSC) database by Spearman correlation analysis. If the correlation result is positive, the high expression of this gene is associated with specific drug resistance. Drug module correlation analyses for all cancer cell lines and other analyses were performed using the KIRP and KIRC TCGA dataset.

Statistical analysis

All statistical analyses were performed using R software (Version 4.0.4). Receiver operating characteristic (ROC) curves were established to evaluate the diagnostic significance of *LAMC1* expression using the "pROC" package of R, and the area under the ROC curve (AUC) indicated the magnitude of diagnostic efficiency. AUC >0.7 indicated good accuracy. Unpaired and paired Student *t*-test were performed to analyze the statistical difference of *LAMC1* gene expression in normal and tumor tissues. The associations between clinical features and *LAMC1* expression were evaluated using the Wilcoxon signed-rank test and logistic regression. Clinical features related to overall survival (OS) in KIRP and KIRC patients were identified using Cox regression and the Kaplan-Meier method. Univariate and multivariate Cox analyses were used to explore the independent prognostic significance of *LAMC1* expression level and clinical features on OS in KIRP and KIRC patients. The correlations of *LAMC1* expression with immune cells infiltration were evaluated using Spearman's correlation analysis. The thresholds were referenced the related methods section. All p-values were adjusted by false discovery rate (FDR)

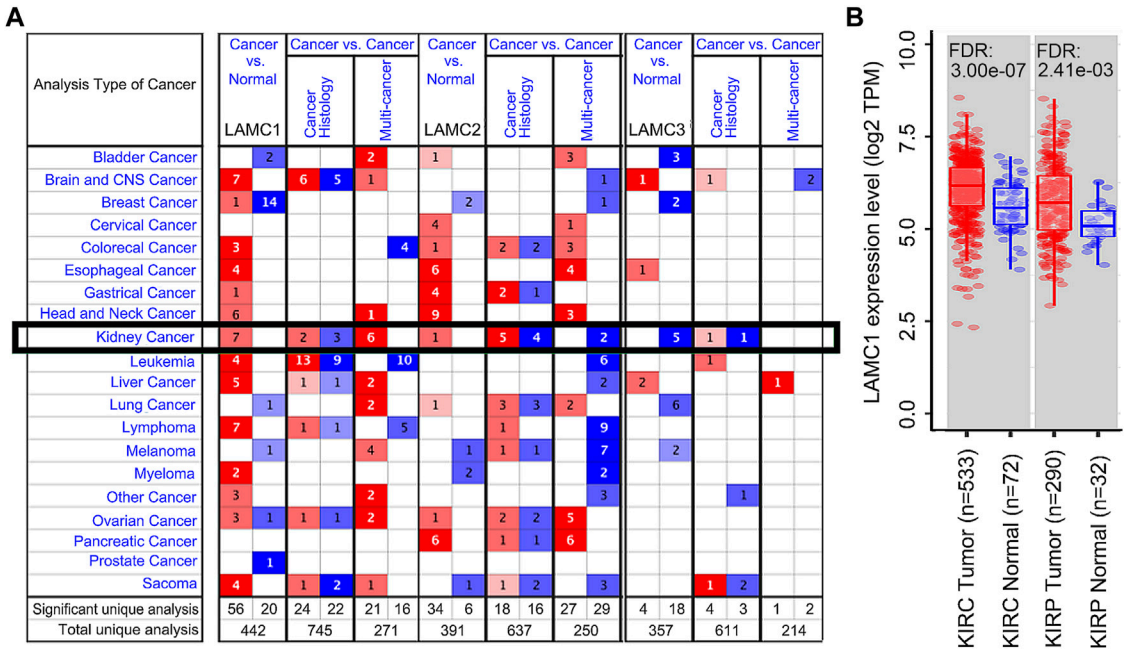

FIGURE 1
The expression levels of *LAMC1* across human cancers at mRNA level. **(A)** The expression levels of Laminin C (*LAMC*) family members in different types of cancers based on Oncomine database. The number in each cell represents significance datasets of genes up-regulated or down-regulated in a particular cancer. Red box represents high expression in tumors, blue box represents low expression in tumors and white box represents no difference in tumors and normal tissues. **(B)** Differential expression levels of *LAMC1* in KIRP and KIRC between tumor groups and normal groups based on TIMER database.

calculated using the Benjamini–Hochberg method, and 5% FDR (q-value <0.05) was set as the threshold.

Results

Expression levels of *LAMC* gene family in kidney cancer patients

Using the Oncomine database, we compared the differential expression levels of *LAMC* family members between cancers and its related normal tissues. Of the three members of the *LAMC* family, *LAMC1* and *LAMC2* were upregulated in kidney cancers, while *LAMC3* was downregulated in kidney cancers (Figure 1A). The significant changes to the expression of the *LAMC* family in different types of kidney cancer and normal kidney tissue are detailed in Supplementary Table S2. Furthermore, expression of *LAMC1* mRNA was found to be significantly higher in KIRP and KIRC samples based on the TIMER database (FDR <0.01, Figure 1B). *LAMC1* mRNA was also upregulated in many other types of tumors besides KIRP and KIRC (Supplementary Figure S1). We further used TCGA database to analyze the expression profile of *LAMC1* in KIRP and KIRC. Our results suggested that the data were of high quality, as the area under the ROC curve was 0.763 (95% CI, 69.5%–83.2%, FDR <0.01) for KIRP (Figure 2A) and 0.750 (95% CI, 69.7%–80.2%, FDR <0.01) for KIRC (Figure 2D). There was significantly enhanced *LAMC1* expression in KIRP compared with normal tissues (FDR = 5.32e-06, Figure 2B), and the result for paired samples also supported this trend (FDR = 8.19e-08, Figure 2C). Similarly, as shown in Figures 2E,F, higher *LAMC1* mRNA expression was also found in KIRC compared with normal tissues (FDR <0.001). We used tissue microarray to validate the LAMC1 protein expression in clinical samples. Three representative images of tissue microarray results are shown in Figure 2G. The analysis of IHC staining data showed that LAMC1 was positively expressed in the nucleus or cytoplasm in renal cancer tissues, and LAMC1 protein staining was stronger in KIRP and KIRC tissues compared with normal renal tissues, indicating higher expression of LAMC1 protein in RCC servers certain pathophysiological role (Figures 2G,H). Additionally, Figure 2H showed that the total immunoreactive scores for different tumor grades in KIRC. We consequently explored the expression of *LAMC1* in different clinicopathological parameters of KIRP and KIRC, including age, gender, nodal metastasis status, and cancer stage, based on the UALCAN database. As shown in Figure 3,

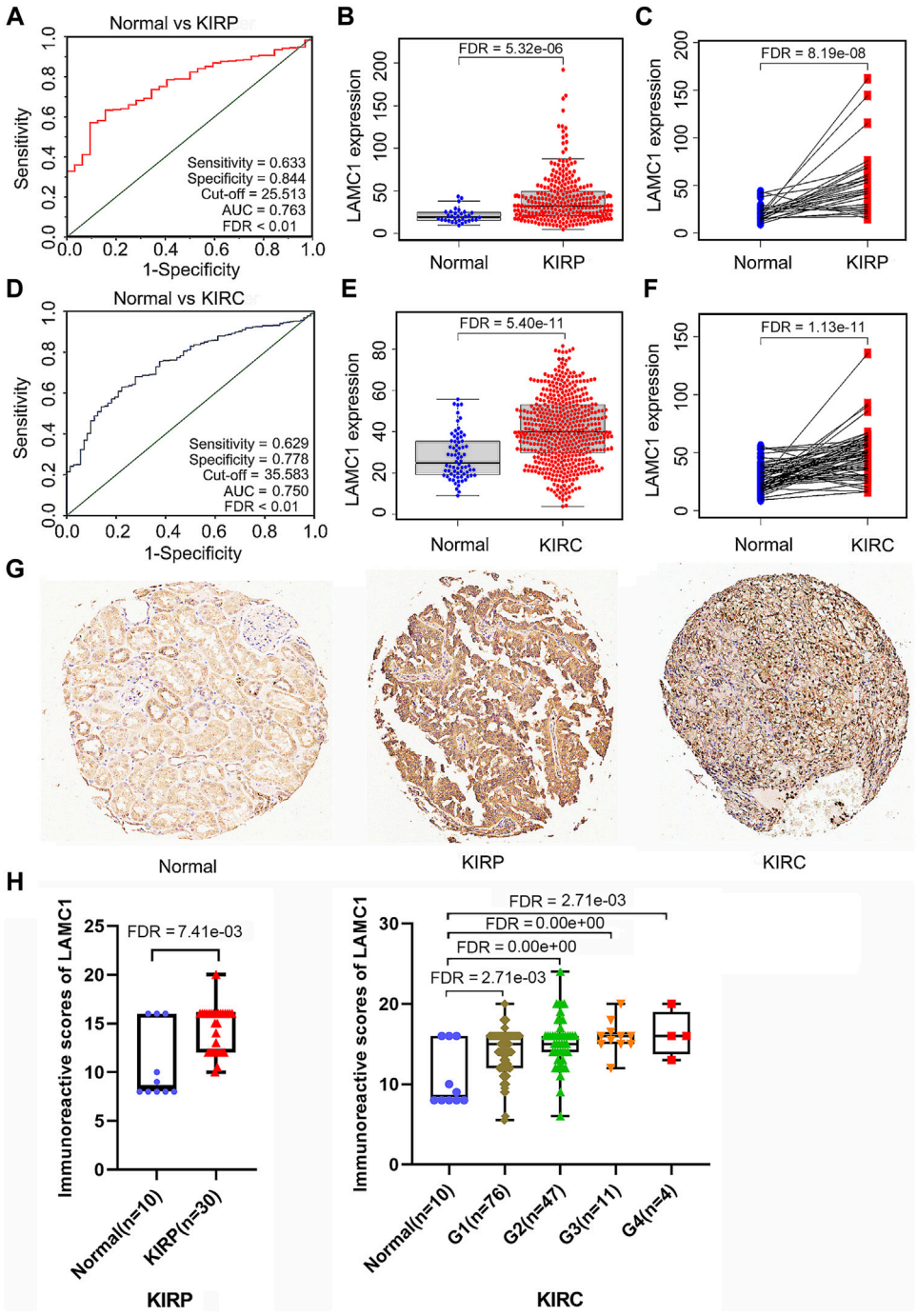

FIGURE 2
LAMC1 mRNA and protein expression levels in two types of renal carcinoma. **(A,D)** The receiver operating characteristic (ROC) curve for *LAMC1* expression in normal kidney tissue and kidney cancer was built based on data downloaded from TCGA database. **(B–C,E–F)** The mRNA level of *LAMC1* in kidney cancer and normal tissues. **(B–C)**, KIRP. **(B)**: N: T = 32:289; **(C)** N: T = 31:31, **(E–F)**, KIRC; **(E)** N: T = 72:532, **(F)** N: T = 72:72; The figure represents the number of the normal(N) or tumor(T) cases; **B** and **E**, unpaired *t*-test; **C** and **F**, paired *t*-test. **(G)** Three representative images of tissue microarray results are used here. Positive immunostaining was located in the nucleus or cytoplasm. Validation of protein expression of *LAMC1* in kidney cancer and normal tissues based on tissue microarray staining data. **(H)** The immunoreactive score of LAMC1 IHC staining presented by boxplot with Student's *t* test or one-way analysis of variance (ANOVA).

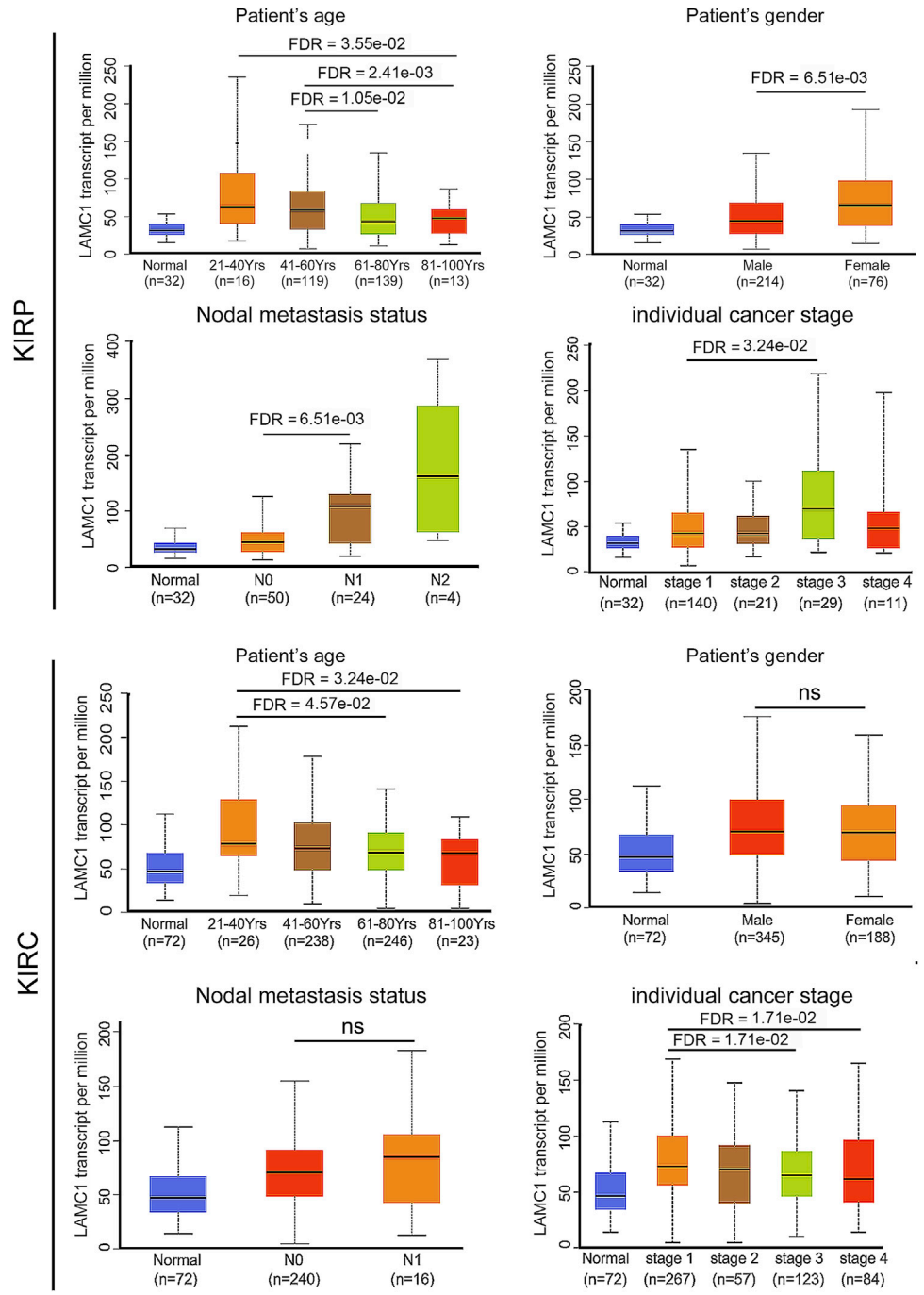

FIGURE 3
The relation of *LAMC1* expression to the clinicopathological features including age, gender, nodal metastasis status, and individual cancer stage in KIRP and KIRC.

patients that showed higher *LAMC1* expression in KIRP were 20–40 years old, female, of advanced nodal metastasis status and advanced stages of cancer (stage 3–4). Patients that showed higher *LAMC1* expression in KIRC were 20–40 years old and in the early stages of cancer (stage 1–2).

Survival outcomes and multivariate analysis

TCGA database was retrieved for further survival analysis. High expression of *LAMC1* was closely associated with poor OS

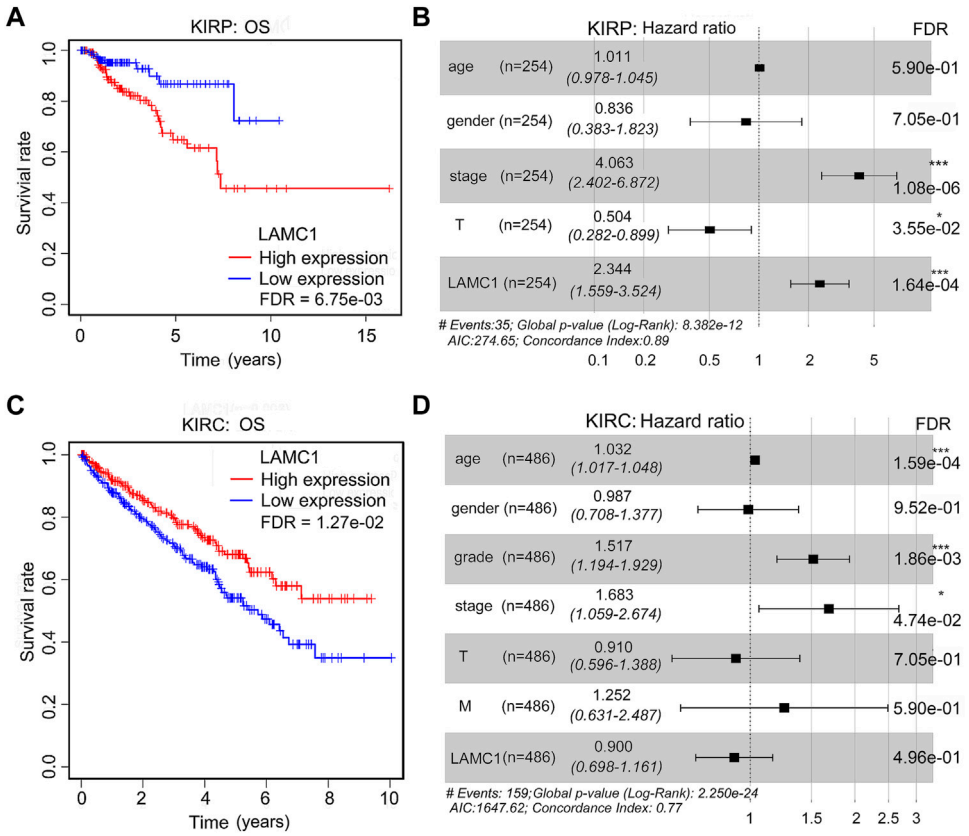

FIGURE 4
The prognostic signatures of *LAMC1* and clinical parameters in KIRP and KIRC patients. Correlation of different expression of *LAMC1* with survival (OS) of KIRP **(A)** and KIRC **(C)** patients. Survival data were analyzed using Kaplan-Meier method. High or low *LAMC1* expression level was determined in relation to its median expression value. The prognostic signatures of *LAMC1* expression and clinical parameters in KIRP**(B)** and KIRC**(D)** patients in the multivariate Cox analysis model presented as the forest plots.

of KIRP patients (FDR = 6.75e-03, Figure 4A) and better OS of KIRC patients (FDR = 1.27e-02, Figure 4C). According to the "survival" package of R calculation, the five-year survival rate of KIRP and KIRC patients with high expression of *LAMC1* was 64.8% and 66.8%, respectively, and the five-year survival rate of KIRP and KIRC patients with low expression of *LAMC1* was 86.8% and 52.9%, respectively (Supplementary Table S3). Using univariate and multivariate Cox analysis, the prognostic signatures of *LAMC1* and other clinical parameters for KIRP and KIRC were analyzed (Supplementary Table S4). The prognostic signatures of *LAMC1* and other clinical parameters in the multivariate Cox analysis model were presented as the forest plots (Figures 4B,D). For KIRP, the *LAMC1* expression level and stage were independent prognostic indicators in both univariate and multivariate Cox analysis models. Considering that the HR values of T classification fluctuates greatly in univariate and multivariate Cox analysis, we did not consider it to be statistically significant in KIRP. For KIRC, age, stage, and grade were the independent prognostic indicators in both univariate and multivariate Cox analysis models, and *LAMC1* lost its independent prognostic signature in KIRC in the multivariate Cox analysis model.

Correlation of *LAMC1* expression, immune infiltration and survival in RCC

Considering that tumor-infiltrating immune cells (TIICs) are potential therapeutic targets for cancer treatment progression (Sanmamed and Chen, 2018), we thus aimed to determine the composition of TIICs in RCC and further reveal the prognostic values. We used the TIMER database to analyze the correlation of *LAMC1* level with immune cell infiltration levels in RCC. For KIRP, *LAMC1* expression was positively correlated with $CD8^+$ T cells (R = 0.201, FDR = 2.83e-03), myeloid dendritic cells (R = 0.259, FDR = 1.10e-04) and neutrophils (R = 0.217, FDR = 1.35e-03) (Figure 5A). For KIRC, the *LAMC1* level showed a positive correlation with infiltrating levels of $CD4^+$ T cells (R = 0.311,

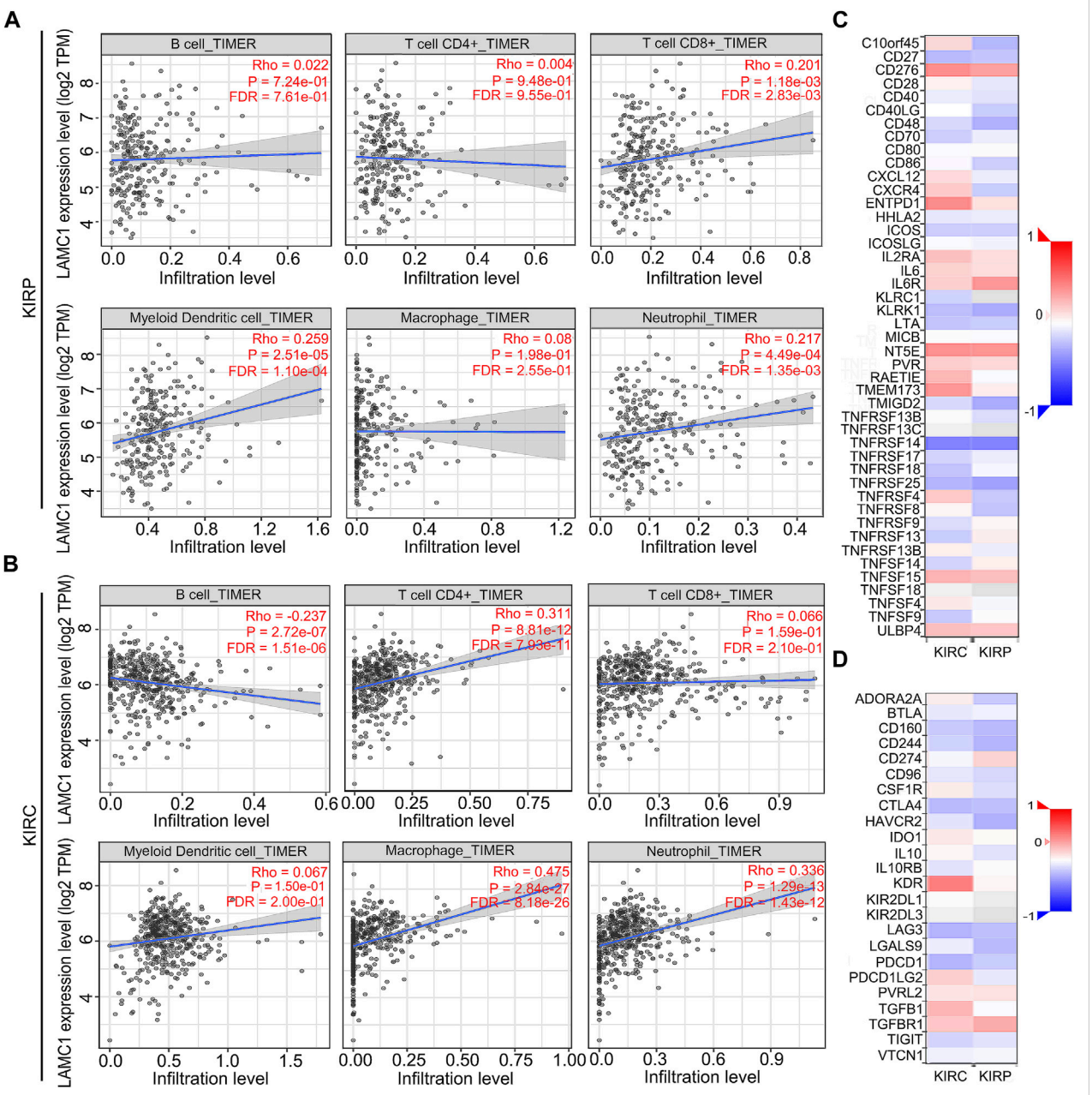

FIGURE 5
Correlation analysis of *LAMC1* expression and immune cell infiltration levels and immunoregulators in KIRP and KIRC. **(A,B)** Correlation between *LAMC1* expression and tumor immune cells in KIRP and KIRC samples identified using the TIMER algorithm. **(C)** Relationships between expression of *LAMC1* and 45 types of immunostimulators in human KIRP and KIRC using TISIDB database. Red color indicates positively related and blue color indicates the negatively related immunostimulators. **(D)** Relationships between expression of *LAMC1* and 24 types of immunoinhibitors in human KIRP and KIRC samples identified using TISIDB database. Red color indicates positively related and blue color indicates the negatively related immunoinhibitors.

FDR = 7.93e-11), macrophages (R = 0.475, FDR = 8.18e-26), and neutrophils (R = 0.336, FDR = 1.43e-12) and a negative correlation with B cells (R = −0.237, FDR = 1.51e-06) (Figure 5B). Similarly, the correlation between *LAMC1* and 45 immunostimulators in RCC is shown in Figure 5C, and the correlation between *LAMC1* and 24 immunoinhibitors in RCC is shown in Figure 5D. We noticed some immunomodulator-related genes with strong or significantly differential correlation with *LAMC1* expression, including *TGFB1*, *CD276*, *NT5E* and *KDR*. We used the GSCALite

TABLE 1 The Cox proportional hazard model of six tumor-infiltrating immune cells in KIRP and KIRC.

Cell type	KIRP				KIRC			
	Coefficient	HR	95% CI	FDR value	Coefficient	HR	95% CI	FDR value
B cell	5.94	378.41	3.01–47528.65	**2.92e-02**	−0.89	0.41	0.02–9.31	6.34e-01
CD8+ T cell	12.53	275289.09	1212.18–62518734.86	**0.00e+00**	−1.95	0.14	0.03–0.66	**2.34e-02**
CD4+ T cell	6.04	419.18	0.27–641305.31	1.48e-01	−0.18	0.84	0.06–11.01	9.20e-01
Macrophage	−3.99	0.02	0.00–2.89	1.66e-01	−2.87	0.06	0.01–0.57	**2.65e-02**
Neutrophil	−3.95	0.02	0.00–7620.69	6.12e-02	4.17	64.50	1.32–3147.94	5.82e-02
Dendritic	−4.47	0.01	0.00–0.78	6.01e-02	1.56	4.73	0.85–26.37	1.12e-01

Bold texts indicate statistically significant according to threshold

database to further explore the expression and prognosis of *LAMC1* and above genes, and provided a potential miRNA regulatory mechanism for gene expression (Supplementary Figure S2, Supporting file 6). Predicted by database analysis, the miR-29 and miR-200 families are prominent in targeting the above-mentioned gene expression. Since microRNAs play important roles in cancer progression, follow-up experimental validation is still required.

Prognostic potential of *LAMC1* expression in RCC based on immune cell infiltration

Given that the *LAMC1* levels are related to TIICs in KIRP and KIRC (Figures 5A,B), we speculated that *LAMC1* may affect the prognosis of KIRP and KIRC patients partly through mediating immune cell infiltration. We examined the prognostic value of tumor infiltrating immune cells in KIRP and KIRC using Cox proportional hazard model by TIMER. The results indicated that B cells (HR = 378.414, FDR = 2.92e-02) and $CD8^+$ T cells (HR = 275289.087, FDR = 0.00) were significantly correlated with clinical prognosis in KIRP (Table 1). Besides, $CD8^+$ T cells (HR = 0.143, FDR = 2.34e-02) and Macrophage (HR = 0.006, FDR = 2.65e-02) were significantly correlated with clinical prognosis in KIRC (Table 1). Kaplan–Meier survival curves for RCC patients with differential *LAMC1* expression were constructed based on immune cells enrichment (Figure 6) or decrease (Figure 7). As shown in Figure 6, high *LAMC1* levels in the KIRP cohorts enriched with B cells (HR = 3.34, FDR = 1.73e-03), $CD4^+$ memory T cells (HR = 3.28, FDR = 4.34e-02), macrophages (HR = 3.13, FDR = 2.04e-03), NK T cells (HR = 2.57, FDR = 2.92e-02), Treg cells (HR = 4.27, FDR = 5.57e-03), and Th1 cells (FDR = 2.20e-02) had a poor OS. Surprisingly, high expression of *LAMC1* had a poor OS in KIRC enriched with Th1 cells (HR = 3.94, FDR = 2.20e-02), but a better OS in $CD8^+$ T cells (HR = 0.56, FDR = 2.24e-03). Similarly, as shown in Figure 7, high *LAMC1* expression in KIRP had a poor OS in the cohorts decreased with $CD4^+$ memory T cells (HR = 3.53, FDR = 1.40e-02), $CD8^+$ T cells (HR = 4.88, FDR = 7.38e-04), Th1 cells (HR = 3.35, FDR = 1.20e-03) and Th2 cells (HR = 2.64, FDR = 6.17e-03). However, high *LAMC1* expression in KIRC had a better OS in the cohorts decreased with $CD4^+$ memory T cells (HR = 0.36, FDR = 1.13e-03), macrophages (HR = 0.23, FDR = 9.60e-04), Treg cells (HR = 0.54, FDR = 2.48e-03), Th1 cells (HR = 0.63, FDR = 9.75e-03) and Th2 cells (HR = 0.57, FDR = 1.91e-03). These results supported our prediction that a high *LAMC1* expression level in KIRP and KIRC affected prognosis partly because of the different TIIC infiltration levels.

The relationships between *LAMC1* expression and immunity, neoantigen and TMB

To further evaluate association of *LAMC1* and immune microenvironment in RCC, we analyzed the relation of *LAMC1* expression to the Cancer-Immunity Cycle, immune neoantigens appearance and tumor mutational burden (TMB). The activities of Cancer-Immunity Cycle can be roughly divided into seven steps. Our results showed that most of activities of Cancer-Immunity Cycle were higher in high *LAMC1* expression groups in KIRC and only just a few steps showed higher immunoactivity in KIRP (Supplementary Figure S3, Supporting file 7). In addition, the ability to recruit $CD8^+$ T cells was significantly enhanced in the KIRC group with high *LAMC1* gene expression. We used GSEABase analysis to evaluate immune, stromal and estimates scores in two types of RCC, depending on *LAMC1* expression. Then we found *LAMC1* gene expression had a weak negative correlation with immune scores in KIRP (R = −0.181, FDR = 4.72e-03) and a moderate positive correlation with stromal scores in KIRC (R = 0.441, FDR = 2.52e-25) (Figures 8A,B). The estimate immune scores also showed a positive correlation in KIRC (R = 0.172, FDR = 2.65e-04) (Figure 8C). Then, we performed the analysis for the association of *LAMC1* expression and the number of immune neoantigens, which showed a weak positive correlation in KIRC (R = 0.101, FDR = 6.89e-02) (Figure 8D). However, *LAMC1* gene expression had no significant correlation with TMB in both types of renal cancer (Figure 8E).

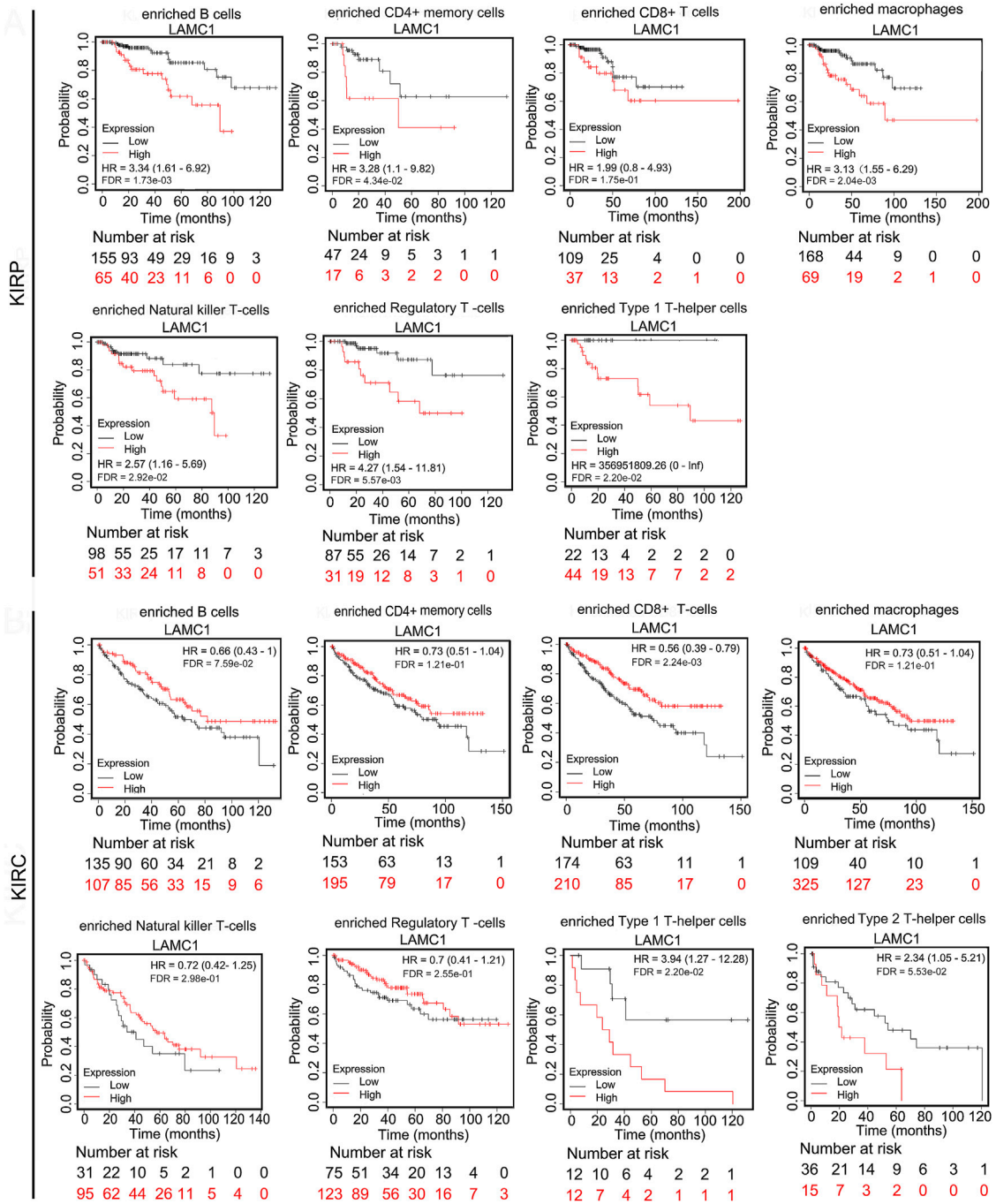

FIGURE 6
Kaplan–Meier survival curves for RCC patients with differential *LAMC1* expression were constructed based on immune cells enrichment in RCC tumors.

Mutation, CNV and methylation analysis of *LAMC1* gene

To assess the cause of elevated *LAMC1* levels in KIRP and KIRC, we used the cBioPortal, UCSC Xena and SurvivalMeth databases to probe the *LAMC1* methylation level, mutations, and CNV status. The results from the cBioPortal dataset showed that *LAMC1* expression was negatively correlated with methylation in KIRP (R = −0.22, FDR = 9.63e-04) and KIRC (R = −0.31, FDR = 1.31e-06) (Supplementary Figure S4A,B, Supporting file 8).

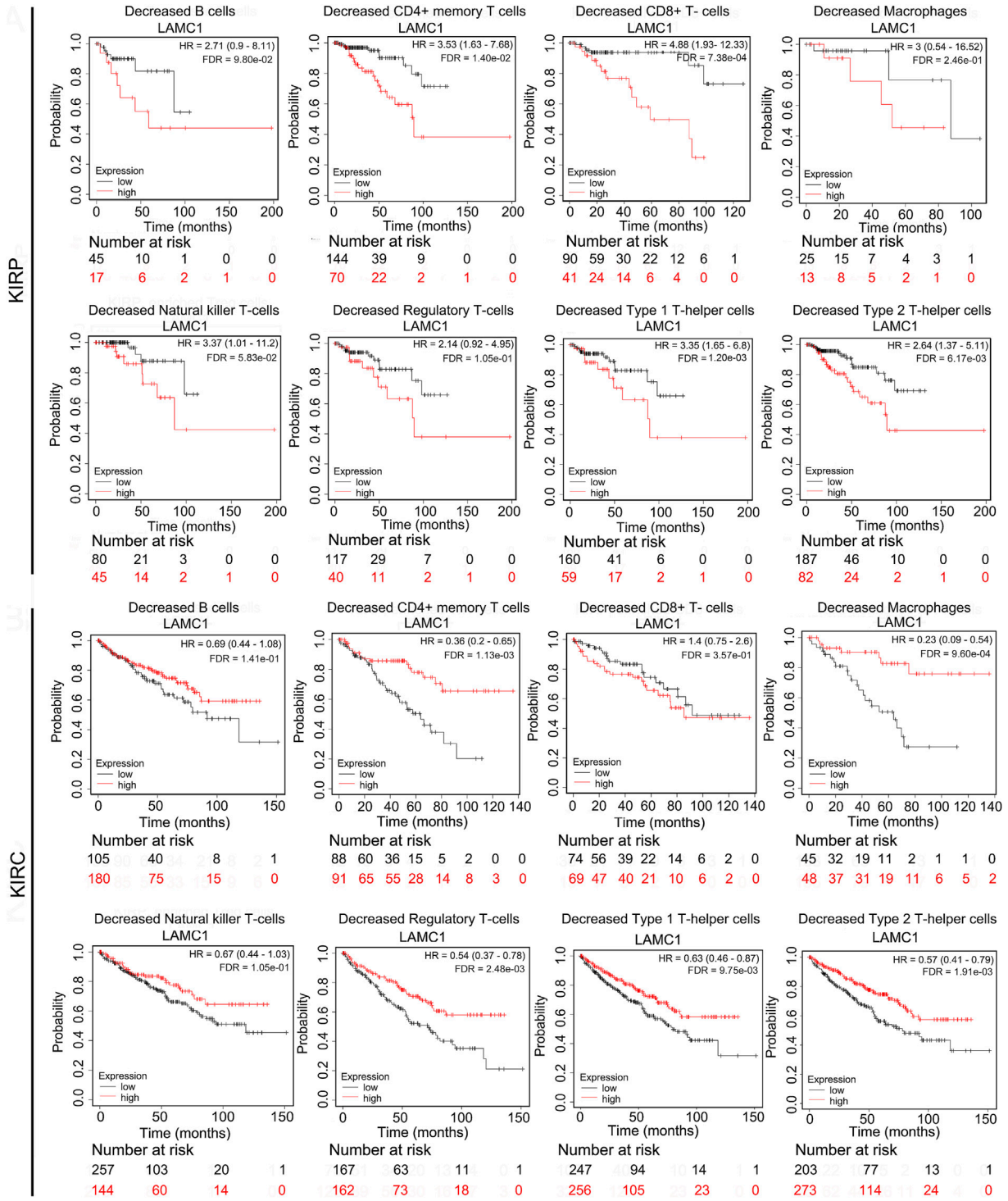

FIGURE 7
Kaplan–Meier survival curves for RCC patients with differential *LAMC1* expression were constructed based on immune cells depletion in RCC tumors.

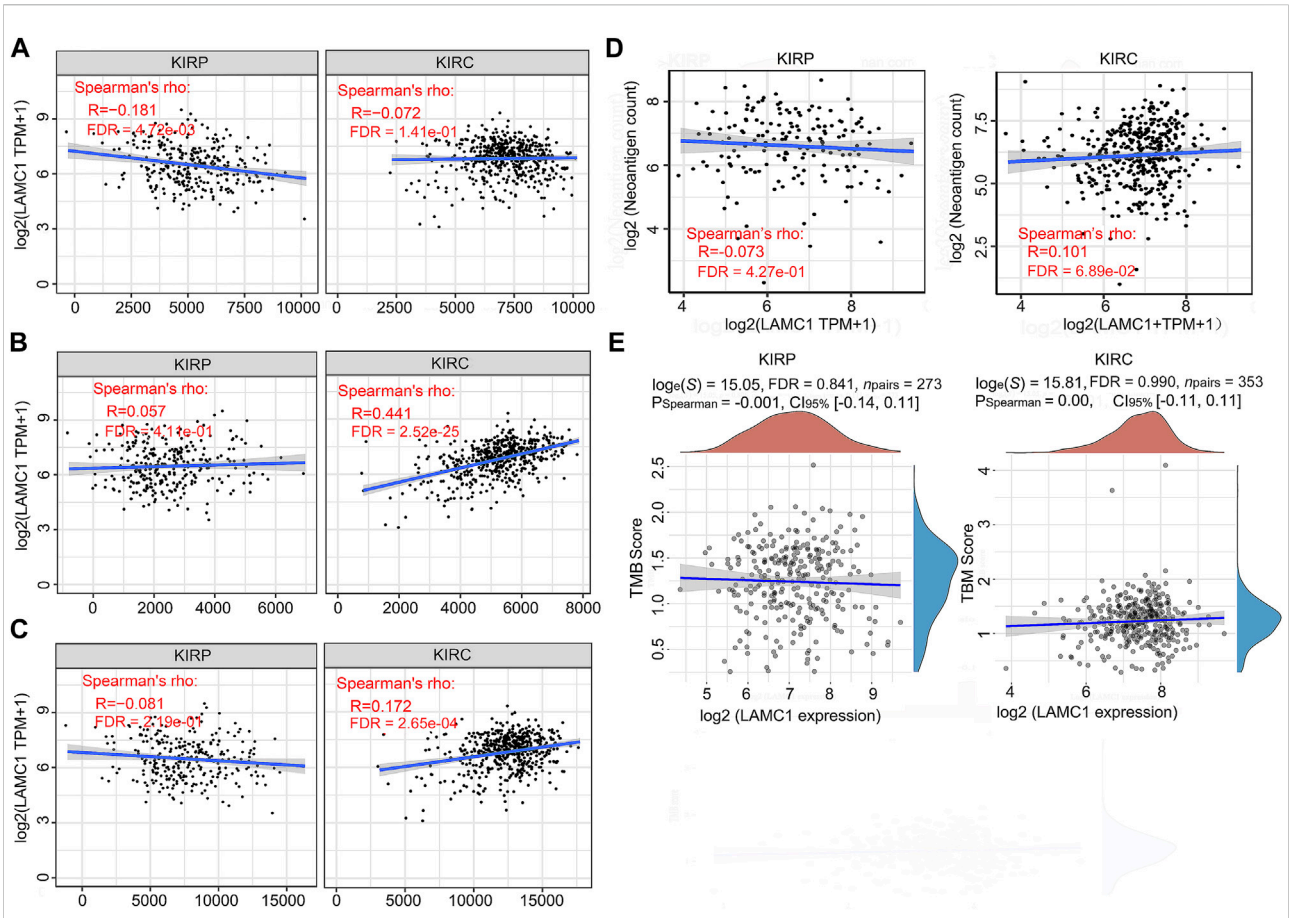

FIGURE 8
The relationships between *LAMC1* expression and tumor immune microenvironment, neoantigens appearance and TMB. **(A)** Correlation analysis between *LAMC1* expression and immune scores in KIRP and KIRC. **(B)** Correlation analysis between *LAMC1* expression and stromal scores in KIRP and KIRC. **(C)** Correlation analysis between *LAMC1* expression and estimate immune scores in KIRP and KIRC. **(D)** Correlation analysis between *LAMC1* expression and the number of neoantigens in KIRP and KIRC. **(E)** Correlation analysis between *LAMC1* expression and TMB scores in KIRP and KIRC. TMB, Tumor mutational burden.

Among the subgroups with different CNV, diploid was the dominant type for both KIRP and KIRC (Supplementary Figure S4C,D, Supporting file 8). We studied 831 samples from TCGA database and showed that the mutation rate of *LAMC1* in KIRP and KIRC was very low (<1%) (Supplementary Figure S4E, Supporting file 8). Heat map of *LAMC1* mRNA expression, methylation and copy number in patients with RCC and normal tissues were showed in Figures 9A,B. We found that *LAMC1* DNA was only locally methylated. Even that the correlation between *LAMC1* expression and methylation may be influenced by few outliers (Supplementary Figure S4B, Supporting file 8), the results of SurvivalMeth database further displayed the lower methylation level of *LAMC1* in both KIRP and KIRC (FDR <0.001, Figures 9C,D). Therefore, we concluded that DNA methylation of *LAMC1* was reduced in KIRP and KIRC tissues compared with that in normal tissues. According to UCSC Xena database, methylation of *LAMC1* was not associated with OS prognosis of KIRP and KIRC (FDR >0.1, Figures 9E,F), while high CNV of *LAMC1* indicated poor OS in both KIRP and KIRC (FRD <0.05, Figures 9G,H).

LAMC1-associated signaling pathways, Co-expression network, functional enrichment, and drug sensitivity in RCC

To screen for differentially activated signaling pathways in KIRP and KIRC, we compared high and low *LAMC1* expression datasets by GSEA analysis. According to the normalized enrichment scores, significantly enriched signaling pathways were identified. Adherens junctions, extracellular matrix receptor interaction, the MAPK (mitogen-activated protein kinase) signaling pathway, the TGF-β (transforming growth factor beta) signaling pathway, and the Wnt signaling

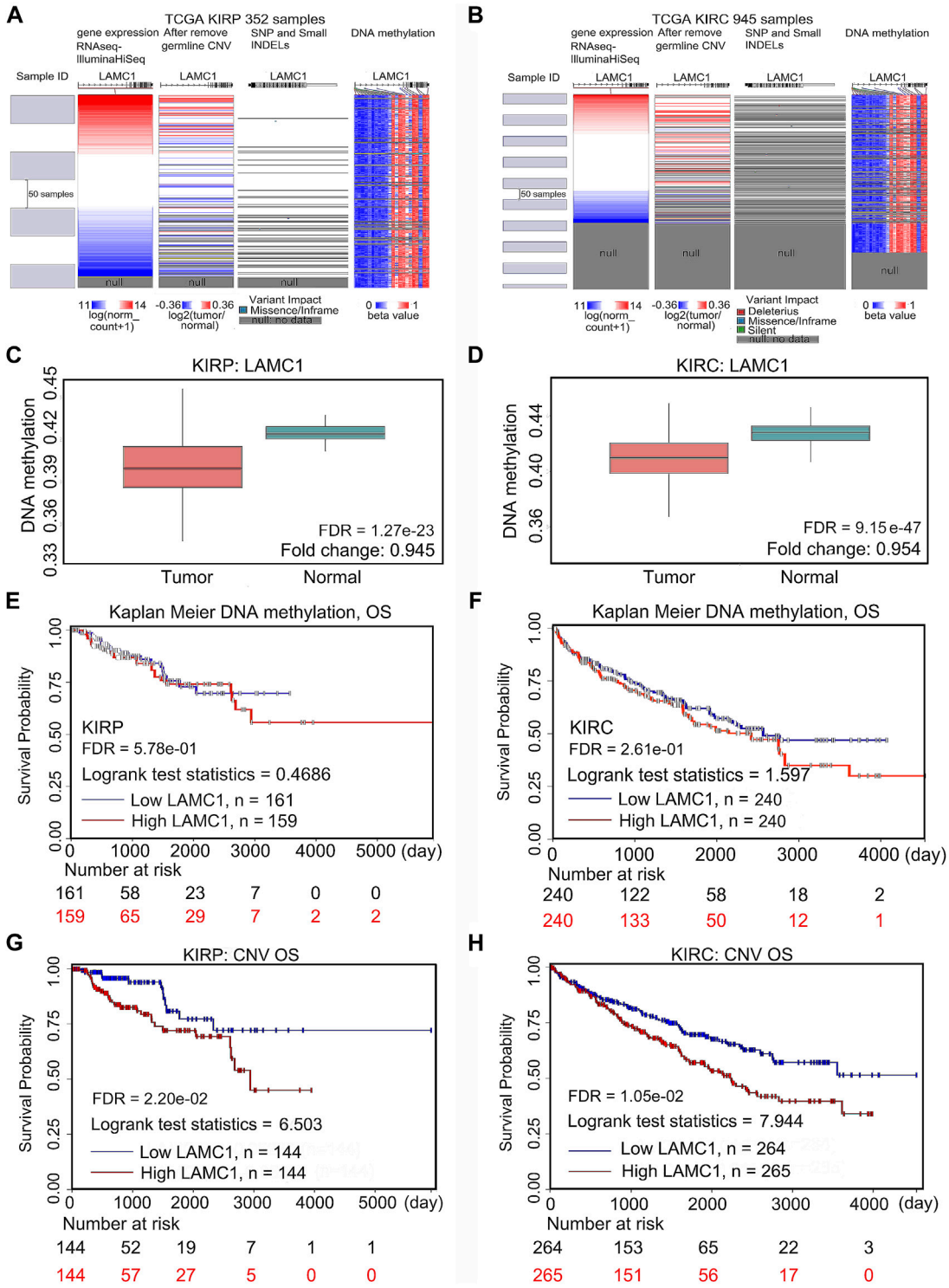

FIGURE 9
Mutation, CNV, and methylation of *LAMC1* and prognostic value of the *LAMC1* gene expression. **(A,B)** Heatmap showing the correlations between *LAMC1* mRNA and somatic mutations, CNV, and methylation in KIRP **(A)** and KIRC **(B)** using UCSC Xena database. **(C,D)** Comparison of *LAMC1* DNA methylation between normal kidney tissues and KIRP **(C)** and KIRC **(D)** tissues using survivalMeth database. **(E,F)** Relationship between *LAMC1* DNA methylation and OS in KIRP **(E)** and KIRC**(F)** using UCSC Xena. **(G,H)** Relationship between *LAMC1* CNV and OS in KIRP**(G)** and KIRC**(H)** using UCSC Xena. OS: overall survival; CNV: copy number variation.

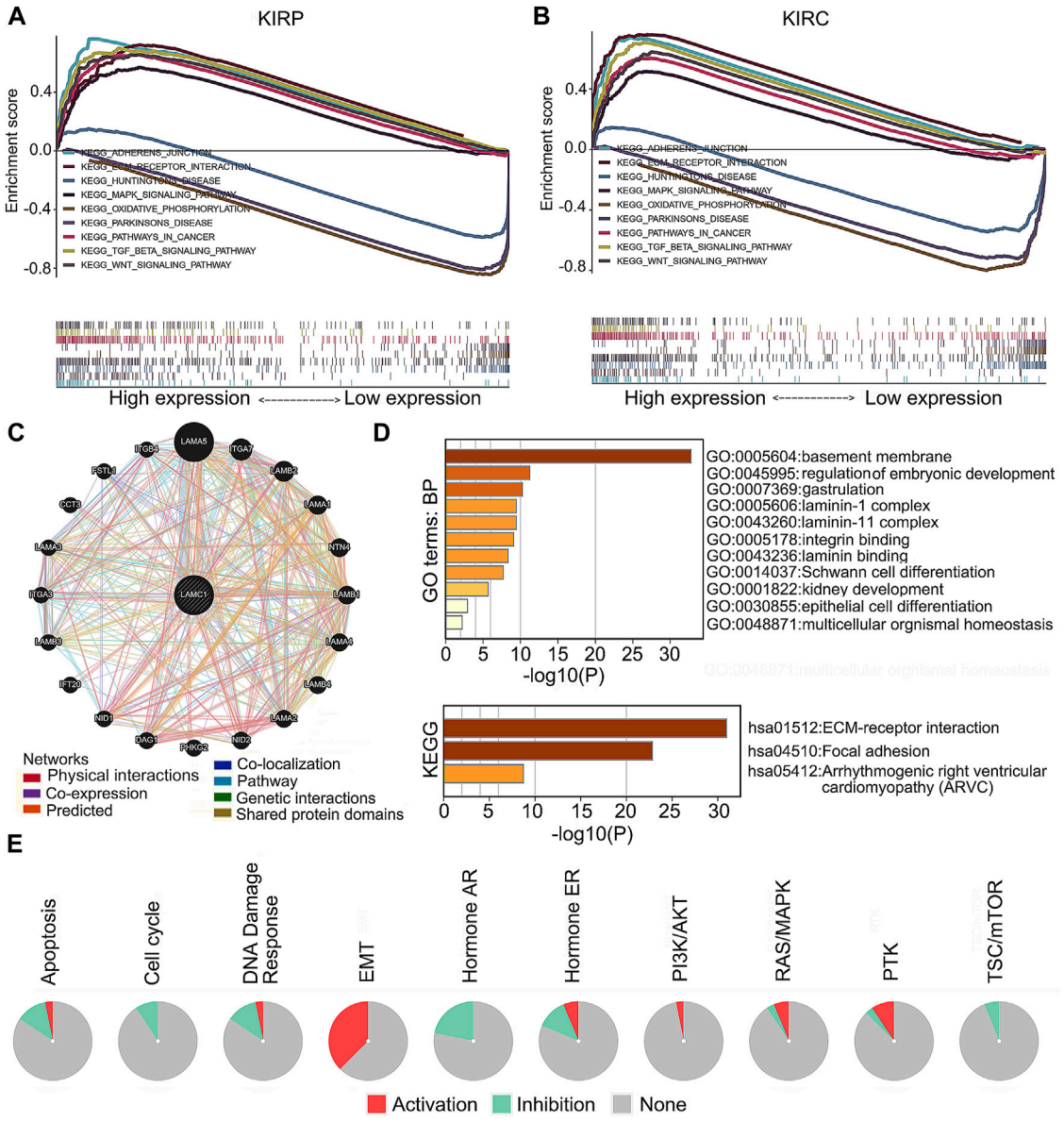

FIGURE 10
LAMC1-associated signaling pathways, co-expression network and functional enrichment. **(A,B)** A pathway enrichment analysis of a rank-ordered gene list using the GSEA software for the high and low *LAMC1* expression in KIRP **(A)** and KIRC **(B)**. **(C)** The co-expression network of *LAMC1* constructed by GeneMANIA. The node size represents the strength of interactions, and the line color represents the types of interactions. **(D)** Effect of *LAMC1* on the biological processes. The histograms show the main biological processes in which *LAMC1* interacting genes (as predicted by the GO and KEGG enrichment analyses) are involved, constructed using the Metascape portal (enrichment conditions: min overlap, three; *p*-value cutoff, 0.01; min enrichment, 1.5). **(E)** Effect of *LAMC1* on the key pathways in cancers detected using GSCALite database. Red represents promotion; green represents inhibition.

pathway were differentially associated with the high *LAMC1* expression phenotype. At the same time, gene sets related to oxidative phosphorylation, Huntington's disease, and Parkinson's disease were differentially associated with the low *LAMC1* expression phenotype (Figures 10A,B). In addition, the functional networks between *LAMC1* and other genes were assessed by GeneMANIA, and LAMA5 displayed the most complex connection with *LAMC1* (Figure 10C). Additionally, biological processes (BP) and pathways of *LAMC1*-interacting genes enriched in GO and KEGG were evaluated by Metascape. We found that the basement membrane formation was the most significantly enriched BP, and signaling initiated by ECM–receptor interaction and focal adhesions formation were the most significant pathways (Figure 10D). We also evaluated

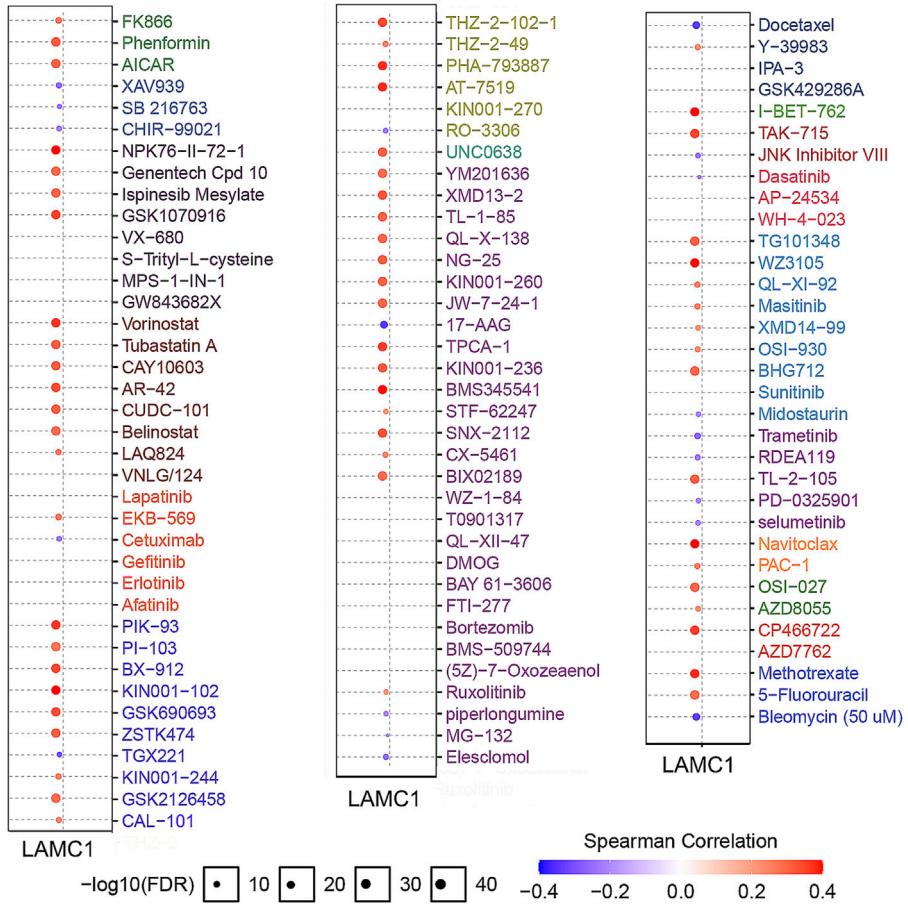

FIGURE 11
Analysis of drug resistance based on IC50 drug data from the GDSC database (GSCALite). A positive Spearman correlation (red) means that high gene expression correlates with drug resistance, a negative Spearman correlation (blue) means that low gene expression correlates with drug resistance.

the role of *LAMC1* in the activity of cancer-related pathways and drug sensitivity in RCC by GSCALite. We found that the epithelial–mesenchymal transition (EMT) process was mainly activated while Hormone AR signaling pathway was most inhibited in RCC (Figure 10E). Finally, when considering the drug sensitivity associated with *LAMC1* expression, RCCs with high *LAMC1* expression were resistant to sets of drugs or small molecules such as phenformin, NPK76-II-72-1, vorinostat, and PIK93, whereas RCCs with lower levels of *LAMC1* expression were resistant to small sets of drugs or small molecules including XAV939, 17-AAG, docetaxel, and bleomycin (Figure 11).

Discussion

LAMC1 is mainly expressed in the basement membrane and participates in several biological and pathological processes, including adhesion, invasion, and migration (Aumailley, 2013; Ke et al., 2013). In addition, LAMC1 may participate in some signaling pathways that affect cell proliferation and migration by activating intracellular downstream effectors (Ke et al., 2013). Interestingly, the *LAMC* gene family is also involved in kidney-related growth, development, and disease. An early report showed that LAMC1 interacts with nidogen to induce ureteric bud protrusion from the Wolffian duct in mammalian renal development (Willem et al., 2002). Besides, increased LAMC1 protein was also detected in glomerular basement membrane of kidney samples from chronic kidney disease (CKD) patients (Setty et al., 2012). A LAMC1 epitope fragment, LG1M, is a marker of remodeling and degradation of the glomerular and tubular basement membrane, and is related to disease progression and mortality in CKD (Holm Nielsen et al., 2018). Furthermore, a gene expression profile analysis identified the *LAMC1* gene as up-regulated in aggressive KIRC and as a candidate gene that differentiate aggressive from indolent KIRC phenotypes (Lane et al., 2009). In line with

these early reports, it appears that high expression of *LAMC1* may be involved in the progression of kidney disease, including cancer. However, the correlation between *LAMC1* expression and the clinicopathological characteristics of RCC, as well as the prognostic significance of *LAMC1* expression for RCC have not been well studied.

In this study, bioinformatics analyses of high-throughput RNA sequencing data from TCGA revealed significantly increased *LAMC1* expression in RCC compared with the adjacent normal renal tissues, and the LAMC1 protein levels in RCC were also increased compared with the normal tissues based on tissue microarray data. Our results summarized for the first time the data on *LAMC1* expression in RCC. To explore the role of high expression of *LAMC1* in RCC, we further evaluated its effect on prognosis. According to the results of the KIRP survival analysis, patients with high *LAMC1* expression had worse survival than those with low expression, whereas in KIRC, high *LAMC1* expression predicted better survival. Univariate and multivariate Cox analysis of the TCGA database showed that *LAMC1* expression is a potential independent marker of poor prognosis in KIRP. Interestingly, KIRC showed the opposite result. The association between *LAMC1* expression and the clinical characteristics of RCC patients also confirmed this observation. These results suggested that *LAMC1* could be used as a marker of the cancer process to distinguish RCC patients from the normal persons; besides, the high expression of *LAMC1* in KIRP and KIRC has completely different clinicopathological significance and prognostic value.

Given that high *LAMC1* expression has significantly different prognostic value in KIRP and KIRC, we next tried to discover its potential regulatory mechanism. By analyzing the correlation between the *LAMC1* gene and immune cells, we found that *LAMC1* expression in KIRP was positively correlated with $CD8^+$ T cells, myeloid dendritic cells and neutrophils. For KIRC, the *LAMC1* expression level showed a positive correlation with infiltrating levels of $CD4^+$ T cells, macrophages, and neutrophils and a negative correlation with B cells. It is known that immune cells infiltrating the tumor, including macrophages, Treg cells, and $CD8^+$ T cells can influence the outcome of RCC treatment (Desar et al., 2011; Cros et al., 2016; Zhu et al., 2019). Thus, the difference in immune cell types present in KIRP and KIRC probably affects the prognosis. In our study, high *LAMC1* expression in the cohort of KIRP patients with enriched Treg cells correlated with worse survival, whereas no such correlation was observed in the cohort of KIRP patients with fewer Treg cells. One of the mechanisms of tumor immune escape is that Treg cells produce immunosuppressive cytokines and receptors, which inhibit T cell activation and anti-tumor response (Sakaguchi et al., 2010; Speiser et al., 2016). The protective role of high levels of activated $CD8^+$ T cells in various tumors have been proposed (Youngblood et al., 2017; Yao et al., 2018). In our study, we found that high *LAMC1* expression in the cohort of KIRC patients with enriched $CD8^+$ T cells correlated with good survival, which was not significant for KIRP patients with high *LAMC1* expression; in contrast, high *LAMC1* expression in the cohort of KIRP patients with reduced $CD8^+$ T cells correlated with poor survival, which was not significant for KIRC patients; on the opposite, *LAMC1* high expression in decreased $CD8^+$ T cells cohort of KIRP showed a well OS but not in KIRC. This result suggests that *LAMC1* overexpression has different prognostic significance in KIRP and KIRC patient cohorts depending on $CD8^+$ cell levels. Notably, KIRP patients with high *LAMC1* expression and reduced numbers of $CD4^+$ memory T cells, Th1 cells, and Th2 cells had a worse prognosis, in contrast to similar cohorts in KIRC. These results indicate the potential functionality of assessing *LAMC1* expression and immune cell infiltration in the prognosis of RCC and treatment efficacy. Thus, KIRP and KIRC have different immune responses. The relationship between this complex immune cell infiltration and *LAMC1* expression affects the prognosis for RCC patients, but the underlined mechanism remains to be clarified, and the single-cell RNA sequencing may provide a potential solution to this problem.

Apart from the immune cells, immune factors also contribute to cancer progression. Using the TIMER database, we identified some of the immunoinhibitors and immunostimulators associated with *LAMC1* in KIRP and KIRC. The biological function of the insertion domain kinase receptor (*KDR*) is to regulate normal/pathological angiogenesis (Hoeben et al., 2004; Takahashi and Shibuya, 2005; Shibuya, 2010). Using the GSCALite database, we tested the correlation of *KDR* with prognosis in KIRC and KIRP, and showed that *KDR* is associated with poor survival in KIRP and better survival in KIRC. Our results are consistent with earlier reports suggesting that high *KDR* levels are significantly associated with poor prognosis for patients with KIRP (Kroeze et al., 2010). However, the positive association of *KDR* expression with survival in patients with KIRC requires further elucidation. Correlation analysis of expression between *LAMC1* and immunostimulators showed that *CD276* (*B7-H3*) and *NT5E* had a higher correlation with KIRP and KIRC. As a member of the B7 family of immunoregulatory ligands, *CD276* (*B7-H3*) plays a role in regulating the immune response (Picarda et al., 2016). High expression of B7-H3 protein correlates with poor outcome in patients with various types of cancer. We also observed that *CD276* is significantly associated with the poor prognosis of two kinds of RCC. Ecto-5′-nucleotidase (*NT5E/CD73*) mediates the sequential dephosphorylation of extracellular ATP to adenosine (Zimmermann, 1992). Increased signaling initiated by adenosine promotes the proliferation of Treg cells, the accumulation of intracellular cAMP, and the differentiation of tumor-associated

macrophages, thereby reducing the anti-tumor immune response (Vigano et al., 2019). The correlation between *LAMC1* expression and these molecules suggests a possible mechanism, signaling pathway, and prognostic value for *LAMC1* in tumor immunity. The current study also showed that tumor neoantigens appearance and TMB have no or very weak association with KIRP and KIRC; we therefore focused on the immune scores, stromal scores and estimate scores in KIRP and KIRC. However, only the results of stroma scores assessment showed KIRC to be moderately positive. These results suggested that the high expression of *LAMC1* in KIRC may be accompanied by a better immune microenvironment. The above results may help to explain the correlation between high *LAMC1* gene expression and the better prognosis in KIRC.

DNA methylation is one of multiple epigenetic marks that regulate gene expression in cells (Ehrlich, 2002). Hypomethylation of the gene body leads to the high expression of oncogenes (Yang et al., 2014). Our study found that hypomethylation of *LAMC1* in two kinds of RCC is related to high expression of the *LAMC1* gene. In the present work, we not only confirmed the hypomethylation of *LAMC1* in KIRC suggested by others (Wu et al., 2018), but additionally found the hypomethylation in the *LAMC1* gene in KIRP. However, *LAMC1* hypomethylation in KIRP and KIRC weakly correlates with prognosis in cancer patients. Thus, although *LAMC1* hypomethylation in KIRP and KIRC is associated with high *LAMC1* expression, alone, it does not contribute significantly to the prognosis of RCC patients. Copy number variations (CNV) influences gene expression in carcinogenesis (Hudler, 2012). In our study, we found that higher CNV values correlated with lower survival in both KIRP and KIRC. Therefore, the CNV of the *LAMC1* gene can be used as a prognostic tool in KIRP and KIRC.

To further evaluate the role of *LAMC1* in KIRP and KIRC, we performed Gene Set Enrichment Analysis (GSEA) using TCGA data. GSEA analysis showed that genes involved in adherens junctions, extracellular matrix receptor interaction, MAPK signaling pathway, TGF-β signaling pathway, and Wnt signaling pathway were differentially associated with the *LAMC1* high expression phenotype. In addition, the mTOR pathway (Motzer et al., 2008) and the VEGF signaling pathway (Turner, 2004; Yildiz et al., 2004) involved in the pathogenesis of renal cancer were also enriched in our current study (data not shown). The results of using two major processes to examine groups of genes involved in common biological activities, Gene Ontology (GO) and KEGG enrichment analyses, using the Metascape portal to identify *LAMC1*-interacting genes, were similar to those of the GSEA analysis. Finally, drug sensitivity analysis revealed that cases with high *LAMC1* expression were resistant to most drugs or small molecules in the GDSC database. These results suggested that expression of *LAMC1* is a potential biomarker for drug screening and might provide a basis for drug-targeted therapy.

In conclusion, we have explored the expression, prognosis, and potential carcinogenic mechanism of *LAMC1* in KIRP and KIRC patients. Enhanced expression of *LAMC1* indicates a poor prognosis in KIRP and a better prognosis in KIRC. These opposite prognostic features of *LAMC1* overexpression in the two types of renal carcinoma may be related to different tumor immune microenvironments and immunomodulator-associated molecules. The results of our study will help clinicians to assess the prognosis and guide treatment of patients with KIRP and KIRC. However, future analysis of an independent patient cohort based on other data sources and experimental validation of the biological significance of *LAMC1* expression in RCC is needed.

Data availability statement

The datasets presented in this study can be found in online repositories. The names of the repository/repositories and accession number(s) can be found in the article/ Supplementary Material.

Ethics statement

Ethical review and approval was not required for the study on human participants in accordance with the local legislation and institutional requirements. Written informed consent for participation was not required for this study in accordance with the national legislation and the institutional requirements.

Author contributions

Conceived and coordinated the study: WJ, BTL and ZHS. Searched literature and performed statistical analyses: JB, AZ, YH, XX, YY, SZ. Drafted the manuscript: JB, BL, YL and WJ. Read and approved the final manuscript: all authors.

Funding

This work was supported by grants from the Yangfan Plan Project of Guangdong Province (No. 4YF16007G). The funders had no role in the design of the study, collection, analysis, and interpretation of data, or writing the manuscript.

Acknowledgments

We thank Catherine Perfect, MA (Cantab), from LiwenBianji (Edanz) (www.liwenbianji.cn/), for editing the English text of a draft of this manuscript.

Conflict of interest

The authors declare that the research was conducted in the absence of any commercial or financial relationships that could be construed as a potential conflict of interest.

Publisher's note

All claims expressed in this article are solely those of the authors and do not necessarily represent those of their affiliated organizations, or those of the publisher, the editors and the reviewers. Any product that may be evaluated in this article, or claim that may be made by its manufacturer, is not guaranteed or endorsed by the publisher.

Supplementary material

The Supplementary Material for this article can be found online at: https://www.frontiersin.org/articles/10.3389/fmolb.2022.988777/full#supplementary-material

References

Aumailley, M. (2013). The laminin family. *Cell adh. Migr.* 7 (1), 48–55. doi:10.4161/cam.22826

Chandrashekar, D. S., Bashel, B., Balasubramanya, S. A. H., Creighton, C. J., Ponce-Rodriguez, I., Chakravarthi, B., et al. (2017). Ualcan: A portal for facilitating tumor subgroup gene expression and survival analyses. *Neoplasia* 19 (8), 649–658. doi:10.1016/j.neo.2017.05.002

Chen, D. S., and Mellman, I. (2013). Oncology meets immunology: The cancer-immunity cycle. *Immunity* 39 (1), 1–10. doi:10.1016/j.immuni.2013.07.012

Cros, J., Sbidian, E., Posseme, K., Letierce, A., Guettier, C., Benoît, G., et al. (2016). Nestin expression on tumour vessels and tumour-infiltrating macrophages define a poor prognosis subgroup of pt1 clear cell renal cell carcinoma. *Virchows Arch.* 469 (3), 331–337. doi:10.1007/s00428-016-1973-2

Desar, I. M., Jacobs, J. H., Hulsbergen-vandeKaa, C. A., Oyen, W. J., Mulders, P. F., van der Graaf, W. T., et al. (2011). Sorafenib reduces the percentage of tumour infiltrating regulatory T cells in renal cell carcinoma patients. *Int. J. Cancer* 129 (2), 507–512. doi:10.1002/ijc.25674

Ehrlich, M. (2002). DNA methylation in cancer: Too much, but also too little. *Oncogene* 21 (35), 5400–5413. doi:10.1038/sj.onc.1205651

Eichelberg, C., Junker, K., Ljungberg, B., and Moch, H. (2009). Diagnostic and prognostic molecular markers for renal cell carcinoma: A critical appraisal of the current state of research and clinical applicability. *Eur. Urol.* 55 (4), 851–863. doi:10.1016/j.eururo.2009.01.003

Engbring, J. A., and Kleinman, H. K. (2003). The basement membrane matrix in malignancy. *J. Pathol.* 200 (4), 465–470. doi:10.1002/path.1396

Escudier, B. (2007). Advanced renal cell carcinoma: Current and emerging management strategies. *Drugs* 67 (9), 1257–1264. doi:10.2165/00003495-200767090-00002

Ferlay, J., Steliarova-Foucher, E., Lortet-Tieulent, J., Rosso, S., Coebergh, J. W., Comber, H., et al. (2013). Cancer incidence and mortality patterns in europe: Estimates for 40 countries in 2012. *Eur. J. Cancer* 49 (6), 1374–1403. doi:10.1016/j.ejca.2012.12.027

Frank, I., Blute, M. L., Cheville, J. C., Lohse, C. M., Weaver, A. L., Leibovich, B. C., et al. (2003). A multifactorial postoperative surveillance model for patients with surgically treated clear cell renal cell carcinoma. *J. Urol.* 170 (6), 2225–2232. doi:10.1097/01.ju.0000095541.10333.a7

Geissler, K., Fornara, P., Lautenschläger, C., Holzhausen, H. J., Seliger, B., and Riemann, D. (2015). Immune signature of tumor infiltrating immune cells in renal cancer. *Oncoimmunology* 4 (1), e985082. doi:10.4161/2162402x.2014.985082

Goldman, M. J., Craft, B., Hastie, M., Repečka, K., McDade, F., Kamath, A., et al. (2020). Visualizing and interpreting cancer genomics data via the Xena platform. *Nat. Biotechnol.* 38 (6), 675–678. doi:10.1038/s41587-020-0546-8

Gritsenko, P. G., Ilina, O., and Friedl, P. (2012). Interstitial guidance of cancer invasion. *J. Pathol.* 226 (2), 185–199. doi:10.1002/path.3031

Han, Z. R., Jiang, X. L., and Fan, W. C. (2021). LAMC1 is related to the poor prognosis of patients with gastric cancer and facilitates cancer cell malignancies. *Neoplasma* 68 (4), 711–718. doi:10.4149/neo_2021_201117N1239

Hoeben, A., Landuyt, B., Highley, M. S., Wildiers, H., Van Oosterom, A. T., and De Bruijn, E. A. (2004). Vascular endothelial growth factor and angiogenesis. *Pharmacol. Rev.* 56 (4), 549–580. doi:10.1124/pr.56.4.3

Holm Nielsen, S., Guldager Kring Rasmussen, D., Brix, S., Fenton, A., Jesky, M., Ferro, C. J., et al. (2018). A novel biomarker of laminin turnover is associated with disease progression and mortality in chronic kidney disease. *PLoS One* 13 (10), e0204239. doi:10.1371/journal.pone.0204239

Hsieh, J. J., Purdue, M. P., Signoretti, S., Swanton, C., Albiges, L., Schmidinger, M., et al. (2017). Renal cell carcinoma. *Nat. Rev. Dis. Prim.* 3, 17009. doi:10.1038/nrdp.2017.9

Hudler, P. (2012). Genetic aspects of gastric cancer instability. *ScientificWorldJournal.* 2012, 761909. doi:10.1100/2012/761909

Jardim, D. L., Goodman, A., de Melo Gagliato, D., and Kurzrock, R. (2021). The challenges of tumor mutational burden as an immunotherapy biomarker. *Cancer Cell* 39 (2), 154–173. doi:10.1016/j.ccell.2020.10.001

Ke, H. L., Ke, R. H., Li, B., Wang, X. H., Wang, Y. N., and Wang, X. Q. (2013). Association between laminin γ1 expression and meningioma grade, recurrence, and progression-free survival. *Acta Neurochir.* 155 (1), 165–171. doi:10.1007/s00701-012-1512-0

Kroeze, S. G., Bijenhof, A. M., Bosch, J. L., and Jans, J. J. (2010). Diagnostic and prognostic tissuemarkers in clear cell and papillary renal cell carcinoma. *Cancer Biomark.* 7 (6), 261–268. doi:10.3233/cbm-2010-0195

Kunitomi, H., Kobayashi, Y., Wu, R. C., Takeda, T., Tominaga, E., Banno, K., et al. (2020). LAMC1 is a prognostic factor and a potential therapeutic target in endometrial cancer. *J. Gynecol. Oncol.* 31 (2), e11. doi:10.3802/jgo.2020.31.e11

Lane, B. R., Li, J., Zhou, M., Babineau, D., Faber, P., Novick, A. C., et al. (2009). Differential expression in clear cell renal cell carcinoma identified by gene expression profiling. *J. Urol.* 181 (2), 849–860. doi:10.1016/j.juro.2008.10.069

Li, T., Fan, J., Wang, B., Traugh, N., Chen, Q., Liu, J. S., et al. (2017). Timer: A web server for comprehensive analysis of tumor-infiltrating immune cells. *Cancer Res.* 77 (21), e108–e110. doi:10.1158/0008-5472.Can-17-0307

Linehan, W. M., and Ricketts, C. J. (2014). Decade in review-kidney cancer: Discoveries, therapies and opportunities. *Nat. Rev. Urol.* 11 (11), 614–616. doi:10.1038/nrurol.2014.262

Liu, C. J., Hu, F. F., Xia, M. X., Han, L., Zhang, Q., and Guo, A. Y. (2018). GSCALite: A web server for gene set cancer analysis. *Bioinformatics* 34 (21), 3771–3772. doi:10.1093/bioinformatics/bty411

Ljungberg, B., Albiges, L., Abu-Ghanem, Y., Bensalah, K., Dabestani, S., Fernández-Pello, S., et al. (2019). European association of urology guidelines on renal cell carcinoma: The 2019 update. *Eur. Urol.* 75 (5), 799–810. doi:10.1016/j.eururo.2019.02.011

Motzer, R. J., Escudier, B., Oudard, S., Hutson, T. E., Porta, C., Bracarda, S., et al. (2008). Efficacy of everolimus in advanced renal cell carcinoma: A double-blind, randomised, placebo-controlled phase III trial. *Lancet* 372 (9637), 449–456. doi:10.1016/s0140-6736(08)61039-9

Motzer, R. J., Rini, B. I., McDermott, D. F., Redman, B. G., Kuzel, T. M., Harrison, M. R., et al. (2015). Nivolumab for metastatic renal cell carcinoma: Results of a randomized phase II trial. *J. Clin. Oncol.* 33 (13), 1430–1437. doi:10.1200/jco.2014.59.0703

Nagy, Á., Munkácsy, G., and Győrffy, B. (2021). Pancancer survival analysis of cancer hallmark genes. *Sci. Rep.* 11 (1), 6047. doi:10.1038/s41598-021-84787-5

Oudard, S., George, D., Medioni, J., and Motzer, R. (2007). Treatment options in renal cell carcinoma: Past, present and future. *Ann. Oncol.* 18 (10), x25–31. doi:10.1093/annonc/mdm411

Picarda, E., Ohaegbulam, K. C., and Zang, X. (2016). Molecular pathways: Targeting B7-H3 (CD276) for human cancer immunotherapy. *Clin. Cancer Res.* 22 (14), 3425–3431. doi:10.1158/1078-0432.Ccr-15-2428

Rhodes, D. R., Kalyana-Sundaram, S., Mahavisno, V., Varambally, R., Yu, J., Briggs, B. B., et al. (2007). Oncomine 3.0: Genes, pathways, and networks in a collection of 18, 000 cancer gene expression profiles. *Neoplasia* 9 (2), 166–180. doi:10.1593/neo.07112

Ru, B., Wong, C. N., Tong, Y., Zhong, J. Y., Zhong, S. S. W., Wu, W. C., et al. (2019). Tisidb: An integrated repository portal for tumor-immune system interactions. *Bioinformatics* 35 (20), 4200–4202. doi:10.1093/bioinformatics/btz210

Sakaguchi, S., Miyara, M., Costantino, C. M., and Hafler, D. A. (2010). FOXP3+ regulatory T cells in the human immune system. *Nat. Rev. Immunol.* 10 (7), 490–500. doi:10.1038/nri2785

Sanmamed, M. F., and Chen, L. (2018). A paradigm shift in cancer immunotherapy: From enhancement to normalization. *Cell* 175 (2), 313–326. doi:10.1016/j.cell.2018.09.035

Schéele, S., Nyström, A., Durbeej, M., Talts, J. F., Ekblom, M., and Ekblom, P. (2007). Laminin isoforms in development and disease. *J. Mol. Med.* 85 (8), 825–836. doi:10.1007/s00109-007-0182-5

Setty, S., Michael, A. A., Fish, A. J., Michael Mauer, S., Butkowski, R. J., Virtanen, I., et al. (2012). Differential expression of laminin isoforms in diabetic nephropathy and other renal diseases. *Mod. Pathol.* 25 (6), 859–868. doi:10.1038/modpathol.2011.216

Shibuya, M. (2010). Tyrosine kinase receptor flt/VEGFR family: Its characterization related to angiogenesis and cancer. *Genes Cancer* 1 (11), 1119–1123. doi:10.1177/1947601910392987

Siegel, R. L., Miller, K. D., and Jemal, A. (2020). Cancer statistics, 2020. *Ca. Cancer J. Clin.* 70 (1), 7–30. doi:10.3322/caac.21590

Sonnenberg, A., Modderman, P. W., and Hogervorst, F. (1988). Laminin receptor on platelets is the integrin VLA-6. *Nature* 336 (6198), 487–489. doi:10.1038/336487a0

Speiser, D. E., Ho, P. C., and Verdeil, G. (2016). Regulatory circuits of T cell function in cancer. *Nat. Rev. Immunol.* 16 (10), 599–611. doi:10.1038/nri.2016.80

Subramanian, A., Tamayo, P., Mootha, V. K., Mukherjee, S., Ebert, B. L., Gillette, M. A., et al. (2005). Gene set enrichment analysis: A knowledge-based approach for interpreting genome-wide expression profiles. *Proc. Natl. Acad. Sci. U. S. A.* 102 (43), 15545–15550. doi:10.1073/pnas.0506580102

Takahashi, H., and Shibuya, M. (2005). The vascular endothelial growth factor (VEGF)/VEGF receptor system and its role under physiological and pathological conditions. *Clin. Sci.* 109 (3), 227–241. doi:10.1042/cs20040370

Topalian, S. L., Hodi, F. S., Brahmer, J. R., Gettinger, S. N., Smith, D. C., McDermott, D. F., et al. (2012). Safety, activity, and immune correlates of anti-PD-1 antibody in cancer. *N. Engl. J. Med.* 366 (26), 2443–2454. doi:10.1056/NEJMoa1200690

Tunuguntla, H. S., and Jorda, M. (2008). Diagnostic and prognostic molecular markers in renal cell carcinoma. *J. Urol.* 179 (6), 2096–2102. doi:10.1016/j.juro.2008.01.083

Turner, K. (2004). Expression of vascular endothelial growth factor protein in human renal cell carcinoma. *BJU Int.* 94 (4), 678. doi:10.1111/j.1464-410x.2003.05067_5.x

Vigano, S., Alatzoglou, D., Irving, M., Ménétrier-Caux, C., Caux, C., Romero, P., et al. (2019). Targeting adenosine in cancer immunotherapy to enhance T-cell function. *Front. Immunol.* 10, 925. doi:10.3389/fimmu.2019.00925

Wang, T. Y., Wang, L., Alam, S. K., Hoeppner, L. H., and Yang, R. (2019). ScanNeo: Identifying indel-derived neoantigens using RNA-seq data. *Bioinformatics* 35 (20), 4159–4161. doi:10.1093/bioinformatics/btz193

Warde-Farley, D., Donaldson, S. L., Comes, O., Zuberi, K., Badrawi, R., Chao, P., et al. (2010). The GeneMANIA prediction server: Biological network integration for gene prioritization and predicting gene function. *Nucleic Acids Res.* 38, W214–W220. Web Server issue. doi:10.1093/nar/gkq537

Weinstein, J. N., Collisson, E. A., Mills, G. B., Shaw, K. R., Ozenberger, B. A., Ellrott, K., et al. (2013). The cancer genome Atlas pan-cancer analysis project. *Nat. Genet.* 45 (10), 1113–1120. doi:10.1038/ng.2764

Willem, M., Miosge, N., Halfter, W., Smyth, N., Jannetti, I., Burghart, E., et al. (2002). Specific ablation of the nidogen-binding site in the laminin gamma1 chain interferes with kidney and lung development. *Development* 129 (11), 2711–2722. doi:10.1242/dev.129.11.2711

Wu, P., Liu, J. L., Pei, S. M., Wu, C. P., Yang, K., Wang, S. P., et al. (2018). Integrated genomic analysis identifies clinically relevant subtypes of renal clear cell carcinoma. *BMC Cancer* 18 (1), 287. doi:10.1186/s12885-018-4176-1

Yang, X., Han, H., De Carvalho, D. D., Lay, F. D., Jones, P. A., and Liang, G. (2014). Gene body methylation can alter gene expression and is a therapeutic target in cancer. *Cancer Cell* 26 (4), 577–590. doi:10.1016/j.ccr.2014.07.028

Yao, J., Xi, W., Zhu, Y., Wang, H., Hu, X., and Guo, J. (2018). Checkpoint molecule PD-1-assisted CD8(+) T lymphocyte count in tumor microenvironment predicts overall survival of patients with metastatic renal cell carcinoma treated with tyrosine kinase inhibitors. *Cancer Manag. Res.* 10, 3419–3431. doi:10.2147/cmar.S172039

Yildiz, E., Gokce, G., Kilicarslan, H., Ayan, S., Goze, O. F., and Gultekin, E. Y. (2004). Prognostic value of the expression of Ki-67, CD44 and vascular endothelial growth factor, and microvessel invasion, in renal cell carcinoma. *BJU Int.* 93 (7), 1087–1093. doi:10.1111/j.1464-410X.2004.04786.x

Yoshihara, K., Shahmoradgoli, M., Martínez, E., Vegesna, R., Kim, H., Torres-Garcia, W., et al. (2013). Inferring tumour purity and stromal and immune cell admixture from expression data. *Nat. Commun.* 4, 2612. doi:10.1038/ncomms3612

Youngblood, B., Hale, J. S., Kissick, H. T., Ahn, E., Xu, X., Wieland, A., et al. (2017). Effector CD8 T cells dedifferentiate into long-lived memory cells. *Nature* 552 (7685), 404–409. doi:10.1038/nature25144

Zhang, C., Zhao, N., Zhang, X., Xiao, J., Li, J., Lv, D., et al. (2021). SurvivalMeth: A web server to investigate the effect of DNA methylation-related functional elements on prognosis. *Brief. Bioinform.* 22 (3), bbaa162. doi:10.1093/bib/bbaa162

Zhang, Y., Xi, S., Chen, J., Zhou, D., Gao, H., Zhou, Z., et al. (2017). Overexpression of LAMC1 predicts poor prognosis and enhances tumor cell invasion and migration in hepatocellular carcinoma. *J. Cancer* 8 (15), 2992–3000. doi:10.7150/jca.21038

Zhou, Y., Zhou, B., Pache, L., Chang, M., Khodabakhshi, A. H., Tanaseichuk, O., et al. (2019). Metascape provides a biologist-oriented resource for the analysis of systems-level datasets. *Nat. Commun.* 10 (1), 1523. doi:10.1038/s41467-019-09234-6

Zhu, Q., Cai, M. Y., Weng, D. S., Zhao, J. J., Pan, Q. Z., Wang, Q. J., et al. (2019). PD-L1 expression patterns in tumour cells and their association with CD8(+) tumour infiltrating lymphocytes in clear cell renal cell carcinoma. *J. Cancer* 10 (5), 1154–1161. doi:10.7150/jca.29052

Zimmermann, H. (1992). 5'-Nucleotidase: Molecular structure and functional aspects. *Biochem. J.* 285 (2), 345–365. doi:10.1042/bj2850345

frontiers | Frontiers in Molecular Biosciences

TYPE Original Research
PUBLISHED 05 October 2022
DOI 10.3389/fmolb.2022.910928

OPEN ACCESS

EDITED BY
Na Luo,
Nankai University, China

REVIEWED BY
Qingyu Luo,
Dana–Farber Cancer Institute,
United States
Leili Saeednejad Zanjani,
Sidney Kimmel Cancer Center,
United States

*CORRESPONDENCE
Xiaoqing Xi,
xixiaoqing500@sina.com

†These authors have contributed equally to this work

SPECIALTY SECTION
This article was submitted to Molecular Diagnostics and Therapeutics, a section of the journal Frontiers in Molecular Biosciences

RECEIVED 01 April 2022
ACCEPTED 20 September 2022
PUBLISHED 05 October 2022

CITATION
Zhang C, Huang R and Xi X (2022), Cuproptosis patterns in papillary renal cell carcinoma are characterized by distinct tumor microenvironment infiltration landscapes.
Front. Mol. Biosci. 9:910928.
doi: 10.3389/fmolb.2022.910928

Cuproptosis patterns in papillary renal cell carcinoma are characterized by distinct tumor microenvironment infiltration landscapes

Chiyu Zhang†, Ruizhen Huang† and Xiaoqing Xi*

Department of Urology, The Second Affiliated Hospital of Nanchang University, Nanchang, China

Cuproptosis is a novel kind of programmed cell death that has been linked to tumor development, prognosis, and responsiveness to therapy. Nevertheless, the precise function of cuproptosis-related genes (CRGs) in the tumor microenvironment (TME) remains unknown. We characterized the genetic and transcriptional changes of CRGs in papillary renal cell carcinoma (PRCC) samples and analyzed the expression patterns in two separate cohorts. We observed that two unique cuproptosis-related subgroups and three separate gene subgroups were connected with clinicopathological, prognostic, and TME features of patients. Then, a risk score for predicting overall survival (OS) was created and validated in patients with PRCC. To make the risk score more clinically useful, we created a nomogram that was very accurate. A lower risk score, which was associated with higher tumor mutation burden, and immune activity, suggested a better prognosis for OS. Additionally, the risk score was shown to be substantially linked with the drug's susceptibility to chemotherapeutic agents. Our extensive research of CRGs in PRCC identified possible roles for them in the TME, clinicopathological features, and overall survival. These findings may help advance our knowledge of CRGs in PRCC and pave the way for improved prognosis and the creation of more effective immunotherapy therapies.

KEYWORDS

cuproptosis, papillary renal cell carcinoma, tumor microenvironment, drug sensitivity, prognostic model

Introduction

Renal cell carcinoma (RCC) is the most common kind of renal tumor, accounting for up to 80% of cases; papillary renal cell carcinoma (PRCC) is the second most prevalent type of RCC, accounting for around one-fifth of all instances (Mendhiratta et al., 2021; Rysz et al., 2021). Patients with localized PRCC have a reported 5-year overall survival rate of 70%, whereas patients with advanced PRCC do not have any feasible therapy choices at this time (Akhtar et al., 2019; Steward et al., 2021; Chan et al., 2022). Currently, an

increasing number of clinical investigations have been conducted on individuals with clear cell RCC and have identified many efficacious treatment targets, including VEGFR and mTOR (Erlmeier et al., 2022; Labaki et al., 2022). Nevertheless, these strategies were less effective in PRCC patients, which may be due to the fact that PRCC carcinogenesis involves distinct genetic alterations and molecular pathways from clear cell RCC tumorigenesis (Paner et al., 2022). As a result, new precise biomarkers and effective treatment techniques for PRCC are required.

Copper (Cu) is a necessary cofactor for all species, but it becomes hazardous when quantities reach a homeostatic threshold (Ruiz et al., 2021). Nevertheless, the mechanism by which excess copper causes cell death is uncertain. In human cells, Tsvetkov et al. demonstrated that Cu-dependent, controlled cell death is unique from other known cell death processes and requires mitochondrial respiration (Tsvetkov et al., 2022). It established that copper-dependent mortality occurs as a result of copper's direct binding to lipoylated tricarboxylic acid (TCA) cycle components. This leads to the aggregation of lipoylated proteins and the loss of iron-sulfur cluster proteins, which causes a lot of stress on the body and eventually cell death. They demonstrated that copper toxicity is unique from all other known processes of controlled cell death, such as apoptosis, ferroptosis, pyroptosis, and necroptosis (Tsvetkov et al., 2022). As a result, they suggest the name "cuprotosis" for this hitherto uncharacterized cell death process. Despite this, a number of associations between illness and Cu have been discovered. Cu levels have been shown to be greater in several cancers than in normal tissues in various investigations (Stepien et al., 2017; Aubert et al., 2020; Saleh et al., 2020; Michniewicz et al., 2021). Cu deposition has been linked to increased proliferation and growth, as well as angiogenesis and metastasis (Oliveri, 2022). Cu dyshomeostasis is clearly important in cancer, although scientists disagree over whether it is a cause or a result of carcinogenesis.

The tumor microenvironment (TME) is a complex and ever-changing milieu that mostly consists of stromal cells and immune cells (Hinshaw and Shevde, 2019). Cancer develops and progresses in conjunction with changes in the surrounding stroma (Wu and Dai, 2017). Through the production of different cytokines, chemokines, and other substances, cancer cells may effectively design their microenvironment (Vitale et al., 2019). This results in the surrounding cells' being reprogrammed, allowing them to play an important part in the proliferation of cancer cells (Kochetkova and Samuel, 2022). Immune cells are essential components of the tumoral microenvironment and are required for this process to occur. The growing body of evidence indicates that when innate and adaptive immune cells interact in the TME, they promote tumor development (Hedrick and Malanchi, 2022). The interaction of cancer cells and their proximal immune cells eventually leads to an environment conducive to tumor development and spread (Burrello and de Visser, 2022). Trying to figure out how this interaction works could lead to better medicines that can affect many parts of the TME at the same time, which could lead to better patient treatment results (Bader et al., 2020).

We conducted a detailed analysis of cuproptosis-related genes and their relationship to the progression, prognosis, and immune response of PRCC in detail. We identified distinct cuproptosis patterns in PRCC using The Cancer Genome Atlas (TCGA) and Gene Expression Omnibus (GEO) datasets and assessed the clinical features, prognostic significance, and immune infiltration degree of the resultant cuproptosis clusters. Additionally, we created a cuproptosis score that accurately predicted patients with PRCC's prognosis and therapy responsiveness. These results may aid in the development of successful immunotherapies for PRCC.

Materials and methods

Obtaining and processing raw data

The transcriptional mRNA sequences (fragments per kilobase of transcript per million, FPKM) and clinicopathological data for PRCC samples were obtained from TCGA and GEO databases. For the following analyses, data from the Cancer Genome Atlas's kidney renal papillary cell carcinoma (TCGA-KIRP) dataset and the Gene Expression Omnibus Series 2748 (GSE 2748) dataset were collected. We used the raw "CELL" files to modify the backdrop and normalize the quantiles. The FPKM values of TCGA-KIRP were converted to transcripts per kilobase million (TPM) and were thought to be equivalent to those from microarray data (Zhao et al., 2021). The batch effects from nonbiological technical biases in the two datasets were removed using the ComBat algorithm from the "SVA" package (Leek et al., 2012). The TCGA database was used to get data on somatic mutations and copy number variation (CNV).

Unsupervised clustering study of cuproptosis-related genes

Thirteen cuproptosis-related genes (CRGs) were extracted from prior studies, including FDX1, LIPT1, LIAS, DLD, DBT, GCSH, DLST, DLAT, PDHA1, PDHB, SLC31A1, ATP7A, and ATP7B(Cobine et al., 2021; Tsvetkov et al., 2022). To categorize individuals into discrete molecular subgroups based on cuproptosis-related gene (CRG) expression, the R package "ConsensusClusterPlus" was used for consensus unsupervised clustering analysis (Wilkerson and Hayes, 2010). This grouping was carried out using the following standards: To begin, the cumulative distribution function (CDF) curve steadily and gently expanded in magnitude. Secondly, there were no small sample sizes in any of the categories. Finally, following clustering, the

correlation inside groups grows and the correlation between groups diminishes. The research was conducted a total of 1000 times to confirm its accuracy as a clustering tool. We investigated the connections between genetic subclusters and clinicopathological features to determine the clinical utility of the two subgroups determined by consensus clustering. Additionally, we utilized Kaplan–Meier curves generated by the R tools "survival" and "survminer" to assess differences in overall survival (OS) among distinct subclusters (Lv et al., 2021).

Correlations between subclusters and the tumor microenvironment

To get a better understanding of the biological roles within distinct CRG subclusters, we utilized the "GSVA" R package to conduct gene set variation analysis (GSVA) analyses on each CRG subcluster (Hänzelmann et al., 2013). The immunological and stromal scores of each patient were calculated using the ESTIMATE method. Additionally, the CIBERSORT method was used to compute the percentages of 23 human immune cell types in each PRCC sample (Chen et al., 2018; Zhang et al., 2021). Additionally, we estimated the levels of immune cell infiltration in the tumor microenvironment using a single-sample gene set enrichment analysis (ssGSEA) approach (Mao et al., 2022).

Identification of DEGs

The R tool "limma" was used to compare differentially expressed genes (DEGs) amongst CRG subclusters (Ritchie et al., 2015). Then, Gene Ontology (GO) enrichment analysis was used to assess biological functions, and Kyoto Encyclopedia of Genes and Genomes (KEGG) enrichment analysis was used to evaluate regulatory pathways (Gene Ontology Consortium, 2015; Kanehisa et al., 2017).

The calculation of risk scores

A scoring system was developed to measure the cuproptosis gene alteration patterns in each PRCC patient. To begin, DEGs were screened across several CRG subclusters, with crossing DEGs maintained for further research. To assess the aforementioned intersecting DEGs and to filter for genes linked with PRCC prognosis, we employed univariate Cox regression techniques. Following that, we employed an unsupervised clustering technique to divide PRCC patients into distinct subclusters for a full systematic analysis based on prognosis-related genes. Additionally, we used Principal Component Analysis (PCA) to identify genes strongly linked with prognosis in order to develop cuproptosis-relevant gene signatures. The PCA approach enabled the scores to be concentrated on highly associated gene modules and downscaled for modules with modest contributions or correlations. Finally, we established cuproptosis scores for each PRCC patient using a mechanism identical to that used to rate gene expression. The following equation was used to get the risk score: Risk score = Σ (Expi * Coefi) (Coefi denotes the risk coefficient and Expi the gene expression).

Developing and validating a nomogram-based scoring system

Based on the conclusion of the independent prognosis study, we utilized the clinical parameters and risk score to build a prediction nomogram using the "rms" software. Each variable was assigned a score in the nomogram scoring method, and the overall score was calculated by summing the scores for all variables for every subject. The nomogram was evaluated using time-dependent receiver operating characteristic (ROC) curves for survivals (Obuchowski and Bullen, 2018). The nomogram's calibration plots were utilized to illustrate the prognostic validity between expected survival events and practically actual outcomes.

Analyses of mutations and drug susceptibility

The "maftools" R package was used to construct the mutation annotation format (MAF) from the TCGA in order to compare the somatic mutations of PRCC patients in two subgroups (Mayakonda et al., 2018; Ferrer-Bonsoms et al., 2021). The tumor mutation burden (TMB) score for each patient with PRCC in the two groups was also computed. To examine whether there were any differences in the therapeutic effects of chemotherapeutic medications in the two subgroups, we utilized the "pRRophetic" package to determine the semi-inhibitory concentration (IC50) values of chemotherapy agents routinely used to treat PRCC (Geeleher et al., 2014; Wang et al., 2021).

Statistical analysis

The Wilcoxon rank-sum test was used to make comparisons between two groups. The Kruskal-Wallis test was used for comparisons of three or more groups. Survival studies including risk scores were carried out using the Kaplan-Meier technique. The log-rank test was used to examine the difference in survival statistics. The function "surv-cutpoint" was used to determine the best cut-off for the cohort in order to categorize patients into high and low-risk score subgroups. The Univariate and multivariate Cox regressions were used to assess the prognostic significance of the risk score. R software version

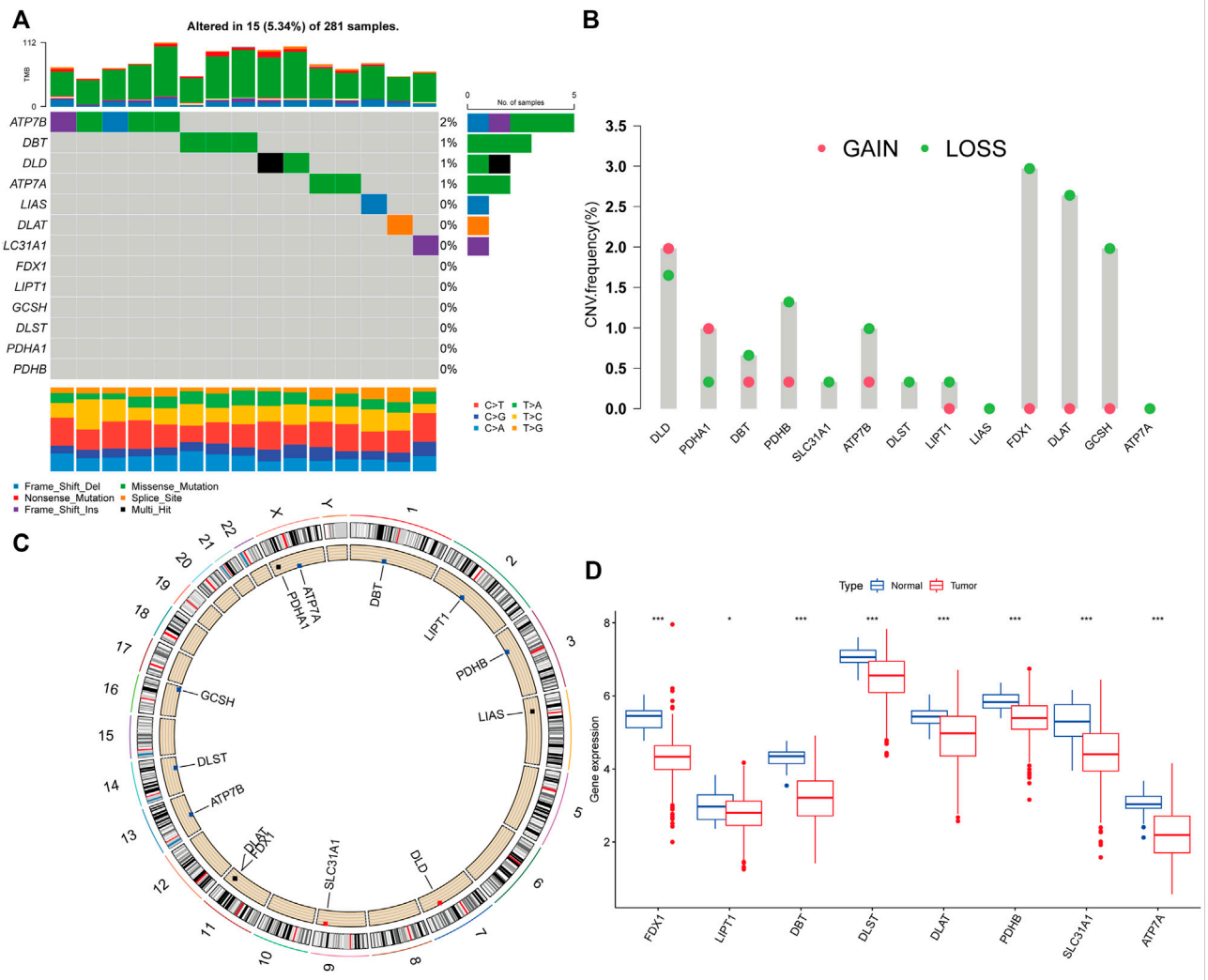

FIGURE 1
Cuproptosis-related genes (CRGs) genetic variation landscape in papillary renal cell carcinoma (PRCC). **(A)**The frequency of CRGs mutations in 281 patients with PRCC. On the right, the number indicated the mutation frequency of the CRGs. **(B)**The CRGs' copy number variation (CNV) frequency. The column indicated the frequency of variation. Red: gain frequency. Green: loss frequency. **(C)**The chromosomal location of the CRGs with a CNV. **(D)** Analysis of the mRNA expression of CRGs in normal and PRCC tissues. Blue: normal renal tissue. Red: tumor tissue. (*$p < 0.05$; ***$p < 0.001$).

4.2.0 was used for all data analysis. A statistically significant p-value of 0.05 was defined.

Results

Cuproptosis-related genes genetic variation landscape in papillary renal cell carcinoma

The TCGA dataset was used to investigate the landscape of genetic variants in 13 CRGs in PRCC, including somatic mutation and CNV. Genetic variations in CRGs were found in 15 out of the 281 samples (5.34 percent), with the majority of the variants being missense mutations (Figure 1A). The most often mutated gene was ATP7B, followed by DBT, DLD, and ATP7A, but PDHB, PDHA1, DLST, GCSH, LIPT1, FDX1, SLC31A1, DLAT, and LIAS did not mutate in PRCC samples. Following that, we examined somatic CNVs in these CRGs and determined that they were widespread in 11 CRGs (Figure 1B). DLD and PDHA1 exhibited increased CNV frequency, but DBT, PDHB, SLC31A1, ATP7B, DLST, LIPT1, FDX1, DLAT, GCSH, and GCSH all had decreased CNV frequency. Each chromosome in Figure 1C has been colored in to illustrate where each CRG has a copy number variation. We also analyzed the transcriptional level of CRGs in PRCC and normal tissues, and discovered that

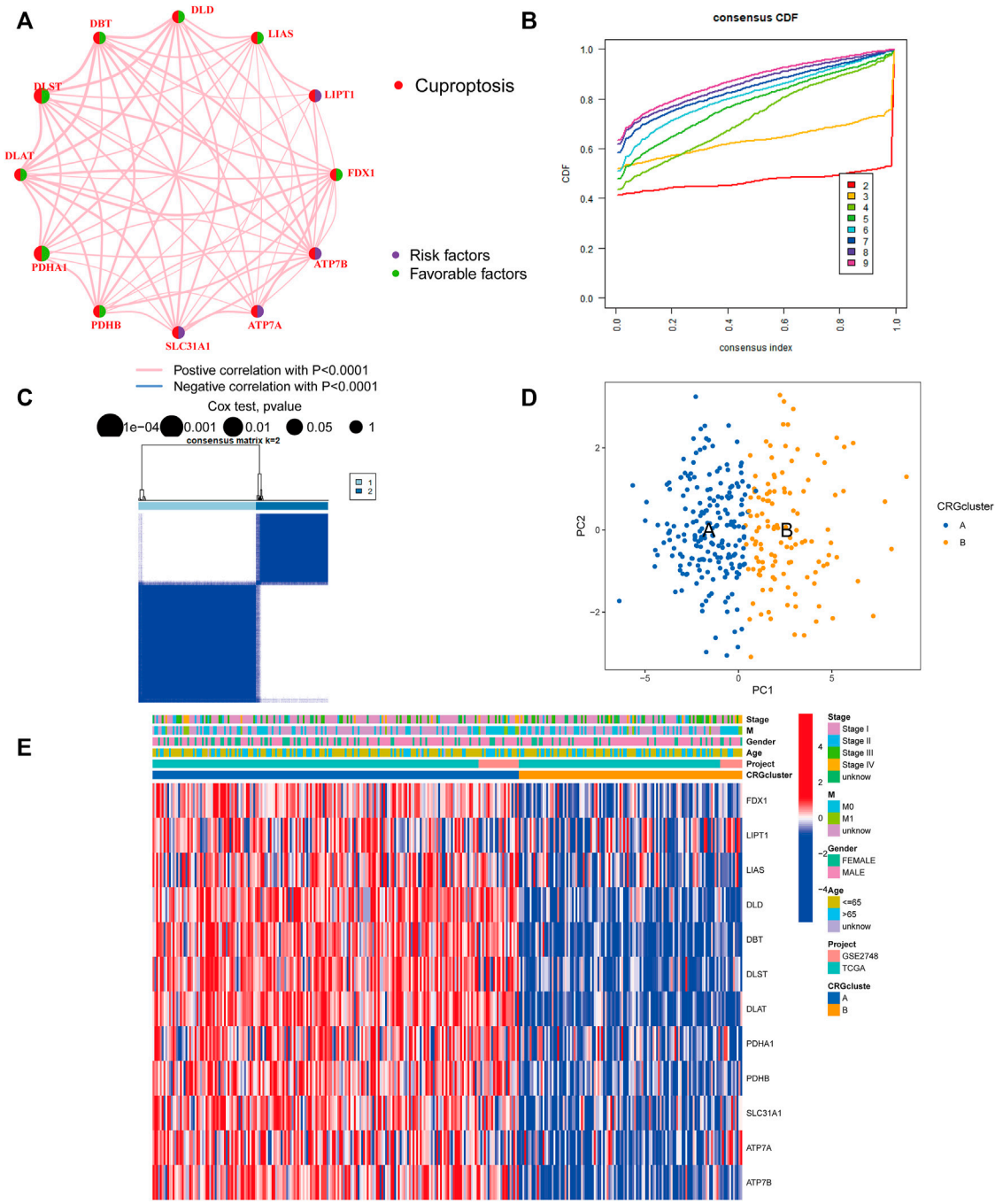

FIGURE 2
Identification of cuproptosis subclusters in PRCC. **(A)** Interactions among CRGs in PRCC. Greater PRCC predictive influence is shown by larger circles. The protective factor is represented by green, and the risk prognostic factor by the dark blue within the circle. **(B)** Consensus clustering cumulative distribution function (CDF) curve when K = 2–9. **(C)** The consensus clustering matrix for CRG modification patterns. At K = 2, the samples are partitioned with reasonable stability. **(D)** Principal component analysis (PCA) of two clusters. Blue indicates CRG cluster A, whereas orange represents CRG cluster B. **(E)** The heatmap depicts the expression of CRGs and clinicopathologic characteristics in different subclusters. Red denotes high CRG expression and blue, low CRG expression.

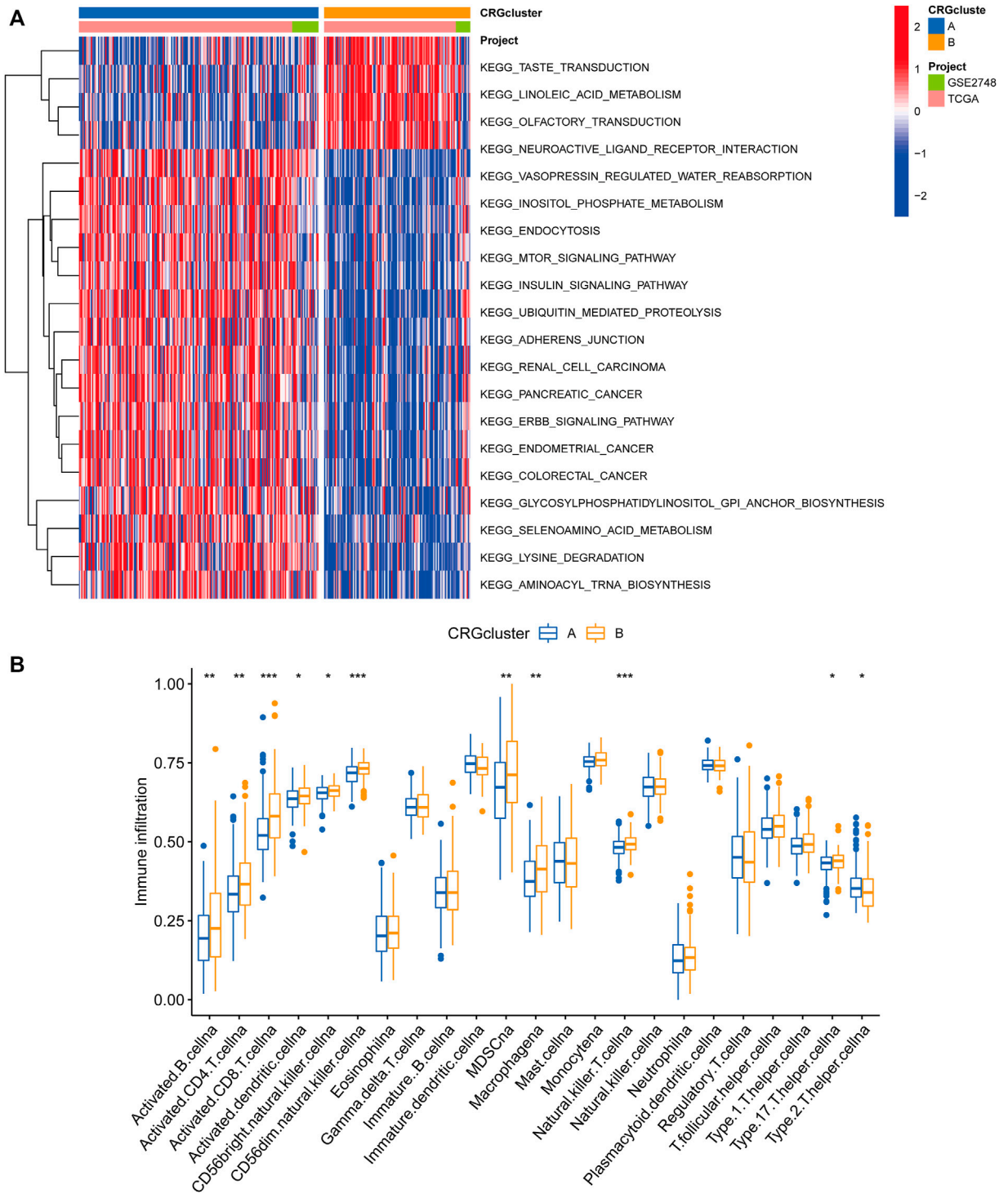

FIGURE 3
Correlations between the microenvironment of tumor immune cells and two PRCC subclusters. **(A)** Gene set variation analysis (GSVA) of biological pathways divided into two separate subclusters, with red denoting active pathways and blue denoting inhibited pathways, respectively. **(B)** The degrees of tumor microenvironment immune cell infiltration between the two CRG clusters. Blue symbolizes cluster A, whereas orange represents cluster B. The median value is indicated by the thick line, and the interquartile range by the bottom and top of the box. The dispersed dots signify anomalies. (*$p < 0.05$; **$p < 0.01$; ***$p < 0.001$).

the transcriptional levels of most CRGs were positively linked with the incidence of CNV. CNV-deficient CRGs, including FDX1, DLAT, DLST, PDHB, SLC31A1, ATP7A, and DBT, were expressed at lower levels in PRCC samples than in renal samples, suggesting that CNVs may regulate CRG mRNA expression (Figure 1D). As a result, the genomic and transcriptome landscape in CRGs is critical for controlling the onset and development of PRCC.

Identification of cuproptosis subclusters in papillary renal cell carcinoma

The TCGA-PRCC and GSE2748 were combined to create a meta-cohort. Each dataset comprised comprehensive clinicopathological information and survival data. The network depicted a full panorama of the CRGs' expression levels, correlations, and prognostic significance in PRCC patients (Figure 2A). These findings suggest that cross-talk between CRGs is crucial for the development of cuproptosis patterns in individuals. To understand more about the CRGs' expression properties in PRCC, we used a consensus clustering approach to identify patients with PRCC based on their transcriptional levels (Figures 2B,C). According to our results, the optimal option for subdividing the whole cohort into subclusters A (n = 199) and B (n = 122) is k = 2. At K = 2, the samples are partitioned with reasonable stability. The cuproptosis transcriptional patterns of the two subclusters differed significantly according to PCA analysis (Figure 2D). Furthermore, evaluating the clinicopathological characteristics of different CRG subclusters revealed significant differences in CRG transcription and pathological stage. Additionally, we detected substantial changes in CRG expression across various cuproptosis patterns, with all CRGs being downregulated in CRG cluster B and upregulated in CRG cluster A (Figure 2E).

Following that, we examined the molecular biological characteristics associated with the two cuproptosis clusters. The GSVA analysis revealed that CRG cluster A was significantly enriched in tumor-associated pathways, including the renal cell carcinoma pathway, pancreatic cancer pathway, endometrial cancer pathway, and colorectal cancer pathway (Figure 3A). Using the CIBERSORT method, we examined the correlations between the two subclusters and 23 human immune cell subtypes of each PRCC sample to explore the involvement of CRGs in the TME of PRCC. According to our findings, the infiltration of most immune cells differed significantly between the two subclusters (Figure 3B). Subcluster B had significantly more activated B cells, CD4 T cells, CD8 T cells, activated dendritic cells, CD56bright natural killer cells, CD56dim natural killer cells, MDSC, Macrophage, and natural killer T cells than subcluster A.

Gene classification based on differentially expressed genes

We used the "limma" R package to search for 3977 cuproptosis subcluster-related DEGs, identified as CRG signature genes, to better understand the probable biological roles across distinct CRG clusters (Figure 4A). The "ClusterProfile" R package was then used to conduct GO functional and KEGG pathway enrichment studies to annotate and show DEGs' biological functions. DEGs were found to be significantly overrepresented in cellular metabolism-associated pathways. In biological processes, DEGs were enriched in Golgi vesicle transport, establishment of organelle localization, and positive regulation of catabolic process. In cellular components, DEGs were highly abundant in focal adhesion, cell–substrate junction, and cell leading edge. DEGs were considerably enriched in ubiquitin–like protein transferase activity, transcription coregulator activity, and ubiquitin–protein transferase activity throughout molecular function processes (Figure 4B). DEGs were also highly enriched in tumor-associated pathways in KEGG analyses: proteoglycans in cancer, prostate cancer, pancreatic cancer, chronic myeloid leukemia and renal cell carcinoma (Figure 4B).

Following that, we used univariate Cox regression to assess the prognostic value of 3977 subcluster-related genes and identified 739 genes linked with OS time for further analysis ($p < 0.05$). We conducted an unsupervised cluster analysis on the 739 DEGs associated with prognosis to group PRCC patients into three distinct gene subclusters: gene subcluster A, gene subcluster B, and gene subcluster C (Figures 5A,B). At K = 3, the samples are partitioned with reasonable stability. Patients with gene subcluster B had the poorest overall survival, while patients in gene subcluster A had the best OS ($p < 0.001$, Figure 5C). CRG expression differed significantly amongst the three cuproptosis gene subclusters, as predicted based on the cuproptosis patterns (Figure 5D). This indicated that greater CRG expression may be associated with a better prognosis for individuals with PRCC. Additionally, the heatmap of gene expression indicated that these differentially expressed genes associated with prognosis were strongly expressed in gene cluster B (Figure 5E).

Developing the prognostic risk score

To begin, we used the R package "caret" to randomly assign patients to one of two subgroups: training (n = 158) or testing (n = 157). The optimum predictive signature for 739 cuproptosis subcluster-related DEGs was further refined using least absolute shrinkage and selection operator (LASSO) regression and multivariate Cox regression analysis. Following LASSO regression analysis, the least partial likelihood deviance revealed that 5 OS-related genes remained (Figures 6A,B). Then, using the

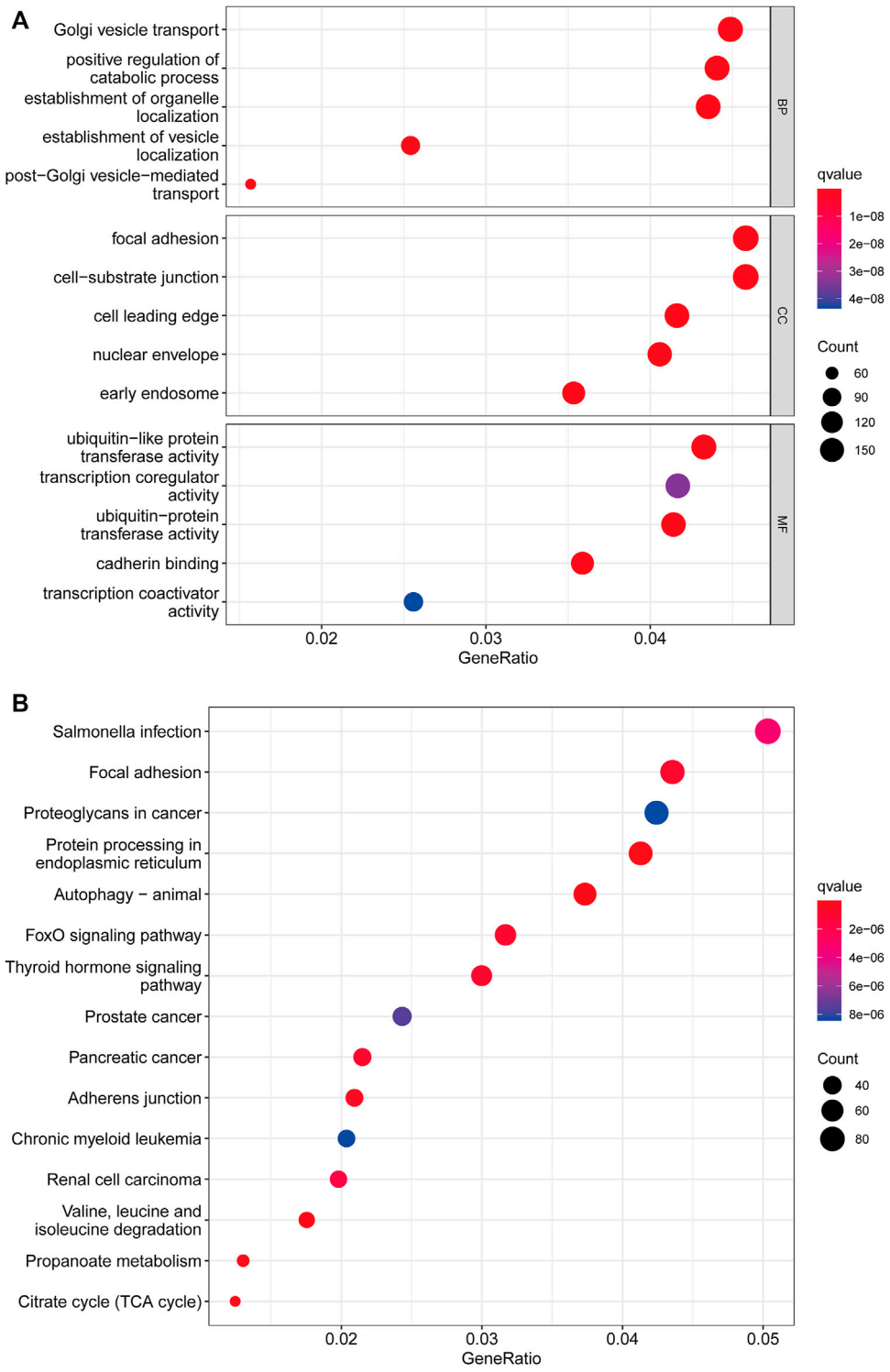

FIGURE 4
Functional enrichment analysis. **(A)** Bubble plot for Gene Ontology (GO) function enrichment analysis. BP: biological processes; CC: cellular components; MF: molecular function. **(B)** Bubble plot for Kyoto Encyclopedia of Genes and Genomes (KEGG) pathway enrichment analysis. The y-axis shows pathway terms, whereas the x-axis denotes gene ratio. The size of each circle represents the number of genes. The hue of the circles symbolizes various q values.

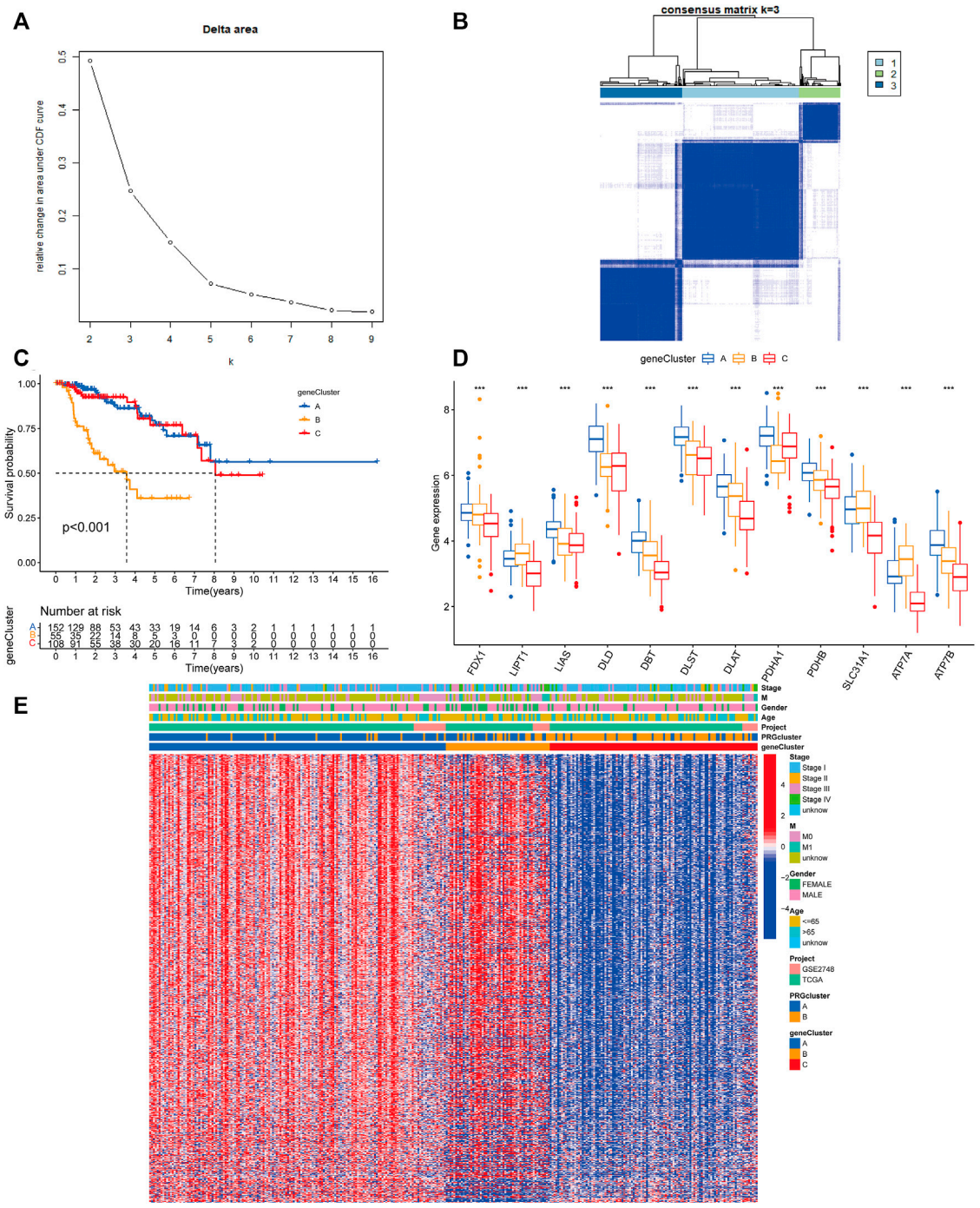

FIGURE 5
Gene classification based on differentially expressed genes. **(A)** For K = 2–9, the relative change in the area under the CDF curve. **(B)** Heatmap of the consensus matrix identifying two clusters (k = 3) and the region of their correlation. At K = 3, the samples are partitioned with reasonable stability. **(C)** Kaplan–Meier curves for the overall survival of the gene subclusters. Blue indicates gene cluster A, orange cluster B, and red cluster C. Log-rank $p < 0.001$, suggesting a substantial difference among the three gene clusters in terms of overall survival. Cluster B's overall survival was much worse than clusters A and C's **(D)** CRG expression differences between gene subclusters. An interquartile range of the data was indicated by the upper and lower ends of the boxes. The boxes' lines indicated the median value. (one-way ANOVA test: ***$p < 0.001$). **(E)** A heat map of the clinical-pathologic correlations between the two gene clusters. Alternate annotations are provided for age, gender, pathologic staging, and gene clusters. Blue denotes low gene expression whereas red denotes high gene expression.

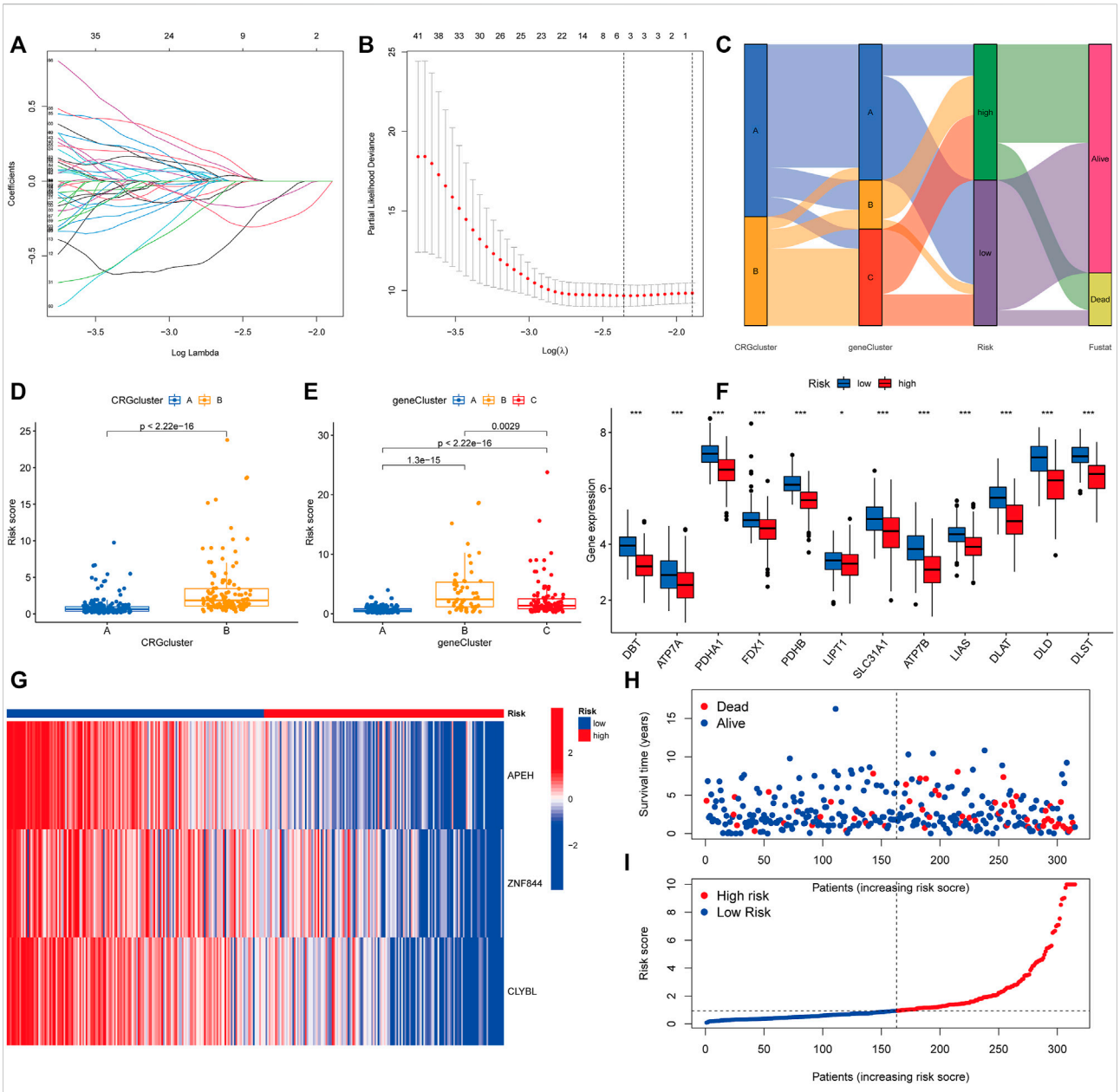

FIGURE 6
Developing the prognostic risk score. **(A,B)** Least absolute shrinkage and selection operator (LASSO) regression and partial likelihood deviance on prognostic genes. **(C)** Distributions of various CRG clusters, gene clusters, risk scores, and survival outcomes are shown in alluvial plots. **(D)** Differences in risk scores between two CRG clusters. The Wilcoxon rank-sum test revealed that the differences between the two clusters were statistically significant ($p < 0.001$). **(E)** Differences in risk scores among three gene clusters. The Kruskal-Wallis test ($p < 0.001$) was used to assess the differences between the three gene clusters. **(F)** Histogram of mRNA expression of CRG between high-risk and low-risk score groups. **(G)** Heatmap of three significant genes across different risk scores. **(H,I)** Distribution of risk scores and patient survival status as shown by dot and scatter plot.

Akaike information criterion (AIC) value, we did multivariate Cox regression analysis on 5 OS-related genes to yield three significant genes (APEH, ZNF844, and CLYBL). The DEGs linked with the subclusters were used to generate the risk score. The distribution of patients into two CRG subclusters, three gene subclusters, and two risk score subgroups is shown in Figure 6C. More crucially, CRG cluster B showed a considerably higher risk score than CRG cluster A (Figure 6D). Between gene subclusters, we discovered a substantial variation in risk score. The risk score for gene subcluster A was the lowest, while that for gene subcluster B was the highest, suggesting that a low-risk score is likely to be

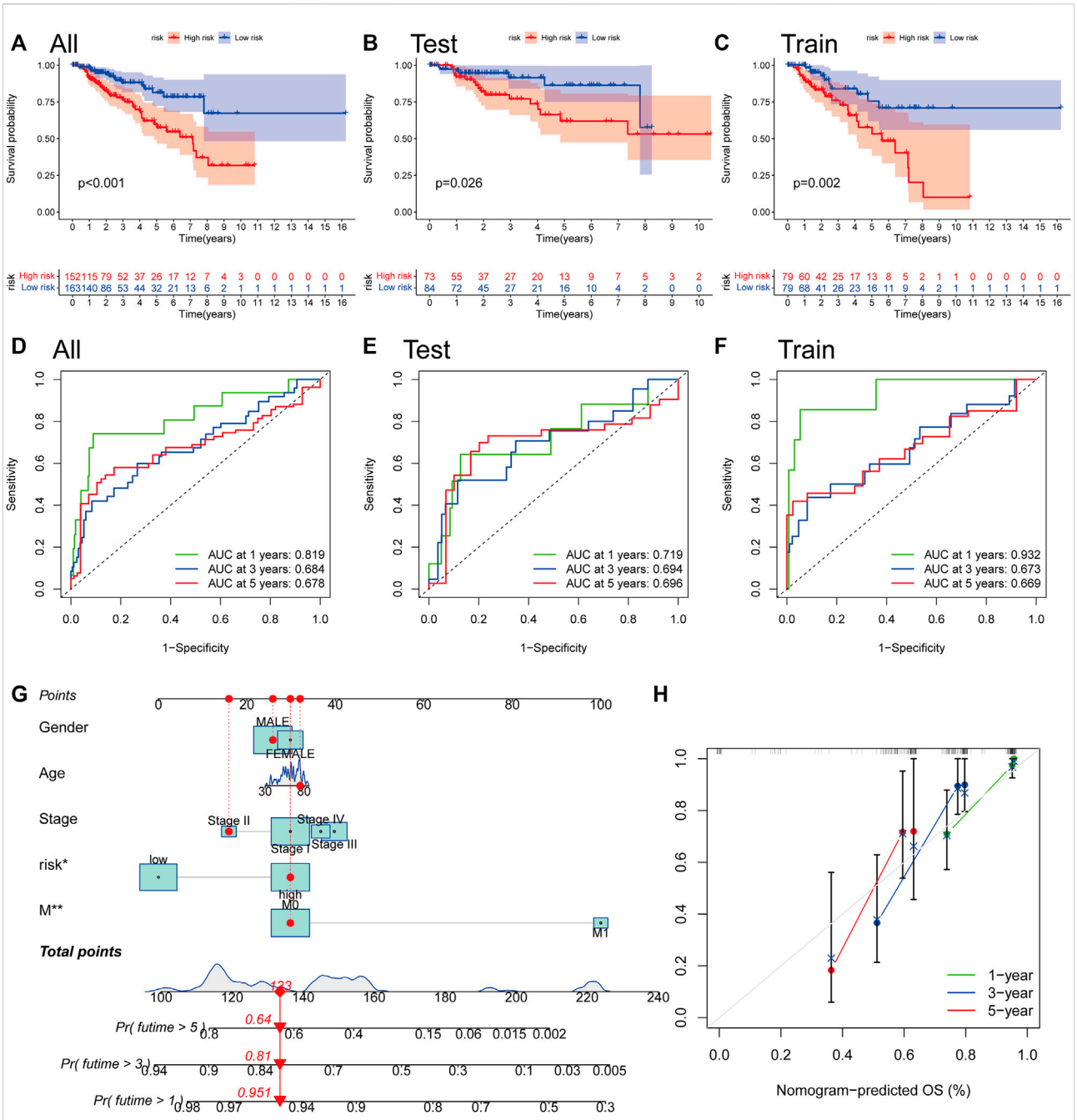

FIGURE 7
The construction of a nomogram for survival prediction. **(A–C)** Overall Survival analysis using the Kaplan–Meier method in all, training, and testing sets. **(D–F)** Time-dependent receiver operating characteristic (ROC) curves to estimate the sensitivity and specificity of survival in all, training, and testing sets based on the risk score. **(G)** Nomogram for predicting overall survival in patients with PRCC. **(H)** The nomogram's calibration curves for predicting overall survival. *$p < 0.05$, **$p < 0.01$.

associated with immunological activation-related characteristics, whilst a high-risk score is likely to be associated with stromal activation-related characteristics (Figure 6E). It was discovered that all CRGs were considerably overexpressed in the low-risk subgroup (Figure 6F). Similarly, as seen in the heatmap, the three genes included in the score were significantly expressed in the low-risk subgroup (Figure 6G). The distribution plot demonstrated that as risk scores climbed, survival times were reduced and recurrence rates increased (Figures 6H,I).

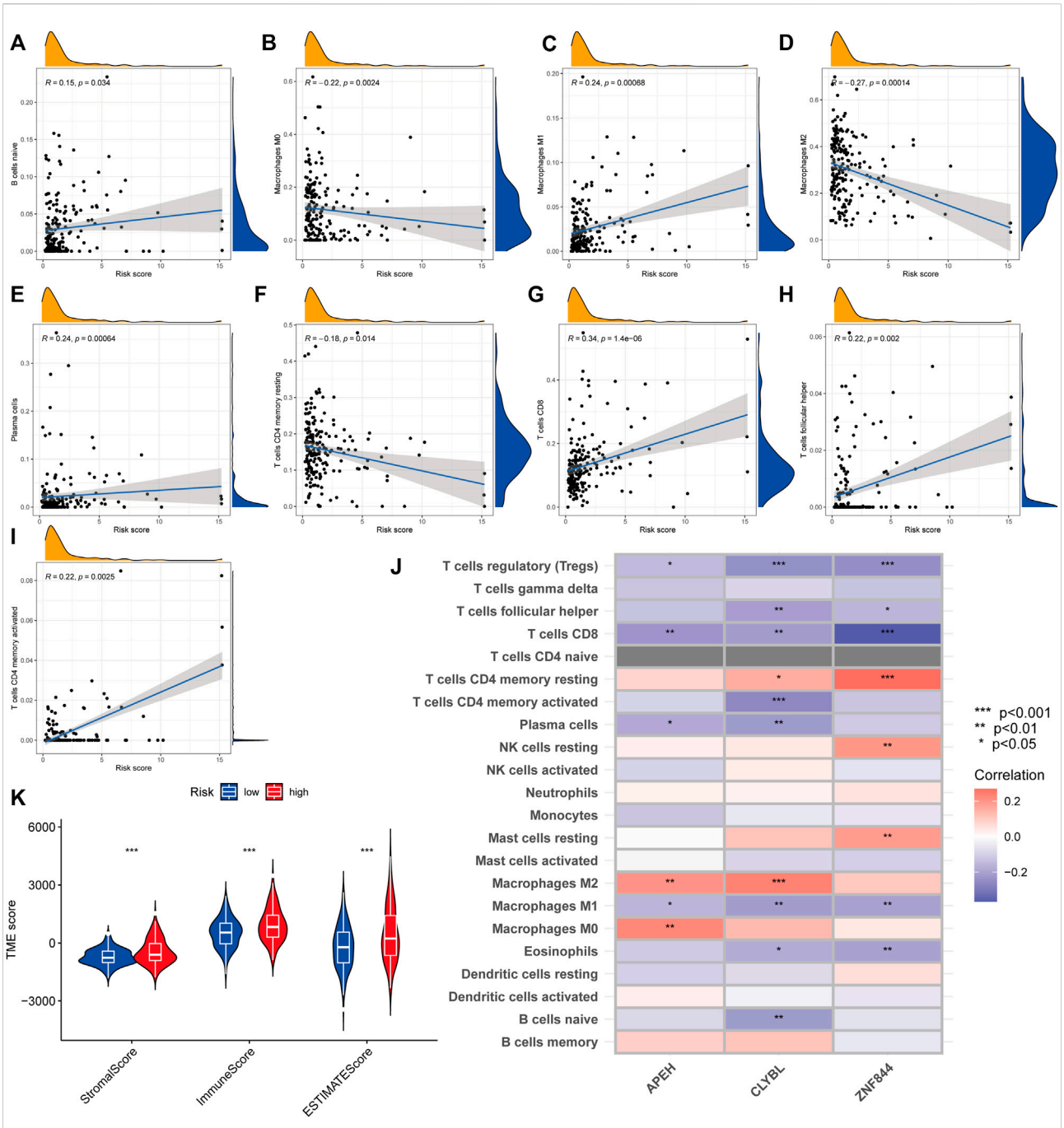

FIGURE 8
Comparative analysis of tumor microenvironment in various risk categories. **(A–I)** Relationship between the risk score and the kind of immune cells. R represents the correlation coefficient, and when it is positive, it means that immune cell infiltration is positively correlated with the risk score, and *vice versa*. **(J)** Relationship between immune cell abundance and three genes included in the suggested model. Red represents a positive correlation between immune cell infiltration and gene expression, and blue represents a negative correlation. The darker the color, the greater the correlation. **(K)** Relationship between risk score and both immune and stromal scores. A greater risk score was shown to be substantially associated with a higher immunological score, stromal score, and ESTIMATE score.

The construction of a nomogram for survival prediction

We computed risk scores across testing and training sets to confirm the risk score's predictive performance. According to the methodology used for the whole set, the patients were likewise divided into two risk categories. Survivability studies showed that patients in the lower-than-normal risk category had a considerably better prognosis (Figures 7A–C). The AUC values for the risk score at 1, 3, and 5 years were 0.819, 0.684, and 0.678, respectively, in the all set (Figure 7D). There were 0.719, 0.694, and 0.696 AUC values for the risk score at 1, 3, and 5 years in the testing set (Figure 7E). Similarly, the training group's AUC values are 0.932, 0.673, and 0.669, correspondingly (Figure 7F). One, three, and five-year prognostic efficiency AUC values for the risk score were demonstrated to be quite high, indicating that the risk score had a remarkable ability to predict the life expectancy of people with PRCC. Because the risk score is difficult to apply in practice, we created a nomogram that combines the risk score with clinicopathological variables to estimate patient survival time. As predictors of the nomogram, we used the risk score, gender, age, tumor metastasis, and cancer stage as variables to consider (Figure 7G). In particular, the calibration plots revealed that the nomograms we developed functioned in a manner comparable to the ideal model, particularly when it came to the one-year survival period (Figure 7H).

A comparative analysis of the tumor microenvironment in various risk categories

We employed the CIBERSORT technique to assess the connection between the risk score and immune cell abundance. As demonstrated in the scatter graphs, the risk score was positively linked with B cells, M1 Macrophages, Plasma cells, CD8 T cells, follicular helper T cells, and CD4 memory activated T cells but negatively associated with M0 Macrophages, M2 Macrophages, and CD4 memory resting T cells (Figures 8A–I). We identified a substantial association between the majority of immune cells and three genes, including APEH and M0 Macrophages, CLYBL and M2 Macrophages, and ZNF844 and CD4 memory resting T cells (Figure 8J). A greater risk score was also shown to be substantially associated with a higher immunological score, stromal score, and ESTIMATE score (Figure 8K).

Analyzing genetic mutations and drug susceptibility

According to accumulating research, due to their large amounts of mutant antigens, people with a high TMB may react better to immunotherapy than those with a low TMB. As a further step, we compared the somatic mutation distribution across two risk score subgroups (Figures 9A,B). The Spearman correlation analysis showed that the risk score and tumor mutational burden were linked in a negative way (R = -0.16, $p = 0.0074$; Figure 9C). Our examination of the mutation datasets revealed that the higher-risk category had a lower TMB than the lower-risk category, suggesting that the lower-risk category may benefit from immunotherapy (Figure 9D). The top twenty mutated genes were similar in both groups, but the majority of genes in the lower-risk subgroup had a higher mutation rate, including TTN, MUC16, MET, MUC4, KMT2D, LRP2, and PCLO. This finding is consistent with previous analyses of gene mutation burden, implying that the lower-risk subgroup may be more responsive to immunotherapy. Following that, we chose medications presently used to treat cancer and assessed their susceptibility in various risk categories (Figure 9E–N). Interestingly, we discovered that patients with a high-risk score had lower IC50 values for the majority of drugs, including A-770041 (Lck targeted inhibitor), ABT-888 (small-molecule inhibitors of PARP, veliparib), AG-014699 (PARP inhibitors, rucaparib), AICAR (5-aminoimidazole-4-carboxamide ribonucleotide), and AMG-706 (a multikinase inhibitor, motesanib). Certain medications' IC50 values were considerably lowered in individuals with low-risk scores, including AKT inhibitors and AS601245 (a selective JNK inhibitor). When these findings are combined, they imply that CRG is linked with medication sensitivity.

Discussion

Although several targeted agents have recently been introduced in clinical applications for patients with high-grade RCC, the evidence for their efficacy in PRCC is not yet strong enough (Motzer et al., 2015; Choueiri and Kaelin, 2020). There are very few cases of PRCC, so the results of genetic tests and randomized control trials are often not included or only make up a very small part of the results of RCC (Courthod et al., 2015). Furthermore, since PRCC is distinct from clear cell RCC, the relevant study findings for clear cell RCC do not apply to PRCC (Massari et al., 2019). As a result, it is important to look into the molecular processes that cause these diseases and to find new biomarkers for targeted therapy. Tsvetkov et al. found that FDX1 and protein acylation (LIPT1, LIAS, DLDDLAT, PDHA1, and PDHB) were the main regulators of copper ionophore-induced cell death, and the knockout of seven genes prevented the killing of two copper ion carriers (Tsvetkov et al., 2022). We began by examining the gene mutation and expression of cuproptosis-related genes using data from the TCGA-PRCC and GSE2748 datasets. CNV-deficient CRGs, such as FDX1, DLAT, and DPT, were expressed at lower levels in PRCC samples than in normal

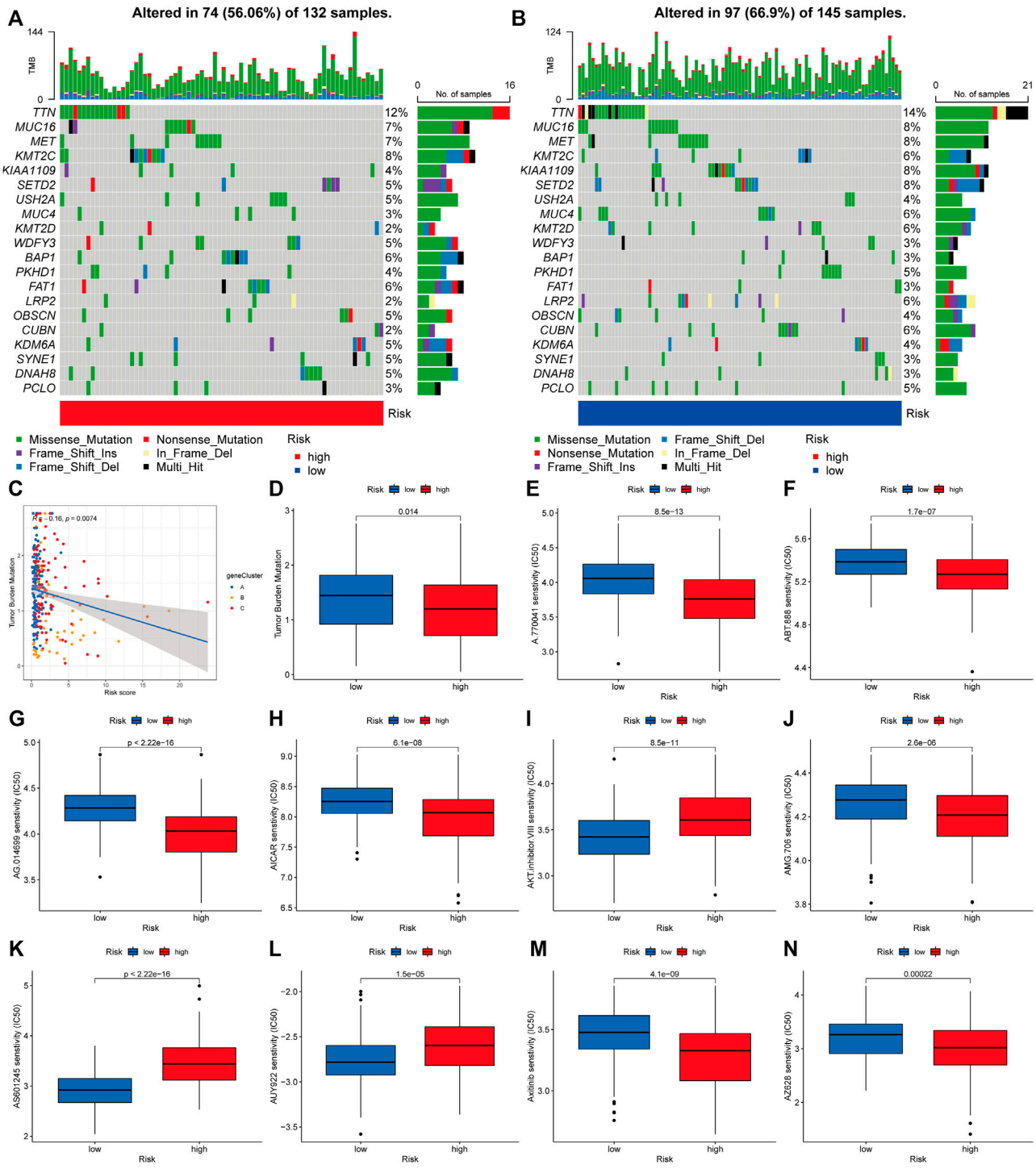

FIGURE 9
Analyzing genetic mutations and drug susceptibility. **(A,B)** The waterfall plot depicting the somatic mutation characteristics associated with various risk scores. The numbers on the graph show the frequency of mutation. The fraction of mutation types is shown by the box on the right. **(C)** Spearman correlation study of risk score and tumor mutational burden. R represents the correlation coefficient, and when it is negative, it means that the tumor burden mutation is negatively correlated with the risk score. **(D)** Tumor mutational burden in several risk score categories. **(E–N)** The relationship between risk score and drug sensitivity. Red represents the high-risk group and blue represents the low-risk group. The lower the half maximal inhibitory concentration (IC50) value, the more sensitive the group of patients to the drug.

renal samples, suggesting that CNV regulates CRG mRNA expression. As a result, the genomic and transcriptome landscape in CRGs is critical for controlling the onset and development of PRCC. CNV are somatic mutations in the DNA sequence that during the course of malignancy. The altered chromosomal structures are produced by an increase or decrease in the copy number of DNA segments, which is common in many types of cancer. In PRCC, somatic CNV identified three distinct tumor groupings. One grouping was often characterized by numerous gains of chromosomes 7p and 17p, deletion of the Y chromosome, and further gains; the majority of these cancers were type 1 and of low grade (Ren et al., 2018). Somatic mutations are non-heritable changes to the human genome that arise in somatic cells on their own accord (Futreal et al., 2004). Linehan et al. indicated that MET mutations are mostly found in type 1 cancers and in the tyrosine kinase domain.

Following that, we grouped PRCC patients according to their expression of cuproptosis-related genes, resulting in two unique pyroptotic patterns. Furthermore, evaluating the clinicopathological characteristics of different CRG subclusters revealed significant differences in CRG transcription and pathological stage. Additionally, we detected substantial changes in CRG expression across various cuproptosis patterns, with all CRGs being downregulated in CRG cluster B and upregulated in CRG cluster A. The GSVA analysis revealed that CRG cluster A was significantly enriched in tumor-associated pathways. According to our findings, the infiltration of most immune cells differed significantly between the two subclusters. Activated B cells, activated CD4 T cells, and natural killer T cells were infiltrated in much greater numbers in subcluster B than in subcluster A. Cellular metabolism-associated pathways were found to be significantly overrepresented by DEGs. Using a combined study of mutation and CNV, numerous pathways were identified as often dysregulated in PRCC. Wnt, Notch, TGF-, and Hedgehog signaling pathways were shown to be enhanced in type 1 PRCC (Saleeb et al., 2018). Additionally, when type 1 tumor tissue is compared to normal renal tissue, numerous intriguing pathways have been found, including adherens junction, focal adhesions, TGF signaling, Wnt signaling, and MAP kinase signaling. We conducted an unsupervised cluster analysis on the 739 DEGs associated with prognosis to group PRCC patients into three distinct gene subclusters. Patients with gene subcluster B had the poorest overall survival, while patients in gene subcluster A had the best OS. CRGs expression differed significantly amongst the three cuproptosis gene subclusters, as predicted based on the cuproptosis patterns. We computed risk scores across testing and training sets to confirm the risk score's predictive performance. Survivability studies showed that patients in the lower-than-normal risk category had a considerably better prognosis. Mei et al. (2022) constructed a cuproptosis-related signature that was used to classify clear cell renal cell carcinoma patients into distinct risk clusters, with low-risk patients having a much better prognosis. Because the risk score is inconvenient to apply in practice, we created a nomogram that combines the risk score with clinicopathological variables to estimate patient survival time.

As demonstrated in the scatter graphs, the risk score was positively linked with B cells, M1 Macrophages, and CD4 memory activated T cells. We identified a substantial association between the majority of immune cells and three genes, including APEH and M0 macrophages, CLYBL and M2 macrophages, and ZNF844 and CD4 memory resting T cells. A greater risk score was also shown to be substantially associated with a higher immunological score, stromal score, and ESTIMATE score. Our examination of the mutation datasets revealed that the higher-risk category had a lower TMB than the lower-risk category, suggesting that the lower-risk category may benefit from immunotherapy. In recent years, renewed interest in immunotherapy has been sparked by the discovery that PD-1 and its ligand PD-L1 are expressed in the majority of RCC (Choueiri and Motzer, 2017). In addition to T- and B-cells, natural killer cells, and macrophages, the PD-1 receptor is found in other immune cells as well. Various malignancies cells may express it, even though it is seldom expressed in healthy cells (Johnson et al., 2018). One study indicated that after initiating therapy with nivolumab in multiple patients with advanced PRCC, computed tomography scans around half a year later revealed a considerable decrease in the size and quantity of systemic metastases (Adrianzen Herrera et al., 2017). Following that, we chose medications presently used to treat cancer and assessed their susceptibility in various risk categories. Interestingly, we discovered that patients with a high-risk score had lower IC50 values for the majority of drugs, including A-770041 (Lck targeted inh ibitor) and AMG-706 (a multikinase inhibitor, motesanib). Certain medications' IC50 values were considerably lowered in individuals with low-risk scores, including AKT inhibitors and AS601245 (a selective JNK inhibitor). When these findings are combined, they imply that CRG is linked with medication sensitivity. In a phase II trial50, Foretinib, a dual MET/VEGFR2 inhibitor, was recently assessed in 74 participants with PRCC (Choueiri et al., 2013). Five out of ten (50%) of these participants had a RECIST partial response, whereas the remaining individuals achieved stable disease as their best response. There are no conventional medicines that have been shown to be effective in the treatment of metastatic PRCC. A clinical experiment at the National Cancer Institute is now evaluating one method that aims to exploit these cancers' reliance on aerobic glycolysis and a high glucose flow (Chen et al., 2019).

Indeed, there is growing evidence that copper is a dynamic signaling molecule that exerts significant control over a varied array of activities, including lipolysis, cellular proliferation, autophagy, and brain activity (Tsang et al., 2020). Copper's growing involvement in maintaining or restoring homeostasis emphasizes the critical nature of controlling its biological

availability both within and outside the cell (Ackerman and Chang, 2018). It is thought that mutations in the ATP7A/B family, which are identical enzymes, cause the hereditary copper transport diseases Menkes and Wilson illness (Kaler, 2013). Genetic investigations have shown unequivocally that export is the primary mechanism of protection against copper toxicity, since cells lacking ATP7A are substantially more susceptible to excess copper than those lacking metallothioneins (Gudekar et al., 2020). Current antineoplastic drugs have significant off-target consequences because they often target fundamental characteristics of cells that are shared by all rapidly reproducing cells (Oliveri, 2022). The goal of developing new therapeutic medicines should be to improve selectivity and thereby minimize adverse effects. Additionally, these drugs should overcome resistance to tumor cells and specifically target tumor stem cells. There are some copper ionophores that have shown promise in this field because they are naturally good at causing cuproptosis in tumor cells instead of healthy ones. Disulfiram (DSF) and other copper ionophores have been looked at as antitumor drugs that can cause cuproptosis (Ge et al., 2022). It has been useful in treating alcoholism for over half a century as a commonly used aldehyde dehydrogenase inhibitor. Since it has various biological functions, it's becoming more popular to repurpose DSF as an anticancer drug (Ekinci et al., 2019). DSF's inexpensive cost, great availability, safety profile, and antitumor efficacy have piqued the curiosity of researchers (Kannappan et al., 2021). A number of cancer cell lines have shown DSF to be an antitumor drug in recent years (Li et al., 2020). Additionally, previous research has shown that co-administration of DSF with copper greatly enhances its antitumor activity since DSF's active form is a copper complex of DTC. DSF's toxic effects seem to be directly connected to the intracellular buildup of copper that DSF promotes (Cen et al., 2004). Despite DSF's good outcomes *in vitro* and *in vivo*, clinical trials in malignancy sufferers were unsuccessful (Kannappan et al., 2021). This discouraging result might be explained by the quick degradation of DSF and its active component or by the use of a distinct route of administration for DSF and copper. It's worth mentioning that long-term use of copper-binding drugs, such as copper ionophores, might disrupt vital metal homeostasis, resulting in significant adverse effects in individuals undergoing the medication. Whereas copper ionophores have demonstrated inherent selectivity against tumor cells, as stated above, their therapeutic window has to be expanded for safer use. As a result, current research has concentrated on establishing logical methodologies and innovative therapeutic modalities to improve tumor cell targeting.

Conclusion

To summarize, the cuproptosis-related gene signature is important for the definition of the TME and the predication of PRCC prognosis. The risk score of a single tumor may help us better understand the peculiarities of TME invasion and aid in the development of more effective immunotherapy tactics.

Data availability statement

The original contributions presented in the study are included in the article/supplementary material, further inquiries can be directed to the corresponding author.

Author contributions

CZ wrote the paper and analyzed the data. RH edited the paper. XX made the images out. Each author contributed to the paper and approved the final version submitted for publication.

Conflict of interest

The authors declare that the research was conducted in the absence of any commercial or financial relationships that could be construed as a potential conflict of interest.

Publisher's note

References

Ackerman, C. M., and Chang, C. J. (2018). Copper signaling in the brain and beyond. *J. Biol. Chem.* 293 (13), 4628–4635. doi:10.1074/jbc.R117.000176

Adrianzen Herrera, D. A., Fleisig, S. B., and Gartrell, B. A. (2017). Impressive and durable response to nivolumab in a patient with metastatic type 2 papillary renal cell carcinoma: On-label but without evidence. *Invest. New Drugs* 35 (5), 665–668. doi:10.1007/s10637-017-0469-5

Akhtar, M., Al-Bozom, I. A., and Al Hussain, T. (2019). Papillary renal cell carcinoma (PRCC): An Update. *Adv. Anat. Pathol.* 26 (2), 124–132. doi:10.1097/pap.0000000000000220

Aubert, L., Nandagopal, N., Steinhart, Z., Lavoie, G., Nourreddine, S., Berman, J., et al. (2020). Copper bioavailability is a KRAS-specific vulnerability in colorectal cancer. *Nat. Commun.* 11 (1), 3701. doi:10.1038/s41467-020-17549-y

Bader, J. E., Voss, K., and Rathmell, J. C. (2020). Targeting metabolism to improve the tumor microenvironment for cancer immunotherapy. *Mol. Cell* 78 (6), 1019–1033. doi:10.1016/j.molcel.2020.05.034

Burrello, C., and de Visser, K. E. (2022). Pulling the Strings of the tumor microenvironment. *Cancer Immunol. Res.* 10 (1), 4. doi:10.1158/2326-6066.Cir-21-0977

Cen, D., Brayton, D., Shahandeh, B., Meyskens, F. L., Jr., and Farmer, P. J. (2004). Disulfiram facilitates intracellular Cu uptake and induces apoptosis in human melanoma cells. *J. Med. Chem.* 47 (27), 6914–6920. doi:10.1021/jm049568z

Chan, E., Stohr, B. A., Butler, R. S., Cox, R. M., Myles, J. L., Nguyen, J. K., et al. (2022). Papillary renal cell carcinoma with Microcystic Architecture is strongly associated with Extrarenal invasion and metastatic disease. *Am. J. Surg. Pathol.* 46 (3), 392–403. doi:10.1097/pas.0000000000001802

Chen, B., Khodadoust, M. S., Liu, C. L., Newman, A. M., and Alizadeh, A. A. (2018). Profiling tumor infiltrating immune cells with CIBERSORT. *Methods Mol. Biol.* 1711, 243–259. doi:10.1007/978-1-4939-7493-1_12

Chen, Q., Cheng, L., and Li, Q. (2019). The molecular characterization and therapeutic strategies of papillary renal cell carcinoma. *Expert Rev. Anticancer Ther.* 19 (2), 169–175. doi:10.1080/14737140.2019.1548939

Choueiri, T. K., and Kaelin, W. G., Jr. (2020). Targeting the HIF2-VEGF axis in renal cell carcinoma. *Nat. Med.* 26 (10), 1519–1530. doi:10.1038/s41591-020-1093-z

Choueiri, T. K., and Motzer, R. J. (2017). Systemic therapy for metastatic renal-cell carcinoma. *N. Engl. J. Med.* 376 (4), 354–366. doi:10.1056/NEJMra1601333

Choueiri, T. K., Vaishampayan, U., Rosenberg, J. E., Logan, T. F., Harzstark, A. L., Bukowski, R. M., et al. (2013). Phase II and biomarker study of the dual MET/VEGFR2 inhibitor foretinib in patients with papillary renal cell carcinoma. *J. Clin. Oncol.* 31 (2), 181–186. doi:10.1200/jco.2012.43.3383

Cobine, P. A., Moore, S. A., and Leary, S. C. (2021). Getting out what you put in: Copper in mitochondria and its impacts on human disease. *Biochim. Biophys. Acta. Mol. Cell Res.* 1868 (1), 118867. doi:10.1016/j.bbamcr.2020.118867

Courthod, G., Tucci, M., Di Maio, M., and Scagliotti, G. V. (2015). Papillary renal cell carcinoma: A review of the current therapeutic landscape. *Crit. Rev. Oncol. Hematol.* 96 (1), 100–112. doi:10.1016/j.critrevonc.2015.05.008

Ekinci, E., Rohondia, S., Khan, R., and Dou, Q. P. (2019). Repurposing Disulfiram as an Anti-cancer agent: Updated review on Literature and Patents. *Recent Pat. anticancer. Drug Discov.* 14 (2), 113–132. doi:10.2174/1574892814666190514104035

Erlmeier, F., Bruecher, B., Stöhr, C., Herrmann, E., Polifka, I., Agaimy, A., et al. (2022). cMET: a prognostic marker in papillary renal cell carcinoma? *Hum. Pathol.* 121, 1–10. doi:10.1016/j.humpath.2021.12.007

Ferrer-Bonsoms, J. A., Jareno, L., and Rubio, A. (2021). Rediscover: an R package to identify mutually exclusive mutations. *Bioinformatics* 38, 844–845. doi:10.1093/bioinformatics/btab709

Futreal, P. A., Coin, L., Marshall, M., Down, T., Hubbard, T., Wooster, R., et al. (2004). A census of human cancer genes. *Nat. Rev. Cancer* 4 (3), 177–183. doi:10.1038/nrc1299

Ge, E. J., Bush, A. I., Casini, A., Cobine, P. A., Cross, J. R., DeNicola, G. M., et al. (2022). Connecting copper and cancer: From transition metal signalling to metalloplasia. *Nat. Rev. Cancer* 22 (2), 102–113. doi:10.1038/s41568-021-00417-2

Geeleher, P., Cox, N., and Huang, R. S. (2014). pRRophetic: an R package for prediction of clinical chemotherapeutic response from tumor gene expression levels. *PLoS One* 9 (9), e107468. doi:10.1371/journal.pone.0107468

Gene Ontology Consortium (2015). Gene Ontology Consortium: Going forward. *Nucleic Acids Res.* 43, D1049–D1056. doi:10.1093/nar/gku1179

Gudekar, N., Shanbhag, V., Wang, Y., Ralle, M., Weisman, G. A., and Petris, M. J. (2020). Metallothioneins regulate ATP7A trafficking and control cell viability during copper deficiency and excess. *Sci. Rep.* 10 (1), 7856. doi:10.1038/s41598-020-64521-3

Hänzelmann, S., Castelo, R., and Guinney, J. (2013). GSVA: Gene set variation analysis for microarray and RNA-seq data. *BMC Bioinforma.* 14, 7. doi:10.1186/1471-2105-14-7

Hedrick, C. C., and Malanchi, I. (2022). Neutrophils in cancer: Heterogeneous and multifaceted. *Nat. Rev. Immunol.* 22 (3), 173–187. doi:10.1038/s41577-021-00571-6

Hinshaw, D. C., and Shevde, L. A. (2019). The tumor microenvironment innately Modulates cancer progression. *Cancer Res.* 79 (18), 4557–4566. doi:10.1158/0008-5472.Can-18-3962

Johnson, D. B., Bordeaux, J., Kim, J. Y., Vaupel, C., Rimm, D. L., Ho, T. H., et al. (2018). Quantitative Spatial profiling of PD-1/PD-L1 interaction and HLA-DR/IDO-1 predicts improved outcomes of Anti-PD-1 therapies in metastatic melanoma. *Clin. Cancer Res.* 24 (21), 5250–5260. doi:10.1158/1078-0432.Ccr-18-0309

Kaler, S. G. (2013). Inborn errors of copper metabolism. *Handb. Clin. Neurol.* 113, 1745–1754. doi:10.1016/b978-0-444-59565-2.00045-9

Kanehisa, M., Furumichi, M., Tanabe, M., Sato, Y., and Morishima, K. (2017). KEGG: New perspectives on genomes, pathways, diseases and drugs. *Nucleic Acids Res.* 45 (D1), D353–D361. doi:10.1093/nar/gkw1092

Kannappan, V., Ali, M., Small, B., Rajendran, G., Elzhenni, S., Taj, H., et al. (2021). Recent advances in repurposing Disulfiram and Disulfiram Derivatives as copper-dependent anticancer agents. *Front. Mol. Biosci.* 8, 741316. doi:10.3389/fmolb.2021.741316

Kochetkova, M., and Samuel, M. S. (2022). Differentiation of the tumor microenvironment: Are CAFs the organizer? *Trends Cell Biol.* 32 (4), 285–294. doi:10.1016/j.tcb.2021.11.008

Labaki, C., Van Allen, E. M., and Choueiri, T. K. (2022). Linking a Trio of molecular features in clear-cell renal cell carcinoma. *Cancer Immunol. Res.* 10 (3), 274. doi:10.1158/2326-6066.Cir-22-0058

Leek, J. T., Johnson, W. E., Parker, H. S., Jaffe, A. E., and Storey, J. D. (2012). The sva package for removing batch effects and other unwanted variation in high-throughput experiments. *Bioinformatics* 28 (6), 882–883. doi:10.1093/bioinformatics/bts034

Li, Y., Chen, F., Chen, J., Chan, S., He, Y., Liu, W., et al. (2020). Disulfiram/copper induces antitumor activity against both Nasopharyngeal cancer cells and cancer-associated Fibroblasts through ROS/MAPK and ferroptosis pathways. *Cancers (Basel)* 12 (1), E138. doi:10.3390/cancers12010138

Lv, X., Jin, Y., Zhang, D., Li, Y., Fu, Y., Wang, S., et al. (2021). Low Circulating Monocytes is in Parallel with Lymphopenia which predicts poor outcome in Anti-melanoma Differentiation-associated gene 5 Antibody-positive Dermatomyositis-associated Interstitial lung disease. *Front. Med.* 8, 808875. doi:10.3389/fmed.2021.808875

Mao, J., Zhang, Q., Wang, Y., Zhuang, Y., Xu, L., Ma, X., et al. (2022). TERT activates endogenous retroviruses to promote an immunosuppressive tumour microenvironment. *EMBO Rep.* 23, e52984. doi:10.15252/embr.202152984

Massari, F., Di Nunno, V., Santoni, M., Gatto, L., Caserta, C., Morelli, F., et al. (2019). Toward a genome-based treatment landscape for renal cell carcinoma. *Crit. Rev. Oncol. Hematol.* 142, 141–152. doi:10.1016/j.critrevonc.2019.07.020

Mayakonda, A., Lin, D. C., Assenov, Y., Plass, C., and Koeffler, H. P. (2018). Maftools: Efficient and comprehensive analysis of somatic variants in cancer. *Genome Res.* 28 (11), 1747–1756. doi:10.1101/gr.239244.118

Mei, W., Liu, X., Jia, X., Jin, L., Xin, S., Sun, X., et al. (2022). A cuproptosis-related gene model for predicting the prognosis of clear cell renal cell carcinoma. *Front. Genet.* 13, 905518. doi:10.3389/fgene.2022.905518

Mendhiratta, N., Muraki, P., Sisk, A. E., Jr., and Shuch, B. (2021). Papillary renal cell carcinoma: Review. *Urol. Oncol.* 39 (6), 327–337. doi:10.1016/j.urolonc.2021.04.013

Michniewicz, F., Saletta, F., Rouaen, J. R. C., Hewavisenti, R. V., Mercatelli, D., Cirillo, G., et al. (2021). Copper: An intracellular Achilles' Heel allowing the targeting of Epigenetics, kinase pathways, and cell metabolism in cancer therapeutics. *ChemMedChem* 16 (15), 2315–2329. doi:10.1002/cmdc.202100172

Motzer, R. J., Hutson, T. E., Glen, H., Michaelson, M. D., Molina, A., Eisen, T., et al. (2015). Lenvatinib, everolimus, and the combination in patients with metastatic renal cell carcinoma: A randomised, phase 2, open-label, multicentre trial. *Lancet. Oncol.* 16 (15), 1473–1482. doi:10.1016/s1470-2045(15)00290-9

Obuchowski, N. A., and Bullen, J. A. (2018). Receiver operating characteristic (ROC) curves: Review of methods with applications in diagnostic medicine. *Phys. Med. Biol.* 63 (7), 07tr01. doi:10.1088/1361-6560/aab4b1

Oliveri, V. (2022). Selective targeting of cancer cells by copper ionophores: An Overview. *Front. Mol. Biosci.* 9, 841814. doi:10.3389/fmolb.2022.841814

Paner, G. P., Chumbalkar, V., Montironi, R., Moch, H., and Amin, M. B. (2022). Updates in grading of renal cell carcinomas beyond clear cell renal cell carcinoma and papillary renal cell carcinoma. *Adv. Anat. Pathol.* 29, 117–130. doi:10.1097/pap.0000000000000341

Ren, Q., Wang, L., Al-Ahmadie, H. A., Fine, S. W., Gopalan, A., Sirintrapun, S. J., et al. (2018). Distinct genomic copy number alterations Distinguish Mucinous Tubular and Spindle cell carcinoma of the kidney from papillary renal cell carcinoma with Overlapping Histologic features. *Am. J. Surg. Pathol.* 42 (6), 767–777. doi:10.1097/pas.0000000000001038

Ritchie, M. E., Phipson, B., Wu, D., Hu, Y., Law, C. W., Shi, W., et al. (2015). Limma powers differential expression analyses for RNA-sequencing and microarray studies. *Nucleic Acids Res.* 43 (7), e47. doi:10.1093/nar/gkv007

Ruiz, L. M., Libedinsky, A., and Elorza, A. A. (2021). Role of copper on mitochondrial function and metabolism. *Front. Mol. Biosci.* 8, 711227. doi:10.3389/fmolb.2021.711227

Rysz, J., Franczyk, B., Ławiński, J., and Gluba-Brzózka, A. (2021). Characteristics of clear cell papillary renal cell carcinoma (ccpRCC). *Int. J. Mol. Sci.* 23 (1), 151. doi:10.3390/ijms23010151

Saleeb, R. M., Plant, P., Tawedrous, E., Krizova, A., Brimo, F., Evans, A. J., et al. (2018). Integrated Phenotypic/Genotypic analysis of papillary renal cell carcinoma subtypes: Identification of prognostic Markers, cancer-related pathways, and implications for therapy. *Eur. Urol. Focus* 4 (5), 740–748. doi:10.1016/j.euf.2016.09.002

Saleh, S. A. K., Adly, H. M., Abdelkhaliq, A. A., and Nassir, A. M. (2020). Serum levels of Selenium, zinc, copper, Manganese, and iron in prostate cancer patients. *Curr. Urol.* 14 (1), 44–49. doi:10.1159/000499261

Stepien, M., Jenab, M., Freisling, H., Becker, N. P., Czuban, M., Tjønneland, A., et al. (2017). Pre-diagnostic copper and zinc biomarkers and colorectal cancer risk in the European Prospective Investigation into Cancer and Nutrition cohort. *Carcinogenesis* 38 (7), 699–707. doi:10.1093/carcin/bgx051

Steward, J. E., Kern, S. Q., Cheng, L., Boris, R. S., Tong, Y., Bahler, C. D., et al. (2021). Clear cell papillary renal cell carcinoma: Characteristics and survival outcomes from a large single institutional series. *Urol. Oncol.* 39 (6), 370.e21–370.370.e25. doi:10.1016/j.urolonc.2021.02.003

Tsang, T., Posimo, J. M., Gudiel, A. A., Cicchini, M., Feldser, D. M., and Brady, D. C. (2020). Copper is an essential regulator of the autophagic kinases ULK1/2 to drive lung adenocarcinoma. *Nat. Cell Biol.* 22 (4), 412–424. doi:10.1038/s41556-020-0481-4

Tsvetkov, P., Coy, S., Petrova, B., Dreishpoon, M., Verma, A., Abdusamad, M., et al. (2022). Copper induces cell death by targeting lipoylated TCA cycle proteins. *Science* 375 (6586), 1254–1261. doi:10.1126/science.abf0529

Vitale, I., Manic, G., Coussens, L. M., Kroemer, G., and Galluzzi, L. (2019). Macrophages and metabolism in the tumor microenvironment. *Cell Metab.* 30 (1), 36–50. doi:10.1016/j.cmet.2019.06.001

Wang, Z., Wang, Y., Yang, T., Xing, H., Wang, Y., Gao, L., et al. (2021). Machine learning revealed stemness features and a novel stemness-based classification with appealing implications in discriminating the prognosis, immunotherapy and temozolomide responses of 906 glioblastoma patients. *Brief. Bioinform.* 22 (5), bbab032. doi:10.1093/bib/bbab032

Wilkerson, M. D., and Hayes, D. N. (2010). ConsensusClusterPlus: A class discovery tool with confidence assessments and item tracking. *Bioinformatics* 26 (12), 1572–1573. doi:10.1093/bioinformatics/btq170

Wu, T., and Dai, Y. (2017). Tumor microenvironment and therapeutic response. *Cancer Lett.* 387, 61–68. doi:10.1016/j.canlet.2016.01.043

Zhang, A. Z., Yuan, X., Liang, W. H., Zhang, H. J., Li, Y., Xie, Y. F., et al. (2021). Immune infiltration in Gastric cancer microenvironment and its clinical significance. *Front. Cell Dev. Biol.* 9, 762029. doi:10.3389/fcell.2021.762029

Zhao, Y., Li, M. C., Konaté, M. M., Chen, L., Das, B., Karlovich, C., et al. (2021). TPM, FPKM, or normalized Counts? A Comparative study of Quantification measures for the analysis of RNA-seq data from the NCI patient-Derived models Repository. *J. Transl. Med.* 19 (1), 269. doi:10.1186/s12967-021-02936-w

frontiers | Frontiers in Molecular Biosciences

TYPE Original Research
PUBLISHED 11 November 2022
DOI 10.3389/fmolb.2022.1034208

OPEN ACCESS

EDITED BY
Na Luo,
Nankai University, China

REVIEWED BY
Ziming Li,
Shanghai Jiao Tong University, China
Yudong Wang,
Fourth Hospital of Hebei Medical University, China
Wanpu Yan,
Beijing Cancer Hospital, China

*CORRESPONDENCE
Jun Chen,
huntercj2004@qq.com
Song Xu,
xusong198@hotmail.com

†These authors have contributed equally to this work

SPECIALTY SECTION
This article was submitted to Molecular Diagnostics and Therapeutics, a section of the journal Frontiers in Molecular Biosciences

RECEIVED 01 September 2022
ACCEPTED 31 October 2022
PUBLISHED 11 November 2022

CITATION
Zhou N, Tang Q, Yu H, Li T, Ren F, Zu L, Chen G, Chen J and Xu S (2022), Comprehensive analyses of one-carbon metabolism related genes and their association with prognosis, tumor microenvironment, chemotherapy resistance and immunotherapy in lung adenocarcinoma.
Front. Mol. Biosci. 9:1034208.
doi: 10.3389/fmolb.2022.1034208

Comprehensive analyses of one-carbon metabolism related genes and their association with prognosis, tumor microenvironment, chemotherapy resistance and immunotherapy in lung adenocarcinoma

Ning Zhou[1,2†], Quanying Tang[1,2†], Haochuan Yu[1,2†], Tong Li[1,2], Fan Ren[1,2], Lingling Zu[1,2], Gang Chen[1,2], Jun Chen[1,2*] and Song Xu[1,2*]

[1]Department of Lung Cancer Surgery, Tianjin Medical University General Hospital, Tianjin, China, [2]Tianjin Key Laboratory of Lung Cancer Metastasis and Tumor Microenvironment, Lung Cancer Institute, Tianjin Medical University General Hospital, Tianjin, China

Background: Lung adenocarcinoma (LUAD) is the most common type of lung cancer and is a global public health concern. One-carbon (1C) metabolism plays a crucial role in the occurrence and development of multiple cancer types. However, there are limited studies investigating 1C metabolism in LUAD. This study aims to evaluate the prognostic value of 1C metabolism-related genes in LUAD and to explore the potential correlation of these genes with gene methylation, the tumor microenvironment, and immunotherapy.

Methods: We identified 26 1C metabolism-related genes and performed a Kaplan-Meier and Cox regression analysis to evaluate the prognostic value of these genes. Consensus clustering was further performed to determine the 1C metabolism-related gene patterns in LUAD. The clinical and molecular characteristics of subgroups were investigated based on consensus clustering. CIBERSORT and ssGSEA algorithms were used to calculate the relative infiltration levels of multiple immune cell subsets. The relationship between 1C metabolism-related genes and drug sensitivity to immunotherapy was evaluated using the CellMiner database and IMvigor210 cohort, respectively.

Results: The expression levels of 23 1C metabolism-related genes were significantly different between LUAD tumor tissues and normal tissues. Seventeen of these genes were related to prognosis. Two clusters (cluster 1 and cluster 2) were identified among 497 LUAD samples based on the expression of 7 prognosis-related genes. Distinct expression patterns were observed between the two clusters. Compared to cluster 2, cluster 1 was

characterized by inferior overall survival (OS) (median OS = 41 vs. 60 months, $p = 0.00031$), increased tumor mutation burden (15.8 vs. 7.5 mut/Mb, $p < 0.001$), high expression of PD-1 ($p < 0.001$) and PD-L1 ($p < 0.001$), as well as enhanced immune infiltration. 1C metabolism-related genes were positively correlated with the expression of methylation enzymes, and a lower methylation level was observed in cluster 1 ($p = 0.0062$). Patients in cluster 1 were resistant to chemotherapy drugs including pemetrexed, gemcitabine, paclitaxel, etoposide, oxaliplatin, and carboplatin. The specific expression pattern of 1C metabolism-related genes was correlated with a better OS in patients treated with immunotherapy (median OS: 11.2 vs. 7.8 months, $p = 0.0034$).

Conclusion: This study highlights that 1C metabolism is correlated with the prognosis of LUAD patients and immunotherapy efficacy. Our findings provide novel insights into the role of 1C metabolism in the occurrence, development, and treatment of LUAD, and can assist in guiding immunotherapy for LUAD patients.

KEYWORDS

one-carbon metabolism, immune cell infiltrate, chemotherapy resistance, immunotherapy, lung adenocarcinoma

Introduction

Lung cancer remains one of the most prevalent cancer types and the most lethal cancer type worldwide (Siegel et al., 2022). Lung cancer is divided into two main forms: non-small cell lung cancer (NSCLC) and small cell lung cancer (SCLC). NSCLC is the most common type of lung cancer and accounts for 85% of all cases (Duma et al., 2019; Wang et al., 2019). Lung adenocarcinoma (LUAD) is the major histopathological subtype of NSCLC and accounts for approximately half of all lung cancer-related deaths (Travis et al., 2015; Behrend et al., 2021). Although several treatments have been confirmed effective in recent years, platinum-based chemotherapy, such as pemetrexed, remains the principal therapeutic for NSCLC (Schiller et al., 2002; Tan et al., 2016).

One-carbon (1C) metabolism, also known as folate metabolism, is involved in multiple physiological processes, such as biosynthesis, amino acid homeostasis, epigenetic maintenance, and redox defense (Ducker and Rabinowitz, 2017). It has been identified that 1C metabolic enzymes are upregulated in numerous cancer types (Mehrmohamadi et al., 2014). *MTHFD2* expression is associated with poor prognosis in hepatocellular carcinoma and colorectal cancer (Liu et al., 2016; Ju et al., 2019). *SHMT2* has also been identified to play a role in colorectal and lung cancer progression (DeNicola et al., 2015; Liu et al., 2021). In addition, *TYMS* is overexpressed in several cancers and is closely associated with a poor prognosis (Sasaki et al., 2013; Fu et al., 2019; Agulló-Ortuño et al., 2020; Song S. et al., 2021). Because of the essential role of 1C metabolism in cancer, inhibition of folate metabolism is regarded as an important therapeutic strategy in cancer. Several drugs targeting 1C metabolic enzymes have been successfully developed, such as methotrexate and pemetrexed (Ducker and Rabinowitz, 2017).

It has been shown that 1C metabolism can affect the function of immune cells, especially the activation of T cell (Ducker and Rabinowitz, 2017). Immune cells play an important role in the tumor microenvironment (TME). The TME includes diverse cell types, including cancer cells, noncancerous cells, as well as many other cellular and noncellular components (Duan et al., 2020). The immune and non-immune cells within the TME have been observed to regulate the proliferation, differentiation, and death of tumor cells (Mu and Najafi, 2021). In recent years, numerous studies have shown the effectiveness of targeting components within the TME alone or in combination with other therapies, including chemotherapy, radiotherapy, and immunotherapy (Hirata and Sahai, 2017; Ozpiskin et al., 2019; Liu et al., 2020).

1C metabolism can support methylation reactions by generating 1C units (also known as methyl groups). DNA and RNA methylation has been widely considered to be the best-characterized epigenetic modifications, and play an important role in the occurrence and development of tumors. DNA methylation occurs at the 5-position of cytosine (5 mC), and transcriptionally regulates the expression of target genes (Robertson and Jones, 2000). RNA methylation mainly includes three types: N6-methyladenosine (m6A), 5-methylcytosine (m5C), and N1-methyladenosine (m1A) (Song P. et al., 2021). Methylation is a reversible modification that is regulated by special enzymes, including methyltransferase (writer), demethylase (eraser), and methylation-dependent binding protein (reader) (Dai et al., 2021).

Although 1C metabolism has been shown to have important functions in the process of methylation and the resistance to

pemetrexed, its role in the occurrence, development, and treatment of LUAD remains unclear. In the present study, we found that 1C metabolism is associated with the prognosis of LUAD and the effect of immunotherapy. 1C metabolism-related genes are potential biomarkers of prognosis of LUAD and can help to guide immunotherapy in LUAD patients.

Materials and methods

Dataset source

RNA-seq profiles (Counts and FPKM format), somatic mutation, DNA methylation, and phenotype data from The Cancer Genome Atlas (TCGA) LUAD cohort were downloaded from the UCSC Xena database (https://xenabrowser.net/datapages/) (Goldman et al., 2020). Six GSE datasets were downloaded from GEO database (https://www.ncbi.nlm.nih.gov/geo/), including GSE3141, GSE29013, GSE31219, GSE31210, GSE37745, and GSE50081. After normalizing the datasets and removing batch effects, the expression profile data was used for the subsequent analysis.

One-carbon metabolism-associated gene collection

Based on the findings of previous studies, 26 1C metabolism-associated genes were identified (Sasaki et al., 2013; Mehrmohamadi et al., 2014; DeNicola et al., 2015; Liu et al., 2016; Ducker and Rabinowitz, 2017; Fu et al., 2019; Ju et al., 2019; Agulló-Ortuño et al., 2020; Liu et al., 2021; Song S. et al., 2021). These genes were used for further analysis, including *PHGDH, PSAT1, PSPH, FTCD, SHMT1, SHMT2, MTHFD2L, MTHFD2, MTHFD1L, MTHFD1, GCAT, SARDH, DMGDH, GNMT, BHMT, ALDH7A1, CHDH, TYMS, MTR, MTHFR, GART, ATIC, ALDH1L1, ALDH1L2, DHFR,* and *MTFMT*.

Gene expression and prognostic analysis

The expression level differences of 1C metabolism-associated genes between 509 LUAD samples and 58 adjacent normal tissues were tested using a Student's *t*-test. A Kaplan-Meier analysis based on the optimal cutoff point was performed using R packages ("survival" and "survminer") to evaluate the clinical relevance of 1C metabolism-associated genes. A univariate Cox proportional hazard regression analysis was performed to identify the risk factors among these genes. Genes with $p < 0.05$ in the Kaplan-Meier analysis or univariate Cox proportional hazard regression analysis were considered prognosis-related genes.

One-carbon metabolism-associated gene-based clustering and least absolute shrinkage and selection operator regression

According to the results of the Kaplan-Meier analysis and univariate Cox proportional hazard regression analysis, 7 prognostic genes in univariate analysis were actually selected based on *p*-value and hazard ratios, including *TYMS, DHFR, MTHFD1L, MTHFD1, ATIC, GNMT,* and *CHDH*. K-means consensus clustering with these 7 genes was performed to identify subgroups in TCGA cohort. Consensus clustering was employed using the R package "ConsensusCluster" (Yu et al., 2012). The details of this process were set as follows: the number of repetitions = 1,000 bootstraps; resample rate = 0.8. LUAD patients were gathered into cluster 1 (n = 248) and cluster 2 (n = 249). Similarly, consensus clustering was also performed in GEO cohort, and patients were divided into two clusters, including cluster 1 (n = 397) and cluster 2 (n = 437). Kaplan-Meier analysis was used to assess OS differences between the two subgroups in TCGA cohort and GEO cohort, respectively.

The least absolute shrinkage and selection operator (LASSO) regression was performed to identify the prognostic genes of 1C metabolism. According to the result of LASSO regression, 7 prognostic genes were finally selected, including *TYMS, DHFR, MTHFD2L, MTHFD1, ATIC, GNMT, and CHDH*. The risk score of each patient was calculated through the equation: risk score = sum of coefficients × expression level of prognostic genes. The LUAD patients were identified as two subgroups based on the median risk score, including high-risk group and low-risk group.

Gene set enrichment analyses

To determine the different biological processes between the two subtypes, a gene set enrichment analyses (GSEA) was conducted in the Hallmark gene set "c5.all.v7.0.entrez.gmt" of MSigDB using the R package "ClusterProfiler" (Yu et al., 2012). The parameters were set as follows: number of permutations = 1,000 and *p*-value cutoff = 0.05.

Immune infiltrate analysis

The infiltration level of immune cells was calculated through cell type identification by estimating relative subsets of RNA transcripts (CIBERSORT) and single-sample gene set enrichment analysis (ssGSEA) (Hänzelmann et al., 2013; Newman et al., 2015). CIBERSORT (http://cibersort.stanford.edu/) was used to assess the abundances of 22 immune cell types based on the RNA-seq profile of LUAD. The relative abundance

of 28 distinct leukocyte subsets was also calculated through ssGSEA using the R package "GSVA". In addition, the immunoscore of each patient was also calculated through the R package "estimate".

Somatic mutations and DNA methylation analysis

To assess somatic mutations between the different subtypes, the somatic mutation profile of LUAD patients was downloaded from the UCSC Xena Database (Goldman et al., 2020). The somatic mutation data were further analyzed with the "maftools" R package. Similarly, the DNA methylation profiles were also downloaded from the UCSC Xena Database and analyzed with the "limma" R package to identify differential methylation sites (Goldman et al., 2020).

Drug sensitivity analysis

Drug sensitivity analysis was performed using the CellMiner Database (Reinhold et al., 2012). The RNA-seq and compound activity data from the DTP NCI-60 dataset was downloaded from the CellMiner Database (https://discover.nci.nih.gov/cellminer/home.do) and was further analyzed with R Software (version 4.1.2). The correlation between 1C metabolism-associated genes and drug sensitivity was calculated. The following selection criteria were used: Food and Drug Administration approval of the therapeutic or inclusion of the therapeutic in clinical trials, and $p < 0.05$.

One-carbon metabolism-associated gene-based immunotherapy response prediction

To validate the value of 1C metabolism-associated genes in immunotherapy prediction, the IMvigor210 cohort was used to investigate the relationships between 1C metabolism-associated genes and immunotherapy response (Mariathasan et al., 2018). Data from 348 patients who were diagnosed with urothelial cancer and treated with atezolizumab were downloaded from the IMvigor210 cohort.

Statistical analysis

Statistical tests were carried out with R (version 4.1.2), SPSS 22.0 (IBM, NY, United States), and GraphPad Prism 9.0. For quantitative data, statistical significance for normally- and nonnormally-distributed variables was estimated using a Student's *t*-test and Wilcoxon rank-sum test, respectively. Two-sided Fisher's exact tests were performed to analyze contingency tables. Survival analyses were performed using the Kaplan-Meier method, and the log-rank test was used to evaluate the difference between groups. A correlation analysis was performed using a Pearson correlation test. Multivariate analyses were conducted using a Cox regression model to identify the independent risk factors. A p-value < 0.05 was considered statistically significant.

Results

Expression of one-carbon metabolism-associated genes

To evaluate the biological function of 1C metabolism-associated genes in the occurrence and development of LUAD, the expression pattern of 26 1C metabolism-associated genes was assessed in LUAD and adjacent normal tissues. Significant differences were observed in the expression levels of 23 genes between LUAD and adjacent normal tissues (Figure 1A). The expression level of 20 genes was upregulated, including *PSAT1, PSPH, FTCD, SHMT1, SHMT2, MTHFD2L, MTHFD2, MTHFD1L, MTHFD1, GCAT, DMGDH, ALDH7A1, CHDH, TYMS, GART, ATIC, ALDH1L1, ALDH1L2, DHFR* and *MTFMT* (Figure 1B). *GNMT* and *MTHFR* were significantly reduced in LUAD compared to adjacent normal tissues (Figure 1B). These results suggest that 1C metabolism-associated genes have important biological roles in LUAD development.

Prognostic value of one-carbon metabolism-associated genes

We further investigated the prognostic significance of 1C metabolism-associated genes in patients of LUAD in TCGA cohort. The Kaplan-Meier analysis based on an optimal cutoff shows that 17 genes were associated with OS, while nine genes were unrelated to prognosis (Figures 2A–C). The nine genes were identified as risk factors and included *ATIC, GART, MTHFD1, MTHFD1L, MTHFD2, PSPH, SHMT2, DHFR*, and *TYMS* (Figure 2A). Several other genes were considered protective factors, such as *CHDH, GCAT, GNMT, MTHFD2L, MTHFR, MTR, SARDH*, and *SHMT1* (Figure 2B). A univariate Cox regression analysis was also performed and 10 genes had a significant prognostic correlation with OS. *MTHFD2, MTHFD1L, MTHFD1, TYMS, DHFR*, and *ATIC* were risk factors, while *SARDH, CHDH, GNMT* and *MTHFR* were protective factors (Figure 2D). In GEO cohort, the Kaplan-Meier analysis which was based on the optimal cut-off revealed that 23 genes were related to OS, including 13 risk factors and

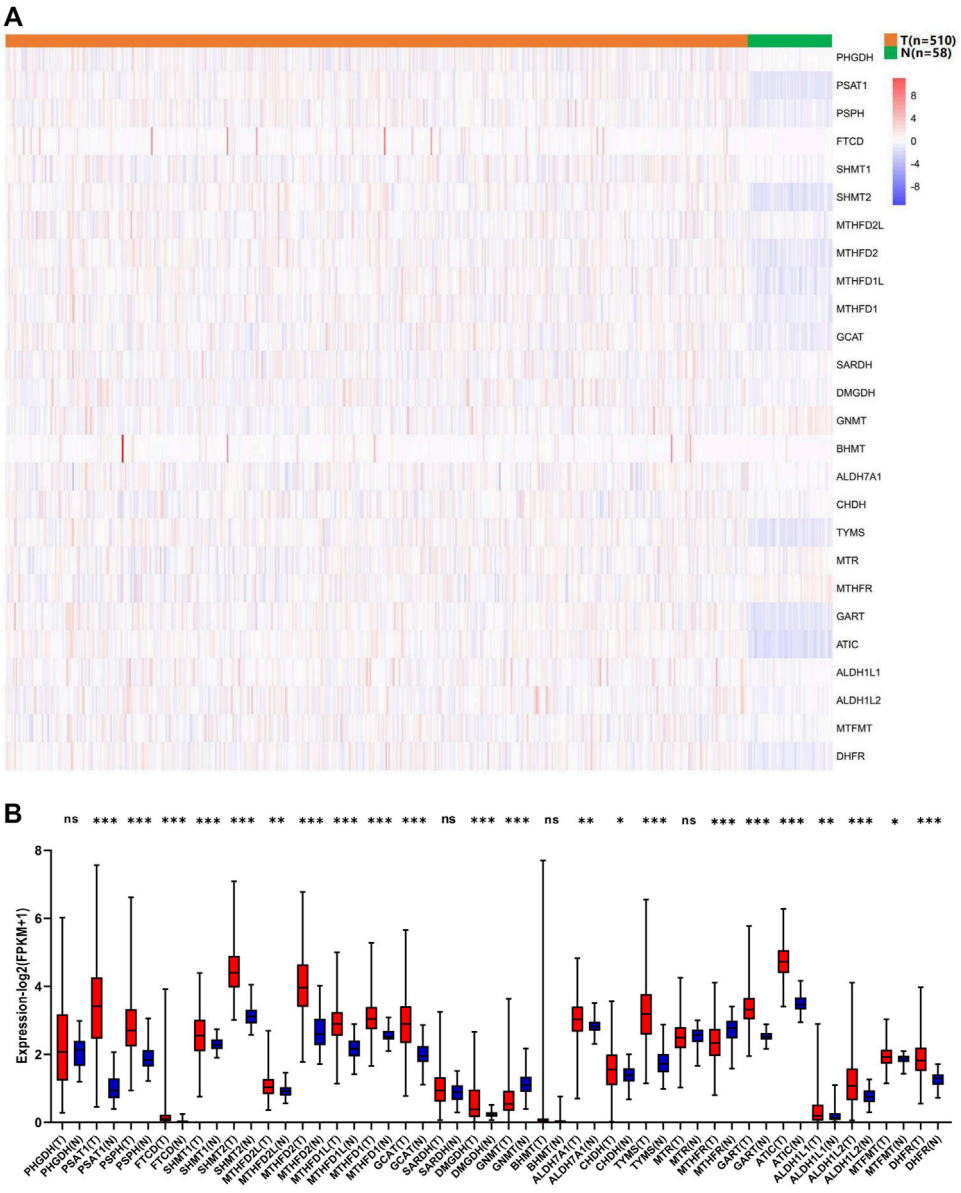

FIGURE 1
Expression levels of one-carbon metabolism associated genes in normal and tumor samples. **(A)** Heatmap of one-carbon metabolism associated genes expression level in each sample; **(B)** The expression difference of one-carbon metabolism associated genes between tumor and normal samples. * means $p < 0.05$; ** means $p < 0.01$; *** means $p < 0.001$; ns means no significant difference.

10 protective factors (Supplementary Figures S1A–C). Univariate Cox regression analysis was also performed and 11 genes were observed associated with OS (Supplementary Figure S1D). In addition, ROC curves were drawn to assess the specificity and sensitivity of 1C metabolism related-genes. The results indicated that the value at 1-, 5- and 10-year were 0.63, 0.67 and 0.74 in TCGA cohort, respectively (Supplementary Figure S2A). The AUC value of 1-year, 5-year and 10-year in GEO cohort were 0.64, 0.65 and 0.63 respectively (Supplementary Figure S2B).

One-carbon metabolism-associated gene-based consensus clustering

Consensus clustering was performed to investigate the heterogeneity of 1C metabolism-associated gene in TCGA cohort. A total of 497 patients with LUAD were clustered into two subtypes. Cluster 1 (n = 248) was characterized by a high expression of high-risk genes while cluster 2 (n = 249) was identified by a high expression level of protective genes (Figure 3A). These two clusters exhibited the opposite

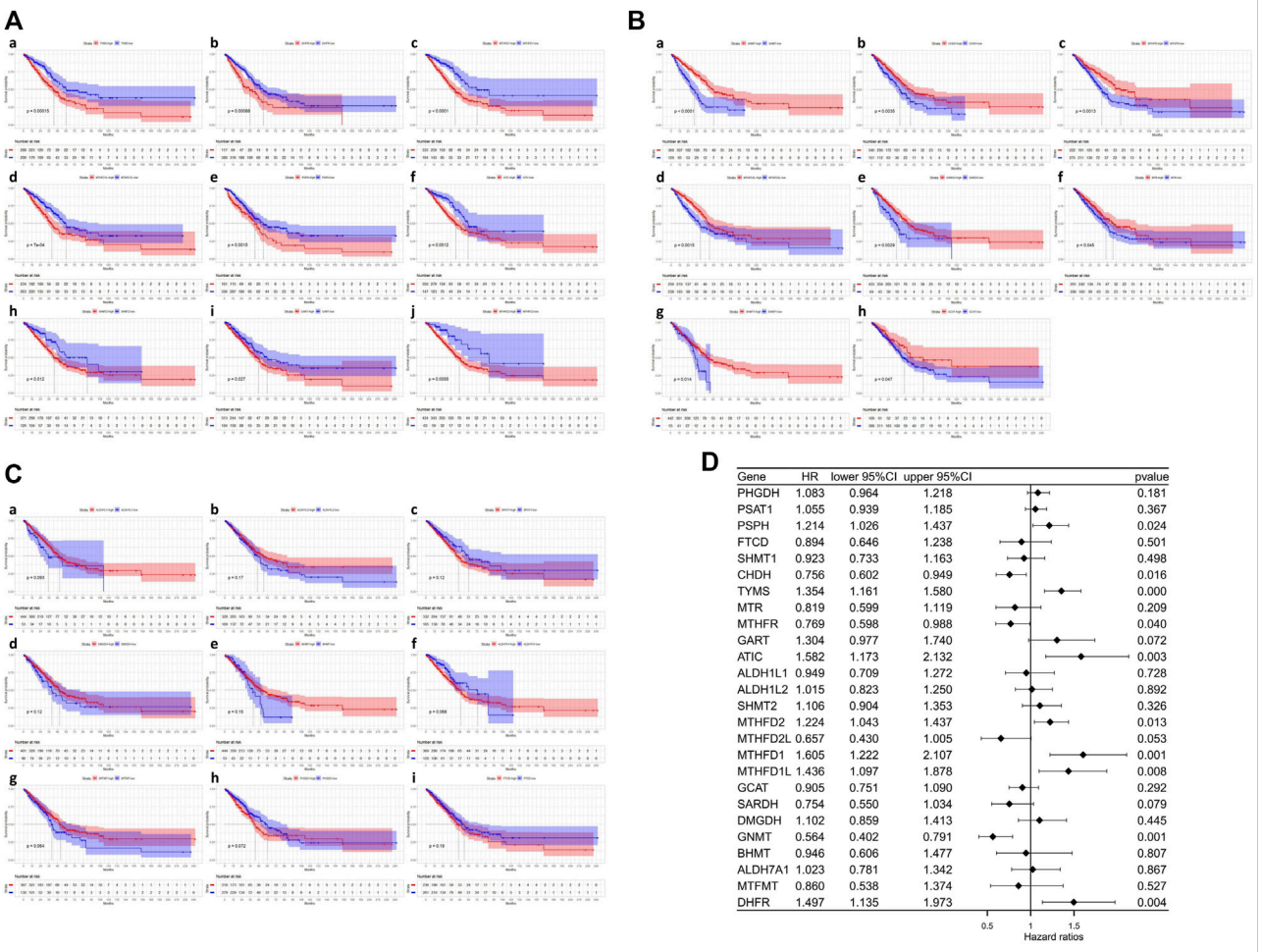

FIGURE 2
Kaplan-Meier survival curves and Univariate Cox regression analysis of one-carbon metabolism associated genes. **(A)** Kaplan-Meier survival curves of nine genes associated with inferior OS; **(B)** Kaplan-Meier survival curves of eight genes associated with superior OS; **(C)** Kaplan-Meier survival curves of nine genes not associated with OS; **(D)** Univariate Cox regression analysis of 26 one-carbon metabolism associated genes.

expression pattern. Cluster 1 was characterized by high expression of *PHSH*, *SHMT2*, *MTHFD2*, *MTHFD1L*, *MTHFD1*, *TYMS*, *GART*, *ATIC*, and *DHFR*, as well as low expression of *SHMT1*, *SARDH*, *GNMT*, *CHDH*, *MTR* and *MTHFR* (Figures 3B,C). A Kaplan-Meier analysis showed that patients who were divided into the cluster 1 subgroup suffered inferior OS (median OS: 41 vs. 60 months, $p = 0.0003$; Figure 3D). Clinical characters between the two clusters were also investigated. Tumor metastasis ($p = 0.016$), advanced stage ($p = 0.036$), and smoking status ($p < 0.001$) were more frequently observed in cluster 1 (Table 1). Similar results were also observed according to LASSO regression and risk score model (Supplementary Figure S3A–H). In addition, consensus clustering was also performed in GEO dataset, and two clusters were identified, including cluster 1 ($n = 397$) and cluster 2 ($n = 437$) (Supplementary Figure S4A). Compared with TCGA cohort, similar expression patterns in two clusters were observed in GEO dataset (Supplementary Figures S4B,C). Kaplan-Meier analysis also revealed that cluster 1 subgroup exhibited an inferior OS in GEO cohort (median OS: 69 vs. 132 months, $p < 0.0001$; Supplementary Figure S4D).

Consensus clustering-based genetic landscape and gene set enrichment analyses

To further investigate the genetic landscape differences between the two subtypes, somatic mutation data in LUAD patients were used. In cluster 1, *TP53* was the most

10.3389/fmolb.2022.1034208

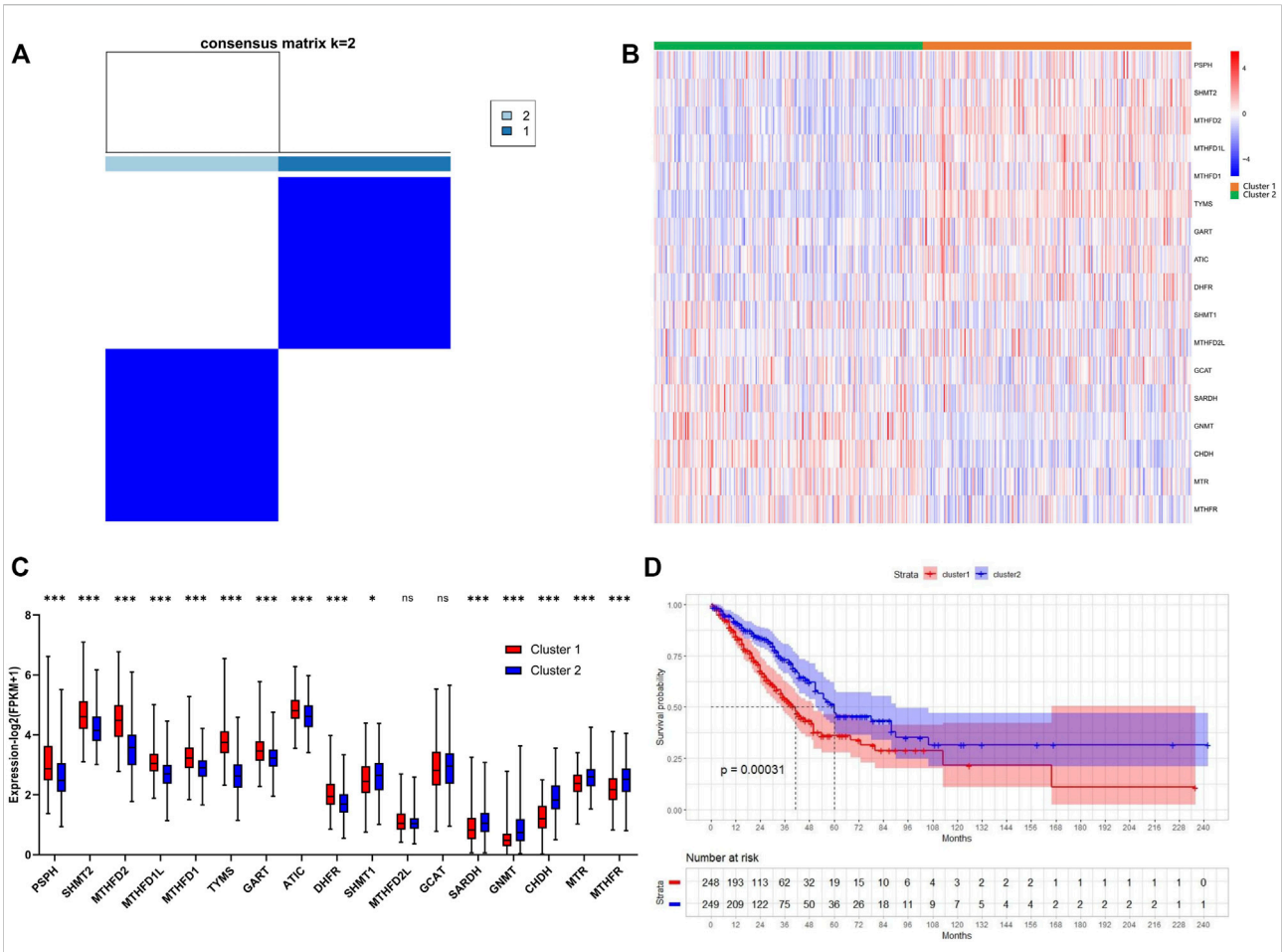

FIGURE 3
Consensus clustering for one-carbon metabolism associated genes in LUAD patients. **(A)** The consensus matrix shows patients with two distinct one-carbon metabolism statuses; **(B)** Heatmap of one-carbon metabolism associated genes expression level in two clusters; **(C)** The expression difference of one-carbon metabolism associated genes in two clusters; **(D)** Kaplan-Meier curves for overall survival in two clusters (Log-rank test). * means $p < 0.05$; ** means $p < 0.01$; *** means $p < 0.001$; ns means no significant difference.

commonly mutated gene—with a frequency of 63%—followed by *TTN, CSMD3, MUC16,* and *RYR2* (Figure 4A). In cluster 2, the top five mutated genes with a relatively low mutation rate were *TTN, TP53, MUC16, KRAS,* and *RYR2* (Figure 4B). Although *TP53* was one of the most frequently mutated genes in both groups, the mutation rate was significantly different between cluster 1 and cluster 2 (63% vs. 33%; Figure 4C). In addition, different mutation frequencies of the same gene between the two clusters were also observed for *TTN, CSMD3, LRP1B, ZFHX4,* and *XIRP2* (Figure 4C), and the tumor mutation burden (TMB) of cluster 1 was significantly higher than in cluster 2 (Figure 4D). GSEA analysis was used to investigate the transcriptomic alterations between these two groups. The most prominent gene ontology terms in cluster 1 were cell cycle, cell cycle procession, chromosome segregation, mitotic cell cycle, and nuclear chromosome segregation (Figure 4E).

Consensus clustering-based immune infiltrate analysis

The infiltration level of immune cells in the TME has been confirmed to play an important role in tumor progression and immunotherapy. To evaluate the difference in immune cell infiltration between the two subgroups, CIBERSORT and ssGSEA were performed in TCGA cohort. The CIBERSORT analysis showed that CD8+ T cells, activated CD4 T cells, M0 macrophages, and M1 macrophages were significantly upregulated in cluster 1, while memory B cells, CD4 memory resting T cells, regulatory T cells, and monocytes were downregulated (Figure 5A). The ssGSEA analysis revealed that activated CD4 T cells, activated CD8 T cells, NK cells, effector memory CD4 T cells, memory B cells, natural killer T cells, and Type 2 T helper cells were significantly upregulated, and Type 17 T helper cells were significantly downregulated, in cluster 1

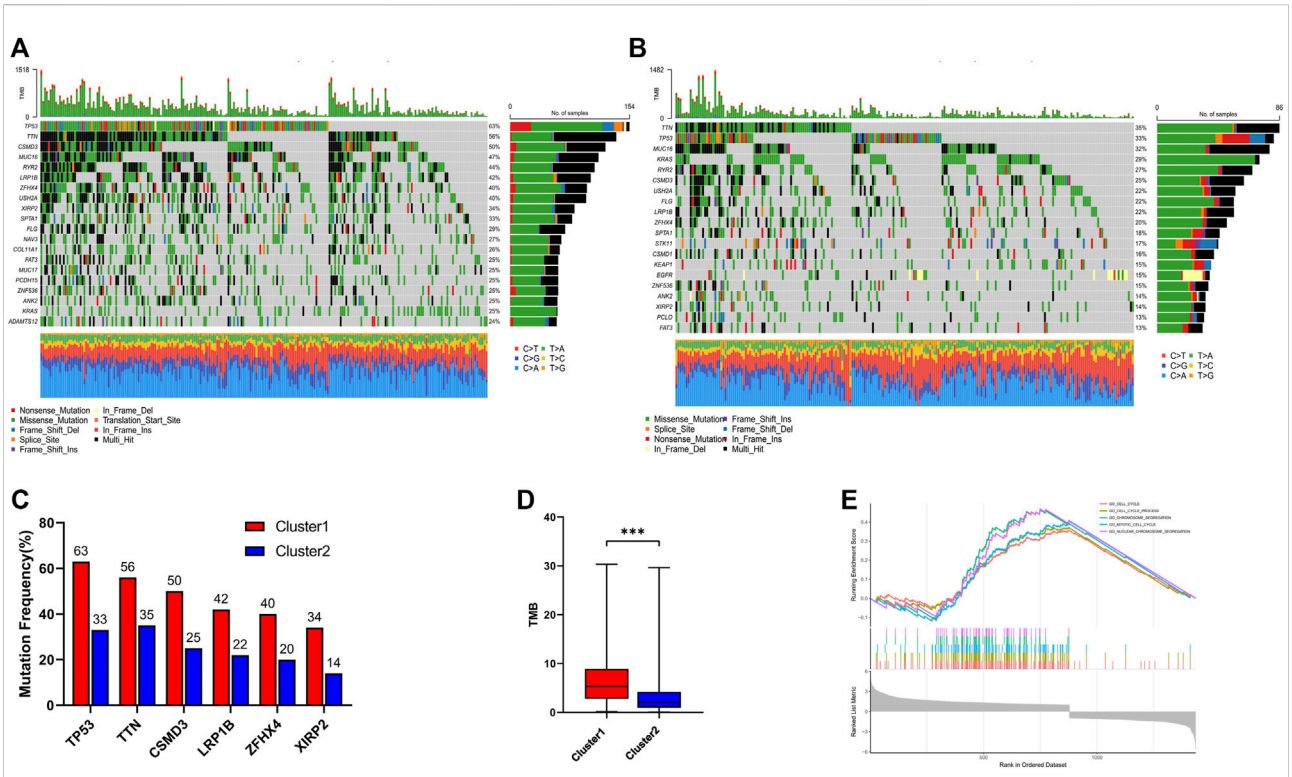

FIGURE 4
Genomic alterations and Gene set enrichment analysis between cluster 1 and cluster 2. **(A)** Landscape of mutation profiles in cluster 1; **(B)** Landscape of mutation profiles in cluster 2; **(C)** The six genes with the greatest variation in mutation frequency between cluster 1 and cluster 2; **(D)** The difference of tumor mutation burden between cluster 1 and cluster 2; **(E)** Top five most significant altered KEGG pathways in cluster 1 compared with cluster 2. *** means $p < 0.001$.

(Figure 5B). Moreover, the expression of PD-1 and PD-L1 was also upregulated in cluster 1 (Figures 5C,D). The correlation of immune cells with 1C metabolism related-genes was also evaluated, and we found that the infiltration level of CD4 T cells was positively related to those genes (Supplementary Figures S5A,B). However, there was no difference was observed between the two clusters on the immune score (Supplementary Figures 6A–D). CIBERSORT and ssGSEA were also performed in GEO cohort. It showed that the infiltration level of immune cells in cluster 1 was higher than in cluster 2 (Supplementary Figures S7A,B).

Correlation analysis of methylation enzymes with one-carbon metabolism-associated genes

1C metabolism supports the biosynthesis and methylation of DNA and RNA by transferring 1C units. To explore the involvement of methylation with 1C metabolism-associated genes, 49 methylation enzymes were selected from previous studies (Zhang and Jia, 2018; Bohnsack et al., 2019; Chen and Zhang, 2020; Zhang C. et al., 2021). In addition, we further evaluated the correlation of methylation enzymes with 1C metabolism-associated genes. The results revealed that the expression of methylation enzymes was significantly positively associated with 1C metabolism-associated genes, such as *TYMS, MTR, MTHFR, SHMT2, MTHFD2L, MTHFD2, MTHFD1L, MTHFD1, GART, ATIC, PSAT1, PSPH, DHFR,* and *FTCD* (Figure 6A). We also investigated the difference in DNA methylation levels between the two groups and observed a significant downregulation of DNA methylation in cluster 1 (Figure 6B). In addition, a further differential analysis revealed that hypermethylation of *SEPT9* and *KLF13* was found in cluster 1, and hypomethylation of *HNRNPR* was also observed (Figure 6C).

One-carbon metabolism-associated gene-based drug sensitivity analysis

To investigate the potential correlation between 1C metabolism-associated genes and drug sensitivity in multiple human tumor cell lines, a correlation analysis was performed in

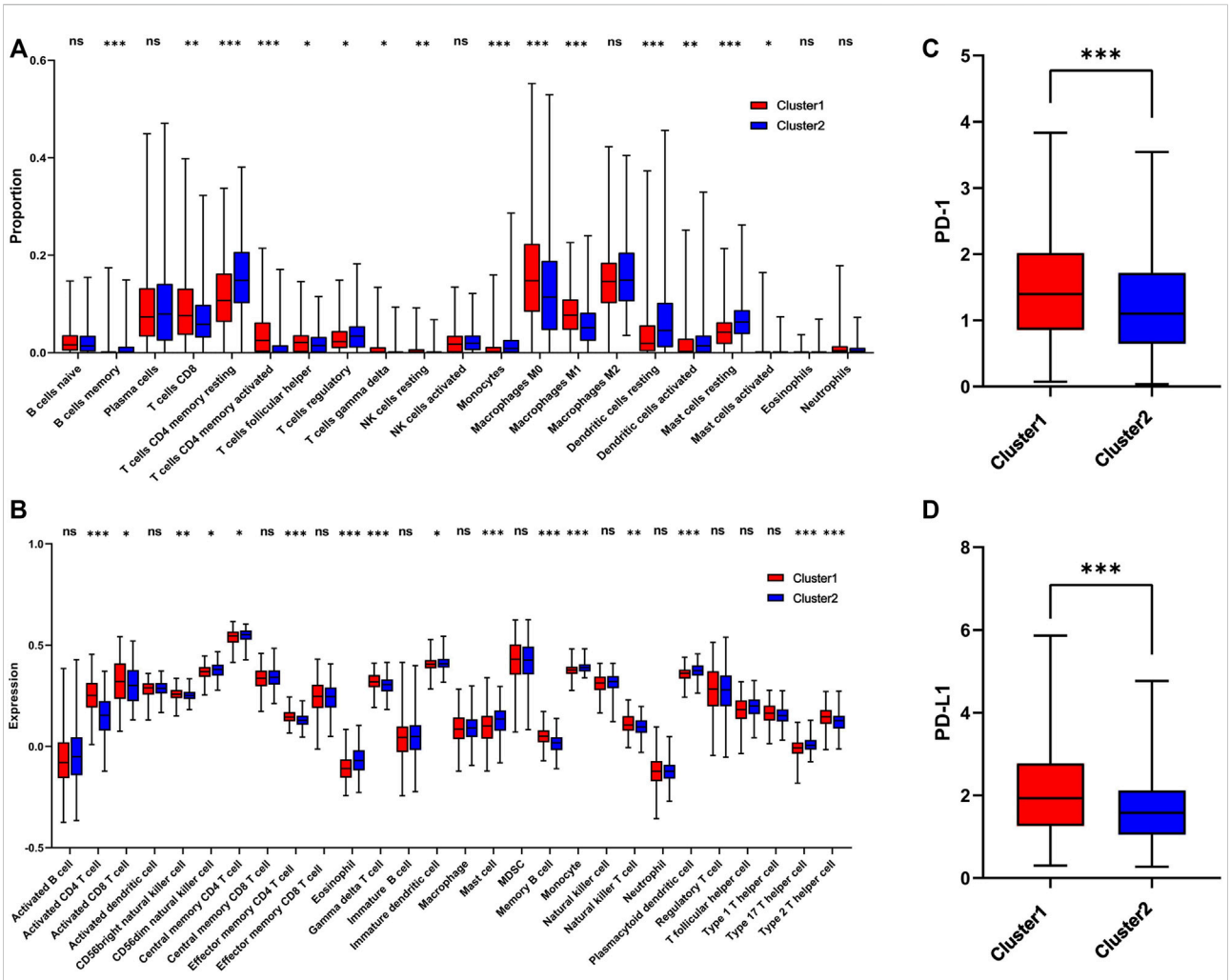

FIGURE 5
Immune profile alterations between cluster 1 and cluster 2. **(A)** The difference of 22 immune cell types between cluster 1 and cluster 2; **(B)** The difference of 28 immune cell types between cluster 1 and cluster 2; **(C)** The difference of PD-1 expression level between the cluster 1 and cluster 2; **(D)** The difference of PD-L1 expression level between cluster 1 and cluster 2. * means $p < 0.05$; ** means $p < 0.01$; *** means $p < 0.001$; ns means no significant difference.

the CellMiner™ database. Cells with the expression pattern of cluster 1 were negatively associated with drug sensitivity to gemcitabine, oxaliplatin, obatoclax, imiquimod, and vorinostat (Figures 7Aa–e), and positively correlated to drug sensitivity to 6-mercaptopurine, vandetanib, copanlisib, AT-9283 and byproducts of CUDC-305 (Figures 7Af–g). Cells with the expression pattern of cluster 2 were negatively correlated with drug sensitivity to etoposide, lapatinib, tepotinib, 6-thioguanine, and uracil mustard (Figures 7Ba–e), but were positively correlated with drug sensitivity to paclitaxel, carboplatin, okadaic acid, pazopanib and alisertib (Figures 7Aa–e). Patients in cluster 1 were also insensitive to paclitaxel and carboplatin, suggesting that patients in cluster 1 are likely resistant to gemcitabine, paclitaxel, oxaliplatin, and carboplatin treatment.

One-carbon metabolism-associated genes are positively correlated with immunotherapy sensitivity

According to the results above, cluster 1 in the LUAD cohort is resistant to chemotherapy but may be sensitive to immunotherapy. We therefore explored the relationship between 1C metabolism-associated genes and immunotherapy in the IMvigor210 cohort. Consensus clustering was also performed, and two clusters (cluster 1 and cluster 2) were identified among patients in the IMvigor210 cohort (Figure 8A). A Kaplan-Meier analysis showed that for patients treated with immunotherapy, cluster 1 had a superior OS compared with cluster 2 (median OS: 11.2 vs. 7.8 months, $p = 0.0034$; Figure 8B). The expression pattern of cluster 1 in the IMvigor210 cohort was similar to that of cluster

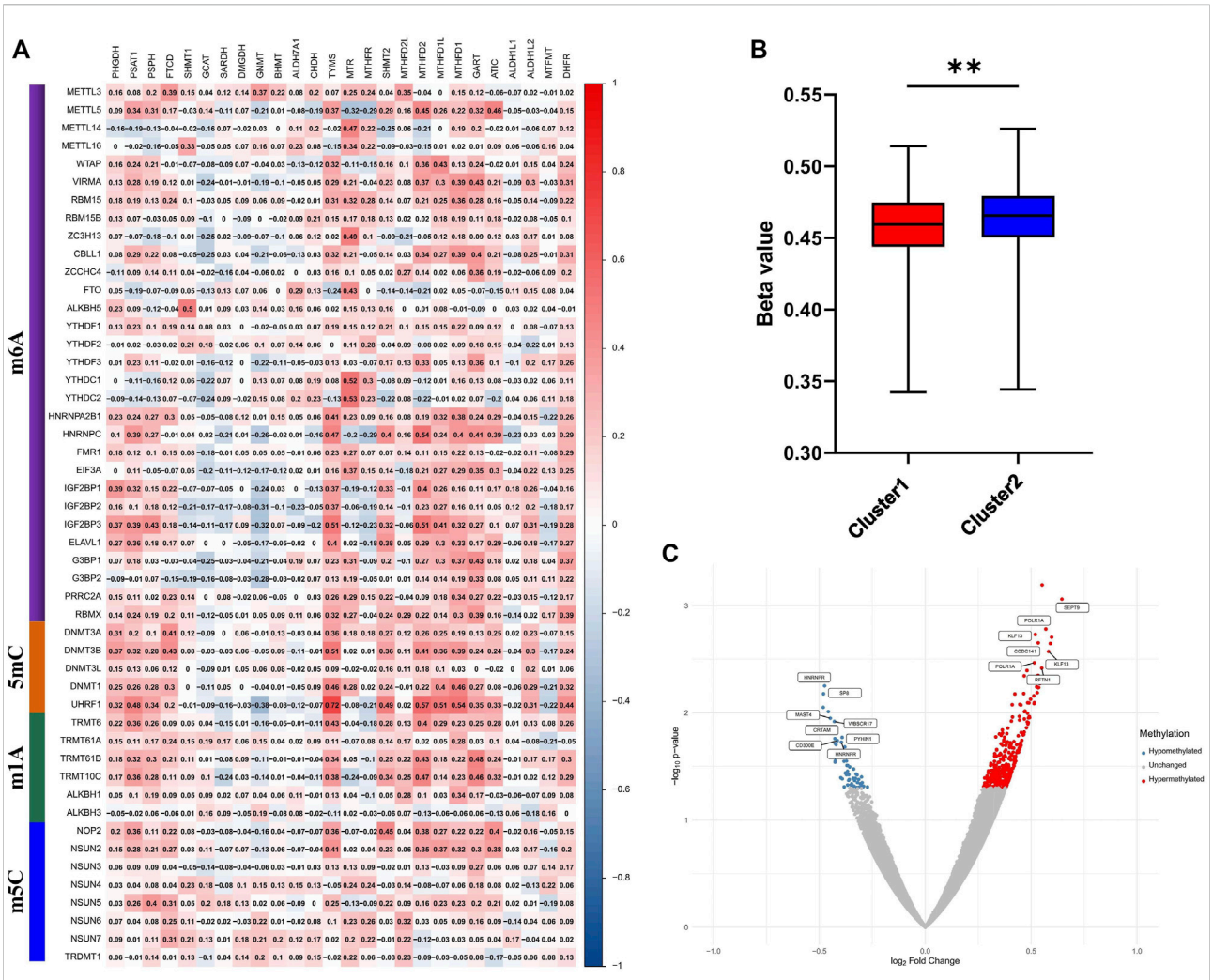

FIGURE 6
Correlation of one-carbon metabolism associated genes with methylation. **(A)** Correlation of 26 one-carbon metabolism associated genes with 49 methylation enzymes; **(B)** The difference of methylation level between cluster 1 and cluster 2; **(C)** Differential analysis of methylation sites between cluster 1 and cluster 2. ** means $p < 0.01$.

1 in the LUAD cohort (Figures 8C,D). A Kaplan-Meier analysis revealed that high expression of *DHFR*, *TYMS*, *GART*, *MTHFD2* and *SHMT1* were correlated with a superior OS (Figure 8E). In addition, the expression levels of *TYMS*, *GART*, and *MTHFD2* in patients with a complete or partial response were higher than for patients with stable or progressive disease (Figure 8F). In addition, ROC curves were drawn to assess the specificity and sensitivity of 1C metabolism related-genes with the value of 0.69 (Supplementary Figure S2C).

Discussion

1C metabolism has been shown to play a role in the occurrence, development, and treatment of multiple cancers. Many 1C metabolic enzymes have been observed upregulated in cancer tissues compared with adjacent normal tissues, and are closely associated with cancer prognosis. However, the literature on 1C metabolism in LUAD patients is sparse. In the present study, we evaluated the expression levels of 1C metabolism-related genes and the correlation with LUAD prognosis. Unsupervised clustering analysis was performed to classify the samples into cluster 1 and cluster 2. We found that cluster 1 was characterized by inferior OS, increased TMB, high PD-1 and PD-L1 expression, as well as enhanced immune infiltration. In addition, 1C metabolism-related genes were positively correlated with the expression of methylation enzymes, and lower methylation levels were observed in cluster 1. Patients in cluster 1 were also resistant to chemotherapy drugs, including pemetrexed, gemcitabine,

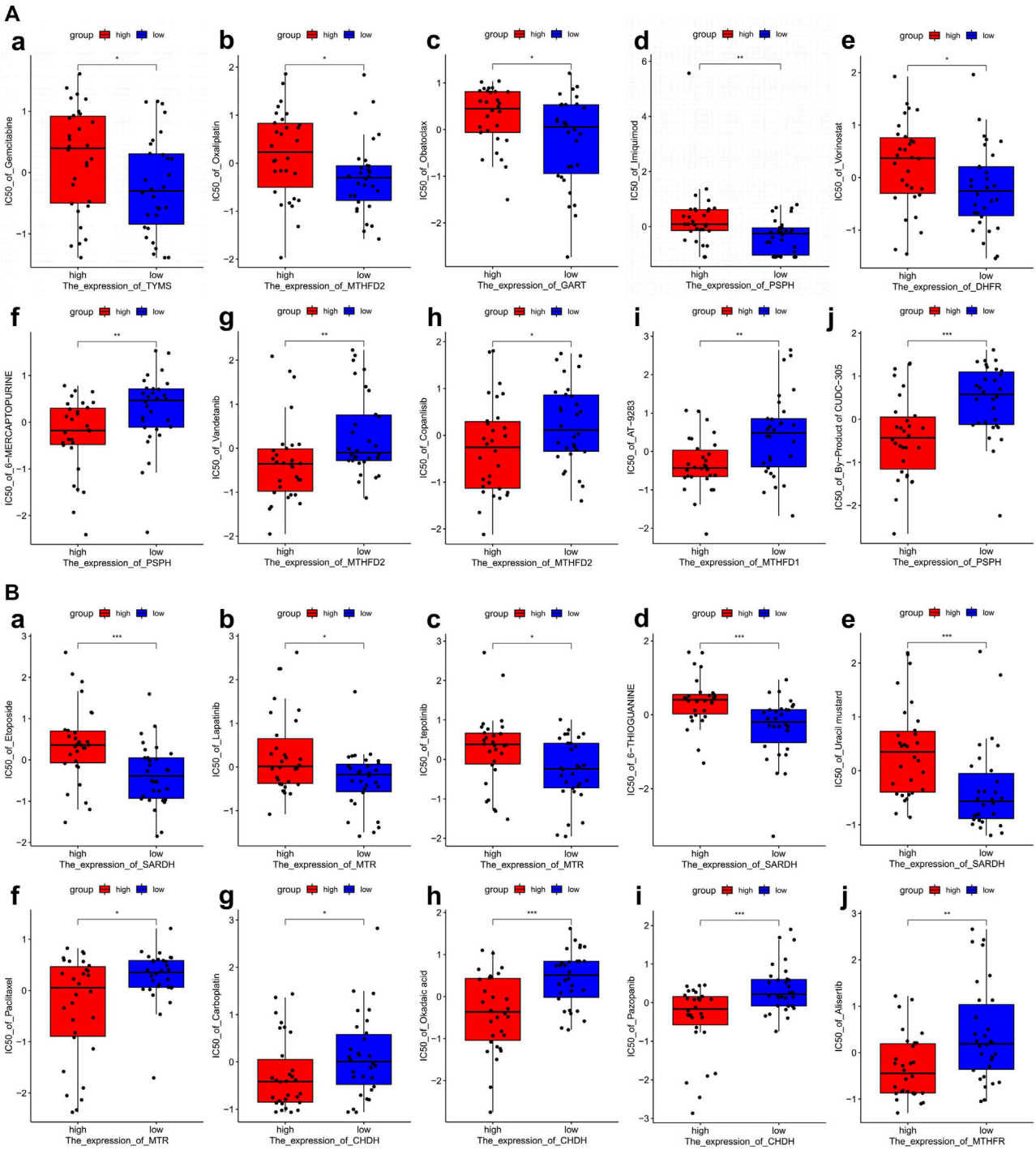

FIGURE 7
Drug sensitivity analysis of one-carbon metabolism associated genes. **(A)** Drug sensitivity analysis based on Cluster 1 expression pattern. (a–e) Five drugs with negatively related sensitivity, (f–j) Five drugs with positively related sensitivity; **(B)** Drug sensitivity analysis based on Cluster 2 expression pattern. (a–e) Five drugs with negatively related sensitivity, (f–j) Five drugs with positively related sensitivity.

paclitaxel, etoposide, oxaliplatin, and carboplatin. We also found that 1C metabolism-related genes were positively correlated with immunotherapy sensitivity.

In our study, 1C metabolism-related genes were selected according to previous studies. The expression levels of these genes were evaluated, and twenty genes were upregulated in

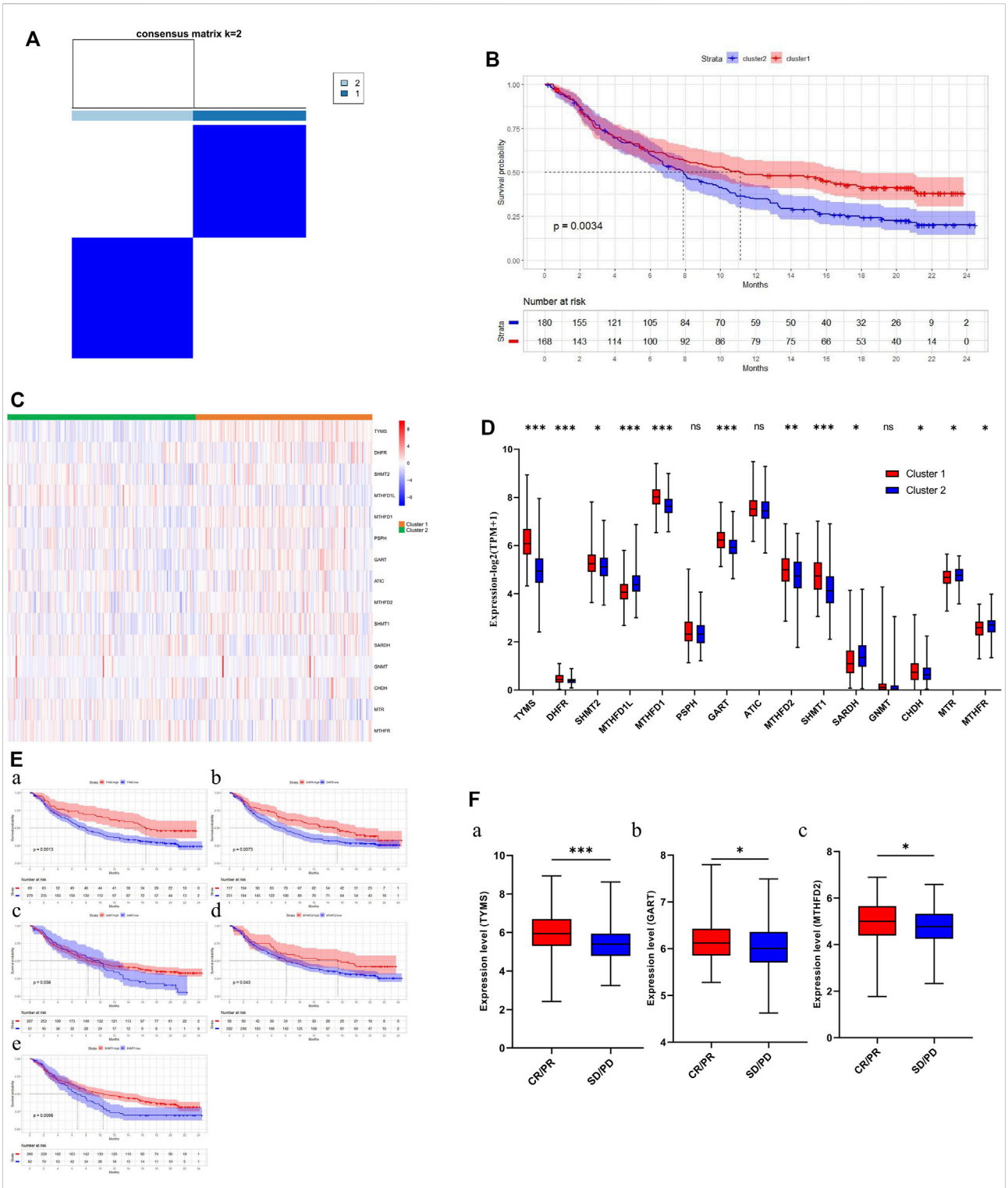

FIGURE 8
Association of one-carbon metabolism related genes with immunotherapy. **(A)** The consensus matrix shows patients with two distinct one-carbon metabolism statuses; **(B)** Kaplan-Meier curves for overall survival in two clusters (Log-rank test); **(C)** Heatmap of one-carbon metabolism associated genes expression level in two clusters; **(D)** The expression difference of one-carbon metabolism associated genes in two clusters; **(E)** Kaplan-Meier survival curves of five genes associated with superior OS; **(F)** The expression difference of three one-carbon metabolism associated genes between CR/PR group and SD/PD group. * means $p < 0.05$; ** means $p < 0.01$; *** means $p < 0.001$; ns means no significant difference.

tumor tissues, while two genes were downregulated. The upregulated genes included *PSAT1, PSPH, FTCD, SHMT1, SHMT2, MTHFD2L, MTHFD2, MTHFD1L, MTHFD1, GCAT, DMGDH, ALDH7A1, CHDH, TYMS, GART, ATIC, ALDH1L1, ALDH1L2, DHFR,* and *MTFMT*, while the downregulated genes included *GNMT* and *MTHFR*. A Kaplan-Meier analysis revealed that 17 genes were associated with prognosis. Among these genes, nine genes were identified as risk factors while the other eight genes were considered protective factors. A univariate Cox regression analysis identified six risk-associated genes and four protective genes. Consensus clustering was performed, and 497 LUAD patients were classified into two clusters. We found that, compared with cluster 2, cluster 1 exhibited the opposite expression pattern and a worse OS.

The genetic landscape of these two groups was also investigated. We observed that somatic mutations were more frequent in the high-risk group. The mutation rates of *TP53, TTN, CSMD3, LRP1B, ZFHX4* and *XIRP2* were significantly higher in the high-risk group compared with the low-risk group. In addition, a heavier TMB was also observed in the high-risk group. Furthermore, the GSEA results suggested that the pathways, which were associated with cell cycle and chromosome segregation, were significantly enriched in the high-risk group. *TP53* (p53) is one of the most common tumor suppressor genes in human cancers. The p53 protein plays an antitumor role by repairing DNA damage, regulating metabolism, normalizing reactive oxygen species levels, modulating expression of non-coding RNAs, and promoting autophagy or ferroptosis (Duffy et al., 2017). TP53 mutations were also positively correlated with PD-L1 expression, TMB, and clinical benefit of PD-1 inhibitors (Dong et al., 2017). In addition, mutant *TTN, CSMD3, LRP1B* was also positively correlated with response rate to immunotherapy (Jia et al., 2019; Brown et al., 2021; Lu et al., 2021). Therefore, LUAD patients in cluster 1 may benefit from immunotherapy treatment.

To investigate the difference in the TME between these two groups, CIBERSORT and ssGSEA were performed. The results revealed that $CD8^+$ T cells, CD4+ T cells, NK cells, Type 2 T helper cells and M1 macrophages were significantly upregulated in the high-risk group, while regulatory T cells were downregulated. Furthermore, the expression of PD-1 and PD-L1 was significantly upregulated. The TME is closely related to the occurrence and progression of tumors, and influences immunotherapy efficacy (Dai et al., 2021). A previous study suggests that CD8+ T cells, CD4+ T cells, NK cells and M1 macrophages influence the clinical benefit of immunotherapy, while Treg cells impair the immunotherapy efficacy (Petitprez et al., 2020). In addition, PD-1 and PD-L1 have also been considered as protective biomarkers for immunotherapy (Petitprez et al., 2020). Previous studies suggested that 1C metabolism was associated the development of immune system (Ducker and Rabinowitz, 2017). The activation of immune cells, especially T cells, required an ample supply of 1C units (Ron-Harel et al., 2016). Therefore, we speculated that 1C metabolism related genes may contribute to the accumulation of folate in TME, which may support the development and activation of immune cells. On the other way, it also may be an underlying competitive absorption of 1C units between the tumor cells and immune cells. Based on these results, we speculate that patients in cluster 1 may benefit from immunotherapy.

1C metabolism generates 1C units to support methylation reactions. To investigate the relationship between 1C metabolism and DNA and RNA methylation, we calculated the correlation of enzymes in the 1C metabolism pathway with 49 methylation enzymes, and the results suggested that 1C metabolism genes are generally positively correlated with methylation enzymes, such as “writers”, “readers”, and “erasers”. A previous review suggests that RNA

TABLE 1 Clinicopathological characteristics of subgroups.

	Cluster 2	Cluster 1	P
Age			0.384
≥70 year	85	75	
<70 year	160	167	
Gender			0.262
Male	108	120	
Female	141	128	
Race			0.590
White	192	192	
Black	27	24	
Other	30	32	
Stage			0.036
I	146	121	
II	55	63	
III	36	44	
IV	7	18	
T stage			0.070
T1	95	71	
T2	119	148	
T3	23	20	
T4	10	8	
N stage			0.079
N0	169	152	
N1–N3	73	92	
M stage			0.016
M0	167	164	
M1	6	18	
Smoking status			<0.001
Non-smoker	47	24	
Current smoker	44	74	
Reformed smoker	152	142	

modifications, including m6A, m1A and m5C, plays an important role in the occurrence and development of lung cancer (Teng et al., 2021). Considering the function of DNA methylation enzymes, we further evaluated the DNA methylation levels between two subgroups and found low methylation levels in the high-risk group. DNA hypomethylation promotes the development of cancer partly by activating oncogenic potential genes (Van Tongelen et al., 2017). A differential analysis suggests that hypermethylation occurs in *SEPT9* and *KLF13*, while hypomethylation occurs in *HNRNPR*. *SEPT9* and *KLF13* have been shown to be antitumor genes in previous studies (Jiao et al., 2019; Yao et al., 2020). The hypermethylation of these genes impairs expression and promotes tumor development. *HNRNPR* contributes to the proliferation and metastasis of gastric cancer (Chen et al., 2019), whereby *HNRNPR* hypomethylation leads to tumor proliferation and metastasis. According to these findings, we speculated that 1C metabolism may play an important role in both methylation and demethylation. On the one hand, the high expression level of 1C metabolism related genes accelerate the generation of 1C units in tumor cells. The abundant methyl groups provide the needs of the methylation of DNA, RNA and proteins, which have been proved by numerous studies (Robertson and Jones, 2000; Van Tongelen et al., 2017; Chen et al., 2019; Jiao et al., 2019; Yao et al., 2020; Dai et al., 2021; Song P. et al., 2021). On the other hand, high expressing 1C metabolism related genes can absorb redundant methyl groups generated by demethylation, thereby promoting the demethylation process. Thus, we speculated that 1C metabolism related genes may contribute to the redistribution of 1C units, by which the important biological processes are influenced. In addition, previous studies indicate that patient tumors with low levels of DNA methylation and high expression of RNA methyltransferases respond better to immunotherapy (Emran et al., 2019; Zhang et al., 2021b). We therefore hypothesized that patients in cluster 1 may benefit from immunotherapy.

We further explored the potential correlation between 1C-related gene expression and drug sensitivity in the CellMiner database. Based on the expression pattern of cluster 1, tumor cells exhibited lower sensitivity to gemcitabine and oxaliplatin, but a higher sensitivity to 6-mercaptopurine. However, tumors with a cluster 2 expression pattern were sensitive to paclitaxel and carboplatin, while resistant to etoposide and lapatinib. Gemcitabine, paclitaxel, etoposide, oxaliplatin, and carboplatin are common drugs for the treatment of NSCLC, however, only a subset of patients benefit from these drugs (Hu et al., 2016; Cui et al., 2020; Esim et al., 2020; Zhang et al., 2021a). Lapatinib is a dual tyrosine kinase inhibitor that has been shown to have promising antitumor effects in NSCLC (Huijberts et al., 2020). 6-mercaptopurine is also an antitumor drug, and the achievement of its therapeutic activity requires the enzymatic conversion to thio-GMP to displace thio-GTP in RNA and DNA (Karran and Attard, 2008). Pemetrexed plays an important role in the treatment of LUAD and has a response rate of 30% (Postmus, 2002). Pemetrexed's antitumor function is achieved by inhibiting three key enzymes in the 1C metabolism pathway: thymidylate synthase (TYMS), dihydrofolate reductase (DHFR), and glycinamide ribonucleotide formyltransferase (GART). A recent study indicates that *MTHFD2* overexpression is involved in resistance to pemetrexed (Yao et al., 2021). We found these four genes to be significantly upregulated in tumor tissues, especially in cluster 1, and were associated with a poor prognosis. Therefore, we can reasonably deduce that LUAD patients with high expression levels of 1C metabolism-related genes may be inherently insensitive to pemetrexed treatment. Likely as a result of the opposite expression pattern of 1C metabolism-related genes in these two groups, the opposite drug sensitivity pattern existed among these two clusters. Patients in cluster 1 were resistant to chemotherapeutic drugs, including pemetrexed, gemcitabine, paclitaxel, oxaliplatin, and carboplatin. Thus, patients in cluster 1 may benefit from immunotherapy.

We speculated that patients in cluster 1 could benefit from immunotherapy. We therefore investigated the relationship between 1C metabolism-related genes and immunotherapy in the IMvigor210 cohort. *DHFR, TYMS, GART, MTHFD2* and *SHMT1* were correlated with a superior OS to immunotherapy. The expression levels of *TYMS, GART,* and *MTHFD2* were also higher in patients with a complete or partial response compared with patients who had stable or progressive disease. Thus, we speculated that 1C metabolism-related genes may play a role in immunotherapy response and lead to a clinical benefit from immunotherapy.

Several limitations exist in our study. Although the results were substantiated in both TCGA and the IMvigor210 cohort, they were not confirmed in LUAD patients who were treated with immunotherapy because of the insufficient transcriptome data from clinical trials. Consequently, different data sets were used in this study. To reduce bias, external validation in larger cohorts is required to validate these findings. Lastly, *in vivo* and *in vitro* experiments are needed to explore the potential mechanisms.

Taken together, our study demonstrates that 1C metabolism-related genes possess potential as therapeutic targets as well as biomarkers of prognosis of immunotherapy in LUAD. Based on the expression pattern of 1C metabolism-related genes, LUAD patients can be classified into two subtypes. Specific subtype characteristics provide information for LUAD clinical management and decision-making. Our findings provide new insight into the mechanisms associated with poor LUAD prognosis, predict efficacy of several therapeutic drug, as well

as assist in identifying biomarkers for immunotherapy in LUAD patients.

Data availability statement

The original contributions presented in the study are included in the article/Supplementary Material, further inquiries can be directed to the corresponding authors.

Author contributions

NZ, QT, and HY contributed to the conception and design of the study. NZ, TL, FR, and LZ contributed to the writing and review of the manuscript. GC, JC, and SX revised the manuscript and finally approved the version to be published. All authors contributed to the article and approved the submitted version.

Funding

The present study was funded by the National Natural Science Foundation of China (82172776), Tianjin Science and Technology Plan Project (19ZXDBSY00060), Tianjin Key Medical Discipline (Specialty) Construction Project (TJYXZDXK-061B), and Diversified Input Project of Tianjin National Natural Science Foundation (21JCYBJC01770).

Conflict of interest

The authors declare that the research was conducted in the absence of any commercial or financial relationships that could be construed as a potential conflict of interest.

Publisher's note

All claims expressed in this article are solely those of the authors and do not necessarily represent those of their affiliated organizations, or those of the publisher, the editors and the reviewers. Any product that may be evaluated in this article, or claim that may be made by its manufacturer, is not guaranteed or endorsed by the publisher.

Supplementary material

The Supplementary Material for this article can be found online at: https://www.frontiersin.org/articles/10.3389/fmolb.2022.1034208/full#supplementary-material

SUPPLEMENTARY FIGURE S1
Kaplan-Meier survival curves and Univariate Cox regression analysis of one-carbon metabolism associated genes. **(A)** Kaplan-Meier survival curves of 13 genes associated with inferior OS; **(B)** Kaplan-Meier survival curves of 10 genes associated with superior OS; **(C)** Kaplan-Meier survival curves of 3 genes not associated with OS; **(D)** Univariate Cox regression analysis of 26 one-carbon metabolism associated genes.

SUPPLEMENTARY FIGURE S2
ROC curves of 1C metabolism related-genes in TCGA, GEO, and IMvigor210 cohort. **(A)** The 1-year, 5-year, and 10-year ROC curve in TCGA cohort; **(B)** The 1-year, 5-year, and 10-year ROC curve in GEO cohort; **(C)** The ROC curve in IMvigor210 cohort.

SUPPLEMENTARY FIGURE S3
Lasso regression and the establishment of risk score model. **(A,B)** Lasso regression for 1C metabolism related-genes in LUAD patients; **(C,D)** The establishment of risk score model in LUAD patients; **(E)** The expression difference of one-carbon metabolism associated genes in high- and low-risk groups; **(F)** Kaplan-Meier curves for overall survival in two subgroups (Log-rank test). * means $p < 0.05$; ** means $p < 0.01$; *** means $p < 0.001$; ns means no significant difference.

SUPPLEMENTARY FIGURE S4
Consensus clustering for one-carbon metabolism associated genes in LUAD patients. **(A)** The consensus matrix shows patients with two distinct one-carbon metabolism statuses; **(B)** Heatmap of one-carbon metabolism associated genes expression level in two clusters; **(C)** The expression difference of one-carbon metabolism associated genes in two clusters; **(D)** Kaplan-Meier curves for overall survival in two clusters (Log-rank test). * means $p < 0.05$; ** means $p < 0.01$; *** means $p < 0.001$; ns means no significant difference.

SUPPLEMENTARY FIGURE S5
Correlation of one-carbon metabolism associated genes with immune cells. **(A)** Correlation of 26 one-carbon metabolism associated genes with 22 immune cells; **(B)** Correlation of 26 one-carbon metabolism associated genes with 28 immune cells.

SUPPLEMENTARY FIGURE S6
ESTIMATE analysis between cluster 1 and cluster 2. **(A)** The ESTIMATE score between cluster 1 and cluster 2; **(B)** The Tumor purity between cluster 1 and cluster 2; **(C)** The immune score between cluster 1 and cluster 2; **(D)** The stromal score between cluster 1 and cluster 2. ns means no significant difference.

SUPPLEMENTARY FIGURE S7
Immune profile alterations between cluster 1 and cluster 2. **(A)** The difference of 22 immune cell types between cluster 1 and cluster 2; **(B)** The difference of 28 immune cell types between cluster 1 and cluster 2. * means $p < 0.05$; ** means $p < 0.01$; *** means $p < 0.001$; ns means no significant difference.

References

Agulló-Ortuño, M. T., García-Ruiz, I., Díaz-García, C. V., Enguita, A. B., Pardo-Marqués, V., Prieto-García, E., et al. (2020). Blood mRNA expression of REV3L and TYMS as potential predictive biomarkers from platinum-based chemotherapy plus pemetrexed in non-small cell lung cancer patients. *Cancer Chemother. Pharmacol.* 85 (3), 525–535. doi:10.1007/s00280-019-04008-9

Behrend, S. J., Giotopoulou, G. A., Spella, M., and Stathopoulos, G. T. (2021). A role for club cells in smoking-associated lung adenocarcinoma. *Eur. Respir. Rev.* 30 (162), 210122. doi:10.1183/16000617.0122-2021

Bohnsack, K. E., Höbartner, C., and Bohnsack, M. T. (2019). Eukaryotic 5-methylcytosine (m^5C) RNA methyltransferases: Mechanisms, cellular functions, and links to disease. *Genes* 10 (2), 102. doi:10.3390/genes10020102

Brown, L. C., Tucker, M. D., Sedhom, R., Schwartz, E. B., Zhu, J., Kao, C., et al. (2021). LRP1B mutations are associated with favorable outcomes to immune checkpoint inhibitors across multiple cancer types. *J. Immunother. Cancer* 9 (3), e001792. doi:10.1136/jitc-2020-001792

Chen, Z., and Zhang, Y. (2020). Role of mammalian DNA methyltransferases in development. *Annu. Rev. Biochem.* 89, 135–158. doi:10.1146/annurev-biochem-103019-102815

Chen, E. B., Qin, X., Peng, K., Li, Q., Tang, C., Wei, Y. C., et al. (2019). HnRNPR-CCNB1/CENPF axis contributes to gastric cancer proliferation and metastasis. *Aging (Albany NY)* 11 (18), 7473–7491. doi:10.18632/aging.102254

Cui, H., Arnst, K., Miller, D. D., and Li, W. (2020). Recent advances in elucidating paclitaxel resistance mechanisms in non-small cell lung cancer and strategies to overcome drug resistance. *Curr. Med. Chem.* 27 (39), 6573–6595. doi:10.2174/0929867326666191016113631

Dai, X., Ren, T., Zhang, Y., and Nan, N. (2021). Methylation multiplicity and its clinical values in cancer. *Expert Rev. Mol. Med.* 23, 23e2. doi:10.1017/erm.2021.4

DeNicola, G. M., Chen, P. H., Mullarky, E., Sudderth, J. A., Hu, Z., Wu, D., et al. (2015). NRF2 regulates serine biosynthesis in non-small cell lung cancer. *Nat. Genet.* 47 (12), 1475–1481. doi:10.1038/ng.3421

Dong, Z. Y., Zhong, W. Z., Zhang, X. C., Su, J., Xie, Z., Liu, S. Y., et al. (2017). Potential predictive value of TP53 and KRAS mutation status for response to PD-1 blockade immunotherapy in lung adenocarcinoma. *Clin. Cancer Res.* 23 (12), 3012–3024. doi:10.1158/1078-0432.CCR-16-2554

Duan, Q., Zhang, H., Zheng, J., and Zhang, L. (2020). Turning cold into hot: Firing up the tumor microenvironment. *Trends Cancer* 6 (7), 605–618. doi:10.1016/j.trecan.2020.02.022

Ducker, G. S., and Rabinowitz, J. D. (2017). One-carbon metabolism in health and disease. *Cell Metab.* 25 (1), 27–42. doi:10.1016/j.cmet.2016.08.009

Duffy, M. J., Synnott, N. C., and Crown, J. (2017). Mutant p53 as a target for cancer treatment. *Eur. J. Cancer* 83, 258–265. doi:10.1016/j.ejca.2017.06.023

Duma, N., Santana-Davila, R., and Molina, J. R. (2019). Non-small cell lung cancer: Epidemiology, screening, diagnosis, and treatment. *Mayo Clin. Proc.* 94 (8), 1623–1640. doi:10.1016/j.mayocp.2019.01.013

Emran, A. A., Chatterjee, A., Rodger, E. J., Tiffen, J. C., Gallagher, S. J., Eccles, M. R., et al. (2019). Targeting DNA methylation and EZH2 activity to overcome melanoma resistance to immunotherapy. *Trends Immunol.* 40 (4), 328–344. doi:10.1016/j.it.2019.02.004

Esim, O., Bakirhan, N. K., Yildirim, N., Sarper, M., Savaser, A., Ozkan, S. A., et al. (2020). Development, optimization and *in vitro* evaluation of oxaliplatin loaded nanoparticles in non-small cell lung cancer. *Daru* 28 (2), 673–684. doi:10.1007/s40199-020-00374-5

Fu, Z., Jiao, Y., Li, Y., Ji, B., Jia, B., and Liu, B. (2019). TYMS presents a novel biomarker for diagnosis and prognosis in patients with pancreatic cancer. *Med. Baltim.* 98 (51), e18487. doi:10.1097/MD.0000000000018487

Goldman, M. J., Craft, B., Hastie, M., Repečka, K., McDade, F., Kamath, A., et al. (2020). Visualizing and interpreting cancer genomics data via the Xena platform. *Nat. Biotechnol.* 38 (6), 675–678. doi:10.1038/s41587-020-0546-8

Hänzelmann, S., Castelo, R., and Guinney, J. (2013). GSVA: Gene set variation analysis for microarray and RNA-seq data. *BMC Bioinforma.* 14, 7. doi:10.1186/1471-2105-14-7

Hirata, E., and Sahai, E. (2017). Tumor microenvironment and differential responses to therapy. *Cold Spring Harb. Perspect. Med.* 7 (7), a026781. doi:10.1101/cshperspect.a026781

Hu, X., Pu, K., Feng, X., Wen, S., Fu, X., Guo, C., et al. (2016). Role of gemcitabine and pemetrexed as maintenance therapy in advanced NSCLC: A systematic review and meta-analysis of randomized controlled trials. *PLoS One* 11 (3), e0149247. doi:10.1371/journal.pone.0149247

Huijberts, S. C. F. A., van Geel, R. M. J. M., van Brummelen, E. M. J., Opdam, F. L., Marchetti, S., Steeghs, N., et al. (2020). Phase I study of lapatinib plus trametinib in patients with KRAS-mutant colorectal, non-small cell lung, and pancreatic cancer. *Cancer Chemother. Pharmacol.* 85 (5), 917–930. doi:10.1007/s00280-020-04066-4

Jia, Q., Wang, J., He, N., He, J., and Zhu, B. (2019). Titin mutation associated with responsiveness to checkpoint blockades in solid tumors. *JCI Insight* 4 (10), e127901. doi:10.1172/jci.insight.127901

Jiao, X., Zhang, S., Jiao, J., Zhang, T., Qu, W., Muloye, G. M., et al. (2019). Promoter methylation of SEPT9 as a potential biomarker for early detection of cervical cancer and its overexpression predicts radioresistance. *Clin. Epigenetics* 11 (1), 120. doi:10.1186/s13148-019-0719-9

Ju, H. Q., Lu, Y. X., Chen, D. L., Zuo, Z. X., Liu, Z. X., Wu, Q. N., et al. (2019). Modulation of redox homeostasis by inhibition of MTHFD2 in colorectal cancer: Mechanisms and therapeutic implications. *J. Natl. Cancer Inst.* 111 (6), 584–596. doi:10.1093/jnci/djy160

Karran, P., and Attard, N. (2008). Thiopurines in current medical practice: molecular mechanisms and contributions to therapy-related cancer. *Nat. Rev. Cancer* 8 (1), 24–36. doi:10.1038/nrc2292

Liu, X., Huang, Y., Jiang, C., Ou, H., Guo, B., Liao, H., et al. (2016). Methylenetetrahydrofolate dehydrogenase 2 overexpression is associated with tumor aggressiveness and poor prognosis in hepatocellular carcinoma. *Dig. Liver Dis.* 48 (8), 953–960. doi:10.1016/j.dld.2016.04.015

Liu, Z., Han, C., and Fu, Y. X. (2020). Targeting innate sensing in the tumor microenvironment to improve immunotherapy. *Cell. Mol. Immunol.* 17 (1), 13–26. doi:10.1038/s41423-019-0341-y

Liu, C., Wang, L., Liu, X., Tan, Y., Tao, L., Xiao, Y., et al. (2021). Cytoplasmic SHMT2 drives the progression and metastasis of colorectal cancer by inhibiting β-catenin degradation. *Theranostics* 11 (6), 2966–2986. doi:10.7150/thno.48699

Lu, N., Liu, J., Xu, M., Liang, J., Wang, Y., Wu, Z., et al. (2021). CSMD3 is associated with tumor mutation burden and immune infiltration in ovarian cancer patients. *Int. J. Gen. Med.* 14, 7647–7657. doi:10.2147/IJGM.S335592

Mariathasan, S., Turley, S. J., Nickles, D., Castiglioni, A., Yuen, K., Wang, Y., et al. (2018). TGFβ attenuates tumour response to PD-L1 blockade by contributing to exclusion of T cells. *Nature* 554 (7693), 544–548. doi:10.1038/nature25501

Mehrmohamadi, M., Liu, X., Shestov, A. A., and Locasale, J. W. (2014). Characterization of the usage of the serine metabolic network in human cancer. *Cell Rep.* 9 (4), 1507–1519. doi:10.1016/j.celrep.2014.10.026

Mu, Q., and Najafi, M. (2021). Modulation of the tumor microenvironment (TME) by melatonin. *Eur. J. Pharmacol.* 907, 174365. doi:10.1016/j.ejphar.2021.174365

Newman, A. M., Liu, C. L., Green, M. R., Gentles, A. J., Feng, W., Xu, Y., et al. (2015). Robust enumeration of cell subsets from tissue expression profiles. *Nat. Methods* 12 (5), 453–457. doi:10.1038/nmeth.3337

Ozpiskin, O. M., Zhang, L., and Li, J. J. (2019). Immune targets in the tumor microenvironment treated by radiotherapy. *Theranostics* 9 (5), 1215–1231. doi:10.7150/thno.32648

Petitprez, F., Meylan, M., de Reyniès, A., Sautès-Fridman, C., and Fridman, W. H. (2020). The tumor microenvironment in the response to immune checkpoint blockade therapies. *Front. Immunol.* 11, 784. doi:10.3389/fimmu.2020.00784

Postmus, P. E. (2002). Activity of pemetrexed (alimta), a new antifolate, against non-small cell lung cancer. *Lung Cancer* 38, S3–S7. doi:10.1016/s0169-5002(02)00350-1

Reinhold, W. C., Sunshine, M., Liu, H., Varma, S., Kohn, K. W., Morris, J., et al. (2012). CellMiner: a web-based suite of genomic and pharmacologic tools to explore transcript and drug patterns in the NCI-60 cell line set. *Cancer Res.* 72 (14), 3499–3511. doi:10.1158/0008-5472.CAN-12-1370

Robertson, K. D., and Jones, P. A. (2000). DNA methylation: past, present and future directions. *Carcinogenesis* 21 (3), 461–467. doi:10.1093/carcin/21.3.461

Ron-Harel, N., Santos, D., Ghergurovich, J. M., Sage, P. T., Reddy, A., Lovitch, S. B., et al. (2016). Mitochondrial biogenesis and proteome remodeling promote one-carbon metabolism for T cell activation. *Cell Metab.* 24 (1), 104–117. doi:10.1016/j.cmet.2016.06.007

Sasaki, S., Watanabe, T., and Nakayama, H. (2013). Analysis of the mRNA expression of chemotherapy-related genes in colorectal carcinoma using the danenberg tumor profile method. *J. Oncol.* 2013, 386906. doi:10.1155/2013/386906

Schiller, J. H., Harrington, D., Belani, C. P., Langer, C., Sandler, A., Krook, J., et al. (2002). Comparison of four chemotherapy regimens for advanced non-small-cell lung cancer. *N. Engl. J. Med.* 346 (2), 92–98. doi:10.1056/NEJMoa011954

Siegel, R. L., Miller, K. D., Fuchs, H. E., and Jemal, A. (2022). Cancer statistics, 2022. *CA Cancer J. Clin.* 72 (1), 7–33. doi:10.3322/caac.21708

Song, P., Tayier, S., Cai, Z., and Jia, G. (2021). RNA methylation in mammalian development and cancer. *Cell Biol. Toxicol.* 37 (6), 811–831. doi:10.1007/s10565-021-09627-8

Song, S., Tian, B., Zhang, M., Gao, X., Jie, L., Liu, P., et al. (2021). Diagnostic and prognostic value of thymidylate synthase expression in breast cancer. *Clin. Exp. Pharmacol. Physiol.* 48 (2), 279–287. doi:10.1111/1440-1681.13415

Tan, W. L., Jain, A., Takano, A., Newell, E. W., Iyer, N. G., Lim, W. T., et al. (2016). Novel therapeutic targets on the horizon for lung cancer. *Lancet. Oncol.* 17 (8), e347–e362. doi:10.1016/S1470-2045(16)30123-1

Teng, P. C., Liang, Y., Yarmishyn, A. A., Hsiao, Y. J., Lin, T. Y., Lin, T. W., et al. (2021). RNA modifications and epigenetics in modulation of lung cancer and pulmonary diseases. *Int. J. Mol. Sci.* 22 (19), 10592. doi:10.3390/ijms221910592

Travis, W. D., Brambilla, E., Burke, A. P., Marx, A., and Nicholson, A. G. (2015). Introduction to the 2015 world health organization classification of tumors of the lung, pleura, thymus, and heart. *J. Thorac. Oncol.* 10 (9), 1240–1242. doi:10.1097/JTO.0000000000000663

Van Tongelen, A., Loriot, A., and De Smet, C. (2017). Oncogenic roles of DNA hypomethylation through the activation of cancer-germline genes. *Cancer Lett.* 396, 130–137. doi:10.1016/j.canlet.2017.03.029

Wang, L., Li, X., Ren, Y., Geng, H., Zhang, Q., Cao, L., et al. (2019). Cancer-associated fibroblasts contribute to cisplatin resistance by modulating ANXA3 in lung cancer cells. *Cancer Sci.* 110 (5), 1609–1620. doi:10.1111/cas.13998

Yao, W., Jiao, Y., Zhou, Y., and Luo, X. (2020). KLF13 suppresses the proliferation and growth of colorectal cancer cells through transcriptionally inhibiting HMGCS1-mediated cholesterol biosynthesis. *Cell Biosci.* 10, 76. doi:10.1186/s13578-020-00440-0

Yao, S., Peng, L., Elakad, O., Küffer, S., Hinterthaner, M., Danner, B. C., et al. (2021). One carbon metabolism in human lung cancer. *Transl. Lung Cancer Res.* 10 (6), 2523–2538. doi:10.21037/tlcr-20-1039

Yu, G., Wang, L. G., Han, Y., and He, Q. Y. (2012). clusterProfiler: an R package for comparing biological themes among gene clusters. *OMICS* 16 (5), 284–287. doi:10.1089/omi.2011.0118

Zhang, C., and Jia, G. (2018). Reversible RNA modification N1-methyladenosine (m1A) in mRNA and tRNA. *Genomics Proteomics Bioinforma.* 16 (3), 155–161. doi:10.1016/j.gpb.2018.03.003

Zhang, C., Zhang, Z., Zhang, Z., Luo, Y., Wu, P., Zhang, G., et al. (2021). The landscape of m6A regulators in small cell lung cancer: molecular characteristics, immuno-oncology features, and clinical relevance. *Mol. Cancer* 20 (1), 122. doi:10.1186/s12943-021-01408-5

Zhang, M., Hagan, C. T., 4th, Foley, H., Tian, X., Yang, F., Au, K. M., et al. (2021a). Co-delivery of etoposide and cisplatin in dual-drug loaded nanoparticles synergistically improves chemoradiotherapy in non-small cell lung cancer models. *Acta Biomater.* 124, 327–335. doi:10.1016/j.actbio.2021.02.001

Zhang, M., Song, J., Yuan, W., Zhang, W., and Sun, Z. (2021). Roles of RNA methylation on tumor immunity and clinical implications. *Front. Immunol.* 12, 641507. doi:10.3389/fimmu.2021.641507

frontiers | Frontiers in Molecular Biosciences

TYPE Review
PUBLISHED 09 January 2023
DOI 10.3389/fmolb.2022.1070383

OPEN ACCESS

EDITED BY
Na Luo,
Nankai University, China

REVIEWED BY
Yu Zhang,
University of Miami, United States
Chien-Feng Li,
National Health Research Institutes, Taiwan

*CORRESPONDENCE
Carmen Jerónimo,
carmenjeronimo@ipoporto.min-saude.pt,
cljeronimo@icbas.up.pt
Margareta P. Correia,
margareta.correia@ipoporto.min-saude.pt

SPECIALTY SECTION
This article was submitted to Molecular Diagnostics and Therapeutics, a section of the journal Frontiers in Molecular Biosciences

RECEIVED 14 October 2022
ACCEPTED 22 November 2022
PUBLISHED 09 January 2023

CITATION
Martins-Lima C, Chianese U, Benedetti R, Altucci L, Jerónimo C and Correia MP (2023), Tumor microenvironment and epithelial-mesenchymal transition in bladder cancer: Cytokines in the game? *Front. Mol. Biosci.* 9:1070383. doi: 10.3389/fmolb.2022.1070383

Tumor microenvironment and epithelial-mesenchymal transition in bladder cancer: Cytokines in the game?

Cláudia Martins-Lima[1,2], Ugo Chianese[2], Rosaria Benedetti[2], Lucia Altucci[2,3,4], Carmen Jerónimo[1,5]* and Margareta P. Correia[1,5]*

[1]Cancer Biology and Epigenetics Group, Research Center of IPO Porto (CI-IPOP)/RISE@CI-IPOP (Health Research Network), Portuguese Oncology Institute of Porto (IPO Porto) and Porto Comprehensive Cancer Center (Porto.CCC) Raquel Seruca, Porto, Portugal, [2]Department of Precision Medicine, University of Campania "Luigi Vanvitelli", Naples, Italy, [3]BIOGEM, Molecular Biology and Genetics Research Institute, Avellino, Italy, [4]IEOS, Institute of Endocrinology and Oncology, Naples, Italy, [5]Department of Pathology and Molecular Immunology at School of Medicine and Biomedical Sciences, University of Porto (ICBAS-UP), Porto, Portugal

Bladder cancer (BlCa) is a highly immunogenic cancer. Bacillus Calmette-Guérin (BCG) is the standard treatment for non-muscle invasive bladder cancer (NMIBC) patients and, recently, second-line immunotherapies have arisen to treat metastatic BlCa patients. Understanding the interactions between tumor cells, immune cells and soluble factors in bladder tumor microenvironment (TME) is crucial. Cytokines and chemokines released in the TME have a dual role, since they can exhibit both a pro-inflammatory and anti-inflammatory potential, driving infiltration and inflammation, and also promoting evasion of immune system and pro-tumoral effects. In BlCa disease, 70–80% are non-muscle invasive bladder cancer, while 20–30% are muscle-invasive bladder cancer (MIBC) at the time of diagnosis. However, during the follow up, about half of treated NMIBC patients recur once or more, with 5–25% progressing to muscle-invasive bladder cancer, which represents a significant concern to the clinic. Epithelial-mesenchymal transition (EMT) is one biological process associated with tumor progression. Specific cytokines present in bladder TME have been related with signaling pathways activation and EMT-related molecules regulation. In this review, we summarized the immune landscape in BlCa TME, along with the most relevant cytokines and their putative role in driving EMT processes, tumor progression, invasion, migration and metastasis formation.

KEYWORDS

tumor microenvironment (TME), bladder cancer, cytokines/chemokines, immune cells, epithelial-mesenchymal transition (EMT)

Introduction

Urothelial cell carcinoma is the most frequent type of bladder cancer (BlCa), corresponding to approximately 90% of the total cases (Cao et al., 2019). 70–80% of the cases are non-muscle invasive bladder cancer (NMIBC), while the remaining 20–30% are muscle-invasive bladder cancer (MIBC) at the time of diagnosis (Yun and Kim, 2013; Chandrasekar et al., 2018). After receiving surgical treatment, almost half of NMIBC patients experience recurrences once or more, with 5–25% of these patients eventually developing to MIBC, the most severe form of the disease (Kamat et al., 2017). Also, a fraction of patients can show metastases at the time of diagnosis, or develop metastatic disease during follow-up, mainly to the bone (Stellato et al., 2021), distant lymph nodes, lung (Dong et al., 2017) and liver (Wang et al., 2020).

BlCa has the highest cumulative treatment cost, compared to other types of cancers (Bryan, 2015). The standard treatment for NMIBCs, except for carcinoma *in situ* (CIS), is transurethral resection of bladder tumor (TURBT). After TURBT, intravesical immunotherapy *Bacillus* Calmette-Guérin (BCG) is usually applied in order to reduce the risk of recurrence and progression (Kamat et al., 2017; Chandrasekar et al., 2018). BCG has a dual role, since it promotes the activation of the immune system and can directly kill tumor cells (Han et al., 2020). Although the mechanisms of BCG-induced immunotherapy are still incompletely understood (Song et al., 2019), it is known that the immune system is triggered when pathogen-associated molecule patterns (PAMPs), located at the bacterium cell wall, are recognized by pattern recognition receptors (PRRs) expressed by antigen-presenting cells (APCs) and bladder tumor cells. This binding promotes MyD88 signaling pathway stimulation, resulting in nuclear factor kappa-B (NF-kB) activation that promotes cytokine transcription (Han et al., 2020). Additionally, BCG-activated skin dendritic cells (DCs) migrate to the draining lymph nodes to activate adaptive $CD4^+$ and $CD8^+$ T cells, and activation of B cells leads to the production of antibodies and memory cells in response to the presence of BCG antigens (Covián et al., 2019).

When tumors progress or are diagnosed as localized MIBC, the recommended treatment is cisplatin-based neoadjuvant chemotherapy (NAC) followed by radical cystectomy (Yafi and Kassouf, 2009; Chandrasekar et al., 2018). Moreover, cisplatin-based chemotherapy is the suggested treatment for individuals who have metastases at the time of diagnosis or develop later on (Chandrasekar et al., 2018). However, most of the times, patients do not respond (Galsky et al., 2012; Minoli et al., 2020) or present several comorbidities impeding the usage of neoadjuvant or adjuvant chemotherapy (Inman et al., 2017). This, alongside with the fact that BlCa is considered as an immunogenic cancer, due to its high tumor mutation burden (TMB) and neoantigens (Hu et al., 2021), led to the Food and Drug Administration (FDA) approving several forms of immunotherapy as second-line treatments for metastatic BlCa patients who had not responded to cisplatin-based chemotherapy (Wołącewicz et al., 2020; Du et al., 2021a). Immune checkpoint blockade (ICB) therapies against PD-L1 (such as atezolizumab, durvalumab and avelumab) or against PD-1 (nivolumab and pembrolizumab) are increasingly promising targets in BlCa (Song et al., 2019; Wołącewicz et al., 2020).

Tumor microenvironment (TME) in BlCa

Bladder tumor microenvironment (TME) has a crucial role in immunotherapy responses (Du et al., 2021a). TME comprise non-cellular components, such as extracellular matrix (ECM) and soluble biological factors or mediators, as cytokines/chemokines, and cellular components, including tumor cells, endothelial cells, stromal cells, and tumor-infiltrating immune cells (TIICs) (Du et al., 2021a; Liu et al., 2021). According to the ESTIMATE algorithm (Yoshihara et al., 2013), patients with high immune score had better prognosis, while patients with high stromal score were associated with shorter survival (Liu et al., 2021). The development of new immunotherapeutic strategies or an improvement in their effectiveness may be aided by a greater comprehension of the bladder TME (Nair et al., 2020).

TME immune cells in BlCa

Macrophages are one the most abundant immune cells in the TME, including in BlCa (Miyake et al., 2016; Du et al., 2021b). Tumor-associated macrophages (TAMs) secrete several soluble molecules, such as cytokines and chemokines, that directly influence tumor growth, metastasis, and drug resistance (Hanada et al., 2000; Pan et al., 2020). In BlCa, higher amounts of $CD68^+$ (pan-macrophage marker) cells, were associated with higher grade and advanced tumors (Huang et al., 2020; Harras and Abo Safia, 2021). Specifically, TAMs ($CD68^+$) number was significantly higher in MIBCs comparing with NMIBCs (Hanada et al., 2000; Viveiros et al., 2022) and higher amounts of $CD68^+$ cells were significantly associated with poorer disease specific survival (DSS) in bladder peritumoral regions and with worse overall survival (OS) and DSS in bladder intratumoral regions (Viveiros et al., 2022). Co-cultures between macrophages and BlCa cell lines showed an increase in colony formation, cell migration and cell invasion (Huang et al., 2020). TME influence macrophage polarization and, consequently, macrophage function (Miyake et al., 2016). Macrophages can be classified in anti-tumor/proinflammatory (M1) and pro-tumor/anti-inflammatory (M2) (Miyake et al., 2016). M2 macrophages ($CD163^+$) are associated with tumorigenesis, tumor growth, angiogenesis, inhibition of immunosurveillance

and ECM degradation (Miyake et al., 2016; Du et al., 2021b; Harras and Abo Safia, 2021). TAMs usually display a bias towards an M2-like phenotype (Takeuchi et al., 2016), as observed in BlCa (Viveiros et al., 2022). Indeed, higher ratio of $CD163^+/CD68^+$ macrophages was correlated with advanced BlCa stage and grade (Takeuchi et al., 2016) and higher amounts of CD163+ were significantly associated with worse DSS and OS (Viveiros et al., 2022).

Fibroblasts are one of the most abundant and active cells in the stroma, performing tissue repair functions (Miyake et al., 2016). Cancer-associated fibroblasts (CAFs) contribute to tumor growth, angiogenesis and treatment resistance by secreting specific cytokines (Miyake et al., 2016). Additionally, CAFs secrete several factors, such as collagen, matrix metalloproteinases (MMPs), chemokines and proteases (Miyake et al., 2016; Du et al., 2021b). Du Y *et al.* demonstrated, *in silico*, that CAFs were abundant in bladder TME. Moreover, the authors showed that higher CAF levels enhanced BlCa progression and were associated with lower OS Du et al. (2021b). Other study demonstrated that co-culture between fibroblasts and BlCa cell lines (UMUC3, T24 and 5637) improved tumor cell invasion (Yeh et al., 2015) and have been associated with cisplatin resistance (Long et al., 2019).

Overall T cells ($CD3^+$) were significant increase in MIBC tumors, comparing with high-grade NMIBCs, although no differences were found in bladder peritumoral areas (Viveiros et al., 2022). It was shown that $CD3^+$ in tumor infiltrating lymphocytes (TILs) were related with poor outcome in BlCa patients (Russo et al., 2022). However, Viveiros N *et al.* proved that an enrichment of $CD3^+$ cells, in the intratumoral area, significantly associated with higher disease-free survival (DFS) (Viveiros et al., 2022) and Sjödahl G *et al.* showed that infiltrating $CD3^+$ cells were significantly associated with good prognosis in the MIBC cases (Sjödahl et al., 2014).

In silico, cytotoxic $CD8^+$ T cells correlated with better patient outcome, being observed a decrease of $CD8^+$ levels in higher BlCa stages (Cao et al., 2019; Zhang et al., 2020). In patient tissues, Zhang S *et al.* and Jóźwicki W *et al.* reported that $CD8^+$ TILs was found mostly in pTa-pT1, comparing with pT2 tumors Jóźwicki et al. (2016), Zhang et al. (2017). Specifically, in Zhang S *et al.* study, higher $CD8^+$ was associated with better OS in non-organ confined disease, but with worse OS in organ-confined disease patients, suggesting that cytotoxic T cells might have anti-tumor activity in non-organ confined disease and a pro-tumor activity in organ-confined disease Zhang et al. (2017). Viveiros N *et al.* observed that MIBC patients presented higher $CD8^+$ expression, comparing with NMIBC high-grade, but, specifically, MIBC tumors with high intratumoral CD8 expression demonstrated higher DFS and OS Viveiros et al. (2022). Additionally, it was shown that poor $CD8^+$ T cell expression, along with type I IFN signature and IFN-inducible inhibitory factors, characterize a non-T cell inflamed bladder TME (Trujillo et al., 2018), usually correlated with poor prognosis and resistance to immunotherapies (Sweis et al., 2016).

In silico, Cao J *et al.* observed that $CD4^+$ memory resting cells decreased with higher BlCa stage, while $CD4^+$ memory activated T cells increased Cao et al. (2019). Zhang Y *et al.* showed, *in silico*, that activated memory $CD4^+$ cells were significantly associated with better outcome, while resting memory $CD4^+$ cells were associated with poor outcome in BlCa patients Zhang et al. (2020). In BlCa tissues, $CD4^+$ levels were significantly higher in pTa-pT1 patients, comparing with most aggressive tumors (Jóźwicki et al., 2016; Viveiros et al., 2022). However, stratifying the tumoral areas, it was observed that $CD4^+$ cells were significantly enriched in high-grade NMIBCs in peritumoral area, while $CD4^+$ levels were significantly abundant in MIBCs in intratumoral area (Viveiros et al., 2022).

Regulatory T (Treg) cells are a subpopulation of $CD4^+$ T cells, characterized by the expression forkhead box protein P3 (FOXP3) transcription factor (Winerdal et al., 2011; Ariafar et al., 2020). Tregs are known to trigger several immunosuppressive mechanisms, both by contact-dependent manner, or indirectly through the secretion of several cytokines, capable of promoting tumor progression (Ariafar et al., 2020). Ariafar A *et al.*, detected a Treg population ($CD4^+CD25+FOXP3+CD127^{low/neg}$) in lymph nodes from BlCa patients, representing about 10% of all $CD4^+$ T cells Ariafar et al. (2020). In this study, Treg cells were significantly higher in patients with at least one involved node, comparing with negative-node patients, although no impact was observed in the survival time (Ariafar et al., 2020), suggesting that Tregs might play a role in tumor metastasis formation (Ariafar et al., 2020). Viveiros N *et al.* observed that Treg cells were significantly lower in the peritumoral area in more advanced stages (pT3 and pT4), but were significantly higher in the intratumoral areas in pTa-pT1 (Viveiros et al., 2022). Moreover, higher Treg amounts in intratumoral areas of high-grade NMIBCs were associated with poor OS and DSS (Viveiros et al., 2022). Jóźwicki W *et al.* showed that Treg amounts were significantly higher in BlCa patients peripheral blood before the surgery, comparing with after surgery (Jóźwicki et al., 2016).

In BlCa, NK cells have been proved to be important in BCG-treatment (Brandau et al., 2001; Esteso et al., 2021), however less is known regarding the role of NK cells in bladder tumor immune surveillance (Sun et al., 2021a). Krpina K *et al.* demonstrated that NMIBC patients with recurrent disease presented significantly higher levels of stromal NK cells, compared with NMIBC patients without recurrence disease (Krpina et al., 2014). Additionally, NMIBC patients with recurrent pTa tumors, recurrent smaller tumors, and recurrent single tumors, presented significantly higher levels of stromal NK cells, than no reccurent NMIBC patients (Krpina et al., 2014). NK cells can be divided in $CD56^{dim}$ NK cells ($CD3^-CD56^{dim}CD16^+$), presenting higher cytolytic activity, and in $CD56^{bright}$ NK cells ($CD3^-CD56^{bright}CD16^-$), presenting immunoregulatory function

through abundant cytokine production (Lin et al., 2004; Poli et al., 2009; Moretta, 2010). In BlCa patients, it was demonstrated that most NK cells were dim NK cells and the proportion of intratumoral dim NK cells were significantly higher in most advanced stages (Mukherjee et al., 2018). Furthermore, higher amounts of $CD56^{bright}$ NK cells were significantly associated with better OS and cancer-specific survival (CSS) (Mukherjee et al., 2018).

DCs are specialized APCs that comprise a rare immune cell population in tumors and in lymphoid organs (Gallo and Gallucci, 2013; Wculek et al., 2020). DCs are essential in trigging antigen-specific immunity and tolerance, since present antigens to T cells and produce immunomodulatory signals by cytokines and cell-cell contacts (Wculek et al., 2020). DCs can be stratified in plasmacytoid (pDC) and in myeloid (mDC) DCs (Martin-Gayo and Yu, 2019). Although DCs are in very low amounts in peripheral blood, Rossi R *et al.* showed a significant decrease of mDCs and pDCs levels in NMIBC patients peripheral blood before TURBT, comparing with healthy donors (Rossi et al., 2013). Also, the authors showed a significant decrease of mDCs in low-grade NMIBC patients before TURBT, compared with high-grade NMIBC patients, while for pDCs no significant differences were observed (Rossi et al., 2013). Patients who received BCG instillations showed peripheral blood evidence of mDC recovery, especially from the third instillation until the completion of the treatment, but no appreciable alterations were detected for pDCs (Rossi et al., 2013). While urine samples did not present mDCs or pDCs before, from third week of BCG instillations mDCs were detected (Rossi et al., 2013). DC cells previously co-cultured with the pumc-91 BlCa cell line resulted in an impaired induction of T cell proliferation. Additionally, a decrease in the levels of T cell-derived cytokines (IL-2, IL-4, IL-6, IL-10, TNF-α, IFN-γ and IL-17A) was observed, compared to control DCs (Xiu et al., 2016), indicating that BlCa cells might induce DC dysfunction, failing to induce T cell responses (Xiu et al., 2016). In patient tissues, high-grade NMIBC and MIBC patients showed similar mature DCs ($CD83^{+}$) levels in bladder peritumoral area and absent expression in intratumoral area (Viveiros et al., 2022).

B cells are important molecules in the adaptive immune response capable of produce both pro- and anti-inflammatory cytokines (Magatti et al., 2020). *In silico* analysis demonstrated that naive B cells were significantly lower in BlCa tumors than in control samples (Zhang et al., 2020). However, Ou Z *et al.* demonstrated that BlCa tissues had more B cells ($CD20^{+}$), than the adjacent normal tissue samples (Ou et al. 2015). Considering high-grade NMIBC and MIBC patients, B cells were only present in bladder peritumoral areas (Viveiros et al., 2022). B cells were significanlty increased in MIBCs, and higher B cell levels were statistically associated with poor DSS (Viveiros et al., 2022). Moreover, Ou Z *et al.* showed that BlCa cell lines' migration and invasion significantly increase after co-culture with B cells and *in vivo*, tumor infiltrating B cells could promote BlCa metastasis Ou et al. (2015).

Immune cells are major cytokines/chemokine producers, playing a role in initiating and triggering immune responses and recruitment of other cell populations to the tumor site. Thus, dysregulations in immune populations in the tumor, can then reflect in the cytokine production in the TME. Those alterations will not only impact in the recruitment and shaping of other immune cells, but also in shaping tumor cells. The impact of TME on driving tumor cell mechanisms that lead to evasion will define tumor development.

Epithelial-mesenchymal transition (EMT) in BlCa

Epithelial-mesenchymal transition (EMT) is a process involved in tumor progression. EMT can be divided in three different types, according to the biological context (Kalluri and Weinberg, 2009). EMT type 1, occurs during embryogenesis, while EMT type 2 relates with inflammation process, wound healing and tissue regeneration (Kalluri and Weinberg, 2009; Yun and Kim, 2013). EMT type 3 is usually associated with tumor progression, particularly in NMIBC to MIBC progression (Kalluri and Weinberg, 2009; Cao et al., 2020). Traditional EMT involves cellular transdifferentiation, which causes changes in desmosomes, adherens junctions, and tight junctions in epithelial cells. A change in the actin cytoskeletal architecture during this phase results in phenotypical changes where front-rear polarity replaces apical-basal polarity. (Koo et al., 2010; Lu and Kang, 2019). Molecularly, it occurs a decrease in epithelial-related genes, such as *CDH1*, *TJP1*, *CLDN1* and specific cytokeratin genes, and an increase in mesenchymal-related genes, such as *VIM*, *CDH2*, *ITGB1* and *ITGB2* (Koo et al., 2010; Lu and Kang, 2019). Additionally, cells exhibiting EMT characteristics can degrade the extracellular matrix by MMPs (Xu et al., 2009; Lu and Kang, 2019). As a result, these cells increase motility, develop resistance to apoptosis, and become isolated, which culminates in cell invasion and migration (Xu et al., 2009; Koo et al., 2010). According to *in silico* analysis, EMT signaling pathways were shown to be significantly activated from NMIBCs to MIBCs (Cao et al., 2020). In this same study, low-risk score patients (based on EMT-related gene signature) showed significantly higher OS and DFS rates than high-risk score, and MIBC samples showed a higher risk-score, comparing with NMIBC patients (Cao et al., 2020). Indeed, in BlCa patient samples, *CDH1* and *TP63* transcript levels were significantly higher in superficial tumors, comparing with MIBCs, while in the most aggressive tumors, *VIM*, *ZEB1*, *ZEB2*, *MMP2* and *MMP9* transcript levels were significantly enhanced (Choi et al., 2012).

It is becoming increasingly evident that cells can undergo rather a partial EMT, exhibiting hybrid epithelial and

mesenchymal features (Lu and Kang, 2019). EMT plasticity involves several epigenetic and genetic alterations, resulting in alterations in the expression of epithelial and mesenchymal markers (Sinha et al., 2020). Cells under partial EMT demonstrate several advantages, comparing with cells with complete EMT phenotypes, such as higher survival mechanisms, tumor-initiating and metastatic potential, which might enhance immune-resistance and chemo-tolerance and increase tumor aggressiveness (Jolly et al., 2015). Indeed, it was shown that there is a "cadherin modulation" in advanced BlCa, where the epithelial marker E-cadherin is expressed at lower levels, simultaneously with high levels of mesenchymal-associated P-cadherin and/or R-cadherin (Martins-Lima et al., 2022).

According to the literature, partial EMT is maintained by phenotypic stability factors (PSFs) and several EMT-inducing transcription factors (EMT-TFs) (Bocci et al., 2019; Sinha et al., 2020). The most well-known EMT-TFs are the zinc-finger-binding transcription factors Snail and Slug, the basic helix-loop-helix (bHLH) factor TWIST1, and the zinc-finger E-box-binding homeobox factors ZEB1 and ZEB2 (Kalluri and Weinberg, 2009; Jolly et al., 2015). Usually, these EMT-TFs are responsible for *CDH1* repression and *CDH2* expression (Wendt et al., 2009). There are specific signaling pathways related with EMT induction, such as transforming growth factor β (TGF-β), bone morphogenetic protein (BMP), Notch, Wnt, hepatocyte growth factor (HGF), epidermal growth factor (EGF), fibroblast growth factor (FGF), platelet-derived growth factor (PDGF), sonic hedehog (Shh), and integrin signaling (Xu et al., 2009; Gonzalez and Medici, 2014; Jolly et al., 2015; Lu and Kang, 2019).

TME cytokines/chemokines in BlCa and impact in EMT modulation

TME has been described to have an important role, not only in EMT induction, but also in the reversion process, mesenchymal-epithelial transition (MET), in distant metastasis (Sinha et al., 2020). Immune cells, besides playing fundamental direct anti-tumoral and pro-tumoral roles, can also display their function through the secretion of cytokines (Zhang and An, 2007; Shelton et al., 2021). Moreover, other types of cells, as endothelial cells, tumor cells, and fibroblasts, are able to produce cytokines (Dunlop and Campbell, 2000; Zhang and An, 2007; Van Linthout et al., 2014). Cytokines are small secreted proteins that participate in cell-cell interaction and communication (Zhang and An, 2007). Cytokine-target cells can be cells that secrete them, in an autocrine action, or the distant cells, in an endocrine action (Zhang and An, 2007). Several cytokines can display both anti-inflammatory and pro-inflammatory potential (Ramesh et al., 2013). Although cytokines participates in tissue damage control and repair (Suarez-Carmona et al., 2017), these soluble molecules can also modulate the TME and, consequently, shape tumor biology (Morizawa et al., 2018), promoting tumor cell survival, proliferation, angiogenesis and immunosuppression (Suarez-Carmona et al., 2017). According to their function and structure, cytokines can be stratified into interferons (IFNs), interleukins (ILs), tumor necrosis factor-alpha (TNFs), transforming growth factors (TGFs), chemotactic cytokines (chemokines), and colony-stimulating factors (CSFs) (Kartikasari et al., 2021).

Chemokines play important roles in inflammatory responses, promoting the recruitment of immune cells responsible for innate and adaptive immune responses (Miyake et al., 2013). There are four chemokine groups, based on two cysteine residue positions, XC, CC, CX3C and CXC (Sokol and Luster, 2015; Kohli et al., 2022). CXC chemokine family can be stratified based on the presence of three amino acid residues (Glu-Leu-Arg; ELR motif), comprising CXCL1, CXCL2, CXCL3, CXCL5, CXCL6, CXCL7, and CXCL8, which are powerful angiogenic molecules and presenting neutrophils chemoattraction abilities (Kawanishi et al., 2008). On the other hand, CXCL4, CXCL9 and CXCL10 are chemokines without ELR motif, displaying chemoattraction capacities for mononuclear cells and can inhibit angiogenesis (Addison et al., 2000; Kawanishi et al., 2008). Chemokines can be cleaved by several molecules, such as, MMPS, cathepsins, thrombin, plasmin and elastase (Hughes and Nibbs, 2018). Chemokines and their receptors can play anti-tumor roles, since these molecules are responsible for the recruitment of immune cells to TME, such as $CD8^+$ T cells, T helper cells and NK (Chow and Luster, 2014; Bule et al., 2021; Kohli et al., 2022). However, chemokine ligands and receptors can play pro-tumoral roles, namely by recruiting pro-tumorigenic immune, such as tumor-associated neutrophils (TAN), TAMs and Treg cells (Bule et al., 2021). Thus, cytokines might also be implicated in the tumor initiation, growth, progression and involved in metastasis formation (Chow and Luster, 2014; Burnier et al., 2015; Kohli et al., 2022).

According to the literature, specific cytokines have been described to be responsible for the transcriptional activation of several genes, including EMT-related genes (Sistigu et al., 2017), consequently contributing to promote BlCa progression, invasion, migration, metastasis formation and angiogenesis (Inoue et al., 2000; Mian et al., 2003; Tsui et al., 2013; Goulet et al., 2019; Zou et al., 2019). Herein, we will focus on some of the most relevant cytokines/chemokines described to be involved in BlCa tumorigenesis and progression and their putative roles in driving EMT processes.

IL-8/CXCL8

IL-8, also known as CXCL8, is an angiogenic factor associated with inflammation and tumorigenesis and it is considered a pro-inflammatory cytokine (Urquidi et al., 2012;

Yao et al., 2020). This chemokine has a powerful leukocyte chemoattraction (Koçak et al., 2004; Jovanović et al., 2010), specially neutrophils attraction (Jovanović et al., 2010). Indeed, in inflammatory regions, IL-8 is responsible to attract and activate neutrophils (Bickel, 1993). Additionally, IL-8 promotes the adhesion of monocytes and neutrophils to endothelial cells, facilitating translocation to inflamed tissues (Gonzalez-Aparicio and Alfaro, 2018). IL-8 can be secreted by lymphocytes, neutrophils, macrophages and by several types of tumor cells (Ou et al., 2015). Furthermore, IL-8 plays an important role in promoting angiogenesis, since contributes to the growth and survival of endothelial cells (Tseng-Rogenski and Liebert, 2009). CXC chemokine receptor 1 (CXCR1) and CXC chemokine receptor 2 (CXCR2), also known as interleukin-8 receptor type beta (IL8RB), are IL-8 receptors, usually expressed in neutrophils and granulocytic myeloid-derived suppressor cells (GR-MDSC) (Miyake et al., 2019; Teijeira et al., 2020). When IL-8 binds to CXCR1 and CXCR2 activates serine/threonine kinases, protein tyrosines and Rho-GTPases, stimulating the expression of proteins related with cell proliferation, survival and cell invasion (Escudero-Lourdes et al., 2012).

In silico GSE32894 database, lower *IL8* levels were associated with improved DSS (Chen et al., 2022). However, in The Cancer Genome Atlas (TCGA) database, it was demonstrated that higher *IL8* levels were significantly associated with basal subtype (usually associated with advanced stage tumors and metastatic disease), comparing with luminal subtype (predominantly associated with papillary histopathological features) (McConkey and Choi, 2018; Chen et al., 2022) (Table 1).

IL-8 urinary protein concentration was found to be significantly higher in bladder tumor patients, comparing with healthy controls (Urquidi et al., 2012; Al-biaty, 2015; Kumari et al., 2017). Furthermore, a significant IL-8 increase was assessed in higher grade and in MIBC tumors, where recurrent disease showed higher IL-8 protein levels, compared with healthy control or newly diagnosed patients (Al-biaty, 2015; Kumari et al., 2017) (Table 1).

Reis ST *et al.* demonstrated that the majority of bladder tumors tissues underexpressed IL-8, comparing with controls (Reis et al., 2012). However, a significant association was established between high-grade tumors and higher *IL8* levels (Reis et al., 2012). Moreover, pT1 and pT2 showed higher *IL8* levels expression than pTa tumors, and recurrent disease patients demonstrated significant higher *IL8* levels, compared to patients that not recurred (Reis et al., 2012) (Table 1).

It was also demonstrated *in vitro* that IL-8 is actually expressed by normal urothelial cells and promotes not only cellular growth, through AKT pathway, but also cellular survival in normal urothelial cells (Tseng-Rogenski and Liebert, 2009). Additionally, *IL8*/IL-8 levels were significantly higher in BlCa cell lines (J82 and TCCSUP) after co-culture with macrophages (Huang et al., 2020). Furthermore, studies *in vitro* suggest a relationship between IL-8 and BCG treatment, since this treatment promotes Ca^{2+} signaling stimulation and NF-kB activation, being responsible for an increase of IL-8 secretion (Ibarra et al., 2019) (Table 1).

According to the literature, in serum samples, IL-8 expression was significantly associated with poor CSS and shorter OS (Morizawa et al., 2018) (Table 1).

In vivo studies demonstrated that IL-8 is able to regulate BlCa tumorigenicity and metastasis formation, and higher IL-8 expression was correlated with higher tumor-induced neovascularization (Inoue et al., 2000). Furthermore, when nude mice implanted with 253J B-V and UMUC3 cell lines in the bladder cell wall were treated with ABX-IL8, an inhibitor of IL-8, it was observed a significant suppression in tumor growth (Mian et al., 2003) (Table 1).

Since IL-8 is upregulated in MIBC tumors (Al-biaty, 2015), and seems to promote tumor growth (Mian et al., 2003) and metastasis formation (Inoue et al., 2000), it suggests that it might play a crucial role in driving EMT. Until now, there are some studies focusing on how deregulation of IL-8 in BlCa might promote alterations in EMT-related molecules and which signaling pathways might be involved in BlCa. It is established that arsenic (As) exposure is a risk factor of BlCa (Escudero-Lourdes et al., 2012). UROtsa, an urothelial cell line, exposed to the arsenic metabolite monomethylarsonous [MMA (III)] undergo malignant transformation. MMA (III) exposure induced *IL8*/IL-8 overexpression, followed by an increase of *CCND1*, *BCL2* and *MMP9* (Escudero-Lourdes et al., 2012). *In vivo*, *IL8* silencing induced a significant decrease of cell proliferation and of tumor formation, while, *in vitro*, was observed a downregulation of *CCND1*, *BCL2* and *MMP9* (Escudero-Lourdes et al., 2012). Furthermore, SVHUC1, a non-malignant BlCa cell line, demonstrated HER2 overexpression and an *IL8*/IL-8 activation upon exposure to As (Zhou et al., 2021). Consequently, IL-8 promoted extracellular signal-regulated kinase (ERK), AKT, and signal transducer and activator of transcription (STAT) 3 signaling activation, resulting in an evident influence in EMT, since the E-cadherin decreased, while Vimentin, Snail, Slug and Twist increased (Zhou et al., 2021). It was shown that a tight junction protein family member, occludin, regulated angiogenesis by controlling IL-8/STAT3 signaling pathway by STAT4 activation (Yang et al., 2022). Retz MM *et al.* showed that co-culture of B cells with the BlCa cell lines, TCCSUP, T24 and J82, increased bladder cell invasion and migration (Ou et al., 2015). The authors suggested that infiltrating B cells can promote IL-8 increase and, consequently, an increase of androgen receptor (AR), leading to MMP-1 and MMP-13 increase (Ou et al., 2015). Corroborating these findings, *in vivo* experiments showed that infiltrating B cells could increase BlCa cell invasion *via* increasing AR signal (Ou et al., 2015). Furthermore, it was

TABLE 1 Cytokines/chemokines levels are deregulated during BlCa progression, growth, invasion, and metastases formation.

	IL-8/CXCL8	CCL2	CXCL1	CXCL12	IL-6	TGF-β1
Receptors	CXCR1; CXCR2/IL8RB (Miyake et al., 2019; Teijeira et al., 2020)	CCR2; CCR4 (Zhang et al., 2010; Gao et al., 2019)	CXCR2 (Kawanishi et al., 2008)	CXCR4; CXCR7 (Shen et al., 2013; Zhang et al., 2018)	IL-6R (Andrews et al., 2002)	TGF-βRI; TGF-βRII (Kim et al., 2001)
Major producing cells	Tumor cells; Lymphocytes; Neutrophils; Macrophages (Ou et al., 2015)	Tumor cells; Macrophages; Fibroblasts; Lymphocytes; Vascular Smooth Muscle (Amann et al., 1998)	Macrophages; Mast cells (De Filippo et al., 2013)	Cancer associated fibroblasts (Du et al., 2021c)	T lymphocytes; Macrophages; Tumor cells; Endothelial cells; Epithelial cells; Muscle cells (Andrews et al., 2002; Rossi et al., 2015; Schuettfort et al., 2022)	Regulatory T cells; Cancer-associated fibroblasts; M2 macrophages; MDSC (Ao et al., 2007; Yu et al., 2014; Yeh et al., 2015; Groth et al., 2019; Efiloğlu et al., 2020; Horibe et al., 2021)
Urine	↑ in BlCa patients than controls (Urquidi et al., 2012; Al-biaty, 2015; Kumari et al., 2017); ↑ in MIBC tumors (Al-biaty, 2015); ↑ in undifferentiated tumors (Al-biaty, 2015; Kumari et al., 2017); ↑ in recurrent disease (Al-biaty, 2015; Kumari et al., 2017)	↑ in pT2-pT4 than pT1 (Amann et al., 1998)	↑ in BlCa patients than controls (Kawanishi et al., 2008; Burnier et al., 2015); ↑ in pT1-pT4 than pTa (Kawanishi et al., 2008)	↓ *CXCL12A* in lower grade (Gosalbez et al., 2014); ↑ *CXCL12B* in higher grade (Gosalbez et al., 2014); CXCL12G was not detected (Gosalbez et al., 2014)	↑ in pT3-pT4 than patients with early stages or than non-malignant disease (Chen et al., 2013); ↑ IL-6 in lower grades (Kumari et al., 2017); ↑ IL-6 associated with ↓ OS (Morizawa et al., 2018)	↑ in BlCa patients than controls or chronic cystitis disease (Helmy et al., 2007)
In vitro	IL-8 promotes cellular growth and cellular survival in normal urothelial cells (Tseng-Rogenski and Liebert, 2009)	↑ in high-grade BlCa cell lines (Chiu et al., 2012); ↓ in low-grade BlCa cell lines (Chiu et al., 2012)	↑ in most aggressive BlCa cell lines (Kawanishi et al., 2008); ↑ CXCL1 increases invasive abilities of BlCa cell lines (Kawanishi et al., 2008; Miyake et al., 2019); ↑ CXCL1 increases angiogenesis abilities of BlCa cell lines (Miyake et al., 2019)	Regulates BlCa cell invasion abilities (Shen et al., 2013); Regulates BlCa cell migration abilities (Retz et al., 2005)	IL-6 was associated with BlCa cell line invasion (Yeh et al., 2015); IL-6 was associated with BlCa cell line growth/proliferation (Okamoto et al., 1997; Miyake et al., 2019)	TGF-β1 was associated ↑ BlCa cell line proliferation; TGF-β1 was associated ↑ BlCa cell line colony formation; TGF-β1 was associated ↑ BlCa cell line invasion; TGF-β1 was associated ↑ BlCa cell line migration (Bian et al., 2013; Zhang et al., 2016; Zou et al., 2019)
Patient tissues	↓ in BlCa patients (Reis et al., 2012); ↑ in undifferentiated tumors (Reis et al., 2012); ↑ in pT1-pT2 than pTa (Reis et al., 2012); ↑ in recurrent disease (Reis et al., 2012)	↑ in BlCa patients than normal/adjacent tissues (Wang et al., 2017); ↑ in undifferentiated tumors (Gao et al., 2019); ↑ in higher stage tumors (Gao et al., 2019); ↑ in lymph node metastasis (Gao et al., 2019); In MIBC patients, ↑ CCL2 in tumor cells was associated with ↓ OS, ↓ DSS and ↓RFS (Eckstein et al., 2020)	Normal or benign tissues did not express CXCL1 (Kawanishi et al., 2008; Miyake et al., 2013); ↑ in undifferentiated tumors (Miyake et al., 2013); ↑ in higher stage tumors (Kawanishi et al., 2008; Miyake et al., 2013); ↑ CXCL1 was associated with ↓ OS (Miyake et al., 2013); ↑ CXCL1 was associated with ↓ DSS (Miyake et al., 2013)	↑ in BlCa patients (Yang et al., 2015) vs. ↓ in BlCa patients (Du et al., 2021c); ↑ in undifferentiated tumors (Batsi et al., 2014); ↑ in higher stage tumors (Batsi et al., 2014); ↑ in recurrent disease (Batsi et al., 2014); Normal tissue did not express *CXCL12* (Yang et al., 2015)	↑ IL-6/*IL6* in BlCa patients than normal tissues or cystitis patients (Chen et al., 2013); ↑ in early stages than non-malignant disease (Chen et al., 2013); ↑ was mostly associated in MIBC tissues (Chen et al., 2013); IL-6 is expressed in non-malignant tissues (Chen et al., 2013)	↓ in normal urothelium (Yang et al., 2018; Zou et al., 2019); ↑ in higher stage tumors (Kim et al., 2001; Yang et al., 2018; Stojnev et al., 2019; Zou et al., 2019); ↑ in undifferentiated tumors (Zou et al., 2019; Stojnev et al., 2019); ↑ was correlated with ↑ cancer-specific death (Stojnev et al., 2019) vs. ↑ *TGFB1* in lower stage tumors (Miyamoto et al., 1995); ↑ *TGFB1* in well-differentiated tumors (Miyamoto et al., 1995); ↑ TGF-β1 in BlCa tumors than normal tissues (Miyamoto et al., 1995)
In silico	↓ *IL8* was associated with ↑ DSS (Chen et al., 2022); ↑*IL8* was associated with basal subtype (Chen et al., 2022)	↓ *CCL2* in BlCa patients than the controls (Li et al., 2021); ↑ *CCL2* associated with better DFS (Li et al., 2021)	↑ *CXCL1* in BlCa tumors than controls (Sun et al., 2021b); ↑ *CXCL1* was associated with ↓ OS (Sun et al., 2021b)	↓ *CXCL12* in BlCa tumors than controls (Sun et al., 2021b; Du et al., 2021c) vs. In tumors, ↑ *CXCL12* was associated with ↑ stage (Sun et al., 2021b; Liu et al., 2021); In tumors, ↑ *CXCL12* was associated with ↑ lymph node (N2 than N0) (Liu et al., 2021); In tumors, ↑ *CXCL12* was associated with ↓ prognosis (Sun et al., 2021b; Liu et al., 2021)	↑ in undifferentiated tumors (Goulet et al., 2019); ↑ in advanced tumors (Goulet et al., 2019)	↑ *TGFB1* in MIBCs, comparing with NMIBCs (Zou et al., 2019); ↑ *TGFB1* was associated with ↑ risk of death (Zou et al., 2019); ↑ *TGFB1* was associated with ↓ DFS (Zou et al., 2019); ↑ *TGFB1* was associated with ↓ OS (Zou et al., 2019)
In vivo	IL-8 regulates tumor growth (Mian et al., 2003); IL-8 regulates BlCa tumorigenicity (Inoue et al., 2000); IL-8 regulates metastasis formation (Inoue et al., 2000); IL-8 regulates neovascularization (Inoue et al., 2000)	Not reported	CXCL1 promotes tumor growth (Miyake et al., 2016); CXCL1 promotes bladder tumor cells attachment to the bladder wall (Miyake et al., 2016); CXCL1 influences proliferation (Miyake et al., 2019); CXCL1 influences angiogenesis (Miyake et al., 2019); CXCL1 influences apoptosis (Miyake et al., 2019)	Influences BlCa cell growth (Zhang et al., 2018)	IL-6 was associated with tumor growth/proliferation (Chen et al., 2013); IL-6 was associated with tumor invasion (Chen et al., 2013); IL-6 was associated with angiogenesis (Chen et al., 2013)	TGF-β1 was associated with ↑ tumor size (Zou et al., 2019); TGF-β1 was associated with ↑ tumor weight (Zou et al., 2019)

(Continued on following page)

10.3389/fmolb.2022.1070383

TABLE 1 (*Continued*) Cytokines/chemokines levels are deregulated during BlCa progression, growth, invasion, and metastases formation.

	IL-8/CXCL8	CCL2	CXCL1	CXCL12	IL-6	TGF-β1
Serum	IL-8 expression was associated with ↓ CSS (Morizawa et al., 2018); IL-8 expression was associated with ↓ OS (Morizawa et al., 2018)	Not reported	Not reported	Not reported	↑ IL-6 in recurrent patients than non-recurrent patients (Kumari et al., 2017); ↑ IL-6 in poor RFS (Kumari et al., 2017); IL-6 was associated with ↓ CSS (Morizawa et al., 2018); ↓ T2-T4 patients than Ta-T1 patients and controls (Yang et al., 2017)	↑ TGF-β1 related with ↓ risk tumor progression (Efiloğlu et al., 2020); ↓ TGF-β1 in pT4 than superficial and invasive tumors (pT2-pT3) (Eder et al., 1996) vs. ↑ TGF-β1 related with ↑ tumor grade and aggressiveness (Eder et al., 1997); ↑ TGF-β1 related with superficial tumors (pTa-pT1) than normal samples (Eder et al., 1997)
Plasma	Not reported	Not reported	Not reported	Not reported	↑ IL-6/IL-6sR median levels in advanced patients (Andrews et al., 2002; Schuettfort et al., 2022); ↑ IL-6/IL-6sR median levels in lymph vascular invasion (Andrews et al., 2002; Schuettfort et al., 2022); ↑ IL-6/IL-6sR median levels in lymph node metastasis (Andrews et al., 2002; Schuettfort et al., 2022); ↑ IL-6/IL-6sR median levels in recurrent disease (Schuettfort et al., 2022); ↑ IL-6/IL-6sR median levels in patients who deceased from BlCa (Schuettfort et al., 2022); ↑ IL-6/IL-6sR median levels associated with ↓ OS, ↓ RFS and ↓CSS (Schuettfort et al., 2022); ↑ IL-6 in BlCa patients than healthy patients (Andrews et al., 2002)	↑ in MIBC patients (Shariat et al., 2001); ↑ in MIBC patients with regional and distant lymph node (Shariat et al., 2001); ↑ related with ↑ risk of disease recurrence (Shariat et al., 2001); ↑ related with ↑ mortality (Shariat et al., 2001)
EMT-related molecules	*IL8* silencing promoted ↓ *MMP9* (Escudero-Lourdes et al., 2012); IL-8 treatment suppresses E-cadherin, while ↑ Vimentin, ↑ Snail, ↑ Slug and ↑ Twist (Zhou et al., 2021); ↑ IL-8 promoted ↑ MMP-1 and ↑ MMP-13 (Ou et al., 2015); IL-8 regulates *MMP9*/MMP-9 and MMP-2 (Inoue et al., 2000; Mian et al., 2003)	↑ CCL2 promoted ↑ MMP-9, ↑ N-cadherin, ↑ Twist, ↑ Snail and ↑ Vimentin (Rao et al., 2016)	Overexpression of CXCL1 in TAMs and CAFs, promoted ↓ E-cadherin and ↑ MMP-2 (Miyake et al., 2016); A significant correlation was established between CXCL1 and MMP-13 (Kawanishi et al., 2008)	Inhibition of CXCR4 promoted ↓ β-catenin, ↓ MMP-2 and ↓ c-Myc and ↑ E-cadherin levels (Zhang et al., 2018); CXCL12/CXCR4 inhibition promoted ↓ E-cadherin and ↑ c-Myc (Zhang et al., 2018); CXCL12/CXCR4 seems to be important in β-catenin regulation (Zhang et al., 2018)	↑ *IL6* promoted ↓ N-cadherin and ↓ Vimentin levels (Tsui et al., 2013); ↓ *IL6* led to ↓ E-cadherin, but ↑ N-cadherin and ↑ Vimentin levels (Tsui et al., 2013) vs. ↓ *IL6* led to ↑ E-cadherin, but ↓ MMP9 (Chen et al., 2013)	↑ TGF-β1 levels promoted ↓ E-cadherin (Chen et al., 2014, Zou et al., 2019), ↓ *miR-200b* (Chen et al., 2014), ↑ N-cadherin (Chen et al., 2014), ↑ Vimentin (Chen et al., 2014, Zou et al., 2019), ↑ MMP-2 (Zou et al., 2019), ↑ MMP-9 (Zou et al., 2019), ↑ Snail (Zou et al., 2019), and ↑ MMP-16 (Chen et al., 2014)
EMT-related signaling pathways	Overexpression of IL-8 promoted ERK, AKT and STAT3 pathways activation (Zhou et al., 2021); IL-8 regulates the expression of MMPs by NF-kB (Mian et al., 2003)	CCL2-CCR2 interaction may facilitate migration by phosphorylating paxillin y118 through a protein kinase C (PKC)-dependent mechanism (Chiu et al., 2012)	Not reported	CXCL12/CXCR4 promotes STAT3 phosphorylation, resulting in BlCa invasion (Shen et al., 2013)	EMT-player alterations, induced by IL-6, might be regulated by STAT3 signaling pathway activation (Chen et al., 2013); E-cadherin expression might be inhibited by IL6-STAT3 signaling pathways (Chen et al., 2020); IL-6-induced STAT3 activation, being able to target *TWIST* promoter (Yao et al., 2020)	TGF-β1 promoted an increase in p-Smad2/3 levels (Geng et al., 2014)

10.3389/fmolb.2022.1070383

demonstrated that IL-8 regulates *MMP9* expression in 253J-P and 253J-BV cells lines (Inoue et al., 2000). Indeed, Mian BM *el al.* showed, *in vitro*, that IL-8 neutralization resulted in a decrease of MMP-2 and MMP-9 expression, in part, through NF-kB, and, consequently, promoted cell invasion decrease (Mian et al., 2003) (Table 1).

CCL2

Monocyte chemoattractant protein -1/chemokine (C-C motif) ligand 2 (MCP-1/CCL2) plays a crucial role in immune responses, regulating infiltration and migration of several immune cells (Xu et al., 2021). CCL2 is a potent chemoattractant for monocytes/macrophages (Li and Tai, 2013) and can activate dendritic cells, memory T cells and basophils (Chiu et al., 2012; Xu et al., 2021). CCL2 is secreted by activated macrophages, fibroblasts, vascular smooth muscle, lymphocytes, and tumor cells (Amann et al., 1998). Usually binds to C-C chemokine receptor type 2 (CCR2), but it also binds to CCR4 (Zhang et al., 2010; Gao et al., 2019). CCL2 expression can be activated by several growth factors and cytokines, such as platelet-derived growth factor (PDGF), TNF-α, IL-1β and IFN-γ (Li and Tai, 2013). Overall, according to the literature, CCL2 in the TME seems to mainly contributes for tumor progression and metastasis formation (Jin et al., 2021).

In silico data analysis showed that *CCL2* expression was significantly lower in BlCa patients than the controls (Li et al., 2021). Additionally, higher *CCL2* levels were associated with better DFS (Li et al., 2021). In patient tissues, CCL2/*CCL2* was described to be significantly higher in tumors, compared with normal and adjacent tissues (Wang et al., 2017). Considering NMIBC and MIBC patients, higher CCL2 levels significantly correlated with higher grade, stage and lymph node metastasis (Gao et al., 2019). Particularly, considering only MIBC patients, a positive CCL2 expression in tumor cells was associated with poor mean OS, DSS and recurrence-free survival (RFS), while expression of CCL2 in immune cells, was associated with longer OS, DSS, and RFS (Eckstein et al., 2020). The role of CCL2 in immune cells is dependent on the lymph node patient's status, as CCL2 in N0 was linked to a good prognosis while N1+N2 was associated with poor prognosis (Eckstein et al., 2020) (Table 1).

In urine samples from BlCa patients, advanced stages (pT2-pT4) presented three to fourfold higher mean concentration, comparing with pT1 stage tumors (Amann et al., 1998) (Table 1).

In vitro, it was demonstrated that higher CCL2 levels were associated with high-grade BlCa cell lines (T24 and J82), while low-grade BlCa cell lines (SVHUC1, RT4 and TSGH8301), showed lower CCL2 levels (Chiu et al., 2012). In addition, higher CCL2 levels were produced in MB49 and MBT-2 cisplatin-resistant cells lines, comparing with parental BlCa cell lines (Takeyama et al., 2020). So far, there is a lack of information about CCL2 expression in plasma, in *in vivo* and in serum of BlCa patients (Table 1).

Besides, in BlCa, the knowledge about the impact of CCL2 in EMT induction and the signaling pathways activated by CCL2 promoting EMT, is still poor, although some studies have been arising. Co-culture of mast cells (HMC-1) with the BlCa cell lines, T24 and 647V, resulted in an increase of the estrogen receptor beta (ERβ) levels and of CCL2 levels in both cell types (Rao et al., 2016). After co-culture, higher CCL2 levels promoted EMT, driving stimulation of MMP-9 expression and enhanced N-cadherin, Twist, Snail and Vimentin expression levels, resulting in higher BlCa cell lines invasion abilities (Rao et al., 2016) (Table 1). Long noncoding RNA Lymph Node Metastasis Associated Transcript 1 (LNMAT1), overexpressed in BlCa tissues comparing with normal adjacent tissues, can directly interact with heterogeneous nuclear ribonucleoprotein L (hnRNPL), resulting in an increase of the H3 lysine four trimethylation (H3K4me3) of the *CCL2* promoter (Chen et al., 2018). *CCL2* overexpression resulted in increased TAM recruitment. Macrophage activation resulted in secretion of lymphangiogenic growth factor (VEGF-C) to the bladder TME, promoting lymphangiogenic and lymphatic metastasis (Chen et al., 2018). In mouse BlCa cell line MBT2, CCL2-CCR2 interaction may facilitate migration by phosphorylating paxillin y118 through a protein kinase C (PKC)-dependent mechanism (Chiu et al., 2012).

CXCL1

CXCL1, also known as MGSA, is a powerful neutrophil chemoattractant chemokine (De Filippo et al., 2013; Boro and Balaji, 2017), interacting with the CXCR2 receptor (Kawanishi et al., 2008). CXCL1 plays a double role in immune responses, since it can recruit and activate neutrophils to the infection area, but can also activate the release of several proteases and reactive oxygen species (ROS) that will result in cell death (Sawant et al., 2016). This chemokine plays important roles in several tumor models, promoting cell migration and invasion (Cheng et al., 2011; Wang et al., 2018). Mast cells, alongside with macrophages are able to produce CXCL1 (De Filippo et al., 2013).

In silico, UALCAN analysis showed higher *CXCL1* transcript levels in BlCa samples compared with normal bladder mucosa tissues, and, according to GEPIA and GEO database analysis, higher *CXCL1* was significantly associated with shorter OS (Sun et al., 2021b) (Table 1).

While benign or normal bladder tissues showed absent CXCL1 levels, higher CXCL1 levels were significantly associated with more undifferentiated tumors and MIBC (Kawanishi et al., 2008; Miyake et al., 2013). Consequently, high amounts of CXCL1 contributed to poor DSS and poor OS (Miyake et al., 2013). Additionally, increased CXCL1 levels in the tumors promoted the recruitment of CAFs and were associated with higher number of TAMs (Miyake et al., 2016) (Table 1).

In *in vitro* studies, higher *CXCL1* expression was observed in the most aggressive BlCa cell lines (UMUC3, 5637 and T24) (Kawanishi et al., 2008). Moreover, CXCL1 could enhance the invasive ability of BlCa cell lines (Kawanishi et al., 2008; Miyake et al., 2019). Additionally, CXCL1 influenced the angiogenesis process and tumor vasculature, since tube structures were significantly lower after treatment with conditioned media from *CXCL1*-knockdown T24 cells (Miyake et al., 2019). Furthermore, higher CXCL1 amounts were obtained with MB49, MBT-2 and T24 cisplatin-resistant cells lines, in comparison with parental BlCa cell lines (Takeyama et al., 2020) (Table 1).

In vivo, it was shown that CXCL1 secreted by TAMs and CAFs enhanced bladder tumor cell attachment to the bladder wall, consequently inducing tumor growth (Miyake et al., 2016). Moreover, by using T24 cell xenografts treated with HL2401, a CXCL1 inhibitor, it was observed a significant increase in the apoptotic index, but a significant decrease in microvessel density and a reduction in proliferation (Miyake et al., 2019).

In liquid biopsies, CXCL1 urinary protein concentrations were significantly higher in BlCa patients comparing with patients without BlCa (Kawanishi et al., 2008; Burnier et al., 2015). Importantly, a significant increase was obtained in stages pT1-pT4, comparing with pTa (Kawanishi et al., 2008) (Table 1).

Information regarding CXCL1 expression in serum and in plasma of BlCa patients is still lacking (Table 1). Also, the role that CXCL1 might have in driving EMT is little explored, as well as the signaling pathways activated by CXCL1 to induce EMT in BlCa. However, it is known, that *in vivo*, overexpression of CXCL1 by TAMs and CAFs, promoted alterations in BLCa EMT, decreasing E-cadherin membrane expression, while increasing MMP-2 expression (Miyake et al., 2016) (Table 1). Furthermore, in tissues, a significant correlation was established between CXCL1 and MMP-13 (Kawanishi et al., 2008) (Table 1). *In silico* analysis, using LinkedOmics database, also showed that microRNA (miR)-200a, an important hallmark in EMT (Adam et al., 2009), interacts with *CXCL1* (Sun et al., 2021b) (Table 1).

CXCL12

CXCL12, also known as stromal cell-derived factor 1 (SDF-1), or pre-B cell stimulating factor (PBSF) (Yang et al., 2015), interacts with CXCR4 and CXCR7 receptors (Shen et al., 2013; Zhang et al., 2018). CAFs are able to secrete CXCL12, being essential for $CD8^+$ T cells recruitment (Du et al., 2021c). This chemokine participates in the homeostatic regulation of leukocyte trafficking and tissue regeneration (Barinov et al., 2017). CXCL12 is also described to be involved in tumor growth, angiogenesis and tumor cell intravasation (Chang et al., 2020).

in silico analyses (GEO, TCGA, ONCOMINE and UALCAN) showed that *CXCL12* was significantly decreased in BlCa samples, comparing with the controls (Sun et al., 2021b; Du et al., 2021c). On the other hand, higher *CXCL12* expression was significantly associated with more advanced stages, worse prognosis, and more lymph node metastasis (N2 showed higher *CXCL12* than N0) (Sun et al., 2021b; Liu et al., 2021).

In accordance with *in silico* data, Du Y *et al.* showed a CXCL12 reduction in BlCa patient tissues comparing with the normal tissues Du et al. (2021c), while Yang DL *et al.* showed a significantly higher expression of CXCR4/CXCL12 in BlCa tissues and no expression in normal tissues Yang et al. (2015). It was demonstrated that CXCL12 positively associated with tumor grade and stage in BlCa patient tissues, being CXCL12 expression more intense in recurrent patients (Batsi et al., 2014). Moreover, Yang DL *et al.* showed that CXCR4/CXCL12 levels strongly associated with tumor progression and invasion, and *CXCL12* transcript levels in tumor tissues increased with tumor aggressiveness.

There are several *CXCL12* mRNA variants depending on alternative splicing (Gosalbez et al., 2014; Chang et al., 2020). CXCL12-α, CXCL12-β and CXCL12-γ are some of the variants, presenting the same first three exons (Chang et al., 2020). According to the literature, CXCL12-α has the strongest affinity to CXCR4, followed by CXCL12-β and CXCL12-γ (Chang et al., 2020). By qPCR, it was demonstrated that CXCL12-α and CXCL12-β levels were higher in metastatic patient tissues compared to non-metastatic patient tissues (Gosalbez et al., 2014). Moreover, only CXCL12-β was significantly higher in tumor patients than normal samples (Gosalbez et al., 2014). In urine, CXCL12-γ was not detected, but CXCL12-α levels were significantly lower in patients with low-grade compared to controls, while CXCL12-β levels were significantly higher in high-grade than the controls (Gosalbez et al., 2014).

There is no information regarding CXCL12 expression in plasma and in serum, similarly to CCL2 and CXCL1 (Table 1). Up till now, CXCL12 has been described to have an important role in regulating some EMT-related molecules in BlCa. Additionally, studies on the signaling pathways that might be activated by this chemokine started to arise. *In vitro,* it was shown that CXCL12 was involved in cell invasion and migration (Retz et al., 2005; Shen et al., 2013). CXCR4 and CXCL12 binding drives the induction of STAT3 phosphorylation (Shen et al., 2013), an important molecule in promoting BlCa growth and survival, and able to work as a transcription factor regulating EMT (Chen et al., 2008; Jin, 2020) (Table 1). This alteration in migration might occur due to an association of CXCR4/CXCL12 with cytoskeletal reorganization, specifically, with a redistribution of F-actin stress fibers (Retz et al., 2005). A study from Zhang T *et al.* reinforced these findings, since SW780 treated with AMD34635, a CXCR4 inhibitor, exhibited growth and colony formation supression, as well as, inhibiton on migration and invasion (Zhang et al., 2018). In addition, *in*

vivo, it was demonstrated that tumors with AMD3465-treatment showed slower growth and lower weight than tumors treated with the vehicle (Zhang et al., 2018). Additionally, *in vitro*, it was also demonstrated that molecular alterations occurred, with a decrease of β-catenin, MMP-2 and c-Myc expression and with an increase in E-cadherin levels (Zhang et al., 2018) (Table 1). However, the effect of AMD3465 was reversed when CXCL12 was added, inducing E-cadherin downregulation and c-Myc upregulation (Zhang et al., 2018) (Table 1). Moreover, SW780 cells treated with FH535, a β-catenin antagonist, also decrease cell proliferation, colony formation, migration and invasion, being these effects once again reverse by CXCL12 treatment. Thus, suggesting that CXCR4/CXCL12 play an important role in regulated β-catenin expression in BlCa progression (Zhang et al., 2018) (Table 1).

IL-6

IL-6 is a pro-inflammatory interleukin (Chen et al., 2013; Morizawa et al., 2018) known to play a major role in inflammatory responses (Chen et al., 2013; Yao et al., 2020), as well as in the maturation of B cells (Andrews et al., 2002; Miyake et al., 2019). IL-6 binds to the receptor IL6-R, present in the extracellular membrane, or secreted in a soluble form (IL-6sR) (Andrews et al., 2002). IL-6 is mainly produced by tumor-infiltrating immune cells, such as T cells and macrophages, by tumor cells, by healthy endothelial tissues, by epithelial cells and by muscle cells (Andrews et al., 2002; Rossi et al., 2015; Schuettfort et al., 2022).

In tissues, Chen MF *et al.* showed that IL-6/*IL6* expression was higher in BlCa tissues, comparing with non-malignant tissues (Chen et al., 2013). The authors demonstrated that non-malignant tissues exhibited IL-6 expression, but in lower levels, compared to early stages, while IL-6 higher levels were mostly associated with MIBC tissues (Chen et al., 2013) (Table 1).

In silico analysis, revealed that *IL6* transcript levels were significantly increased in higher stages (stages III and IV), comparing with lower stages (stages I and II) (Goulet et al., 2019). Moreover, *IL6* was significantly enhanced in high-grade patients, comparing with low-grade patients (Goulet et al., 2019) (Table 1).

In urine samples, IL-6 levels were significantly higher in advanced stage patients (pT3-pT4), comparing with patients with early stage tumors or non-malignant samples (Chen et al., 2013). Kumari N *et al.* showed that higher IL-6 concentration was significantly associated with lower disease grade Kumari et al. (2017). Furthermore, it was demonstrated that IL-6 levels in urine were associated with shorter OS (Morizawa et al., 2018) (Table 1).

Using preoperative plasma samples, Schuettfort VM *et al.* and Andrews B *et al.* demonstrated that IL-6 and IL-6sR were significantly higher in patients with advanced stages, lymph vascular invasion and lymph node metastasis Andrews et al. (2002), Schuettfort et al. (2022). Dmytryk V *et al.* also observed significantly higher IL-6 leveles in pT3-pT4 samples, comparing with control samples Dmytryk et al. (2020). Moreover, patients with recurrent disease or patients who deceased due to BlCa disease presented higher IL-6 and IL-6sR levels (Schuettfort et al., 2022). Higher IL-6 and IL-6sR levels were associated with poor RFS, CSS and OS (Schuettfort et al., 2022). Andrews B *et al.* showed that plasma IL-6 levels were significantly higher in BlCa than in healthy patients, however IL-6sR levels did not present statitiscal differences bteween the two groups (Andrews et al., 2002) (Table 1).

In serum BlCa samples, collected prior to surgery, IL-6 levels were significantly higher in recurrent patients, comparing with non-recurrent patients and were significantly associated with poor RFS (Kumari et al., 2017). Similar to IL-8, IL-6 expression was significantly associated with shorter CSS (Morizawa et al., 2018). However, Yang G *et al.* described a descrease of IL-6 levels in T2-T4 patient samples, comparing with Ta-T1 samples and healthly controls (Yang et al., 2017) (Table 1).

Regarding the literature, BlCa cell lines produced high IL-6 levels, while normal cell lines expressed only low IL-6 levels (Okamoto et al., 1997). Upon IL-6 treatment, BlCa cell lines (253J, RT4 and T24) presented enhanced cellular growth, comparing with normal cell lines (Okamoto et al., 1997). Moreover, the cell growth was significantly inhibited upon anti-IL-6 neutralizing antibody treatment, suggesting that IL-6 provides autocrine growth advantages to the BlCa cell lines (Okamoto et al., 1997). Additionally, Yeh CR *et al.* suggested that, *in vitro*, ERα overexpression in fibroblasts may increase BlCa cell invasion through IL-6 expression in BlCa cells (Yeh et al., 2015). Miyake M *et al.* demonstrated, *in vivo* and *in vitro*, that CXCL1 had an important impact in BlCa tumor growth, since promoted IL-6 induction and repressed tissue inhibitor of metalloproteinase 4 (TIMP4) inhibition Miyake et al. (2019). Chen MF *et al.* showed that *IL6* silencing contributed to a decrease in tumor invasion and tumor growth/proliferation, both *in vivo* and *in vitro* (HT1197 and HT1376 cell lines) Chen et al. (2013).

Overall, IL-6 has been described to be upregulated in advanced BlCa patients (Chen et al., 2013; Goulet et al., 2019) and in lymph node metastasis (Andrews et al., 2002; Schuettfort et al., 2022). Thus, the association between IL-6 and EMT induction starts to be studied in BlCa, along with which signaling pathways can be activated by IL-6. Indeed, *IL6* overexpression in HT1376 cells promoted a decrease in N-cadherin and Vimentin levels, while the *IL6* knockdown in T24 cells led to a decrease in E-cadherin, but an increase in N-cadherin and Vimentin levels (Tsui et al., 2013) (Table 1). However, it was demonstrated that *IL6* silencing was able to

increase E-cadherin levels, but decreased MMP-9 levels and attenuated angiogenesis, since it led to a decrease of CD31 and vascular endothelial growth factor (VEGF) levels (Chen et al., 2013) (Table 1). EMT-player alterations, induced by IL-6, might be regulated by STAT3 signaling pathway activation (Chen et al., 2013) (Table 1). In patient tissues, it was demonstrated a significant positive correlation between p-STAT3 Y705 and IL-6, and a significant negative correlation between p-STAT3 Y705 and E-cadherin, suggesting that E-cadherin expression might be inhibited by IL6-STAT3 signaling pathway (Chen et al., 2020). *In vitro*, it was demonstrated that IL-6-induced STAT3 is able to target *TWIST* promoter, modulating EMT and BlCa cell invasion (Yao et al., 2020).

TGF-β1

TGF-β1 is the most well studied isoform and its receptors are membrane serine-threonine kinase receptors I and II (TGF-βRI and TGF-βRII) (Kim et al., 2001). This cytokine has been described as playing a dual role in tumorigenesis, displaying a tumor suppressor role in normal cells or in early tumor stages, inducing cell cycle arrest and apoptosis, while in late stages can promote cell motility and invasion (Eder et al., 1997; Jakowlew, 2006; Lebrun, 2012; Stojnev et al., 2019). Overall, TGF-β1 is mainly released by regulatory T cells (Efiloğlu et al., 2020) and CAFs (Ao et al., 2007; Yu et al., 2014; Yeh et al., 2015), M2 macrophages (Horibe et al., 2021) and MDSC (Groth et al., 2019). TGF-β1 can activate both SMAD-dependent or SMAD-independent signaling (Hata and Chen, 2016). TGFRβII point mutations have been reported, not only in the BlCa cell line T24, but also in BlCa patients, being associated with higher pathologic T category and tumor grade (Bian et al., 2013).

In silico analysis, it was demonstrated that *TGFB1* is upregulated in MIBC compared to NMIBC and patients with higher *TGFB1* expression presented higher risk of death, lower DFS and lower OS (Zou et al., 2019) (Table 1).

In BlCa patient samples, TGF-β1 is expressed in normal urothelium, although at lower levels (Yang et al., 2018; Zou et al., 2019). Within tumors, higher TGF-β1 levels were significantly associated with higher tumor stage and grade and correlated with cancer-specific death (Kim et al., 2001; Yang et al., 2018; Stojnev et al., 2019; Zou et al., 2019). On the other hand, although Miyamoto H *et al.* also found that *TGFB1* transcript levels were higher in tumor tissues, than in normal samples, *TGFB1* transcript levels were significantly associated with low-grade and stage Miyamoto et al. (1995) (Table 1).

In BlCa patient serum samples, Efiloğlu Ö *et al.* described that higher TGF-β1 was associated with a low risk of tumor progression (Efiloğlu et al., 2020). Indeed, Eder IE *et al.*, using serum samples, mentioned that TGF-β1 levels were significantly lower in T4 tumors than superficial and invasive (T2-T3) tumors Eder et al. (1997). However, Eder IE *et al.* demonstrated that superficial tumors (Ta-T1) had significantly TGF-β1 higher levels, than normal samples (Eder et al., 1997). Another study from Eder IE *et al.* mentioned that serum TGF-β1 were elevated in the most aggressive BlCa cases compared to controls, and in the most undifferentiated tumors, than with lower grade tumors (Eder et al., 1996) (Table 1).

Also in preoperative plasma, TGF-β1 levels were significantly higher in MIBC patients with regional and distant lymph node, comparing with non-metastatic MIBC and controls (Shariat et al., 2001). An increase of TGF-β1 was found in MIBC, comparing with less aggressive tumors, with patients with higher TGF-β1 demonstrating increased risk of disease recurrence and mortality (Shariat et al., 2001). On the other hand, no significant differences were found between controls and patients with early stages (Shariat et al., 2001) (Table 1).

In urine samples, it was observed a significantly higher number of BlCa samples expressing TGF-β1 comparing with chronic cystitis disease cases or the control group (Helmy et al., 2007) (Table 1).

In vivo, it was observed an increase of, not only in tumor size, but also in tumor weight (Zou et al., 2019) when the 5637 cell line overexpressing TGF-β1 was transplanted into mice, compared with the parental cell line (Zou et al., 2019) (Table 1).

As mentioned above, TGF-β1 is an important inducer and regulator of EMT (Stojnev et al., 2019). EMT-related molecules regulated by TGF-β1 and the signaling pathways activated by this cytokine have been well described in several models, including in BlCa. Both *in vitro and in vivo*, an increase of TGF-β1 reflected in an upregulation of EMT-related molecule levels, such as Slug, Vimentin, Snail, MMP-2, MMP-9 and E-cadherin (Zou et al., 2019). Additionally, TGF-β1 has been associated with proliferation, colony formation, migration and invasion in BlCa cell lines (Bian et al., 2013; Zhang et al., 2016; Zou et al., 2019). HTB9 and T24 cell lines treated with TGF-β1 resulted in E-cadherin/*CDH1* decrease, and a N-cadherin/*CDH2* and Vimentin/*VIM* increase (Chen et al., 2014). Upon TGF-β1 treatment, it was shown *miR-200b* downregulation and MMP-16 upregulation, due to miR-200b targeting of MMP-16 (Chen et al., 2014). TGF-β1 treatment of T24 and BIU87 BlCa cell lines resulted in increased fascin1 levels, an important molecule in tumor migration and invasion (Zhang et al., 2016). Finally, AY-27, a rat cell line, treated with TGF-β1 resulted in alterations in morphology, with the increase of spindle shaped cells, while the polygonal shaped cells decreased, as well as cell-to-cell contact (Koo et al., 2010). In Smad-dependent signaling, it occurs recruitment and phosphorylation of SMAD2 and SMAD3 (Heldin et al., 2012; Gonzalez and Medici, 2014; Papageorgis, 2015; Gupta et al., 2016). Then, SMAD4 is recruited, forming a trimeric complex capable to be translocated to the nucleus (Bian et al., 2013; Gonzalez and Medici, 2014; Gupta et al., 2016). In BlCa samples, Smad2 and Smad4 expression were associated with low-grade and superficial tumors, and better overall survival of the patients (Stojnev et al., 2019). However, it was observed an increase of p-SMAD2 in

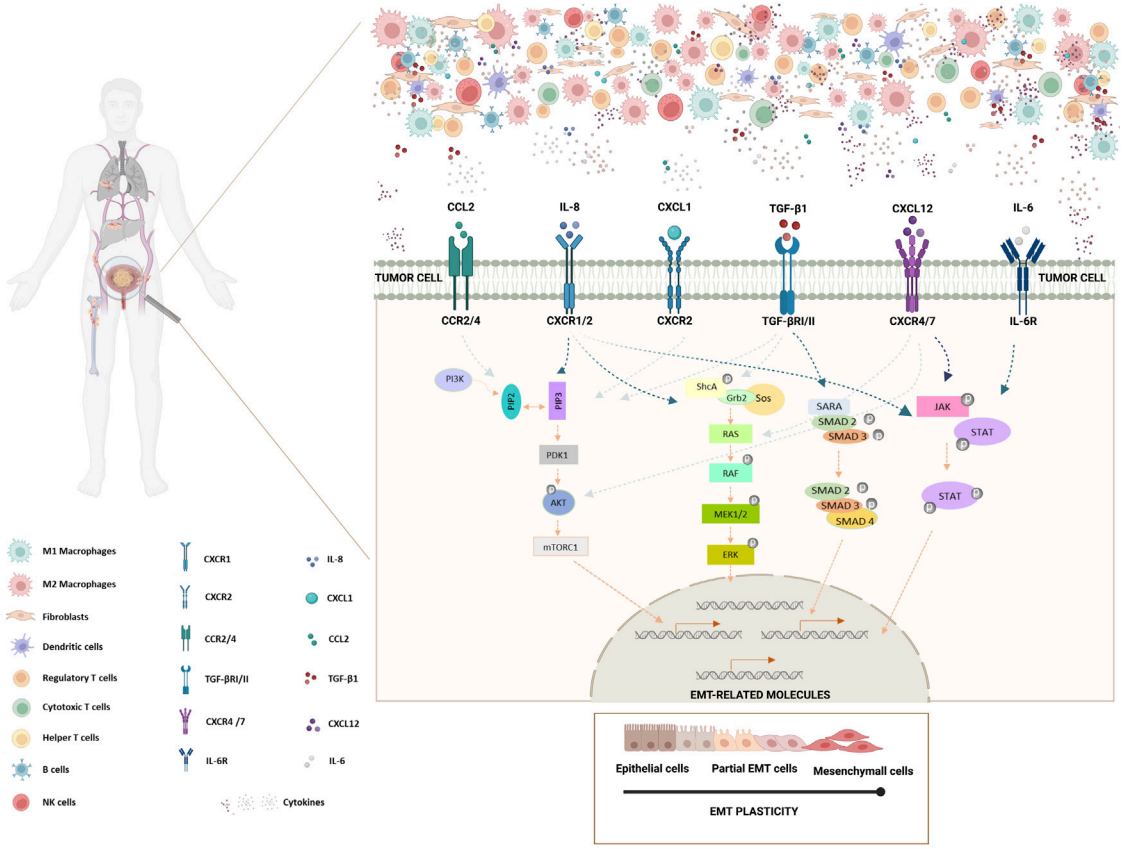

FIGURE 1
Schematic representation of the impact of BlCa TME cytokines/chemokines in EMT induction in bladder tumor cells. Bladder tumor microenvironment is comprised by tumor cells and several tumor-infiltrating immune cells, such as, M1 and M2 macrophages, dendritic cells, regulatory T cells, cytotoxic T cells, helper T cells, B cells and NK cells. Furthermore, TME includes stromal cells, like fibroblasts, and non-cellular components, including soluble biological factors or mediators, as cytokines/chemokines. Cytokines/chemokines are mainly produced by several immune cells and fibroblasts, but they also can be produced by tumor cells. Tumor cells present several cytokine/chemokine receptors. IL-8 binds to CXCR1/CXCR2 receptors, CCL2 binds to CCR2/CCR4 receptor, TGF-β1 binds to TGF-βRI/II receptors, CXCL1 binds to CXCR2 receptor, CXCL12 binds to CXCR4/7 receptors and IL-6 binds to IL-6R receptor. Cytokine/receptor binding on tumor cells can drive the deregulation of specific molecules, including the triggering of EMT signaling pathways. Here, are depicted the most relevant signaling pathways involved in driving EMT that have been described to be deregulated in BlCa upon cytokine binding. JAK-STAT, RAS-RAF-ERK and AKT signaling pathways and TGF-β SMAD-dependent pathway are described to play roles in the activation of EMT-related molecules, driving EMT processes in tumor cells. Bladder tumor cells presenting partial EMT demonstrate a higher survival mechanism and a higher tumor-initiating and metastatic potential. In this way, bladder tumor cells are able to metastasize to the bones, lungs and liver (Created with BioRender.com).

invasive bladder tumors (Gupta et al., 2016). Knockdown of *PPM1A*, an antagonist of TGF-β signaling by dephosphorylating TGF-β-activated Smad2/3, resulted in an increase in p-Smad2/3 levels upon TGF-β1 treatment, in 5637 and T24 cell lines (Geng et al., 2014).

Conclusion

In this review, we focused on the dysregulation of several immune cells, and of key cytokines/chemokines in the bladder cancer TME. In BlCa, IL-6, CCL2, CXCL1, CXCL12, IL-8 and TGF-β1 play putative roles in promoting tumor progression, growth, invasion, and metastases formation (Figure 1). The cytokine-driven modulation of the transcription of specific EMT-related molecules in BlCa starts to be unravel (Figure 1). However, the mechanisms involved in the axis TME-EMT signaling pathway activation in BlCa remains to be further exploited. Therefore, finding novel cytokines/chemokines present in bladder TME driving EMT induction and, simultaneously, decipher crucial players involved in BlCa tumorigenesis and progression.

Author contributions

CM-L and MPC conceptualized the paper. CM-L collected, analyzed the information, wrote the manuscript and elaborated the

figure and the table. MPC and CJ drafted and revised the paper. RB, UC, and LA revised the paper. All authors read and approved the final manuscript.

Funding

This study was funded by the Research Center of Portuguese Institute of Porto (CI-IPOP-FBGEBC-27 and CI-IPOP-PI 137), and also by Associazione Italiana per la Ricerca sul Cancro (AIRC IG17217 to LA); the Italian Ministry for University and Research (PRIN 2015-20152TE5PK, to LA); the project "Epigenetic Hallmarks of Multiple Sclerosis" (acronym Epi-MS) (id:415, Merit Ranking Area ERC LS) in VALERE 2019 Program (to RB); Blueprint 282510 (to LA); Campania Regional Government Technology Platform Lotta alle Patologie Oncologiche: iCURE (to LA); Campania Regional Government FASE2: IDEAL (to LA); MIUR, Proof of Concept POC01_00043 (to LA); Programma V:ALERE 2020 - Progetto competitivo "CIRCE" in risposta al bando D.R. n. 138 del 17/02/2020 (to RB). CM-L is fellow from a grant of UniCampania, Naples, IT (2020-UNA2CLE-0203198) enrolled in the PhD program in Translational Medicine, Department of Precision Medicine, University of Campania "Luigi Vanvitelli", Italy. MPC is funded by FCT (CEECINST/00091/2018).

Acknowledgments

The authors would like to thank the Cancer Biology and Epigenetics Group members.

Conflict of interest

The authors declare that the research was conducted in the absence of any commercial or financial relationships that could be construed as a potential conflict of interest.

Publisher's note

References

Adam, L., Zhong, M., Choi, W., Qi, W., Nicoloso, M., Arora, A., et al. (2009). miR-200 expression regulates epithelial-to-mesenchymal transition in bladder cancer cells and reverses resistance to epidermal growth factor receptor therapy. *Clin. Cancer Res.* 15, 5060–5072. doi:10.1158/1078-0432.CCR-08-2245

Addison, C. L., Daniel, T. O., Burdick, M. D., Liu, H., Ehlert, J. E., Xue, Y. Y., et al. (2000). The CXC chemokine receptor 2, CXCR2, is the putative receptor for ELR+ CXC chemokine-induced angiogenic activity. *J. Immunol.* 165, 5269–5277. doi:10.4049/jimmunol.165.9.5269

Al-biaty, H. S. J. (2015). Urinary IL-8 and BLCA-4 in detection of bladder cancer and their clinical significant. *Iraqi J. Cancer Med. Genet.* 8.

Amann, B., Perabo, F. G., Wirger, A., Hugenschmidt, H., and Schultze-Seemann, W. (1998). Urinary levels of monocyte chemo-attractant protein-1 correlate with tumour stage and grade in patients with bladder cancer. *Br. J. Urol.* 82, 118–121. doi:10.1046/j.1464-410x.1998.00675.x

Andrews, B., Shariat, S. F., Kim, J. H., Wheeler, T. M., Slawin, K. M., and Lerner, S. P. (2002). Preoperative plasma levels of interleukin-6 and its soluble receptor predict disease recurrence and survival of patients with bladder cancer. *J. Urology* 167, 1475–1481. doi:10.1097/00005392-200203000-00083

Ao, M., Franco, O. E., Park, D., Raman, D., Williams, K., and Hayward, S. W. (2007). Cross-talk between paracrine-acting cytokine and chemokine pathways promotes malignancy in benign human prostatic epithelium. *Cancer Res.* 67, 4244–4253. doi:10.1158/0008-5472.CAN-06-3946

Ariafar, A., Vahidi, Y., Fakhimi, M., Asadollahpour, A., Erfani, N., and Faghih, Z. (2020). Prognostic significance of CD4-positive regulatory T cells in tumor draining lymph nodes from patients with bladder cancer. *Heliyon* 6, e05556. doi:10.1016/j.heliyon.2020.e05556

Barinov, A., Luo, L., Gasse, P., Meas-Yedid, V., Donnadieu, E., Arenzana-Seisdedos, F., et al. (2017). Essential role of immobilized chemokine CXCL12 in the regulation of the humoral immune response. *Proc. Natl. Acad. Sci. U. S. A.* 114, 2319–2324. doi:10.1073/pnas.1611958114

Batsi, O., Giannopoulou, I., Nesseris, I., Valavanis, C., Gakiopoulou, H., Patsouris, E. S., et al. (2014). Immunohistochemical evaluation of CXCL12-CXCR4 axis and VEGFR3 expression in primary urothelial cancer and its recurrence. *Anticancer Res.* 34, 3537–3542.

Bian, J., Li, B., Zeng, X., Hu, H., Hong, Y., Ouyang, H., et al. (2013). Mutation of TGF-β receptor II facilitates human bladder cancer progression through altered TGF-β1 signaling pathway. *Int. J. Oncol.* 43, 1549–1559. doi:10.3892/ijo.2013.2065

Bickel, M. (1993). The role of interleukin-8 in inflammation and mechanisms of regulation. *J. Periodontol.* 64, 456–460.

Bocci, F., Tripathi, S. C., Vilchez Mercedes, S. A., George, J. T., Casabar, J. P., Wong, P. K., et al. (2019). NRF2 activates a partial epithelial-mesenchymal transition and is maximally present in a hybrid epithelial/mesenchymal phenotype. *Integr. Biol.* 11, 251–263. doi:10.1093/intbio/zyz021

Boro, M., and Balaji, K. N. (2017). CXCL1 and CXCL2 regulate NLRP3 inflammasome activation via G-protein–coupled receptor CXCR2. *J. Immunol.* 199, 1660–1671. doi:10.4049/jimmunol.1700129

Brandau, S., Riemensberger, J., Jacobsen, M., Kemp, D., Zhao, W., Zhao, X., et al. (2001). NK cells are essential for effective BCG immunotherapy. *Int. J. Cancer* 92, 697–702. doi:10.1002/1097-0215(20010601)92:5<697:aid-ijc1245>3.0.co;2-z

Bryan, R. T. (2015). Cell adhesion and urothelial bladder cancer: The role of cadherin switching and related phenomena. *Philos. Trans. R. Soc. Lond. B Biol. Sci.* 370, 20140042. doi:10.1098/rstb.2014.0042

Bule, P., Aguiar, S. I., Aires-Da-Silva, F., and Dias, J. N. R. (2021). Chemokine-directed tumor microenvironment modulation in cancer immunotherapy. *Int. J. Mol. Sci.* 22, 9804. doi:10.3390/ijms22189804

Burnier, A., Shimizu, Y., Dai, Y., Nakashima, M., Matsui, Y., Ogawa, O., et al. (2015). CXCL1 is elevated in the urine of bladder cancer patients. *Springerplus* 4, 610. doi:10.1186/s40064-015-1393-9

Cao, J., Yang, X., Li, J., Wu, H., Li, P., Yao, Z., et al. (2019). Screening and identifying immune-related cells and genes in the tumor microenvironment of bladder urothelial carcinoma: Based on TCGA database and bioinformatics. *Front. Oncol.* 9, 1533. doi:10.3389/fonc.2019.01533

Cao, R., Yuan, L., Ma, B., Wang, G., Qiu, W., and Tian, Y. (2020). An EMT-related gene signature for the prognosis of human bladder cancer. *J. Cell. Mol. Med.* 24, 605–617. doi:10.1111/jcmm.14767

Chandrasekar, T., Erlich, A., and Zlotta, A. R. (2018). Molecular characterization of bladder cancer. *Curr. Urol. Rep.* 19, 107. doi:10.1007/s11934-018-0853-5

Chang, C.-W., Seibel, A. J., Avendano, A., Cortes-Medina, M. G., and Song, J. W. (2020). Distinguishing specific CXCL12 isoforms on their angiogenesis and vascular permeability promoting properties. *Adv. Healthc. Mat.* 9, 1901399. doi:10.1002/adhm.201901399

Chen, C., He, W., Huang, J., Wang, B., Li, H., Cai, Q., et al. (2018). LNMAT1 promotes lymphatic metastasis of bladder cancer via CCL2 dependent macrophage recruitment. *Nat. Commun.* 9, 3826. doi:10.1038/s41467-018-06152-x

Chen, C. L., Cen, L., Kohout, J., Hutzen, B., Chan, C., Hsieh, F. C., et al. (2008). Signal transducer and activator of transcription 3 activation is associated with bladder cancer cell growth and survival. *Mol. Cancer* 7, 78. doi:10.1186/1476-4598-7-78

Chen, M. F., Lin, P. Y., Wu, C. F., Chen, W. C., and Wu, C. T. (2013). IL-6 expression regulates tumorigenicity and correlates with prognosis in bladder cancer. *PLoS One* 8, e61901. doi:10.1371/journal.pone.0061901

Chen, M. F., Zeng, F., Qi, L., Zu, X. B., Wang, J., Liu, L. F., et al. (2014). Transforming growth factor-β1 induces epithelial-mesenchymal transition and increased expression of matrix metalloproteinase-16 via miR-200b downregulation in bladder cancer cells. *Mol. Med. Rep.* 10, 1549–1554. doi:10.3892/mmr.2014.2366

Chen, R., Pagano, I., Sun, Y., Murakami, K., Goodison, S., Vairavan, R., et al. (2022). A diagnostic gene expression signature for bladder cancer can stratify cases into prescribed molecular subtypes and predict outcome. *Diagn. (Basel)* 12, 1801. doi:10.3390/diagnostics12081801

Chen, Y., Lv, W., Yang, W., Chen, J., Pei, X., Luo, L., et al. (2020). Loss of E-cadherin expression in bladder cancer is associated with IL6-STAT3 signaling pathway activation. *Int. J. Clin. Exp. Med.* 13, 1519–1527.

Cheng, W. L., Wang, C. S., Huang, Y. H., Tsai, M. M., Liang, Y., and Lin, K. H. (2011). Overexpression of CXCL1 and its receptor CXCR2 promote tumor invasion in gastric cancer. *Ann. Oncol.* 22, 2267–2276. doi:10.1093/annonc/mdq739

Chiu, H. Y., Sun, K. H., Chen, S. Y., Wang, H. H., Lee, M. Y., Tsou, Y. C., et al. (2012). Autocrine CCL2 promotes cell migration and invasion via PKC activation and tyrosine phosphorylation of paxillin in bladder cancer cells. *Cytokine* 59, 423–432. doi:10.1016/j.cyto.2012.04.017

Choi, W., Shah, J. B., Tran, M., Svatek, R., Marquis, L., Lee, I. L., et al. (2012). p63 expression defines a lethal subset of muscle-invasive bladder cancers. *PLoS One* 7, e30206. doi:10.1371/journal.pone.0030206

Chow, M. T., and Luster, A. D. (2014). Chemokines in cancer. *Cancer Immunol. Res.* 2, 1125–1131. doi:10.1158/2326-6066.CIR-14-0160

Covián, C., Fernández-Fierro, A., Retamal-Díaz, A., Díaz, F. E., Vasquez, A. E., Lay, M. K., et al. (2019). BCG-induced cross-protection and development of trained immunity: Implication for vaccine design. *Front. Immunol.* 10, 2806. doi:10.3389/fimmu.2019.02806

De Filippo, K., Dudeck, A., Hasenberg, M., Nye, E., van Rooijen, N., Hartmann, K., et al. (2013). Mast cell and macrophage chemokines CXCL1/CXCL2 control the early stage of neutrophil recruitment during tissue inflammation. *Blood* 121, 4930–4937. doi:10.1182/blood-2013-02-486217

Dmytryk, V., Luhovska, T., Yakovlev, P., Savchuk, O., Ostapchenko, L., Halenova, T., et al. (2020). Elevated levels of proinflammatory and anti-inflammatory cytokines in patients with bladder cancer depending on a tumor stage. *J. Biol. Res.* 93. 8632. doi:10.4081/jbr.2020.8632

Dong, F., Shen, Y., Gao, F., Xu, T., Wang, X., Zhang, X., et al. (2017). Prognostic value of site-specific metastases and therapeutic roles of surgery for patients with metastatic bladder cancer: A population-based study. *Cancer Manag. Res.* 9, 611–626. doi:10.2147/CMAR.S148856

Du, Y., Cao, J., Jiang, X., Cai, X., Wang, B., Wang, Y., et al. (2021). Comprehensive analysis of CXCL12 expression reveals the significance of inflammatory fibroblasts in bladder cancer carcinogenesis and progression. *Cancer Cell Int.* 21, 613. doi:10.1186/s12935-021-02314-y

Du, Y., Jiang, X., Wang, B., Cao, J., Wang, Y., Yu, J., et al. (2021). The cancer-associated fibroblasts related gene CALD1 is a prognostic biomarker and correlated with immune infiltration in bladder cancer. *Cancer Cell Int.* 21, 283. doi:10.1186/s12935-021-01896-x

Du, Y., Miao, W., Jiang, X., Cao, J., Wang, B., Wang, Y., et al. (2021). The epithelial to mesenchymal transition related gene calumenin is an adverse prognostic factor of bladder cancer correlated with tumor microenvironment remodeling, gene mutation, and ferroptosis. *Front. Oncol.* 11, 683951. doi:10.3389/fonc.2021.683951

Dunlop, R. J., and Campbell, C. W. (2000). Cytokines and advanced cancer. *J. Pain Symptom Manage.* 20, 214–232. doi:10.1016/s0885-3924(00)00199-8

Eckstein, M., Epple, E., Jung, R., Weigelt, K., Lieb, V., Sikic, D., et al. (2020). CCL2 expression in tumor cells and tumor-infiltrating immune cells shows divergent prognostic potential for bladder cancer patients depending on lymph node stage. *Cancers (Basel)* 12, E1253. doi:10.3390/cancers12051253

Eder, I. E., Stenzl, A., Hobisch, A., Cronauer, M. V., Bartsch, G., and Klocker, H. (1997). Expression of transforming growth factors beta-1, beta 2 and beta 3 in human bladder carcinomas. *Br. J. Cancer* 75, 1753–1760. doi:10.1038/bjc.1997.299

Eder, I. E., Stenzl, A., Hobisch, A., Cronauer, M. V., Bartsch, G., and Klocker, H. (1996). Transforming growth factors-beta 1 and beta 2 in serum and urine from patients with bladder carcinoma. *J. Urology* 156, 953–957. doi:10.1097/00005392-199609000-00029

Efiloğlu, Ö., Başok, B., Turan, T., Toprak, T., Erol, B., Çaşkurlu, T., et al. (2020). Role of serum and urine transforming growth factor beta 1, matrix metallopeptidase 9, tissue inhibitor of metalloproteinase 2, and nerve growth factor beta levels and serum neutrophil-to-lymphocyte ratio in predicting recurrence and progression risks in patients with primary non-muscle invasive bladder cancer. *Turk. J. Urol.* 46, 206–212. doi:10.5152/tud.2020.19186

Escudero-Lourdes, C., Wu, T., Camarillo, J. M., and Gandolfi, A. J. (2012). Interleukin-8 (IL-8) over-production and autocrine cell activation are key factors in monomethylarsonous acid [MMA(III)]-induced malignant transformation of urothelial cells. *Toxicol. Appl. Pharmacol.* 258, 10–18. doi:10.1016/j.taap.2011.10.002

Esteso, G., Aguiló, N., Julián, E., Ashiru, O., Ho, M. M., Martín, C., et al. (2021). Natural killer anti-tumor activity can Be achieved by *in vitro* incubation with heat-killed BCG. *Front. Immunol.* 12, 622995. doi:10.3389/fimmu.2021.622995

Gallo, P. M., and Gallucci, S. (2013). The dendritic cell response to classic, emerging, and homeostatic danger signals. Implications for autoimmunity. *Front. Immunol.* 4, 138. doi:10.3389/fimmu.2013.00138

Galsky, M. D., Chen, G. J., Oh, W. K., Bellmunt, J., Roth, B. J., Petrioli, R., et al. (2012). Comparative effectiveness of cisplatin-based and carboplatin-based chemotherapy for treatment of advanced urothelial carcinoma. *Ann. Oncol.* 23, 406–410. doi:10.1093/annonc/mdr156

Gao, W., Zhang, Q., Zhang, L., Liu, Q., Duan, X., Bo, J., et al. (2019). *CCL2 is associated with metastasis and poor prognosis of bladder cancer*. Durham, North Carolina, United States: Research Square.

Geng, J., Fan, J., Ouyang, Q., Zhang, X., Zhang, X., Yu, J., et al. (2014). Loss of PPM1A expression enhances invasion and the epithelial-to-mesenchymal transition in bladder cancer by activating the TGF-β/Smad signaling pathway. *Oncotarget* 5, 5700–5711. doi:10.18632/oncotarget.2144

Gonzalez, D. M., and Medici, D. (2014). Signaling mechanisms of the epithelial-mesenchymal transition. *Sci. Signal.* 7, re8. doi:10.1126/scisignal.2005189

Gonzalez-Aparicio, M., and Alfaro, C. (2018). The role of IL-8 in the immune response associated to cancer development. *Clin. Res. Trial.* 5. 1000245. doi:10.15761/crt.1000245

Gosalbez, M., Hupe, M. C., Lokeshwar, S. D., Yates, T. J., Shields, J., Veerapen, M. K., et al. (2014). Differential expression of SDF-1 isoforms in bladder cancer. *J. Urol.* 191, 1899–1905. doi:10.1016/j.juro.2013.11.053

Goulet, C. R., Champagne, A., Bernard, G., Vandal, D., Chabaud, S., Pouliot, F., et al. (2019). Cancer-associated fibroblasts induce epithelial-mesenchymal transition of bladder cancer cells through paracrine IL-6 signalling. *BMC Cancer* 19, 137. doi:10.1186/s12885-019-5353-6

Groth, C., Hu, X., Weber, R., Fleming, V., Altevogt, P., Utikal, J., et al. (2019). Immunosuppression mediated by myeloid-derived suppressor cells (MDSCs) during tumour progression. *Br. J. Cancer* 120, 16–25. doi:10.1038/s41416-018-0333-1

Gupta, S., Hau, A. M., Al-Ahmadie, H. A., Harwalkar, J., Shoskes, A. C., Elson, P., et al. (2016). Transforming growth factor-β is an upstream regulator of mammalian target of rapamycin complex 2-dependent bladder cancer cell migration and invasion. *Am. J. Pathol.* 186, 1351–1360. doi:10.1016/j.ajpath.2016.01.008

Han, J., Gu, X., Li, Y., and Wu, Q. (2020). Mechanisms of BCG in the treatment of bladder cancer-current understanding and the prospect. *Biomed. Pharmacother.* 129, 110393. doi:10.1016/j.biopha.2020.110393

Hanada, T., Nakagawa, M., Emoto, A., Nomura, T., Nasu, N., and Nomura, Y. (2000). Prognostic value of tumor-associated macrophage count in human bladder cancer. *Int. J. Urol.* 7, 263–269. doi:10.1046/j.1442-2042.2000.00190.x

Harras, H., and Abo Safia, H. (2021). Role of tumor-associated macrophages in relation to angiogenesis in urothelial bladder carcinoma. *Int. J. Cancer Biomed. Res.* 5, 0–160. doi:10.21608/jcbr.2021.66740.1188

Hata, A., and Chen, Y. G. (2016). TGF-B signaling from receptors to smads. *Cold Spring Harb. Perspect. Biol.* 8, a022061. doi:10.1101/cshperspect.a022061

Heldin, C. H., Vanlandewijck, M., and Moustakas, A. (2012). Regulation of EMT by TGFβ in cancer. *FEBS Lett.* 586, 1959–1970. doi:10.1016/j.febslet.2012.02.037

Helmy, A., Hammam, O. A., El Lithy, T. R., and El Deen Wishahi, M. M. (2007). The role of TGF-beta-1 protein and TGF-beta-R-1 receptor in immune escape mechanism in bladder cancer. *MedGenMed.* 9, 34.

Horibe, K., Hara, M., and Nakamura, H. (2021). M2-like macrophage infiltration and transforming growth factor-β secretion during socket healing process in mice. *Arch. Oral Biol.* 123, 105042. doi:10.1016/j.archoralbio.2021.105042

Hu, J., Yu, A., Othmane, B., Qiu, D., Li, H., Li, C., et al. (2021). Siglec15 shapes a non-inflamed tumor microenvironment and predicts the molecular subtype in bladder cancer. *Theranostics* 11, 3089–3108. doi:10.7150/thno.53649

Huang, C. P., Liu, L. X., and Shyr, C. R. (2020). Tumor-associated macrophages facilitate bladder cancer progression by increasing cell growth, migration, invasion and cytokine expression. *Anticancer Res.* 40, 2715–2724. doi:10.21873/anticanres.14243

Hughes, C. E., and Nibbs, R. J. B. (2018). A guide to chemokines and their receptors. *Febs J.* 285, 2944–2971. doi:10.1111/febs.14466

Ibarra, C., Karlsson, M., Codeluppi, S., Varas-Godoy, M., Zhang, S., Louhivuori, L., et al. (2019). BCG-induced cytokine release in bladder cancer cells is regulated by Ca(2+) signaling. *Mol. Oncol.* 13, 202–211. doi:10.1002/1878-0261.12397

Inman, B. A., Longo, T. A., Ramalingam, S., and Harrison, M. R. (2017). Atezolizumab: A PD-L1-blocking antibody for bladder cancer. *Clin. Cancer Res.* 23, 1886–1890. doi:10.1158/1078-0432.CCR-16-1417

Inoue, K., Slaton, J. W., Kim, S. J., Perrotte, P., Eve, B. Y., Bar-Eli, M., et al. (2000). Interleukin 8 expression regulates tumorigenicity and metastasis in human bladder cancer. *Cancer Res.* 60, 2290–2299.

Jakowlew, S. B. (2006). Transforming growth factor-beta in cancer and metastasis. *Cancer Metastasis Rev.* 25, 435–457. doi:10.1007/s10555-006-9006-2

Jin, J., Lin, J., Xu, A., Lou, J., Qian, C., Li, X., et al. (2021). CCL2: An important mediator between tumor cells and host cells in tumor microenvironment. *Front. Oncol.* 11, 722916. doi:10.3389/fonc.2021.722916

Jin, W. (2020). Role of JAK/STAT3 signaling in the regulation of metastasis, the transition of cancer stem cells, and chemoresistance of cancer by epithelial-mesenchymal transition. *Cells* 9, E217. doi:10.3390/cells9010217

Jolly, M. K., Boareto, M., Huang, B., Jia, D., Lu, M., Ben-Jacob, E., et al. (2015). Implications of the hybrid epithelial/mesenchymal phenotype in metastasis. *Front. Oncol.* 5, 155. doi:10.3389/fonc.2015.00155

Jovanović, M., Stefanoska, I., Radojcić, L., and Vićovac, L. (2010). Interleukin-8 (CXCL8) stimulates trophoblast cell migration and invasion by increasing levels of matrix metalloproteinase (MMP)2 and MMP9 and integrins alpha5 and beta1. *Reproduction* 139, 789–798. doi:10.1530/REP-09-0341

Jóźwicki, W., Brożyna, A. A., Siekiera, J., and Slominski, A. T. (2016). Frequency of CD4+CD25+Foxp3+ cells in peripheral blood in relation to urinary bladder cancer malignancy indicators before and after surgical removal. *Oncotarget* 7, 11450–11462. doi:10.18632/oncotarget.7199

Kalluri, R., and Weinberg, R. A. (2009). The basics of epithelial-mesenchymal transition. *J. Clin. Invest.* 119, 1420–1428. doi:10.1172/JCI39104

Kamat, A. M., Bağcıoğlu, M., and Huri, E. (2017). What is new in non-muscle-invasive bladder cancer in 2016? *Turk. J. Urol.* 43, 9–13. doi:10.5152/tud.2017.60376

Kartikasari, A. E. R., Huertas, C. S., Mitchell, A., and Plebanski, M. (2021). Tumor-induced inflammatory cytokines and the emerging diagnostic devices for cancer detection and prognosis. *Front. Oncol.* 11, 692142. doi:10.3389/fonc.2021.692142

Kawanishi, H., Matsui, Y., Ito, M., Watanabe, J., Takahashi, T., Nishizawa, K., et al. (2008). Secreted CXCL1 is a potential mediator and marker of the tumor invasion of bladder cancer. *Clin. Cancer Res.* 14, 2579–2587. doi:10.1158/1078-0432.CCR-07-1922

Kim, J. H., Shariat, S. F., Kim, I. Y., Menesses-Diaz, A., Tokunaga, H., Wheeler, T. M., et al. (2001). Predictive value of expression of transforming growth factor-beta(1) and its receptors in transitional cell carcinoma of the urinary bladder. *Cancer* 92, 1475–1483. doi:10.1002/1097-0142(20010915)92:6<1475:aid-cncr1472>3.0.co;2-x

Koçak, H., Öner-İyidoğan, Y., Koçak, T., and Öner, P. (2004). Determination of diagnostic and prognostic values of urinary interleukin-8, tumor necrosis factor-α, and leukocyte arylsulfatase-A activity in patients with bladder cancer. *Clin. Biochem.* 37, 673–678. doi:10.1016/j.clinbiochem.2004.02.005

Kohli, K., Pillarisetty, V. G., and Kim, T. S. (2022). Key chemokines direct migration of immune cells in solid tumors. *Cancer Gene Ther.* 29, 10–21. doi:10.1038/s41417-021-00303-x

Koo, V., El Mekabaty, A., Hamilton, P., Maxwell, P., Sharaf, O., Diamond, J., et al. (2010). Novel *in vitro* assays for the characterization of EMT in tumourigenesis. *Cell. Oncol.* 32, 67–76. doi:10.3233/CLO-2009-0501

Krpina, K., Babarović, E., Đordević, G., Markić, D., Maricić, A., and Jonjić, N. (2014). Impact of NK cell count on bladder cancer recurrence. *Urologia* 81, 233–236. doi:10.5301/uro.5000063

Kumari, N., Agrawal, U., Mishra, A. K., Kumar, A., Vasudeva, P., Mohanty, N. K., et al. (2017). Predictive role of serum and urinary cytokines in invasion and recurrence of bladder cancer. *Tumour Biol.* 39, 1010428317697552. doi:10.1177/1010428317697552

Lebrun, J. J. (2012). The dual role of TGFβ in human cancer: From tumor suppression to cancer metastasis. *ISRN Mol. Biol.* 2012, 381428. doi:10.5402/2012/381428

Li, X., and Tai, H.-H. (2013). Activation of thromboxane A2 receptor (TP) increases the expression of monocyte chemoattractant protein -1 (MCP-1)/Chemokine (C-C motif) ligand 2 (CCL2) and recruits macrophages to promote invasion of lung cancer cells. *PLOS ONE* 8, e54073. doi:10.1371/journal.pone.0054073

Li, Y., Chen, X., Li, D., Yang, Z., Bai, Y., Hu, S., et al. (2021). Identification of prognostic and therapeutic value of CC chemokines in urothelial bladder cancer: Evidence from comprehensive bioinformatic analysis. *BMC Urol.* 21, 173. doi:10.1186/s12894-021-00938-w

Lin, A. W., Gonzalez, S. A., Cunningham-Rundles, S., Dorante, G., Marshall, S., Tignor, A., et al. (2004). CD56(+dim) and CD56(+bright) cell activation and apoptosis in hepatitis C virus infection. *Clin. Exp. Immunol.* 137, 408–416. doi:10.1111/j.1365-2249.2004.02523.x

Liu, Y., Wu, Y., Zhang, P., Xu, C., Liu, Z., He, C., et al. (2021). CXCL12 and CD3E as indicators for tumor microenvironment modulation in bladder cancer and their correlations with immune infiltration and molecular subtypes. *Front. Oncol.* 11, 636870. doi:10.3389/fonc.2021.636870

Long, X., Xiong, W., Zeng, X., Qi, L., Cai, Y., Mo, M., et al. (2019). Cancer-associated fibroblasts promote cisplatin resistance in bladder cancer cells by increasing IGF-1/ERβ/Bcl-2 signalling. *Cell Death Dis.* 10, 375. doi:10.1038/s41419-019-1581-6

Lu, W., and Kang, Y. (2019). Epithelial-mesenchymal plasticity in cancer progression and metastasis. *Dev. Cell* 49, 361–374. doi:10.1016/j.devcel.2019.04.010

Magatti, M., Masserdotti, A., Bonassi Signoroni, P., Vertua, E., Stefani, F. R., Silini, A. R., et al. (2020). B lymphocytes as targets of the immunomodulatory properties of human amniotic mesenchymal stromal cells. *Front. Immunol.* 11, 1156. doi:10.3389/fimmu.2020.01156

Martin-Gayo, E., and Yu, X. G. (2019). Role of dendritic cells in natural immune control of HIV-1 infection. *Front. Immunol.* 10, 1306. doi:10.3389/fimmu.2019.01306

Martins-Lima, C., Miranda-Gonçalves, V., Lobo, J., Constâncio, V., Leite-Silva, P., Guimarães-Teixeira, C., et al. (2022). Cadherin switches during epithelial-mesenchymal transition: CDH4/RCAD downregulation reduces bladder cancer progression. *Cell. Oncol.* 45, 135–149. doi:10.1007/s13402-021-00657-2

McConkey, D. J., and Choi, W. (2018). Molecular subtypes of bladder cancer. *Curr. Oncol. Rep.* 20, 77. doi:10.1007/s11912-018-0727-5

Mian, B. M., Dinney, C. P., Bermejo, C. E., Sweeney, P., Tellez, C., Yang, X. D., et al. (2003). Fully human anti-interleukin 8 antibody inhibits tumor growth in orthotopic bladder cancer xenografts via down-regulation of matrix metalloproteases and nuclear factor-kappaB. *Clin. Cancer Res.* 9, 3167–3175.

Minoli, M., Kiener, M., Thalmann, G. N., Kruithof-de Julio, M., and Seiler, R. (2020). Evolution of urothelial bladder cancer in the context of molecular classifications. *Int. J. Mol. Sci.* 21, 5670. doi:10.3390/ijms21165670

Miyake, M., Furuya, H., Onishi, S., Hokutan, K., Anai, S., Chan, O., et al. (2019). Monoclonal antibody against CXCL1 (HL2401) as a novel agent in suppressing IL6 expression and tumoral growth. *Theranostics* 9, 853–867. doi:10.7150/thno.29553

Miyake, M., Hori, S., Morizawa, Y., Tatsumi, Y., Nakai, Y., Anai, S., et al. (2016). CXCL1-Mediated interaction of cancer cells with tumor-associated macrophages and cancer-associated fibroblasts promotes tumor progression in human bladder cancer. *Neoplasia* 18, 636–646. doi:10.1016/j.neo.2016.08.002

Miyake, M., Lawton, A., Goodison, S., Urquidi, V., Gomes-Giacoia, E., Zhang, G., et al. (2013). Chemokine (C-X-C) ligand 1 (CXCL1) protein expression is increased in aggressive bladder cancers. *BMC Cancer* 13, 322. doi:10.1186/1471-2407-13-322

Miyamoto, H., Kubota, Y., Shuin, T., Torigoe, S., Dobashi, Y., and Hosaka, M. (1995). Expression of transforming growth factor-beta 1 in human bladder cancer. *Cancer* 75, 2565–2570. doi:10.1002/1097-0142(19950515)75:10<2565:aid-cncr2820751025>3.0.co;2-m

Moretta, L. (2010). Dissecting CD56dim human NK cells. *Blood* 116, 3689–3691. doi:10.1182/blood-2010-09-303057

Morizawa, Y., Miyake, M., Shimada, K., Hori, S., Tatsumi, Y., Nakai, Y., et al. (2018). Correlation of immune cells and cytokines in the tumor microenvironment with elevated neutrophil-to-lymphocyte ratio in blood: An analysis of muscle-invasive bladder cancer. *Cancer Invest.* 36, 395–405. doi:10.1080/07357907.2018.1506800

Mukherjee, N., Ji, N., Hurez, V., Curiel, T. J., Montgomery, M. O., Braun, A. J., et al. (2018). Intratumoral CD56(bright) natural killer cells are associated with improved survival in bladder cancer. *Oncotarget* 9, 36492–36502. doi:10.18632/oncotarget.26362

Nair, S. S., Weil, R., Dovey, Z., Davis, A., and Tewari, A. K. (2020). The tumor microenvironment and immunotherapy in prostate and bladder cancer. *Urol. Clin. North Am.* 47, e17–e54. doi:10.1016/j.ucl.2020.10.005

Okamoto, M., Hattori, K., and Oyasu, R. (1997). Interleukin-6 functions as an autocrine growth factor in human bladder carcinoma cell lines *in vitro*. *Int. J. Cancer* 72, 149–154. doi:10.1002/(sici)1097-0215(19970703)72:1<149:aid-ijc21>3.0.co;2-d

Ou, Z., Wang, Y., Liu, L., Li, L., Yeh, S., Qi, L., et al. (2015). Tumor microenvironment B cells increase bladder cancer metastasis via modulation of the IL-8/androgen receptor (AR)/MMPs signals. *Oncotarget* 6, 26065–26078. doi:10.18632/oncotarget.4569

Pan, Y., Yu, Y., Wang, X., and Zhang, T. (2020). Tumor-associated macrophages in tumor immunity. *Front. Immunol.* 11. 587193. doi:10.3389/fimmu.2020.583084

Papageorgis, P. (2015). TGFβ signaling in tumor initiation, epithelial-to-mesenchymal transition, and metastasis. *J. Oncol.* 2015, 587193. doi:10.1155/2015/587193

Poli, A., Michel, T., Thérésine, M., Andrès, E., Hentges, F., and Zimmer, J. (2009). CD56bright natural killer (NK) cells: An important NK cell subset. *Immunology* 126, 458–465. doi:10.1111/j.1365-2567.2008.03027.x

Ramesh, G., MacLean, A. G., and Philipp, M. T. (2013). Cytokines and chemokines at the crossroads of neuroinflammation, neurodegeneration, and neuropathic pain. *Mediat. Inflamm.* 2013, 480739. doi:10.1155/2013/480739

Rao, Q., Chen, Y., Yeh, C. R., Ding, J., Li, L., Chang, C., et al. (2016). Recruited mast cells in the tumor microenvironment enhance bladder cancer metastasis via modulation of ERβ/CCL2/CCR2 EMT/MMP9 signals. *Oncotarget* 7, 7842–7855. doi:10.18632/oncotarget.5467

Reis, S. T., Leite, K. R. M., Piovesan, L. F., Pontes-Junior, J., Viana, N. I., Abe, D. K., et al. (2012). Increased expression of MMP-9 and IL-8 are correlated with poor prognosis of Bladder Cancer. *BMC Urol.* 12, 18. doi:10.1186/1471-2490-12-18

Retz, M. M., Sidhu, S. S., Blaveri, E., Kerr, S. C., Dolganov, G. M., Lehmann, J., et al. (2005). CXCR4 expression reflects tumor progression and regulates motility of bladder cancer cells. *Int. J. Cancer* 114, 182–189. doi:10.1002/ijc.20729

Rossi, J. F., Lu, Z. Y., Jourdan, M., and Klein, B. (2015). Interleukin-6 as a therapeutic target. *Clin. Cancer Res.* 21, 1248–1257. doi:10.1158/1078-0432.CCR-14-2291

Rossi, R., Lichtner, M., Iori, F., Ermocida, A., Mascia, C., Mengoni, F., et al. (2013). Dendritic cells in blood and urine samples from bladder cancer patients undergoing BCG immunotherapy. *Arch. Ital. Urol. Androl.* 85, 157–163. doi:10.4081/aiua.2013.4.157

Russo, G. I., Musso, N., Lo Giudice, A., Asmundo, M. G., Di Mauro, M., Bonacci, P. G., et al. (2022). PD-1, PD-L1 and cAMP immunohistochemical expressions are associated with worse oncological outcome in patients with bladder cancer. *J. Cancer Res. Clin. Oncol.* doi:10.1007/s00432-022-04262-0

Sawant, K. V., Poluri, K. M., Dutta, A. K., Sepuru, K. M., Troshkina, A., Garofalo, R. P., et al. (2016). Chemokine CXCL1 mediated neutrophil recruitment: Role of glycosaminoglycan interactions. *Sci. Rep.* 6, 33123. doi:10.1038/srep33123

Schuettfort, V. M., Pradere, B., Trinh, Q. D., D'Andrea, D., Quhal, F., Mostafaei, H., et al. (2022). Impact of preoperative plasma levels of interleukin 6 and interleukin 6 soluble receptor on disease outcomes after radical cystectomy for bladder cancer. *Cancer Immunol. Immunother.* 71, 85–95. doi:10.1007/s00262-021-02953-0

Shariat, S. F., Kim, J. H., Andrews, B., Kattan, M. W., Wheeler, T. M., Kim, I. Y., et al. (2001). Preoperative plasma levels of transforming growth factor beta(1) strongly predict clinical outcome in patients with bladder carcinoma. *Cancer* 92, 2985–2992. doi:10.1002/1097-0142(20011215)92:12<2985:aid-cncr10175>3.0.co;2-5

Shelton, S. E., Nguyen, H. T., Barbie, D. A., and Kamm, R. D. (2021). Engineering approaches for studying immune-tumor cell interactions and immunotherapy. *iScience* 24, 101985. doi:10.1016/j.isci.2020.101985

Shen, H. B., Gu, Z. Q., Jian, K., and Qi, J. (2013). CXCR4-mediated Stat3 activation is essential for CXCL12-induced cell invasion in bladder cancer. *Tumour Biol.* 34, 1839–1845. doi:10.1007/s13277-013-0725-z

Sinha, D., Saha, P., Samanta, A., and Bishayee, A. (2020). Emerging concepts of hybrid epithelial-to-mesenchymal transition in cancer progression. *Biomolecules* 10, E1561. doi:10.3390/biom10111561

Sistigu, A., Di Modugno, F., Manic, G., and Nisticò, P. (2017). Deciphering the loop of epithelial-mesenchymal transition, inflammatory cytokines and cancer immunoediting. *Cytokine Growth Factor Rev.* 36, 67–77. doi:10.1016/j.cytogfr.2017.05.008

Sjödahl, G., Lövgren, K., Lauss, M., Chebil, G., Patschan, O., Gudjonsson, S., et al. (2014). Infiltration of $CD3^+$ and $CD68^+$ cells in bladder cancer is subtype specific and affects the outcome of patients with muscle-invasive tumors. *Urol. Oncol.* 32, 791–797. doi:10.1016/j.urolonc.2014.02.007

Sokol, C. L., and Luster, A. D. (2015). The chemokine system in innate immunity. *Cold Spring Harb. Perspect. Biol.* 7, a016303. doi:10.1101/cshperspect.a016303

Song, D., Powles, T., Shi, L., Zhang, L., Ingersoll, M. A., and Lu, Y. J. (2019). Bladder cancer, a unique model to understand cancer immunity and develop immunotherapy approaches. *J. Pathol.* 249, 151–165. doi:10.1002/path.5306

Stellato, M., Santini, D., Cursano, M. C., Foderaro, S., Tonini, G., and Procopio, G. (2021). Bone metastases from urothelial carcinoma. The dark side of the moon. *J. Bone Oncol.* 31, 100405. doi:10.1016/j.jbo.2021.100405

Stojnev, S., Krstić, M., Čukuranović Kokoris, J., Conić, I., Petković, I., Ilić, S., et al. (2019). Prognostic impact of canonical TGF-β signaling in urothelial bladder cancer. *Med. Kaunas.* 55, E302. doi:10.3390/medicina55060302

Suarez-Carmona, M., Lesage, J., Cataldo, D., and Gilles, C. (2017). EMT and inflammation: Inseparable actors of cancer progression. *Mol. Oncol.* 11, 805–823. doi:10.1002/1878-0261.12095

Sun, X., Chen, Q., Zhang, L., Chen, J., and Zhang, X. (2021). Exploration of prognostic biomarkers and therapeutic targets in the microenvironment of bladder cancer based on CXC chemokines. *Math. Biosci. Eng.* 18, 6262–6287. doi:10.3934/mbe.2021313

Sun, Y., Sedgwick, A. J., Khan, M. A.-A.-K., Palarasah, Y., Mangiola, S., and Barrow, A. D. (2021). A transcriptional signature of IL-2 expanded natural killer cells predicts more favorable prognosis in bladder cancer. *Front. Immunol.* 12, 724107. doi:10.3389/fimmu.2021.724107

Sweis, R. F., Spranger, S., Bao, R., Paner, G. P., Stadler, W. M., Steinberg, G., et al. (2016). Molecular drivers of the non-T-cell-inflamed tumor microenvironment in urothelial bladder cancer. *Cancer Immunol. Res.* 4, 563–568. doi:10.1158/2326-6066.CIR-15-0274

Takeuchi, H., Tanaka, M., Tanaka, A., Tsunemi, A., and Yamamoto, H. (2016). Predominance of M2-polarized macrophages in bladder cancer affects angiogenesis, tumor grade and invasiveness. *Oncol. Lett.* 11, 3403–3408. doi:10.3892/ol.2016.4392

Takeyama, Y., Kato, M., Tamada, S., Azuma, Y., Shimizu, Y., Iguchi, T., et al. (2020). Myeloid-derived suppressor cells are essential partners for immune checkpoint inhibitors in the treatment of cisplatin-resistant bladder cancer. *Cancer Lett.* 479, 89–99. doi:10.1016/j.canlet.2020.03.013

Teijeira, Á., Garasa, S., Gato, M., Alfaro, C., Migueliz, I., Cirella, A., et al. (2020). CXCR1 and CXCR2 chemokine receptor agonists produced by tumors induce neutrophil extracellular traps that interfere with immune cytotoxicity. *Immunity* 52, 856–871. e8. doi:10.1016/j.immuni.2020.03.001

Trujillo, J. A., Sweis, R. F., Bao, R., and Luke, J. J. (2018). T cell-inflamed versus non-T cell-inflamed tumors: A conceptual framework for cancer immunotherapy drug development and combination therapy selection. *Cancer Immunol. Res.* 6, 990–1000. doi:10.1158/2326-6066.CIR-18-0277

Tseng-Rogenski, S., and Liebert, M. (2009). Interleukin-8 is essential for normal urothelial cell survival. *Am. J. Physiol. Ren. Physiol.* 297, F816–F821. doi:10.1152/ajprenal.90733.2008

Tsui, K. H., Wang, S. W., Chung, L. C., Feng, T. H., Lee, T. Y., Chang, P. L., et al. (2013). Mechanisms by which interleukin-6 attenuates cell invasion and tumorigenesis in human bladder carcinoma cells. *Biomed. Res. Int.* 2013, 791212. doi:10.1155/2013/791212

Urquidi, V., Chang, M., Dai, Y., Kim, J., Wolfson, E. D., Goodison, S., et al. (2012). IL-8 as a urinary biomarker for the detection of bladder cancer. *BMC Urol.* 12, 12. doi:10.1186/1471-2490-12-12

Van Linthout, S., Miteva, K., and Tschöpe, C. (2014). Crosstalk between fibroblasts and inflammatory cells. *Cardiovasc. Res.* 102, 258–269. doi:10.1093/cvr/cvu062

Viveiros, N., Flores, B. C., Lobo, J., Martins-Lima, C., Cantante, M., Lopes, P., et al. (2022). Detailed bladder cancer immunoprofiling reveals new clues for immunotherapeutic strategies. *Clin. Transl. Immunol.* 11, e1402. doi:10.1002/cti2.1402

Wang, N., Liu, W., Zheng, Y., Wang, S., Yang, B., Li, M., et al. (2018). CXCL1 derived from tumor-associated macrophages promotes breast cancer

metastasis via activating NF-κB/SOX4 signaling. *Cell Death Dis.* 9, 880. doi:10.1038/s41419-018-0876-3

Wang, P., Zang, S., Li, G., Qu, W., Li, S., Qiao, Q., et al. (2020). The role of surgery on the primary tumor site in bladder cancer with distant metastasis: Significance of histology type and metastatic pattern. *Cancer Med.* 9, 9293–9302. doi:10.1002/cam4.3560

Wang, W., Shen, F., Wang, C., Lu, W., Wei, J., Shang, A., et al. (2017). MiR-1-3p inhibits the proliferation and invasion of bladder cancer cells by suppressing CCL2 expression. *Tumour Biol.* 39, 1010428317698383. doi:10.1177/1010428317698383

Wculek, S. K., Cueto, F. J., Mujal, A. M., Melero, I., Krummel, M. F., and Sancho, D. (2020). Dendritic cells in cancer immunology and immunotherapy. *Nat. Rev. Immunol.* 20, 7–24. doi:10.1038/s41577-019-0210-z

Wendt, M. K., Allington, T. M., and Schiemann, W. P. (2009). Mechanisms of the epithelial-mesenchymal transition by TGF-beta. *Future Oncol.* 5, 1145–1168. doi:10.2217/fon.09.90

Winerdal, M. E., Marits, P., Winerdal, M., Hasan, M., Rosenblatt, R., Tolf, A., et al. (2011). FOXP3 and survival in urinary bladder cancer. *BJU Int.* 108, 1672–1678. doi:10.1111/j.1464-410X.2010.10020.x

Wołącewicz, M., Hrynkiewicz, R., Grywalska, E., Suchojad, T., Leksowski, T., Roliński, J., et al. (2020). Immunotherapy in bladder cancer: Current methods and future perspectives. *Cancers (Basel)* 12, E1181. doi:10.3390/cancers12051181

Xiu, W., Ma, J., Lei, T., Zhang, M., and Zhou, S. (2016). Immunosuppressive effect of bladder cancer on function of dendritic cells involving of Jak2/STAT3 pathway. *Oncotarget* 7, 63204–63214. doi:10.18632/oncotarget.11434

Xu, J., Lamouille, S., and Derynck, R. (2009). TGF-beta-induced epithelial to mesenchymal transition. *Cell Res.* 19, 156–172. doi:10.1038/cr.2009.5

Xu, M., Wang, Y., Xia, R., Wei, Y., and Wei, X. (2021). Role of the CCL2-CCR2 signalling axis in cancer: Mechanisms and therapeutic targeting. *Cell Prolif.* 54, e13115. doi:10.1111/cpr.13115

Yafi, F. A., and Kassouf, W. (2009). Radical cystectomy is the treatment of choice for invasive bladder cancer. *Can. Urological Assoc. J. = J. de l'Association des urologues du Can.* 3, 409–412. doi:10.5489/cuaj.1156

Yang, D. L., Xin, M. M., Wang, J. S., Xu, H. Y., Huo, Q., Tang, Z. R., et al. (2015). Chemokine receptor CXCR4 and its ligand CXCL12 expressions and clinical significance in bladder cancer. *Genet. Mol. Res.* 14, 17699–17707. doi:10.4238/2015.December.21.43

Yang, F., Liu, X.-Q., He, J.-Z., Xian, S.-P., Yang, P.-F., Mai, Z.-Y., et al. (2022). Occludin facilitates tumour angiogenesis in bladder cancer by regulating IL8/STAT3 through STAT4. *J. Cell. Mol. Med.* 26, 2363–2376. doi:10.1111/jcmm.17257

Yang, G., Shen, W., Zhang, Y., Liu, M., Zhang, L., Liu, Q., et al. (2017). Accumulation of myeloid-derived suppressor cells (MDSCs) induced by low levels of IL-6 correlates with poor prognosis in bladder cancer. *Oncotarget* 8, 38378–38388. doi:10.18632/oncotarget.16386

Yang, H. J., Liu, G. L., Liu, B., and Liu, T. (2018). GP73 promotes invasion and metastasis of bladder cancer by regulating the epithelial-mesenchymal transition through the TGF-β1/Smad2 signalling pathway. *J. Cell. Mol. Med.* 22, 1650–1665. doi:10.1111/jcmm.13442

Yao, K., He, L., Gan, Y., Liu, J., Tang, J., Long, Z., et al. (2020). HMGN5 promotes IL-6-induced epithelial-mesenchymal transition of bladder cancer by interacting with Hsp27. *Aging (Albany NY)* 12, 7282–7298. doi:10.18632/aging.103076

Yeh, C. R., Hsu, I., Song, W., Chang, H., Miyamoto, H., Xiao, G. Q., et al. (2015). Fibroblast ERα promotes bladder cancer invasion via increasing the CCL1 and IL-6 signals in the tumor microenvironment. *Am. J. Cancer Res.* 5, 1146–1157.

Yoshihara, K., Shahmoradgoli, M., Martínez, E., Vegesna, R., Kim, H., Torres-Garcia, W., et al. (2013). Inferring tumour purity and stromal and immune cell admixture from expression data. *Nat. Commun.* 4, 2612. doi:10.1038/ncomms3612

Yu, Y., Xiao, C. H., Tan, L. D., Wang, Q. S., Li, X. Q., and Feng, Y. M. (2014). Cancer-associated fibroblasts induce epithelial–mesenchymal transition of breast cancer cells through paracrine TGF-β signalling. *Br. J. Cancer* 110, 724–732. doi:10.1038/bjc.2013.768

Yun, S. J., and Kim, W. J. (2013). Role of the epithelial-mesenchymal transition in bladder cancer: From prognosis to therapeutic target. *Korean J. Urol.* 54, 645–650. doi:10.4111/kju.2013.54.10.645

Zhang, J. M., and An, J. (2007). Cytokines, inflammation, and pain. *Int. Anesthesiol. Clin.* 45, 27–37. doi:10.1097/AIA.0b013e318034194e

Zhang, J., Patel, L., and Pienta, K. J. (2010). Targeting chemokine (C-C motif) ligand 2 (CCL2) as an example of translation of cancer molecular biology to the clinic. *Prog. Mol. Biol. Transl. Sci.* 95, 31–53. doi:10.1016/B978-0-12-385071-3.00003-4

Zhang, N., Bi, X., Zeng, Y., Zhu, Y., Zhang, Z., Liu, Y., et al. (2016). TGF-β1 promotes the migration and invasion of bladder carcinoma cells by increasing fascin1 expression. *Oncol. Rep.* 36, 977–983. doi:10.3892/or.2016.4889

Zhang, S., Wang, J., Zhang, X., and Zhou, F. (2017). Tumor-infiltrating CD8+ lymphocytes predict different clinical outcomes in organ- and non-organ-confined urothelial carcinoma of the bladder following radical cystectomy. *PeerJ* 5, e3921. doi:10.7717/peerj.3921

Zhang, T., Yang, F., Li, W., Liu, B., Li, W., Chen, Z., et al. (2018). Suppression of the SDF-1/CXCR4/β-catenin axis contributes to bladder cancer cell growth inhibition *in vitro* and *in vivo*. *Oncol. Rep.* 40, 1666–1674. doi:10.3892/or.2018.6546

Zhang, Y., Ou, D. H., Zhuang, D. W., Zheng, Z. F., and Lin, M. E. (2020). *In silico* analysis of the immune microenvironment in bladder cancer. *BMC Cancer* 20, 265. doi:10.1186/s12885-020-06740-5

Zhou, Q., Jin, P., Liu, J., Li, S., Liu, W., and Xi, S. (2021). HER2 overexpression triggers the IL-8 to promote arsenic-induced EMT and stem cell-like phenotypes in human bladder epithelial cells. *Ecotoxicol. Environ. Saf.* 208, 111693. doi:10.1016/j.ecoenv.2020.111693

Zou, J., Huang, R., Li, H., Wang, B., Chen, Y., Chen, S., et al. (2019). Secreted TGF-beta-induced protein promotes aggressive progression in bladder cancer cells. *Cancer Manag. Res.* 11, 6995–7006. doi:10.2147/CMAR.S208984

Frontiers in
Molecular Biosciences

Explores biological processes in living organisms on a molecular scale

Focuses on the molecular mechanisms underpinning and regulating biological processes in organisms across all branches of life.

Discover the latest Research Topics

See more →

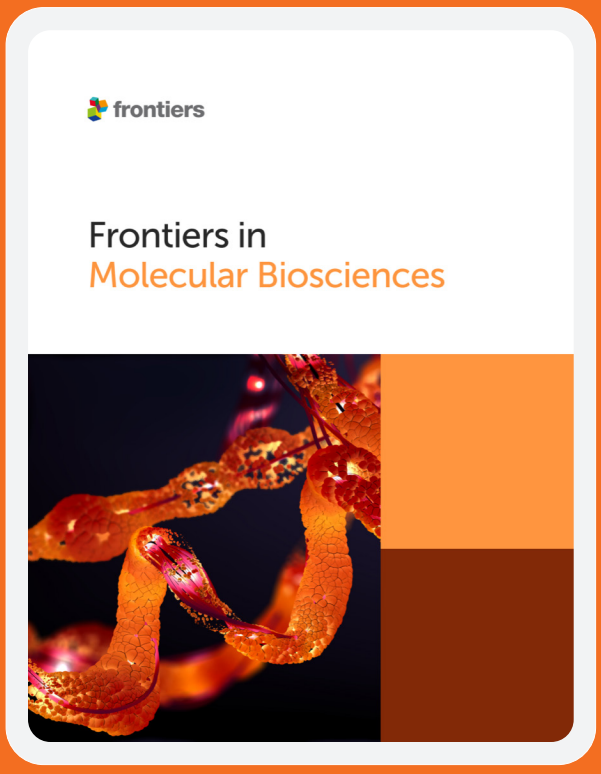

Frontiers

Avenue du Tribunal-Fédéral 34
1005 Lausanne, Switzerland
frontiersin.org

Contact us

+41 (0)21 510 17 00
frontiersin.org/about/contact